



# MOLECULAR SIGNALLING AND PATHWAYS EDITOR'S PICKS 2021

EDITED BY: Jean-Marc Taymans

PUBLISHED IN: Frontiers in Molecular Neuroscience



**frontiers** Research Topics



# frontiers

## Frontiers eBook Copyright Statement

The copyright in the text of individual articles in this eBook is the property of their respective authors or their respective institutions or funders. The copyright in graphics and images within each article may be subject to copyright of other parties. In both cases this is subject to a license granted to Frontiers.

The compilation of articles constituting this eBook is the property of Frontiers.

Each article within this eBook, and the eBook itself, are published under the most recent version of the Creative Commons CC-BY licence.

The version current at the date of publication of this eBook is CC-BY 4.0. If the CC-BY licence is updated, the licence granted by Frontiers is automatically updated to the new version.

When exercising any right under the CC-BY licence, Frontiers must be attributed as the original publisher of the article or eBook, as applicable.

Authors have the responsibility of ensuring that any graphics or other materials which are the property of others may be included in the CC-BY licence, but this should be checked before relying on the CC-BY licence to reproduce those materials. Any copyright notices relating to those materials must be complied with.

Copyright and source acknowledgement notices may not be removed and must be displayed in any copy, derivative work or partial copy which includes the elements in question.

All copyright, and all rights therein, are protected by national and international copyright laws. The above represents a summary only. For further information please read Frontiers' Conditions for Website Use and Copyright Statement, and the applicable CC-BY licence.

ISSN 1664-8714  
ISBN 978-2-88971-112-3  
DOI 10.3389/978-2-88971-112-3

## About Frontiers

Frontiers is more than just an open-access publisher of scholarly articles: it is a pioneering approach to the world of academia, radically improving the way scholarly research is managed. The grand vision of Frontiers is a world where all people have an equal opportunity to seek, share and generate knowledge. Frontiers provides immediate and permanent online open access to all its publications, but this alone is not enough to realize our grand goals.

## Frontiers Journal Series

The Frontiers Journal Series is a multi-tier and interdisciplinary set of open-access, online journals, promising a paradigm shift from the current review, selection and dissemination processes in academic publishing. All Frontiers journals are driven by researchers for researchers; therefore, they constitute a service to the scholarly community. At the same time, the Frontiers Journal Series operates on a revolutionary invention, the tiered publishing system, initially addressing specific communities of scholars, and gradually climbing up to broader public understanding, thus serving the interests of the lay society, too.

## Dedication to Quality

Each Frontiers article is a landmark of the highest quality, thanks to genuinely collaborative interactions between authors and review editors, who include some of the world's best academicians. Research must be certified by peers before entering a stream of knowledge that may eventually reach the public - and shape society; therefore, Frontiers only applies the most rigorous and unbiased reviews. Frontiers revolutionizes research publishing by freely delivering the most outstanding research, evaluated with no bias from both the academic and social point of view. By applying the most advanced information technologies, Frontiers is catapulting scholarly publishing into a new generation.

## What are Frontiers Research Topics?

Frontiers Research Topics are very popular trademarks of the Frontiers Journals Series: they are collections of at least ten articles, all centered on a particular subject. With their unique mix of varied contributions from Original Research to Review Articles, Frontiers Research Topics unify the most influential researchers, the latest key findings and historical advances in a hot research area! Find out more on how to host your own Frontiers Research Topic or contribute to one as an author by contacting the Frontiers Editorial Office: [frontiersin.org/about/contact](https://frontiersin.org/about/contact)



# MOLECULAR SIGNALLING AND PATHWAYS EDITOR'S PICKS 2021

Topic Editor:

**Jean-Marc Taymans**, Institut National de la Santé et de la Recherche Médicale (INSERM), France

**Citation:** Taymans, J.-M., ed. (2021). Molecular Signalling and Pathways Editor's Picks 2021. Lausanne: Frontiers Media SA. doi: 10.3389/978-2-88971-112-3

# Table of Contents

- 05** *Differences in Gene Expression Profiles and Phenotypes of Differentiated SH-SY5Y Neurons Stably Overexpressing Mitochondrial Ferritin*  
Anarmaa Mendsaikhan, Shigeko Takeuchi, Douglas G. Walker and Ikuo Tooyama
- 27** *PKR: A Kinase to Remember*  
Shunit Gal-Ben-Ari, Iliana Barrera, Marcelo Ehrlich and Kobi Rosenblum
- 47** *Small Molecule Modulators of the Circadian Molecular Clock With Implications for Neuropsychiatric Diseases*  
Hyo Kyeong Cha, Sooyoung Chung, Hye Young Lim, Jong-Wha Jung and Gi Hoon Son
- 57** *Connexin Hemichannels in Astrocytes: Role in CNS Disorders*  
LingYan Xing, Tuo Yang, ShuSen Cui and Gang Chen
- 67** *An IQSEC2 Mutation Associated With Intellectual Disability and Autism Results in Decreased Surface AMPA Receptors*  
Eli J. Rogers, Reem Jada, Kinneret Schragenheim-Rozales, Megha Sah, Marisol Cortes, Matthew Florence, Nina S. Levy, Rachel Moss, Randall S. Walikonis, Raz Palty, Reut Shalgi, Daniela Lichtman, Alexandra Kavushansky, Nashaat Z. Gerges, Itamar Kahn, George K. E. Umanah and Andrew P. Levyi
- 85** *27-Hydroxycholesterol Contributes to Lysosomal Membrane Permeabilization-Mediated Pyroptosis in Co-cultured SH-SY5Y Cells and C6 Cells*  
Si Chen, Cui Zhou, Huiyan Yu, Lingwei Tao, Yu An, Xiaona Zhang, Ying Wang, Yushan Wang and Rong Xiao
- 96** *MicroRNAs in Microglia: How do MicroRNAs Affect Activation, Inflammation, Polarization of Microglia and Mediate the Interaction Between Microglia and Glioma?*  
Yawei Guo, Wenming Hong, Xinming Wang, Pengying Zhang, Heinrich Körner, Jiajie Tu and Wei Wei
- 110** *Monoamine Oxidases (MAOs) as Privileged Molecular Targets in Neuroscience: Research Literature Analysis*  
Andy Wai Kan Yeung, Maya G. Georgieva, Atanas G. Atanasov and Nikolay T. Tzvetkov
- 122** *Inhibition of nSMase2 Reduces the Transfer of Oligomeric  $\alpha$ -Synuclein Irrespective of Hypoxia*  
Valerie Sackmann, Maitrayee Sardar Sinha, Christopher Sackmann, Livia Civitelli, Joakim Bergström, Anna Ansell-Schultz and Martin Hallbeck
- 137** *Glucocorticoid-Driven NLRP3 Inflammasome Activation in Hippocampal Microglia Mediates Chronic Stress-Induced Depressive-Like Behaviors*  
Xiujing Feng, Yuan Zhao, Tianyuan Yang, Manyu Song, Chaoran Wang, Yujie Yao and Honggang Fan

**152   *Structural Insights Into TDP-43 and Effects of Post-translational Modifications***

Liberty François-Moutal, Samantha Perez-Miller, David D. Scott, Victor G. Miranda, Niloufar Mollasalehi and May Khanna

**174   *Circulating Exosomal miRNA as Diagnostic Biomarkers of Neurodegenerative Diseases***

Lin Wang and Lijuan Zhang



# Differences in Gene Expression Profiles and Phenotypes of Differentiated SH-SY5Y Neurons Stably Overexpressing Mitochondrial Ferritin

Anarmaa Mendsaikhan, Shigeko Takeuchi, Douglas G. Walker\* and Ikuo Tooyama\*

Molecular Neuroscience Research Center, Shiga University of Medical Science, Otsu, Japan

## OPEN ACCESS

### Edited by:

Christian Gonzalez-Billault,  
Universidad de Chile, Chile

### Reviewed by:

Patrizia Longone,  
Fondazione Santa Lucia (IRCCS), Italy  
Mariapaola Nitti,  
Università di Genova, Italy

### \*Correspondence:

Douglas G. Walker  
walker@belle.shiga-med.ac.jp  
Ikuo Tooyama  
kinchan@belle.shiga-med.ac.jp

**Received:** 19 June 2018

**Accepted:** 04 December 2018

**Published:** 08 January 2019

### Citation:

Mendsaikhan A, Takeuchi S,  
Walker DG and Tooyama I (2019)  
Differences in Gene Expression  
Profiles and Phenotypes of  
Differentiated SH-SY5Y Neurons  
Stably Overexpressing Mitochondrial  
Ferritin. *Front. Mol. Neurosci.* 11:470.  
doi: 10.3389/fnmol.2018.00470

Mitochondrial ferritin (FtMt) is an iron-transport protein with ferroxidase properties localized to mitochondria. Levels are generally low in all tissues, while increasing the expression of FtMt in neuronal-like cells has been shown to be protective. To determine whether FtMt has potential as a therapeutic approach, there remains the question of how much FtMt is protective. To address this issue, we transfected SH-SY5Y neuroblastoma cells with a FtMt expression plasmid and isolated cell lines with stable expression of FtMt at high, medium and low levels. Using these cell lines, we examined effects of FtMt on neuronal phenotype, neuroprotective activity and gene expression profiles. The phenotypic properties of high, medium and low FtMt expressors were compared with native untransfected SH-SY5Y cells after differentiation with retinoic acid to a neuronal phenotype. Overexpression of FtMt, even in low expressing cells, showed significant protection from oxidative stress induced by hydrogen peroxide or cobalt chloride. Higher levels of FtMt expression did not appear to offer greater protection, and did not have toxic consequences to cells, even though there were significantly more aggregated mitochondria in the highest expressing clone. The phenotypes differed between cell clones when assessed by cell growth, neurite outgrowth, and expression of neuronal proteins including those associated with neurodegenerative diseases. Microarray analysis of high, medium and negative FtMt-expressing cells identified different patterns of expression of certain genes associated with oxidative stress and neuronal development, amongst others. Validation of microarray analyses was carried out by real time polymerase chain reaction. The results showed significant differences in expression of thioredoxin-interacting protein (TXNIP) and microsomal glutathione transfer-1 (MGST-1), which can have critical roles in the regulation of oxidative stress. Differences in expression of calcitonin-related polypeptide alpha (CALCA), growth differentiation factor-15 (GDF-15) and secretogranin II (SCG2) were also observed. Our findings indicate that even low levels of increased FtMt expression can be protective

possibly by alterations of some oxidative stress-related and growth factor genes, while high levels of expression did not appear to offer greater protection from oxidative stress or induce significant toxicity in cells. These experiments provide supporting data that increasing FtMt might be a feasible strategy for therapeutics in certain neurodegenerative and neurological diseases.

**Keywords:** neuroprotection, free radical, mitochondria, iron, neurodegeneration, cell culture

## INTRODUCTION

Age-associated neurodegenerative diseases, particularly Alzheimer's disease (AD) and Parkinson's disease (PD), have proven resistant to effective therapies as the pathological processes are complex and still incompletely understood. There have been multiple approaches aimed at slowing down the degenerative processes, but they have primarily focused on inhibiting the formation or promoting the removal of toxic forms of amyloid beta (A $\beta$ ) peptide or tau (for AD) or  $\alpha$ -synuclein (for PD) (Brundin et al., 2017; Jan et al., 2017). Although these diseases have significant clinical and pathological differences, one common feature is increased oxidative stress through elevated levels of damaging reactive oxygen species (ROS) (Nesi et al., 2017; Lang and Espay, 2018). Effective regulation of intracellular iron plays a critical role in controlling generation of ROS. Ferritin-H is the major cellular regulator of iron in most cells, but a significant role has been identified for mitochondrial ferritin (FtMt), a ferritin-H-like molecule that is targeted to mitochondria (Arosio et al., 2009).

FtMt has roles that overlap with ferritin, but its expression in normal tissue is very low and restricted to testis, brain, heart, and erythroblasts (Levi and Arosio, 2004; Santambrogio et al., 2007). FtMt expression is highest in cells of tissues with high oxygen demand, including neurons in brain (Gao and Chang, 2014). FtMt has multiple properties, in particular ferroxidase activity to reduce reactive ferrous ions to less reactive ferric ions. Within the realm of biological processes, it participates in oxidation-reduction, iron transport across membranes and cellular iron homeostasis. FtMt is synthesized as a 30 kDa polypeptide that is cleaved once the protein is translocated to the mitochondria matrix and assembles into a "ferritin-shell" of 24 of 22 kDa polypeptide chains (Levi et al., 2001; Drysdale et al., 2002). FtMt binds iron with similar properties to ferritin, but has particularly important function of regulating reactive iron species in mitochondria (Yang et al., 2013; Wang Y. Q. et al., 2016). In contrast to ferritin, FtMt mRNA lacks an iron-response element indicating a different mechanism of regulation (Drysdale et al., 2002). Recently, the FtMt gene promoter was shown to contain positive regulatory sequences for cyclic-AMP response element-binding protein (CREB), YY1 and SP1 transcription factors, and C/EBP $\beta$ , GATA2 and FOXA1 sequences as negative regulators (Gualdo et al., 2016).

With reference to the involvement of FtMt in diseases, it has been associated with Friedreich's Ataxia, restless leg syndrome and macular degeneration (Huang et al., 2009; Snyder et al., 2009; Stenirri et al., 2012; Wang X. et al., 2016). Overexpression

of FtMt significantly slowed the replication of FtMt transfected SH-SY5Y neuroblastoma cells, both in culture and after *in vivo* transplantation of overexpressing cells to immune-deficient mice (Gong et al., 2017). Increased expression of FtMt has been demonstrated in neurons in regions of human brains affected by AD and PD pathology (Wang et al., 2011; Yang et al., 2017).

A number of studies using overexpression or knockdown models employing neuronal-like cells, particularly SH-SY5Y cells, demonstrated that FtMt protected against oxidative stressors and A $\beta$  neurotoxicity (Shi et al., 2015; Gao et al., 2017; Li X. et al., 2017; Wang et al., 2017), (Wu et al., 2013; Wang Y. Q. et al., 2016; Gao et al., 2017; Guan et al., 2017). The potential therapeutic benefits of FtMt have also been suggested from different animal models for AD or PD. Using a line of mice with deletion of FtMt gene, it was shown that intracerebroventricular administration of the toxic A $\beta$ 25-35 fragment exacerbated memory deficits, with enhanced caspase activation in the gene deletion mice compared to mice expressing FtMt (Wang et al., 2017). Such studies will be enhanced with a transgenic mouse line that overexpresses FtMt. In models of PD, increased expression of FtMt was shown in mice treated with the dopaminergic toxins 6-OHDA and MPTP, while similarly treated FtMt gene deletion mice had higher levels of dopaminergic cell loss (Shi et al., 2010; You et al., 2016).

To determine whether FtMt has potential as a therapeutic approach, possibly by gene delivery methods, there remains the question of how much FtMt is protective and if mitochondrial damage can occur if levels are too high. Our previous paper showed that overexpression of FtMt in the ARPE-13 line of retinol epithelium cells caused several effects on mitochondrial function including increased mitochondrial fission and mitophagy (Wang X. et al., 2016). In order to clarify these issues, we established neuronal cell lines with stable expression of high, medium and low FtMt levels. Using these cell lines, we examined effects of overexpression of FtMt on neuronal phenotype, neuroprotective activity, and gene expression profiles.

## MATERIALS AND METHODS

### Cell Culture

The human neuroblastoma SH-SY5Y cell line was obtained from the American Type Culture Collection (Gaithersburg, MD, USA) (Ross et al., 1983). Cells were grown in Dulbecco's Modified Eagle's Medium (DMEM) with high glucose and supplemented with 5% fetal bovine serum (FBS) and 50  $\mu$ g/ml gentamicin. All

cell culture reagents were obtained from Nacalai-Tesque, Kyoto, Japan. Cells were routinely subcultured with 0.1% trypsin/1 mM EDTA in Hanks Balanced Salt Solution (HBSS) before reaching confluency, but in some circumstances during earlier stages of clone establishment, cells were subcultured with PBS without trypsin to separate the neuroblast from epithelial-type cells. After initial isolation of FtMt-expressing clones, all experiments were carried out with differentiated cells with the exception of studies on cell growth. To produce differentiated cells with neuronal features, untransfected and isolated clones were treated with retinoic acid (10  $\mu$ M) (Sigma-Aldrich, St. Louis, MO, USA) for 7 days in DMEM with 0.5–1.0 % FBS. Media was refreshed after 3 days of culture.

## Transfection

Cells were transfected with a pEGFP-FTMT plasmid whose construction and characterization has been described (Wang et al., 2011). All recombinant DNA experiments were carried out with appropriate institutional approvals. To isolate stably-expressing SH-SY5Y cells, cells were plated at  $2 \times 10^5$  cells/well in 12 well-plates in growth media. After 24 h, media was replaced with serum-free DMEM, and transfection was carried out in triplicate using 0.5–1  $\mu$ g plasmid DNA mixed with Viofectin (Viogen, New Taipei City, Taiwan) according to the manufacturer's instructions. After 6 h, serum was added to media to 5% final concentration, and cells allowed to recover for 18 h. The cultures were then subcultured with cells from each well-being transferred to a 60 mm diameter petri dish. The following day, media was replaced with growth media (DMEM + 5% FBS) containing 500  $\mu$ g/ml G418 (Selection Media) (Nacalai-Tesque, Kyoto, Japan). The progress of the cultures were followed with twice-weekly media changes until growing colonies could be identified on plates. Individual colonies were selected using trypsin-soaked cloning discs (approximately 0.5 cm diameter), and these were transferred to individual T25 flasks in selection media for expansion. A number of separate colonies of G418-resistant cells were grown until cell numbers were sufficient to permit screening for FtMt expression and freezing in liquid nitrogen. A total of 26 isolated clones were isolated, screened and stored (Supplemental Figure 1).

## Western Blot Screening Colonies for FtMt Expression

Western blots were used to screen isolated clones for expression of FtMt protein in selected clones. Initial screening was carried out using undifferentiated cells. Cell pellets were briefly disrupted by sonication in RIPA buffer (50 mM Tris-HCl, pH 7.6, 1% sodium deoxycholate, 1% NP40, 0.1% sodium dodecyl sulfate (SDS) and a cocktail of protease inhibitors). Protein concentrations in samples were measured using a MicroBCA Protein assay kit (Thermo Scientific, USA). Samples were prepared for SDS-polyacrylamide gel electrophoresis by dissolving in SDS-sample buffer containing 0.1M dithiothreitol (DTT). Equal amounts of protein were loaded on precast 5–20% SDS gradient gels (Wako, Japan or Nacalai-Tesque, Japan). After separation, proteins were transferred to Immobilon P (Millipore,

MA, USA) PVDF membrane using semi-dry electroblotting apparatus.

## Western Blot Detection and Quantification

The following procedures were used for all western blot in the analyses in this report. PVDF membranes were blocked for 1 h with 5% skim milk dissolved in Tris-buffered saline (50 mM Tris-HCl, pH 7.5, 150 mM NaCl) containing 0.05% Tween 20 (TBST). Membranes were subsequently incubated at room temperature for 18 h in optimal antibody dilution in 2% skim milk in TBST containing 0.005% sodium azide. The production and characterization of the custom rabbit polyclonal antibody to FtMt has previously been described (Yang et al., 2015). The antibodies used in this report are listed in **Table 1**. After antibody incubation, membranes were sequentially washed  $3 \times 10$  min in TBST, and incubated in the appropriate horseradish peroxidase (HRP)-conjugated anti-immunoglobulin for 2 h. Membranes were imaged using Chemi-Lumi-One HRP chemiluminescence substrate (Nacalai-Tesque) with a LAS4000 Imaging system (GE Biosciences, U.S.A.). Some membranes were reprobed with different antibodies after treatment with Stripping Agent-Strong (Nacalai-Tesque). For normalization and loading control, membranes were subsequently incubated with an HRP-conjugated antibody to  $\beta$ -actin (FujiFilm/Wako, Japan) at 1:15,000 for 1 h. All images were quantified using Image Studio Lite software (Licor, NE, USA). Results are calculated as relative expression after normalization for levels of  $\beta$ -actin.

## Immunocytochemistry

Immunocytochemistry was used to demonstrate expression and localization of FtMt, neurofilaments, and mitochondrial cyclooxygenase 1 (MtCox-1) in differentiated FtMt expressing clones. Different clones were plated onto chamber slides (Nunc) at  $10^4$  cells/well and differentiated for 7 days in RA-containing media. After that period, cells were rinsed with PBS, and fixed with 70% ethanol at  $-20^\circ\text{C}$  for 30 min. The fixative solution was removed and cells dried to ensure attachment. Cells were incubated in optimal dilutions of antibody (**Table 1**) diluted in TBST overnight at room temperature. After washing three times with TBST, cells were incubated with optimal dilution of anti-species immunoglobulin conjugated with fluorophore (dyes used indicated in Figure legends). Cells were counterstained with DAPI to allow identification of nuclei and coverslipped with fluorescent mounting agent. Stained cells were examined using a FV1000 Olympus confocal microscope. Photos were taken from three randomly selected fields for each experiment of three independent experiments.

## Cellular Fractionation and Mitochondria Isolation

To measure the subcellular localization of overexpressed FtMt, differentiated cells were fractionated using the Mitochondria Isolation kit for Mammalian Cells (Thermo Fisher, USA) to isolate a mitochondria-enriched fraction. FtMt expressors and untransfected cells were grown in T75 flasks and differentiated for 7 days with RA treatment. Mitochondria fractions were



**TABLE 1** | Description of reagents used in study.

Antigen	Supplier/Cat.no	Description	Species	Application	Dilution
<b>ANTIBODIES</b>					
FtMt	Custom	Polyclonal	Rabbit	WB, ICC	1/5000
NFH/M	Biologend (837904)	Monoclonals	Mouse	WB, ICC	1/2000
PSD95	Abcam (ab126732)	Monoclonal	Rabbit	WB	1/2000
SNAP25	Abcam (ab109105)	Monoclonal	Rabbit	WB	1/10000
APP	Abcam (ab126732)	Monoclonal	Rabbit	WB	1/3000
Tau	Pierce (MN1000)	Monoclonal	Mouse	WB	1/2000
$\alpha$ -synuclein	Covance 4B12	Monoclonal	Mouse	WB	1/2000
TXNIP	Abcam (ab188865)	Monoclonal	Rabbit	WB	1/2000
Mt-Cox-1	Abcam (ab14705)	Monoclonal	Mouse	WB, ICC	1/2000
Histone H3	Abcam (ab21054)	HRP Polyclonal	Rabbit	WB	1/10000
$\beta$ -actin	Fujifilm (017-24573)	HRP Monoclonal	Mouse	WB	1/10000

WB, Western blot; ICC, Immunocytochemistry.

Gene	Sequence	Amplicon (bp)	Ref.Seq.
<b>PCR PRIMER SEQUENCES</b>			
FTMT sense	CCCATTTGTGCGATTTCC	166	NM_177478.1
FTMT antisense	TTCTGCTTGTTCATTTCCA		
MGST-1 sense	GAAAGGTTTTTGCCAATCCA	186	XM_011520674
MGST-1 antisense	TTCCTGCCATTCTCATTTCC		
TXNIP sense	TCGTGTCAAAGCCGTTAGGA	228	NM_006472.5
TXNIP antisense	TTGAAGGATGTTCCAGAGGC		
TXN sense	GCCTTCTTTTCATTCCCTCTCT	145	NM_003329.3
TXN antisense	ACCCACCTTTTGTCCCTTCT		
CALCA sense	GTCAAGGCACAGCATTACCA	95	XM_017018283.1
CALCA antisense	CCCTATTGACATTGGTGGCTCT		
SCG2 sense	AGATGAAACGCTCAGGGCAG	147	NM_003469.4
SCG2 antisense	GCCCATCTGTAACTCCCA		
GDF-15 sense	CTCTCAGATGCTCCTGGTGT	159	AF003934.1
GDF-15 antisense	AGCAGGTCCTCGTAGCGTTT		
TFRC sense	GCCAATGTCACAAAACCAA	188	NM_003234.3
TFRC antisense	AAGTCCTCTCCTGGCTCCTC		
$\beta$ actin sense	CCTATGTGGGCGACGAG	242	NM_001101.3
$\beta$ actin antisense	ATGGCTGGGGTGTGAAG		

isolated from collected cells following a modification of the manufacturer's recommended protocol. In brief, cell pellets containing approximately  $1.5 \times 10^7$  cells were resuspended in Reagent A (with added protease inhibitors) (400  $\mu$ l) and incubated on ice for 2 min. 5  $\mu$ l of Reagent B was then added and pellets were gently sonicated for 5 s to ensure complete cell lysis without damaging nuclei. The lysates were centrifuged for 10 min at 700 g and the supernatants transferred to new tubes. This step was repeated to remove all nuclear material. The supernatants were then centrifuged at 12,000 g for 15 min. The pellets were resuspended in 500  $\mu$ l of Reagent C and centrifuged for the same period as a wash step, while the supernatants were saved as cytosolic fractions. The protein concentration was determined for each fraction, and samples processed for western blot analysis.

## Cell Replication and Neurite Elongation Measurements

Similar analysis methods were used to determine the rate of replication of undifferentiated FtMt clones compared to untransfected cells, and development of neurites of differentiated FtMt clones compared to untransfected cells. For measuring cell replication,  $10^4$  cells from different clones were plated into T25 flasks in growth media. Phase contrast images were recorded at Day 1, Day 3, Day 5, and Day 7 using an Olympus phase contrast microscope. Area occupied was used as the measure of cell numbers. The area of cells in 20x images were measured using image J software (NIH, USA). Five images taken at random were recorded at each time point for each clone. Each experiment was repeated three times. Results recorded show mean values  $\pm$  standard error of mean (SEM).

For measuring neurite formation,  $10^4$  cells from each clone were plated into wells of 12-well plates in triplicate. The following day media was exchanged for differentiation media containing RA. Five images/well were recorded and analyzed for neurite elongation after 7 days using Image J software plugin NeuronJ (<https://imagescience.org/meijering/>). The area occupied by neurites in each field was measured and data analyzed as described above.

## Cell Viability Measurements

For assessing responses to oxidative stress caused by hydrogen peroxide or cobalt chloride, a microtiter assay was used. Using 96-well-tissue culture microtiter plates,  $1.5 \times 10^4$  cells/well were plated in 100  $\mu$ l of media. After attachment, media was exchanged for differentiation media and cells were treated for 7 days to develop a neuronal phenotype. For assessing treatments, media was exchanged for DMEM + 1% FBS to which different concentrations of hydrogen peroxide (0–250  $\mu$ M) or cobalt chloride (0–200  $\mu$ M) were added. Cells were incubated for 24 h and then 10  $\mu$ l of cell viability reagent WST-1 (Cell Count Reagent, Nacalai-Tesque, Japan) was added to each well. Absorbance at 450 nm was recorded using a Tecan 2000 plate reader after 1, 2 and 4 h of further incubation. Changes in absorbance were calculated after subtraction of absorbance from cell-free wells. Degree of protection was calculated as percentage changes relative to untreated cells for each clone.

## RNA Preparation

RNA was prepared from 7 day RA-differentiated neuronal-like cells (FtMt clones and untransfected cells) using the RNeasy plus Mini kit (Qiagen, Hilden, Germany) according to the manufacturer's instructions. RNA yield was assessed using a Nanodrop spectrophotometer (Thermo Scientific, USA), and integrity with an Agilent Bioanalyzer and RNA 6000 Nano kit (Agilent Inc, Palo Alto, USA). All RNA samples had RIN values >9 and were considered suitable for microarray analysis.

## Microarray Analysis

Microarray analysis using the Applied Biosystems Human Genome U133 Plus 2.0 array (ThermoFisher Scientific, USA) was carried out as a contract analyses by Takara Bio Inc. (Kusatsu, Japan) using RNA isolated from the clone with the highest expression of FtMt, the medium expression FtMt clone, and untransfected control cells. Labeled cRNA probes from RNA were prepared using the 3' IVT Plus transcription kit (Thermo Fisher Scientific). The array contained 11 separate oligonucleotide probes to represent each of over 47,000 transcripts. Data was extracted and analyzed using Affymetrix Signal Console software. Signal intensity for each gene oligonucleotide probe was obtained based on the mean of oligonucleotide replicates after correction for normalization controls.

## Microarray Data Analysis

Results of analysis of gene expression were prepared by pairwise comparison of untransfected (negative) to high FtMt expression; untransfected (negative) to medium FtMt expressor, and medium to high FtMt expressors. Intensity data for each clone for each gene probe was  $\log_2$  transformed. Significant differences between gene expression values were highlighted when the difference in  $\log_2$  values varied by +1 or -1 (reflecting 2.7 fold increase or decrease in expression). Adjusted *p*-values were provided that reflect significant differences in expression based on the 11 oligonucleotide/transcript technical replicates. Tables were prepared that highlighted significant differences in gene expression, but excluding low expressing genes marked as Absent (below background), and genes with no assigned identity. Different processes of data analysis were examined to demonstrate how altered levels of FtMt affect cellular phenotypes. Particular emphasis was placed on data mining for genes important for protection from oxidative stress, iron transport, and those involved in neuronal differentiation and phenotypes.

## Real Time Reverse Transcription-Polymerase Chain Reaction

Quantification of FtMt gene expression and validation of identified genes with differential expression was carried out by real time RT-PCR with SYBR green detection using RNA from the high and medium FtMt overexpressing clones used for microarray analysis and untransfected cells, and also one additional high expressor and one low FtMt expressor clone. RNA was isolated as described above, and equal amount of RNA (0.75–1  $\mu$ g total cellular RNA) from each sample was reverse transcribed using the PrimeScript RT kit with genomic DNA eraser (Takara Bio, Japan). Appropriate numbers of samples that were not reverse transcribed were analyzed to verify that amplification signal was not due to contaminating DNA.

Real time PCR was carried out using a relative standard curve method (Walker et al., 2009) for analysis using Thunderbird SYBR QPCR master mix supplemented with Rox reference dye (Toyobo, Inc, Japan). Primers (listed in **Table 1**) were used at 12.5 pmol/reaction, and each sample was analyzed in duplicate using triplicate biological replicates on the Roche Light Cycler 480 qPCR machine using the following program: 95°C 60 s denaturation/activation, followed by amplification program of 95°C for 15 s, 60°C for 20 s and 72°C for 30 s for 45 cycles. PCR experimental design followed most of the criteria for Minimum Information for Publication of Quantitative Real time PCR Experiments (MIQE) (Bustin et al., 2009). Primers were designed and analyzed to show absence of self-dimers or cross dimers, and this was verified by demonstration of melting curves that showed single bands.

## Statistical Analysis

Statistical analyses were carried out using Graphpad Prism 7 software (La Jolla, CA). Analysis between groups and treatments were carried out by One-way or Two-Way Analysis of Variance (ANOVA) with Tukey's test of multiple comparisons to examine significance between groups. Significance was assessed if *p* < 0.05.

## RESULTS

### Isolation of Mitochondrial Ferritin Overexpressing SH-SY5Y Cells

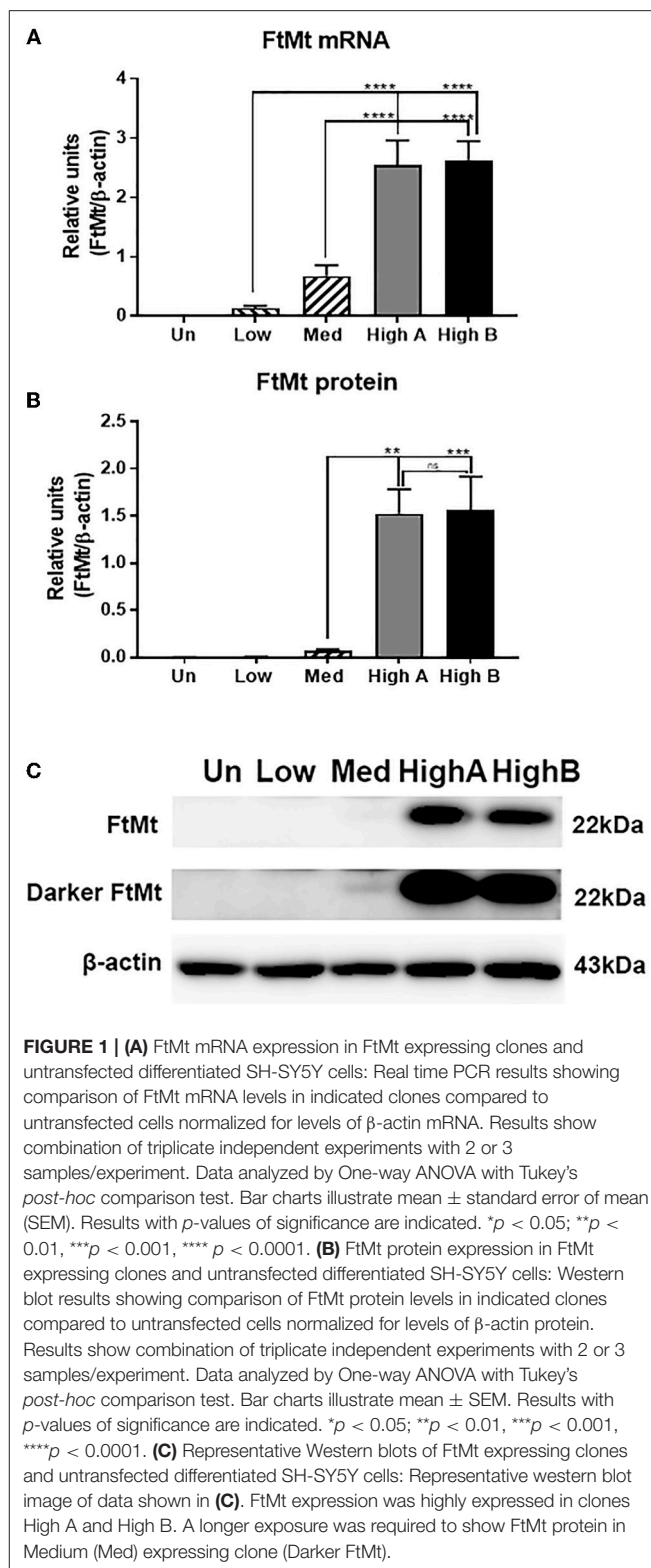
Using standard cell transfection methodology and a plasmid that expressed the human FtMt gene using the CMV immediate early gene promoter, we isolated by disc cloning 26 separate G418-resistant colonies and expanded them in separate cultures. These were screened for expression of FtMt protein by western blot (Supplemental Figure 1). As this image was obtained during the screening process, it used protein extracts from undifferentiated cells. As shown, there was a wide range of FtMt expression levels ranging from undetectable to high levels of expression. Isolated clones were expanded and then frozen, and for subsequent experiments, each clone was used for 6–8 passages before a new frozen vial was revived. Expression and growth of some of the highest expressors proved unstable, but final characterization was carried out on 4 separate clones as their growth and different FtMt expression levels were stable with passage.

Relative levels of FtMt mRNA and protein were measured by real time polymerase chain reaction (qPCR) and western blot. Two clones had high levels of expression of FtMt mRNA and protein (Figures 1A,B), while one had medium level of FtMt mRNA expression and low levels of detectable protein, and one had low level of FtMt mRNA expression but with no detectable protein (representative western blot: Figure 1C). The difference in mRNA expression between the low and high clones was 20-fold, and 4-fold between medium and high, but for protein levels, the difference in expression between medium and high was 22-fold. Considering the differences in mRNA expression, it might be expected that FtMt protein should be detectable in the low expressor clone. These differences between mRNA and protein would suggest that FtMt protein was being rapidly degraded. It should be noted that untransfected SH-SY5Y differentiated cells used in these experiments did not contain detectable levels of FtMt mRNA or protein.

### Phenotyping of FtMt Overexpressing Clones

#### Characterization of FtMt Expressing Clones

As elevated amounts of FtMt will increase the levels of potentially toxic iron in mitochondria, a series of experiments were carried out to determine how overexpression affected the phenotype and gene expression of clones differentiated to a neuronal phenotype. Staining of cells with antibody to FtMt showed expected clear differences in immunoreactivity intensity between medium and high expressor cells (Figures 2B,C), while the untransfected cells only showed some background staining (Figure 2A). Higher magnification images are shown in Figures 2D–E. All cells of the high expressor clone showed FtMt immunoreactivity (Figures 2C,F). The punctate immunoreactivities are consistent with mitochondrial localization. Staining of cells with pan-neurofilament antibody (SMI312) showed that all cells produced the characteristic processes of neurons (Figures 2G–I). Staining of cultures with an antibody to mitochondrial cytochrome oxidase I (MtCox-1) showed an unexpected gradation of distribution and intensity of mitochondria in the untransfected,



medium expressor and high expressor cells (Figures 2J–L). Many of the high FtMt expressing cells showed MtCox1 staining consistent with an aggregated morphology. This

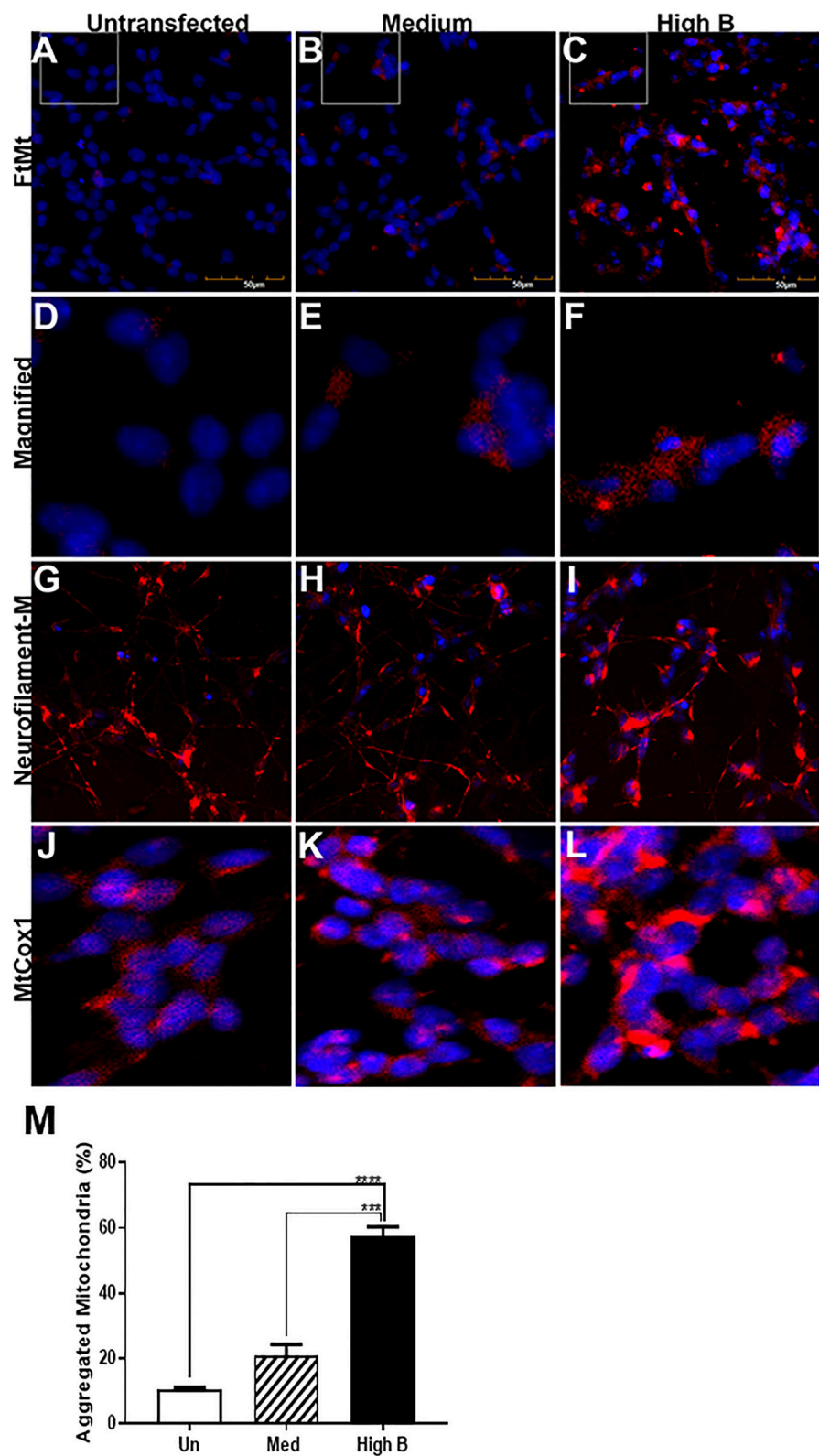


**FIGURE 2 |** Immunocytochemistry of FtMt expressing clones. (A–C). Untransfected (A), Medium (B), and High B (C) clones differentiated for 7 days stained with antibody to FtMt to identify positive expressing cells. Positive staining is observed for Medium and High B clone, but not untransfected cells. Antibody reacted cells were identified by reaction with Alexa568 labeled-anti rabbit immunoglobulin G. All images were recorded using an Olympus FV1000 laser confocal

(Continued)



**FIGURE 2 |** microscope. (D–F). Higher magnification images of FtMt antibody reacted cells. Images from areas indicated with white lines on (A–C). (G–I) Untransfected (G), Medium (H), and High B (I) clones differentiated for 7 days stained with antibody SMI-312 that stains neurofilament proteins, but predominantly NF-M. All cells showed SMI-312 positive neuronal processes consistent with differentiated morphology. Undifferentiated cells show no staining for SMI312 (not shown). Antibody-reacted cells were identified by reaction with Alexa568 labeled-anti mouse immunoglobulin (G). (J–L). Untransfected (J), Medium (K), and High B (L) clones differentiated for 7 days stained with antibody MtCox1 that stains mitochondrial cytochrome oxidase-1. Morphology of MtCox1 immunoreactive mitochondria in FtMt expressing clones (K–Medium and L– High B) compared to untransfected cells (J). Antibody reacted cells were identified by reaction with Alexa568-labeled anti mouse immunoglobulin (G). (M) Quantitative estimation of aggregated/abnormal mitochondria. Estimation of percentage of aggregated mitochondria in untransfected (Un), Med, and High B expressing clones. The numbers were estimated by visual examination of 3 fields/image and 3 images for each clone at magnification shown in (A–C). Results show mean  $\pm$  SEM, with standard significance levels indicated from data analyzed by one way ANOVA with Tukey post-hoc test. \*\*\* $p < 0.001$ , \*\*\*\* $p < 0.0001$ .

was confirmed by determining the percentage of cells with aggregated morphology of MtCox-1 immunoreactivity. This showed significant increase between the untransfected and high expressing clone (Figure 2M).

### Subcellular Localization of Mitochondrial Ferritin

Quantification of MtCox-1 expression by western blots of total cell lysates detected the opposite pattern with significantly higher levels in untransfected neurons (Figures 3A,B). The reason for this discrepancy requires further investigation, but both data suggest abnormalities of mitochondria.

The levels of FtMt protein in different cellular fractions, particularly mitochondria, were measured by western blot. The method used produced a mitochondria-enriched fraction, and also a nuclear and cytosolic fraction, from each cell extract. The question being asked was whether the considerably increased amounts of FtMt being produced by overexpressing cells accumulated predominantly in the mitochondria fraction. The western blots were representative of distinct experiments carried out in triplicate (Figure 3C). The results showed that FtMt was predominantly detected in the mitochondria fraction, but a certain amount could also be detected in the nuclear fraction of the highest expressing clone (Figure 3C - HighB). The levels of FtMt in the nuclear fraction of this clone were higher than might be expected from contamination of this fraction by mitochondria. In the cytosolic fraction, we detected two polypeptide bands of slightly higher molecular weight than processed FtMt. As these were also detected in the untransfected cells that lack FtMt RNA, these bands were considered as non-specific. Similar to Figure 3B, the western blots showing levels of MtCox1 in the different fractions showed larger amounts of this protein in the untransfected cells. The relative intensities of FtMt in the different fractions are illustrated in Figure 3D.

### Alteration in Expression of Neuronal Proteins

To determine if FtMt overexpression affects neuronal phenotype upon differentiation, expression levels of key neuronal proteins-neurofilament M (NF-M); synapse-associated proteins, postsynaptic density protein 95 (PSD95) and synaptosomal-associated protein-25 (SNAP-25)- were measured by western blotting (Figure 4). To confirm the effect of retinoic acid differentiation on expression of proteins, differentiated, and undifferentiated cells from untransfected and High B FtMt clone were analyzed for NF-M, PSD-95, SNAP-25 and FtMt (Figure 4A), which shows that these neuronal proteins were

upregulated by RA differentiation. Surprisingly, it was also observed that there was increased amounts of FtMt in the overexpressing clone following RA treatment. This was unexpected as FtMt in these clones was being expressed using the plasmid CMV IE promoter not the native FtMt promoter.

There were significantly higher levels of NF-M in higher FtMt overexpressing clones compared to the untransfected and low expressor (Figure 4B). By comparison the low expressor had significantly higher levels of the synaptic proteins PSD-95 (Figure 4C) and SNAP25 (Figure 4D). The pattern of expression for both proteins between the different cell types analyzed was similar with decreasing expression from low to high. A composite western blot showing these three proteins along with  $\beta$ -actin normalization for one representative experiment is shown (Figure 4E). NF-M, PSD-95, SNAP-25, and  $\beta$ -actin were sequentially detected on the same membrane. Although we could not detect FtMt protein by western blot in the analyses made in the low FtMt expressing clone, we did show significant expression of FtMt mRNA in these cells compared to untransfected cells, and assume that small amounts of FtMt protein are functional in this clone, but the turnover of this protein makes it undetectable. Further investigations are needed to improve sensitivity of detection, but these results and subsequent data suggest this low FtMt expressing clone has significant differences from untransfected cells.

### Alteration in Expression of Amyloid Precursor Protein, Tau, and $\alpha$ -synuclein

Similar analyses were carried out for expression of amyloid precursor protein (APP) and microtubule associated protein tau, proteins associated with AD pathology, and  $\alpha$ -synuclein, which is associated with PD (Figure 5). Expression of APP was generally higher in FtMt-expressing clones with highest levels of expression in the lowest expressing clone (Figure 5A). By contrast, a different pattern was seen for tau, with significantly increased expression in the medium FtMt expressor (Figure 5B). Highest  $\alpha$ -synuclein expression was also observed in this clone, but the magnitude of change was less than for tau (Figure 5C). A composite western blot showing these three proteins along with  $\beta$ -actin normalization for one representative experiment is shown (Figure 5D). APP, tau,  $\alpha$ -synuclein and  $\beta$ -actin were sequentially detected on the same membrane. The pattern of expression for tau was also observed in the gene expression analyses of these clones (see Table 7—MAPT).

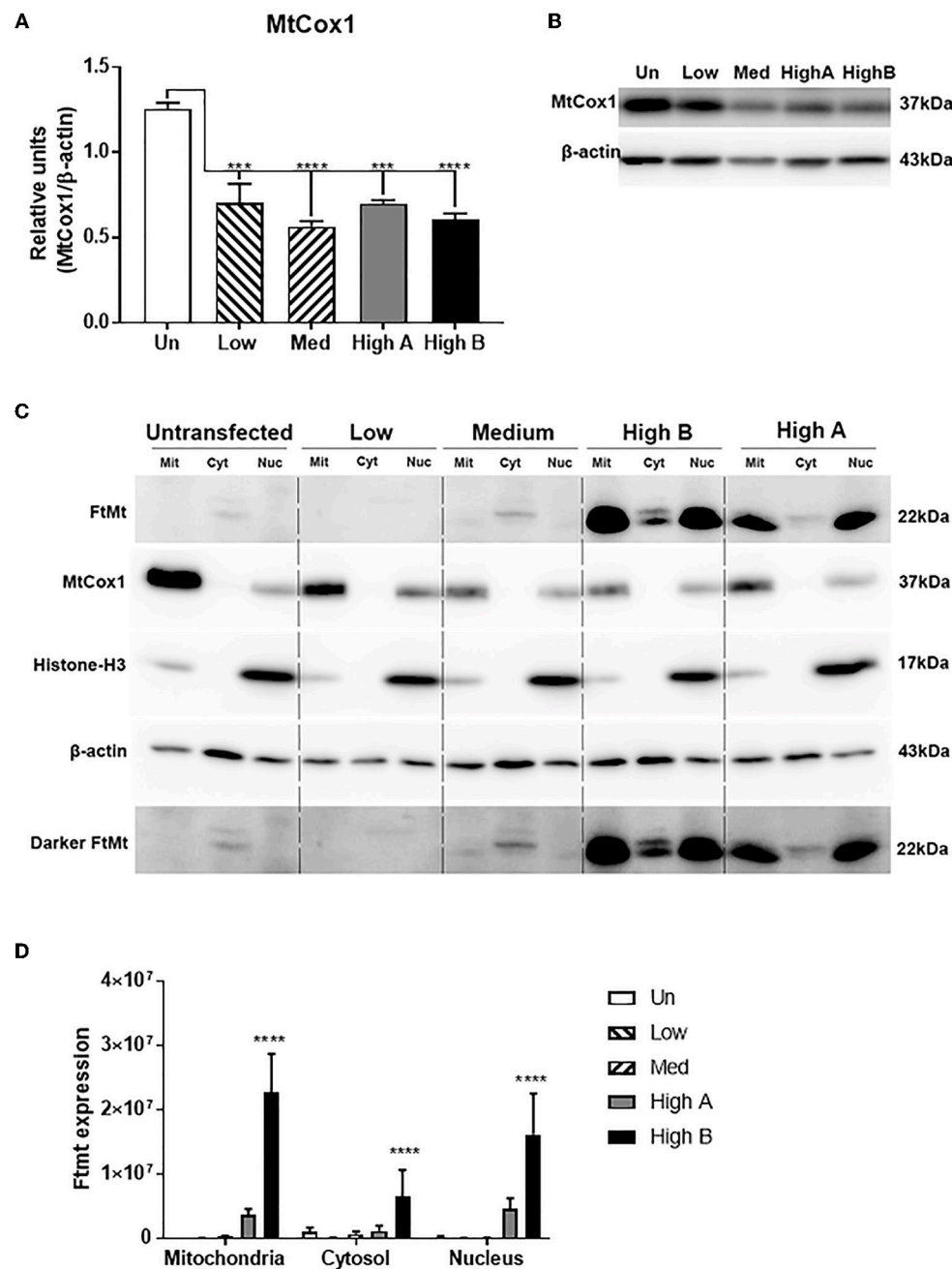


**FIGURE 3 |** Characterization of mitochondria in FtMt expressing clones. **(A,B)** Western blot measurements of MtCox-1 in whole cell extracts. Measurement of Mt Cox-1 in total cell lysates by western blots gave the reverse result compared to immunocytochemistry. There were significantly reduced levels of MtCox-1 protein in FtMt expressing clones. Results based on triplicate determinations. The different patterns of expression are shown in representative western blot. **(C)** Composite western blot panel of subcellular fractions from FtMt expressing clones. Cell extracts from differentiated clones fractionated into mitochondria (Mit), cytosol (Cyt), and nucleus (Nuc) fractions were analyzed by western blot and probed with antibodies to FtMt, MtCox1, Histone-H3, and  $\beta$ -actin. The results for MtCox1 and Histone-H3 indicate that the mitochondria contain some contaminating nuclei, and the nuclei contain some contaminating mitochondria. The results show that the majority of overexpressed FtMt is present in mitochondria though the abundance in nucleus is higher than might be expected from mitochondria contamination. Enhanced exposure was needed to demonstrate FtMt in Med clone (Darker FtMt). A non-specific band of higher molecular weight than FtMt is detected in cytosol fraction. **(D)** Quantitative estimation of results in **(A)**. Results show relative levels of FtMt protein in different fractions from FtMt expressing clones. Results are not normalized and represent signal intensities from triplicate experiments. Results show mean  $\pm$  SEM, with standard significance levels indicated from data analyzed by one way ANOVA with Tukey's *post-hoc* test. \*\*\* $p < 0.001$ , \*\*\*\* $p < 0.0001$ .



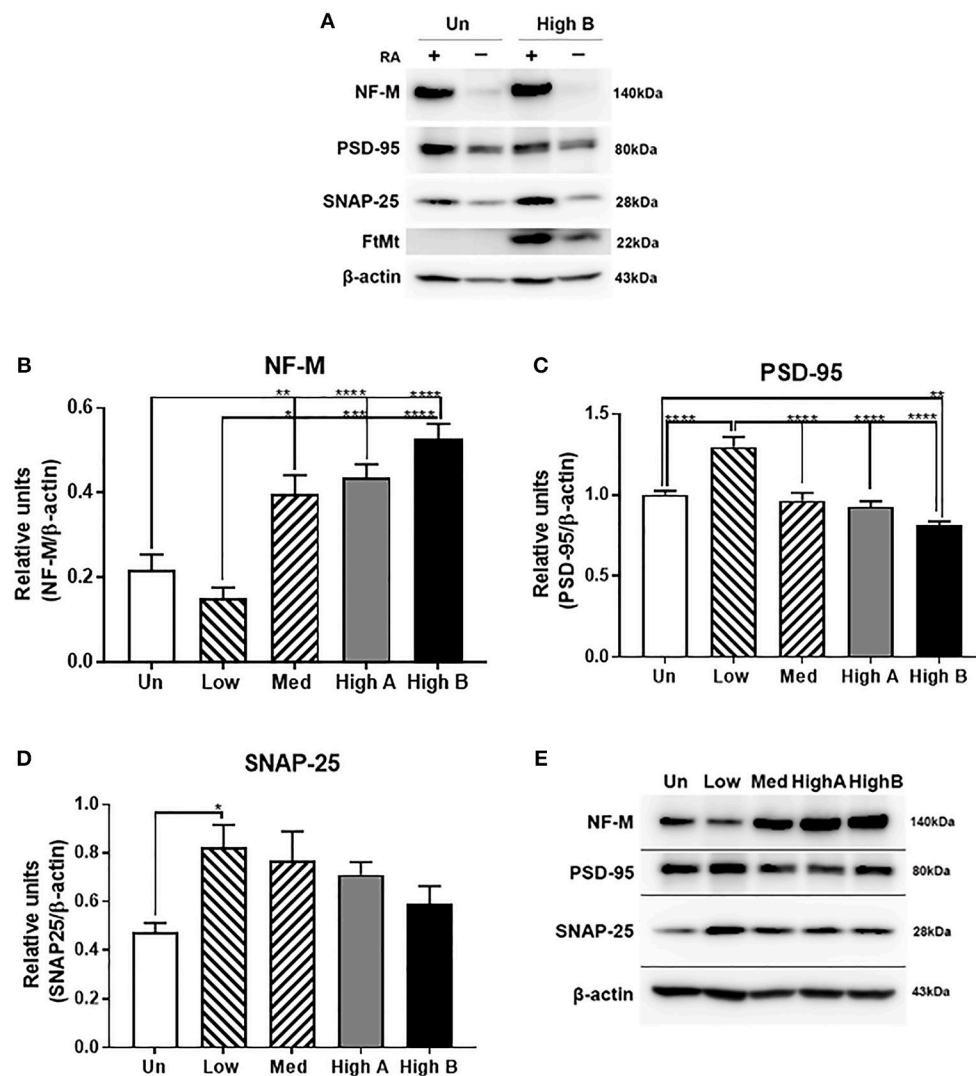


**FIGURE 4 |** Expression of neuronal proteins in FtMt clones. **(A)** Composite picture of western blots showing the differences in levels of NF-M, PSD-95, SNAP-25, and FtMt between undifferentiated (-) and RA differentiated (+) of untransfected (Un) and FtMt high expressing clone (High B). It was noticed in all experiments that FtMt expression was increased with differentiation RA treatment, even though the expression vector was using the CMV immediate-early promoter, and not the native FtMt promoter. **(B)** Relative levels of NF-M **(B)** in different FtMt clones. Results shown in B represent mean  $\pm$  SEM of triplicate experiments. Data analyzed by One way ANOVA with Tukey's *post hoc* test of significance. Results indicate level of significance. \* $p < 0.05$ ; \*\* $p < 0.01$ ; \*\*\* $p < 0.001$ ; \*\*\*\* $p < 0.0001$ . **(C)** Relative levels of PSD-95 **(C)** in different FtMt clones. Results shown in C represent mean  $\pm$  SEM of triplicate experiments. Data analyzed by One way ANOVA with Tukey's *post-hoc* test of significance. Results indicate level of significance. \* $p < 0.05$ ; \*\* $p < 0.01$ ; \*\*\* $p < 0.001$ ; \*\*\*\* $p < 0.0001$ . **(D)** Relative levels of SNAP-25 **(D)** expression in different FtMt clones. Results shown in -D represent mean  $\pm$  SEM of triplicate experiments. Data analyzed by One way ANOVA with Tukey's *post-hoc* test of significance. Results indicate level of significance. \* $p < 0.05$ . **(E)** Composite Western blot showing pattern of expression for NF-M, PSD-95, and SNAP-25. Representative western blots of one experiment showing patterns of expression in untransfected and different FtMt clones. Experiment represents the sequential probing of single membrane for NF-M, PSD-95, and SNAP-25 followed by normalization for  $\beta$ -actin.

## Effect of FtMt Overexpression on Neuronal Phenotypes

### Cell Division and Neurite Formation

Comparison was made between undifferentiated clones of their rate of growth (Figure 6A) (Table 2A) and neurite formation (Figure 6C) (Table 2B). Representative photomicrographs for these experiments are shown in Figures 6B,D. These analyses showed that FtMt expressing clones replicated at a slightly faster rate over 7 days than the untransfected parent cells. By

comparison, the medium expressor and high expressor clones produced significantly less density of neurites after retinoic acid differentiation for 7 days.

### Resistance to Oxidative Stress From Hydrogen Peroxide or Cobalt Chloride

Cytotoxicity assays were carried out using hydrogen peroxide and cobalt chloride as inducers of oxidative stress to determine if the FtMt expressing clones showed more resistance to these

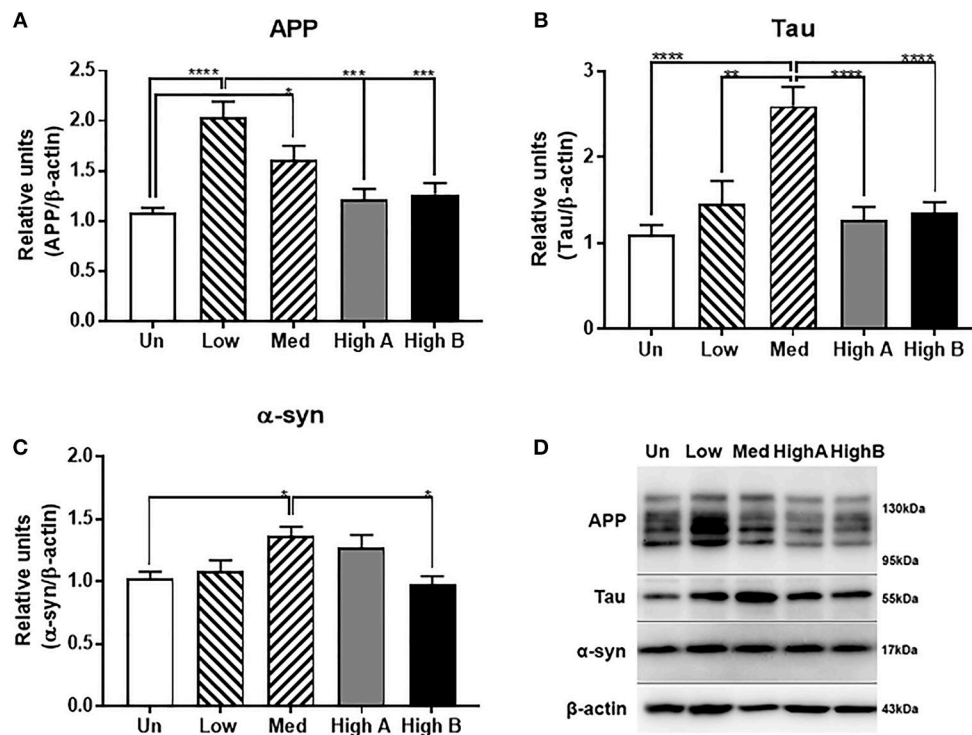


**FIGURE 5 |** Expression of neuronal disease-associated proteins in FtMt clones. **(A)** Relative levels of amyloid precursor protein (APP) in different FtMt clones. Results shown represent mean  $\pm$  SEM of triplicate experiments. Data analyzed by One way ANOVA with Tukey's *post-hoc* test of significance. Results indicate level of significance. \* $p < 0.05$ ; \*\* $p < 0.01$ , \*\*\* $p < 0.001$ , \*\*\*\* $p < 0.0001$ . **(B)** Relative levels of Tau in different FtMt clones. Results shown represent mean  $\pm$  SEM of triplicate experiments. Data analyzed by One way ANOVA with Tukey's *post-hoc* test of significance. Results indicate level of significance. \* $p < 0.05$ ; \*\* $p < 0.01$ , \*\*\* $p < 0.001$ , \*\*\*\* $p < 0.0001$ . **(C)** Relative levels of  $\alpha$ -synuclein ( $\alpha$ -syn) in different FtMt clones. Results shown represent mean  $\pm$  SEM of triplicate experiments. Data analyzed by One way ANOVA with Tukey's *post-hoc* test of significance. Results indicate level of significance. \* $p < 0.05$ . **(D)** Composite Western blot showing pattern of expression for APP, tau, and  $\alpha$ -synuclein. Representative western blots of one experiment showing patterns of expression in untransfected and different FtMt clones. Experiment represents the sequential probing of single membrane for APP, tau, and  $\alpha$ -synuclein followed by normalization for  $\beta$ -actin.

agents. These agents induce oxidative stress through different mechanisms, with hydrogen peroxide being a direct source of reactive oxygen species and cobalt chloride modeling oxidative stress caused by hypoxia (Yu and Gao, 2013). FtMt expressing clones appeared significantly more resistant to the toxic effects of hydrogen peroxide compared to untransfected cells (Figure 6E). Summary of statistical pairwise comparison for different doses of hydrogen peroxide is shown in Table 3A. These results confirm an earlier observation that differentiated cells are more resistant to different oxidative stress inducing factors (Cecchi et al., 2008; Cheung et al., 2009; Lee et al., 2015; Forster et al., 2016). A similar pattern of resistance was shown to cobalt chloride with significant protection in FtMt overexpressing clone (Figure 6F). Summary of statistical pairwise comparison for different doses of cobalt chloride is shown in Table 3B.

### Gene Expression Profiling of FtMt Overexpressing Neuronal Cells

Gene expression profiling using microarrays was carried out with RNA derived from High (B) expressor, medium expressor and untransfected RA-differentiated neurons. Complete results are provided in a searchable Microsoft Excel file

(Supplemental File 1) that shows all expression intensities of indicated genes for these clones. For analysis of differential gene expression, expression intensities were  $\log_2$  transformed and differences of 1  $\log_2$  or greater (more than 2.7 fold) were considered of significance. The microarray platform used for these analyses did not include probes for FtMt, so we cannot directly compare gene expression values with levels of FtMt expression.

Initial inspection of this large dataset revealed that expression of many genes were marked as absent (below the level of detection). It was decided not to consider results from any genes where one or more of the values were tagged as absent. Another noticeable feature was that a number of genes had multiple results that were attributed to different Genbank accession numbers. This indicated different results depending on the gene sequence used to design the oligonucleotide probes on the microarray. Our analysis only considered the gene set with the highest expression values as low expression values tended to be highly variable and therefore less reliable. Finally, we excluded from analyses unassigned or uncharacterized genes even though some showed significant differential expression. Expression of commonly used housekeeping genes (ACTB,

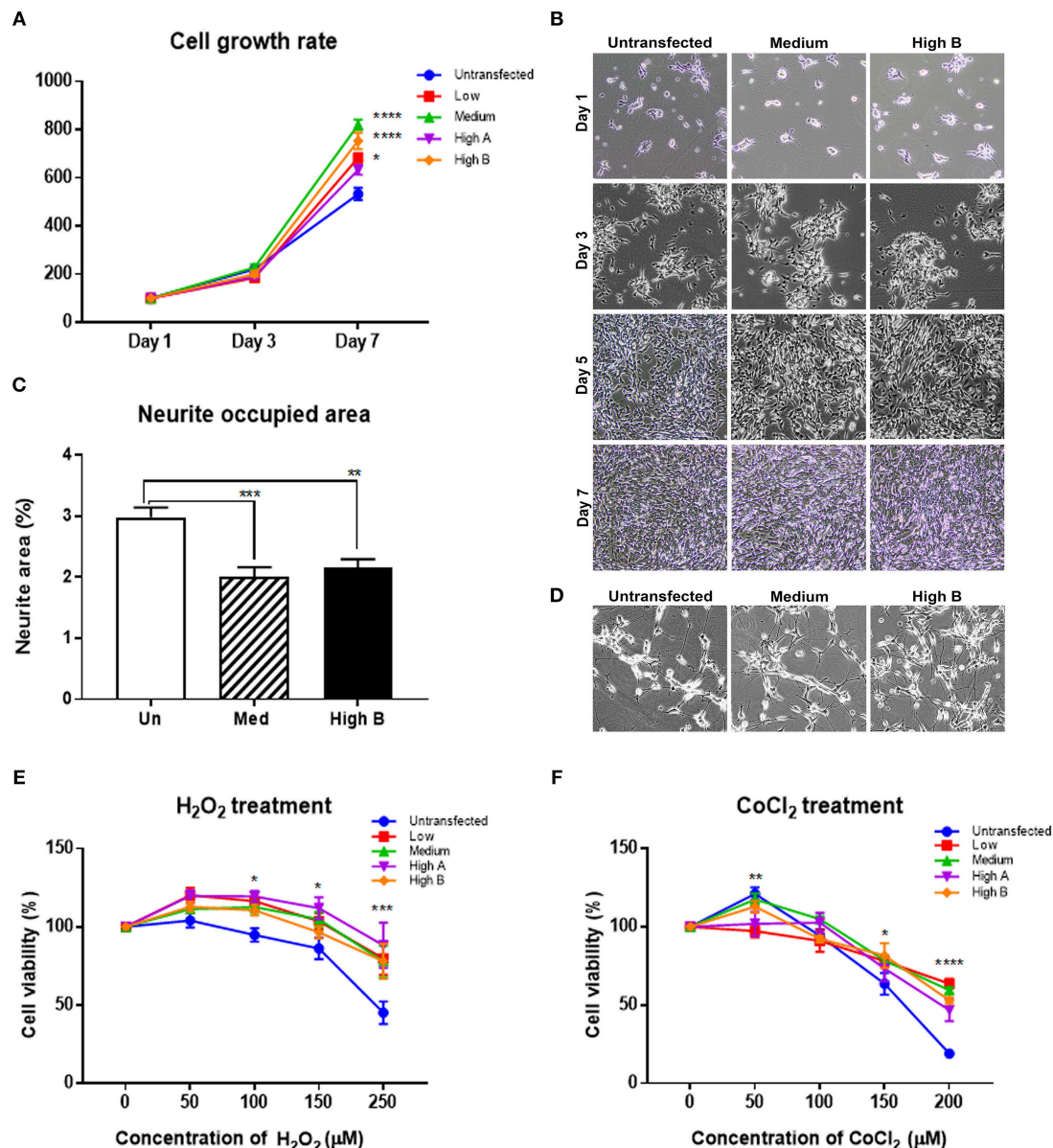


**FIGURE 6 |** Phenotyping of FtMt expressing neuronal cells. **(A,B)** Measurements of Cell Growth Rates of Undifferentiated FtMt clones. **(A)** Results showing relative increase in cell area occupied as percentage of Day 1 of FtMt clones and untransfected cells. Results show analyses at Day 7. Measurements involved area occupied of growing clones identified using Image J image analysis software. Data analyzed by Two-way ANOVA. Relative statistical differences between clones and are listed in **Table 2A**. **(B)** Representative photomicrographs of proliferating clones untransfected, Medium FtMt expressor and High B FtMt expressor at Day 1, Day 3, Day 5, and Day 7. **(C,D)** Measurements of Neurite formation of Differentiated FtMt clones. **(C)** Results showing relative area occupied of neuritic processes at day 7 of untransfected (Un), Medium FtMt expressor (Med) and High Ft expressor (High B). Measurements involved measuring area occupied of neurites identified using NeuronJ plugin of Image J image analysis software. Results are representative of triplicate experiments. Relative statistical differences between clones listed in **Table 2B**. **(D)** Representative photomicrographs of differentiated, untransfected, Medium FtMt expressor and High B FtMt expressor at Day 7. **(E,F)** Responses of FtMt overexpressing clones to oxidative stress. **(E)** Changes in cell viability (as percentage of untreated cultures) with increasing doses of hydrogen peroxide (H<sub>2</sub>O<sub>2</sub>) (0–250 μM). Untransfected and FtMt expressing clones were differentiated in microtiter plate wells for 7 days. Treatments added to media lacking RA containing 1% FBS on day 7 for 24 h. Cell viability assessed by added WST-1 reagent after 24 h. Absorbance (450 nm) measured after 1, 2, and 4 h. Results presented (mean ± SEM) of six wells/treatment and combination of three independent experiments. Data analyzed by Two Way ANOVA. Relative statistical differences between clones and treatments are listed in **Table 3A**. **(F)** Changes in cell viability (as percentage of untreated cultures) with increasing doses of Cobalt Chloride (CoCl<sub>2</sub>) (0–200 μM). Untransfected and FtMt expressing clones were differentiated in microtiter plate wells for 7 days. Treatments added to media lacking RA containing 1% FBS on day 7 for 24 h. Cell viability assessed by added WST-1 reagent after 24 h. Absorbance (450 nm) measured after 1, 2, and 4 h. Results presented (mean ± SEM) of six wells/treatment and combination of three independent experiments. Data analyzed by Two-way ANOVA. Results indicate level of significance. \**p* < 0.05; \*\**p* < 0.01, \*\*\**p* < 0.001, \*\*\*\**p* < 0.0001. Relative statistical differences between clones and treatments are listed in **Table 3B**.

**TABLE 2 |** Effect of FtMt overexpression on Cell division and differentiation.

Sample	P-values
<b>(A) EFFECT OF FtMt ON CELL REPLICATION OF ISOLATED CLONES</b>	
Untransfected vs. Low	0.026
Untransfected vs. Medium	<0.0001
Untransfected vs. High A	0.3530
Untransfected vs. High B	<0.0001
<b>(B) EFFECT OF FtMt OVEREXPRESSION ON NEURITE FORMATION OF DIFFERENTIATED CELLS</b>	
Untransfected vs. Medium	0.0002
Untransfected vs. High B	0.0013
Medium vs. High B	0.7856

Summary of results at day 7 between clones as illustrated in **Figure 6B**. Areas occupied by non-differentiated cells were measured using ImageJ from 5 separate random fields of each cell type. Results analyzed by Two Way Analysis of Variance with Tukey's post-hoc test. Results are compiled from three separate experiments.

Summary of results at day 7 between clones as illustrated in **Figure 6D**. Areas occupied by neurites formed from retinoic acid differentiated cells were measured using ImageJ with NeuronJ plugin from 5 separate random fields of each cell type. Results analyzed by Two Way Analysis of Variance with Tukey's post-hoc test. Results are compiled from three separate experiments.

GAPDH, TUBB, PPIA, HPRT1, G6PD, B2M) showed no significant differences ( $<1 \log_2$  difference) between the different analyzed cells.

**Table 4** presents the top 20 upregulated and downregulated genes selected in order between the high FtMt expressor and untransfected neurons (left columns) and in adjacent columns, the differences between medium expressor and untransfected (middle columns) and between high and medium expressors (right columns). A complete list is presented in **Supplemental Data** that lists all genes with differential expression of  $>1 \log_2$  (**Supplemental File 2**). **Table 5** presents the top 20 upregulated and downregulated genes selected in order between the medium FtMt expressor and untransfected neurons (left columns) and in adjacent columns, the differences between high expressor and untransfected (middle columns) and between high and medium expressors. **Table 6** presents the top 20 upregulated and downregulated genes selected in order between the high FtMt expressor and medium FtMt expressor (left columns), and in adjacent columns, the differences between high expressor and untransfected cells (middle columns) and between medium and untransfected cells (right column). Most of these genes followed the pattern of highest or lowest expression in high FtMt expressor, followed by moderate FtMt expressor, followed by untransfected cells (Complete gene lists for **Table 5**, **6** are included in **Supplemental Files 3, 4**).

### Genes Associated With Neuronal Structure and Differentiation

Further data mining of the gene expression profiling data had revealed changes in a class of differentiation genes designated Inhibitor of Differentiation or Inhibitor of DNA-binding (ID) 1-4. These genes have been shown to be downregulated with RA treatment of neuroblastomas (Lopez-Carballo et al., 2002;

Peddada et al., 2006). The data show increased expression between high expressor FtMt and untransfected neurons for ID1, ID2, and ID3, but reduced expression for ID4 (**Table 7**). For all of these listed genes, there were intermediate levels of expression in medium expressor FtMt clone. **Table 7** also shows the gene expression results for a number of neuronal structural genes that were measured by western blot. Two tables of genes of interest related to iron metabolism and oxidative stress are also presented as **Supplemental File 5**). The majority of these genes did not show significant changes, but are involved in many of the key processes associated with FtMt function.

### Validation of Genes Associated With Oxidative Stress

Although there are multiple criteria available for selecting genes of interest to study further, one of the central goals of the experiments was to investigate novel mechanisms associated with FtMt protection from oxidative stress. With this in mind, examination of the expression data indicated significant changes in expression of thioredoxin-interacting protein (TXNIP). This protein has multiple functions, but one key role is binding and inactivating reduced thioredoxin, a major cellular antioxidant. Increased amounts of cellular TXNIP will reduce the protective effects of thioredoxin. Gene expression data indicated relatively high expression in untransfected SH-SY5Y neurons, and considerable reduction in FtMt expressing clones. The highest reduction in TXNIP mRNA was in the high FtMt expressor, with less reduced in medium FtMt expressor, compared to untransfected cells. Three separate analysis for TXNIP were carried out on the microarray using separate probe sequences, but all showed similar results with reduction ranging from 5.5 fold to 3.8 fold. To confirm these findings, qPCR validation was carried out for TXNIP and TXN1 (**Figures 7A,C**). It is noticeable the considerable difference in TXNIP expression between the two different high FtMt expression clones. Both confirmed considerable reduction compared to untransfected cells (**Figure 7A**). For TXN, consistent with the microarray data that indicated a small non-significant increase in TXN expression in the high expressor clone, PCR validation produced similar result (**Figures 7B,C**); confirming that TXN expression is relatively unchanged. This is consistent with a protective mechanism involving reduced TXNIP levels. We have observed these differences in expression patterns between the two high expressor clones for TXNIP as well as some other genes that have to be further investigated. A western blot for TXNIP protein in these cells confirmed highest levels in untransfected cells, and least in the high expressor clones (High A and High B) (**Figure 7B**).

Another gene target of interest was microsomal glutathione transferase-1 (MGST1), which is localized to mitochondria, and is protective from oxidative stress (**Figure 7D**). Increased expression of MGST1 would also be protective from oxidative stress. Although the microarray data showed significant differences in expression of transferrin receptor (TFRC) between clones, this was not validated by qPCR analyses (data not shown).



**TABLE 3 |** Effect of FtMt overexpression on resistance to oxidative stress by hydrogen peroxide and cobalt chloride.

Samples	Significance ( <i>P</i> -values)				
Dose ( $\mu$ M) Hydrogen Peroxide	0	50	100	150	250
Untransfected vs. Low	0.99 (NS)	0.15 (NS)	0.028	0.106 (NS)	0.0001
Untransfected vs. Medium	0.99 (NS)	0.80 (NS)	0.1 (NS)	0.086 (NS)	0.0004
Untransfected vs. High A	0.99 (NS)	0.22 (NS)	0.019	0.013	0.0001
Untransfected vs. High B	0.99 (NS)	0.66 (NS)	0.16	0.52 (NS)	0.0003
Dose ( $\mu$ M) Cobalt Chloride	0	50	100	150	200
Untransfected vs. Low	0.99 (NS)	0.0005	0.98 (NS)	0.058 (NS)	0.0001
Untransfected vs. Medium	0.99 (NS)	0.94 (NS)	0.4 (NS)	0.048	0.0001
Untransfected vs. High A	0.99 (NS)	0.006	0.61 (NS)	0.30 (NS)	0.0001
Untransfected vs. High B	0.99 (NS)	0.46 (NS)	0.99 (NS)	0.01(NS)	0.0001

Summary of results between clones as illustrated in **Figure 6E** (hydrogen peroxide) and **Figure 6F** (cobalt chloride) after 24 h treatment. Results analyzed by Two-Way Analysis of Variance with Tukey's post-hoc test. Results are compiled from three separate experiments. NS, not significant statistically.

### Validation of Growth Factor Associated Genes

Three genes belonging to different classes of growth factor/neuroendocrine factors with the significant levels of differential expression (see **Tables 4–6**) were identified for validation. The genes GDF15 (growth differentiation factor 15), CALCA, SCG2, and CHGA share some common functions but were shown to have different expression profiles by microarray. Changes in expression of GDF15 (**Figure 7E**), CALCA (**Figure 7F**), and SCG2 (**Figure 7G**) for separate clones are shown with indicated significance between groups share common functions.

## DISCUSSION

A number of studies have demonstrated that increased levels of FtMt in cells have significant protective effect from a range of insults linked to production of ROS, including those associated with neurodegenerative disease mechanisms. These previous studies have shown that protection can be conferred even with small levels of increased FtMt (Shi et al., 2010; Wang Y. Q. et al., 2016; You et al., 2016; Gao et al., 2017; Li J. et al., 2017). Although expressed at low levels compared to ubiquitous iron binding proteins such as ferritin, the protective effect would appear to come from its specific localization to mitochondria, the major cellular source of ROS (Nesi et al., 2017).

The significant protective effects of FtMt from insults associated with AD and PD have indicated that this protein might be a therapeutic target for these diseases. Gene delivery methods are feasible for targeted delivery to involved tissues, but it does raise the question about the consequences of overexpression of a protein that could be toxic to mitochondria. Several studies have utilized the widely used SH-SY5Y neuroblastoma cell as a model to study effects of FtMt, but all of these studies

used undifferentiated cells. Some studies employed the mouse FtMt gene for overexpression in SH-SY5Y cells (Shi et al., 2010). The cleaved FtMt proteins only show 88% homology at the amino acid level and within this sequence, the human FtMt only has 2 cysteines while the mouse FtMt protein has 4. This difference can not only affect the redox properties of the protein but also its secondary structure. Because of these features, some differences in function are possible. For this study, we attempted to advance the previous models by establishing stable overexpression of human FtMt in SH-SY5Y, and then study them in a differentiated state as a simplified model of human neurons. Earlier studies have shown increase in mature neuronal features if SH-SY5Y cells were differentiated with retinoic acid (Nicolini et al., 1998; Simpson et al., 2001; Lopez-Carballo et al., 2002), and that differentiated SH-SY5Y neurons are more resistant to oxidative stress inducing toxins (Cecchi et al., 2008; Cheung et al., 2009; Lee et al., 2015; Forster et al., 2016) than undifferentiated cells. Retinoic acid differentiated SH-SY5Y cells were shown to express a significantly larger panel of mature neuronal genes (Pezzini et al., 2017).

In this study, we isolated a number of FtMt-expressing SH-SY5Y clones. Some of the clones proved unstable, but several clones that had relatively stable levels of FtMt expression after 2–3 passages showed normal cell growth and replicated at a significantly higher rate than untransfected cells. This finding is in contrast to one study that concluded that FtMt overexpression slowed the rate of neuroblastoma cell division (Shi et al., 2015). The overexpressing clones produced neurites at a lower density than untransfected cells. High FtMt expression did not affect the viability of cultures, but immunocytochemical staining for FtMt and the mitochondrial marker MtCox1 showed a higher number of aggregated mitochondria, a possible sign of mitochondrial damage. Analysis of nuclear, mitochondrial, and cytosolic fractions from the highest expressor FtMt clones

**TABLE 4 |** Differential Genes expressed by FtMt overexpressing SH-SY5Y neuronal cells.

GeneSymbol	RefSeq		Log2	Fold	Log2	Fold	Log2	Fold
			Diff	Change	Diff	Change	Diff	Change
			HighB vs. Un		Med vs. Un		HighB vs. Med	
UPREGULATED GENES								
GDF15	AF003934		4.39	21.02	1.85	3.60	2.55	5.84
SGK1	NM_005627		3.35	10.22	2.88	7.34	0.48	1.39
TFPI2	L27624		3.03	8.17	2.30	4.91	0.74	1.66
TENM1	AL022718		3.02	8.13	2.05	4.15	0.97	1.96
MSN	NM_002444		2.96	7.78	1.31	2.47	1.65	3.15
CDKN1A	NM_000389		2.83	7.11	1.84	3.58	0.99	1.99
VIP	NM_003381		2.82	7.08	2.55	5.87	0.27	1.21
ZDHHC2	AK001608		2.69	6.44	2.52	5.75	0.16	1.12
ACTA2	NM_001613		2.47	5.53	1.59	3.00	0.88	1.84
TFPI2	AL574096		2.42	5.37	1.80	3.48	0.63	1.54
ID1	D13889		2.40	5.28	0.78	1.72	1.62	3.07
SPATA18	AI559300		2.37	5.17	1.13	2.18	1.25	2.37
FRMD3	BF589413		2.24	4.73	1.68	3.21	0.56	1.47
FN1	AK026737		2.21	4.63	2.20	4.61	0.01	1.00
ZDHHC2	AI814257		2.21	4.63	2.00	3.99	0.21	1.16
FN1	BC005858		2.20	4.61	2.67	6.36	-0.46	1.38
SLC35F1	AI809083		2.17	4.51	1.46	2.74	0.72	1.64
KITLG	AI446414		2.16	4.48	1.55	2.94	0.61	1.53
IL13RA1	U81380		2.07	4.21	1.91	3.77	0.16	1.12
DOWNREGULATED GENES								
CARTPT	NM_004291		-3.36	10.25	-3.48	11.14	0.12	1.09
TMEM100	NM_018286		-3.15	8.90	-0.70	1.62	-2.46	5.48
AJAP1	AF052109		-2.84	7.17	-1.30	2.46	-1.54	2.92
ID4	AL022726		-2.77	6.81	-0.74	1.67	-2.03	4.09
HIF3A	BC026308		-2.51	5.71	-0.55	1.47	-1.96	3.89
SLC8A1	AI741439		-2.51	5.70	-0.64	1.56	-1.87	3.66
TXNIP	NM_006472		-2.45	5.48	-1.70	3.24	-0.76	1.69
IGF2	X07868		-2.45	5.46	-3.00	8.00	0.55	1.47
KIT	NM_000222		-2.41	5.32	-0.41	1.33	-2.00	4.00
LPAR1	AW269335		-2.34	5.07	-1.33	2.51	-1.01	2.02
TMEM178A	AA058832		-2.31	4.96	-0.43	1.34	-1.88	3.69
LINC01105	NM_153011		-2.25	4.77	-2.07	4.21	-0.18	1.13
WNT2B	BF961733		-2.25	4.75	-0.25	1.19	-1.99	3.98
SEMA6A	AB002438		-2.25	4.75	-2.11	4.31	-0.14	1.10
IGFBP7	NM_001553		-2.20	4.59	-2.64	6.23	0.44	1.36
GRIA2	NM_000826		-2.15	4.43	-1.22	2.33	-0.93	1.91
AJAP1	AA835004		-2.11	4.31	-0.29	1.23	-1.82	3.52
DMD	NM_004010		-2.10	4.29	-1.54	2.91	-0.56	1.47
NPY2R	U32500		-2.04	4.12	-1.50	2.83	-0.54	1.46

Genes ordered for High expressing vs. Untransfected, compared to other comparison pairs.

showed that the majority of overexpressed FtMt was localized to mitochondria, though some could be detected in the nuclear fraction.

The value of the clones isolated for future studies is their expression of different levels of FtMt mRNA. The difference in expression ranged was 20-fold from lowest to highest. The

lowest FtMt expressor expressed readily detectable mRNA by qPCR, but we were unable to detect protein in these cells. This is unexpected as the difference in mRNA expression levels would indicate that protein should be detectable. It is possible that some mechanism is involved in the rapid degradation of the low level of protein. This is being investigated, but



**TABLE 5 |** Differential Genes expressed by FtMt overexpressing SH-SY5Y neuronal cells.

GeneSymbol	RefSeq		Log2	Fold	Log2	Fold	Log2	Fold
			Diff	Change	Diff	Change	Diff	Change
			Med vs. Un		HighB vs. Un		HighB vs. Med	
UPREGULATED GENES								
CALCA	BF447272		5.61	48.77	1.26	2.40	−4.34	20.31
CALCB	AA747379		3.83	14.22	0.58	1.49	−3.26	9.55
RGS13	AF030107		2.95	7.73	2.07	4.20	−0.88	1.84
SGK1	NM_005627		2.88	7.34	3.35	10.22	0.48	1.39
FN1	BC005858		2.67	6.36	2.20	4.61	−0.46	1.38
PLK2	NM_006622		2.59	6.02	1.71	3.27	−0.88	1.84
VIP	NM_003381		2.55	5.87	2.82	7.08	0.27	1.21
ZDHHC2	AK001608		2.52	5.75	2.69	6.44	0.16	1.12
RGS13	BC036950		2.50	5.64	1.78	3.44	−0.71	1.64
TMEM74	BC030710		2.48	5.58	−0.43	1.35	−2.91	7.53
CPED1	BF724137		2.47	5.55	1.64	3.12	−0.83	1.78
TFPI2	L27624		2.30	4.91	3.03	8.17	0.74	1.66
PRKCH	NM_006255		2.29	4.91	1.59	3.02	−0.70	1.62
EDIL3	AA053711		2.29	4.89	1.05	2.08	−1.23	2.35
FN1	AK026737		2.20	4.61	2.21	4.63	0.01	1.00
SMIM3	AF313413		2.14	4.40	0.96	1.94	−1.18	2.26
IGSF11	BE221674		2.12	4.34	1.21	2.31	−0.91	1.88
EGR1	AI459194		2.07	4.19	2.03	4.09	−0.03	1.02
TENM1	AL022718		2.05	4.15	3.02	8.13	0.97	1.96
DOWNREGULATED GENES								
CARTPT	NM_004291		−3.48	11.14	−3.36	10.25	−3.48	11.14
IGF2 /// INS-IGF2	X07868		−3.00	8.00	−2.45	5.46	−3.00	8.00
DLK1	U15979		−2.88	7.35	−2.63	6.19	−2.88	7.35
NAALAD2	BC038840		−2.74	6.69	−1.29	2.44	−2.74	6.69
IGFBP7	NM_001553		−2.64	6.23	−2.20	4.59	−2.64	6.23
SOX9	NM_000346		−2.33	5.03	−1.96	3.88	−2.33	5.03
INSM2	AA046951		−2.32	5.01	−1.54	2.90	−2.32	5.01
ABI3BP	AB056106		−2.25	4.77	−1.55	2.94	−2.25	4.77
KCNQ5	BF513800		−2.18	4.55	−1.32	2.50	−2.18	4.55
SEMA6A	AB002438		−2.11	4.31	−2.25	4.75	−2.11	4.31
SPOCK1	AF231124		−2.09	4.25	−2.00	4.01	−2.09	4.25
HIST1H4	NM_003542		−1.99	3.97	−0.62	1.54	−1.99	3.97
UTRN	N66570		−1.97	3.93	−1.00	2.00	−1.97	3.93
AQP1	AL518391		−1.96	3.88	−1.31	2.48	−1.96	3.88
PDZRN3	AL569804		−1.93	3.81	−0.85	1.81	−1.93	3.81
ZNF229	AA180985		−1.91	3.77	−0.75	1.68	−1.91	3.77
SLC16A10	AI935541		−1.86	3.64	−1.19	2.28	−1.86	3.64
SYTL4	AL391688		−1.82	3.54	−1.68	3.21	−1.82	3.54
SCAF11	AA679858		−1.81	3.50	−1.83	3.56	−1.81	3.50

Genes ordered for Medium expressing vs. Untransfected, compared to other comparison pairs.

to date the mechanisms of FtMt processing and degradation have not been identified. This hypothesis is strengthened if you consider the medium expressor clone, which expressed 3.9-fold less RNA than the highest expressor, but 22.1-fold less protein. Future experiments will include the use of inhibitors of proteosomal degradation and autophagy to determine if these

affect cellular FtMt levels. Unlike in some other studies, the untransfected isolate of SH-SY5Y cells used to produce the transfected clones expressed no detectable FtMt RNA or protein. These experiments used a different SH-SY5Y isolate compared to experiments which we previously reported (Guan et al., 2017).

**TABLE 6 |** Differential Genes expressed by FtMT overexpressing SH-SY5Y neuronal cells.

GeneSymbol	RefSeq		Log2	Fold	Log2	Fold	Log2	Fold
			Diff	Change	Diff	Change	Diff	Change
			HighB vs. Med		HighB vs. Un		Med vs. Un	
UPREGULATED GENES								
GDF15	AF003934		2.55	5.84	4.39	21.02	1.85	3.60
FAM162B	AI540210		2.13	4.37	0.96	1.94	-1.17	2.25
TNFRSF10A	W65310		1.90	3.72	0.64	1.56	-1.25	2.38
NHLH2	AA166895		1.82	3.54	1.54	2.91	-0.28	1.22
MBNL3	AI197932		1.79	3.46	1.34	2.53	-0.46	1.37
CD99	NM_002414		1.70	3.24	0.51	1.43	-1.18	2.27
GALNT6	NM_007210		1.66	3.15	0.43	1.35	-1.23	2.34
MSN	NM_002444		1.65	3.15	2.96	7.78	1.31	2.47
SFXN4	AI346445		1.63	3.09	0.36	1.29	-1.26	2.40
ID1	D13889		1.62	3.07	2.40	5.28	0.78	1.72
RBPMS2	BE348466		1.55	2.93	0.96	1.95	-0.59	1.51
ITGB5	NM_002213		1.55	2.92	0.10	1.07	-1.44	2.72
CD99	U82164		1.54	2.92	0.50	1.41	-1.05	2.07
MYBL2	NM_002466		1.51	2.86	0.59	1.51	-0.92	1.89
ITPR1	L38019		1.49	2.81	1.22	2.33	-0.27	1.21
PTPRM	BC029442		1.48	2.78	0.28	1.21	-1.20	2.30
RIT2	NM_002930		1.46	2.76	0.74	1.67	-0.72	1.65
NAALAD2	BC038840		1.46	2.74	-1.29	2.44	-2.74	6.69
OSBPL3	AI202969		1.45	2.73	1.99	3.97	0.54	1.46
LYN	NM_002350		1.44	2.71	0.61	1.53	-0.82	1.77
DOWNREGULATED GENES								
CALCA	BF447272		-4.34	20.31	1.26	2.40	5.61	48.77
PPP2R2B	AA974416		-3.37	10.31	-1.58	2.98	1.79	3.46
CALCB	AA747379		-3.26	9.55	0.58	1.49	3.83	14.22
TMEM74	BC030710		-2.91	7.53	-0.43	1.35	2.48	5.58
NEGR1	AI123532		-2.65	6.26	-1.57	2.97	1.08	2.11
LDLRAD4	NM_004338		-2.51	5.69	-0.97	1.96	1.54	2.91
TMEM100	NM_018286		-2.46	5.48	-3.15	8.90	-0.70	1.62
PLD5	R38585		-2.24	4.74	-1.16	2.23	1.09	2.13
MMP28	NM_024302		-2.08	4.24	-0.58	1.49	1.50	2.84
ID4	AL022726		-2.03	4.09	-2.77	6.81	-0.74	1.67
KIT	NM_000222		-2.00	4.00	-2.41	5.32	-0.41	1.33
WNT2B	BF961733		-1.99	3.98	-2.25	4.75	-0.25	1.19
HIF3A	BC026308		-1.96	3.89	-2.51	5.71	-0.55	1.47
GRIA3	AW294729		-1.95	3.86	-1.27	2.41	0.68	1.60
FAM19A4	AA757457		-1.92	3.79	-1.32	2.50	0.60	1.52
DST	AL049215		-1.90	3.72	-1.62	3.07	0.28	1.21
TMEM178A	AA058832		-1.88	3.69	-2.31	4.96	-0.43	1.34
CADPS	BE467579		-1.88	3.67	-1.25	2.37	0.63	1.55
MRAP2	AA418816		-1.88	3.67	-1.06	2.08	0.82	1.76
SLC8A1	AI741439		-1.87	3.66	-2.51	5.70	-0.64	1.56

Genes ordered for High B expressing vs. Medium, compared to other comparison pairs.

The characterization of FtMt overexpressing cells showed differences in expression of mature neuronal proteins. The differences in levels of NF-M, PSD-95, and SNAP-25, along with the disease-associated proteins APP, tau, and  $\alpha$ -synuclein suggest

changes in neuronal properties. Further studies will determine if FtMt overexpression affects cellular production of the A $\beta$  peptide from APP, or the levels of phosphorylated tau or  $\alpha$ -synuclein, which are associated with AD or PD pathology. The use of

**TABLE 7** | Differential expression of genes associated with neuronal structure and differentiation.

Gene Symbol	RefSeq	Intensity	Intensity	Intensity	Log2	Fold
		<i>Un</i>	<i>Med</i>	<i>HighB</i>	<i>Un vs. HighB</i>	
ID1	D13889	168	289	889	1.7	5.3
ID2	NM_002166	786	1229	2038	0.95	2.6
ID3	NM_002167	181	551	1591	2.2	8.9
ID4	AW157094	520	409	172	−1.1	0.33
MYC	NM_002467	300	365	300	0	1
MYCN	BC002712	821	335	248	−1.2	0.3
PCNA	NM_002592	10,090	7,301	12,037	0.18	1.2
NEFL	AL566528	1,785	2,116	1,543	−0.14	0.86
<b>NEFM</b>	<b>NM_005382</b>	<b>11,227</b>	<b>16,853</b>	<b>16,335</b>	<b>0.38</b>	<b>1.45</b>
NEFH	NM_021076	1,076	905	1,249	0.37	1.45
<b>SNAP25</b>	<b>L19760</b>	<b>3,932</b>	<b>4,469</b>	<b>4,322</b>	<b>0.15</b>	<b>1.16</b>
<b>MAPT</b>	<b>J03778</b>	<b>1,117</b>	<b>1,763</b>	<b>1,053</b>	<b>−0.06</b>	<b>0.94</b>
MAP2	BF342661	7,218	6,353	7,384	0.02	1.02
TH	NM_000360	113	ND	ND	ND	
DBH	NM_000787	5,988	2,991	6,630	0.1	1.1
<b>APP</b>	<b>NM_000484</b>	<b>4,606</b>	<b>4,285</b>	<b>3,415</b>	<b>−0.3</b>	<b>0.74</b>
<b>SNCA</b>	<b>NM_000345</b>	<b>468</b>	<b>981</b>	<b>569</b>	<b>0.2</b>	<b>1.2</b>

Data shows raw intensity values (Intensity) between untransfected (*Un*), Medium FtMt expressing clone (*Med*) and High FtMt expressing clone (*HighB*).

Log<sub>2</sub> difference and Fold change between untransfected (*Un*) and High B clone are included to indicate which genes met the 1log<sub>2</sub> difference criteria used for differential expression.

ND: Not detected.

Results in bold refer to genes that were analyzed at protein level by western blot.

these experimental models of stable FtMt overexpression for studying changes in aggregation or phosphorylation of tau and  $\alpha$ -synuclein would be feasible.

A potentially significant new finding from the gene array data has been linking overexpression of FtMt to downregulation of TXNIP expression. TXNIP is a member of the alpha arrestin protein family that regulates and binds to reduced thioredoxin (TXN) and can be induced in response to oxidative stress, calcium influx and hyperglycemia (Kim et al., 2012). TXNIP has many identified functions, but is an important regulator of thioredoxin activity. Thioredoxin, a thiol-oxidoreductase, is a major regulator of cellular redox signaling which protects cells from oxidative stress (Mahmood et al., 2013). Binding of thioredoxin and TXNIP inhibits the anti-oxidative function resulting in the greater accumulation of reactive oxygen species and cellular stress. Increased levels of TXNIP has been associated with many diseases of oxidative stress including ischemic heart disease, diabetes, cancer, AD, and PD (Zhou et al., 2010; Li J. et al., 2017; Duan et al., 2018; Melone et al., 2018). Thioredoxin-TXNIP is a major regulator of mitochondrial-mediated oxidative stress in many pathologies including cerebrovascular and neurodegenerative diseases (Nasoohi et al., 2018). Areas with the highest level of thioredoxin activity in brain are those with the highest level of metabolic and oxidative burden (Aon-Bertolino et al., 2011), similar to FtMt. One recent study that linked TXNIP to AD pathology showed that inhibiting TXNIP expression in SH-SY5Y cells and AD model mice using a pharmaceutical agent directly inhibited the phosphorylation of the microtubule associated protein tau (Melone et al., 2018).

Increased phosphorylation of tau is a key pathological event in AD, and its inhibition due to reduced TXNIP expression that can be caused by FtMt overexpression could provide further rationale for this therapeutic approach for AD.

TXNIP expression is induced in neurons after oxidative or glucose stress in either ischemic or hyperglycemic-ischemic condition (Kim et al., 2012). Induction of TXNIP can be pro-apoptotic under these conditions. The changes in TXNIP protein levels in these overexpressing clones followed the same pattern as TXNIP mRNA expression. Downregulation of TXNIP while maintaining levels of thioredoxin-1 and -2 will provide protection from oxidative stress. Another factor shown to be protective is microsomal glutathione transferase-1 (MGST1), which accumulates in mitochondria and is protective from oxidative stress (Siritantikorn et al., 2007). It has been observed that MGST1 expression was very low in neuroblastomas and neuroblastoma cell line (Bjorkhem-Bergman et al., 2014). These authors hypothesized that this could explain the extreme sensitivity of neuroblastomas to oxidative stress. Increasing MGST1 expression resulted in significant protection of MCF-2 cells from lipid peroxidation (Siritantikorn et al., 2007), while downregulating expression increased PC12 cells susceptibility to toxic stress (Sobczak et al., 2014).

Three other groups of genes that coded for growth factor and cytokine molecules were investigated as they had shown significant differences between FtMt expressing clones by microarray analysis. Growth differentiation factor-15 (GDF-15), also called macrophage inhibitory cytokine-1 (MIC-1), was strongly upregulated in FtMt expressing clones.

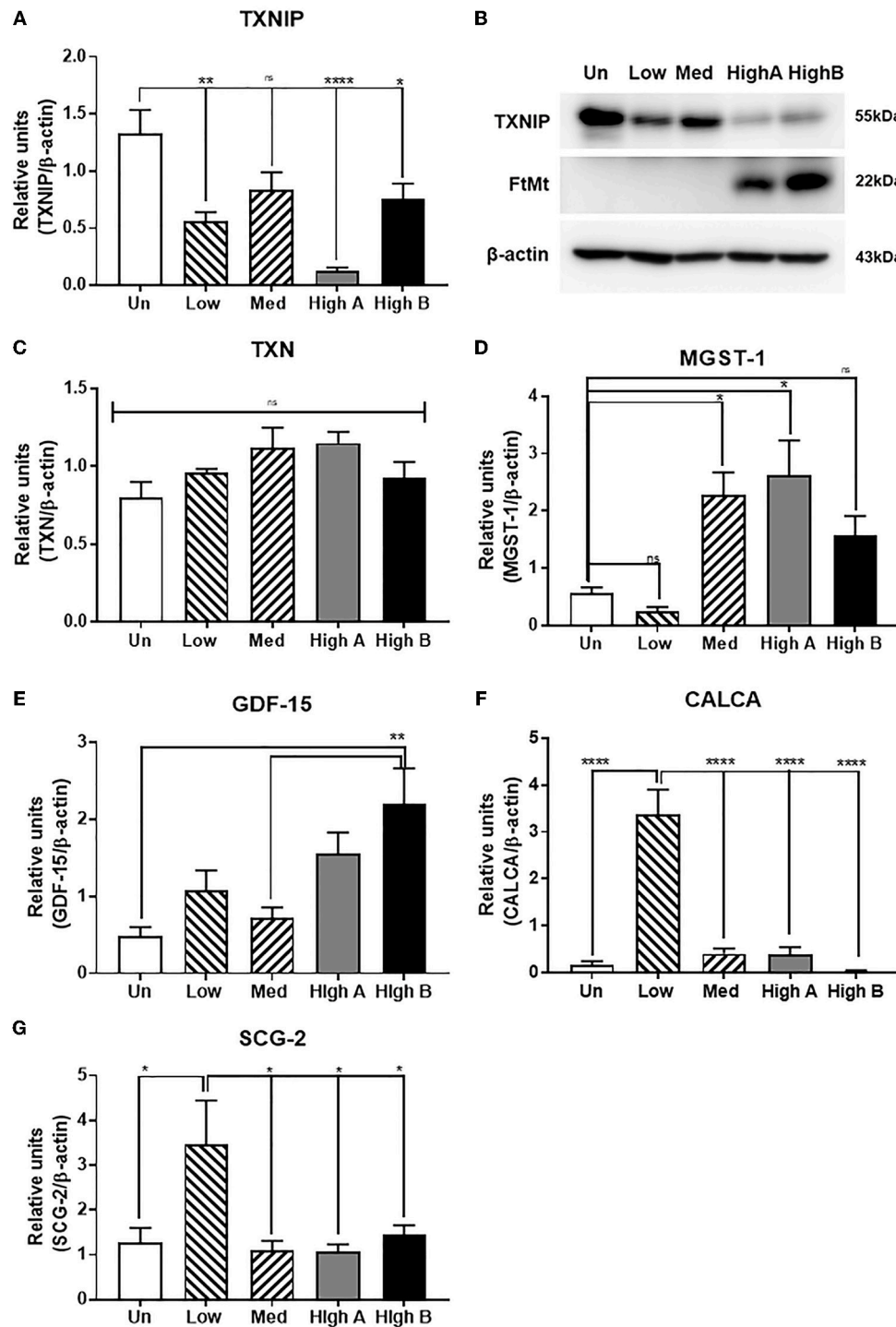


**FIGURE 7 |** Validation of expression of key differentially expressed genes identified by microarray. **(A)** Real time PCR measurement of expression of thioredoxin-interacting protein (TXNIP) in different clones. Results are combined of three independent experiments. Data analyzed by one-way ANOVA with Tukey's *post-hoc* test of significance. Results indicate level of significance. \* $p < 0.05$ ; \*\* $p < 0.01$ , \*\*\* $p < 0.001$ , \*\*\*\* $p < 0.0001$ . **(B)** Western blot showing relative levels of TXNIP protein in different clones compared to expression of FtMt and β-actin. ns: not significantly different **(C)** Real time PCR measurement of expression of thioredoxin (TXN) in different clones. Results are combined of three independent experiments. Data show no significant differences between expression levels of different clones. **(D)** Real time PCR measurement of expression of microsomal glutathione transferase (MGST)–1 in different clones. Results are combined of three independent experiments. Data analyzed by one-way

(Continued)

**FIGURE 7 |** ANOVA with Tukey's *post-hoc* test of significance. Results indicate level of significance. \* $p < 0.05$ ; \*\* $p < 0.01$ . **(E)** Real time PCR measurement of expression of growth differentiation factor-15 (GDF-15) in different clones. Results are combined of three independent experiments. Data analyzed by one-way ANOVA with Tukey's *post-hoc* test of significance. Results indicate level of significance. \*\* $p < 0.01$ . **(F)** Real time PCR measurement of expression of calcitonin gene related peptide alpha (CALCA) in different clones. Results are combined of three independent experiments. Data analyzed by one-way ANOVA with Tukey's *post-hoc* test of significance. Results indicate level of significance. \*\* $p < 0.01$ . **(G)** Real time PCR measurement of expression of secretogranin-2/chromogranin C (SCG-2) in different clones. Results are combined of three independent experiments. Data analyzed by one-way ANOVA with Tukey's *post-hoc* test of significance. Results indicate level of significance. \* $p < 0.05$ .

It was initially identified as a powerful protective factor for cultured dopaminergic neurons exposed to toxic doses of iron and other toxins (Strelau et al., 2000, 2003). Deficiency of GDF-15 has been shown to increase the vulnerability of dopaminergic neurons to 6-OHDA administration in mice (Machado et al., 2016). GDF-15 was shown to have a role in normal erythropoiesis, and its expression was increased in erythroblasts from patients with refractory anemia, which is associated with large increase in iron in mitochondria (Ramirez et al., 2009). GDF-15 can regulate energy homeostasis in mitochondria in muscle through elevation of oxidative metabolism (Cheung et al., 2009). Expression of calcitonin gene related polypeptide alpha (CALCA) and beta (CALCB) genes were significantly altered. These genes produce pro-peptides that are cleaved to neuroactive peptide hormones calcitonin and calcitonin gene related polypeptide (CGRP), which are involved in calcium homeostasis, including vasodilation. CGRP expression is high in the CNS suggesting neurotransmitter activity. CGRP was shown to provide significant protective properties in different experimental systems, including heat injury and ischemia/reperfusion in rats and overexpression in Schwann cells subject to oxidative stress (Russell et al., 2014; Wu et al., 2015; Yang et al., 2016; Lu et al., 2017). Secretogranin II (SCG2)(Chromogranin C) is also a neuroendocrine secretory protein that is cleaved to form the peptide secretoneurin. Expression of SCG2 is modulated by extracellular calcium (Zhan et al., 2008), and it can induce expression of the anti-apoptotic protein Bcl2 through activation of JAK2/STAT3 signaling, providing protection in a murine stroke model (Shyu et al., 2008). This gene is involved in neuronal differentiation and resistance to apoptosis. Due to the large amount of data generated by the microarray profiling of different FtMt clones, there are a number of other genes of potential interest to neuronal phenotype and differentiation that can be explored.

In conclusion, our data have identified that FtMt overexpression has significant effects on neuronal-like cells. The results indicate that the protective effect is not dependent on amount of FtMt expression. High levels of expression did not appear to harm the viability of cells in terms of growth and differentiation, but some mitochondria abnormalities were observed in the highest expressing clone. There was a clear difference in expression of many genes between low and high expressing clones that suggest a dose effect. cells. The data

provides a framework for investigating novel mechanisms concerning FtMt expression in diseases such as AD, and whether FtMt could be considered as a candidate for use in gene therapy for diseases involving mitochondrial oxidative stress.

## AUTHOR CONTRIBUTIONS

AM performed all experiments, analyzed data and assisted in manuscript preparation. ST assisted in experiments and data acquisition. DGW planned experiments, supervised experiments, assisted in data analyses and wrote manuscript. IT initiated experiments, provided funding and intellectual input to data interpretation and manuscript. All authors read and approved all versions of manuscript.

## FUNDING

This study was supported by JSPS KAKENHI Grant Numbers JP17H03560 and JP26290022 (IT) from Japan Society for the Promotion of Science.

## SUPPLEMENTARY MATERIAL

The Supplementary Material for this article can be found online at: <https://www.frontiersin.org/articles/10.3389/fnmol.2018.00470/full#supplementary-material>

**Supplemental Figure 1 |** Western blot panel showing FtMt expression in all isolated clones of SH-SY5Y cells transfected with FtMt expression plasmid. Results are shown for FtMt expression in undifferentiated cells.

**Supplemental File 1 |** Zipped Microsoft Excel File showing complete results of all expression intensities for analyzed clones. File is searchable.

**Supplemental File 2 |** Microsoft Excel File complete results of expression intensities with changes up or down by more than 1 log2 comparing between highest expressing clone (HighB) and untransfected cells.

**Supplemental File 3 |** Microsoft Excel File complete results of expression intensities with changes up or down by more than 1 log2 comparing between medium expressing clone and untransfected cells.

**Supplemental File 4 |** Microsoft Excel File complete results of expression intensities with changes up or down by more than 1 log2 comparing between highest expressing (high B) and medium FtMt expressing clones.

**Supplemental File 5 |** Microsoft word table listing expression differences of key genes related to Iron Metabolism and to Oxidative Stress.

## REFERENCES

Aon-Bertolino, M. L., Romero, J. I., Galeano, P., Holubiec, M., Badorrey, M. S., Saraceno, G. E., et al. (2011). Thioredoxin and glutaredoxin system

proteins-immunolocalization in the rat central nervous system. *Biochim. Biophys. Acta* 1810, 93–110. doi: 10.1016/j.bbagen.2010.06.011  
Arosio, P., Ingrassia, R., and Cavadini, P. (2009). Ferritins: a family of molecules for iron storage, antioxidation and more.



- Biochim. Biophys. Acta* 1790, 589–599. doi: 10.1016/j.bbagen.2008.09.004
- Bjorkhem-Bergman, L., Johansson, M., Morgenstern, R., Rane, A., and Ekstrom, L. (2014). Prenatal expression of thioredoxin reductase 1 (TRXR1) and microsomal glutathione transferase 1 (MGST1) in humans. *FEBS Open Bio* 4, 886–891. doi: 10.1016/j.fob.2014.10.005
- Brundin, P., Dave, K. D., and Kordower, J. H. (2017). Therapeutic approaches to target alpha-synuclein pathology. *Exp. Neurol.* 298, 225–235. doi: 10.1016/j.expneurol.2017.10.003
- Bustin, S. A., Benes, V., Garson, J. A., Hellems, J., Huggett, J., Kubista, M., et al. (2009). The MIQE guidelines: minimum information for publication of quantitative real-time PCR experiments. *Clin. Chem.* 55, 611–622. doi: 10.1373/clinchem.2008.112797
- Cecchi, C., Pensalfini, A., Liguri, G., Baglioni, S., Fiorillo, C., Guadagna, S., et al. (2008). Differentiation increases the resistance of neuronal cells to amyloid toxicity. *Neurochem. Res.* 33, 2516–2531. doi: 10.1007/s11064-008-9627-7
- Cheung, Y.-T., Lau, W. K.-W., Yu, M.-S., Lai, C. S.-W., Yeung, S.-C., So, K.-F., et al. (2009). Effects of all-trans-retinoic acid on human SH-SY5Y neuroblastoma as in vitro model in neurotoxicity research. *Neurotoxicology* 30, 127–135. doi: 10.1016/j.neuro.2008.11.001
- Drysdale, J., Arosio, P., Invernizzi, R., Cazzola, M., Volz, A., Corsi, B., et al. (2002). Mitochondrial ferritin: a new player in iron metabolism. *Blood Cells. Mol. Dis.* 29, 376–383. doi: 10.1006/bcmd.2002.0577
- Duan, J., Du, C., Shi, Y., Liu, D., and Ma, J. (2018). Thioredoxin-interacting protein deficiency ameliorates diabetic retinal angiogenesis. *Int. J. Biochem. Cell Biol.* 94, 61–70. doi: 10.1016/j.biocel.2017.11.013
- Forster, J. I., Koglsberger, S., Trefois, C., Boyd, O., Baumuratov, A. S., Buck, L. et al. (2016). Characterization of differentiated SH-SY5Y as neuronal screening model reveals increased oxidative vulnerability. *J. Biomol. Screen.* 21, 496–509. doi: 10.1177/1087057115625190
- Gao, G., and Chang, Y.-Z. (2014). Mitochondrial ferritin in the regulation of brain iron homeostasis and neurodegenerative diseases. *Front. Pharmacol.* 5:19. doi: 10.3389/fphar.2014.00019
- Gao, G., Zhang, N., Wang, Y.-Q., Wu, Q., Yu, P., Shi, Z.-H., et al. (2017). Mitochondrial ferritin protects hydrogen peroxide-induced neuronal cell damage. *Aging Dis.* 8, 458–470. doi: 10.14336/AD.2016.1108
- Gong, S., Chen, Y., Meng, F., Zhang, Y., Wu, H., and Wu, F. (2017). Roflumilast restores cAMP/PKA/CREB signaling axis for FtMt-mediated tumor inhibition of ovarian cancer. *Oncotarget* 8, 112341–112353. doi: 10.18632/oncotarget.22866
- Guan, H., Yang, H., Yang, M., Yanagisawa, D., Bellier, J.-P., Mori, M., et al. (2017). Mitochondrial ferritin protects SH-SY5Y cells against H<sub>2</sub>O<sub>2</sub>-induced oxidative stress and modulates alpha-synuclein expression. *Exp. Neurol.* 291, 51–61. doi: 10.1016/j.expneurol.2017.02.001
- Guaraldo, M., Santambrogio, P., Rovelli, E., Di Savino, A., Saglio, G., Cittaro, D., et al. (2016). Characterization of human mitochondrial ferritin promoter: identification of transcription factors and evidences of epigenetic control. *Sci. Rep.* 6:33432. doi: 10.1038/srep33432
- Huang, M. L.-H., Becker, E. M., Whitnall, M., Suryo Rahmanto, Y., Ponka, P., and Richardson, D. R. (2009). Elucidation of the mechanism of mitochondrial iron loading in Friedreich's ataxia by analysis of a mouse mutant. *Proc. Natl. Acad. Sci. U.S.A.* 106, 16381–16386. doi: 10.1073/pnas.0906784106
- Jan, A. T., Azam, M., Rahman, S., Almigeiti, A. M. S., Choi, D. H., Lee, E. J., et al. (2017). Perspective insights into disease progression, diagnostics, and therapeutic approaches in alzheimer's disease: a judicious update. *Front. Aging Neurosci.* 9:356. doi: 10.3389/fnagi.2017.00356
- Kim, G. S., Jung, J. E., Narasimhan, P., Sakata, H., and Chan, P. H. (2012). Induction of thioredoxin-interacting protein is mediated by oxidative stress, calcium, and glucose after brain injury in mice. *Neurobiol. Dis.* 46, 440–449. doi: 10.1016/j.nbd.2012.02.008
- Lang, A. E., and Espay, A. J. (2018). Disease modification in Parkinson's disease: current approaches, challenges, and future considerations. *Mov. Disord.* 33, 660–677. doi: 10.1002/mds.27360
- Lee, C.-I., Perng, J.-H., Chen, H.-Y., Hong, Y.-R., Wang, J.-J., (2015). Undifferentiated neuroblastoma cells are more sensitive to photogenerated oxidative stress than differentiated cells. *J. Cell. Biochem.* 116, 2074–2085. doi: 10.1002/jcb.25165
- Levi, S., and Arosio, P. (2004). Mitochondrial ferritin. *Int. J. Biochem. Cell Biol.* 36, 1887–1889. doi: 10.1016/j.biocel.2003.10.020
- Levi, S., Corsi, B., Bosio, M., Invernizzi, R., Volz, A., Sanford, D., et al. (2001). A human mitochondrial ferritin encoded by an intronless gene. *J. Biol. Chem.* 276, 24437–24440. doi: 10.1074/jbc.C100141200
- Li, J., Yue, Z., Xiong, W., Sun, P., You, K., and Wang, J. (2017). TXNIP overexpression suppresses proliferation and induces apoptosis in SMMC7221 cells through ROS generation and MAPK pathway activation. *Oncol. Rep.* 37, 3369–3376. doi: 10.3892/or.2017.5577
- Li, X., Wang, P., Wu, Q., Xie, L., Cui, Y., Li, H., et al. (2017). The construction and characterization of mitochondrial ferritin overexpressing mice. *Int. J. Mol. Sci.* 18:1518. doi: 10.3390/ijms18071518
- Lopez-Carballo, G., Moreno, L., Masia, S., Perez, P., and Baretino, D. (2002). Activation of the phosphatidylinositol 3-kinase/Akt signaling pathway by retinoic acid is required for neural differentiation of SH-SY5Y human neuroblastoma cells. *J. Biol. Chem.* 277, 25297–25304. doi: 10.1074/jbc.M201869200
- Lu, C.-X., Qiu, T., Liu, Z.-F., Su, L., and Cheng, B. (2017). Calcitonin gene-related peptide has protective effect on brain injury induced by heat stroke in rats. *Exp. Ther. Med.* 14, 4935–4941. doi: 10.3892/etm.2017.5126
- Machado, V., Haas, S. J.-P., von Bohlen Und Halbach, O., Wree, A., Kriegelstein, K., Unsicker, K., et al. (2016). Growth/differentiation factor-15 deficiency compromises dopaminergic neuron survival and microglial response in the 6-hydroxydopamine mouse model of Parkinson's disease. *Neurobiol. Dis.* 88, 1–15. doi: 10.1016/j.nbd.2015.12.016
- Mahmood, D. F. D., Abderrazak, A., El Hadri, K., Simmet, T., and Rouis, M. (2013). The thioredoxin system as a therapeutic target in human health and disease. *Antioxid. Redox Signal.* 19, 1266–1303. doi: 10.1089/ars.2012.4757
- Melone, M. A. B., Dato, C., Paladino, S., Coppola, C., Trebbini, C., Giordana, M. T., et al. (2018). Verapamil Inhibits Ser202/Thr205 phosphorylation of tau by blocking TXNIP/ROS/p38 MAPK pathway. *Pharm. Res.* 35:44. doi: 10.1007/s11095-017-2276-2
- Nasoohi, S., Ismael, S., and Ishrat, T. (2018). Thioredoxin-Interacting Protein (TXNIP) in cerebrovascular and neurodegenerative diseases: regulation and implication. *Mol. Neurobiol.* 55, 7900–7920. doi: 10.1007/s12035-018-0917-z
- Nesi, G., Sestito, S., Digiacomo, M., and Rapposelli, S. (2017). Oxidative stress, mitochondrial abnormalities and proteins deposition: multitarget approaches in Alzheimer's disease. *Curr. Top. Med. Chem.* 17, 3062–3079. doi: 10.2174/1568026617666170607114232
- Nicolini, G., Miloso, M., Zoia, C., Di Silvestro, A., Cavaletti, G., and Tredici, G. (1998). Retinoic acid differentiated SH-SY5Y human neuroblastoma cells: an *in vitro* model to assess drug neurotoxicity. *Anticancer Res.* 18, 2477–2481.
- Peddada, S., Yasui, D. H., LaSalle, J. M., (2006). Inhibitors of differentiation (ID1, ID2, ID3 and ID4) genes are neuronal targets of MeCP2 that are elevated in Rett syndrome. *Hum. Mol. Genet.* 15, 2003–2014. doi: 10.1093/hmg/ddl124
- Pezzini, F., Bettinetti, L., Di Leva, F., Bianchi, M., Zoratti, E., Carrozzo, R., et al. (2017). Transcriptomic profiling discloses molecular and cellular events related to neuronal differentiation in SH-SY5Y neuroblastoma cells. *Cell. Mol. Neurobiol.* 37, 665–682. doi: 10.1007/s10571-016-0403-y
- Ramirez, J.-M., Schaad, O., Durual, S., Cossali, D., Docquier, M., Beris, P., et al. (2009). Growth differentiation factor 15 production is necessary for normal erythroid differentiation and is increased in refractory anaemia with ring-sideroblasts. *Br. J. Haematol.* 144, 251–262. doi: 10.1111/j.1365-2141.2008.07441.x
- Ross, R. A., Spengler, B. A., and Biedler, J. L. (1983). Coordinate morphological and biochemical interconversion of human neuroblastoma cells. *J. Natl. Cancer Inst.* 71, 741–747.
- Russell, F. A., King, R., Smillie, S.-J., Kodji, X., and Brain, S. D. (2014). Calcitonin gene-related peptide: physiology and pathophysiology. *Physiol. Rev.* 94, 1099–1142. doi: 10.1152/physrev.00034.2013
- Santambrogio, P., Biasotto, G., Sanvito, F., Olivieri, S., Arosio, P., and Levi, S. (2007). Mitochondrial ferritin expression in adult mouse tissues. *J. Histochem. Cytochem.* 55, 1129–1137. doi: 10.1369/jhc.7A7273.2007
- Shi, Z.-H., Nie, G., Duan, X.-L., Rouault, T., Wu, W.-S., Ning, B., Zhang, N., Chang, Y.-Z., and Zhao, B.-L. (2010). Neuroprotective mechanism of mitochondrial ferritin on 6-hydroxydopamine-induced dopaminergic cell damage: implication for neuroprotection in Parkinson's



- disease. *Antioxid. Redox Signal.* 13, 783–796. doi: 10.1089/ars.2009.3018
- Shi, Z.-H., Shi, F.-F., Wang, Y.-Q., Sheftel, A. D., Nie, G., Zhao, Y.-S., et al. (2015). Mitochondrial ferritin, a new target for inhibiting neuronal tumor cell proliferation. *Cell. Mol. Life Sci.* 72, 983–997. doi: 10.1007/s00018-014-1730-0
- Shyu, W.-C., Lin, S.-Z., Chiang, M.-F., Chen, D.-C., Su, C.-Y., Wang, H.-J., et al. (2008). Secretoneurin promotes neuroprotection and neuronal plasticity via the Jak2/Stat3 pathway in murine models of stroke. *J. Clin. Invest.* 118, 133–148. doi: 10.1172/JCI32723
- Simpson, P. B., Bacha, J. I., Palfreyman, E. L., Woollacott, A. J., McKernan, R. M., and Kerby, J. (2001). Retinoic acid evoked-differentiation of neuroblastoma cells predominates over growth factor stimulation: an automated image capture and quantitation approach to neuritogenesis. *Anal. Biochem.* 298, 163–169. doi: 10.1006/abio.2001.5346
- Siritantikorn, A., Johansson, K., Ahlen, K., Rinaldi, R., Suthiphongchai, T., Wilairat, P., et al. (2007). Protection of cells from oxidative stress by microsomal glutathione transferase 1. *Biochem. Biophys. Res. Commun.* 355, 592–596. doi: 10.1016/j.bbrc.2007.02.018
- Snyder, A. M., Wang, X., Patton, S. M., Arosio, P., Levi, S., Earley, C. J., et al. (2009). Mitochondrial ferritin in the substantia nigra in restless legs syndrome. *J. Neuropathol. Exp. Neurol.* 68, 1193–1199. doi: 10.1097/NEN.0b013e3181bdc44f
- Sobczak, M., Boczek, T., Kowalski, A., Wiktorska, M., Niewiarowska, J., and Zylinska, L. (2014). Downregulation of microsomal glutathione-S-transferase 1 modulates protective mechanisms in differentiated PC12 cells. *J. Physiol. Biochem.* 70, 375–383. doi: 10.1007/s13105-014-0312-9
- Stenirri, S., Santambrogio, P., Setaccioli, M., Erba, B. G., Pia Manitto, M., Rovida, E., et al. (2012). Study of FTMT and ABCA4 genes in a patient affected by age-related macular degeneration: identification and analysis of new mutations. *Clin. Chem. Lab. Med.* 50, 1021–1029. doi: 10.1515/cclm-2011-0854
- Strelau, J., Bottner, M., Lingor, P., Suter-Crazzolara, C., Galter, D., Jaszi, J., et al. (2000). GDF-15/MIC-1 a novel member of the TGF-beta superfamily. *J. Neural Transm.* 60, 273–276.
- Strelau, J., Schober, A., Sullivan, A., Schilling, L., and Unsicker, K. (2003). Growth/differentiation factor-15 (GDF-15), a novel member of the TGF-beta superfamily, promotes survival of lesioned mesencephalic dopaminergic neurons *in vitro* and *in vivo* and is induced in neurons following cortical lesioning. *J. Neural Transm.* 65, 197–203.
- Walker, D. G., Dalsing-Hernandez, J. E., Campbell, N. A., and Lue, L.-F. (2009). Decreased expression of CD200 and CD200 receptor in Alzheimer's disease: a potential mechanism leading to chronic inflammation. *Exp. Neurol.* 215, 5–19. doi: 10.1016/j.expneurol.2008.09.003
- Wang, L., Yang, H., Zhao, S., Sato, H., Konishi, Y., Beach, T. G., et al. (2011). Expression and localization of mitochondrial ferritin mRNA in Alzheimer's disease cerebral cortex. *PLoS ONE* 6:e22325. doi: 10.1371/journal.pone.0022325
- Wang, P., Wu, Q., Wu, W., Li, H., Guo, Y., Yu, P., et al. (2017). Mitochondrial ferritin deletion exacerbates beta-amyloid-induced neurotoxicity in mice. *Oxid. Med. Cell. Longev.* 2017:1020357. doi: 10.1155/2017/1020357
- Wang, X., Yang, H., Yanagisawa, D., Bellier, J.-P., Morino, K., Zhao, S., et al. (2016). Mitochondrial ferritin affects mitochondria by stabilizing HIF-1alpha in retinal pigment epithelium: implications for the pathophysiology of age-related macular degeneration. *Neurobiol. Aging* 47, 168–179. doi: 10.1016/j.neurobiolaging.2016.07.025
- Wang, Y.-Q., Chang, S.-Y., Wu, Q., Gou, Y.-J., Jia, L., Cui, Y.-M., et al. (2016). The protective role of mitochondrial ferritin on erastin-induced ferroptosis. *Front. Aging Neurosci.* 8:308. doi: 10.3389/fnagi.2016.00308
- Wu, W.-S., Zhao, Y.-S., Shi, Z.-H., Chang, S.-Y., Nie, G.-J., Duan, X.-L., et al. (2013). Mitochondrial ferritin attenuates beta-amyloid-induced neurotoxicity: reduction in oxidative damage through the Erk/P38 mitogen-activated protein kinase pathways. *Antioxid. Redox Signal.* 18, 158–169. doi: 10.1089/ars.2011.4285
- Wu, Y., Hao, G.-M., He, J., Lv, T.-T., Wang, H.-L., Mao, Y.-Q., et al. (2015). Lentivirus mediated over expression of CGRP inhibited oxidative stress in Schwann cell line. *Neurosci. Lett.* 598, 52–58. doi: 10.1016/j.neulet.2015.05.009
- Yang, H., Guan, H., Yang, M., Liu, Z., Takeuchi, S., Yanagisawa, D., et al. (2015). Upregulation of mitochondrial ferritin by proinflammatory cytokines: implications for a role in Alzheimer's disease. *J. Alzheimers. Dis.* 45, 797–811. doi: 10.3233/JAD-142595
- Yang, H., Yang, M., Guan, H., Liu, Z., Zhao, S., Takeuchi, S., et al. (2013). Mitochondrial ferritin in neurodegenerative diseases. *Neurosci. Res.* 77, 1–7. doi: 10.1016/j.neures.2013.07.005
- Yang, M., Yang, H., Guan, H., Kato, T., Mukaisho, K., Sugihara, H., et al. (2017). Characterization of a novel monoclonal antibody against human mitochondrial ferritin and its immunohistochemical application in human and monkey Substantia Nigra. *Acta Histochem. Cytochem.* 50, 49–55. doi: 10.1267/ahc.16034
- Yang, S. I., Yuan, Y., Jiao, S., Luo, Q. I., and Yu, J. (2016). Calcitonin gene-related peptide protects rats from cerebral ischemia/reperfusion injury via a mechanism of action in the MAPK pathway. *Biomed. Rep.* 4, 699–703. doi: 10.3892/br.2016.658
- You, L.-H., Li, Z., Duan, X.-L., Zhao, B.-L., Chang, Y.-Z., and Shi, Z.-H. (2016). Mitochondrial ferritin suppresses MPTP-induced cell damage by regulating iron metabolism and attenuating oxidative stress. *Brain Res.* 1642, 33–42. doi: 10.1016/j.brainres.2016.03.023
- Yu, X., and Gao, D. (2013). Overexpression of cytoglobin gene inhibits hypoxic injury to SH-SY5Y neuroblastoma cells. *Neural Regen. Res.* 8, 2198–2203. doi: 10.3969/j.issn.1673-5374.2013.23.010
- Zhan, X., Li, F., Chu, Q., Pang, H., Kim, H. J., Denli, A. M., et al. (2008). Cellular expression and subcellular localization of secretogranin II in the mouse hippocampus and cerebellum. *Exp. Gerontol.* 497, 53–63. doi: 10.1016/j.bbrc.2018.02.130
- Zhou, R., Tardivel, A., Thorens, B., Choi, I., and Tschopp, J. (2010). Thioredoxin-interacting protein links oxidative stress to inflammasome activation. *Nat. Immunol.* 11, 136–140. doi: 10.1038/ni.1831

**Conflict of Interest Statement:** The authors declare that the research was conducted in the absence of any commercial or financial relationships that could be construed as a potential conflict of interest.

Copyright © 2019 Mendsaikhan, Takeuchi, Walker and Tooyama. This is an open-access article distributed under the terms of the Creative Commons Attribution License (CC BY). The use, distribution or reproduction in other forums is permitted, provided the original author(s) and the copyright owner(s) are credited and that the original publication in this journal is cited, in accordance with accepted academic practice. No use, distribution or reproduction is permitted which does not comply with these terms.



# PKR: A Kinase to Remember

Shunit Gal-Ben-Ari<sup>1</sup>, Iliana Barrera<sup>1</sup>, Marcelo Ehrlich<sup>2</sup> and Kobi Rosenblum<sup>1,3\*</sup>

<sup>1</sup> Laboratory of Molecular and Cellular Mechanisms Underlying Learning and Memory, Sagol Department of Neurobiology, University of Haifa, Haifa, Israel, <sup>2</sup> Laboratory of Intracellular Trafficking and Signaling, School of Molecular Cell Biology & Biotechnology, The George S. Wise Faculty of Life Sciences, Tel Aviv University, Tel Aviv, Israel, <sup>3</sup> Center for Gene Manipulation in the Brain, University of Haifa, Haifa, Israel

Aging is a major risk factor for many diseases including metabolic syndrome, cancer, inflammation, and neurodegeneration. Identifying mechanistic common denominators underlying the impact of aging is essential for our fundamental understanding of age-related diseases and the possibility to propose new ways to fight them. One can define aging biochemically as prolonged metabolic stress, the innate cellular and molecular programs responding to it, and the new stable or unstable state of equilibrium between the two. A candidate to play a role in the process is protein kinase R (PKR), first identified as a cellular protector against viral infection and today known as a major regulator of central cellular processes including mRNA translation, transcriptional control, regulation of apoptosis, and cell proliferation. Prolonged imbalance in PKR activation is both affected by biochemical and metabolic parameters and affects them in turn to create a feedforward loop. Here, we portray the central role of PKR in transferring metabolic information and regulating cellular function with a focus on cancer, inflammation, and brain function. Later, we integrate information from open data sources and discuss current knowledge and gaps in the literature about the signaling cascades upstream and downstream of PKR in different cell types and function. Finally, we summarize current major points and biological means to manipulate PKR expression and/or activation and propose PKR as a therapeutic target to shift age/metabolic-dependent undesired steady states.

**Keywords:** PKR, protein synthesis, learning and memory, signal transduction, metabolic stress, aging, cancer, Alzheimer's disease

## OPEN ACCESS

### Edited by:

Christian Gonzalez-Billault,  
Universidad de Chile, Chile

### Reviewed by:

Constanze I. Seidenbecher,  
Leibniz Institute for Neurobiology (LG),  
Germany  
Alexandre Henriques,  
Neuro-Sys, France

### \*Correspondence:

Kobi Rosenblum  
kobir@psy.haifa.ac.il

**Received:** 18 September 2018

**Accepted:** 10 December 2018

**Published:** 09 January 2019

### Citation:

Gal-Ben-Ari S, Barrera I, Ehrlich M  
and Rosenblum K (2019) PKR: A  
Kinase to Remember.  
Front. Mol. Neurosci. 11:480.  
doi: 10.3389/fnmol.2018.00480

## INTRODUCTION

Protein kinase R (PKR) is a serine-threonine kinase (551 amino acid long) encoded in humans by the EIF2AK2 gene [located on chromosome 2 (Feng et al., 1992)], which plays a major role in central cellular processes such as mRNA translation, transcriptional control, regulation of apoptosis, and proliferation (García et al., 2007). In accordance with such preponderant role, PKR dysregulation (see **Figure 1**) has been implicated in cancer, neurodegeneration (Segev et al., 2013, 2015; Stern et al., 2013), inflammation, and metabolic disorders (Segev et al., 2016; Garcia-Ortega et al., 2017). This kinase, which is constitutively and ubiquitously expressed in vertebrate cells, is not found in plants, fungi, protists, or invertebrates (Taniuchi et al., 2016). PKR was first cloned in 1990 at the Pasteur Institute (Meurs et al., 1990; Watanabe et al., 2018), and is also known as Protein kinase RNA-activated; and interferon-induced, double-stranded RNA-domain kinase (Hugon et al., 2009).

The structural composition of PKR consists of an N-terminal double stranded RNA binding domain composed of two tandem repeats of a conserved double stranded RNA binding motif (dsRBM1 and dsRBM2) interspaced by a 23 amino acid linker, and followed by a flexible linker connecting to a C-terminal kinase domain (Meurs et al., 1990). Both dsRBMs are required for the high-affinity interaction with double stranded RNA (dsRNA) (McKenna et al., 2006). The catalytic domain of PKR, where its dimerization takes place, has a typical protein kinase fold formed between its  $\beta$ -sheet N-terminal lobe and its  $\alpha$ -helical C-terminal lobe (Dzananovic et al., 2018). However, while the catalytic domain structure is similar to other protein kinases, the interaction of PKR with its best-characterized substrate, the eukaryotic initiation factor 2 $\alpha$  (eIF2 $\alpha$ ), requires a specific  $\alpha$ -helix unique to PKR ( $\alpha$ G), which is located on the surface of the C-terminal lobe of the kinase domain (Dar et al., 2005).

While the best-described transcriptional motif in the PKR promoter is an IFN-stimulated response element (ISRE), allowing it to be transcribed in response to type I IFN (Kuhlen and Samuel, 1997), numerous transcription factors have been identified as binders of the promoter region of the EIF2AK2 gene [e.g., 92 different factors identified by CHIP-Seq assays in the context of the ENCODE project (Rouillard et al., 2016)]. This scenario supports the notion of PKR as an interferon stimulated gene (ISG), while also allowing for the modulation of PKR expression in cellular programs involving the activation of different repertoires of transcription. Activation of PKR results in a number of conformational changes, the most important of which is its homodimerization, based on biochemical and genetic analyses (Dey et al., 2005). As a result of its homodimerization, PKR is autophosphorylated at multiple serine and threonine sites, including Ser242, Thr255, Thr258, Ser83, Thr88, Thr89, Thr90, Thr446, and Thr451 (Taylor et al., 2001). The latter two, namely, the Thr 446 and Thr 451 sites, are consistently phosphorylated during PKR activation, resulting in further stabilization of its homodimerization and increased catalytic activity (Hugon et al., 2009; Watanabe et al., 2018).

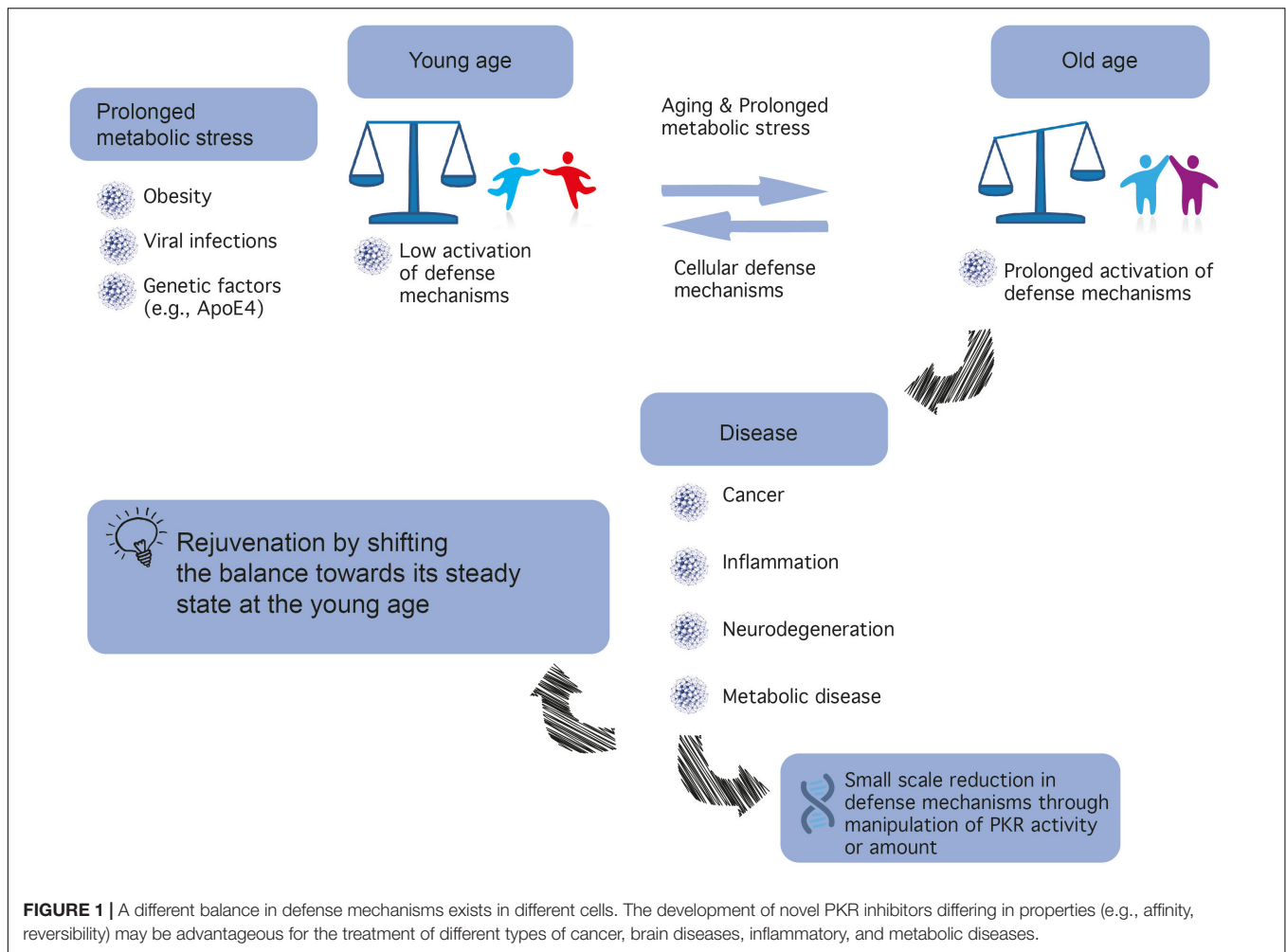
Protein kinase R serves as a central hub for the detection of cellular stress signals and response to them, and is thus expected to be regulated by different stress-response pathways. In accord with this notion, the canonical activator of PKR is double-stranded RNA (an obligatory feature of the replication process of RNA viruses), rendering PKR as a pattern recognition receptor endowed with cell function modulatory abilities. The central role of PKR in mediating anti-viral responses is also evidenced by the high degree of positive selection exhibited by coding sequence, indicative of the arms race against the pathogens it encounters and combats (Elde et al., 2009; Rothenburg et al., 2009; Carpentier et al., 2016). However, PKR can also be activated by other factors, for example, heat shock proteins, growth factors (e.g., PDGF), and heparin (Li et al., 2006). PKR is also activated in response to numerous insults, including non-viral pathogens (bacterial lipopolysaccharide, which activates the toll-like receptor 4 pathway), nutrition or energy excess, cytokines (e.g., TNF- $\alpha$ , IL-1, IFN- $\gamma$ ), calcium, reactive oxygen species, irradiation (presumably by inducing DNA damage), mechanical stress, and endoplasmic reticulum

stress resulting from the presence of a large quantity of unfolded proteins [caused, e.g., by tunicamycin, arsenite, thapsigargin, or H<sub>2</sub>O<sub>2</sub>, which in turn activate the PKR activator protein (PACT; RAX in mice)] (Gil and Esteban, 2000; García et al., 2007; Hugon et al., 2017; Watanabe et al., 2018). **Figure 2** summarizes molecular pathways upstream and downstream of PKR, and **Figure 3** presents interaction partners and substrates of PKR.

PKR is one of four kinases that regulate protein synthesis via the eIF2 $\alpha$  pathway. These kinases include, apart from PKR, the (PKR)-like endoplasmic reticulum kinase (PERK); general control non-derepressible 2 kinase (GCN2), and heme-regulated eIF2 $\alpha$  kinase (HRI). All four kinases regulate the phosphorylation of eukaryotic initiation factor 2 on its  $\alpha$  subunit (eIF2 $\alpha$ ), a major regulator of the initiation phase of mRNA translation, the rate limiting step of protein synthesis. Phosphorylation of eIF2 $\alpha$  on Ser 51 by any of the four kinases leads to its inhibition and a consequent transient suppression of general protein synthesis, up to its complete blockade, concomitant with translation of mRNAs that encode for antiviral factors and/or mediate the integrated stress response (Hoang et al., 2018). Such blockade of protein synthesis results in the decrease or prevention of viral replication, and may result in apoptosis (García et al., 2007). PKR can also induce apoptosis independently of eIF2 $\alpha$  phosphorylation, by activation of the FADD/caspase-8/caspase-3 and caspase-9 APAF pathways (Gil et al., 2002; von Roretz and Gallouzi, 2010).

Both PKR-dependent apoptosis strategies, either with or without blockade of protein synthesis, serve as anti-viral responses. Consequently, many viruses have developed mechanisms which prevent the establishment of an anti-viral state, by inhibiting components of the PKR pathway. These mechanisms include viral proteins that serve as inhibitors of PKR, which inhibit it by direct binding of PKR (thereby preventing autophosphorylation; e.g., Hepatitis C virus, Herpes simplex 1, and Kaposi's sarcoma VRF-2), changing its subcellular localization (e.g., Human and Murine Cytomegalovirus), directing it for degradation (e.g., Rift valley fever virus), or regulating its activity. Regulation of PKR activity is done by expression of proteins that disrupt PKR RNA binding sites by dsRNA sequestration, direct obstruction of these sites (e.g., Vaccinia virus, Influenza virus), or interference with the phosphorylation of eIF2 $\alpha$  (e.g., Human Immunodeficiency Virus 1) (Dzananovic et al., 2018). Specifically, adenovirus and Epstein-Barr virus transcribe dsRNAs with structural elements required for binding the dsRBMs and a stem-loop structure that inhibits PKR autophosphorylation (McKenna et al., 2006; Wahid et al., 2009; Dzananovic et al., 2014).

In addition to its ability to sense dsRNA, primarily of viral origin, PKR is also activated in response to endogenous RNA. Many of these are non-coding RNAs and/or regulatory RNAs such as microRNAs (miRNAs). For example, the non-coding nc886 miRNA functions as a suppressor of PKR by interacting with it directly (Lee et al., 2011), and its expression is increased in some malignancies but reduced others (Lee et al., 2016). In accordance, its suppression or epigenetic silencing result in induction of apoptosis and increased expression of



oncogenes in certain models of cancer (Lee et al., 2014; Hu et al., 2017), and a protective effect in other models of cancer *in vitro* (Lee et al., 2016). Additionally, overexpression of miR-29b in developing cerebellar granular neurons confers protection against ethanol neurotoxicity leading to apoptosis through the SP1/RAX/PKR cascade (Qi et al., 2014). Another example is the long non-coding RNA HOX antisense intergenic RNA (HOTAIR), whose overexpression in keratinocytes resulted in increased expression of PKR and, as a result, decreased cell viability, increased levels of apoptosis, and increased expression of inflammatory factors in ultraviolet B (UVB)-treated cells (Liu and Zhang, 2018). Furthermore, a recent study has shown that PKR binds other non-coding RNAs such as retrotransposons, satellite RNAs, and mitochondrial RNAs (which can form intermolecular dsRNAs through bidirectional transcription of the mitochondrial genome). In fact, in a screen for molecules which bind PKR, done using the formaldehyde-mediated crosslinking and immunoprecipitation sequencing, mitochondrial RNA constituted the majority of endogenous molecules that bind PKR (Kim et al., 2018). In addition, PKR has been proposed to bind dsRNAs formed by inverted Alu repeats (IRAlus), upon disruption of the nuclear membrane in mitosis,

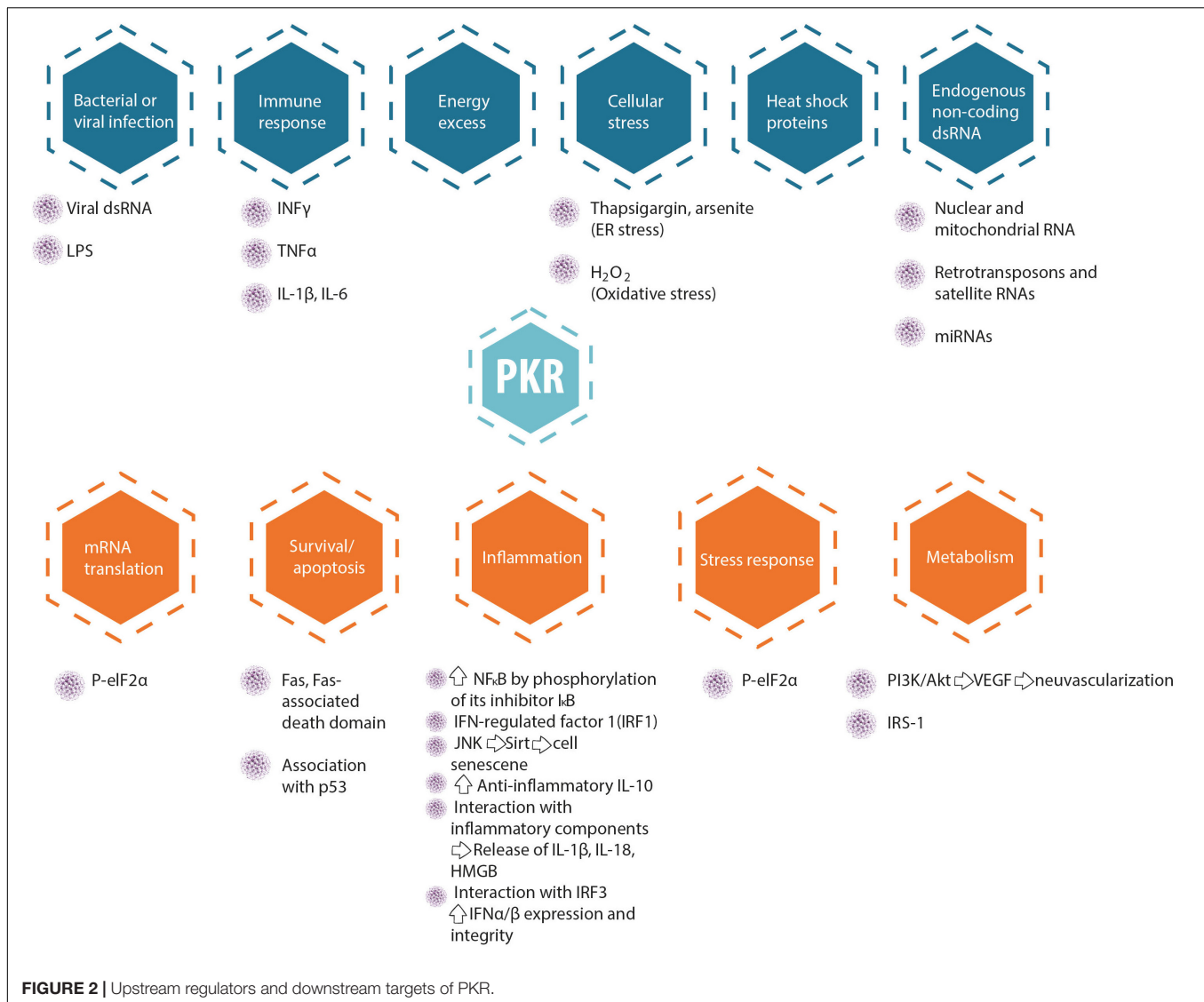
leading to the phosphorylation of eIF2 $\alpha$  in this phase of the cell cycle (Kim et al., 2014).

## PKR IN THE BRAIN

### Neurodegeneration

In the past two decades, increased levels of PKR phosphorylation have been detected in the brains of patients with HIV and neurodegenerative diseases such as Alzheimer's disease (AD) (Chang et al., 2002), Parkinson's disease, Huntington's disease (Peel et al., 2001), dementia, and prion disease (Hugon et al., 2009). Furthermore, elevated levels of p-PKR and p-eIF2 $\alpha$  have been observed in several mouse and monkey models of AD, including wild-type mice and cynomolgus monkeys injected with A $\beta$ <sub>1–42</sub> oligomers (i.c.v.), APPSwe/PS1DE9 mice, and ApoE4 mice (Lourenco et al., 2013; Segev et al., 2016). In both AD and Huntington's disease, PKR has been implicated as mediating an ER stress-induced cell death (Peel and Bredesen, 2003; Bando et al., 2005), and it is possible that this is also the case regarding other neurological disorders where PKR levels are elevated. In the case of AD, increased staining of phosphorylated

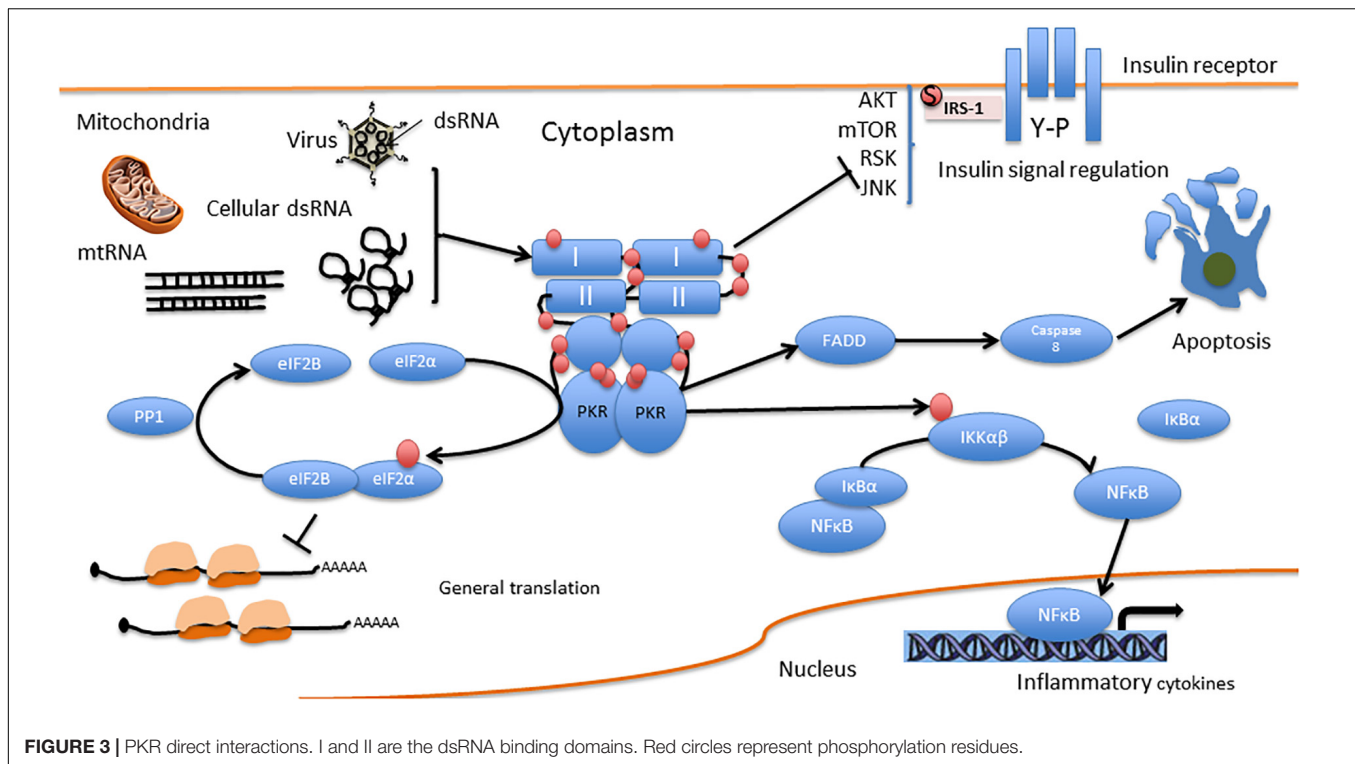




PKR (p-PKR) and phosphorylated eIF2 $\alpha$  (p-eIF2 $\alpha$ ) have been observed mainly in degenerating hippocampal neurons, partially colocalized with hyperphosphorylated tau, a major hallmark of AD, and p-PKR levels are increased in cerebrospinal fluid from patients with AD and mild cognitive impairment (Mouton-Liger et al., 2012; Hugon et al., 2017), in positive correlation with cognitive decline in AD (Dumurgier et al., 2013). According to another study, increased levels of p-PKR, p-eIF2 $\alpha$ , and p-mTOR were found in peripheral blood lymphocytes derived from AD patients compared to healthy subjects, in correlation with cognitive decline, further supporting the use of these molecules as biomarkers for the diagnosis of AD progression (Paccalin et al., 2006). Moreover, sporadic cases of AD constitute approximately 95% of AD cases, while the rest are familial ones. The sporadic cases are hypothesized to result from interaction between genetic and environmental factors, such as virus infections. Indeed, a study that analyzed human genes involved in the cell response to the herpes simplex virus type 1 (HSV-1) in AD samples compared

to healthy subjects identified a SNP (rs2254958) located on the 5'UTR region of EIF2AK2, the gene encoding to PKR. This SNP, found within an exonic splicing enhancer, was found to be associated with AD, and homozygous carriers showed slightly earlier onset of AD (3.3 years), especially in the absence of the APOE4 allele (Bullido et al., 2008).

It has also been shown that in neuroblastoma cells overexpressing PKR, incubation with A $\beta$  peptide resulted in increased phosphorylation levels of eIF2 $\alpha$ , concomitant with an increase in the number of apoptotic cells (Chang et al., 2002). In a reciprocal experiment, incubation of PKR<sup>-/-</sup> neuroblastoma cells with A $\beta$  peptide resulted in reduced levels of p-eIF2 $\alpha$  and apoptosis, and in accordance, primary culture cells derived from PKR KO mice were less sensitive to A $\beta$ -induced toxicity (Chang et al., 2002). Finally, treatment with C16, the most widely used PKR inhibitor, in 12-month-old 5XFAD AD model mice rescued fear memory deficits almost fully, and restored LTP impairment in these mice. This was shown to occur without affecting A $\beta$ <sub>1-42</sub>



levels in these mice. Similar cognitive rescue effects were induced by C16 in  $A\beta_{1-42}$ -injected mice in the novel object recognition task and LTP impairment (Hwang et al., 2017).

The link between neurodegenerative diseases and oxidative stress has been a prevailing dogma in neurodegeneration research in the past three decades. Recent studies suggest a link between oxidative stress and PKR. Specifically, the anti-oxidant drug gastrodin (a phenolic glucoside), which suppresses BACE1 expression has been shown to enhance long term memory in the Tg2576 mouse model of AD in the Morris water maze paradigm of spatial learning. While induction of oxidative stress using  $H_2O_2$  in neuroblastoma cells led to increased levels of pPKR, p-eIF2 $\alpha$ , and BACE1, in accordance with the literature, treatment with either gastrodin or a peptide PKR inhibitor prevented the increased elevation in all three parameters, indicating that gastrodin exerts its neuroprotective effect by inhibition of the PKR/eIF2 $\alpha$  pathway (Zhang et al., 2016). Another study has identified PKR as an inducer of apoptosis in response to oxidative stress. The authors showed that oxidative stress induced by nicotinamide adenine dinucleotide phosphate reduced oxidase (NADPH oxidase; NOX), an enzyme activated downstream of ER-stress, leads to the activation of PKR and amplification of its downstream target CCAAT/enhancer binding protein homologous protein (CHOP), resulting in apoptosis (Li et al., 2010).

## Learning and Memory

Protein kinase R has also been directly implicated in learning and memory. Cumulative evidence suggests that *de novo* global protein synthesis is a prerequisite for the consolidation of

labile, short-term memory into more stable, long-term memory (Rosenblum et al., 1993; Klann and Richter, 2007; Gkogkas et al., 2010; Alberini and Chen, 2012; Gal-Ben-Ari et al., 2012). Since the rate-limiting step of most protein synthesis through mRNA translation is the initiation phase, it is plausible that global protein synthesis during memory consolidation involves the eIF2 $\alpha$  pathway. Global protein synthesis is increased when phosphorylation levels of eIF2 $\alpha$  are decreased. Indeed, enhancement of long term memory has been shown in both mice and rats, in cortical- and hippocampal-dependent learning paradigms, using genetic and pharmacological methods for decreasing eIF2 $\alpha$  phosphorylation directly or indirectly, by reducing expression levels or activity levels of any of its four regulatory kinases, including PKR. For example, eIF2 $\alpha^{+/S51A}$  mice (where Ser51 is replaced with alanine, preventing the phosphorylation of eIF2 $\alpha$ ) show enhanced performance in hippocampal-dependent spatial memory and contextual and auditory fear conditioning, and cortical-dependent conditioned taste aversion (CTA). The reciprocal experiment of stereotaxic administration of Sal003 (a derivative of salubrin, which inhibits eIF2 $\alpha$  dephosphorylation) into the rat hippocampus resulted in impaired contextual fear learning (Costa-Mattioli et al., 2007). However, these findings may be ascribed to PERK, rather than PKR, since similar memory enhancement has been observed by PERK genetic reduction (viral vectors and PERK KO mice) or pharmacological inhibition (using PERK inhibitor GSK2606414) (Trinh et al., 2012; Ounallah-Saad et al., 2014; Trinh et al., 2014; Sharma et al., 2018; Zimmermann et al., 2018), and also in a mouse model of AD (Ma et al., 2013; Yang et al., 2016). It is important to note that the main kinase to



determine the basal phosphorylation state of eIF2 $\alpha$  in the brain and primary culture is PERK (80%), while the other three eIF2 $\alpha$  kinases including PKR determine the remaining 20% (Ounallah-Saad et al., 2014). Below we list findings supporting the beneficial effects of inhibiting or suppressing PKR specifically.

Similarly, in rats, pharmacological inhibition of PKR using C16 (aka PKRi) resulted in enhanced cortical-dependent novel taste learning (insular cortex-dependent positive, incidental learning) and CTA (negative, insular cortex dependent taste-malaise associative learning) when administered either i.p. or stereotactically into the insular cortex prior to the taste stimulus. Similar results were obtained in mice using these paradigms. This effect of C16 on memory enhancement was shown to be PKR-specific, since it did not occur when PKR<sup>-/-</sup> mice were administered C16 either in the novel taste learning or the CTA paradigm. However, administration of C16 did not affect phosphorylation levels of eIF2 $\alpha$  either in the hippocampus or the cortex, in WT or PKR KO mice (Jiang et al., 2010; Stern et al., 2013). This point has been neglected in the literature thus far, and is in line with the fact that PERK is the major kinase to determine levels of eIF2 $\alpha$  phosphorylation in the brain (Ounallah-Saad et al., 2014). We deem it important to explicitly state that, contrary to our simplistic view, C16 administration usually does not decrease p-eIF2 $\alpha$  levels either *in vivo* or in cell culture [e.g., Hwang et al., 2017; 5XFAD mice treated with A $\beta$ <sub>1–42</sub> and PKRi (0.335 mg/kg, i.p.)]. In fact, to the best of our knowledge, in certain cases, p-eIF2 $\alpha$  levels can be decreased by C16 only by pushing cells to extreme conditions involving massive cell death, such as prolonged incubation with toxic agents and/or high concentrations of C16 *in vivo* [e.g., striatal quinolinic acid administration combined with C16 (600 mg/Kg, i.p.) (Tronel et al., 2014)], *ex vivo* [e.g., bath treatment of brain slices; C16 (50  $\mu$ M) for 2 h (Stern et al., 2013)], or in culture [e.g., PKRi 500 nM (C16) in cerebellar granular neurons from rats treated with amprolium (1.5 mM) for 24 h; amprolium is a thiamine competitor and depletes its intracellular levels (Wang et al., 2007); hippocampal neurons treated with A $\beta$  oligomers for 3 h and PKRi (C16) 1  $\mu$ M (Lourenco et al., 2013)]. C16 has an IC<sub>50</sub> of 210 nM (Jammi et al., 2003).

A major current advancement in neuroscience is the ability to zoom in molecularly on specific cell/neuronal types. Zhu et al. (2011) have shown that PKR<sup>-/-</sup> mice or WT mice treated with PKR inhibitor C16 have enhanced long-term memory and synaptic plasticity in inhibitory neurons, while synaptic plasticity in excitatory neurons is unaltered. Furthermore, the authors demonstrated that IFN- $\gamma$  was increased in PKR<sup>-/-</sup> mice. In addition, hippocampal-dependent memory enhancement, as measured in the contextual fear conditioning paradigm, was observed following administration of PKR inhibitor C16 and was abolished in IFN- $\gamma$ <sup>-/-</sup> mice. In accordance, treatment of mouse hippocampal slices with C16 led to sustained L-LTP in slices derived from WT mice, but not IFN- $\gamma$ <sup>-/-</sup> mice. The authors concluded that IFN- $\gamma$  mediates disinhibition, which underlies the enhanced cognitive performance and synaptic plasticity when PKR is suppressed genetically or pharmacologically (Zhu et al., 2011). Importantly, the effect downstream of PKR is unclear, since levels of eIF2 $\alpha$  phosphorylation in general or in the relevant

GABAergic neurons were not measured. Further research using neuronal-specific manipulation is needed to better understand the possible differential role of PKR and/or the eIF2 $\alpha$  pathway in different neuronal subtypes.

Other studies have also shown the direct involvement of IFN- $\gamma$  in learning and memory and in synaptic plasticity. For example, the production of IFN- $\gamma$  is altered in many conditions accompanied by cognitive deficits. A recent study has shown that hippocampal-dependent tasks such as spatial memory and recognition memory are enhanced in IFN- $\gamma$  KO mice (while other functions, such as motor function or anxiety, for example, are unaltered). These IFN- $\gamma$  KO mice were also shown to have increased DG neurogenesis, along with enlarged dendritic trees, characterized by longer dendrites in this brain subregion, as well as changes in cell volume and number, restricted to the dorsal part of the hippocampus (Monteiro et al., 2016).

## PKR IN NEUROINFLAMMATORY PROCESSES

As mentioned above, PKR is activated by pro-inflammatory cytokines (e.g., TNF- $\alpha$ , IL-1, and IFN- $\gamma$ ) (Khandelwal et al., 2011), and in turn, activates inflammation-related pathways, including the pro-apoptotic c-Jun N-terminal kinases (JNK) pathway (Bonnet et al., 2000; De Felice and Ferreira, 2014) and the pro-inflammatory NF- $\kappa$ B pathway (by direct interaction with I $\kappa$ B, an inhibitor of the NF- $\kappa$ B  $\beta$  subunit) (Bonnet et al., 2000). Activated PKR enhances IFN- $\alpha/\beta$  expression by IRF3 activation (Zhang and Samuel, 2008) and contributes to IFN- $\alpha/\beta$  mRNA integrity (Schulz et al., 2010). Activation of both IFN- $\alpha/\beta$  and NF- $\kappa$ B occurs downstream of toll-like receptor 3 (TLR3) activation in response to dsRNA. The signaling cascade, as demonstrated using poly I:C, involves (TLR3)-mediated activation of NF- $\kappa$ B and MAP kinase through the signaling components TLR3-TRAF6-TAK1-TAB2-PKR (Jiang et al., 2003). Depending on the cell type and insult activating PKR, it also induces the release of pro-inflammatory IL-1 $\beta$ , IL-18, and high mobility group box 1 (HMGB1) protein (Lu et al., 2012). However, in addition to its pro-inflammatory activity, PKR also activates anti-inflammatory IL-10 (Cheung et al., 2005; Chakrabarti et al., 2008) and reduces CD8 T cell proliferation in several models (Grolleau et al., 2000; Kadereit et al., 2000). In addition, PKR promotes apoptosis by interacting with the Fas-associated death domain protein (Couturier et al., 2010; von Roretz and Gallouzi, 2010) and upregulation of the proapoptotic factor Bax (Balachandran et al., 1998).

Indeed, neuroinflammation and activation of microglia are molecular hallmarks of AD, alongside neuronal loss, A $\beta$  senile plaques (which are surrounded by reactive microglia and astrocytes), and neurofibrillary tangles of hyperphosphorylated tau protein (Duyckaerts et al., 2009). In addition, it has been shown in mice that inflammation, even if external to the brain, may lead to neuroinflammation and increased brain levels of A $\beta$  (Kahn et al., 2012; Krstic et al., 2012), whereas treatment of brain-external inflammation may halt or even reverse the progression of this neuropathology. Increased brain levels of A $\beta$ , in turn,

may lead to exacerbation of inflammation, since A $\beta$  peptide can activate microglia and lead to further release of pro-inflammatory cytokines, e.g., TNF- $\alpha$  or IL-1 $\beta$  (Kahn et al., 2012; Krstic et al., 2012; Carret-Rebillat et al., 2015). PKR contributes directly to neurotoxicity by activating pro-apoptotic caspase 3 and caspase 8, as shown in A $\beta$ -treated cells and the APPSLPS1 knock-in mouse model of AD (Couturier et al., 2010).

A recent study has uncovered at least some of the molecular mechanisms underlying PKR-mediated neuroinflammation. In this study, the authors injected lipopolysaccharide (LPS; present in bacteria and used to induce inflammation) intraperitoneally to WT or PKR-KO mice, and measured inflammation-related parameters in the cortex and the hippocampus. These authors showed that many of the inflammation-related parameters were PKR-dependent, since these phenomena were not observed in PKR knockout mice, as opposed to WT mice, including LPS-induced increase in hippocampal neuroinflammation (measured by IBA1, a marker of microglia activation), cytokine release (TNF- $\alpha$  and IL-6), as well as BACE1, A $\beta$ <sub>42</sub>, and phosphorylated STAT3 (BACE1 transcription regulator) protein expression levels (Carret-Rebillat et al., 2015).

In another study using PKR KO mice, 7-week-old mice were challenged with intracranial administration (into the left hemisphere) of the neurovirulent JHM strain of mouse hepatitis virus, JHMV, which induces encephalitis. In this model, too, the increase in brain levels of pro-inflammatory genes observed in WT mice was prevented in PKR KO mice (e.g., IL-6, *Ccl5*, and *Cxcl10*) (Kapil et al., 2014). However, no such PKR KO vs. WT mouse differences were observed in the respective proteins encoded by these genes, or IL-1 $\beta$  levels (Taga et al., 2017). By contrast, other inflammation-related genes and their respective proteins were matched in the impaired pro-inflammatory response in PKR KO mice compared to WT mice, for example, IL-10 and TIMP1. Notably, IFN- $\gamma$  levels (gene and protein) were higher in PKR KO mice compared with WT ones (Kapil et al., 2014). It should be noted that both IL-1 $\beta$  and IL-6 are upregulated following neuroinflammation, and both cytokines promote disruption of the blood-brain barrier (BBB) and recruitment of lymphocytes (Hopkins and Rothwell, 1995; Erta et al., 2012).

These data suggest that pharmacological inhibition of PKR or its downregulation, e.g., by a virus, may also protect against neuroinflammation and its exacerbation. Indeed, injection of C16 (600  $\mu$ g/kg, i.p.), the currently most potent PKR inhibitor (IC<sub>50</sub> = 210 nM; Jammi et al., 2003), to a rat model (10 weeks old) of acute inflammation, induced by unilateral stereotaxic administration of quinolinic acid (QA), decreased neuronal loss. Furthermore, it ameliorated neuroinflammation, as demonstrated by reduced levels of pro-inflammatory IL-1 $\beta$  and cleaved caspase 3, a marker of apoptosis and increased levels of anti-inflammatory IL-10 (Lu et al., 2012; Tronel et al., 2014). However, no significant differences were detected in TNF- $\alpha$  or IL-4 in the QA-treated animals following C16 treatment. In another study, treatment with C16 (100  $\mu$ g/kg) was shown to prevent neonatal hypoxia-ischemia brain damages by inhibiting neuroinflammation, reducing pro-inflammatory TNF- $\alpha$ , IL-6, and IL-1 $\beta$  mRNA expression levels in neonate (7 days old) rats

(Xiao et al., 2016). In both studies, less tissue damage was evident in C16-treated animals (Tronel et al., 2014; Xiao et al., 2016).

## THE ROLE OF PKR IN METABOLISM

### PKR in Whole-Body Metabolism

Evidence suggests that PKR constitutes the link binding metabolic stress, obesity, diabetes, and inflammation, although this is controversial across the literature. PKR is apparently involved in metabolism throughout the body, and increased phosphorylation of eIF2 $\alpha$  is a hallmark of obesity and diabetes-related insulin resistance (Nakamura et al., 2010, 2014; Carvalho-Filho et al., 2012). Furthermore, in culture, PKR inhibits pancreatic  $\beta$ -cell proliferation (Song et al., 2015), whereas insulin treatment elevates PKR phosphorylation on tyrosine residues, while inhibiting poly I:C-induced PKR phosphorylation on threonine residues (Swetha and Ramaiah, 2015). Additionally, high glucose impairs insulin signaling by activation of the PKR pathway (Udumula et al., 2017), whereas PKR activation induces insulin resistance in peripheral tissues (Nakamura et al., 2010, 2014; Carvalho-Filho et al., 2012; Carvalho et al., 2013). In a recent study, PKR was shown to interact with TAR RNA-binding protein (TRBP) under conditions of metabolic stress, and that phosphorylation of TRBP results in the activation of PKR, which in turn leads to JNK activation. While overexpression of TRBP in obese mice resulted in exacerbation of glucose metabolism, inhibition of TRBP phosphorylation in the liver had beneficial effects, including improved insulin resistance and glucose metabolism as well as reduced inflammation (Nakamura et al., 2015).

In another study, where PKR KO mice were fed on a high fat diet (HFD), insulin levels were markedly higher compared to PKR KO mice fed on control diet or WT mice fed on either diet. However, no significant differences between WT and PKR KO mice fed on HFD were noted in other parameters measured, such as body weight or glucose levels (Taga et al., 2018). Similar findings were reported by Lancaster et al. (2016) regarding these parameters in HFD-fed PKR KO mice. However, Lancaster and colleagues reported that PKR does have a role in T-lymphocyte recruitment, and PKR KO mice had less T cells in adipose tissue, which was thought to protect them from inflammation. However, this was not the case, and the authors showed that genetic deletion of PKR did not protect these mice against saturated fatty acid-induced inflammation or inflammasome activation. Furthermore, contrary to the studies presented above, injection of poly I:C in order to increase PKR did not result in impaired glucose tolerance (Lancaster et al., 2016).

These contradictory findings may be explained by different transgenic mouse models used. The widely used PKR KO mouse models have a deletion either in the N terminal or C terminal of PKR, and cells derived from these models were shown to express truncated forms of PKR (Baltzis et al., 2002), which retain partial functionality, and studies have shown that different domains of PKR are required for its different functions. Indeed, the catalytic domain is necessary for suppression of mRNA translation regulation and induction of inflammation in response

to excessive consumption of nutrients and energy (Garcia-Ortega et al., 2017); the dsRNA binding domain is required for the activation of PKR by snoRNA under conditions of metabolic stress (Youssef et al., 2015); and the protein binding domain of PKR (but not its dsRNA binding domain) is required for other functions, e.g., as an adaptor protein. For example, a catalytically inactive PKR with intact protein binding was shown to promote  $\beta$ -cell proliferation via the TRAF2/RIP1/NF- $\kappa$ B/c-Myc pathways (Gao et al., 2015). However, this finding is inconsistent with those reported by Song et al. (2015), where PKR was reported to inhibit  $\beta$ -cell proliferation through sumoylation-dependent stabilization of P53. Of note, most kinase inhibitor compounds, including inhibitors of PKR, target only the catalytic domain (Garcia-Ortega et al., 2017).

## PKR Metabolism in the Brain

Insulin plays a major role in orchestrating energy availability in the body, as well as in the brain, a high-energy demanding organ (Fernandez and Torres-Alemán, 2012). In recent years, it has become increasingly clear that metabolic dysregulation in the brain underlies cognitive disorders, including AD, now considered type III diabetes (de la Monte and Wands, 2008). Such metabolic dysregulation or metabolic stress may result from aging, particularly when combined with high caloric intake and lack of physical exercise, which may lead to health problems spanning obesity, cardiovascular diseases, and diabetes (see Figure 1).

Metabolic stress also plays a role in AD, *inter alia*, through the Apolipoprotein E (ApoE) protein, which plays a role in lipid metabolism and transport in the liver and the brain, including clearance of A $\beta$  peptide from the synapse (Li et al., 1988). The ApoE4  $\epsilon$ 4 allele (ApoE4) is currently the best studied risk factor for late-onset, sporadic AD, with a prevalence of 20% in the general population, compared to 50% in AD patients, although estimates vary between different sources (Ward et al., 2012).

A recent study examined the interplay of PKR, metabolic stress, and ApoE4. Following prolonged metabolic stress, induced via HFD (60% fat for 3 months), higher levels of anxiety behavior were observed in ApoE4 mice compared to control ApoE3 mice fed on the same HFD. Furthermore, maintenance on HFD led to poorer levels of metabolic parameters in ApoE4 compared to ApoE3 mice, resembling diabetes mellitus-like characteristics, manifested as more rapid weight gain, lower serum and plasma insulin levels, and higher serum glucose levels in ApoE4 compared to ApoE3 mice. Furthermore, this HFD protocol led to higher hippocampal levels of  $\beta$ -site amyloid precursor protein-cleaving enzyme1 (BACE1) and p-eIF2 $\alpha$  protein expression levels, as well as higher hippocampal levels of ATF4 mRNA in ApoE4 compared to ApoE3 mice (Segev et al., 2016). However, the increase observed in p-eIF2 $\alpha$  protein expression levels may be ascribed to eIF2 $\alpha$  regulatory kinases other than PKR, especially PERK, the predominant kinase to affect p-eIF2 $\alpha$ , and the main kinase to respond to ER stress (Ounallah-Saad et al., 2014).

In another study, ApoE4 mice were shown to have poorer long-term memory compared to ApoE3 mice, as measured by freezing in the fear conditioning paradigm. However, a single-dose treatment with the PKR inhibitor C16 (0.335  $\mu$ g/g body

weight, 1 h before conditioning) resulted in restoration of long term memory in ApoE4 mice, with freezing levels similar to ApoE3 mice in the fear conditioning paradigm. In addition, hippocampal ATF4 mRNA levels were found to be higher in ApoE4 mice compared to ApoE3 mice, whose ATF4 levels were similar to those of C57BL/6 mice. Hippocampal ATF4 mRNA levels were further elevated in aged ApoE3 and ApoE4 mice (12 months old) compared to their younger (4 months old) counterparts. Similar findings were observed in humans, where ATF4 mRNA levels were higher in ApoE4 carriers (67–98 years old) compared to non-carrier age-matched controls (Segev et al., 2015).

While immune system aspects are discussed in the section above, the interplay of PKR, the immune system, and metabolism has been shown in several studies. For example, A $\beta$  oligomers have been shown to remove insulin receptors from the neuronal surface, which in turn leads to activation of c-Jun N-terminal kinase (JNK). This is followed by inhibition of the insulin receptor substrate (IRS-1) and, in cultured hippocampal neurons, this inhibition was shown to be mediated both by JNK/TNF $\alpha$  and PKR (Bomfim et al., 2012). This is supported by the finding that elevated levels of serine phosphorylation of IRS-1 and activated JNK were found in brains of both AD and diabetes patients (Bomfim et al., 2012). In addition, JNK/TNF $\alpha$  signaling leads to peripheral insulin resistance (Gregor and Hotamisligil, 2011), and this may also be the case in AD. Recent studies have shown that while i.c.v. administration of A $\beta$ <sub>1–42</sub> oligomers to mice resulted in long term memory impairment, this impairment was prevented both in PKR<sup>−/−</sup> mice and in TNFR<sup>−/−</sup> mice, and mice treated with either PKR inhibitor C16 or TNF- $\alpha$  neutralizing antibody, infliximab (Lourenco et al., 2013; Hwang et al., 2017). Furthermore, treatment of hippocampal cultures with insulin prevented A $\beta$ <sub>1–42</sub> oligomer-induced phosphorylation of PKR (Lourenco et al., 2013).

## PKR IN ENDOTHELIAL CELLS

Protein kinase R has multiple effects in the vascular system in general and in endothelium cells in particular. One mechanism through which PKR exerts its effect in the vascular system is by modulating the expression of adhesion molecules in endothelial cells in the vascular system, thereby leading to the onset and development of inflammation (Osborn, 1990; Carlos and Harlan, 1994). For example, the adhesion molecule E-selectin is expressed on endothelial cells during inflammation, and its transcription can be induced by TNF- $\alpha$  or IL-1 (Ghersa et al., 1992). The activation of E-selectin by these cytokines is mediated by NF- $\kappa$ B in conjunction with endothelial leukocyte adhesion molecule 1 (ELAM-1) (Schindler and Baichwal, 1994). In aortic endothelial cells derived from PKR<sup>−/−</sup> mice, the induction of E-selectin by either TNF- $\alpha$  or PKR-specific inducer was attenuated, supporting the idea described above, that PKR functions downstream of TNF- $\alpha$ , and additionally, demonstrating that PKR mediates the role of the adhesion molecule E-selectin in inflammation. Furthermore, the authors showed that the attenuation of E-selectin activation in the PKR deficient mice was caused by a



reduction in the formation of the NF-ELAM-1 complex, as well as reduced activation of NF- $\kappa$ B (Bandyopadhyay et al., 2000).

As mentioned above, PKR is activated in response to mechanical stress, and plays a central role in determining cell fate, whether toward apoptosis or survival (Gil and Esteban, 2000; García et al., 2007; Hugon et al., 2017; Watanabe et al., 2018). Furthermore, many of the factors known to promote or exacerbate congestive heart failure, which constitutes mechanical stress due to hemodynamic overload, are also known to activate PKR, including oxidative stress, Toll receptor activation, and low-grade chronic inflammation (Kadokami et al., 2001; Lu et al., 2010). In a recent study, it was shown that PKR activation is increased both in a model of chronic transverse aortic constriction in mice, a mechanically induced simulation of congestive heart failure, and in human samples of congestive heart failure. Moreover, PKR<sup>-/-</sup> mice were protected from transverse aortic constriction-induced pulmonary congestion, cardiac dysfunction, elevation in inflammatory cytokines (TNF- $\alpha$  and IL-1 $\beta$ ), and apoptosis (as measured by the TUNEL assay and mRNA and protein expression levels of pro-apoptotic Bax and Caspase-3) (Wang et al., 2014).

Many studies have shown that PKR plays a central role in angiogenesis, which in turn plays a central role in cancer, neurodegeneration, and inflammation, cardiovascular diseases, as well as age-related macular degeneration, a common cause for blindness in the elderly. In two independent studies using *in vitro* and *in vivo* models (each) for cardiovascular diseases mediated by hypoxia and mechanical stress caused by hemodynamic pressure, similar results were obtained, showing that PKR is necessary for angiogenesis and neovascularization. Specifically, Zhu et al. (2016) used the RF/6A rhesus choroid-retinal endothelial cell line, where hypoxia was chemically induced using cobalt chloride (CoCl<sub>2</sub>). In this system, PKR expression was upregulated in parallel with p-PI3K, p-Akt, and VEGF expression, all of which were downregulated using siRNA directed against PKR (Zhu et al., 2016). The authors demonstrated that PKR is upstream of p-PI3K, p-Akt, and VEGF using a p-PI3K inhibitor, which affected p-PI3K, p-Akt, and VEGF, but not PKR. In addition, the knockdown of PKR using siRNA in a co-culture of RF/6A and ARPE-19 cells resulted in decreased cell migration and tube formation, strongly implicating the necessity of PKR in the formation of vasculature. In a mouse model of choroidal neovascularization (CNV), which mimics age-related macular degeneration, PKR was colocalized with CD31, a marker of vascular epithelium. In this model, treatment with monoclonal antibodies directed against PKR resulted in decreased progression of CNV. These findings were supported by another study, focusing on peripheral artery disease (Zhu et al., 2015), where PKR<sup>-/-</sup> mice were shown to have delayed blood flow recovery, with a 34% decrease in CD31 in the ischemic tissue, indicating a reduced number of endothelial cells. *In vitro*, the authors demonstrated in a model of human umbilical vein endothelial cells (HUVECs) that pPKR expression was increased in response to hypoxia, whereas inhibition of PKR using siRNA resulted in reduced microtubule formation and migration. Furthermore, VEGF expression was reduced both in PKR<sup>-/-</sup> mice and in HUVECs treated with PKR

siRNA, supporting the findings of the study above regarding the necessity of PKR for VEGF-mediated angiogenesis under hypoxia conditions.

Other studies have shown the role of PKR in angiogenesis in the context of hypoxia in tumors. For example, PKR was shown to function as a tumor suppressor, downregulating transcription of hypoxia-inducible factor 1 $\alpha$  (HIF-1 $\alpha$ ) under hypoxia conditions. This was shown to occur by PKR-regulated activation of T-cell protein tyrosine phosphatase, which in turn suppresses signal transducer and activator of transcription 3 (Stat3) (Papadakis et al., 2010). The role of PKR in cancer is discussed in further detail below.

Aging, as a risk factor for cancer, cardiovascular diseases, and neurodegeneration, is also related to senescence of endothelial cells. A recent study has shown that PKR inhibition (either by siRNA for PKR or inhibition of its phosphorylation using 2-AP) can reverse palmitate-induced (an independent risk factor of cardiovascular diseases) senescence of HUVECs, by activating JNK. JNK activation results in inhibition of silent information regulator 1 (Sirt1), which serves as an anti-senescent factor (Li et al., 2018), by affecting downstream targets such as histones, transcription factors, and many other aging proteins, one of which is the tumor suppressor p53 (Volonte et al., 2015). Taken together, these studies point to PKR as an attractive target for the treatment of cardiovascular diseases.

## PKR IN CANCER

### PKR, an Enzyme With Contentious Roles in Cancer

While the role of PKR in metabolic stress and brain function is well established and described above, the role of PKR in cancer biology remains a subject of debate, as both tumor-suppressive and tumor-stimulatory functions have been attributed to this enzyme. The attribution of different and even contradictory roles for PKR in tumorigenesis reflect its involvement in the regulation of diverse cellular processes which may differentially affect the cancer cell and its interaction with the tumor microenvironment. Such processes include cell autonomous events such as the negative regulation of protein synthesis through eIF2 $\alpha$  phosphorylation or signal transduction through different pathways including NF- $\kappa$ B, which alter the susceptibility of the cell to apoptosis and modulate the expression of inflammatory cytokines. Thus, variations in PKR expression and activity are predicted to affect both cancer-cell-autonomous and non-cell-autonomous aspects of the developing tumor.

This duality of effects is predicted to be a source of differences in experimental results and in their ensuing interpretation, with dependence on tumor type, tumor stage, or experimental model. Thus, results may differ between *in vitro* vs. *in vivo* studies, immune-deficient vs. immunocompetent mouse models, and tumors driven or not by inflammation. Also, the regulatory role performed by PKR in transduction of oncogenic/tumor suppressor signals may serve as a source for dual roles in tumor progression. This is exemplified by the PKR-mediated activation of NF $\kappa$ B (Maran et al., 1994). PKR was shown to

activate NF- $\kappa$ B in diverse cellular contexts, with a differential dependence on its enzymatic activity (Kumar et al., 1994; Bonnet et al., 2000; Bonnet et al., 2006). As NF- $\kappa$ B may have powerful, albeit contradictory (double-edged sword) roles in cancer, mediating either tumor promotion or tumor suppression in different tumor settings (Pikarsky and Ben-Neriah, 2006), one can imagine similarly dual roles for PKR. Moreover, the proposed non-enzymatic activity of PKR may support the distinction between pro- or anti-tumorigenic roles, alternatively resulting from modifications in PKR expression or activity. In this context, functional interactions between PKR and pro-tumorigenic signaling pathways [e.g., STAT3 (Shen et al., 2012) or v-mos (Dagon et al., 2001)] were proposed to inhibit PKR activity, resulting in a scenario where increased PKR expression may not necessarily coincide with its increased activity.

## Tumor Suppressor Roles of PKR

The notion that PKR functions as a tumor suppressor is supported by: (i) Cell growth inhibition upon PKR overexpression (Chong et al., 1992; Meurs et al., 1993). In this context, PKR-mediated regulation of cellular replication may occur either through the inhibitory effect of PKR on protein synthesis, an essential resource for cell growth, or through PKR-dependent phosphorylation of cell cycle regulators. Of note, the expression and activity of PKR are differentially regulated in the cell cycle (Zamanian-Daryoush et al., 1999), and exposure to dsRNA upon mitotic breakdown of the nuclear envelope and exposure of dsRNA was proposed as a mechanism for PKR activation in mitosis (Kim et al., 2014). However, both stimulatory (Kim et al., 2014) and inhibitory (Dagon et al., 2001; Yoon et al., 2010) roles have been proposed for PKR in mitotic progression, underscoring the putative dual role of PKR in cancer. (ii) PKR-mediated stimulation of apoptosis through different molecular mechanisms (Jagus et al., 1999; Gil and Esteban, 2000) including transcription- and translation-mediated increases in expression of receptors that mediate programmed cell death (e.g., Fas (CD95/Apo-1) and/or pro-apoptotic Bcl2 effector proteins (Balachandran et al., 1998), which result in increased caspase activity (Gil et al., 2002). (iii) Functional interactions between PKR and tumor suppressors which regulate apoptosis (e.g., p53). Indeed, PKR is a p53 target gene (Yoon et al., 2009). Moreover, Type I interferon increases expression of both p53 (Takaoka et al., 2003) and PKR, and PKR amplifies interferon  $\beta$  induction by dsRNA (McAllister et al., 2012). Furthermore, PKR and p53 physically interact, and PKR positively regulates p53 transcriptional activity (Cuddihy et al., 1999a,b), while p53 positively regulates gene induction by dsRNA (Hummer et al., 2001). Together, these data suggest that PKR and p53 are intertwined in a positive feedback loop. However, other studies show that dsRNA stimulates p53 degradation (Marques et al., 2005; Baltzis et al., 2007), suggesting a negative feedback loop involving p53 and PKR, and underscoring the complexity of their functional interactions. (iv) *In vivo* experiments demonstrating an inverse correlation between PKR expression and/or activity and tumorigenicity. For example, knockdown of PKR in HCT116 human colon cancer cells supported rapid tumor growth and resistance to

genotoxic drugs in nude mice (Yoon et al., 2009). Similarly, expression of dominant-negative mutants of PKR resulted in malignant transformation of NIH 3T3 cells and endowed these cells with the ability to generate tumors in nude mice (Koromilas et al., 1992; Meurs et al., 1993; Barber et al., 1995). (v) Reduced expression and/or activity of PKR in tumors. For example, in head and neck carcinoma, PKR and the proliferation marker PCNA exhibited inversely correlated expression patterns, suggesting a proliferation-inhibitory role for PKR (Haines et al., 1998). Furthermore, in myelodysplastic syndrome (a slow growing form of blood cancer), deletion of chromosome 5q, and the ensuing lack of IRF1 expression, lead to reduced PKR expression (Beretta et al., 1996). In addition to reduced expression, inactivation of PKR, similarly to what occurs in cells of patients with B-cell chronic lymphocytic leukemia (Hii et al., 2004), was also suggested to support tumorigenesis.

## PKR and Tumor Promotion

The established roles of inflammation in cancer progression (Coussens and Werb, 2002; Hanahan and Weinberg, 2011), the pro-inflammatory nature of NF- $\kappa$ B signaling and its multiple roles in cancer development (Taniguchi and Karin, 2018), and the identification of PKR as a stimulator of NF- $\kappa$ B activity (Kumar et al., 1994; Maran et al., 1994; Bonnet et al., 2000, 2006) form a strong rationale for pro-tumorigenic signaling by PKR. Indeed, PKR has been identified as overexpressed and activated in several cancers including hematopoietic malignancies (Basu et al., 1997), breast cancer (Kim et al., 2000), melanoma, and colon cancer (Kim et al., 2002). For example, in melanoma, eIF2 $\alpha$  phosphorylation and the ensuing translation reprogramming were recently described as drivers of phenotypic plasticity, invasiveness and therapeutic resistance in melanoma (Falletta et al., 2017). These studies suggest that eIF2 $\alpha$  kinases, such as PKR, may switch melanoma from a proliferative to an invasive cancer cell, driving metastasis in this manner. Indeed, interference with PKR reduced the growth and metastatic potential of murine melanoma (Delgado André and De Lucca, 2007; André et al., 2014). Moreover, and in accord with a correlation between PKR expression and tumor progression, primary melanomas revealed minimal PKR immunoreactivity, while melanoma lymph node metastases expressed high levels of PKR (Kim et al., 2002).

Recent transcriptomic studies in multiple cancer types (e.g., The Cancer Genome Atlas, TCGA) and their compilation into accessible public databases [e.g., cBio Portal, (Cerami et al., 2012; Gao et al., 2013)] allow for a global assessment of PKR expression in human tumors. The picture that emerges is one in which PKR (EIF2AK2) is broadly expressed across different cancer types, individual patients within a defined cancer type show considerably variable (up to 10-fold) levels of PKR expression (**Figure 4A**), PKR is rarely mutated, and 5–10% of patients show overexpression of PKR. Visualization of publically accessible TCGA data with the UCSC Xena browser<sup>1</sup> shows survival data (Kaplan–Meier curves for overall survival) across multiple cancer types (TCGA PanCanAtlas, 12830 patients). These data revealed

<sup>1</sup><https://xenabrowser.net>



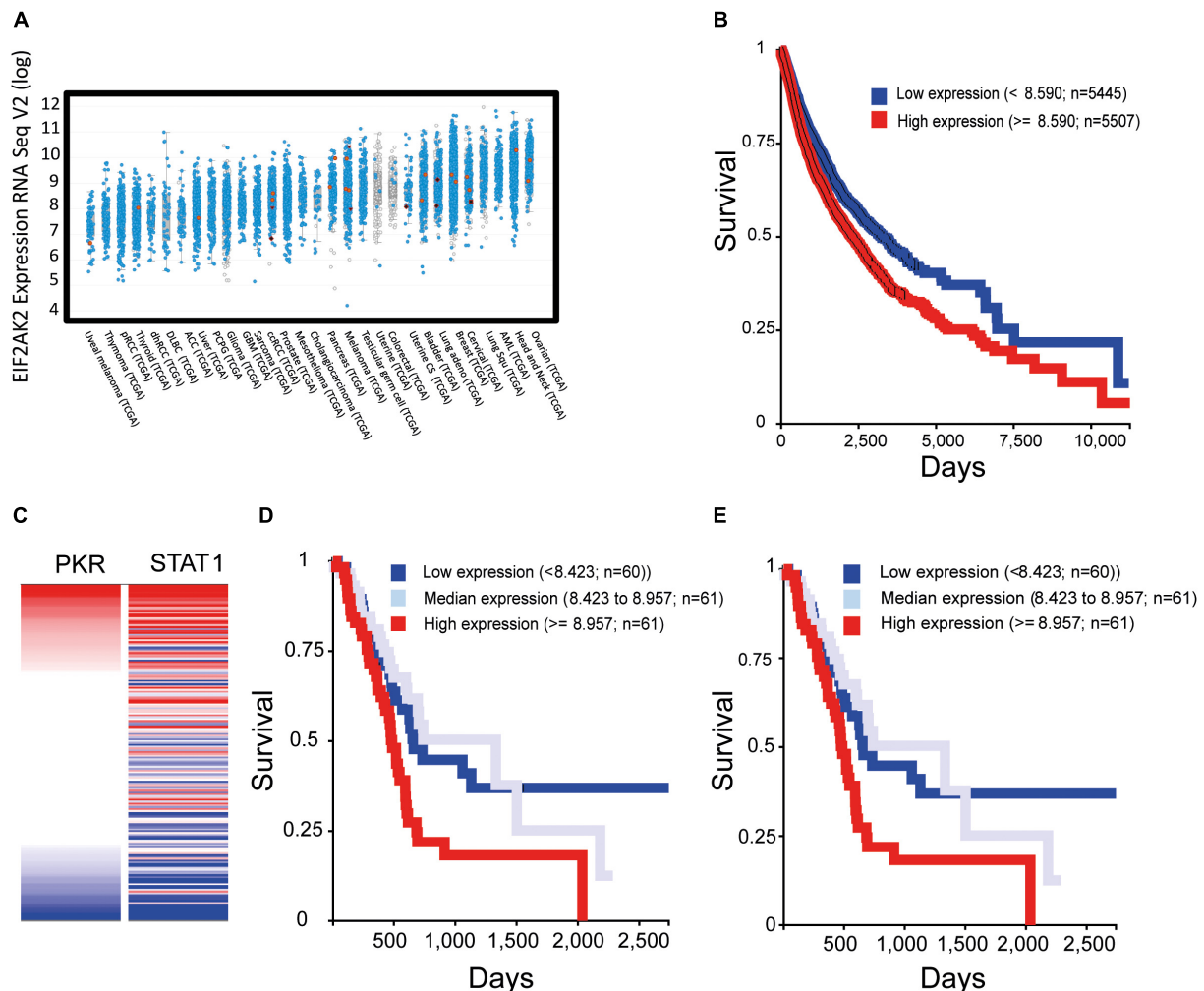


**FIGURE 4 |** Increased expression of PKR correlates with activation of interferon-STAT1 signaling and with poor prognosis in multiple cancer types. To evaluate the expression of EIF2AK2 (PKR) in samples of cancer patients, we employed cBio Portal to assess studies of The Cancer Genome Atlas (TCGA). **(A)** Expression of EIF2AK2. Graph depicts the RPKM value of EIF2AK2 expression in different patient samples, ordered according to the median value of expression in the given cancer type. Blue puncta are samples where the EIF2AK2 sequence is wild type, red are samples in which EIF2AK2 is mutated. **(B)** Analysis of survival of cancer patients according to EIF2AK2 expression. Graph depicts the survival of patients (12830 patients from the PANCAN TCGA database, assessed and visualized with the UCSC Xena browser) classified according to a threshold of EIF2AK2 expression (blue, low expression; red, high expression). **(C)** Correlation of expression of EIF2AK2 and STAT1 in pancreatic cancer patients (196 cases, PAAD TCGA study, visualized with the UCSC Xena browser). **(D,E)** Analysis of survival of pancreatic cancer patients according to EIF2AK2 **(D)** or STAT1 **(E)** expression. Graph depicts the survival of patients (196 patients from the PAAD TCGA database, assessed and visualized with the UCSC Xena browser) classified according to threshold expression (blue, low expression; gray, median expression; red, high expression).

that higher levels of PKR expression correlated with poor survival (**Figure 4B**,  $p = 4.441 \times 10^{-16}$ ). For example, in pancreatic cancer (PAAD study, TCGA pancreatic cancer database, 196 cases), EIF2AK2 expression is considered as an unfavorable prognostic marker<sup>2</sup>; and data depiction with the UCSC Xena browser shows a negative correlation between PKR expression and survival ( $p = 0.001$ , **Figure 4C**). Indeed, expression of STAT1 (an interferon stimulated gene, and a mediator of interferon-transcriptional activity) and its correlation with survival in this cohort revealed a similar scenario to the one observed with PKR (**Figures 4D,E**). Together, these data support the notions of a

pro-tumorigenic association of PKR expression and cancer, and of the regulation of its expression by JAK-STAT signaling in cancer cells. Of note, JAK-STAT signaling pathway is intimately associated with the transduction of signals from inflammatory cytokines (e.g., interferon gamma), suggesting that the pro-tumorigenic role of PKR occurs within the context of tumor-related inflammation.

**PKR in cancer therapy.** Due to its roles as a mediator of apoptosis and anti-viral responses, PKR expression and function have been implicated in two forms of anti-cancer therapy: chemotherapy and oncolytic virotherapy. In the former, PKR expression and activity have been positively associated with the therapeutic effects of 5-Fluorouracil [5-FU, (García et al., 2011)],

<sup>2</sup><https://www.proteinatlas.org>

**TABLE 1** | Summary of publications that used PKR inhibitor imidazole-oxindole compound also known as C16 or Imoxim, which acts as an ATP-binding site directed inhibitor of PKR.

Field	Mode of administration	Concentration used	Model	Readout	Disease	Reference
Metabolism	Not given	5 $\mu$ M for cells treatments	H9C2 cells treated with high concentrated glucose	Levels of pJNK/JNK $\downarrow$ , PKR $\downarrow$ and Caspase 3 $\downarrow$ , mRNA levels of NF $\kappa$ B $\downarrow$ , JNK $\downarrow$ and caspase-3 $\downarrow$ . Measurements of ROS $\downarrow$ , nitrite levels $\downarrow$ , LDH $\downarrow$	Diabetes	Udumula et al., 2018
	NA	5 $\mu$ M (Imoxim)	NRK-52E cells treated with high fructose	Levels of PKR $\downarrow$ , caspase 3 $\downarrow$ , Measurements of ROS levels $\downarrow$ , Apoptosis $\downarrow$ , JNK $\downarrow$	Hypertension	Kaira et al., 2018
	Subcutaneous injection (Imoxim)	0.5 mg/kg (Imoxim)	Lean and obese male mice and MEF with TNF $\alpha$	Glucose homeostasis $\uparrow$ TNF $\alpha$ $\downarrow$ and IL-6 $\downarrow$ mRNA in WTA. In MEF pPKR/PKR $\downarrow$ , pJNK/JNK $\downarrow$ , pIRS1 <sup>S307</sup> /IRS1 $\downarrow$	Obesity	Nakamura et al., 2014
Immunology	NA	C16 400nM	THP1 macrophages	mRNA levels of GADD34 $\downarrow$ , IL-8 $\downarrow$ , IL- $\beta$ $\downarrow$	Inflammation	Dabo et al., 2017
	i.p.	100–500 $\mu$ g/kg	Male BALB/C mice (7–8 weeks old) treated with intratracheal administration of LPS	Levels of TNF- $\alpha$ $\downarrow$ , IL-1 $\beta$ $\downarrow$ , IL-6 $\downarrow$ , pPKR/actin $\downarrow$ , pIKK/JKK $\downarrow$ , pIKB $\alpha$ /IKB $\downarrow$ , pNF $\kappa$ B/actin $\downarrow$ , caspase3 $\downarrow$ . Apoptosis $\downarrow$ assessed by TUNEL $\downarrow$ and pPKR $\downarrow$ and pNF $\kappa$ B $\downarrow$ by immunohistochemistry analysis. Analysis of lung injury $\downarrow$ by hematoxylin and eosin stain	Acute lung injury	Li et al., 2017
	i.p.	150 $\mu$ g/kg	Male SD Rats treated with Freund's adjuvant	Limb swelling $\downarrow$ . Protein and mRNA levels of HMGB1 $\downarrow$ and PKR $\downarrow$ in blood and synovium	Rheumatoid arthritis	Wang et al., 2015
Neuroscience	NA	500 nM	mDC and BMDM derived from cybb <sup>+/+</sup> , cybb <sup>-/-</sup> mice, pkr <sup>+/+</sup> and pkr <sup>-/-</sup>	IFN $\beta$ mRNA $\downarrow$ and pPKR/PKR $\downarrow$	Parasite infection ( <i>Chlamydia trachomatis</i> )	Webster et al., 2016
	NA	500 nM	SH-SY5Y and UM1242-G cells exposed to EtOH	Cell viability $\uparrow$	Alcohol use	Duncan et al., 2016
	i.p.	600 $\mu$ g/kg	Male Wistar rats treated with QA	Levels of pPKR/PKR $\downarrow$ , pelf2 $\alpha$ /elf2 $\alpha$ $\downarrow$ . Assessment of neurodegeneration by hematoxylin and eosin stain $\downarrow$ . Immunofluorescence of cleaved caspase-3 $\downarrow$	Neuroinflammation	Tronel et al., 2014
	NA	1 $\mu$ M	Hippocampus-derived neuronal culture treated with A $\beta$ O	Synapse loss $\downarrow$ assessed by immunocytochemistry against synapsin and PSD95	Alzheimer's disease and diabetes	Lourenco et al., 2013
	i.p.	0.5 $\mu$ g/kg	APPswPS1dE9	Levels of pPKR <sup>T451</sup> /PKR $\downarrow$ , pNF $\kappa$ B <sup>S536</sup> /NF $\kappa$ B $\downarrow$ , BACE $\downarrow$ and TNF $\alpha$ mRNA $\downarrow$ , IL-1 $\beta$ mRNA $\downarrow$	Alzheimer's disease	Couturier et al., 2012
	NA	210 nM	Primary murine mixed co-cultures treated with A $\beta$ 42	Levels of pPKR <sup>T451</sup> /Actin $\downarrow$ , pNF $\kappa$ B <sup>S536</sup> /NF $\kappa$ B $\downarrow$ , pIKB <sup>32/36</sup> /IKB $\downarrow$ , pro-caspase3/cleaved caspase3 $\downarrow$ and levels of TNF $\alpha$ $\downarrow$ , IL-1 $\beta$ $\downarrow$ , IL-6 $\downarrow$	Alzheimer's disease	Couturier et al., 2011
	i.p.	0.27 mg/kg	Mice treated with 3-NP	Assessment of neurodegeneration $\downarrow$ by Cresyl violet staining	Huntington's disease	Chen et al., 2008

(Continued)

TABLE 1 | Continued

Field	Mode of administration	Concentration used	Model	Readout	Disease	Reference
	NA	500 nM	Cerebellar granular neurons from rats treated with amprolium (thiamine depletion)	Levels of pelf2α/elf2α↓ and cell viability↑	Vitamin B1 deficiency	Wang et al., 2007
	i.p.	0.335, 3.35, 33.5, or 167.5 μg/kg	Sprague-Dawley rats (7 days old, 1, 2, 4, 6, 9, and 12 months old)	Levels of pPKR <sup>Thr446</sup> /PKR↓, pelf2α/elf2α↓, pmTOR/mTOR (–), p70S6K <sup>Thr389</sup> /p70S6K (–) and pPERK/PERK (–)	Neuroprotection	Ingrand et al., 2007
	i.p. and local microinjection	167.5 μg/kg, 50 μM for hippocampal slices and local injection	Male Wistar rats, PKR-KO and WT (129SvEv) Hippocampal slices	CTA↑, NT↑ Levels of pelf2α/elf2α↓, pPKR <sup>Thr446</sup> /PKR↓	Memory	Stern et al., 2013
	i.p.	0.1 mg/kg	lfn-γ <sup>-/-</sup> and WT CF57BL/6 mice	Synchronized EEG and inhibition↓, FC (Auditory and Context)↑	Memory	Zhu et al., 2011

The inhibitor C16 was acquired from Calbiochem (cat. # 527450) or from Sigma Aldrich (cat. # I9785). ↑ up-regulation, ↓ down-regulation, (–) no change, NOR, Novel Object Recognition; FC, Fear conditioning; MWM, Morris Water Maze; mDC, human monocyte-derived dendritic cells; BMDM, murine bone marrow derived monocytes; CTA, Conditioned taste aversion; NT, Novel taste; WAT, white adipose tissue; MEF, Mice Embryonic Fibroblasts; QA, quolinolic acid; NA, not applicable; AβQ, Aβ oligomers.

doxorubicin (Peidis et al., 2011), bozepinib (Marchal et al., 2013), and histone deacetylase inhibitors [HDACi, (Peidis et al., 2010)]. Concerning oncolytic virotherapy, which aims at the specific infection and killing of cancer cells (oncolysis) and the activation of anti-tumor immunity, defects in interferon signaling in cancer cells expose these cells to viral oncolysis (Stojdl et al., 2000; Danziger et al., 2016). Specifically, defects in PKR activation were identified as a central mechanism by which oncogenic Ras enables oncolysis of transformed cells with oncolytic reovirus (Strong et al., 1998). In addition to oncolysis resulting from productive infection (a scenario which may benefit from defects in PKR expression or function), we have recently identified a novel form of viral oncolysis (oncolysis by non-productive viral infection, ONPVI) in which the combined exposure of interferon-responsive prostate cancer cells to a novel oncolytic virus (epizootic hemorrhagic disease virus-Tel Aviv University, EHDV-TAU) and interleukin-6, induced caspase-mediated cell death. ONPVI occurred in the context of STAT-1-dependent upregulation of multiple anti-viral gene products, including PKR (Danziger et al., 2018); opening the possibility that PKR may contribute to virally induced cancer cell death. Given the dependency of anti-immune checkpoint therapy on functional interferon-gamma/JAK-STAT signaling (Zaretsky et al., 2016; Sharma et al., 2017), and the positive feedback loop involving interferon signaling and PKR expression/function, we speculate that PKR may also play roles in this form of therapy. Together, these data suggest that the assessment of the status of PKR expression and function in cancer cells may be important for the choice of optimal therapeutic options, and that the development of means to manipulate its expression and function may have future applications in combination therapy settings.

## TOOLS FOR INHIBITING PKR

Taken together, the studies above point to PKR as a hub for co-morbidity and an attractive target for the treatment of metabolic diseases, cardiovascular diseases, neurodegenerative diseases, inflammation, and cancer. Moreover, when it comes to aging and correlated cognitive decline (Segev et al., 2015), PKR inhibition should serve both as an anti-neurodegenerative disorders agent and a pro-cognitive agent. The main obstacles to better understand PKR are (i) the available tools to inhibit PKR activity in general and specific functions of PKR in particular, (ii) the differences in expression levels between different cells, and (iii) the ability to manipulate PKR in specific cell types within a tissue. The most widely used pharmacological PKR inhibitor is the highly potent small molecule imidazolo-oxindole C16, also known as PKRi, which targets the ATP binding site of PKR. C16 has an IC<sub>50</sub> of 210 nM *in vitro* (Jammi et al., 2003), and is typically used at doses of 210–500 nM *in vitro* for 1 h (Table 1). Incubation of cells with high concentrations of C16 induces high cell toxicity (see PKR in Learning and Memory section above). C16 has been successfully used by i.p. administration in mice and rats to elicit memory enhancement, indicating that the compound can cross the blood brain barrier.

**Table 1** shows that inhibition of PKR with C16 rarely inhibits eIF2 $\alpha$  phosphorylation, the most known and cited substrate of PKR. It is clear that, in the brain, PERK is the dominant kinase to control basal levels of eIF2 $\alpha$  phosphorylation (Ounallah-Saad et al., 2014); however, we do not know if this is the case in different neuronal subtypes (e.g., inhibitory versus excitatory neurons). Another less specific pharmacological inhibitor of PKR is the 2-aminopurine (2-AP) compound, which competes for ATP at the ATP binding site of PKR, and thereby inhibits its phosphorylation (Hu and Conway, 1993). This compound is less potent than C16, and is used *in vitro* at doses of 4–10 mM for 4 h (Endoh et al., 2009). Other inhibitors of PKR have been developed, although these were less potent than C16 (Weintraub et al., 2016).

The PKR can also be inhibited by monoclonal antibodies and using genetic tools such as siRNA or viral vectors harboring an shRNA sequence directed against PKR, and both approaches have been successfully used *in vitro* and *in vivo* (André et al., 2014; Zhu et al., 2015, 2016). However, a new direction with promising high specificity is the use of biological, custom-designed peptides, whose advantages include high potency, high specificity, relative lack of toxicity, predictable metabolism, and selective targeting of specific functions (Kaidanovich-Beilin and Eldar-Finkelman, 2006; Eldar-Finkelman and Eisenstein, 2009; Fosgerau and Hoffmann, 2015). Indeed, some peptide drugs have already been FDA approved (Kaspar and Reichert, 2013). Still, peptides suffer from disadvantages, which include instability, high susceptibility to degradation, susceptibility to hydrolysis and oxidation, tendency for aggregation, short half-life, limited bioavailability due to their low membrane permeability, and consequently, the inability to administer them orally (Fosgerau and Hoffmann, 2015). However, in recent years there have been technological developments allowing to overcome some of the drawbacks of peptides, such as conferring membrane permeability by fusion to the Tat peptide or insertion of peptides into liposomes, micelles, nano-emulsions, or polymer nanoparticles to confer membrane permeability (Kaidanovich-Beilin and Eldar-Finkelman, 2006). Nevertheless, this strategy is still under development.

## SUMMARY AND FUTURE

As can be clearly understood from the review above, we, the authors, recognize the complexity of PKR-mediated signaling in different cells and/or body/organs at different developmental stages and cellular compartments (**Figures 2, 3**). The main points we conclude from the many excellent papers summarized above are:

(1) PKR level and post-translation modifications are excellent biomarkers for neurodegenerative diseases (e.g., AD, dementia, Parkinson's disease, Huntington's disease, and prion disease) and cancer (**Figure 4**, based on open source data).

(2) Inhibition of PKR is predicted to be highly beneficial in age-related neurodegenerative diseases. PKR is positioned in the center of metabolic syndrome disease, including glucose or A $\beta$

load and inflammation and its inactivation reduces the insult (**Figure 1**).

(3) PKR inhibition contributes positively and directly to cognitive function in young and old mice.

(4) Inhibition of PKR is beneficial in certain cases of cancer. However, here, the situation is more complex as the role of PKR in tumors (pro- or anti-tumorigenic) may differ according to tumor type and/or stage.

(5) PKR inhibition or deletion is not essential for an organism response to viral infection as detected in PKR KO mice or prolonged treatments with the best-known PKR inhibitor, C16, and thus has the potential to serve as medical treatment.

(6) Treatment with C16 following different stimulations in most cases does not affect eIF2 $\alpha$  phosphorylation levels, although many publications are trying to explain the phenotypes of PKR inhibition via regulation of mRNA translation (**Table 1**). Moreover, brains of PKR KO mice do not show significant change in eIF2 $\alpha$  phosphorylation. On the other hand, most papers do show a clear effect of PKR inhibition on the NF- $\kappa$ B pathway (**Table 1**).

(7) The recent findings that PKR detects not only exogenous, viral dsRNA but also endogenous dsRNA, such as mitochondrial RNA, point to it as a new target for reducing oxidative stress and apoptosis in disease states and specifically in neurodegenerative diseases.

We hypothesize that better understanding of PKR equilibrium and function in different scenarios, in addition to its 'traditional' role in cellular viral response, can be extremely important in understanding basic related biological processes such as inflammation, metabolism, aging, cancer, and brain function in normal and pathological states. Moreover, we predict that potent, non-toxic, specific inhibition of PKR function/s will serve as treatment for different diseases in certain situations. The most plausible steps in order test our hypotheses are:

(1) Identify small molecule inhibitors for PKR. Weintraub and colleagues (2016) employed a computational chemistry screening approach, which yielded interesting but unsatisfactory results. Screening small molecule libraries is the next reasonable step.

(2) Better understanding of the interplay of levels of PKR expression, function, and cell states.

(3) Identifying new tools (i.e., non-small molecule inhibitor), such as peptides, to inhibit specific functions of PKR.

(4) Understanding the role of PKR in specific cellular and subcellular compartments (e.g., neuronal dendrites) and cellular-specific context using genetics and/or pharmacokinetic tools.

We believe that the steps proposed above together with the new tools of omics and precision biology will allow better fundamental understanding of PKR functions to be translated into treatment of currently incurable diseases.

## AUTHOR CONTRIBUTIONS

All the authors contributed equally to this work.



## FUNDING

This work was supported by a grant from the Canadian Institutes of Health Research (CIHR), the International Development Research Centre (IDRC), the Israel Science Foundation (ISF) and the Azrieli Foundation (ISF-IDRC 2395/2015 to KR); ISF 946/17 to KR, Israeli Ministry of Science, Technology, and Space (MOST 3-12080 and MOST 3-14761 to KR); TransNeuro ERANET JPND

supported by the Israel Ministry of Health grant 3-14616 to KR; and ISF grant 1966/18 to ME.

## ACKNOWLEDGMENTS

The authors wish to thank Jessica Barrera for the graphic design of **Figures 1–3**.

## REFERENCES

- Alberini, C. M., and Chen, D. Y. (2012). Memory enhancement: consolidation, reconsolidation and insulin-like growth factor 2. *Trends Neurosci.* 35, 274–283. doi: 10.1016/j.tins.2011.12.007
- André, N. D., Silva, V. A. O., Watanabe, M. A. E., and De Lucca, F. L. (2014). Intratumoral injection of PKR shRNA expressing plasmid inhibits B16-F10 melanoma growth. *Oncol. Rep.* 32, 2267–2273. doi: 10.3892/or.2014.3410
- Balachandran, S., Kim, C. N., Yeh, W. C., Mak, T. W., Bhalla, K., and Barber, G. N. (1998). Activation of the dsRNA-dependent protein kinase, PKR, induces apoptosis through FADD-mediated death signaling. *EMBO J.* 17, 6888–6902. doi: 10.1093/emboj/17.23.6888
- Baltzis, D., Li, S., and Koromilas, A. E. (2002). Functional characterization of pkr gene products expressed in cells from mice with a targeted deletion of the N terminus or C terminus domain of PKR. *J. Biol. Chem.* 277, 38364–38372. doi: 10.1074/jbc.M203564200
- Baltzis, D., Pluquet, O., Papadakis, A. I., Kazemi, S., Qu, L., and Koromilas, A. E. (2007). The eIF2 $\alpha$  kinases PERK and PKR activate glycogen synthase kinase 3 to promote the proteasomal degradation of p53. *J. Biol. Chem.* 282, 31675–31687. doi: 10.1074/jbc.M704491200
- Bando, Y., Onuki, R., Katayama, T., Manabe, T., Kudo, T., Taira, K., et al. (2005). Double-strand RNA dependent protein kinase (PKR) is involved in the extrastriatal degeneration in Parkinson's disease and Huntington's disease. *Neurochem. Int.* 46, 11–18. doi: 10.1016/j.neuint.2004.07.005
- Bandyopadhyay, S. K., de La Motte, C. A., and Williams, B. R. (2000). Induction of E-selectin expression by double-stranded RNA and TNF- $\alpha$  is attenuated in murine aortic endothelial cells derived from double-stranded RNA-activated kinase (PKR)-null mice. *J. Immunol.* 164, 2077–2083. doi: 10.4049/jimmunol.164.4.2077
- Barber, G. N., Jagus, R., Meurs, E. F., Hovanessian, A. G., and Katze, M. G. (1995). Molecular mechanisms responsible for malignant transformation by regulatory and catalytic domain variants of the interferon-induced enzyme RNA-dependent protein kinase. *J. Biol. Chem.* 270, 17423–17428. doi: 10.1074/jbc.270.29.17423
- Basu, S., Panayiotidis, P., Hart, S. M., He, L. Z., Man, A., Hoffbrand, A. V., et al. (1997). Role of double-stranded RNA-activated protein kinase in human hematological malignancies. *Cancer Res.* 57, 943–947.
- Beretta, L., Gabbay, M., Berger, R., Hanash, S. M., and Sonenberg, N. (1996). Expression of the protein kinase PKR in modulated by IRF-1 and is reduced in 5q- associated leukemias. *Oncogene* 12, 1593–1596.
- Bomfim, T. R., Fornly-Germano, L., Sathler, L. B., Brito-Moreira, J., Houzel, J., Decker, H., et al. (2012). An anti-diabetes agent protects the mouse brain from defective insulin signaling caused by Alzheimer's disease- associated A $\beta$  oligomers. *J. Clin. Invest.* 122, 1339–1353. doi: 10.1172/JCI57256
- Bonnet, M. C., Daurat, C., Ottone, C., and Meurs, E. F. (2006). The N-terminus of PKR is responsible for the activation of the NF- $\kappa$ B signaling pathway by interacting with the IKK complex. *Cell Signal.* 18, 1865–1875. doi: 10.1016/j.cellsig.2006.02.010
- Bonnet, M. C., Weil, R., Dam, E., Hovanessian, A. G., and Meurs, E. F. (2000). PKR stimulates NF- $\kappa$ B irrespective of its kinase function by interacting with the IkappaB kinase complex. *Mol. Cell. Biol.* 20, 4532–4542. doi: 10.1128/MCB.20.13.4532-4542.2000
- Bullido, M. J., Martinez-Garcia, A., Tenorio, R., Sastre, I., Munoz, D. G., Frank, A., et al. (2008). Double stranded RNA activated EIF2 alpha kinase (EIF2AK2; PKR) is associated with Alzheimer's disease. *Neurobiol. Aging* 29, 1160–1166. doi: 10.1016/j.neurobiolaging.2007.02.023
- Carlos, T. M., and Harlan, J. M. (1994). Leukocyte-endothelial adhesion molecules. *Blood* 84, 2068–2101.
- Carpentier, K. S., Esparo, N. M., Child, S. J., and Geballe, A. P. (2016). A single amino acid dictates protein kinase R susceptibility to unrelated viral antagonists. *PLoS Pathog.* 12:e1005966. doi: 10.1371/journal.ppat.1005966
- Carret-Rebillat, A., Pace, C., Gourmaud, S., Ravasi, L., Montagne-Stora, S., Longueville, S., et al. (2015). Neuroinflammation and A $\beta$  accumulation linked to systemic inflammation are decreased by genetic PKR down-regulation. *Sci. Rep.* 5:8489. doi: 10.1038/srep08489
- Carvalho, B. M., Oliveira, A. G., Ueno, M., Araújo, T. G., Guadagnini, D., Carvalho-Filho, M. A., et al. (2013). Modulation of double-stranded RNA-activated protein kinase in insulin sensitive tissues of obese humans. *Obesity (Silver Spring)* 21, 2452–2457. doi: 10.1002/oby.20410
- Carvalho-Filho, M. A., Carvalho, B. M., Oliveira, A. G., Guadagnini, D., Ueno, M., Dias, M. M., et al. (2012). Double-stranded RNA-activated protein kinase is a key modulator of insulin sensitivity in physiological conditions and in obesity in mice. *Endocrinology* 153, 5261–5274. doi: 10.1210/en.2012-1400
- Cerami, E., Gao, J., Dogrusoz, U., Gross, B. E., Sumer, S. O., Aksoy, B. A., et al. (2012). The cBio cancer genomics portal: an open platform for exploring multidimensional cancer genomics data. *Cancer Discov.* 2, 401–404. doi: 10.1158/2159-8290.CD-12-0095
- Chakrabarti, A., Sadler, A. J., Kar, N., Young, H. A., Silverman, R. H., and Williams, B. R. G. (2008). Protein kinase R-dependent regulation of interleukin-10 in response to double-stranded RNA. *J. Biol. Chem.* 283, 25132–25139. doi: 10.1074/jbc.M804770200
- Chang, R. C., Suen, K., Ma, C., Elyaman, W., Ng, H., and Hugon, J. (2002). Involvement of double-stranded RNA-dependent protein kinase and phosphorylation of eukaryotic initiation factor-2 $\alpha$  in neuronal degeneration. *J. Neurochem.* 83, 1215–1225. doi: 10.1046/j.1471-4159.2002.01237.x
- Chen, H., Wang, L., and D'Mello, S. R. (2008). A chemical compound commonly used to inhibit PKR, {8-(imidazol-4-ylmethylene)-6H-azolidino[5,4-g]benzothiazol-7-one}, protects neurons by inhibiting cyclin-dependent kinase. *Eur. J. Neurosci.* 28, 2003–2016. doi: 10.1111/j.1460-9568.2008.06491.x
- Cheung, B. K. W., Lee, D. C. W., Li, J. C. B., Lau, Y., and Lau, A. S. Y. (2005). A role for double-stranded RNA-activated protein kinase PKR in *Mycobacterium*-induced cytokine expression. *J. Immunol.* 175, 7218–7225. doi: 10.4049/jimmunol.175.11.7218
- Chong, K. L., Feng, L., Schappert, K., Meurs, E., Donahue, T. F., Friesen, J. D., et al. (1992). Human p68 kinase exhibits growth suppression in yeast and homology to the translational regulator GCN2. *EMBO J.* 11, 1553–1562. doi: 10.1002/j.1460-2075.1992.tb05200.x
- Costa-Mattioli, M., Gobert, D., Stern, E., Gamache, K., Colina, R., Cuello, C., et al. (2007). eIF2 $\alpha$  phosphorylation bidirectionally regulates the switch from short- to long-term synaptic plasticity and memory. *Cell* 129, 195–206. doi: 10.1016/j.cell.2007.01.050
- Coussens, L. M., and Werb, Z. (2002). Inflammation and cancer. *Nature* 420, 860–867. doi: 10.1038/nature01322
- Couturier, J., Morel, M., Pontcharraud, R., Gontier, V., Fauconneau, B., Paccalin, M., et al. (2010). Interaction of double-stranded RNA-dependent protein kinase (PKR) with the death receptor signaling pathway in amyloid beta (A $\beta$ )-treated cells and in APPSLPS1 knock-in mice. *J. Biol. Chem.* 285, 1272–1282. doi: 10.1074/jbc.M109.041954
- Couturier, J., Paccalin, M., Lafay-Chebassier, C., Chalou, S., Ingrand, I., Pinguet, J., et al. (2012). Pharmacological inhibition of PKR in APPswePS1dE9 mice



- transiently prevents inflammation at 12 months of age but increases A $\beta$ 42 levels in the late stages of the Alzheimer's disease. *Curr. Alzheimer Res.* 9, 344–360. doi: 10.2174/156720512800107582
- Couturier, J., Paccalin, M., Morel, M., Terro, F., Milin, S., Pontcharraud, R., et al. (2011). Prevention of the beta-amyloid peptide-induced inflammatory process by inhibition of double-stranded RNA-dependent protein kinase in primary murine mixed co-cultures. *J. Neuroinflamm.* 8:72. doi: 10.1186/1742-2094-8-72
- Cuddihy, A. R., Li, S., Tam, N. W., Wong, A. H., Taya, Y., Abraham, N., et al. (1999a). Double-stranded-RNA-activated protein kinase PKR enhances transcriptional activation by tumor suppressor p53. *Mol. Cell. Biol.* 19, 2475–2484. doi: 10.1128/MCB.19.4.2475
- Cuddihy, A. R., Wong, A. H., Tam, N. W., Li, S., and Koromilas, A. E. (1999b). The double-stranded RNA activated protein kinase PKR physically associates with the tumor suppressor p53 protein and phosphorylates human p53 on serine 392 in vitro. *Oncogene* 18, 2690–2702. doi: 10.1038/sj.onc.1202620
- Dabo, S., Maillard, P., Collados Rodriguez, M., Hansen, M. D., Mazouz, S., Bigot, D., et al. (2017). Inhibition of the inflammatory response to stress by targeting interaction between PKR and its cellular activator PACT. *Sci. Rep.* 7:16129. doi: 10.1038/s41598-017-16089-8
- Dagon, Y., Dovrat, S., Vilchik, S., Hacohen, D., Shlomo, G., Sredni, B., et al. (2001). Double-stranded RNA-dependent protein kinase, PKR, down-regulates CDC2/cyclin B1 and induces apoptosis in non-transformed but not in v-mos transformed cells. *Oncogene* 20, 8045–8056. doi: 10.1038/sj.onc.1204945
- Danziger, O., Pupko, T., Bacharach, E., and Ehrlich, M. (2018). Interleukin-6 and interferon- $\alpha$  signaling via JAK1-STAT differentially regulate oncolytic versus cytoprotective antiviral states. *Front. Immunol.* 9:94. doi: 10.3389/fimmu.2018.00094
- Danziger, O., Shai, B., Sabo, Y., Bacharach, E., and Ehrlich, M. (2016). Combined genetic and epigenetic interferences with interferon signaling expose prostate cancer cells to viral infection. *Oncotarget* 7, 52115–52134. doi: 10.18632/oncotarget.10313
- Dar, A. C., Dever, T. E., and Sicheri, F. (2005). Higher-order substrate recognition of eIF2 $\alpha$  by the RNA-dependent protein kinase PKR. *Cell* 122, 887–900. doi: 10.1016/j.cell.2005.06.044
- De Felice, F. G., and Ferreira, S. T. (2014). Inflammation, defective insulin signaling, and mitochondrial dysfunction as common molecular denominators connecting type 2 diabetes to Alzheimer disease. *Diabetes Metab. Res. Rev.* 63, 2262–2272. doi: 10.2337/db13-1954
- de la Monte, S. M., and Wands, J. R., (2008). Alzheimer's disease is type 3 diabetes-evidence reviewed. *J. Diabetes Sci. Technol.* 2, 1101–1113. doi: 10.1177/193229680800200619
- Delgado André, N., and De Lucca, F. L. (2007). Knockdown of PKR expression by RNAi reduces pulmonary metastatic potential of B16-F10 melanoma cells in mice: possible role of NF-kappaB. *Cancer Lett.* 258, 118–125. doi: 10.1016/j.canlet.2007.08.021
- Dey, M., Cao, C., Dar, A. C., Tamura, T., Ozato, K., Sicheri, F., et al. (2005). Mechanistic link between PKR dimerization, autophosphorylation, and eIF2 $\alpha$  substrate recognition. *Cell* 122, 901–913. doi: 10.1016/j.cell.2005.06.041
- Dumurgier, J., Mouton-Liger, F., Lapalus, P., Prevot, M., Laplanche, J. L., Hugon, J., et al. (2013). Cerebrospinal fluid PKR level predicts cognitive decline in Alzheimer's disease. *PLoS One* 8:e53587. doi: 10.1371/journal.pone.0053587
- Duncan, J. W., Johnson, S., Zhang, X., Zheng, B., Luo, J., Ou, X., et al. (2016). Up-regulation of PKR signaling pathway by ethanol displays an age of onset-dependent relationship. *Alcohol. Clin. Exp. Res.* 40, 2320–2328. doi: 10.1111/acer.13209
- Duyckaerts, C., Delatour, B., and Potier, M. (2009). Classification and basic pathology of Alzheimer disease. *Acta Neuropathol.* 118, 5–36. doi: 10.1007/s00401-009-0532-1
- Dzananovic, E., McKenna, S. A., and Patel, T. R. (2018). Viral proteins targeting host protein kinase R to evade an innate immune response: a mini review. *Biotechnol. Genet. Eng. Rev.* 34, 33–59. doi: 10.1080/02648725.2018.1467151
- Dzananovic, E., Patel, T. R., Chojnowski, G., Boniecki, M. J., Deo, S., McEleney, K., et al. (2014). Solution conformation of adenovirus virus associated RNA-I and its interaction with PKR. *J. Struct. Biol.* 185, 48–57. doi: 10.1016/j.jsb.2013.11.007
- Eldar-Finkelman, H., and Eisenstein, M. (2009). Peptide inhibitors targeting protein kinases. *Curr. Pharm. Des.* 15, 2463–2470. doi: 10.2174/138161209788682253
- Elde, N. C., Child, S. J., Geballe, A. P., and Malik, H. S. (2009). Protein kinase R reveals an evolutionary model for defeating viral mimicry. *Nature* 457, 485–489. doi: 10.1038/nature07529
- Endoh, Y., Chung, Y. M., Clark, I. A., Geczy, C. L., and Hsu, K. (2009). IL-10-dependent S100A8 gene induction in monocytes/macrophages by double-stranded RNA. *J. Immunol.* 182, 2258–2268. doi: 10.4049/jimmunol.0802683
- Erta, M., Quintana, A., and Hidalgo, J. (2012). Interleukin-6, a major cytokine in the central nervous system. *Int. J. Biol. Sci.* 8, 1254–1266. doi: 10.7150/ijbs.4679
- Falletta, P., Sanchez-Del-Campo, L., Chauhan, J., Efferm, M., Kenyon, A., Kershaw, C. J., et al. (2017). Translation reprogramming is an evolutionarily conserved driver of phenotypic plasticity and therapeutic resistance in melanoma. *Genes Dev.* 31, 18–33. doi: 10.1101/gad.290940.116
- Feng, G. S., Chong, K., Kumar, A., and Williams, B. R. (1992). Identification of double-stranded RNA-binding domains in the interferon-induced double-stranded RNA-activated p68 kinase. *Proc. Natl. Acad. Sci. U.S.A.* 89, 5447–5451. doi: 10.1073/pnas.89.12.5447
- Fernandez, A. M., and Torres-Alemán, I. (2012). The many faces of insulin-like peptide signalling in the brain. *Nat. Rev. Neurosci.* 13, 225–239. doi: 10.1038/nrn3209
- Fosgerau, K., and Hoffmann, T. (2015). Peptide therapeutics: current status and future directions. *Drug Discov. Today* 20, 122–128. doi: 10.1016/j.drudis.2014.10.003
- Gal-Ben-Ari, S., Kenney, J. W., Ounalla-Saad, H., Taha, E., David, O., Levitan, D., et al. (2012). Consolidation and translation regulation. *Learn. Mem.* 19, 410–422. doi: 10.1101/lm.026849.112
- Gao, J., Aksoy, B. A., Dogrusoz, U., Dresdner, G., Gross, B., Sumer, S. O., et al. (2013). Integrative analysis of complex cancer genomics and clinical profiles using the cBioPortal. *Sci. Signal.* 6:11. doi: 10.1126/scisignal.2004088
- Gao, L., Tang, W., Ding, Z., Wang, D., Qi, X., Wu, H., et al. (2015). Protein-binding function of RNA-dependent protein kinase promotes proliferation through TRAF2/RIP1/NF- $\kappa$ B/c-Myc pathway in pancreatic  $\beta$  cells. *Mol. Med.* 21, 154–166.
- García, M. A., Carrasco, E., Aguilera, M., Alvarez, P., Rivas, C., Campos, J. M., et al. (2011). The chemotherapeutic drug 5-fluorouracil promotes PKR-mediated apoptosis in a p53-independent manner in colon and breast cancer cells. *PLoS One* 6:e23887. doi: 10.1371/journal.pone.0023887
- García, M. A., Meurs, E. F., and Esteban, M. (2007). The dsRNA protein kinase PKR: virus and cell control. *Biochimie* 89, 799–811. doi: 10.1016/j.biochi.2007.03.001
- Garcia-Ortega, M. B., Lopez, G. J., Jimenez, G., Garcia-Garcia, J. A., Conde, V., Boulaiz, H., et al. (2017). Clinical and therapeutic potential of protein kinase PKR in cancer and metabolism. *Expert Rev. Mol. Med.* 19:e9. doi: 10.1017/erm.2017.11
- Ghersa, P., Hooft van Huijsduijnen, R., Whelan, J., and DeLamarter, J. F. (1992). Labile proteins play a dual role in the control of endothelial leukocyte adhesion molecule-1 (ELAM-1) gene regulation. *J. Biol. Chem.* 267, 19226–19232.
- Gil, J., and Esteban, M. (2000). Induction of apoptosis by the dsRNA-dependent protein kinase (PKR): mechanism of action. *Apoptosis* 5, 107–114. doi: 10.1023/A:1009664109241
- Gil, J., García, M. A., and Esteban, M. (2002). Caspase 9 activation by the dsRNA-dependent protein kinase, PKR: molecular mechanism and relevance. *FEBS Lett.* 529, 249–255. doi: 10.1016/S0014-5793(02)03348-3
- Gkogkas, C., Sonenberg, N., and Costa-Mattioli, M. (2010). Translational control mechanisms in long-lasting synaptic plasticity and memory. *J. Biol. Chem.* 285, 31913–31917. doi: 10.1074/jbc.R110.154476
- Gregor, M. F., and Hotamisligil, G. S. (2011). Inflammatory mechanisms in obesity. *Annu. Rev. Immunol.* 29, 415–445. doi: 10.1146/annurev-immunol-031210-101322
- Grolleau, A., Kaplan, M. J., Hanash, S. M., Beretta, L., and Richardson, B. (2000). Impaired translational response and increased protein kinase PKR expression in T cells from lupus patients. *J. Clin. Invest.* 106, 1561–1568. doi: 10.1172/JCI9352
- Haines, G. K., Panos, R. J., Bak, P. M., Brown, T., Zielinski, M., Leyland, J., et al. (1998). Interferon-responsive protein kinase (p68) and proliferating cell nuclear

- antigen are inversely distributed in head and neck squamous cell carcinoma. *Tumour Biol.* 19, 52–59. doi: 10.1159/000029974
- Hanahan, D., and Weinberg, R. A. (2011). Hallmarks of cancer: the next generation. *Cell* 144, 646–674. doi: 10.1016/j.cell.2011.02.013
- Hii, S. I., Hardy, L., Crough, T., Payne, E. J., Grimmett, K., Gill, D., et al. (2004). Loss of PKR activity in chronic lymphocytic leukemia. *Int. J. Cancer* 109, 329–335. doi: 10.1002/ijc.11714
- Hoang, H., Graber, T. E., and Alain, T. (2018). Battling for ribosomes: translational control at the forefront of the antiviral response. *J. Mol. Biol.* 430, 1965–1992. doi: 10.1016/j.jmb.2018.04.040
- Hopkins, S. J., and Rothwell, N. J. (1995). Cytokines and the nervous system. I: Expression and recognition. *Trends Neurosci.* 18, 83–88.
- Hu, Y., and Conway, T. W. (1993). 2-Aminopurine inhibits the double-stranded RNA-dependent protein kinase both in vitro and in vivo. *J. Interferon Res.* 13, 323–328. doi: 10.1089/jir.1993.13.323
- Hu, Z., Zhang, H., Tang, L., Lou, M., and Geng, Y. (2017). Silencing nc886, a non-coding RNA, induces apoptosis of human endometrial cancer cells-1A in vitro. *Med. Sci. Monit.* 23, 1317–1324. doi: 10.12659/MSM.900320
- Hugon, J., Mouton-Liger, F., Dumurgier, J., and Paquet, C. (2017). PKR involvement in Alzheimer's disease. *Alzheimers Res. Ther.* 9:83. doi: 10.1186/s13195-017-0308-0
- Hugon, J., Paquet, C., and Chang, R. C. (2009). Could PKR inhibition modulate human neurodegeneration? *Exp. Rev. Neurother.* 9, 1455–1457. doi: 10.1586/ern.09.92
- Hummer, B. T., Li, X. L., and Hassel, B. A. (2001). Role for p53 in gene induction by double-stranded RNA. *J. Virol.* 75, 7774–7777. doi: 10.1128/JVI.75.16.7774-7777.2001
- Hwang, K., Bak, M. S., Kim, S. J., Rhee, S., and Lee, Y. (2017). Restoring synaptic plasticity and memory in mouse models of Alzheimer's disease by PKR inhibition. *Mol. Brain* 10:57. doi: 10.1186/s13041-017-0338-3
- Ingrand, S., Barrier, L., Lafay-Chebassier, C., Fauconneau, B., Page, G., and Hugon, J. (2007). The oxindole/imidazole derivative C16 reduces in vivo brain PKR activation. *FEBS Lett.* 581, 4473–4478. doi: 10.1016/j.febslet.2007.08.022
- Jagus, R., Joshi, B., and Barber, G. N. (1999). PKR, apoptosis and cancer. *Int. J. Biochem. Cell Biol.* 31, 123–138. doi: 10.1016/S1357-2725(98)00136-8
- Jammi, N. V., Whitby, L. R., and Beal, P. A. (2003). Small molecule inhibitors of the RNA-dependent protein kinase. *Biochem. Biophys. Res. Commun.* 308, 50–57. doi: 10.1016/S0006-291X(03)01318-4
- Jiang, Z., Belforte, J. E., Lu, Y., Yabe, Y., Pickel, J., Smith, C. B., et al. (2010). eIF2 $\alpha$  Phosphorylation-dependent translation in CA1 pyramidal cells impairs hippocampal memory consolidation without affecting general translation. *J. Neurosci.* 30, 2582–2594. doi: 10.1523/JNEUROSCI.3971-09.2010
- Jiang, Z., Zamanian-Daryoush, M., Nie, H., Silva, A. M., Williams, B. R. G., and Li, X. (2003). Poly(I-C)-induced Toll-like receptor 3 (TLR3)-mediated activation of NF $\kappa$ B and MAP kinase is through an interleukin-1 receptor-associated kinase (IRAK)-independent pathway employing the signaling components TLR3-TRAF6-TAK1-TAB2-PKR. *J. Biol. Chem.* 278, 16713–16719. doi: 10.1074/jbc.M300562200
- Kadereit, S., Xu, H., Engeman, T. M., Yang, Y. L., Fairchild, R. L., and Williams, B. R. (2000). Negative regulation of CD8 $^{+}$  T cell function by the IFN-induced and double-stranded RNA-activated kinase PKR. *J. Immunol.* 165, 6896–6901. doi: 10.4049/jimmunol.165.12.6896
- Kadokami, T., Frye, C., Lemster, B., Wagner, C. L., Feldman, A. M., and McTiernan, C. F. (2001). Anti-tumor necrosis factor- $\alpha$  antibody limits heart failure in a transgenic model. *Circulation* 104, 1094–1097. doi: 10.1161/hc3501.096063
- Kahn, M. S., Kranjac, D., Alonzo, C. A., Haase, J. H., Cedillos, R. O., McLinden, K. A., et al. (2012). Prolonged elevation in hippocampal A $\beta$  and cognitive deficits following repeated endotoxin exposure in the mouse. *Behav. Brain Res.* 229, 176–184. doi: 10.1016/j.bbr.2012.01.010
- Kaidanovich-Beilin, O., and Eldar-Finkelman, H. (2006). Peptides targeting protein kinases: strategies and implications. *Physiology (Bethesda)* 21, 411–418. doi: 10.1152/physiol.00022.2006
- Kalra, J., Mangali, S. B., Bhat, A., Dhar, I., Udumula, M. P., and Dhar, A. (2018). Imoxin attenuates high fructose-induced oxidative stress and apoptosis in renal epithelial cells via downregulation of protein kinase R pathway. *Fundam. Clin. Pharmacol.* 32, 297–305. doi: 10.1111/fcp.12352
- Kapil, P., Stohlman, S. A., Hinton, D. R., and Bergmann, C. C. (2014). PKR mediated regulation of inflammation and IL-10 during viral encephalomyelitis. *J. Neuroimmunol.* 270, 1–12. doi: 10.1016/j.jneuroim.2014.02.012
- Kaspar, A. A., and Reichert, J. M. (2013). Future directions for peptide therapeutics development. *Drug Discov. Today* 18, 807–817. doi: 10.1016/j.drudis.2013.05.011
- Khandelwal, P. J., Herman, A. M., and Moussa, C. E. (2011). Inflammation in the early stages of neurodegenerative pathology. *J. Neuroimmunol.* 238, 1–11. doi: 10.1016/j.jneuroim.2011.07.002
- Kim, S. H., Forman, A. P., Mathews, M. B., and Gunnery, S. (2000). Human breast cancer cells contain elevated levels and activity of the protein kinase. *PKR Oncogene* 19, 3086–3094. doi: 10.1038/sj.onc.1203632
- Kim, S. H., Gunnery, S., Choe, J. K., and Mathews, M. B. (2002). Neoplastic progression in melanoma and colon cancer is associated with increased expression and activity of the interferon-inducible protein kinase. *PKR Oncogene* 21, 8741–8748. doi: 10.1038/sj.onc.1205987
- Kim, Y., Lee, J. H., Park, J., Cho, J., Yi, H., and Kim, V. N. (2014). PKR is activated by cellular dsRNAs during mitosis and acts as a mitotic regulator. *Genes Dev.* 28, 1310–1322. doi: 10.1101/gad.242644.114
- Kim, Y., Park, J., Kim, S., Kim, M., Kim, M., Kang, M. G., Kwak, C., et al. (2018). PKR senses nuclear and mitochondrial signals by interacting with endogenous double-stranded RNAs. *Mol. Cell.* 71, 1051.e6–1063.e6 doi: 10.1016/j.molcel.2018.07.029
- Klann, E., and Richter, J. D. (2007). “Translational control of synaptic plasticity and learning and memory,” in eds *Translational Control in Biology and Medicine*, eds N. Sonenberg, J. W. B. Hershey, and M. B. Matthews (Cold Spring Harbor, NY: Cold Spring Harbor Laboratory Press), 485–506
- Koromilas, A. E., Roy, S., Barber, G. N., Katze, M. G., and Sonenberg, N. (1992). Malignant transformation by a mutant of the IFN-inducible dsRNA-dependent protein kinase. *Science* 257, 1685–1689. doi: 10.1126/science.1382315
- Krstic, D., Madhusudan, A., Doehner, J., Vogel, P., Nötter, T., Imhof, C., et al. (2012). Systemic immune challenges trigger and drive Alzheimer-like neuropathology in mice. *J. Neuroinflamm.* 9:151. doi: 10.1186/1742-2094-9-151
- Kuhen, K. L., and Samuel, C. E. (1997). Isolation of the interferon-inducible RNA-dependent protein kinase Pkr promoter and identification of a novel DNA element within the 5'-flanking region of human and mouse Pkr genes. *Virology* 227, 119–130. doi: 10.1006/viro.1996.8306
- Kumar, A., Haque, J., Lacoste, J., Hiscott, J., and Williams, B. R. (1994). Double-stranded RNA-dependent protein kinase activates transcription factor NF- $\kappa$ B by phosphorylating I  $\kappa$ B. *Proc. Natl. Acad. Sci. U.S.A.* 91, 6288–6292. doi: 10.1073/pnas.91.14.6288
- Lancaster, G. I., Kammoun, H. L., Kraakman, M. J., Kowalski, G. M., Bruce, C. R., and Febbraio, M. A. (2016). PKR is not obligatory for high-fat diet-induced obesity and its associated metabolic and inflammatory complications. *Nat. Commun.* 7:10626. doi: 10.1038/ncomms10626
- Lee, E. K., Hong, S., Shin, S., Lee, H., Lee, J., Park, E. J., et al. (2016). nc886, a non-coding RNA and suppressor of PKR, exerts an oncogenic function in thyroid cancer. *Oncotarget* 7, 75000–75012. doi: 10.18632/oncotarget.11852
- Lee, H., Lee, K., Jang, H., Lee, G. K., Park, J., Kim, S. Y., et al. (2014). Epigenetic silencing of the non-coding RNA nc886 provokes oncogenes during human esophageal tumorigenesis. *Oncotarget* 5, 3472–3481. doi: 10.18632/oncotarget.1927
- Lee, K., Kunkeaw, N., Jeon, S. H., Lee, I., Johnson, B. H., Kang, G., et al. (2011). Precursor miR-886, a novel noncoding RNA repressed in cancer, associates with PKR and modulates its activity. *RNA* 17, 1076–1089. doi: 10.1261/rna.2701111
- Li, G., Scull, C., Ozcan, L., and Tabas, I. (2010). NADPH oxidase links endoplasmic reticulum stress, oxidative stress, and PKR activation to induce apoptosis. *J. Cell Biol.* 191, 1113–1125. doi: 10.1083/jcb.201006121
- Li, S., Peters, G. A., Ding, K., Zhang, X., Qin, J., and Sen, G. C. (2006). Molecular basis for PKR activation by PACT or dsRNA. *Proc. Natl. Acad. Sci. U.S.A.* 103, 10005–10010. doi: 10.1073/pnas.0602317103
- Li, W. H., Tanimura, M., Luo, C. C., Datta, S., and Chan, L. (1988). The apolipoprotein multigene family: biosynthesis, structure, structure-function relationships and evolution. *J. Lipid Res.* 29, 245–271.
- Li, Y., Xiao, J., Tan, Y., Wang, J., Zhang, Y., Deng, X., et al. (2017). Inhibition of PKR ameliorates lipopolysaccharide-induced acute lung injury by suppressing

- NF- $\kappa$ B pathway in mice. *Immunopharmacol. Immunotoxicol.* 39, 165–172. doi: 10.1080/08923973.2017.1303839
- Li, Y., Peng Zhou, Y., Wang, C., Li, L., Leng, Y., Chen, R., et al. (2018). Novel role of PKR in palmitate-induced Sirt1 inactivation and endothelial cell senescence. *Am. J. Physiol. Heart Circ. Physiol.* 315, H571–H580. doi: 10.1152/ajpheart.00038.2018
- Liu, G., and Zhang, W. (2018). Long non-coding RNA HOTAIR promotes UVB-induced apoptosis and inflammatory injury by up-regulation of PKR in keratinocytes. *Braz. J. Med. Biol. Res.* 51:e6896. doi: 10.1590/1414-431x20186896
- Lourenco, M. V., Clarke, J. R., Frozza, R. L., Bomfim, T. R., Forny-Germano, L., Batista, A. F., et al. (2013). TNF- $\alpha$  mediates PKR-dependent memory impairment and brain IRS-1 inhibition induced by Alzheimer's beta-amyloid oligomers in mice and monkeys. *Cell. Metab.* 18, 831–843. doi: 10.1016/j.cmet.2013.11.002
- Lu, B., Nakamura, T., Inouye, K., Li, J., Tang, Y., Lundbäck, P., et al. (2012). Novel role of PKR in inflammasome activation and HMGB1 release. *Nature* 488, 670–674. doi: 10.1038/nature11290
- Lu, Z., Xu, X., Hu, X., Lee, S., Traverse, J. H., Zhu, G., et al. (2010). Oxidative stress regulates left ventricular PDE5 expression in the failing heart. *Circulation* 121, 1474–1483. doi: 10.1161/CIRCULATIONAHA.109.906818
- Ma, T., Trinh, M. A., Wexler, A. J., Bourbon, C., Gatti, E., Pierre, P., et al. (2013). Suppression of eIF2 $\alpha$  kinases alleviates Alzheimer's disease-related plasticity and memory deficits. *Nat. Neurosci.* 2013, 1299–1305. doi: 10.1038/nn.3486
- Maran, A., Maitra, R. K., Kumar, A., Dong, B., Xiao, W., Li, G., et al. (1994). Blockage of NF- $\kappa$ B signaling by selective ablation of an mRNA target by 2-5A antisense chimeras. *Science* 265, 789–792. doi: 10.1126/science.7914032
- Marchal, J. A., Carrasco, E., Ramirez, A., Jiménez, G., Olmedo, C., Peran, M., et al. (2013). Bocepinib, a novel small antitumor agent, induces PKR-mediated apoptosis and synergizes with IFN $\alpha$  triggering apoptosis, autophagy and senescence. *Drug Des. Dev. Ther.* 7, 1301–1313.
- Marques, J. T., Rebouillat, D., Ramana, C. V., Murakami, J., Hill, J. E., Gudkov, A., et al. (2005). Down-regulation of p53 by double-stranded RNA modulates the antiviral response. *J. Virol.* 79, 11105–11114. doi: 10.1128/JVI.79.17.11105-11114.2005
- McAllister, C. S., Taghavi, N., and Samuel, C. E. (2012). Protein kinase PKR amplification of interferon  $\beta$  induction occurs through initiation factor eIF-2 $\alpha$ -mediated translational control. *J. Biol. Chem.* 287, 36384–36392. doi: 10.1074/jbc.M112.390039
- McKenna, S. A., Kim, I., Liu, C. W., and Puglisi, J. D. (2006). Uncoupling of RNA binding and PKR kinase activation by viral inhibitor RNAs. *J. Mol. Biol.* 358, 1270–1285. doi: 10.1016/j.jmb.2006.03.003
- Meurs, E., Chong, K., Galabru, J., Thomas, N. S., Kerr, I. M., Williams, B. R., et al. (1990). Molecular cloning and characterization of the human double-stranded RNA-activated protein kinase induced by interferon. *Cell* 62, 379–390. doi: 10.1016/0092-8674(90)90374-N
- Meurs, E. F., Galabru, J., Barber, G. N., Katze, M. G., and Hovanessian, A. G. (1993). Tumor suppressor function of the interferon-induced double-stranded RNA-activated protein kinase. *Proc. Natl. Acad. Sci. U.S.A.* 90, 232–236. doi: 10.1073/pnas.90.1.232
- Monteiro, S., Ferreira, F. M., Pinto, V., Roque, S., Morais, M., de Sá-Calçada, D., et al. (2016). Absence of IFN $\gamma$  promotes hippocampal plasticity and enhances cognitive performance. *Transl. Psychiatry* 6:e707. doi: 10.1038/tp.2015.194
- Mouton-Liger, F., Paquet, C., Dumurgier, J., Lapalus, P., Gray, F., Laplanche, J. L., et al. (2012). Increased cerebrospinal fluid levels of double-stranded RNA-dependant protein kinase in Alzheimer's disease. *Biol. Psychiatry* 71, 829–835. doi: 10.1016/j.biopsych.2011.11.031
- Nakamura, T., Arduini, A., Baccaro, B., Furuhashi, M., and Hotamisligil, G. S. (2014). Small-molecule inhibitors of PKR improve glucose homeostasis in obese diabetic mice. *Diabetes Metab. Res. Rev.* 63, 526–534. doi: 10.2337/db13-1019
- Nakamura, T., Furuhashi, M., Li, P., Cao, H., Tuncman, G., Sonenberg, N., et al. (2010). Double-stranded RNA-dependent protein kinase links pathogen sensing with stress and metabolic homeostasis. *Cell* 140, 338–348. doi: 10.1016/j.cell.2010.01.001
- Nakamura, T., Kunz, R. C., Zhang, C., Kimura, T., Yuan, C. L., Baccaro, B., et al. (2015). A critical role for PKR complexes with TRBP in immunometabolic regulation and eIF2 $\alpha$  phosphorylation in obesity. *Cell Rep.* 11, 295–307. doi: 10.1016/j.celrep.2015.03.021
- Osborn, L. (1990). Leukocyte adhesion to endothelium in inflammation. *Cell* 62, 3–6. doi: 10.1016/0092-8674(90)90230-C
- Ounallah-Saad, H., Sharma, V., Edry, E., and Rosenblum, K. (2014). Genetic or pharmacological reduction of PERK enhances cortical-dependent taste learning. *J. Neurosci.* 34, 14624–14632. doi: 10.1523/JNEUROSCI.2117-14.2014
- Paccalin, M., Pain-Barc, S., Pluchon, C., Paul, C., Besson, M., Carret-Rebillat, A., et al. (2006). Activated mTOR and PKR kinases in lymphocytes correlate with memory and cognitive decline in Alzheimer's disease. *Dement. Geriatr. Cogn. Disord.* 22, 320–326. doi: 10.1159/000095562
- Papadakis, A. I., Paraskeva, E., Peidis, P., Muaddi, H., Li, S., Raptis, L., et al. (2010). eIF2 $\alpha$  Kinase PKR modulates the hypoxic response by Stat3-dependent transcriptional suppression of HIF-1 $\alpha$ . *Cancer Res.* 70, 7820–7829. doi: 10.1158/0008-5472.CAN-10-0215
- Peel, A. L., and Bredesen, D. E. (2003). Activation of the cell stress kinase PKR in Alzheimer's disease and human amyloid precursor protein transgenic mice. *Neurobiol. Dis.* 14, 52–62. doi: 10.1016/S0969-9961(03)00086-X
- Peel, A. L., Rao, R. V., Cottrell, B. A., Hayden, M. R., Ellerby, L. M., and Bredesen, D. E. (2001). Double-stranded RNA-dependent protein kinase, PKR, binds preferentially to Huntington's disease (HD) transcripts and is activated in HD tissue. *Hum. Mol. Genet.* 10, 1531–1538. doi: 10.1093/hmg/10.15.1531
- Peidis, P., Papadakis, A. I., Muaddi, H., Richard, S., and Koromilas, A. E. (2011). Doxorubicin bypasses the cytoprotective effects of eIF2 $\alpha$  phosphorylation and promotes PKR-mediated cell death. *Cell Death. Differ.* 18, 145–154. doi: 10.1038/cdd.2010.76
- Peidis, P., Papadakis, A. I., Rajesh, K., and Koromilas, A. E. (2010). HDAC pharmacological inhibition promotes cell death through the eIF2 $\alpha$  kinases PKR and GCN2. *Aging (Albany NY)* 2, 669–677. doi: 10.18632/aging.100216
- Pikarsky, E., and Ben-Neriah, Y. (2006). NF- $\kappa$ B inhibition: a double-edged sword in cancer? *Eur. J. Cancer* 42, 779–784. doi: 10.1016/j.ejca.2006.01.011
- Qi, Y., Zhang, M., Li, H., Frank, J. A., Dai, L., Liu, H., et al. (2014). MicroRNA-29b regulates ethanol-induced neuronal apoptosis in the developing cerebellum through SP1/RAX/PKR cascade. *J. Biol. Chem.* 289, 10201–10210. doi: 10.1074/jbc.M113.535195
- Rosenblum, K., Meiri, N., and Dudai, Y. (1993). Taste memory: the role of protein synthesis in gustatory cortex. *Behav. Neural Biol.* 59, 49–56. doi: 10.1016/0163-1047(93)91145-D
- Rothenburg, S., Seo, E. J., Gibbs, J. S., Dever, T. E., and Dittmar, K. (2009). Rapid evolution of protein kinase PKR alters sensitivity to viral inhibitors. *Nat. Struct. Mol. Biol.* 16, 63–70. doi: 10.1038/nsmb.1529
- Rouillard, A. D., Gundersen, G. W., Fernandez, N. F., Wang, Z., Monteiro, C. D., McDermott, M. G., et al. (2016). The harmonizome: a collection of processed datasets gathered to serve and mine knowledge about genes and proteins. *Database (Oxford)* 3:2016. doi: 10.1093/database/baw100
- Schindler, U., and Baichwal, V. R. (1994). Three NF- $\kappa$ B binding sites in the human E-selectin gene required for maximal tumor necrosis factor  $\alpha$ -induced expression. *Mol. Cell. Biol.* 14, 5820–5831. doi: 10.1128/MCB.14.9.5820
- Schulz, O., Pichlmair, A., Rehwinkel, J., Rogers, N. C., Scheuner, D., Kato, H., et al. (2010). Protein kinase R contributes to immunity against specific viruses by regulating interferon mRNA integrity. *Cell. Host. Microbe.* 7, 354–361. doi: 10.1016/j.chom.2010.04.007
- Segev, Y., Barrera, I., Ounallah-Saad, H., Wibrand, K., Sporild, I., Livne, A., et al. (2015). PKR inhibition rescues memory deficit and ATF4 overexpression in ApoE epsilon4 human replacement mice. *J. Neurosci.* 35, 12986–12993. doi: 10.1523/JNEUROSCI.5241-14.2015
- Segev, Y., Livne, A., Mints, M., and Rosenblum, K. (2016). Concurrence of high fat diet and APOE gene induces allele specific metabolic and mental stress changes in a mouse model of Alzheimer's disease. *Front. Behav. Neurosci.* 10:170. doi: 10.3389/fnbeh.2016.00170
- Segev, Y., Michaelson, D. M., and Rosenblum, K. (2013). ApoE epsilon4 is associated with eIF2 $\alpha$  phosphorylation and impaired learning in young mice. *Neurobiol. Aging* 34, 863–872. doi: 10.1016/j.neurobiolaging.2012.06.020
- Sharma, P., Hu-Lieskova, S., Wargo, J. A., and Ribas, A. (2017). Primary, adaptive, and acquired resistance to cancer immunotherapy. *Cell* 168, 707–723. doi: 10.1016/j.cell.2017.01.017



- Sharma, V., Ounallah-Saad, H., Chakraborty, D., Hleihil, M., Sood, R., Barrera, I., et al. (2018). Local inhibition of PERK enhances memory and reverses age-related deterioration of cognitive and neuronal properties. *J. Neurosci.* 38, 648–658. doi: 10.1523/JNEUROSCI.0628-17.2017
- Shen, S., Niso-Santano, M., Adjemian, S., Takehara, T., Malik, S. A., Minoux, H., et al. (2012). Cytoplasmic STAT3 represses autophagy by inhibiting PKR activity. *Mol. Cell* 48, 667–680. doi: 10.1016/j.molcel.2012.09.013
- Song, Y., Wan, X., Gao, L., Pan, Y., Xie, W., Wang, H., et al. (2015). Activated PKR inhibits pancreatic  $\beta$ -cell proliferation through sumoylation-dependent stabilization of P53. *Mol. Immunol.* 68, 341–349. doi: 10.1016/j.molimm.2015.09.007
- Stern, E., Chinnakkaruppan, A., David, O., Sonenberg, N., and Rosenblum, K. (2013). Blocking the eIF2 $\alpha$  kinase (PKR) enhances positive and negative forms of cortex-dependent taste memory. *J. Neurosci.* 33, 2517–2525. doi: 10.1523/JNEUROSCI.2322-12.2013
- Stojdl, D. F., Lichty, B., Knowles, S., Marius, R., Atkins, H., Sonenberg, N., et al. (2000). Exploiting tumor-specific defects in the interferon pathway with a previously unknown oncolytic virus. *Nat. Med.* 6, 821–825. doi: 10.1038/77588
- Strong, J. E., Coffey, M. C., Tang, D., Sabinin, P., and Lee, P. W. (1998). The molecular basis of viral oncolysis: usurpation of the Ras signaling pathway by reovirus. *EMBO J.* 17, 3351–3362. doi: 10.1093/emboj/17.12.3351
- Swetha, M., and Ramaiah, K. V. A. (2015). Insulin treatment promotes tyrosine phosphorylation of PKR and inhibits polyIC induced PKR threonine phosphorylation. *Arch. Biochem. Biophys.* 585, 98–108. doi: 10.1016/j.abb.2015.07.012
- Taga, M., Minett, T., Classey, J., Matthews, F. E., Brayne, C., Ince, P. G., et al. (2017). Metaflammasome components in the human brain: a role in dementia with Alzheimer's pathology? *Brain Pathol.* 27, 266–275. doi: 10.1111/bpa.12388
- Taga, M., Mouton-Liger, F., Sadoune, M., Gourmaud, S., Norman, J., Tible, M., et al. (2018). PKR modulates abnormal brain signaling in experimental obesity. *PLoS One* 13:e0196983. doi: 10.1371/journal.pone.0196983
- Takaoka, A., Hayakawa, S., Yanai, H., Stoiber, D., Negishi, H., Kikuchi, H., et al. (2003). Integration of interferon- $\alpha$ /beta signalling to p53 responses in tumour suppression and antiviral defence. *Nature* 424, 516–523. doi: 10.1038/nature01850
- Taniguchi, K., and Karin, M. (2018). NF- $\kappa$ B, inflammation, immunity and cancer: coming of age. *Nat. Rev. Immunol.* 18, 309–324. doi: 10.1038/nri.2017.142
- Taniuchi, S., Miyake, M., Tsugawa, K., Oyadomari, M., and Oyadomari, S. (2016). Integrated stress response of vertebrates is regulated by four eIF2 $\alpha$  kinases. *Sci. Rep.* 6:32886. doi: 10.1038/srep32886
- Taylor, D. R., Tian, B., Romano, P. R., Hinnebusch, A. G., Lai, M. M., and Mathews, M. B. (2001). Hepatitis C virus envelope protein E2 does not inhibit PKR by simple competition with autophosphorylation sites in the RNA-binding domain. *J. Virol.* 75, 1265–1273. doi: 10.1128/JVI.75.3.1265-1273.2001
- Trinh, M. A., Kaphzan, H., Wek, R. C., Pierre, P., Cavener, D. R., and Klann, E. (2012). Brain-specific disruption of the eIF2 $\alpha$  kinase PERK decreases ATF4 expression and impairs behavioral flexibility. *Cell Rep.* 1, 676–688. doi: 10.1016/j.celrep.2012.04.010
- Trinh, M. A., Ma, T., Kaphzan, H., Bhattacharya, A., Antion, M. D., Cavener, D. R., et al. (2014). The eIF2 $\alpha$  kinase PERK limits the expression of hippocampal metabotropic glutamate receptor-dependent long-term depression. *Learn. Mem.* 21, 298–304. doi: 10.1101/lm.032219.113
- Tronel, C., Page, G., Bodard, S., Chalon, S., and Antier, D. (2014). The specific PKR inhibitor C16 prevents apoptosis and IL-1 $\beta$  production in an acute excitotoxic rat model with a neuroinflammatory component. *Neurochem. Int.* 64, 73–83. doi: 10.1016/j.neuint.2013.10.012
- Udumula, M. P., Babu, M. S., Bhat, A., Dhar, I., Sriram, D., and Dhar, A. (2017). High glucose impairs insulin signaling via activation of PKR pathway in L6 muscle cells. *Biochem. Biophys. Res. Commun.* 486, 645–651. doi: 10.1016/j.bbrc.2017.03.078
- Udumula, M. P., Bhat, A., Mangali, S., Kalra, J., Dhar, I., Sriram, D., et al. (2018). Pharmacological evaluation of novel PKR inhibitor indirubin-3-hydrazone in vitro in cardiac myocytes and in vivo in wistar rats. *Life Sci.* 209, 85–96. doi: 10.1016/j.lfs.2018.07.055
- Volonte, D., Zou, H., Bartholomew, J. N., Liu, Z., Morel, P. A., and Galbiati, F. (2015). Oxidative stress-induced inhibition of Sirt1 by caveolin-1 promotes p53-dependent premature senescence and stimulates the secretion of interleukin 6 (IL-6). *J. Biol. Chem.* 290, 4202–4214. doi: 10.1074/jbc.M114.598268
- von Roretz, C., and Gallouzi, I. (2010). Protein kinase RNA/FADD/caspase-8 pathway mediates the proapoptotic activity of the RNA-binding protein human antigen R (HuR). *J. Biol. Chem.* 285, 16806–16813. doi: 10.1074/jbc.M109.087320
- Wahid, A. M., Coventry, V. K., and Conn, G. L. (2009). The PKR-binding domain of adenovirus VA RNAI exists as a mixture of two functionally non-equivalent structures. *Nucleic Acids Res.* 37, 5830–5837. doi: 10.1093/nar/gkp595
- Wang, H., Xu, X., Fassett, J., Kwak, D., Liu, X., Hu, X., et al. (2014). Double-stranded RNA-dependent protein kinase deficiency protects the heart from systolic overload-induced congestive heart failure. *Circulation* 129, 1397–1406. doi: 10.1161/CIRCULATIONAHA.113.002209
- Wang, W. J., Yin, S. J., and Rong, R. Q. (2015). PKR and HMGB1 expression and function in rheumatoid arthritis. *Genet. Mol. Res.* 14, 17864–17870. doi: 10.4238/2015.December.22.11
- Wang, X., Fan, Z., Wang, B., Luo, J., and Ke, Z. (2007). Activation of double-stranded RNA-activated protein kinase by mild impairment of oxidative metabolism in neurons. *J. Neurochem.* 103, 2380–2390. doi: 10.1111/j.1471-4159.2007.04978.x
- Ward, A., Crean, S., Mercaldi, C. J., Collins, J. M., Boyd, D., Cook, M. N., et al. (2012). Prevalence of apolipoprotein E4 genotype and homozygotes (APOE e4/e4) among patients diagnosed with Alzheimer's disease: a systematic review and meta-analysis. *Neuroepidemiology* 38, 1–17. doi: 10.1159/000334607
- Watanabe, T., Imamura, T., and Hiasa, Y. (2018). Roles of protein kinase R in cancer: potential as a therapeutic target. *Cancer Sci.* 109, 919–925. doi: 10.1111/cas.13551
- Webster, S. J., Ellis, L., O'Brien, L. M., Tyrrell, B., Fitzmaurice, T. J., Elder, M. J., et al. (2016). IRE1 $\alpha$  mediates PKR activation in response to *Chlamydia trachomatis* infection. *Microbes Infect.* 18, 472–483. doi: 10.1016/j.micinf.2016.03.010
- Weintraub, S., Yarnitzky, T., Kahremany, S., Barrera, I., Viskind, O., Rosenblum, K., et al. (2016). Design and synthesis of novel protein kinase R (PKR) inhibitors. *Mol. Divers.* 20, 805–819. doi: 10.1007/s11030-016-9689-4
- Xiao, J., Tan, Y., Li, Y., and Luo, Y. (2016). The specific protein kinase R (PKR) inhibitor C16 protects neonatal hypoxia-ischemia brain damages by inhibiting neuroinflammation in a neonatal rat model. *Med. Sci. Monit.* 22, 5074–5081. doi: 10.12659/MSM.898139
- Yang, W., Zhou, X., Zimmermann, H. R., Cavener, D. R., Klann, E., and Ma, T. (2016). Repression of the eIF2 $\alpha$  kinase PERK alleviates mGluR-LTD impairments in a mouse model of Alzheimer's disease. *Neurobiol. Aging* 41, 19–24. doi: 10.1016/j.neurobiolaging.2016.02.005
- Yoon, C., Lee, E., Lim, D., and Bae, Y. (2009). PKR, a p53 target gene, plays a crucial role in the tumor-suppressor function of p53. *Proc. Natl. Acad. Sci. U.S.A.* 106, 7852–7857. doi: 10.1073/pnas.0812148106
- Yoon, C., Miah, M. A., Kim, K. P., and Bae, Y. (2010). New Cdc2 Tyr 4 phosphorylation by dsRNA-activated protein kinase triggers Cdc2 polyubiquitination and G2 arrest under genotoxic stresses. *EMBO Rep.* 11, 393–399. doi: 10.1038/embor.2010.45
- Youssef, O. A., Safran, S. A., Nakamura, T., Nix, D. A., Hotamisligil, G. S., and Bass, B. L. (2015). Potential role for snoRNAs in PKR activation during metabolic stress. *Proc. Natl. Acad. Sci. U.S.A.* 112, 5023–5028. doi: 10.1073/pnas.1424044112
- Zamanian-Daryoush, M., Der, S. D., and Williams, B. R. (1999). Cell cycle regulation of the double stranded RNA activated protein kinase. *PKR Oncogene* 18, 315–326. doi: 10.1038/sj.onc.1202293
- Zaretsky, J. M., Garcia-Diaz, A., Shin, D. S., Escuin-Ordinas, H., Hugo, W., Hu-Lieskovan, S., et al. (2016). Mutations associated with acquired resistance to PD-1 blockade in melanoma. *N. Engl. J. Med.* 375, 819–829. doi: 10.1056/NEJMoa1604958
- Zhang, J. S., Zhou, S. F., Wang, Q., Guo, J. N., Liang, H. M., Deng, J. B., et al. (2016). Gastrodin suppresses BACE1 expression under oxidative stress condition via inhibition of the PKR/eIF2 $\alpha$  pathway in Alzheimer's disease. *Neuroscience* 325, 1–9. doi: 10.1016/j.neuroscience.2016.03.024
- Zhang, P., and Samuel, C. E. (2008). Induction of protein kinase PKR-dependent activation of interferon regulatory factor 3 by vaccinia virus occurs through adapter IPS-1 signaling. *J. Biol. Chem.* 283, 34580–34587. doi: 10.1074/jbc.M807029200

- Zhu, M., Liu, X., Wang, S., Miao, J., Wu, L., Yang, X., et al. (2016). PKR promotes choroidal neovascularization via upregulating the PI3K/Akt signaling pathway in VEGF expression. *Mol. Vis.* 22, 1361–1374.
- Zhu, P. J., Huang, W., Kalikulov, D., Yoo, J. W., Placzek, A. N., Stoica, L., et al. (2011). Suppression of PKR promotes network excitability and enhanced cognition by interferon-gamma-mediated disinhibition. *Cell* 147, 1384–1396. doi: 10.1016/j.cell.2011.11.029
- Zhu, Z., Zhong, H., Zhou, Q., Hu, X., Chen, D., Wang, J., et al. (2015). Inhibition of PKR impairs angiogenesis through a VEGF pathway. *Am. J. Physiol. Endocrinol. Metab.* 308, 518. doi: 10.1152/ajpendo.00469.2014
- Zimmermann, H. R., Yang, W., Beckelman, B. C., Kasica, N. P., Zhou, X., Galli, L. D., et al. (2018). Genetic removal of eIF2 $\alpha$  kinase PERK in mice enables hippocampal L-LTP independent of mTORC1 activity. *J. Neurochem.* 146, 133–144. doi: 10.1111/jnc.14306

**Conflict of Interest Statement:** KR serves as Chief Scientific Officer at Protekt Therapeutics Ltd.

The remaining authors declare that the research was conducted in the absence of any commercial or financial relationships that could be construed as a potential conflict of interest.

Copyright © 2019 Gal-Ben-Ari, Barrera, Ehrlich and Rosenblum. This is an open-access article distributed under the terms of the Creative Commons Attribution License (CC BY). The use, distribution or reproduction in other forums is permitted, provided the original author(s) and the copyright owner(s) are credited and that the original publication in this journal is cited, in accordance with accepted academic practice. No use, distribution or reproduction is permitted which does not comply with these terms.





# Small Molecule Modulators of the Circadian Molecular Clock With Implications for Neuropsychiatric Diseases

Hyo Kyeong Cha<sup>1†</sup>, Sooyoung Chung<sup>2†</sup>, Hye Young Lim<sup>1†</sup>, Jong-Wha Jung<sup>3</sup> and Gi Hoon Son<sup>1\*</sup>

<sup>1</sup> Department of Biomedical Sciences, College of Medicine, Korea University, Seoul, South Korea, <sup>2</sup> Department of Brain and Cognitive Sciences, Scranton College, Ewha Womans University, Seoul, South Korea, <sup>3</sup> College of Pharmacy, Research Institute of Pharmaceutical Sciences, Kyungpook National University, Daegu, South Korea

## OPEN ACCESS

### Edited by:

Urs Albrecht,  
Université de Fribourg, Switzerland

### Reviewed by:

Etienne Challet,  
The National Center for Scientific  
Research (CNRS), France  
Henrik Oster,  
Universität zu Lübeck, Germany

### \*Correspondence:

Gi Hoon Son  
songh@korea.ac.kr

<sup>†</sup>These authors have contributed  
equally to this work

**Received:** 10 October 2018

**Accepted:** 28 December 2018

**Published:** 21 January 2019

### Citation:

Cha HK, Chung S, Lim HY,  
Jung J-W and Son GH (2019) Small  
Molecule Modulators of the Circadian  
Molecular Clock With Implications  
for Neuropsychiatric Diseases.  
*Front. Mol. Neurosci.* 11:496.  
doi: 10.3389/fnmol.2018.00496

Circadian rhythms regulate many biological processes and play fundamental roles in behavior, physiology, and metabolism. Such periodicity is critical for homeostasis because disruption or misalignment of the intrinsic rhythms is associated with the onset and progression of various human diseases and often directly leads to pathological states. Since the first identification of mammalian circadian clock genes, numerous genetic and biochemical studies have revealed the molecular basis of these cell-autonomous and self-sustainable rhythms. Specifically, these rhythms are generated by two interlocking transcription/translation feedback loops of clock proteins. As our understanding of these underlying mechanisms and their functional outputs has expanded, strategies have emerged to pharmacologically control the circadian molecular clock. Small molecules that target the molecular clock may present novel therapeutic strategies to treat chronic circadian rhythm-related diseases. These pharmaceutical approaches may include the development of new drugs to treat circadian clock-related disorders or combinational use with existing therapeutic strategies to improve efficacy via intrinsic clock-dependent mechanisms. Importantly, circadian rhythm disruptions correlate with, and often precede, many symptoms of various neuropsychiatric disorders such as sleep disorders, affective disorders, addiction-related disorders, and neurodegeneration. In this mini-review, we focus on recent discoveries of small molecules that pharmacologically modulate the core components of the circadian clock and their potential as preventive and/or therapeutic strategies for circadian clock-related neuropsychiatric diseases.

**Keywords:** circadian rhythm, circadian clock, cryptochrome, REV-ERB, ROR, small molecule, circadian rhythm-related disease

## INTRODUCTION

Circadian rhythms are ubiquitous biological oscillations with an approximate 24-h period. These evolutionarily well-conserved rhythms arise from an intrinsic timekeeping system known as the “circadian clock”, which allows organisms to anticipate environmental cycling and coordinate biological processes. This clock is self-sustainable through an elaborate cooperation of genetic

components and is hierarchically organized into a circadian timing system. In mammals, the apex of this system is the suprachiasmatic nucleus (SCN) of the hypothalamus, which is considered the central or master clock (Ralph et al., 1990; Reppert and Weaver, 2002). The SCN integrates environmental cues such as light into time information to entrain its phase and then conveys this information to other oscillators in extra-SCN brain regions and peripheral tissues. Indeed, in multicellular organisms, most cells harbor cell-autonomous oscillators. These so-called local or peripheral clocks contribute to overt circadian rhythms, including the rest-activity cycle, periodic daily variations in metabolism and body temperature, as well as rhythmic hormone secretion (Dibner et al., 2010; Son et al., 2011).

Robust circadian timing is required for health, and disruption of these intrinsic rhythms causes diverse pathologies. For instance, circadian disruption caused by shift-work, jet-lag, or mis-timed food intake is considered a risk factor for various chronic diseases, including sleep disorders, metabolic syndromes, cardiovascular diseases, affective disorders, neurodegeneration, and tumorigenesis (Takahashi et al., 2008; Bechtold et al., 2010). To develop treatments for these disorders, extensive studies have identified several small molecule compounds that can directly modulate circadian clocks. In this mini-review, we will discuss recent investigations of the most promising of these small chemical compounds and their therapeutic implications in neuropsychiatric diseases.

## THE MAMMALIAN CIRCADIAN MOLECULAR CLOCK

The self-sustainable nature of the circadian system is primarily attributed to circadian molecular oscillators. The molecular clock is composed of several clock proteins that are required for the generation and maintenance of cell-autonomous rhythms (Dibner et al., 2010). Clock proteins form two interlocking positive and negative transcription/translation feedback loops that drive periodic expression of their target genes (**Figure 1**). The primary regulators are Circadian Locomotor Output Cycle Kaput (CLOCK) and Brain Muscle Aryl Hydrocarbon Receptor Nuclear Translocator-Like 1 (BMAL1, encoded by the *ARNTL* gene). They belong to the basic helix-loop-helix-PER-ARNT-SIM (bHLH-PAS) transcription factor family. CLOCK and BMAL1 activate transcription of target genes by forming heterodimers and binding to E-box enhancer elements (5'-CACGTG-3') in the promoter/enhancer regions. In addition to CLOCK, Neuronal PAS 2 (NPAS2) is another bHLH-PAS protein enriched in forebrain regions that can also form heterodimers with BMAL1 to control E-box element-dependent gene transcription (Asher and Schibler, 2006). The targets include proteins that form a negative feedback loop such as PERIODs (PERs: PER1, 2, and 3) and CRYPTOCHROMEs (CRYs: CRY1 and 2). Accumulated PER and CRY proteins form repressive complexes that suppress E-box-mediated transcription by binding to CLOCK/BMAL1 heterodimers, whereas PER and CRY degradation terminates this repression and reinitiates transcription (Gekakis et al., 1998; Hogenesch et al., 1998;

Kume et al., 1999; Shearman et al., 2000). Stability of PER and CRY proteins is linked with their post-translational modifications and is crucial for proper circadian period length. It is well known that the *Tau*-mutant hamster, bearing a mutation in the casein kinase 1 $\epsilon$  (CK1 $\epsilon$ ) gene, displays a shortened free-running period in locomotor activities (Ralph and Menaker, 1988). In accordance, PER proteins are phosphorylated by CK1s prior to their proteasomal degradation, contributing to regulation of circadian period lengths (Eide et al., 2005; Shirogane et al., 2005). Similarly, CRY protein phosphorylation by adenosine monophosphate-activated protein kinase (AMPK) or glycogen synthase kinase 3 $\beta$  (GSK3 $\beta$ ) leads to degradation mediated by paralogous F-box proteins, FBXL3 and FBXL21 (Busino et al., 2007; Lamia et al., 2009; Kurabayashi et al., 2010; Hirano et al., 2013; Yoo et al., 2013). Mutations in the *Fbxl3* gene result in long-period phenotypes in mice, whereas *Fbxl21*-mutant mice display short-period phenotypes (Godinho et al., 2007; Siepka et al., 2007; Hirano et al., 2013; Yoo et al., 2013). This CLOCK/BMAL1-initiated loop is considered the core loop of the mammalian clock.

An additional stabilizing loop adjusts the amounts of bHLH-PAS proteins. This secondary loop consists of sets of the circadian nuclear receptors, in particular REV-ERBs (REV-ERB $\alpha$  and  $\beta$ , encoded by *NR1D1* and *NR1D2*, respectively) and retinoic acid receptor-related orphan nuclear receptors (RORs: ROR $\alpha$ - $\gamma$ ), that are also under the transcriptional control of CLOCK/BMAL1 heterodimers. REV-ERBs and RORs compete to occupy the RORs/REV-ERBs-responsive elements (RREs) located in the promoter/enhancer regions of their target genes. RORs usually activate RRE-mediated transcription, whereas REV-ERBs strongly suppress it (Preitner et al., 2002; Ueda et al., 2002; Sato et al., 2004). This stabilizing loop was originally considered as accessory because only moderate phenotypes were observed in mutant mice bearing null alleles of any of these genes. However, more recent studies using inducible double knockouts for both *Nr1d1* and 2 revealed that their compensatory activity yielded these subtle phenotypes and that REV-ERBs are required for normal period regulation (Cho et al., 2012). REV-ERBs also control circadian outputs by cooperating with cell type-specific transcriptional regulators (Chung et al., 2014; Zhang et al., 2015). Additional feedback loops involving the proline and acidic amino acid-rich basic leucine zipper proteins (PARbZip), such as D-box binding protein (DBP) and E4 promoter-binding protein 4 (E4BP4), as well as several members of bHLH transcription factors (BHLHE40 and BHLHE41), also intersect with the main loops to confer further regulation and mediate circadian expression of subsets of clock-controlled genes (Mitsui et al., 2001; Honma et al., 2002).

## SMALL MOLECULES TARGETING CLOCK PROTEINS

As noted earlier, circadian disruptions are pivotal in various biological dysfunctions. Subsequent studies have attempted to correct these dysfunctions by exploring pharmacological

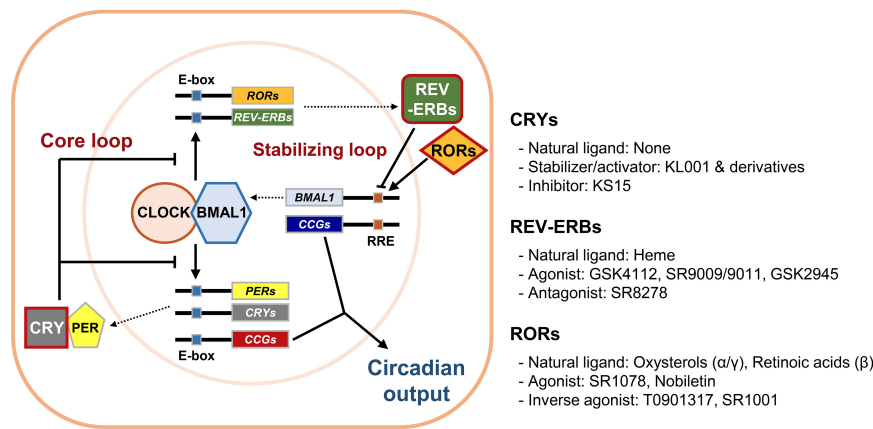


**FIGURE 1 |** The mammalian circadian molecular clock and its potential drug targets. The mammalian circadian clock is composed of two interlocking transcription/translation feedback loops, the core and stabilizing/auxiliary loops, respectively. The integral components of the core loop are CLOCK (or NPAS2) and BMAL1, which form a heterodimer and then induce E-box-mediated transcription of their negative regulators *Periods* (PERs) and *Cryptochromes* (CRYs). Accumulated PER and CRY proteins repress E-box-mediated transcription until they are sufficiently cleared by proteasome-mediated degradation. CLOCK and BMAL1 also control expression of circadian nuclear receptors such as RORs and REV-ERBs, which modulate *Bmal1* mRNA levels by competitive actions on the RORs/REV-ERBs-responsive elements (RREs) in the *Bmal1* promoter. Collectively, cycling of clock components determines the periodic mRNA expression levels of various clock-controlled genes (CCGs) through E-box, RRE, and/or other *cis*-elements recognized by secondary circadian transcription factors, thus generating rhythmic physiological outputs. Of these core clock proteins, we focused primarily on CRYs, REV-ERBs, and RORs (red boxes), which were recently identified as targets for small molecule modifiers of the circadian clock.

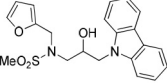
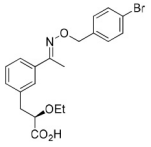
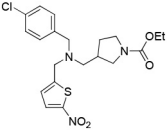
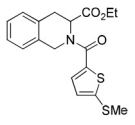
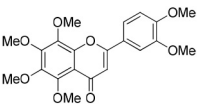
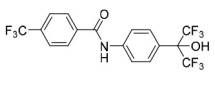
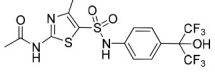
strategies (Schroeder and Colwell, 2013). Initially, high-throughput screening studies identified several compounds that influence circadian oscillators by acting on post-translational regulators, including CK1s, CK2, GSK3 $\beta$ , and AMPK (Chen et al., 2018). These studies have advanced our understanding of the post-translational mechanisms underlying the circadian clock and uncovered novel clock-regulatory pathways. Additionally, some of the clock modulators that target these signaling pathways have already been recognized for their therapeutic implications (He and Chen, 2016; Chen et al., 2018). For example, lithium, a widely used mood stabilizer, inhibits GSK3 $\beta$  and lengthens the circadian period; however, some synthetic inhibitors exhibited opposite effects (Hirota et al., 2008; Li et al., 2012). Also, AMPK activators with a wide range of beneficial metabolic and physiological effects also altered circadian gene expression, as demonstrated both *in vivo* and *in vitro* (Um et al., 2007; Lamia et al., 2009). These observations suggest that modulation of the circadian clock may have beneficial effects on circadian rhythm-related chronic diseases. In this regard, recent investigations have attempted to directly target core components of the mammalian circadian clock by using small-molecule modifiers. Representative small molecules that bind to core clock components are summarized in **Table 1**. Pharmacological targets of these small molecules include CRYs, REV-ERBs, and RORs, which are described below.

## CRYs: Key Targets of Small Molecules That Act Directly on the Core Loop

A carbazole derivative, KL001, and its analogs are the first-in-class small molecules that target the core components of the mammalian clock (Hirota et al., 2012). In cultured

SCN explants and fibroblasts, continuous treatment with these compounds significantly lengthens the circadian period and reduces amplitude of both *Bmal1* and *Per2* promoter activity, implying CRY protein activation. KL001 binds to CRY through the FAD-binding pocket, which is known to be recognized by FBXL3 and mediate proteasomal degradation (Xing et al., 2013). The co-crystal structure of the KL001–CRY2 complex revealed that KL001 competes with FAD and interferes with binding of the FBXL3 C-terminal to CRY, thereby stabilizing CRY proteins (Hirota et al., 2012; Nangle et al., 2013). Alternatively, we identified a derivative of 2-ethoxypropanoic acid (designated as KS15) that inhibits CRY-mediated feedback on CLOCK/BMAL1-mediated transcription (Chun et al., 2014). KS15 directly binds to CRY C-terminal domains, enhancing E-box-mediated transcription in a CRY-dependent manner, and attenuates the circadian oscillations of *Bmal1* and *Per2* promoter activity (Chun et al., 2014; Jang et al., 2018). Thus, while KL001 and its derivatives strengthen CRY-mediated feedback, KS15 increases basal promoter activity by inhibiting the repressive actions of CRYs on CLOCK/BMAL1-mediated transcription. CRYs are composed of highly conserved N-terminal photolyase homology regions and variable C-terminal extension domains (Chaves et al., 2006). The putative coiled-coil (CC) domain is located in the C-terminal tail and is highly conserved between CRY1 and CRY2. Previous studies have suggested that CRY C-terminal tails, including the CC domain, are important for nuclear localization and interactions with other core clock proteins (Chaves et al., 2006; van der Schalie et al., 2007). We found that KS15 binding of CRY C-terminal domains significantly inhibits CRY-BMAL1 interactions, but barely affects CRY-PER associations. Thus, KS15 can be used as a distinct scaffold to develop additional derivatives with improved pharmacokinetics, although further SAR studies

**TABLE 1** | Representative small molecule clock modulators.

Name	Structure	Actions	Potential applications	Reference
KL001 and analogs		CRY stabilizer Suppresses E-box-mediated transcription Alters period	Metabolic disorders	Hirota et al., 2012; Nangle et al., 2013
KS15		CRY inhibitor Enhances E-box-mediated transcription	Cancer	Chun et al., 2014, 2015; Jang et al., 2018
SR9009 and related compounds		REV-ERB agonist Suppresses RRE-mediated transcription	<b>Sleep disorders</b> <b>Anxiety disorders</b> Metabolic disorders Cancer	Solt et al., 2012; Banerjee et al., 2014; Sulli et al., 2018b
SR8278		REV-ERB antagonist Enhances RRE-mediated transcription	<b>Depressive disorders</b> <b>Risk of bipolarity</b>	Kojetin et al., 2011; Chung et al., 2014; Guo et al., 2018
Nobiletin		ROR $\alpha/\gamma$ agonist Enhances RRE-mediated transcription Increases amplitude	<b>Depressive disorders</b> <b>Neurodegeneration</b> Metabolic disorders	Onozuka et al., 2008; Yi et al., 2011; Yabuki et al., 2014; Nakajima et al., 2015; He et al., 2016
SR1078 and related compounds		ROR $\alpha/\gamma$ agonist Enhances RRE-mediated transcription	<b>Autism-spectrum disorders</b> Diabetic cardiomyopathy	Wang et al., 2010, 2016; Zhao et al., 2017
SR1001 and related compounds		ROR $\alpha/\gamma$ inverse agonist Suppresses RRE-mediated transcription	Metabolic disorders Atherosclerosis Autoimmunity Anti-inflammation	Solt et al., 2011; Billon et al., 2016; Dai et al., 2017

CRY, cryptochrome; ROR, retinoic acid receptor-related orphan nuclear receptor; RRE, RORs/REV-ERBs-responsive element.

are required to determine its mechanism of action (Jang et al., 2018).

## Circadian Nuclear Receptors as Small Molecule Probe Targets

The circadian nuclear receptors, REV-ERBs and RORs, mediate many physiological processes, including circadian rhythms, development, metabolism, immunity, and even various brain functions. Members of the nuclear receptor superfamily are ligand-activated transcription factors that act as intracellular receptors for cell-permeable ligands. Thus, nuclear receptors are considered as one of the primary molecular classes suitable for drug targets. Interestingly, REV-ERBs contain atypical ligand-binding domains (LBDs) and lack C-terminal transactivation domains, which are used for interactions with transcriptional co-activators. These features provide a structural basis for constitutively repressive action of REV-ERBs upon binding their target genes transcription. Recent studies have identified endogenous ligands for these circadian nuclear receptors, thereby stimulating the development of synthetic ligands with therapeutic

applications to circadian rhythm-related diseases (Kojetin and Burris, 2014).

Although REV-ERBs were initially identified as orphan nuclear receptors, subsequent studies revealed that heme binds to the LBD of REV-ERBs (Raghuram et al., 2007; Yin et al., 2007). The discovery of endogenous REV-ERBs ligands led to the identification of chemical scaffolds that can act as synthetic ligands. The first identified synthetic REV-ERB ligand was GSK4112 (Meng et al., 2008). Specifically, GSK4112 is a REV-ERB agonist that enhances recruitment of NCoR and HDAC3 to their target promoters and then represses target gene transcription (Grant et al., 2010). While GSK4112 did not exhibit favorable pharmacokinetics, it paved the way for the subsequent development of synthetic REV-ERBs ligands. To improve potency, efficacy, and pharmacokinetics, Burris and colleagues developed additional REV-ERB agonists, such as SR9009 and SR9011, that were more suitable for *in vivo* applications. Both compounds demonstrated therapeutic efficacy of small molecule REV-ERB modulators in the treatment of circadian-related metabolic diseases and sleep disorders (Solt et al., 2012). Although there are several REV-ERBs agonists,



SR8278 is the only antagonist that has been identified thus far. SR8278 inhibits the transcriptional repression activity of both REV-ERBs, thereby enhancing RRE-mediated transcription (Kojetin et al., 2011). So far, SR8278 applications *in vivo* have been limited; however, it provides a convenient tool to temporally inhibit REV-ERB activity in target cells or tissues.

Cholesterol and some of its metabolites were initially shown to act as natural ROR ligands. Recent studies revealed that several oxysterols are high-affinity endogenous ROR modulators. Oxysterol ligands bind directly to the ROR $\alpha/\gamma$  LBD and act as inverse agonists by modulating the interaction of co-regulators. As indicated by their names, RORs are evolutionarily related to retinoic acid receptors. Interestingly, all-*trans* retinoic acids recognize the LBD of ROR $\beta$ , but not ROR $\alpha/\gamma$ , suggesting subtype specificity. Alternatively, the liver X receptor agonist, T0901317, was the first synthetic ligand and inverse agonist identified for ROR $\alpha/\gamma$  (Kumar et al., 2010). Subsequently, a series of ROR $\alpha/\gamma$  agonists or inverse agonists were developed as reviewed in more detail elsewhere (Kojetin and Burris, 2014). In a more recent study, Chen et al. identified that nobiletin, a natural polymethoxylated flavone, enhances circadian molecular rhythm amplitudes by acting on RORs (He et al., 2016).

## IMPLICATIONS IN CIRCADIAN RHYTHM-RELATED NEUROPSYCHIATRIC DISEASES

Considering the impact of the circadian system on a wide range of biological processes, small-molecule circadian modifiers may be used to optimize internal timing for pharmacological treatment and/or to rescue the desynchrony underlying circadian-related diseases. For example, SR9009/9011 and nobiletin have beneficial effects on high-fat diet-induced metabolic disturbances that affect a wide range of molecular, metabolic, and behavioral rhythms (Kohsaka et al., 2007; Solt et al., 2012; He et al., 2016). Dysregulation of circadian rhythmicity is also associated with various neuropsychiatric disorders, including sleep disorders, affective disorders, substance use disorders, schizophrenia, and neurodegeneration (Jagannath et al., 2013). However, determining whether the changes in brain function associated with these disorders manifest because of circadian dysregulation or additional malfunctions is controversial. Compelling evidence suggests that the effects of circadian disruption on brain function are attributable to both the SCN and local oscillators in discrete brain regions. Here, we will discuss how the circadian clock is involved in neuropsychiatric disorders and the potential implications of clock modulators for those diseases.

### Sleep Disorders

Given that the circadian system constitutes one of the two major mechanistic facets of sleep, small molecule clock modulators may be applicable for circadian rhythm-related sleep disorders. Indeed, abnormal sleep phenotypes have been reported in mutant mice with defective alleles of core clock genes as well as genes mediating post-translational modification of clock proteins (Sehgal and Mignot, 2011). For example, familial advanced

sleep phase syndrome can be caused by either phosphorylation-defective mutations in human *PER2* or by mutant alleles for protein kinases such as CK1 $\delta$  (Toh et al., 2001; Xu et al., 2005). A variation in human *PER3* is also associated with differential sleep homeostasis, particularly after sleep deprivation (Viola et al., 2007). Furthermore, REV-ERBs appear to have a certain role in both homeostatic and circadian regulation of sleep. In mutant mice with a defective allele of *Rev-erba* gene, sleep/wake distributions are advanced in comparison with the environmental light-dark cycle. Moreover, both electroencephalogram delta power and sleep consolidation were also significantly reduced after sleep onset, suggesting a slower increase of homeostatic sleep need during wakefulness in the mutant mice (Mang et al., 2016). Interestingly, daytime administration of REV-ERB agonists induced wakefulness and suppressed both slow-wave and rapid eye movement sleep (Banerjee et al., 2014). Thus, pharmacological manipulation of the circadian clock may be used to treat circadian rhythm-related sleep disorders, such as sleep fragmentation, abnormal sleep phase syndromes, and non-24-h sleep-wake rhythm disorders.

### Mood-Related Psychiatric Disorders

Mood spectrum disorders, including major depression, bipolar disorder, seasonal affective disorder, and various addiction-related diseases, are the most attractive targets for clock modulators. Patients with mood disorders commonly suffer from disrupted sleep/wake cycles and dysregulated diurnal mood variations. Furthermore, several genetics studies have reported significant associations of clock genes with the onset and symptoms of affective disorders (Wulff et al., 2010; McCarthy and Welsh, 2012). Similarly, mutant mice with defective clock genes exhibit behavioral phenotypes linked with abnormal despair, anxiety, and reward responses (McClung et al., 2005; Hampp et al., 2008; Chung et al., 2014; Schnell et al., 2015). The key mediators of circadian mood regulation are central monoamine systems, making them ideal therapeutic targets for affective disorders. These monoamine systems are related to circadian disruption, as mutant mice bearing defective *Clock $\Delta$ 19* demonstrate mania-like behaviors characterized by hyperactivity, as well as decreased depression- and anxiety-related behaviors. They also demonstrate increased cocaine sensitization with enhanced dopamine (DA) transmission (McClung et al., 2005). More recently, our data demonstrating mania-like phenotypes in *Rev-erba*-deficient mice revealed that REV-ERB $\alpha$  connects the molecular clock with the midbrain DA system (Chung et al., 2014). CLOCK and REV-ERB $\alpha$  expression in DA neurons evokes daily variations in DA biosynthesis and transmission in mesocorticolimbic DA circuits, particularly through transcriptional control of tyrosine hydroxylase, a rate-limiting enzyme for catecholamine biosynthesis. Monoamine oxidase-mediated DA clearance in post-synaptic sites is also reported to be under the circadian control of NPAS2 and BMAL1 (Hampp et al., 2008). Taken together, these findings indicate that the circadian clock tightly controls DA biosynthesis, transmission, and turnover.

Interestingly, acute administration of the REV-ERB antagonist, SR8278, to the ventral midbrain produces mania-like behaviors with increased DA production and release (Chung

et al., 2014). While both REV-ERB agonists and antagonists reduce anxiety-like behaviors in mice, REV-ERB agonists do not significantly affect despair-based behaviors (Banerjee et al., 2014; Chung et al., 2014). This discrepancy may arise from the presence of two REV-ERB isoforms that could interact with synthetic ligands. Although SR8278 promotes mania in wild-type mice, it acts as an anti-depressant in a mouse genetic model of depression (Guo et al., 2018). Nobiletin also has anti-depressant-like effects that are comparable with those of fluoxetine. These effects are also prevented by inhibitors for monoamine transmission (Yi et al., 2011). These findings strongly suggest that circadian clock modulators have therapeutic potential for mood-related psychiatric disorders, but also warn of potential risks in their clinical applications to circadian rhythm-related sleep and metabolic diseases.

## Neurodegenerative Diseases

Circadian disruptions are common among patients with neurodegenerative diseases, including Alzheimer's disease (AD), Parkinson's disease (PD), and Huntington's disease, despite the range in pathogenesis and associated symptoms of these diseases (Hood and Amir, 2017). Circadian disturbances manifesting as alterations in sleep-wake cycles, hormone secretion, and diurnal mood regulation precede the cognitive and motor symptoms characteristic of these diseases. Indeed, various forms of AD models have exhibited phenotypes linked with circadian and/or sleep abnormalities (Wisor et al., 2005; Gorman and Yellon, 2010; Sterniczuk et al., 2010; Koss et al., 2016), and neurodegenerative lesions in the SCN have been proposed as a possible underlying mechanism (Sterniczuk et al., 2010; Zhou et al., 2016). Conversely, amyloid-beta ( $A\beta$ ) pathologies are affected by the sleep-wake cycle in both mice and humans (Kang et al., 2009; Ooms et al., 2014). The sleep-wake cycle controls a diurnal rhythm found in  $A\beta$  levels in brain interstitial fluid (ISF) and sleep deprivation exacerbated  $A\beta$  plaque burden in an AD mouse model (Kang et al., 2009). These findings collectively suggest mutual interactions between circadian disturbances and neurodegenerative pathologies.

Considerable evidence suggests that circadian disturbances may play more direct roles in the progression of neurodegenerative diseases, particularly in sporadic disease forms (Musiek and Holtzman, 2016; Videnovic and Willis, 2016). Specifically, genetic variations in clock gene loci are associated with neurodegenerative diseases (Gu et al., 2015). Furthermore, the absence of functional BMAL1 is associated with various phenotypes of premature aging, increased oxidative stress, induced age-dependent gliosis, and neurodegeneration in the presence of neurotoxic assaults (Kondratov et al., 2006; Musiek et al., 2013). Recently, Musiek et al. (2013) demonstrated that loss of central circadian rhythms accelerates amyloid plaque accumulation along with disruption of daily  $A\beta$  oscillations in hippocampal ISF, whereas loss of local BMAL1 in extra-SCN brain regions promotes fibrillar plaque deposition and increased APOE expression, suggesting both central and local brain clock influence AD pathogenesis (Kress et al., 2018). It was also demonstrated that the expression of several AD risk genes, including *Bace1* and *Bace2*, are under the control of cellular clockworks (Ma et al., 2016). In addition

to AD, genetic abrogation of REV-ERB $\alpha$  and chronic circadian disruption were shown to exacerbate neurotoxin-induced PD-like phenotypes and neuroinflammation-mediated DA neuron loss (Lauretti et al., 2017; Kim et al., 2018). Thus, chronic circadian disruption by either environmental or genetic causes is likely a risk factor for sporadic forms of neurodegenerative diseases, and neuroinflammatory dysregulation could be a link between circadian dysfunction and neurodegeneration (Musiek et al., 2013; Lauretti et al., 2017).

These findings also suggest that circadian rhythm-based therapeutics may delay the progression and severity of neurodegenerative diseases. Such chronobiological interventions for neuropsychiatric disorders, such as affective disorders and neurodegeneration, include bright-light therapy and timed melatonin administration (Forbes et al., 2014). Previous studies have suggested that timed light exposure and/or melatonin administration partially improve sleep- and circadian rhythm-related symptoms of AD and PD (Ancoli-Israel et al., 2003; Riemersma-van der Lek et al., 2008; Videnovic et al., 2017). However, whether bright light has long-lasting beneficial effects on cognitive or motor-skill impairments in AD or PD patients remains unclear. Alternatively, these impairments may be treated with small-molecule modulators of clock proteins. Indeed, nobiletin attenuated memory impairments and amyloid pathology in transgenic mouse models of AD (Onozuka et al., 2008; Nakajima et al., 2015) and ameliorated motor and cognitive deficits in MPTP-induced PD mice (Yabuki et al., 2014). Considering that clock proteins have been implicated in cellular antioxidant responses (Lee et al., 2013; Woldt et al., 2013), amelioration of oxidative damage may be an additional potential mechanism by which clock modulators delay neurodegeneration.

## Possible Mode of Actions: Brain Region-Specific and Systemic Mechanisms

Although still in preclinical development, small-molecule modifiers of clock components may exert beneficial effects at multiple levels (Sulli et al., 2018a). The simplest modes of action could involve cellular clock-dependent modulation of transcriptional networks or signaling pathways that are responsible for pathological states due to malfunction. Considering that the cellular clock coordinates diverse cellular pathways, pharmacological manipulation of clock components may have pleiotropic benefits, comparable to combination-therapy approaches. For example, a REV-ERBs antagonist enhanced both DA biosynthesis and activity-dependent neurotransmitter release, which may both contribute to its anti-depressant-like effects (Chung et al., 2014; Guo et al., 2018). In this context, it should be also noted that some molecular targets of established drugs have been identified to follow oscillatory expression or to be directly controlled by the cellular clock. Hogenesch et al. (1998) identified sets of oscillatory genes across multiple tissues in mice. Additionally, they found that more than 20% of the 100 best-selling drugs with short half-lives involved circadian gene targets; these drugs included widely used drugs for neuropsychiatric disorders such as insomnia, depressive disorders, and attention-deficit

hyperactivity disorders (Zhang et al., 2014). These findings imply therapeutic potential of clock modulators that can be also considered for combinational therapy with existing treatments to improve their efficacy.

Systemic restoration or stabilization of the circadian system may also mediate therapeutic effects of clock modulators, plausibly by strengthening the autonomous oscillations of the SCN pacemaker and/or by helping the synchronization between brain clocks. As noted earlier, behavioral interventions to restore circadian rhythm and sleep have been reported to ameliorate some symptoms of affective disorders and neurodegeneration (Forbes et al., 2014; Sulli et al., 2018a). Furthermore, co-morbidities among circadian rhythm-related diseases are frequently found. For example, there is a bi-directional association between metabolic syndromes and mental health disorders including bipolar disorder, major depression, anxiety, attention-deficit hyperactivity disorder, schizophrenia, and autism spectrum disorders (Nousen et al., 2013). Because circadian rhythms coordinate the multiple brain systems responsible for affective, cognitive, and metabolic functions, dysregulation of circadian clocks has been proposed to play a central role in cardio-metabolic co-morbidity in psychiatric disorders (Barandas et al., 2015). It can be, therefore suggested that systemic actions of clock-targeting pharmaceuticals may provide additional distinct preventive or therapeutic strategies for co-morbid disorders.

## CONCLUDING REMARKS

Circadian clocks govern a wide spectrum of biochemical, physiological, and behavioral processes. Disruption or

misalignment of the intrinsic rhythms are considered as a risk for the pathogenesis of various chronic diseases. Therefore, improving our understanding of the impact of the circadian system on brain functions may lead to the development of novel treatment schemes, increase efficacious therapeutic delivery, and improve preventative strategies for circadian rhythm-related brain disorders. In this context, development of chemical clock modulators may primarily contribute to revealing the functional relevance of the molecular clock across discrete brain regions because these small molecules can be used to dynamically control location-specific cellular clocks in the brain. More importantly, these molecules could provide lead structures for novel therapeutics for prevention and treatment of neuropsychiatric disorders.

## AUTHOR CONTRIBUTIONS

All authors listed have made a substantial, direct and intellectual contribution to the work, and approved it for publication.

## FUNDING

This work was supported by the Ministry of Science, the ICT, and the Ministry of Education through the National Research Foundation of Korea (NRF-2015M3A9E7029176 and NRF-2016M3C7A1904340 to GHS, NRF-2014R1A6A3A04054863 to SC). GHS was supported by the Korea University Research Grant.

## REFERENCES

- Ancoli-Israel, S., Gehrman, P., Martin, J. L., Shochat, T., Marler, M., Corey-Bloom, J., et al. (2003). Increased light exposure consolidates sleep and strengthens circadian rhythms in severe Alzheimer's disease patients. *Behav. Sleep Med.* 1, 22–36. doi: 10.1207/S15402010BSM0101-4
- Asher, G., and Schibler, U. (2006). A clock-less clock. *Trends Cell Biol.* 16, 547–549. doi: 10.1016/j.tcb.2006.09.005
- Banerjee, S., Wang, Y., Solt, L. A., Griffett, K., Kazantzis, M., Amador, A., et al. (2014). Pharmacological targeting of the mammalian clock regulates sleep architecture and emotional behaviour. *Nat. Commun.* 5:5759. doi: 10.1038/ncomms6759
- Barandas, R., Landgraf, D., McCarthy, M. J., and Welsh, D. K. (2015). Circadian clocks as modulators of metabolic comorbidity in psychiatric disorders. *Curr. Psychiatry Rep.* 17:98. doi: 10.1007/s11920-015-0637-2
- Bechtold, D. A., Gibbs, J. E., and Loudon, A. S. (2010). Circadian dysfunction in disease. *Trends Pharmacol. Sci.* 31, 191–198. doi: 10.1016/j.tips.2010.01.002
- Billon, C., Sitaula, S., and Burris, T. P. (2016). Inhibition of ROR $\alpha$ / $\gamma$  suppresses atherosclerosis via inhibition of both cholesterol absorption and inflammation. *Mol. Metab.* 5, 997–1005. doi: 10.1016/j.molmet.2016.07.001
- Busino, L., Bassermann, F., Maiolica, A., Lee, C., Nolan, P. M., Godinho, S. I., et al. (2007). SCFFbx13 controls the oscillation of the circadian clock by directing the degradation of cryptochrome proteins. *Science* 316, 900–904. doi: 10.1126/science.1141194
- Chaves, I., Yagita, K., Barnhoorn, S., Okamura, H., van der Horst, G. T., and Tamanini, F. (2006). Functional evolution of the photolyase/cryptochrome protein family importance of the C terminus of mammalian CRY1 for circadian core oscillator performance. *Mol. Cell. Biol.* 26, 1743–1753. doi: 10.1128/MCB.26.5.1743-1753.2006
- Chen, Z., Yoo, S. H., and Takahashi, J. S. (2018). Development and therapeutic potential of small-molecule modulators of circadian systems. *Annu. Rev. Pharmacol. Toxicol.* 58, 231–252. doi: 10.1146/annurev-pharmtox-010617-052645
- Cho, H., Zhao, X., Hatori, M., Yu, R. T., Barish, G. D., Lam, M. T., et al. (2012). Regulation of circadian behaviour and metabolism by REV-ERB- $\alpha$  and REV-ERB- $\beta$ . *Nature* 485, 123–127. doi: 10.1038/nature11030
- Chun, S. K., Chung, S., Kim, H. D., Lee, J. H., Jang, J., Kim, J., et al. (2015). A synthetic cryptochrome inhibitor induces anti-proliferative effects and increases chemosensitivity in human breast cancer cells. *Biochem. Biophys. Res. Commun.* 467, 441–446. doi: 10.1016/j.bbrc.2015.09.103
- Chun, S. K., Jang, J., Chung, S., Yun, H., Kim, N. J., Jung, J. W., et al. (2014). Identification and validation of cryptochrome inhibitors that modulate the molecular circadian clock. *ACS Chem. Biol.* 9, 703–710. doi: 10.1021/cb400752k
- Chung, S., Lee, E. J., Yun, S., Choe, H. K., Park, S. B., Son, H. J., et al. (2014). Impact of circadian nuclear receptor REV-ERB $\alpha$  on midbrain dopamine production and mood regulation. *Cell* 157, 858–868. doi: 10.1016/j.cell.2014.03.039
- Dai, J., Choo, M. K., Park, J. M., and Fisher, D. E. (2017). Topical ROR inverse agonists suppress inflammation in mouse models of atopic dermatitis and acute irritant dermatitis. *J. Invest. Dermatol.* 137, 2523–2531. doi: 10.1016/j.jid.2017.07.819
- Dibner, C., Schibler, U., and Albrecht, U. (2010). The mammalian circadian timing system: organization and coordination of central and peripheral clocks. *Annu. Rev. Physiol.* 72, 517–549. doi: 10.1146/annurev-physiol-021909-135821
- Eide, E. J., Woolf, M. F., Kang, H., Woolf, P., Hurst, W., Camacho, F., et al. (2005). Control of mammalian circadian rhythm by CKIepsilon-regulated



- proteasome-mediated PER2 degradation. *Mol. Cell. Biol.* 25, 2795–2807. doi: 10.1128/MCB.25.7.2795-2807.2005
- Forbes, D., Blake, C. M., Thiessen, E. J., Peacock, S., and Hawranik, P. (2014). Light therapy for improving cognition, activities of daily living, sleep, challenging behaviour and psychiatric disturbances in dementia. *Cochrane Database Syst. Rev.* 26:CD003946. doi: 10.1002/14651858.CD003946.pub4
- Gekakis, N., Staknis, D., Nguyen, H. B., Davis, F. C., Wilsbacher, L. D., King, D. P., et al. (1998). Role of the CLOCK protein in the mammalian circadian mechanism. *Science* 280, 564–569. doi: 10.1126/science.280.5369.1564
- Godinho, S. I., Maywood, E. S., Shaw, L., Tucci, V., Barnard, A. R., Busino, L., et al. (2007). The after-hours mutant reveals a role for Fbxl3 in determining mammalian circadian period. *Science* 316, 897–900. doi: 10.1126/science.1141138
- Gorman, M. R., and Yellon, S. (2010). Lifespan daily locomotor activity rhythms in a mouse model of amyloid-induced neuropathology. *Chronobiol. Int.* 27, 1159–1177. doi: 10.3109/07420528.2010.485711
- Grant, D., Yin, L., Collins, J. L., Parks, D. J., Orband-Miller, L. A., Wisely, G. B., et al. (2010). GSK4112, a small molecule chemical probe for the cell biology of the nuclear heme receptor Rev-erb $\alpha$ . *ACS Chem. Biol.* 5, 925–932. doi: 10.1021/cb100141y
- Gu, Z., Wang, B., Zhang, Y. B., Ding, H., Zhang, Y., Yu, J., et al. (2015). Association of ARNTL and PER1 genes with Parkinson's disease: a case-control study of han chinese. *Sci. Rep.* 5:15891. doi: 10.1038/srep15891
- Guo, D., Zhang, S., Sun, H., Xu, X., Hao, Z., Mu, C., et al. (2018). Tyrosine hydroxylase down-regulation after loss of Abelson helper integration site 1 (AHI1) promotes depression via the circadian clock pathway in mice. *J. Biol. Chem.* 293, 5090–5101. doi: 10.1074/jbc.RA117.000618
- Hamp, G., Ripperger, J. A., Houben, T., Schmutz, I., Blex, C., Perreau-Lenz, S., et al. (2008). Regulation of monoamine oxidase A by circadian-clock components implies clock influence on mood. *Curr. Biol.* 18, 678–683. doi: 10.1016/j.cub.2008.04.012
- He, B., and Chen, Z. (2016). Molecular targets for small-molecule modulators of circadian clocks. *Curr. Drug Metab.* 17, 503–512. doi: 10.2174/138920021766616011124439
- He, B., Nohara, K., Park, N., Park, Y. S., Guillory, B., Zhao, Z., et al. (2016). The small molecule nobletin targets the molecular oscillator to enhance circadian rhythms and protect against metabolic syndrome. *Cell Metab.* 23, 610–621. doi: 10.1016/j.cmet.2016.03.007
- Hirano, A., Yumimoto, K., Tsunematsu, R., Matsumoto, M., Oyama, M., Kozuka-Hata, H., et al. (2013). FBXL21 regulates oscillation of the circadian clock through ubiquitination and stabilization of cryptochromes. *Cell* 152, 1106–1118. doi: 10.1016/j.cell.2013.01.054
- Hirota, T., Lee, J. W., St. John, P. C., Sawa, M., Iwaisako, K., Noguchi, T., et al. (2012). Identification of small molecule activators of cryptochrome. *Science* 337, 1094–1097. doi: 10.1126/science.1223710
- Hirota, T., Lewis, W. G., Liu, A. C., Lee, J. W., Schultz, P. G., and Kay, S. A. (2008). A chemical biology approach reveals period shortening of the mammalian circadian clock by specific inhibition of GSK-3 $\beta$ . *Proc. Natl. Acad. Sci. U.S.A.* 105, 20746–20751. doi: 10.1073/pnas.0811410106
- Hogenesch, J. B., Gu, Y. Z., Jain, S., and Bradfield, C. A. (1998). The basic-helix-loop-helix-PAS orphan MOP3 forms transcriptionally active complexes with circadian and hypoxia factors. *Proc. Natl. Acad. Sci. U.S.A.* 95, 5474–5479. doi: 10.1073/pnas.95.10.5474
- Honma, S., Kawamoto, T., Takagi, Y., Fujimoto, K., Sato, F., Noshiro, M., et al. (2002). Dec1 and Dec2 are regulators of the mammalian molecular clock. *Nature* 419, 841–844. doi: 10.1038/nature01123
- Hood, S., and Amir, S. (2017). Neurodegeneration and the circadian clock. *Front. Aging Neurosci.* 9:170. doi: 10.3389/fnagi.2017.00170
- Jagannath, A., Peirson, S. N., and Foster, R. G. (2013). Sleep and circadian rhythm disruption in neuropsychiatric illness. *Curr. Opin. Neurobiol.* 23, 888–894. doi: 10.1016/j.conb.2013.03.008
- Jang, J., Chung, S., Choi, Y., Lim, H. Y., Son, Y., Chun, S. K., et al. (2018). The cryptochrome inhibitor KS15 enhances E-box-mediated transcription by disrupting the feedback action of a circadian transcription-repressor complex. *Life Sci.* 200, 49–55. doi: 10.1016/j.lfs.2018.03.022
- Kang, J. E., Lim, M. M., Bateman, R. J., Lee, J. J., Smyth, L. P., Cirrito, J. R., et al. (2009). Amyloid-beta dynamics are regulated by orexin and the sleep-wake cycle. *Science* 326, 1005–1007. doi: 10.1126/science.1180962
- Kim, J., Jang, S., Choi, M., Chung, S., Choe, Y., Choe, H. K., et al. (2018). Abrogation of the circadian nuclear receptor REV-ERB $\alpha$  exacerbates 6-hydroxydopamine-induced dopaminergic neurodegeneration. *Mol. Cells* 41, 742–752. doi: 10.14348/molcells.2018.0201
- Kohsaka, A., Laposky, A. D., Ramsey, K. M., Estrada, C., Joshu, C., Kobayashi, Y., et al. (2007). High-fat diet disrupts behavioral and molecular circadian rhythms in mice. *Cell Metab.* 6, 414–421. doi: 10.1016/j.cmet.2007.09.006
- Kojetin, D., Wang, Y., Kamenecka, T. M., and Burris, T. P. (2011). Identification of SR8278, a synthetic antagonist of the nuclear heme receptor REV-ERB. *ACS Chem. Biol.* 6, 131–134. doi: 10.1021/cb1002575
- Kojetin, D. J., and Burris, T. P. (2014). REV-ERB and ROR nuclear receptors as drug targets. *Nat. Rev. Drug Discov.* 13, 197–216. doi: 10.1038/nrd4100
- Kondratov, R. V., Kondratova, A. A., Gorbacheva, V. Y., Vykhovanets, O. V., and Antoch, M. P. (2006). Early aging and age-related pathologies in mice deficient in BMAL1, the core component of the circadian clock. *Genes Dev.* 20, 1868–1873. doi: 10.1101/gad.1432206
- Koss, D. J., Robinson, L., Drever, B. D., Plucińska, K., Stoppelkamp, S., Veselcic, P., et al. (2016). Mutant Tau knock-in mice display frontotemporal dementia relevant behaviour and histopathology. *Neurobiol. Dis.* 91, 105–123. doi: 10.1016/j.nbd.2016.03.002
- Kress, G. J., Liao, F., Dimitry, J., Cedeno, M. R., FitzGerald, G. A., Holtzman, D. M., et al. (2018). Regulation of amyloid- $\beta$  dynamics and pathology by the circadian clock. *J. Exp. Med.* 215, 1059–1068. doi: 10.1084/jem.20172347
- Kumar, N., Solt, L. A., Konkright, J. J., Wang, Y., Istrate, M. A., Busby, S. A., et al. (2010). The benzenesulfoamide T0901317 [N-(2,2,2-trifluoroethyl)-N-[4-[2,2,2-trifluoro-1-hydroxy-1-(trifluoromethyl)ethyl]phenyl]-benzenesulfonamide] is a novel retinoic acid receptor-related orphan receptor- $\alpha$ /gamma inverse agonist. *Mol. Pharmacol.* 77, 228–236. doi: 10.1124/mol.109.060905
- Kume, K., Zylka, M. J., Sriram, S., Shearman, L. P., Weaver, D. R., Jin, X., et al. (1999). mCRY1 and mCRY2 are essential components of the negative limb of the circadian clock feedback loop. *Cell* 98, 193–205. doi: 10.1016/S0092-8674(00)81014-4
- Kurabayashi, N., Hirota, T., Sakai, M., Sanada, K., and Fukada, Y. (2010). DYRK1A and glycogen synthase kinase 3 $\beta$ , a dual-kinase mechanism directing proteasomal degradation of CRY2 for circadian timekeeping. *Mol. Cell. Biol.* 30, 1757–1768. doi: 10.1128/MCB.01047-09
- Lamia, K. A., Sachdeva, U. M., DiTacchio, L., Williams, E. C., Alvarez, J. G., Egan, D. F., et al. (2009). AMPK regulates the circadian clock by cryptochrome phosphorylation and degradation. *Science* 326, 437–440. doi: 10.1126/science.1172156
- Lauretti, E., Di Meco, A., Merali, S., and Praticò, D. (2017). Circadian rhythm dysfunction: a novel environmental risk factor for Parkinson's disease. *Mol. Psychiatry* 22, 280–286. doi: 10.1038/mp.2016.47
- Lee, J., Moulik, M., Fang, Z., Saha, P., Zou, F., Xu, Y., et al. (2013). Bmal1 and  $\beta$ -cell clock are required for adaptation to circadian disruption and their loss of function leads to oxidative stress-induced  $\beta$ -cell failure in mice. *Mol. Cell. Biol.* 33, 2327–2338. doi: 10.1128/MCB.014210-12
- Li, J., Lu, W. Q., Beesley, S., Loudon, A. S., and Meng, Q. J. (2012). Lithium impacts on the amplitude and period of the molecular circadian clockwork. *PLoS One* 7:e33292. doi: 10.1371/journal.pone.0033292
- Ma, Z., Jiang, W., and Zhang, E. E. (2016). Orexin signaling regulates both the hippocampal clock and the circadian oscillation of Alzheimer's disease-risk genes. *Sci. Rep.* 6:36035. doi: 10.1038/srep36035
- Mang, G. M., La Spada, F., Emmenegger, Y., Chappuis, S., Ripperger, J. A., Albrecht, U., et al. (2016). Altered sleep homeostasis in rev-erb $\alpha$  knockout mice. *Sleep* 39, 589–601. doi: 10.5665/sleep.5534
- McCarthy, M. J., and Welsh, D. K. (2012). Cellular circadian clocks in mood disorders. *J. Biol. Rhythms* 27, 339–352. doi: 10.1177/0748730412456367
- McClung, C. A., Sidiropoulou, K., Vitaterna, M., Takahashi, J. S., White, F. J., Cooper, D. C., et al. (2005). Regulation of dopaminergic transmission and cocaine reward by the Clock gene. *Proc. Natl. Acad. Sci. U.S.A.* 102, 9377–9381. doi: 10.1073/pnas.0503584102
- Meng, Q. J., McMaster, A., Beesley, S., Lu, W. Q., Gibbs, J., Parks, D., et al. (2008). Ligand modulation of REV-ERB $\alpha$  function resets the peripheral circadian clock in a phasic manner. *J. Cell. Sci.* 121, 3629–3635. doi: 10.1242/jcs.035048
- Mitsui, S., Yamaguchi, S., Matsuo, T., Ishida, Y., and Okamura, H. (2001). Antagonistic role of E4BP4 and PAR proteins in the circadian



- oscillatory mechanism. *Genes Dev.* 15, 995–1006. doi: 10.1101/gad.873501
- Musiek, E. S., and Holtzman, D. M. (2016). Mechanisms linking circadian clocks, sleep, and neurodegeneration. *Science* 354, 1004–1008. doi: 10.1126/science.aah4968
- Musiek, E. S., Lim, M. M., Yang, G., Bauer, A. Q., Qi, L., Lee, Y., et al. (2013). Circadian clock proteins regulate neuronal redox homeostasis and neurodegeneration. *J. Clin. Invest.* 123, 5389–5400. doi: 10.1172/JCI70317
- Nakajima, A., Aoyama, Y., Shin, E.-J., Nam, Y., Kim, H.-C., Nagai, T., et al. (2015). Nobiletin, a citrus flavonoid, improves cognitive impairment and reduces soluble A $\beta$  levels in a triple transgenic mouse model of Alzheimer's disease. *Behav. Brain Res.* 289, 69–77. doi: 10.1016/j.bbr.2015.04.028
- Nangle, S., Xing, W., and Zheng, N. (2013). Crystal structure of mammalian cryptochrome in complex with a small molecule competitor of its ubiquitin ligase. *Cell Res.* 23, 1417–1419. doi: 10.1038/cr.2013.136
- Nousen, E. K., Franco, J. G., and Sullivan, E. L. (2013). Unraveling the mechanisms responsible for the comorbidity between metabolic syndrome and mental health disorders. *Neuroendocrinology* 98, 254–266. doi: 10.1159/000355632
- Onozuka, H., Nakajima, A., Matsuzaki, K., Shin, R.-W., Ogino, K., Saigusa, D., et al. (2008). Nobiletin, a citrus flavonoid, improves memory impairment and A $\beta$  pathology in a transgenic mouse model of Alzheimer's disease. *J. Pharmacol. Exp. Ther.* 326, 739–744. doi: 10.1124/jpet.108.140293
- Ooms, S., Overeem, S., Besse, K., Rikkert, M. O., Verbeek, M., and Claassen, J. A. (2014). Effect of 1 night of total sleep deprivation on cerebrospinal fluid  $\beta$ -amyloid 42 in healthy middle-aged men: a randomized clinical trial. *JAMA Neurol.* 71, 971–977. doi: 10.1001/jamaneurol.2014.1173
- Preitner, N., Damiola, F., Lopez-Molina, L., Zakany, J., Duboule, D., Albrecht, U., et al. (2002). The orphan nuclear receptor REV-ERB $\alpha$  controls circadian transcription within the positive limb of the mammalian circadian oscillator. *Cell* 110, 251–260. doi: 10.1016/S0092-8674(02)00825-5
- Raghuram, S., Stayrook, K. R., Huang, P., Rogers, P. M., Nosie, A. K., McClure, D. B., et al. (2007). Identification of heme as the ligand for the orphan nuclear receptors REV-ERB $\alpha$  and REV-ERB $\beta$ . *Nat. Struct. Mol. Biol.* 14, 1207–1213. doi: 10.1038/nsmb1344
- Ralph, M. R., Foster, R. G., Davis, F. C., and Menaker, M. (1990). Transplanted suprachiasmatic nucleus determines circadian period. *Science* 247, 975–978. doi: 10.1126/science.2305266
- Ralph, M. R., and Menaker, M. (1988). A mutation of the circadian system in golden hamsters. *Science* 241, 1225–1227. doi: 10.1126/science.3413487
- Reppert, S. M., and Weaver, D. R. (2002). Coordination of circadian timing in mammals. *Nature* 418, 935–941. doi: 10.1038/nature00965
- Riemersma-van der Lek, R. F., Swaab, D. F., Twisk, J., Hol, E. M., Hoogendijk, W. J., and Van Someren, E. J. (2008). Effect of bright light and melatonin on cognitive and noncognitive function in elderly residents of group care facilities: a randomized controlled trial. *JAMA* 299, 2642–2655. doi: 10.1001/jama.299.22.2642
- Sato, T. K., Panda, S., Miraglia, L. J., Reyes, T. M., Rudic, R. D., McNamara, P., et al. (2004). A functional genomics strategy reveals Rora as a component of the mammalian circadian clock. *Neuron* 43, 527–537. doi: 10.1016/j.neuron.2004.07.018
- Schnell, A., Sandrelli, F., Ranc, V., Ripperger, J. A., Brai, E., Alberi, L., et al. (2015). Mice lacking circadian clock components display different mood-related behaviors and do not respond uniformly to chronic lithium treatment. *Chronobiol. Int.* 32, 1075–1089. doi: 10.3109/07420528.2015.1062024
- Schroeder, A. M., and Colwell, C. S. (2013). How to fix a broken clock. *Trends Pharmacol. Sci.* 34, 605–619. doi: 10.1016/j.tips.2013.09.002
- Sehgal, A., and Mignot, E. (2011). Genetics of sleep and sleep disorders. *Cell* 146, 194–207. doi: 10.1016/j.cell.2011.07.004
- Shearman, L. P., Sriram, S., Weaver, D. R., Maywood, E. S., Chaves, I., Zheng, B., et al. (2000). Interacting molecular loops in the mammalian circadian clock. *Science* 288, 1013–1019. doi: 10.1126/science.288.5468.1013
- Shirogane, T., Jin, J., Ang, X. L., and Harper, J. W. (2005). SCF $\beta$ -TRCP controls clock-dependent transcription via casein kinase 1-dependent degradation of the mammalian period-1 (Per1) protein. *J. Biol. Chem.* 280, 26863–26872. doi: 10.1074/jbc.M502862200
- Siepkka, S. M., Yoo, S. H., Park, J., Song, W., Kumar, V., Hu, Y., et al. (2007). Circadian mutant overtime reveals F-box protein FBXL3 regulation of cryptochrome and period gene expression. *Cell* 129, 1011–1023. doi: 10.1016/j.cell.2007.04.030
- Solt, L. A., Kumar, N., Nuhant, P., Wang, Y., Lauer, J. L., Liu, J., et al. (2011). Suppression of TH17 differentiation and autoimmunity by a synthetic ROR ligand. *Nature* 472, 491–494. doi: 10.1038/nature10075
- Solt, L. A., Wang, Y., Banerjee, S., Hughes, T., Kojetin, D. J., Lundasen, T., et al. (2012). Regulation of circadian behaviour and metabolism by synthetic REV-ERB agonists. *Nature* 485, 62–68. doi: 10.1038/nature11030
- Son, G. H., Chung, S., and Kim, K. (2011). The adrenal peripheral clock: glucocorticoid and the circadian timing system. *Front. Neuroendocrinol.* 32, 451–465. doi: 10.1016/j.yfrne.2011.07.003
- Sterniczuk, R., Dyck, R. H., Laferla, F. M., and Antle, M. C. (2010). Characterization of the 3xTg-AD mouse model of Alzheimer's disease: part 1. circadian changes. *Brain Res.* 1348, 139–148. doi: 10.1016/j.brainres.2010.05.013
- Sulli, G., Manoogian, E. N. C., Taub, P. R., and Panda, S. (2018a). Training the circadian clock, clocking the drugs, and drugging the clock to prevent, manage, and treat chronic diseases. *Trends Pharmacol. Sci.* 39, 812–827. doi: 10.1016/j.tips.2018.07.003
- Sulli, G., Rommel, A., Wang, X., Kolar, M. J., Puca, F., Saghatelian, A., et al. (2018b). Pharmacological activation of REV-ERBs is lethal in cancer and oncogene-induced senescence. *Nature* 553, 351–355. doi: 10.1038/nature25170
- Takahashi, J. S., Hong, H. K., Ko, C. H., and McDearmon, E. L. (2008). The genetics of mammalian circadian order and disorder: implications for physiology and disease. *Nat. Rev. Genet.* 9, 764–775. doi: 10.1038/nrg2430
- Toh, K. L., Jones, C. R., He, Y., Eide, E. J., Hinz, W. A., Virshup, D. M., et al. (2001). An hPer2 phosphorylation site mutation in familial advanced sleep phase syndrome. *Science* 291, 1040–1043. doi: 10.1126/science.1057499
- Ueda, H. R., Chen, W., Adachi, A., Wakamatsu, H., Hayashi, S., Takasugi, T., et al. (2002). A transcription factor response element for gene expression during circadian night. *Nature* 418, 534–539. doi: 10.1038/nature00906
- Um, J. H., Yang, S., Yamazaki, S., Kang, H., Viollet, B., Foretz, M., et al. (2007). Activation of 5'-AMP-activated kinase with diabetes drug metformin induces casein kinase Iepsilon (CKIepsilon)-dependent degradation of clock protein mPer2. *J. Biol. Chem.* 282, 20794–20798. doi: 10.1074/jbc.C700070200
- van der Schalie, E. A., Conte, F. E., Marz, K. E., and Green, C. B. (2007). Structure/function analysis of xenopus cryptochromes 1 and 2 reveals differential nuclear localization mechanisms and functional domains important for interaction with and repression of CLOCK/BMAL1. *Mol. Cell. Biol.* 27, 2120–2129. doi: 10.1128/MCB.01638-06
- Videnovic, A., Klerman, E. B., Wang, W., Marconi, A., Kuhta, T., and Zee, P. C. (2017). Timed light therapy for sleep and daytime sleepiness associated with Parkinson disease: a randomized clinical trial. *JAMA Neurol.* 74, 411–418. doi: 10.1001/jamaneurol.2016.5192
- Videnovic, A., and Willis, G. L. (2016). Circadian system - a novel diagnostic and therapeutic target in Parkinson's disease? *Mov. Disord.* 31, 260–269. doi: 10.1002/mds.26509
- Viola, A. U., Archer, S. N., James, L. M., Groeger, J. A., Lo, J. C., Skene, D. J., et al. (2007). PER3 polymorphism predicts sleep structure and waking performance. *Curr. Biol.* 17, 613–618. doi: 10.1016/j.cub.2007.01.073
- Wang, Y., Billon, C., Walker, J. K., and Burris, T. P. (2016). Therapeutic effect of a synthetic ROR $\alpha$ / $\gamma$  agonist in an animal model of autism. *ACS Chem. Neurosci.* 7, 143–148. doi: 10.1021/acschemneuro.5b00159
- Wang, Y., Kumar, N., Nuhant, P., Cameron, M. D., Istrate, M. A., Roush, W. R., et al. (2010). Identification of SR1078, a synthetic agonist for the orphan nuclear receptors ROR $\alpha$  and ROR $\gamma$ . *ACS Chem. Biol.* 5, 1029–1034. doi: 10.1021/cb100223d
- Wisor, J. P., Edgar, D. M., Yesavage, J., Ryan, H. S., McCormick, C. M., Lapustea, N., et al. (2005). Sleep and circadian abnormalities in a transgenic mouse model of Alzheimer's disease: a role for cholinergic transmission. *Neuroscience* 131, 375–385. doi: 10.1016/j.neuroscience.2004.11.018
- Woldt, E., Sebt, Y., Solt, L. A., Duhem, C., Lancel, S., Eeckhoutte, J., et al. (2013). Rev-erb- $\alpha$  modulates skeletal muscle oxidative capacity by regulating mitochondrial biogenesis and autophagy. *Nat. Med.* 19, 1039–1046. doi: 10.1038/nm.3213
- Wulff, K., Gatti, S., Wettstein, J. G., and Foster, R. G. (2010). Sleep and circadian rhythm disruption in psychiatric and neurodegenerative disease. *Nat. Rev. Neurosci.* 11, 589–599. doi: 10.1038/nrn2868

- Xing, W., Busino, L., Hinds, T. R., Marionni, S. T., Saifee, N. H., Bush, M. F., et al. (2013). SCF(FBXL3) ubiquitin ligase targets cryptochromes at their cofactor pocket. *Nature* 496, 64–68. doi: 10.1038/nature11964
- Xu, Y., Padiath, Q. S., Shapiro, R. E., Jones, C. R., Wu, S. C., Saigoh, N., et al. (2005). Functional consequences of a CK1delta mutation causing familial advanced sleep phase syndrome. *Nature* 434, 640–644. doi: 10.1038/nature03453
- Yabuki, Y., Ohizumi, Y., Yokosuka, A., Mimaki, Y., and Fukunaga, K. (2014). Nobiletin treatment improves motor and cognitive deficits seen in MPTP-induced Parkinson model mice. *Neuroscience* 259, 126–141. doi: 10.1016/j.neuroscience.2013.11.051
- Yi, L. T., Xu, H. L., Feng, J., Zhan, X., Zhou, L. P., and Cui, C. C. (2011). Involvement of monoaminergic systems in the antidepressant-like effect of nobiletin. *Physiol. Behav.* 102, 1–6. doi: 10.1016/j.physbeh.2010.10.008
- Yin, L., Wu, N., Curtin, J. C., Qatanani, M., Szwergold, N. R., Reid, R. A., et al. (2007). Rev-erbalpha, a heme sensor that coordinates metabolic and circadian pathways. *Science* 318, 1786–1789. doi: 10.1126/science.1150179
- Yoo, S. H., Mohawk, J. A., Siepka, S. M., Shan, Y., Huh, S. K., Hong, H. K., et al. (2013). Competing E3 ubiquitin ligases govern circadian periodicity by degradation of CRY in nucleus and cytoplasm. *Cell* 152, 1091–1105. doi: 10.1016/j.cell.2013.01.055
- Zhang, R., Lahens, N. F., Balance, H. I., Hughes, M. E., and Hogenesch, J. B. (2014). A circadian gene expression atlas in mammals: implications for biology and medicine. *Proc. Natl. Acad. Sci. U.S.A.* 111, 16219–16224. doi: 10.1073/pnas.1408886111
- Zhang, Y., Fang, B., Emmett, M. J., Damle, M., Sun, Z., Feng, D., et al. (2015). Discrete functions of nuclear receptor Rev-erb $\alpha$  couple metabolism to the clock. *Science* 348, 1488–1492. doi: 10.1126/science.aab3021
- Zhao, Y., Xu, L., Ding, S., Lin, N., Ji, Q., Gao, L., et al. (2017). Novel protective role of the circadian nuclear receptor retinoic acid-related orphan receptor- $\alpha$  in diabetic cardiomyopathy. *J. Pineal Res.* 62:e12378. doi: 10.1111/jpi.12378
- Zhou, L., Gao, Q., Nie, M., Gu, J. L., Hao, W., Wang, L., et al. (2016). Degeneration and energy shortage in the suprachiasmatic nucleus underlies the circadian rhythm disturbance in ApoE $^{-/-}$  mice: implications for Alzheimer's disease. *Sci. Rep.* 6:36335. doi: 10.1038/srep36335

**Conflict of Interest Statement:** The authors declare that the research was conducted in the absence of any commercial or financial relationships that could be construed as a potential conflict of interest.

Copyright © 2019 Cha, Chung, Lim, Jung and Son. This is an open-access article distributed under the terms of the Creative Commons Attribution License (CC BY). The use, distribution or reproduction in other forums is permitted, provided the original author(s) and the copyright owner(s) are credited and that the original publication in this journal is cited, in accordance with accepted academic practice. No use, distribution or reproduction is permitted which does not comply with these terms.



# Connexin Hemichannels in Astrocytes: Role in CNS Disorders

LingYan Xing<sup>1†</sup>, Tuo Yang<sup>2†</sup>, ShuSen Cui<sup>2\*</sup> and Gang Chen<sup>1,3\*</sup>

<sup>1</sup> Key Laboratory of Neuroregeneration of Jiangsu and Ministry of Education, Co-innovation Center of Neuroregeneration, Nantong University, Nantong, China, <sup>2</sup> Department of Hand Surgery, China-Japan Union Hospital of Jilin University, Changchun, China, <sup>3</sup> Department of Anesthesiology, Affiliated Hospital of Nantong University, Nantong, China

In the central nervous system (CNS), astrocytes form networks interconnected by gap junctions made from connexins of the subtypes Cx30 and Cx43. When unopposed by an adjoining hemichannel, astrocytic connexins can act as hemichannels to control the release of small molecules such as ATP and glutamate into the extracellular space. Accumulating evidence indicates that astrocytic connexins are crucial for the coordination and maintenance of physiologic CNS activity. Here we provide an update on the role of astrocytic connexins in neurodegenerative disorders, glioma, and ischemia. In addition, we address the regulation of Cx43 in chronic pain.

**Keywords:** astrocyte, connexin 43, Alzheimer's disease, glioma, ischemia, neuropathic pain

## OPEN ACCESS

### Edited by:

Michele Papa,  
Università degli Studi della Campania  
Luigi Vanvitelli Caserta, Italy

### Reviewed by:

Fabrizio Michetti,  
Catholic University of Sacred Heart,  
Italy

Won-Suk Chung,

Korea Advanced Institute of Science  
& Technology (KAIST), South Korea

### \*Correspondence:

ShuSen Cui  
cuiss@jlu.edu.cn  
Gang Chen  
chengang6626@ntu.edu.cn

<sup>†</sup>These authors have contributed  
equally to this work

**Received:** 24 October 2018

**Accepted:** 21 January 2019

**Published:** 06 February 2019

### Citation:

Xing L, Yang T, Cui S and Chen G  
(2019) Connexin Hemichannels  
in Astrocytes: Role in CNS Disorders.  
*Front. Mol. Neurosci.* 12:23.  
doi: 10.3389/fnmol.2019.00023

## INTRODUCTION

As the most abundant cells in the central nervous system, astrocytes are critical for synaptic transmission and homeostasis maintenance. Astrocyte dysfunction has been associated with many neurological disorders, including but not limited to neurodegenerative diseases, gliomas, and ischemia (Verkhratsky et al., 2010; Yang et al., 2013; Hirayama and Koizumi, 2018). Over the last two decades, accumulating evidence has shown that astrocytes are also key mediators in pain development and maintenance (Ji et al., 2013).

Astrocytes in the CNS form a highly interconnected network via gap junctions or hemichannels. Each connexin hemichannel consists of six protein subunits termed connexins, which belong to a protein family encoded by 20–21 genes in mammals (Scott et al., 2012). An individual subunit possesses four alpha-helical transmembrane domains, connected by two extracellular loops and one intracellular loop, with cytoplasmic carboxyl and amine terminals (Bennett et al., 2016). When one hemichannel docks to its counterpart on the apposed cells, a gap junction is formed. Gap junctions of astrocytes allow rapid intercellular exchange of ions and metabolites, which is critical for K<sup>+</sup> and glutamate buffering, calcium wave propagation, and synaptic plasticity (Li et al., 2014; Lapato and Tiwari-Woodruff, 2018). Unpaired connexins can act as hemichannels, which are responsible for the release of gliotransmitters, including ATP, glutamate, nicotinamide adenine dinucleotide (NAD), and D-serine to the extracellular milieu (Saez et al., 2003; Retamal et al., 2014). This offers a new exchange route between neurons and glia.

Accruing evidence suggests that connexin hemichannels can open at both physiological and pathological conditions (Saez et al., 2003). The opening of hemichannels is highly dynamic and can be controlled by multiple regulators. Lower or higher intercellular Ca<sup>2+</sup> can increase the opening probability of hemichannels (Decrock et al., 2011). In addition, pathological conditions, such as oxidative stress, lower pH, mechanical stimulation, and inflammation can significantly enhance the hemichannel opening (Johansen et al., 2011; Batra et al., 2014; Castellano and Eugenin, 2014;

Retamal et al., 2015). The uncontrolled opening of hemichannels can lead to cell damage and homeostatic imbalance (Orellana, 2016). It is accepted that excessive release of ATP and glutamate or overload of intracellular free  $\text{Ca}^{2+}$  are toxic to neighboring cells or trigger secondary damages to distant cells (Takeuchi et al., 2006; Orellana et al., 2011). Of note, dysregulation of hemichannels permeability can also induce excessive influx of  $\text{Na}^+$  and  $\text{Cl}^-$ , leading to osmotic and ionic imbalance (Orellana et al., 2016). In astrocytes, the predominant connexins are connexin 43 (Cx43), though Cx26 and Cx30 are also detectable (Rash et al., 2001a,b). This review will focus on the role of astrocytic Cx43 in the regulation of CNS disorders (Table 1, Figure 1). Furthermore, we also discuss an emerging role of astrocyte Cx43 in chronic pain (Table 2).

## Cx43 IN NEURODEGENERATIVE DISEASES

Alzheimer's disease (AD), a representative CNS neurodegenerative disease characterized by plaques and tangles in the brain (Ballard et al., 2011), is the leading cause of dementia worldwide. Until recently, the role of astrocytes in AD has been appreciated, though astrocytic modification was discovered in AD decades ago (Nagy et al., 1996; Rodríguez et al., 2009; Verkhratsky et al., 2010). Astroglial and  $\beta$ -amyloid ( $\text{A}\beta$ ) plaque, two prominent pathologic features of AD, are both highly associated with astrocytic connexins, which offer a novel pathological mechanism and a potential therapeutic target for AD (Yi et al., 2017b). Altered expression of astrocytic connexins have been observed in the brains of both AD patients and mice (Nagy et al., 1996; Mei et al., 2010), though the mechanisms by which connexins expression is changed, remain controversial. For example, the expression of Cx43 in astrocytic gap junctions of AD patients is upregulated in the cortical regions with  $\text{A}\beta$  plaques, and some plaques corresponded exactly to the potentiated Cx43 immunoreactive sites (Nagy et al., 1996). In older APP/PS1 mice, a murine model of familial AD, an increase of Cx43 and Cx30 immunoreactivity was found in 60–70%  $\text{A}\beta$  plaques of reactive astrocytes. However, a decrease in the expression of Cx43 and Cx30 was also found in a few newly formed plaques (<10%) (Mei et al., 2010). This discrepancy indicates that the alteration of Cx43 expression in AD depends on the amyloid pathology and local inflammatory status of the plaque sites (Koulakoff et al., 2012). The increase in Cx43 expression promotes astroglial activation and further alters astroglial channel function and the pathologic process of AD.

Studies have been performed to investigate the role of Cx43 in AD, either as gap junction channels or hemichannels. Interestingly, the reactive astroglial does not affect astroglial gap junctional communication in APP/PS1 mice (Yi et al., 2017b). Hemichannels in astrocytes, however, can be activated during the pathologic process of AD and are critical for the neuronal damage (Orellana et al., 2011). The activated hemichannels increase the release of ATP and glutamate from astrocytes around the amyloid plaques, leading to overload of neuronal  $\text{Ca}^{2+}$ , synaptic depression (Pascual, 2005), and final

neuronal damage (Yi et al., 2016). Neuronal damages in the process could be alleviated by Cx43 hemichannel blocker boldine or cannabinoids (Gajardo-Gómez et al., 2017; Yi et al., 2017a). In addition, in APP/PS1 mice, a specific deletion of astroglial Cx43 could significantly reduce astroglial and increase synapse numbers, though it had no effects on amyloid plaque formation or inflammatory response (Ren et al., 2018). These results indicate that Cx43 could be a novel therapeutic target for AD.

As the second most common chronic neurodegenerative disorder in the CNS, Parkinson's disease (PD) possesses reactive astrocytes in the substantia nigra (Fernandez, 2012; Cabezas et al., 2014). Rotenone is a common neurotoxic substance used for generating PD experimental models. In both rotenone-treated rats and *in vitro* astrocytes, levels of both total Cx43 and phosphorylated Cx43 were elevated (Wang Y. et al., 2013). Additionally, gatrodin from a Chinese herbal medicine can ameliorate PD by downregulating Cx43 (Wang Y. et al., 2013). Cx43 expression was also found upregulated in patients with amyotrophic lateral sclerosis (ALS) or related models (Almad et al., 2016). This upregulated Cx43 expression led to elevated hemichannel activity, enhanced gap junction coupling and increased intracellular  $\text{Ca}^{2+}$  concentration, which contributed to motor neuron toxicity. Furthermore, it was conferred that Cx43 blocker or Cx43 hemichannel blocker provided protection against this neuron toxicity (Almad et al., 2016).

Overall, the role of astrocytes as well as astrocytic connexins has attracted more attention in the field of neurodegenerative diseases in recent years, due to their critical role in gliosis, inflammation, and neuronal damage (Freitas-Andrade and Naus, 2016). Here we pose several questions and perspectives for further study. First, in-depth studies may be needed to apply and clarify the targets of these interventions, for example, R76W mutant which specifically block gap junction channels (Xu et al., 2015), Gap19 (a specific Cx43 hemichannel blocker) (Wang N. et al., 2013) and non-selective peptides. Second, the discrepancy of Cx43 immunoreactivity in neurodegenerative diseases was found in a previous study (Mei et al., 2010), which may lead us to test how Cx43 works in a time-dependent manner.

## Cx43 IN GLIOMA

Glioblastoma (GBM), a representative type of malignant glioma, is the most common and aggressive CNS malignant tumor (Sontheimer, 2015). Both the expression changes of Cx43 and its role in glioma progression are controversial, which may be attribute to high heterogeneity of this tumor (Sin et al., 2012). The expression of Cx43 varies with grades, stages, and locations of tumors. For example, Cx43 generally exhibits a lower expression in the tumor core within high-grade gliomas compared with low-grade ones (Sin et al., 2016). As a conventional therapeutic strategy, surgical resection supplemented with chemotherapy and radiotherapy confers a poor prognosis in patients with gliomas (Stupp et al., 2005). This poor prognosis is mainly caused by the resistance to the chemotherapeutic alkylating agents such as temozolomide (TMZ), and the invasive nature of the tumor cells (Sin et al., 2012, 2016; Wang et al., 2018).



**TABLE 1** | Cx43 in the regulation of CNS disorders.

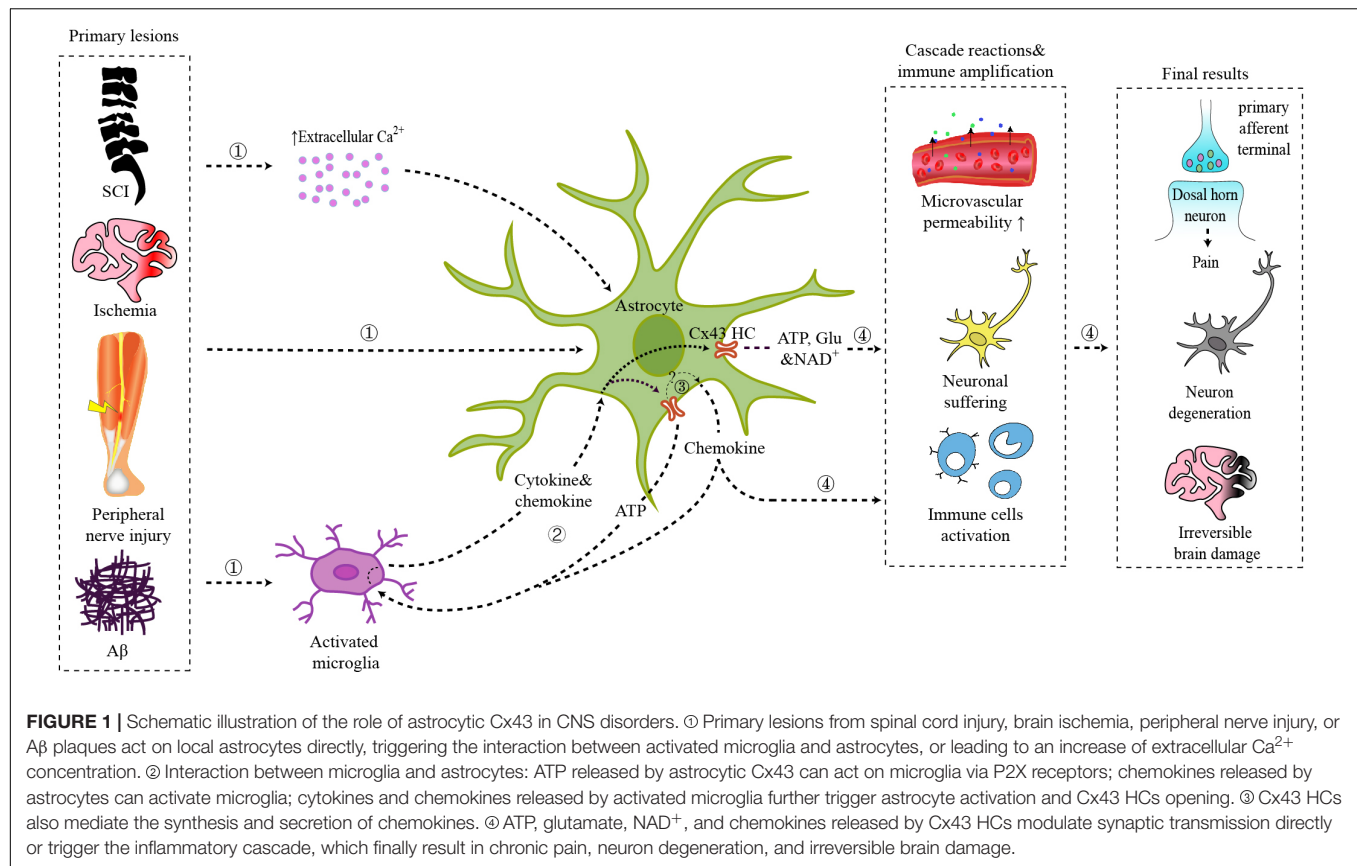
Diseases and models		Cx43 expression changes	Manipulations and drugs	Target channel	Mechanism	Outcomes	Reference
AD	APP/PS1/Gfap-Cx43 KO mice	↑	Astrocyte Cx43 KO	HC and GJC	APPswe/PS1dE9 + Gfap-Cx43 KO	↑cognitive function	Ren et al., 2018
	APP/PS1/Gfap-Cx43 KO mice	↑	Astrocyte Cx43 KO	HC and GJC	APPswe/PS1dE9 + Gfap-Cx43 KO	↓astrogliosis ↓gliotransmitter release	Yi et al., 2016
	APPswe/PS1dE9 mice	↑	boldine	HC	HC blockade	↓neuronal damages ↓hippocampal neuronal suffering	Yi et al., 2017a
	Astrocytes and acute hippocampal slices treated with the active fragment of Aβ ( <i>in vitro</i> )	—	cannabinoids	HC	HC blockade	↓inflammatory profile evoked by Aβ	Gajardo-Gómez et al., 2017
Cerebral ischemia	Astrocyte from Wistar rats	Cx43 expression varies according to the time points and p-Cx43↑	carbenoxolone	GJC	GJC blockade	↑protective effects of ischemic preconditioning	Ma et al., 2018
	Neonatal SD rats	↑	Cx43 mimetic peptides Gap26 and Gap27	HC	Extracellular loop peptides	↓cerebral infarct volume	Li et al., 2015
Retinal ischemia-reperfusion	Wistar rats ( <i>in vivo</i> ) and endothelial cell ( <i>in vitro</i> )	↑	Cx43 mimetic peptide5	HC	Extracellular loop peptides	↓dye leak ( <i>in vivo</i> ) ↑retinal ganglion cell survival ( <i>in vitro</i> )	Danesh-Meyer et al., 2012
Glioma (glioblastoma)	Cx43 KO mice and Cx43 truncated mutant mice (Cx43K258stop)	↓as the glioma grade increases	Cx43 KO and Cx43 truncated	HC and GJC	Gfap:Cre+Cx43fl/fl; C-terminal truncation at amino acid 258	↓glioma invasion	Sin et al., 2016
	GBM cells ( <i>in vitro</i> )	↑in the TMZ-resistant GBM cells	Cx43 siRNA	HC and GJC	RNA interference	↓TMZ resistance	Munoz et al., 2014
	BALB/c nude mice injected with LN229 human GBM stem cells	↑	αCT1	HC	Cx43 C-terminus mimetic peptide	↓TMZ resistance	Murphy et al., 2016
Myocardial ischemia	Intact heart of rats	—	Cx43 mimetic peptide Gap26	HC	Extracellular loop peptides	↑protection against myocardial ischemia-reperfusion injury	Hawat et al., 2010
Amyotrophic Lateral Sclerosis	SOD1 mice and SOD1 <sup>G93A</sup> mice	↑	Cx43 mimetic peptide Gap26	HC	Extracellular loop peptides	↑motor neurons survive	Almad et al., 2016

↑denotes upregulation; ↓denotes downregulation; — denotes data unavailable.

**TABLE 2 |** Expression changes of Cx43 in different pain models.

Pain models and species	Cx43 expression changes	Manipulations and drugs	Target channel	Mechanism	Effects on pain	Reference
Spinal cord injury, mouse	↑	Cx43 <sup>-/-</sup> -Cx30 <sup>-/-</sup> , double knockout	HC and GJC	Cx30-KO + Gfap:Cre Cx43 <sup>fl/fl</sup>	↓heat hyperalgesia and mechanical allodynia	Chen et al., 2012
Spinal cord injury (thoracic spinal cord hemisection), mouse	↑	Intrathecal injection of fluorocitrate and carbenoxolone and Gap26	HC and GJC	astrocyte metabolic inhibitor; gap junction/hemichannel blocker; Cx43 extracellular loop peptides	↓SCI-induced bilateral below-level mechanical allodynia	Choi et al., 2016
Spinal cord contusion, rat	↑	Intraperitoneal injection of Peptide5	HC	Cx43 extracellular loop peptides	↓at-level mechanical allodynia	Mao et al., 2017b
Chronic constriction injury (CCI) of the sciatic nerves, mouse	↑	Intrathecal injection of CBX, Gap26 or Gap27, astroglial toxin pretreatment of astrocytes, or Cx43 siRNA	HC and GJC	GJC blockade; Cx43 extracellular loop peptides; RNA interference	↓mechanical allodynia	Chen et al., 2014
CCI, mouse	↑	—	—	—	—	Neumann et al., 2015
Spinal nerve ligation (SNL), rat	↓	Intrathecal Cx43 siRNA	HC and GJC	RNA interference	↓mechanical hypersensitivity	Xu et al., 2014
Spinal nerve ligation (SNL), rat	↑	Intrathecal CORM-2 administration	HC	Release CO as HC inhibitor	↓hyperalgesia and allodynia	Wang and Sun, 2017
Partial sciatic nerve ligation (PSNL), mouse	↓	Intrathecal injection of an adenovirus vector expressing Cx43	HC and GJC	RNA interference	↓PSNL-induced mechanical hypersensitivity	Morioka et al., 2015
PSNL, mouse	↓	Intrathecal injection of lycopene	HC and GJC	Reversed TNF-induced downregulation of Cx43 expression	↓mechanical hypersensitivity	Zhang et al., 2016
Inferior alveolar nerve injury, rat	↑	Administration of Gap27 in the trigeminal ganglion	HC	Cx43 extracellular loop peptides	↓mechanical hypersensitivity	Kaji et al., 2016
Chemotherapy (bortezomib -induced peripheral neuropathy), rat	↑	Intraperitoneal injection of minocycline and CBX	GJC	Glial activation inhibitor and gap junction decoupler	—	Robinson and Dougherty, 2015
Opioid intrathecal (i.t.) administration of morphine, rat	↑	Intrathecal injection of Gap26	HC	Cx43 extracellular loop peptides	↓morphine antinociceptive tolerance,	Shen et al., 2014
Inflammation (unilateral carrageenan (CA) injection), rat	↑	Intrathecal injection of CBX or Gap26	HC and GJC	Gap junction decoupler and Cx43 extracellular loop peptides	↓contralateral paw withdrawal frequency (PWF), while the ipsilateral PWF was not affected	Choi et al., 2017
Bone Cancer Walker 256 tumor cells inoculation into the tibia, rat	p-Cx43↑	Intrathecal injection of Gap26	HC	Cx43 extracellular loop peptides	↓mechanical allodynia	Hang et al., 2016
Bone Cancer (intra-femoral inoculation of Lewis lung carcinoma cells), mouse	↑	Intrathecal injection of CBX	GJC	Gap junction decoupler	↓pain hypersensitivity	Yang et al., 2018
Breakthrough cancer pain (BTcP), mouse	Cx43 protein↑ p-Cx43↓	Intrathecal injection of Gap26	HC	Cx43 extracellular loop peptides	↓pain hypersensitivity	Li et al., 2017

↑denotes upregulation; ↓denotes downregulation; — denotes data unavailable.



In the TMZ-resistant GBM cells, Cx43 expression showed a significant upregulation. Studies suggested that an increase of functional EGFR expression activated the JNK-ERK1/2-AP-1 axis to upregulate Cx43 expression in the TMZ-resistant GBM cells (Munoz et al., 2014). TMZ-resistance was significantly reduced when Cx43 was suppressed by peptides targeting Cx43 channels or Cx43 C-terminal (Gielen et al., 2013; Murphy et al., 2016; Grek et al., 2018), which implies TMZ-resistance is highly dependent on Cx43 in gliomas.

Temozolomide resistance may be mediated by Cx43 via the mitochondrial apoptosis pathway (Gielen et al., 2013), or interactions between Cx43 carboxyl terminus and actin cytoskeleton (Crespin et al., 2010). GBM cells treated with za restored TMZ sensitivity (Gielen et al., 2013; Murphy et al., 2016). These results indicated that Cx43 carboxyl terminus confers TMZ-resistance in gliomas. Cx43 carboxyl terminus promotes tumor cell migration, and therefore may contribute to glioma invasion (Bates et al., 2007). However, another study showed that Cx43 can promote tumor invasion via a carboxyl terminus-independent manner, since Cx43 without carboxyl terminus can also increase migration (Crespin et al., 2010), which may be derived from connexin-based  $\text{Ca}^{2+}$  signaling and ATP release (Sin et al., 2016). Notably, utilizing Cx43 peptidomimetics as an adjuvant for TMZ resistance has been proposed (Grek et al., 2018).

Not only does the expression of Cx43 change, but its role may also vary with grades, stages, and locations of the tumors. Since

many studies focused on Cx43 in gliomas, many new therapeutic targets have been proposed (e.g., Cx43 extracellular loop, Cx43 loop/tail interactions, Cx43 C-terminal) (Delvaeye et al., 2018). The diverse effects of these drugs are needed to testify to different conditions. In addition, specific drugs targeting Cx43 for varying glioma, may be a better solution based on the dynamic changes of Cx43.

## Cx43 IN BRAIN ISCHEMIA

Brain ischemia is a leading cause of long-term disability or even mortality in adults. Insufficient blood flow, which fails to meet the high metabolic demands of the brain, will trigger the cascade reaction including tissue ischemia, reperfusion injury, inflammatory activity, leading to irreversible brain damage (Kim et al., 2018). Accumulating evidence suggests that astrocytic Cx43 expression is increased after hypoxia/ischemia injury and that Cx43 plays an important role in cell death and neuronal damage induced by cerebral ischemia (Davidson et al., 2012a,b, 2013, 2014; Ma et al., 2018). Ischemia/reperfusion injury and the following inflammatory activation can activate the astrocytic hemichannels via the increased extracellular  $\text{Ca}^{2+}$  and inflammatory factors released (Davidson et al., 2013). For instance, inflammatory factors just like IL-1 $\beta$  could reverse the inhibition of hemichannel activity caused by epidermal growth factor (EGF) (Morita et al., 2007); Cx43 hemichannels can

also be triggered via p38 kinase by pro-inflammatory cytokines including IL-1 $\beta$  and TNF- $\alpha$  released by activated microglia (Retamal et al., 2007; Giaume et al., 2013). These abnormally opened hemichannels subsequently cause an uncontrolled release of ATP, glutamate, and an overload of Ca<sup>2+</sup>, leading to tissue excitotoxicity, amplification of the inflammation (Kim et al., 2018), and ultimately irreversible brain damage. The treatment of Cx43 mimetic peptide Gap26 leads to a reduction in both Cx43 expression and Cx43 hemichannels activity, which improve neurological function and reduce infarct volume (Li et al., 2015). According to this evidence, targeting to Cx43 might be a promising therapeutic strategy for brain ischemia, but more efforts are needed to develop specific inhibitors which can penetrate the blood-brain barrier.

## ASTROCYTES AND Cx43 IN CHRONIC PAIN

Astrocytes are reactive in multiple types of conditioning-induced chronic pain, including peripheral and central nerve trauma, inflammation, chronic opioid exposure, etc. (Song and Zhao, 2001; Okada-Ogawa et al., 2009; Ren and Dubner, 2010; Chiang et al., 2012; Ji et al., 2013). Consistently, inhibiting the activity of astrocytes in the spinal cord can ameliorate chronic pain (Tsuda et al., 2011). Different from rapid activation of microglia, reactive astrocytes are usually found several days after injury and persist for a longer time (Mika et al., 2009; Old et al., 2015). This indicates that astrocytes might mainly contribute to the development and maintenance of chronic pain. The following mechanisms have been discussed in the astrocyte-mediated pain: (1) astrocytes can release multiple inflammatory mediators and neuromodulators, such as cytokines IL-1 $\beta$ , chemokines CCL2, and CXCL1; (2) a variety of receptors and transports, for example, ATP receptors P2XR and P2Y, glutamate transporter-1 (GLT-1), and glutamate and aspartic acid transporter (GLAST) can be activated in astrocytes; (3) the mitogen activated protein kinases (MAPKs) are also activated and further induce downstream signaling critical for pain; (4) reactive astrocytes also regulate the opening states of gap junctions or hemichannels, which further control the release of ATP, glutamate, and NAD<sup>+</sup>. These signaling pathways coordinate or interact with each other in response to pain. The role of Cx43 in pain is acknowledged by the study that Cx43/Cx30 deletion, instead of Cx30 single knockout, can alleviate the neuropathic pain developed between 4 and 8 weeks following spinal cord injury (Chen et al., 2012). Here, we will comprehensively discuss the role of Cx43 in chronic pain.

Studies have shown that Cx43 can act as a non-ligated hemichannel releasing small mediators or gliotransmitters, such as ATP and glutamate, into the extracellular environment (Bennett et al., 2003; D'hondt et al., 2014), which modulate synaptic transmission by directly interacting with nociceptive neurons, further contributing to pain. In addition, extracellular ATP also acts via its receptor P2X on non-neuronal cells, which contribute to pain by inducing the release of cytokines and chemokines.

Studies have shown that Cx43 can also regulate the expression or secretion of cytokines and chemokines in multiple systems. Although it is generally believed that hemichannels only allow passage of small molecules and ions, it has been reported that Cx43 can control the secretion of chemokine CXCL12 in bone marrow stromal cells (Schajnovitz et al., 2011). In the rat arthritis model, LPS treatment significantly enhanced Cx43 gene expression in rat fibroblast-like synoviocytes, whereas transfection of siCx43 inhibited the LPS-induced overexpression of pro-inflammatory cytokines and chemokines (Tsuchida et al., 2013). Furthermore, CBX (carbenoxolone, a non-selective gap-junction inhibitor) reduces the increase of IL-1 $\beta$  and IL6 in cerebrospinal fluid caused by intrathecal injection of HIV1 gp120 (Spataro et al., 2004). The expression and secretion of cytokines or chemokines are up-regulated in TNF- $\alpha$ -activated astrocytes, which are important in the induction and maintenance of pain hypersensitivity (Gao et al., 2009; Huh et al., 2017). Our previous study has shown that TNF- $\alpha$ -induced CXCL1 and CCL2 release from astrocytes, were blocked by Cx43 small interfering RNA, CBX and <sup>43</sup>Gap26 or <sup>37,43</sup>Gap27 (two Cx43 mimetic peptides that blocks hemichannels), indicating that astrocytic Cx43 hemichannels are responsible for the release of the chemokines (Chen et al., 2014). Another study showed that intrathecal injection of <sup>43</sup>Gap26 markedly attenuated mechanical allodynia in rat bone cancer model and reduced CXCL12 production from spinal dorsal horn in astrocytes (Hang et al., 2016). Although this evidence suggests that Cx43 hemichannels mediate the synthesis and secretion of chemokines, the mechanism remains unclear as chemokines are too large to directly efflux through the Cx43 hemichannels. One possible explanation is that activated calcium signaling contributes to CXCL12 secretion via the GTPase RalA (Schajnovitz et al., 2011). Another possibility is that an increase of purine induced by Cx43 may regulate the release of chemokines, based on the role of purinergic signaling in astrocytic release (Chen et al., 2014). Moreover, the Cx43 hemichannel may be hyperactive in pathological conditions, thereby causing chemokines to "leak" out of astrocytes through cytoskeletal changes (Cotrina et al., 2000).

The expression changes of Cx43 following pain is still inconclusive (Table 2). Multiple studies have shown that Cx43 is upregulated in astrocytes following nerve ligation and spinal cord injury, and that inhibition of Cx43 can attenuate pain hypersensitivity (Wu et al., 2011; Chen et al., 2012, 2014, 2018; Shen et al., 2014; Neumann et al., 2015; Robinson and Dougherty, 2015; Choi et al., 2016; Hang et al., 2016; Kaji et al., 2016; Mao et al., 2017a,b; Wang and Sun, 2017; Yang et al., 2018). On the contrary, few studies showed that a decrease of Cx43 following nerve injury could contribute to pain hypersensitivity (Xu et al., 2014; Morioka et al., 2015; Zhang et al., 2016). Interestingly, in a mouse model of breakthrough cancer pain, Cx43 protein level is upregulated while phosphorylation of Cx43 (p-Cx43) is downregulated (Li et al., 2017). The conflict might come from distinct pain conditions or models. Additionally, it might not be the Cx43 expression level alone that determines the enhanced or attenuated function of hemichannels or gap junctions, because even in the pain model with decreased CX43



expression, inhibition of CX43 function can still relieve pain (Xu et al., 2014).

Studies have shown that Cx43 can be highly regulated by astrocytic inflammatory mediators, growth factors, or receptors. TNF- $\alpha$  and IL-1 $\beta$ , inflammatory mediators produced by astrocytes in pain, can modulate the expression of Cx43 (Morioka et al., 2015; Choi et al., 2017). For example, TNF decreases Cx43 expression in naive mice, which can be reversed by the TNF inhibitor (Morioka et al., 2015). Reactive astrocytes also lead to an increase in the basic fibroblast growth factor (bFGF or FGF-2) in the late phase following nerve injury. bFGF increases the expression of Cx43 and enhances intercellular communication of Cx43 gap junction in cardiac fibroblasts (Doble and Kardami, 1995), though the study of the role of bFGF in astrocytic Cx43 is lacking. In addition, the sigma-1 receptor activated by astrocytes in both peripheral and central neuropathy, could also modulate the activation of Cx43. The increase in Cx43 expression can be reversed by a sigma-1 receptor blocker (Choi et al., 2016).

Increasing evidence has shown that mitogen-activated protein kinases (MAPKs) can also regulate the opening states of Cx43 channels in astrocytes. Activation of MAPKs family members contribute to pain sensitization. For instance, extracellular signal-regulated kinases (ERKs) is significantly upregulated in astrocytes when animals were injected with complete Freund's adjuvant (CFA), a drug inducing inflammation and pain (Weyerbacher et al., 2010). Phosphorylation of C-Jun N-terminal kinases (JNKs), predominantly JNK-1, is observed in spinal astrocytes in a persistent pain condition (Gao et al., 2010). MAPKs lead to a closure of CX43 gap junction and hemichannels, while MAPK phosphatase make Cx43 preferentially open (Kim et al., 1999; Goodenough and Paul, 2003; Solan and Lampe, 2005). Notably, phosphorylation and dephosphorylation events not only regulate the gating of channels, but also the trafficking and assembly of connexins (Ribeiro-Rodrigues et al., 2017), indicating the complicated effects of MAPKs on Cx43.

Though the interaction between Cx43 and molecules involved in pain offers a complicated feedback loop in pain development and maintenance, based on the current studies, strategies to suppress the function of Cx43 may be a robust approach for pain relief (Wu et al., 2011; Chen et al., 2012, 2014; Shen et al., 2014; Xu et al., 2014; Neumann et al., 2015; Robinson and Dougherty, 2015; Choi et al., 2016; Hang et al., 2016; Kaji et al., 2016; Mao et al., 2017a,b; Wang and Sun, 2017; Yang et al., 2018).

Cx43 might function as hemichannels or a gap junction, which has not been clearly characterized in every single study (Tables 1, 2). A non-selective gap-junction inhibitor carbenoxolone (CBX) can reduce neuropathic pain (Wang et al., 2014), supporting the ideas that Cx43 can function as a gap junction. On the other hand, studies proposed a model in which Cx43 can function as a non-junctional hemichannel to release mediators such as ATP and glutamate (Bennett et al., 2003; D'hondt et al., 2014). There are a few ways to distinguish hemichannels and gap junctions. For example, when used for short incubation time or at a low concentration, peptide 5, a mimetic of Cx43, can only inhibit hemichannels, but when applied for a long incubation time or at a long concentration, can attenuate both hemichannels and gap

junctions (Choi et al., 2016; Mao et al., 2017a). Another approach to distinguish Cx43 gap junction and hemichannels are using the dyes uptaken. Lucifer yellow, only permeable to the gap junction, while ethidium bromide is considered exclusively uptaken by hemichannels. The diffusion rates of these dyes will differentiate hemichannel and gap junction. Interestingly, a peptide derived from the cytoplasmic loop of Cx43 termed Gap19 can specifically function in Cx43 hemichannels while not affecting gap junctions (Abudara et al., 2014). In addition, La3+ can specifically block hemichannels rather than gap junctions. Typically, the use of these drugs is accompanied by other blockers or dyes, however, thus far no drugs that only target to Cx43 are available.

The enriched expression of Cx43 and wide distribution of astrocytes in the brain and spinal cord might explain the complicated phenotypes observed in animals with Cx43 manipulation. Though changes of either ATP, glutamate, or Ca<sup>2+</sup> can be detected when Cx43 is manipulated, it is hard to tell how each molecule contributes to the system since (1) few studies have systematically tested all changes of these molecules; (2) not only local signaling is affected by these small molecules.

## CONCLUSION AND PERSPECTIVES

Astrocytes modulate extrasynaptic or synaptic milieu to further enhance or dampen electrochemical signaling propagating in neurons. As the major connexin altered following nerve injury, Cx43 can be regulated by multiple signals under pathological conditions, which in turn, modulate several downstream signals critical for neuronal activity, and further contribute to a variety of CNS disorders, including pain. So far, up to 21 phosphorylation sites have been reported in Cx43 (Pogoda et al., 2016), indicating a complex post-translational modification. Further studies might be necessary to characterize how these phosphorylation sites contribute to specific CNS disorders. Of note, besides connexin hemichannels, pannexin is also detectable in astrocytes (Garre et al., 2010). Pannexin-1, like Cx43, can also be inhibited by the non-selective gap-junction blocker CBX (Garre et al., 2010). Therefore, the role of Pannexin-1 in pain control could be an interesting topic to explore. In addition, how connexins interact with pannexins and the signaling pathways mediated by connexins or pannexins need further investigation. Selective manipulation of connexins might be a potential therapeutic approach in some CNS disorders.

## AUTHOR CONTRIBUTIONS

LX and TY wrote and drafted the manuscript. All authors contributed to manuscript revision, read and approved the submitted version.

## FUNDING

This study was supported by The National Key Research and Development Program of China (2017YFA0104704 and

2016YFC1101602), The National Natural Science Foundation of China (31872773, 81701127, and 81671220), The Natural Science Foundation of JiangSu of China (BK20170446 and BK20181460), The Natural Science Foundation of the JiangSu Higher Education

Institutions of China (17KJA180009), the Jilin Scientific and Technological Development Program (20160101077JC), and the Jilin Provincial School Joint Construction Special Project (SXGJQY2017-13).

## REFERENCES

- Abudara, V., Bechberger, J., Freitas-Andrade, M., De Bock, M., Wang, N., Bultynck, G., et al. (2014). The connexin43 mimetic peptide Gap19 inhibits hemichannels without altering gap junctional communication in astrocytes. *Front. Cell. Neurosci.* 8:306. doi: 10.3389/fncel.2014.00306
- Almad, A. A., Doreswamy, A., Gross, S. K., Richard, J. P., Huo, Y., Haughey, N., et al. (2016). Connexin 43 in astrocytes contributes to motor neuron toxicity in amyotrophic lateral sclerosis. *Glia* 64, 1154–1169. doi: 10.1002/glia.22989
- Ballard, C., Gauthier, S., Corbett, A., Brayne, C., Aarsland, D., and Jones, E. (2011). Alzheimer's disease. *Lancet* 377, 1019–1031. doi: 10.1016/S0140-6736(10)61349-9
- Bates, D. C., Sin, W. C., Aftab, Q., and Naus, C. C. (2007). Connexin43 enhances glioma invasion by a mechanism involving the carboxy terminus. *Glia* 55, 1554–1564. doi: 10.1002/glia.20569
- Batra, N., Riquelme, M. A., Burra, S., and Jiang, J. X. (2014). 14-3-3 $\sigma$  facilitates plasma membrane delivery and function of mechanosensitive connexin 43 hemichannels. *J. Cell Sci.* 127, 137–146. doi: 10.1242/jcs.133553
- Bennett, B. C., Purdy, M. D., Baker, K. A., Acharya, C., McIntire, W. E., Stevens, R. C., et al. (2016). An electrostatic mechanism for Ca<sup>2+</sup> mediated regulation of gap junction channels. *Nat. Commun.* 7:8770. doi: 10.1038/ncomms9770
- Bennett, M. V. L., Contreras, J. E., Bukauskas, F. F., and Sáez, J. C. (2003). New roles for astrocytes: gap junction hemichannels have something to communicate. *Trends Neurosci.* 26, 610–617. doi: 10.1016/j.tins.2003.09.008
- Cabezas, R., Avila, M., Gonzalez, J., El-Bachá, R. S., Báez, E., Garcá-A-Segura, L. M., et al. (2014). Astrocytic modulation of blood brain barrier: perspectives on Parkinson's disease. *Front. Cell. Neurosci.* 8:211. doi: 10.3389/fncel.2014.00211
- Castellano, P., and Eugenin, E. A. (2014). Regulation of gap junction channels by infectious agents and inflammation in the CNS. *Front. Cell. Neurosci.* 8:122. doi: 10.3389/fncel.2014.00122
- Chen, G., Luo, X., Qadri, M. Y., Berta, T., and Ji, R. R. (2018). Sex-dependent glial signaling in pathological pain: distinct roles of spinal microglia and astrocytes. *Neurosci. Bull.* 34, 98–108. doi: 10.1007/s12264-017-0145-y
- Chen, G., Park, C. K., Xie, R. G., Berta, T., Nedergaard, M., and Ji, R. R. (2014). Connexin-43 induces chemokine release from spinal cord astrocytes to maintain late-phase neuropathic pain in mice. *Brain* 137, 2193–2209. doi: 10.1093/brain/awu140
- Chen, M. J., Kress, B., Han, X., Moll, K., Peng, W., Ji, R.-R., et al. (2012). Astrocytic Cx43 hemichannels and gap junctions play a crucial role in development of chronic neuropathic pain following spinal cord injury. *Glia* 60, 1660–1670. doi: 10.1002/glia.22384
- Chiang, C.-Y., Sessle, B. J., and Dostrovsky, J. O. (2012). Role of astrocytes in pain. *Neurochem. Res.* 37, 2419–2431. doi: 10.1007/s11064-012-0801-6
- Choi, H.-S., Roh, D.-H., Yoon, S.-Y., Kwon, S.-G., Choi, S.-R., Kang, S.-Y., et al. (2017). The role of spinal interleukin-1 $\beta$  and astrocyte connexin 43 in the development of mirror-image pain in an inflammatory pain model. *Exp. Neurol.* 287, 1–13. doi: 10.1016/j.expneurol.2016.10.012
- Choi, S.-R., Roh, D.-H., Yoon, S.-Y., Kwon, S.-G., Choi, H.-S., Han, H.-J., et al. (2016). Astrocyte sigma-1 receptors modulate connexin 43 expression leading to the induction of below-level mechanical allodynia in spinal cord injured mice. *Neuropharmacology* 111, 34–46. doi: 10.1016/j.neuropharm.2016.08.027
- Cotrina, M. L., Lin, J. H., López-García, J. C., Naus, C. C., and Nedergaard, M. (2000). ATP-mediated glia signaling. *J. Neurosci.* 20, 2835–2844. doi: 10.1523/JNEUROSCI.20-08-02835.2000
- Crespin, S., Bechberger, J., Mesnil, M., Naus, C. C., and Sin, W. C. (2010). The carboxy-terminal tail of connexin43 gap junction protein is sufficient to mediate cytoskeleton changes in human glioma cells. *J. Cell. Biochem.* 110, 589–597. doi: 10.1002/jcb.22554
- Danesh-Meyer, H. V., Kerr, N. M., Zhang, J., Eady, E. K., O'Carroll, S. J., Nicholson, L. F. B., et al. (2012). Connexin43 mimetic peptide reduces vascular leak and retinal ganglion cell death following retinal ischaemia. *Brain*, 135, 506–520. doi: 10.1093/brain/awr338
- Davidson, J. O., Drury, P. P., Green, C. R., Nicholson, L. F., Bennet, L., and Gunn, A. J. (2014). Connexin hemichannel blockade is neuroprotective after asphyxia in preterm fetal sheep. *PLoS One* 9:e96558. doi: 10.1371/journal.pone.0096558
- Davidson, J. O., Green, C. R., Bennet, L., Nicholson, L. F., Danesh-Meyer, H., O'Carroll, S. J., et al. (2013). A key role for connexin hemichannels in spreading ischemic brain injury. *Curr. Drug Targets* 14, 36–46. doi: 10.2174/138945013804806479
- Davidson, J. O., Green, C. R., Louise, L. F., O'Carroll, S. J., Fraser, M., Bennet, L., et al. (2012a). Connexin hemichannel blockade improves outcomes in a model of fetal ischemia. *Ann. Neurol.* 71, 121–132. doi: 10.1002/ana.22654
- Davidson, J. O., Green, C. R., Nicholson, L. F. B., Bennet, L., and Gunn, A. J. (2012b). Deleterious effects of high dose connexin 43 mimetic peptide infusion after cerebral ischaemia in near-term fetal sheep. *Int. J. Mol. Sci.* 13, 6303–6319. doi: 10.3390/ijms13056303
- Decroock, E., Vinken, M., Bol, M., D'Herde, K., Rogiers, V., Vandenabeele, P., et al. (2011). Calcium and connexin-based intercellular communication, a deadly catch? *Cell Calcium* 50, 310–321. doi: 10.1016/j.ceca.2011.05.007
- Delaeye, T., Vandenabeele, P., Bultynck, G., Leybaert, L., and Krysko, D. V. (2018). Therapeutic targeting of connexin channels: new views and challenges. *Trends Mol. Med.* 24, 1036–1053. doi: 10.1016/j.molmed.2018.10.005
- D'hondt, C., Iyyathurai, J., Himpens, B., Leybaert, L., and Bultynck, G. (2014). Cx43-hemichannel function and regulation in physiology and pathophysiology: insights from the bovine corneal endothelial cell system and beyond. *Front. Physiol.* 5:348. doi: 10.3389/fphys.2014.00348
- Doble, B. W., and Kardami, E. (1995). Basic fibroblast growth factor stimulates connexin-43 expression and intercellular communication of cardiac fibroblasts. *Mol. Cell. Biochem.* 143, 81–87. doi: 10.1007/BF00925930
- Fernandez, H. H. (2012). Updates in the medical management of Parkinson disease. *Cleve. Clin. J. Med.* 79, 28–35. doi: 10.3949/ccjm.78gr.11005
- Freitas-Andrade, M., and Naus, C. C. (2016). Astrocytes in neuroprotection and neurodegeneration: the role of connexin43 and pannexin1. *Neuroscience* 323, 207–221. doi: 10.1016/j.neuroscience.2015.04.035
- Gajardo-Gómez, R., Labra, V. C., Maturana, C. J., Shoji, K. F., Santibañez, C. A., Sáez, J. C., et al. (2017). Cannabinoids prevent the amyloid  $\beta$ -induced activation of astroglial hemichannels: a neuroprotective mechanism. *Glia* 65, 122–137. doi: 10.1002/glia.23080
- Gao, Y.-J., Xu, Z.-Z., Liu, Y.-C., Wen, Y.-R., Decosterd, I., and Ji, R.-R. (2010). The c-Jun N-terminal kinase 1 (JNK1) in spinal astrocytes is required for the maintenance of bilateral mechanical allodynia under a persistent inflammatory pain condition. *Pain* 148, 309–319. doi: 10.1016/j.pain.2009.11.017
- Gao, Y.-J., Zhang, L., Samad, O. A., Suter, M. R., Yasuhiko, K., Xu, Z.-Z., et al. (2009). JNK-induced MCP-1 production in spinal cord astrocytes contributes to central sensitization and neuropathic pain. *J. Neurosci.* 29, 4096–4108. doi: 10.1523/JNEUROSCI.3623-08.2009
- Garre, J. M., Retamal, M. A., Cassina, P., Barbeito, L., Bukauskas, F. F., Sáez, J. C., et al. (2010). FGF-1 induces ATP release from spinal astrocytes in culture and opens pannexin and connexin hemichannels. *Proc. Natl. Acad. Sci. U.S.A.* 107, 22659–22664. doi: 10.1073/pnas.1013793107
- Giaume, C., Leybaert, L., Naus, C. C., and Sáez, J. C. (2013). Connexin and pannexin hemichannels in brain glial cells: properties, pharmacology, and roles. *Front. Pharmacol.* 4:88. doi: 10.3389/fphar.2013.00088
- Gielen, P. R., Aftab, Q., Ma, N., Chen, V. C., Hong, X., Lozinsky, S., et al. (2013). Connexin43 confers temozolomide resistance in human glioma cells by modulating the mitochondrial apoptosis pathway. *Neuropharmacology* 75, 539–548. doi: 10.1016/j.neuropharm.2013.05.002
- Goodenough, D. A., and Paul, D. L. (2003). Beyond the gap: functions of unpaired connexon channels. *Nat. Rev. Mol. Cell Biol.* 4, 285–295. doi: 10.1038/nrm1072

- Grek, C. L., Sheng, Z., Naus, C. C., Sin, W. C., Gourdie, R. G., and Ghatnekar, G. G. (2018). Novel approach to temozolomide resistance in malignant glioma: connexin43-directed therapeutics. *Curr. Opin. Pharmacol.* 41, 79–88. doi: 10.1016/j.coph.2018.05.002
- Hang, L.-H., Li, S.-N., Luo, H., Shu, W.-W., Mao, Z.-M., Chen, Y.-F., et al. (2016). Connexin 43 mediates CXCL12 production from spinal dorsal horn to maintain bone cancer pain in rats. *Neurochem. Res.* 41, 1200–1208. doi: 10.1007/s11064-015-1815-7
- Hawat, G., Benderdour, M., Rousseau, G., and Baroudi, G. (2010). Connexin 43 mimetic peptide Gap26 confers protection to intact heart against myocardial ischemia injury. *Pflugers Arch. Eur. J. Physiol.* 460, 583–592. doi: 10.1007/s00424-010-0849-6
- Hirayama, Y., and Koizumi, S. (2018). Astrocytes and ischemic tolerance. *Neurosci. Res.* 126, 53–59. doi: 10.1016/j.neures.2017.11.013
- Huh, Y., Ji, R.-R., and Chen, G. (2017). Neuroinflammation, bone marrow stem cells, and chronic pain. *Front. Immunol.* 8:1014. doi: 10.3389/fimmu.2017.01014
- Ji, R.-R., Berta, T., and Nedergaard, M. (2013). Glia and pain: is chronic pain a gliopathy? *Pain* 154(Suppl.), S10–28. doi: 10.1016/j.pain.2013.06.022
- Johansen, D., Cruciani, V., Sundset, R., Ytrehus, K., and Mikalsen, S.-O. (2011). Ischemia induces closure of gap junctional channels and opening of hemichannels in heart-derived cells and tissue. *Cell. Physiol. Biochem.* 28, 103–114. doi: 10.1159/000331719
- Kaji, K., Shinoda, M., Honda, K., Unno, S., Shimizu, N., and Iwata, K. (2016). Connexin 43 contributes to ectopic orofacial pain following inferior alveolar nerve injury. *Mol. Pain* 12, 1–12. doi: 10.1177/1744806916633704
- Kim, D. Y., Kam, Y., Koo, S. K., and Joe, C. O. (1999). Gating connexin 43 channels reconstituted in lipid vesicles by mitogen-activated protein kinase phosphorylation. *J. Biol. Chem.* 274, 5581–5587. doi: 10.1074/jbc.274.9.5581
- Kim, Y., Davidson, J. O., Green, C. R., Nicholson, L. F. B., O'Carroll, S. J., and Zhang, J. (2018). Connexins and pannexins in cerebral ischemia. *Biochim. Biophys. Acta – Biomembr.* 1860, 224–236. doi: 10.1016/j.bbamem.2017.03.018
- Koulakoff, A., Mei, X., Orellana, J. A., Sáez, J. C., and Giaume, C. (2012). Glial connexin expression and function in the context of Alzheimer's disease. *Biochim. Biophys. Acta – Biomembr.* 1818, 2048–2057. doi: 10.1016/j.bbamem.2011.10.001
- Lapato, A. S., and Tiwari-Woodruff, S. K. (2018). Connexins and pannexins: at the junction of neuro-glial homeostasis & disease. *J. Neurosci. Res.* 96, 31–44. doi: 10.1002/jnr.24088
- Li, T., Giaume, C., and Xiao, L. (2014). Connexins-mediated glia networking impacts myelination and remyelination in the central nervous system. *Mol. Neurobiol.* 49, 1460–1471. doi: 10.1007/s12035-013-8625-1
- Li, X., Jiang, S., Yang, H., Liao, Q., Cao, S., Yan, X., et al. (2017). Breakthrough cancer pain is associated with spinal gap junction activation via regulation of connexin 43 in a mouse model. *Front. Cell. Neurosci.* 11:207. doi: 10.3389/fncel.2017.00207
- Li, X., Zhao, H., Tan, X., Kostrzewa, R. M., Du, G., Chen, Y., et al. (2015). Inhibition of connexin43 improves functional recovery after ischemic brain injury in neonatal rats. *Glia* 63, 1553–1567. doi: 10.1002/glia.22826
- Ma, D., Feng, L., Cheng, Y., Xin, M., You, J., Yin, X., et al. (2018). Astrocytic gap junction inhibition by carbenoxolone enhances the protective effects of ischemic preconditioning following cerebral ischemia. *J. Neuroinflamm.* 15, 1–12. doi: 10.1186/s12974-018-1230-5
- Mao, Y., Nguyen, T., Tonkin, R. S., Lees, J. G., Warren, C., O'Carroll, S. J., et al. (2017a). Characterisation of Peptide5 systemic administration for treating traumatic spinal cord injured rats. *Exp. Brain Res.* 235, 3033–3048. doi: 10.1007/s00221-017-5023-3
- Mao, Y., Tonkin, R. S., Nguyen, T., O'Carroll, S. J., Nicholson, L. F. B., Green, C. R., et al. (2017b). Systemic administration of connexin43 mimetic peptide improves functional recovery after traumatic spinal cord injury in adult rats. *J. Neurotrauma* 34, 707–719. doi: 10.1089/neu.2016.4625
- Mei, X., Ezan, P., Giaume, C., and Koulakoff, A. (2010). Astroglial connexin immunoreactivity is specifically altered at  $\beta$ -amyloid plaques in  $\beta$ -amyloid precursor protein/presenilin1 mice. *Neuroscience* 171, 92–105. doi: 10.1016/j.neuroscience.2010.08.001
- Mika, J., Osikowicz, M., Rojewska, E., Korostynski, M., Wawrzczak-Bargiela, A., Przewlocki, R., et al. (2009). Differential activation of spinal microglial and astroglial cells in a mouse model of peripheral neuropathic pain. *Eur. J. Pharmacol.* 623, 65–72. doi: 10.1016/j.ejphar.2009.09.030
- Morioka, N., Zhang, F. F., Nakamura, Y., Kitamura, T., Hisaoka-Nakashima, K., and Nakata, Y. (2015). Tumor necrosis factor-mediated downregulation of spinal astrocytic connexin43 leads to increased glutamatergic neurotransmission and neuropathic pain in mice. *Brain. Behav. Immun.* 49, 293–310. doi: 10.1016/j.bbi.2015.06.015
- Morita, M., Saruta, C., Kozuka, N., Okubo, Y., Itakura, M., Takahashi, M., et al. (2007). Dual regulation of astrocyte gap junction hemichannels by growth factors and a pro-inflammatory cytokine via the mitogen-activated protein kinase cascade. *Glia* 55, 508–515. doi: 10.1002/glia.20471
- Munoz, J. L., Rodriguez-Cruz, V., Greco, S. J., Ramkissoon, S. H., Ligon, K. L., and Rameshwar, P. (2014). Temozolomide resistance in glioblastoma cells occurs partly through epidermal growth factor receptor-mediated induction of connexin 43. *Cell Death Dis.* 5:e1145. doi: 10.1038/cddis.2014.111
- Murphy, S. F., Varghese, R. T., Lamouille, S., Guo, S., Pridham, K. J., Kanabur, P., et al. (2016). Connexin 43 inhibition sensitizes chemoresistant glioblastoma cells to temozolomide. *Cancer Res.* 76, 139–149. doi: 10.1158/0008-5472.CAN-15-1286
- Nagy, J. I., Li, W., Hertzberg, E. L., and Marotta, C. A. (1996). Elevated connexin43 immunoreactivity at sites of amyloid plaques in Alzheimer's disease. *Brain Res.* 717, 173–178. doi: 10.1016/0006-8993(95)01526-4
- Neumann, E., Hermanns, H., Barthel, F., Werdehausen, R., and Brandenburger, T. (2015). Expression changes of microRNA-1 and its targets connexin 43 and brain-derived neurotrophic factor in the peripheral nervous system of chronic neuropathic rats. *Mol. Pain* 11, 1–9. doi: 10.1186/s12990-015-0045-y
- Okada-Ogawa, A., Suzuki, I., Sessle, B. J., Chiang, C.-Y., Salter, M. W., Dostrovsky, J. O., et al. (2009). Astroglia in medullary dorsal horn (trigeminal spinal subnucleus caudalis) are involved in trigeminal neuropathic pain mechanisms. *J. Neurosci.* 29, 11161–11171. doi: 10.1523/JNEUROSCI.3365-09.2009
- Old, E. A., Clark, A. K., and Malcangio, M. (2015). The role of glia in the spinal cord in neuropathic and inflammatory pain. *Handb. Exp. Pharmacol.* 227, 145–170. doi: 10.1007/978-3-662-46450-2\_8
- Orellana, J. A. (2016). Physiological functions of glial cell hemichannels. *Adv. Exp. Med. Biol.* 949, 93–108. doi: 10.1007/978-3-319-40764-7\_5
- Orellana, J. A., Retamal, M. A., Moraga-Amaro, R., and Stehberg, J. (2016). Role of astroglial hemichannels and pannexons in memory and neurodegenerative diseases. *Front. Integr. Neurosci.* 10:26. doi: 10.3389/fnint.2016.00026
- Orellana, J. A., Shoji, K. F., Abudara, V., Ezan, P., Amigou, E., Saez, P. J., et al. (2011). Amyloid-induced death in neurons involves glial and neuronal hemichannels. *J. Neurosci.* 31, 4962–4977. doi: 10.1523/JNEUROSCI.6417-10.2011
- Pascual, O. (2005). Astrocytic purinergic signaling coordinates synaptic networks. *Science* (80-). 310, 113–116. doi: 10.1126/science.1116916
- Pogoda, K., Kameritsch, P., Retamal, M. A., and Vega, J. L. (2016). Regulation of gap junction channels and hemichannels by phosphorylation and redox changes: a revision. *BMC Cell Biol.* 17:11. doi: 10.1186/s12860-016-0099-3
- Rash, J. E., Yasumura, T., Davidson, K. G., Furman, C. S., Dudek, F. E., and Nagy, J. I. (2001a). Identification of cells expressing Cx43, Cx30, Cx26, Cx32 and Cx36 in gap junctions of rat brain and spinal cord. *Cell Commun. Adhes.* 8, 315–320. doi: 10.3109/15419060109080745
- Rash, J. E., Yasumura, T., Dudek, F. E., and Nagy, J. I. (2001b). Cell-specific expression of connexins and evidence of restricted gap junctional coupling between glial cells and between neurons. *J. Neurosci.* 21, 1983–2000. doi: 10.1523/JNEUROSCI.21-06-01983.2001
- Ren, K., and Dubner, R. (2010). Interactions between the immune and nervous systems in pain. *Nat. Med.* 16, 1267–1276. doi: 10.1038/nm.2234
- Ren, R., Zhang, L., and Wang, M. (2018). Specific deletion connexin43 in astrocyte ameliorates cognitive dysfunction in APP/PS1 mice. *Life Sci.* 208, 175–191. doi: 10.1016/j.lfs.2018.07.033
- Retamal, M. A., Alcayaga, J., Verdugo, C. A., Bultynck, G., Leybaert, L., Sáez, P. J., et al. (2014). Opening of pannexin- and connexin-based channels increases the excitability of nodose ganglion sensory neurons. *Front. Cell. Neurosci.* 8:158. doi: 10.3389/fncel.2014.00158
- Retamal, M. A., Froger, N., Palacios-Prado, N., Ezan, P., Saez, P. J., Saez, J. C., et al. (2007). Cx43 hemichannels and gap junction channels in astrocytes are regulated oppositely by proinflammatory cytokines released from activated microglia. *J. Neurosci.* 27, 13781–13792. doi: 10.1523/JNEUROSCI.2042-07.2007



- Retamal, M. A., Reyes, E. P., García, I. E., Pinto, B., Martínez, A. D., and González, C. (2015). Diseases associated with leaky hemichannels. *Front. Cell. Neurosci.* 9:267. doi: 10.3389/fncel.2015.00267
- Ribeiro-Rodrigues, T. M., Nia Martins-Marques, T., Morel, S., Kwak, B. R., and Gira, H. (2017). Role of connexin 43 in different forms of intercellular communication-gap junctions, extracellular vesicles and tunnelling nanotubes. *J. Cell Sci.* 130, 3619–3630. doi: 10.1242/jcs.200667
- Robinson, C. R., and Dougherty, P. M. (2015). Spinal astrocyte gap junction and glutamate transporter expression contributes to a rat model of bortezomib-induced peripheral neuropathy. *Neuroscience* 285, 1–10. doi: 10.1016/j.neuroscience.2014.11.009
- Rodríguez, J. J., Olabarria, M., Chvatal, A., and Verkhratsky, A. (2009). Astroglia in dementia and Alzheimer's disease. *Cell Death Differ.* 16, 378–385. doi: 10.1038/cdd.2008.172
- Saez, J. C., Berthoud, V. M., Branes, M. C., Martinez, A. D., and Beyer, E. C. (2003). Plasma membrane channels formed by connexins: their regulation and functions. *Physiol. Rev.* 83, 1359–1400. doi: 10.1152/physrev.00007.2003
- Schajnovitz, A., Itkin, T., D'Uva, G., Kalinkovich, A., Golan, K., Ludin, A., et al. (2011). CXCL12 secretion by bone marrow stromal cells is dependent on cell contact and mediated by connexin-43 and connexin-45 gap junctions. *Nat. Immunol.* 12, 391–398. doi: 10.1038/ni.2017
- Scott, C. A., Tattersall, D., O'Toole, E. A., and Kelsell, D. P. (2012). Connexins in epidermal homeostasis and skin disease. *Biochim. Biophys. Acta – Biomembr.* 1818, 1952–1961. doi: 10.1016/j.bbamem.2011.09.004
- Shen, N., Mo, L.-Q., Hu, F., Chen, P.-X., Guo, R.-X., and Feng, J.-Q. (2014). A novel role of spinal astrocytic connexin 43: mediating morphine antinociceptive tolerance by activation of NMDA receptors and inhibition of glutamate transporter-1 in rats. *CNS Neurosci. Ther.* 20, 728–736. doi: 10.1111/cns.12244
- Sin, W. C., Aftab, Q., Bechberger, J. F., Leung, J. H., Chen, H., and Naus, C. C. (2016). Astrocytes promote glioma invasion via the gap junction protein connexin43. *Oncogene* 35, 1504–1516. doi: 10.1038/onc.2015.210
- Sin, W. C., Crespin, S., and Mesnil, M. (2012). Opposing roles of connexin43 in glioma progression. *Biochim. Biophys. Acta – Biomembr.* 1818, 2058–2067. doi: 10.1016/j.bbamem.2011.10.022
- Solan, J. L., and Lampe, P. D. (2005). Connexin phosphorylation as a regulatory event linked to gap junction channel assembly. *Biochim. Biophys. Acta – Biomembr.* 1711, 154–163. doi: 10.1016/j.bbamem.2004.09.013
- Song, P., and Zhao, Z. Q. (2001). The involvement of glial cells in the development of morphine tolerance. *Neurosci. Res.* 39, 281–286. doi: 10.1016/S0168-0102(00)00226-1
- Sontheimer, H. (2015). Brain cancer: tumour cells on neighbourhood watch. *Nature* 528, 49–50. doi: 10.1038/nature15649
- Spataro, L. E., Sloane, E. M., Milligan, E. D., Wieseler-Frank, J., Schoeniger, D., Jekich, B. M., et al. (2004). Spinal gap junctions: potential involvement in pain facilitation. *J. Pain* 5, 392–405. doi: 10.1016/j.jpain.2004.06.006
- Stupp, R., Mason, W., van den Bent, M., Weller, M., Fisher, B., Taphoorn, M., et al. (2005). Radiotherapy plus concomitant and adjuvant temozolomide for glioblastoma. *N. Engl. J. Med.* 352, 987–996. doi: 10.1016/j.canrad.2005.05.001
- Takeuchi, H., Jin, S., Wang, J., Zhang, G., Kawanokuchi, J., Kuno, R., et al. (2006). Tumor Necrosis factor- $\alpha$  induces neurotoxicity via glutamate release from hemichannels of activated microglia in an autocrine manner. *J. Biol. Chem.* 281, 21362–21368. doi: 10.1074/jbc.M600504200
- Tsushida, S., Arai, Y., Kishida, T., Takahashi, K. A., Honjo, K., Terauchi, R., et al. (2013). Silencing the expression of connexin 43 decreases inflammation and joint destruction in experimental arthritis. *J. Orthop. Res.* doi: 10.1002/jor.22263
- Tsuda, M., Kohro, Y., Yano, T., Tsujikawa, T., Kitano, J., Tozaki-Saitoh, H., et al. (2011). JAK-STAT3 pathway regulates spinal astrocyte proliferation and neuropathic pain maintenance in rats. *Brain* 134, 1127–1139. doi: 10.1093/brain/awr025
- Verkhratsky, A., Olabarria, M., Noristani, H. N., Yeh, C.-Y., and Rodriguez, J. J. (2010). Astrocytes in Alzheimer's disease. *Neurotherapeutics* 7, 399–412. doi: 10.1016/j.nurt.2010.05.017
- Wang, H., Cao, Y., Chiang, C.-Y., Dostrovsky, J. O., and Sessle, B. J. (2014). The gap junction blocker carbenoxolone attenuates nociceptive behavior and medullary dorsal horn central sensitization induced by partial infraorbital nerve transection in rats. *Pain* 155, 429–435. doi: 10.1016/j.pain.2013.11.004
- Wang, H., and Sun, X. (2017). Carbon monoxide-releasing molecule-2 inhibits connexin 43-hemichannel activity in spinal cord astrocytes to attenuate neuropathic pain. *J. Mol. Neurosci.* 63, 58–69. doi: 10.1007/s12031-017-0957-2
- Wang, L., Peng, Y., Peng, J., Shao, M., Ma, L., Zhu, Z., et al. (2018). Tramadol attenuates the sensitivity of glioblastoma to temozolomide through the suppression of Cx43-mediated gap junction intercellular communication. *Int. J. Oncol.* 52, 295–304. doi: 10.3892/ijo.2017.4188
- Wang, N., De Vuyst, E., Ponsaerts, R., Boengler, K., Palacios-Prado, N., Wauman, J., et al. (2013). Selective inhibition of Cx43 hemichannels by Gap19 and its impact on myocardial ischemia/reperfusion injury. *Basic Res. Cardiol.* 108:309. doi: 10.1007/s00395-012-0309-x
- Wang, Y., Wu, Z., Liu, X., and Fu, Q. (2013). Lamina gastrodin ameliorates Parkinson's disease by downregulating connexin 43. *Mol. Med. Rep.* 8, 585–590. doi: 10.3892/mmr.2013.1535
- Weyerbacher, A. R., Xu, Q., Tamasdan, C., Shin, S. J., and Inturrisi, C. E. (2010). N-Methyl-D-aspartate receptor (NMDAR) independent maintenance of inflammatory pain. *Pain* 148, 237–246. doi: 10.1016/j.pain.2009.11.003
- Wu, X. F., Liu, W. T., Liu, Y. P., Huang, Z. J., Zhang, Y. K., and Song, X. J. (2011). Reopening of ATP-sensitive potassium channels reduces neuropathic pain and regulates astroglial gap junctions in the rat spinal cord. *Pain* 152, 2605–2615. doi: 10.1016/j.pain.2011.08.003
- Xu, H., Gu, S., Riquelme, M. A., Burra, S., Callaway, D., Cheng, H., et al. (2015). Connexin 43 channels are essential for normal bone structure and osteocyte viability. *J. Bone Miner. Res.* 30, 436–448. doi: 10.1002/jbmr.2374
- Xu, Q., Cheong, Y.-K., He, S.-Q., Tiwari, V., Liu, J., Wang, Y., et al. (2014). Suppression of spinal connexin 43 expression attenuates mechanical hypersensitivity in rats after an L5 spinal nerve injury. *Neurosci. Lett.* 566, 194–199. doi: 10.1016/j.neulet.2014.03.004
- Yang, C., Rahimpour, S., Yu, A. C. H., Lonser, R. R., and Zhuang, Z. (2013). Regulation and dysregulation of astrocyte activation and implications in tumor formation. *Cell. Mol. Life Sci.* 70, 4201–4211. doi: 10.1007/s00018-013-1274-8
- Yang, H., Yan, H., Li, X., Liu, J., Cao, S., Huang, B., et al. (2018). Inhibition of connexin 43 and phosphorylated NR2B in spinal astrocytes attenuates bone cancer pain in mice. *Front. Cell. Neurosci.* 12:129. doi: 10.3389/fncel.2018.00129
- Yi, C., Ezan, P., Fernández, P., Schmitt, J., Sáez, J. C., Giaume, C., et al. (2017a). Inhibition of glial hemichannels by boldine treatment reduces neuronal suffering in a murine model of Alzheimer's disease. *Glia* 65, 1607–1625. doi: 10.1002/glia.23182
- Yi, C., Koulakoff, A., and Giaume, C. (2017b). Astroglial connexins as a therapeutic target for Alzheimer's disease. *Curr. Pharm. Des.* 23, 4985–4968. doi: 10.2174/1381612823666171004151215
- Yi, C., Mei, X., Ezan, P., Mato, S., Matias, I., Giaume, C., et al. (2016). Astroglial connexin43 contributes to neuronal suffering in a mouse model of Alzheimer's disease. *Cell Death Differ.* 23, 1691–1701. doi: 10.1038/cdd.2016.63
- Zhang, F. F., Morioka, N., Kitamura, T., Fujii, S., Miyauchi, K., Nakamura, Y., et al. (2016). Lycopene ameliorates neuropathic pain by upregulating spinal astrocytic connexin 43 expression. *Life Sci.* 155, 116–122. doi: 10.1016/j.lfs.2016.05.021

**Conflict of Interest Statement:** The authors declare that the research was conducted in the absence of any commercial or financial relationships that could be construed as a potential conflict of interest.

Copyright © 2019 Xing, Yang, Cui and Chen. This is an open-access article distributed under the terms of the Creative Commons Attribution License (CC BY). The use, distribution or reproduction in other forums is permitted, provided the original author(s) and the copyright owner(s) are credited and that the original publication in this journal is cited, in accordance with accepted academic practice. No use, distribution or reproduction is permitted which does not comply with these terms.





# An IQSEC2 Mutation Associated With Intellectual Disability and Autism Results in Decreased Surface AMPA Receptors

Eli J. Rogers<sup>1†</sup>, Reem Jada<sup>1†</sup>, Kinneret Schragenheim-Rozales<sup>1†</sup>, Megha Sah<sup>2</sup>, Marisol Cortes<sup>3</sup>, Matthew Florence<sup>4</sup>, Nina S. Levy<sup>1</sup>, Rachel Moss<sup>1</sup>, Randall S. Walikonis<sup>2</sup>, Raz Palty<sup>1</sup>, Reut Shalgi<sup>1</sup>, Daniela Lichtman<sup>1</sup>, Alexandra Kavushansky<sup>1</sup>, Nashaat Z. Gerges<sup>4</sup>, Itamar Kahn<sup>1</sup>, George K. E. Umanah<sup>3</sup> and Andrew P. Levy<sup>1\*</sup>

<sup>1</sup> Technion Faculty of Medicine, Technion Israel Institute of Technology, Haifa, Israel, <sup>2</sup> Department of Physiology and Neurobiology, University of Connecticut, Storrs, CT, United States, <sup>3</sup> Department of Neurology, Johns Hopkins University, Baltimore, MD, United States, <sup>4</sup> Department of Biopharmaceutical Sciences and Department of Cell Biology, Neurobiology and Anatomy, Medical College of Wisconsin, Milwaukee, WI, United States

## OPEN ACCESS

### Edited by:

Deepak Prakash Srivastava,  
King's College London,  
United Kingdom

### Reviewed by:

Jeongyeon Kim,  
Korea Brain Research Institute,  
South Korea  
Michael E. Cahill,  
University of Wisconsin-Madison,  
United States

### \*Correspondence:

Andrew P. Levy  
alevy@technion.ac.il

<sup>†</sup> These authors have contributed  
equally to this work

**Received:** 29 October 2018

**Accepted:** 01 February 2019

**Published:** 20 February 2019

### Citation:

Rogers EJ, Jada R, Schragenheim-Rozales K, Sah M, Cortes M, Florence M, Levy NS, Moss R, Walikonis RS, Palty R, Shalgi R, Lichtman D, Kavushansky A, Gerges NZ, Kahn I, Umanah GKE and Levy AP (2019) An IQSEC2 Mutation Associated With Intellectual Disability and Autism Results in Decreased Surface AMPA Receptors. *Front. Mol. Neurosci.* 12:43. doi: 10.3389/fnmol.2019.00043

We have recently described an A350V mutation in IQSEC2 associated with intellectual disability, autism and epilepsy. We sought to understand the molecular pathophysiology of this mutation with the goal of developing targets for drug intervention. We demonstrate here that the A350V mutation results in interference with the binding of apocalmodulin to the IQ domain of IQSEC2. We further demonstrate that this mutation results in constitutive activation of the guanine nucleotide exchange factor (GEF) activity of IQSEC2 resulting in increased production of the active form of Arf6. In a CRISPR generated mouse model of the A350V IQSEC2 mutation, we demonstrate that the surface expression of GluA2 AMPA receptors in mouse hippocampal tissue was significantly reduced in A350V IQSEC2 mutant mice compared to wild type IQSEC2 mice and that there is a significant reduction in basal synaptic transmission in the hippocampus of A350V IQSEC2 mice compared to wild type IQSEC2 mice. Finally, the A350V IQSEC2 mice demonstrated increased activity, abnormal social behavior and learning as compared to wild type IQSEC2 mice. These findings suggest a model of how the A350V mutation in IQSEC2 may mediate disease with implications for targets for drug therapy. These studies provide a paradigm for a personalized approach to precision therapy for a disease that heretofore has no therapy.

**Keywords:** IQSEC2, Arf6, GEF, AMPA, calmodulin, IQ domain, intellectual disability, autism

## INTRODUCTION

IQSEC2 is an X-linked gene which has been previously associated with intellectual disability (ID), autism and epilepsy (Shoubridge et al., 2010, 2019; Fieremans et al., 2015; Alexander-Bloch et al., 2016; Kalscheuer et al., 2016; Zerem et al., 2016; Mignot and Depienne, 2018) with mutations in IQSEC2 accounting for approximately 2% of patients with ID and epilepsy referred for exome sequencing (Heyne et al., 2018). Understanding the molecular pathophysiology of IQSEC2 mutations may allow for a personalized treatment program to provide much-needed hope and help to affected children and their families.

The IQSEC2 protein is localized in excitatory synapses as part of the NMDA receptor complex via interaction with post-synaptic density proteins DLG1, DLG2, and DLG4 and has been proposed to play a role in synaptic plasticity and dendritic spine formation (Murphy et al., 2006; Sakagami et al., 2008; Hinze et al., 2017). Biochemically IQSEC2 is a member of the GEF (guanine nucleotide exchange factor) family of proteins whose role is to promote exchange of GDP for GTP on specific Arfs (ADP ribosylation factors) and thereby activate the Arf. The target Arf for IQSEC2 is not known but binding of IQSEC2 to Arf6 has been demonstrated *in vitro* (Sakagami et al., 2008). Arf6, similar to other Arfs, regulates actin dynamics in dendritic spines and membrane trafficking, and is the only Arf which regulates trafficking between the cell surface membrane and endocytotic membranes (Donaldson, 2003; Choi et al., 2006; Jaworski, 2007). The GEF activity of IQSEC2, mediated through ARF6, has recently been demonstrated to be required for the activity dependent removal of  $\alpha$ -amino-3-hydroxyl-5-methyl-4-isoxazolepropionic acid (AMPA) receptors (Brown et al., 2016; Petersen et al., 2018) from the surface of hippocampal neurons. The regulation of surface synaptic AMPA receptors has been shown to be critically involved in learning and memory processes with alterations in AMPA trafficking being associated with cognitive impairment and social behavioral abnormalities (Awasthi et al., 2018; Medin et al., 2018; Parkinson and Hanley, 2018). Demonstration that IQSEC2 can regulate AMPA trafficking (Brown et al., 2016) may therefore provide a mechanistic link for the severe intellectual disability and abnormalities in social behavior associated with mutations in IQSEC2.

The IQSEC2 gene contains 15 exons and codes for a protein of 1488 amino acids (long isoform) with 98.5% homology between murine IQSEC2 and human IQSEC2. The coding sequence contains several canonical domains notably a catalytic domain (SEC7) [aa 746–939] characteristic of all GEFs promoting GTP exchange and an IQ like domain [aa 347–376] which has been suggested to bind calmodulin and thereby modulate the GEF activity of IQSEC2 (Shoubridge et al., 2010).

At least 70 different mutations have been described in the IQSEC2 gene all associated with moderate to severe intellectual disability, with variable seizures and autistic traits (Shoubridge et al., 2019). The genotype-phenotype relationship for these mutations is not understood. Many of these mutations cluster in recognized functional domains of IQSEC2 such as the Sec7 and IQ domains thereby providing a possible mechanism by which they produce disease (Mignot and Depienne, 2018; Shoubridge et al., 2019). There have been no reports in animal models on how altered IQSEC2 function for any of these mutations may influence cognition or social behavior.

We have recently reported on the ID and associated disorders in a child resulting from a *de novo* mutation identified by exome sequencing in the IQSEC2 gene (A350V, i.e., valine for alanine substitution in amino acid residue 350) (Zipper et al., 2017). In this study we set out to characterize the molecular mechanisms underlying the pathophysiology of the A350V IQSEC2 mutation *in vitro* and in a CRISPR murine model with the goal of developing precise therapies to alleviate at least in part the

severe clinical syndrome associated with the mutation. First, as the A350V mutation is in the IQ calmodulin binding domain of IQSEC2 we set out to define how this mutation may affect the interaction of IQSEC2 with calmodulin. Second, as other mutations in the IQ domain have been associated with changes in the ability of IQSEC2 to promote GTP exchange on Arf6 in response to calcium (Shoubridge et al., 2010; Myers et al., 2012) we investigated whether the A350V mutation may also alter Arf6 activity and whether this regulation was sensitive to calcium. Third, as IQSEC2 induced activation of Arf6 has been shown to modulate AMPA receptor trafficking (Brown et al., 2016) we sought to determine how the A350V mutation may affect this trafficking in our CRISPR model and specifically surface AMPA receptors which have been linked to learning and memory (Parkinson and Hanley, 2018). Fourth, we set out to determine whether the A350V mutation may affect basal hippocampal synaptic transmission. Finally, in an attempt to recapitulate the clinical phenotype in the CRISPR model we have assessed the effects of the A350V IQSEC2 mutation on behavioral phenotypes focusing on tests assessing locomotion, social interactions and learning.

## MATERIALS AND METHODS

### DNA Constructs Used in This Study

The IQSEC2 wild type gene was cloned 3' to renilla luciferase and three copies of the HA tag in pcDNA3.1 Zeo (Genscript) or 3' to a FLAG tag in pCAGGS. The pcDNA3.1 construct expresses full length (1488aa) human IQSEC2 with an N-terminal renilla luciferase and HAX3 tag under the control of a CMV promoter, and also contains a zeocin (Zeo) gene allowing for selection of stable transformants expressing the IQSEC2 gene. Specific mutations were introduced into the renilla luciferase-wild type (WT) IQSEC2 vector or the FLAG wild type IQSEC2 vector for the studies described herein (GenScript) (**Figure 1A**). For production of the A350V mutation we changed the corresponding codon for IQSEC2 amino acid residue 350 from GCT (Alanine) to GTT (Valine). We also generated two additional mutant constructs in the IQ domain of IQSEC2: (1) a previously described IQSEC2 R359C mutation associated with ID (Shoubridge et al., 2010) and (2) a previously described engineered mutation containing three alanine substitutions in the IQ region at amino acid residues 354, 355 and 359 (herein called 3A) (Myers et al., 2012). All IQSEC2 constructs were verified by DNA sequencing. The genes for calmodulin (human Calm1 (NM\_006888), Calm2 (NM\_001743) and Calm3 (NM\_005184) were obtained from a human ORFeome library (Yang et al., 2011) and subcloned into pcDNA3 to have a C-terminal triple FLAG tag.

### Cell Culture and Stable Cell Lines Expressing IQSEC2

HEK293T cells were propagated in DMEM with low glucose and 10% fetal calf serum (FCS). Stable cell lines (expressing either wild type or mutant A350V IQSEC2) were produced in 293T

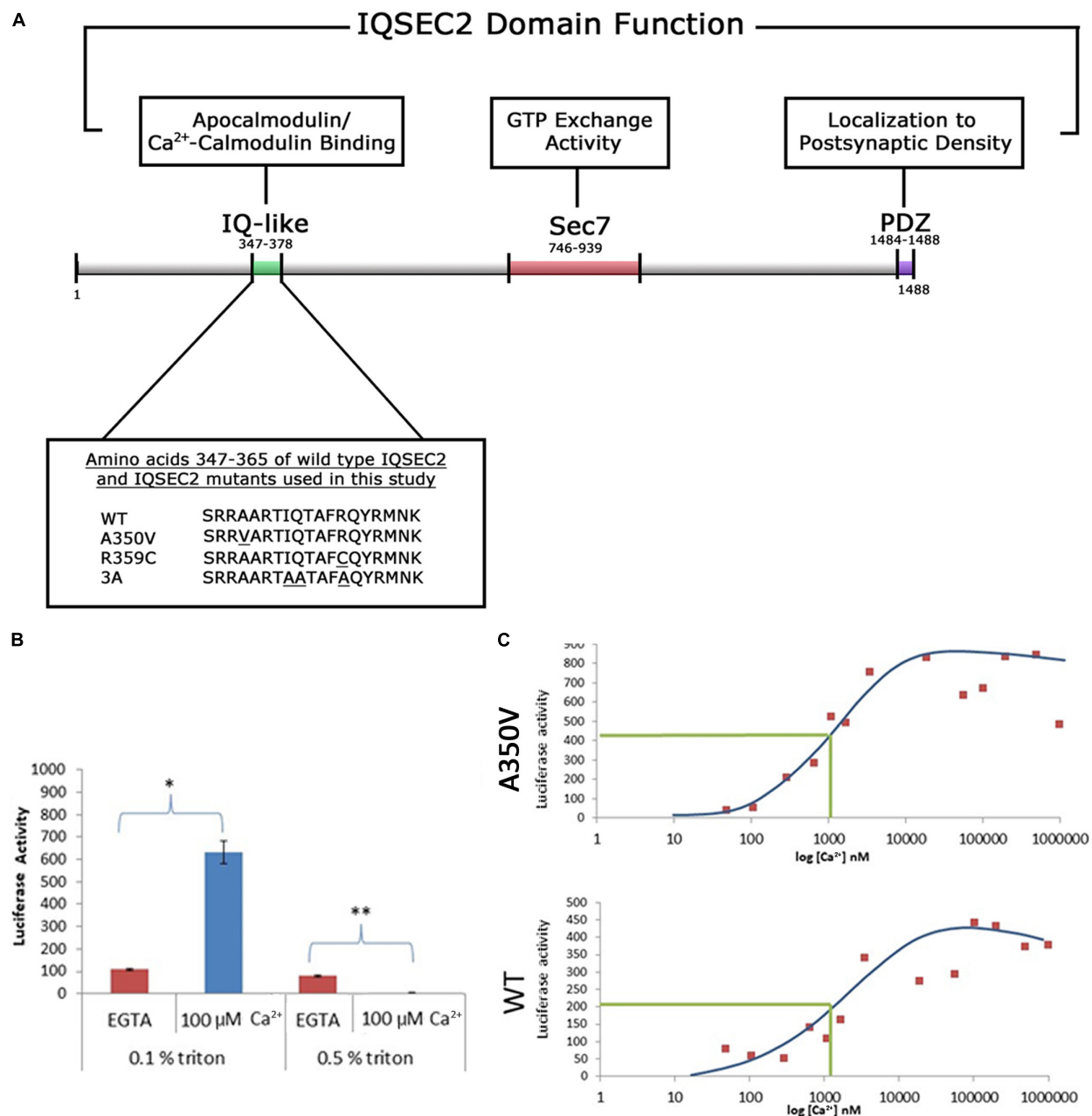


**FIGURE 1 | (A)** Functional domain organization of the IQSEC2 gene and amino acid sequence of IQSEC2 IQ motif mutants used in this study. IQ-like, IQ homology motif thought to be site for interaction of IQSEC2 with calmodulin (Shoubridge et al., 2010). SEC7, catalytic domain responsible for the GEF activity of IQSEC2 (Shoubridge et al., 2010). PDZ, domain reported to mediate interaction of IQSEC2 with the post-synaptic protein PSD-95 thereby localizing IQSEC2 to the post-synaptic density (Brown et al., 2016). Inset demonstrates the amino acid sequence within the IQSEC2 IQ domain of wild type IQSEC2 and sequence variants in this region, including A350V, used in this study. Underlined residues indicate site of sequence variance from the wild type. **(B)** The effect of calcium on the binding of IQSEC2 to calmodulin depends on the triton concentration in the cell extracts. Luciferase activity of the CM sepharose beads was used as a readout of the calmodulin IQSEC2-luciferase interaction. 293T cell extracts containing wild type IQSEC2 were prepared in low (0.1%) or high (0.5%) triton and used for binding studies with calmodulin sepharose as described in methods. In the presence of low triton concentration in the extracts, calcium resulted in a significant increase in the interaction between calmodulin and IQSEC2 (indicated by \*, unpaired *t*-test,  $p < 0.001$ ,  $n = 6$ ), while in the presence of high triton calcium resulted in a significant decrease in the interaction between calmodulin and IQSEC2 (indicated by \*\*, unpaired *t*-test,  $p < 0.001$ ,  $n = 6$ ). **(C)** The binding of calmodulin to wild type and A350V IQSEC2 is increased by calcium. Cell extracts containing wild type or A350V IQSEC2 and binding studies between IQSEC2 and calmodulin sepharose under defined calcium concentrations were performed as described in methods. As shown for a representative experiment for both wild type and A350V IQSEC2, calcium resulted in an increase in binding of calmodulin to IQSEC2 with a similar calcium dose-response relationship [half-maximal binding (indicated by green line) of calcium-calmodulin for IQSEC2 at a free calcium concentration of approximately 1  $\mu$ M for both wild type and A350V IQSEC2]. The binding of calcium calmodulin was significantly increased for A350V IQSEC2 as compared to wild type IQSEC2 at all calcium concentrations greater than 200 nM (A350V  $594 \pm 59.6$  vs. wild type  $271 \pm 41$  luciferase units,  $n = 11$ , unpaired *t*-test,  $p < 0.0005$ ).

cells using selection with Zeo (200 µg/ml) after transfection with calcium phosphate.

## Arf6 Activation Assay

For the assessment of Arf6-GTP by ELISA, cell extracts were prepared from HEK293T cells stably expressing either wild type or A350V IQSEC2. ELISA was performed exactly according to manufacturer's protocol (G-LISA Arf6 activation assay, Cytoskeleton Inc). The amount of Arf6-GTP was assessed using immobilized GGA peptide. Normalization was by total protein and/or luciferase as described in results.

For the assessment of Arf6-GTP using a GGA-3 pulldown assay and western blot, HEK293T cells were transfected with FLAG-tagged WT, A350V, or R359C IQSEC2 in pCAGGS vector by calcium phosphate. Twenty-four hours after transfection, the cultures were treated with 5 µM ionomycin or ethanol vehicle for 5 min, then lysed in 50 mM Tris-HCl, pH 7.5, 100 mM NaCl, 2 mM MgCl<sub>2</sub>, 0.2% SDS, 0.5% sodium deoxycholate, 1% Triton X-100, 10% glycerol, and 1x Halt protease inhibitor cocktail. An Arf6-GTP pull-down assay was carried out as described (Shoubridge et al., 2010). Briefly, lysates were cleared by centrifugation at 10,000 rpm for 10 min and incubated with GGA3:GST on glutathione-sepharose beads for 5 h at 4°C. The beads were washed and bound proteins were eluted and probed by immunoblot with rabbit anti-Arf6 (1:750, Cell Signaling #5740). Lysates were also probed against total Arf6 and with rabbit anti-FLAG (1:1000; Covance # PRB-132P) to detect expression of FLAG-IQSEC2. Bands were visualized with the use of a LiCor Odyssey imaging system and quantified with Image Studio Lite. Each band was normalized to the untreated sham-transfected control. The data were statistically analyzed by one-way ANOVA followed by Tukey's Multiple Comparison Test for *post hoc* analysis.

## Assessment of Binding of IQSEC2 to Calmodulin *in vitro*

The binding of wild type and mutant IQSEC2 to calmodulin was assessed *in vitro* using calmodulin-sepharose (BioVision, Milpitas, CA, United States). Extracts from stably transfected cells were prepared in either buffer A [50 mM Tris pH 7.5; 150 mM NaCl, 10 mg/ml BSA; 5 mM EGTA and 0.1% Triton X-100] or buffer B [10 mM Tris pH 7.5; 150 mM NaCl, 5 mM EGTA, 5% glycerol, 0.5% Triton X-100]. Extracts were clarified by centrifugation at 14000 rpm at 4°C to remove insoluble debris and the amount of luciferase activity in the extract assessed using the Promega luciferase assay system and a Turner TD 20/20 luminometer. Extracts (10,000–100,000 luciferase units) were then incubated in buffer A or buffer B with or without CaCl<sub>2</sub> in a total volume of 1 cc. The concentration of free calcium in the incubation conditions was calculated using the maxchelator algorithm<sup>1</sup> which is based on the ionic strength, pH, temperature and dissociation constant of EGTA for calcium. The concentration of free calcium used in these studies ranged from 0.73 nM to 2 mM. 10 µl of calmodulin-sepharose was added

to the incubation and mixed on a rotary apparatus for 3–4 h. The calmodulin-sepharose was washed twice with binding buffer, resuspended in 100 µl of luciferase reagent lysis buffer and 20 µl was assessed for luciferase activity.

## Assessment of Binding of IQSEC2 to Calmodulin in Cells

Assessment of an interaction between wild type and mutant renilla luciferase IQSEC2 constructs (wild type or mutants) and 3xFLAG tagged candidate interactors (calmodulin proteins Calm1 (NM\_006888), Calm2 (NM\_001743), and Calm3 (NM\_005184) in HEK293T cells was performed using the Lumier assay (Taipale et al., 2012), with an automated robotic system. Briefly, constructs were cotransfected using polyethylenimine (PEI), in 96 well plates. Cells were lysed at 48 h in lysis/wash buffer [50 mM Hepes pH 7.9; 150 mM NaCl; 2 mM EDTA; 0.5% Triton X-100, 5% glycerol] and candidate interactors were pulled down in anti-FLAG antibody (Sigma, F1804) coated 384 well plates for 3 h at 4°C. The amount of renilla luciferase activity in anti-FLAG captured protein was used as a readout of the strength of the interaction between renilla-IQSEC2 and interactor-FLAG. Interaction scores designate renilla activity after pulldown normalized to FLAG ELISA, to account for potential variability in interactor levels. GFP-FLAG was used as a negative control interactor and its interaction strength and score were considered background levels. Each experiment was performed with 2–4 replicate wells for each pair of IQSEC2 (wild type or mutant) and each calmodulin. In addition, independent replicate experiments were performed on different days, four repeat experiments for the wild type IQSEC2 and the A350V mutant and two repeat experiments for the R359C and 3A mutants. Renilla activity was also measured in whole cell lysates (negative control cells, cotransfected with GFP-FLAG) in order to verify that the observed differences in interaction scores between wild type and mutant IQSEC2 and the calmodulins were not due to differences in cell viability or transfection efficiency.

## Generation of A350V IQSEC2 Mice by CRISPR

Mice were generated by CRISPR at Applied Stem Cells (Milpitas, CA, United States). We targeted murine IQSEC2 (NM\_001005475.2) with the goal of generating an A350V mutation identical to that found in the human index case in which the codon GCT (Ala) at amino acid 350 is mutated to GTT (Val) with an additional AGG to CGT silent mutation (R349) in order to prevent the guide RNA g20 GGCAGCCCTGCGGCTCAGGA from targeting the same allele after repair. A single stranded oligonucleotide donor (ssODN) was synthesized with two homology arms flanking the GCT to GTT mutation site (5'CTGAGCT GCGCAGCCGCTCAAAGTTCCTATTTCATACGGTACTGTGCG AAAGGCTGTCTGGATGGTCTGGCAACACGGCGGCTCA GGAAGGAGCCCCCATACTTCCTCTCCAGCATTTCACCT GTCAGAGGAACAAGTTCAGAAAG3') serving as the repair template during the process of homology directed repair (HDR). Synthesized ssODN donor, g20 gRNA transcripts and Cas9

<sup>1</sup><https://somapp.ucdmc.ucdavis.edu/pharmacology/bers/maxchelator/CaEGTA-TS.htm>



mRNA were microinjected into the cytoplasm of C57BL/6J embryos. Identification of F0 successfully targeted mice were identified by Sanger sequencing. Germline transmitted F1s containing the mutation were used to generate the A350V colony used for all additional studies and continued breeding of the mice was done in a C57BL/6J background. Approximately 1 kb of DNA was sequenced on both sides of the mutation with no other changes detected. Wild type (WT) and A350V IQSEC2 protein were also assessed by western blot from mouse brains and they were found to be of the same size as predicted. MRI structural analysis of both wild type and A350V mice revealed no gross differences in brain volume or gross structural differences in A350V mice. Hemizygous males, heterozygous and homozygous females were fertile and were housed in a germ-free animal facility and used for breeding and the studies described.

All studies for which the mice were used were approved by the Institutional Animal Care and Use Committees of the institutions in which they were performed (Technion Faculty of Medicine (IL0360212; IL1691117) and Medical College of Wisconsin (AUA1650).

### Flow Cytometry Analysis for Surface AMPA Receptors of Hippocampal Neurons From Wild Type and A350V IQSEC2 Mutant Mice

A single cell suspension from the mouse hippocampus was prepared by mechanical dissociation using the gentleMACS dissociator (Miltenyi Biotec, Gladbach, Germany) coupled with tissue enzymatic degradation using the Adult Brain Dissociation Kit (Miltenyi Biotec). The cell suspension was mesh-filtered (70 micron) to remove clumps and debris and red blood cells were removed by a Red Blood Cell Removal Solution (Miltenyi Biotec). A highly enriched population of neurons were obtained from this cell suspension by depleting non-neuronal cells using the Neuron Isolation Kit (Miltenyi Biotec). Non-neuronal cells are removed in this method using biotin-conjugated monoclonal antibodies specific for non-neuronal cells followed by anti-biotin monoclonal antibodies coupled to magnetic microbeads.

For flow cytometric analysis of membrane bound GluA1/2 we used the Alex Fluor 647 fluorochrome –conjugated to Anti-GluA1/2 antibody (Santa Cruz, sc-517265). This antibody recognizes an epitope present in both GluA1 and GluA2. Neurons were incubated with the antibody for 30 min at 4°C and were then washed with a phosphate-buffered staining solution (Dulbecco's phosphate buffered saline with calcium, magnesium, glucose, pyruvate and 0.5% bovine serum albumin). Samples were analyzed on a LSRFortessa cell analyzer using FlowJo software.

### Surface Protein Cross-Linking Assay to Detect Surface AMPA Receptors in Hippocampal Tissue From Wild Type and A350V IQSEC2 Mice

To determine the relative distribution of surface AMPA receptors in the hippocampus of IQSEC2 A350V as compared to wild type IQSEC2 a surface protein-crosslinking assay was

performed using membrane-impermeant crosslinking agent, Bis(sulphosuccinimidyl)suberate (BS<sub>3</sub>, Sigma) as previously described (Umanah et al., 2017) with some modifications. Bis(sulphosuccinimidyl)suberate (BS<sub>3</sub>) is a membrane-impermeant crosslinking agent that selectively crosslinks cell-surface proteins, forming high-molecular-mass aggregates. Non-crosslinked intracellular proteins still retain their normal molecular mass. Brains from wild type or IQSEC2 A350V mice littermates were rapidly removed and the hippocampi were dissected on ice and stored at –80°C until further processing. The frozen tissue was cut into small pieces. Each sample was divided into two and transferred to 1.5 ml Eppendorf tubes containing ice-cold PBS buffer with or without 2 mM BS<sub>3</sub> followed by 3 h incubation at 4°C with gentle agitation. Tissues were quenched with 0.1 M glycine in PBS (10 min, 4°C) and lysed in ice-cold lysis buffer (PBS with 1% Triton-X100, 0.5% SDS, 5 mM EDTA, pH 7.4, and protease inhibitor cocktail). The lysates were homogenized and centrifuged at 15,000 × g for 5 min. The total protein concentrations in the supernatants were determined. 20 ug of total protein from each sample was resolved on 10% SDS-PAGE and western immunoblotting was performed to analyze the surface and intracellular pools of AMPA receptors using anti-GluA1 (rabbit monoclonal, Abcam, Ab109450) (1:1,000), anti-GluA2 (rabbit monoclonal, Abcam Ab150387) (1:2,000), anti-GluA3 (rabbit monoclonal, Abcam Ab40845) (1:1,000), anti-GluA4 (goat polyclonal, Abcam Ab115322) (1:1,000), HRP conjugated polyclonal goat anti-rabbit (Cell signaling 7074), HRP conjugated polyclonal rabbit anti-goat (Invitrogen 611620) and HRP conjugated monoclonal mouse anti-beta-actin (Millipore-SIGMA, A3854) (1:5,000). The signal on blots were generated with VisiGlo™ HRP Chemiluminescent Substrate Kits (1B1583, AMRESCO) and imaged captured by Amersham Imager 600. The band intensities of all blots were measured using NIH ImageJ software (Rasband, W.S., NIH<sup>2</sup>). All experiments were performed with five biological replicates and quantitative data are presented as the mean ± standard error of the mean (SEM) performed by GraphPad prism6 software (Instat, GraphPad Software). Statistical significance was assessed by *t*-test (two-tailed). Assessments were considered significant with a *p* < 0.05.

### Immunocytochemistry of Hippocampus for Surface AMPA Receptor GluA2 From Wild Type and A350V Mice

Mice were anesthetized and transcardially perfused with 4% paraformaldehyde (PFA) in PBS after a brief vascular system washing with PBS as previously described (Umanah et al., 2017). After perfusion, brains were removed and postfixed overnight with 4% PFA plus 4% sucrose in PBS. Brains were paraffinized and sectioned. Brain sections were then deparaffinized and blocked with 5% normal goat serum for 1 h at room temperature (RT). To label surface GluA2, sections were incubated at 4°C overnight in PBS containing mouse monoclonal anti-N-terminal GluA2 Alexa 488- conjugated

<sup>2</sup><http://rsb.info.nih.gov/ij/>

antibody (Millipore-SIGMA, MAB397A4). After four washes with PBS, sections were incubated with permeabilization buffer with 0.3% Triton X-100, 2.5% normal goat serum in PBS, and rabbit monoclonal anti-C-terminal GluA2 antibody (Abcam, Ab150387) to label total GluA2 for 4 h. The sections were then incubated in PBS containing goat anti-rabbit IgG Alexa Fluor Plus 555 conjugated secondary antibody (Thermo Fisher Scientific, A32732) for 1 h at RT after four washes with PBS. Sections were then stained with DAPI for 5 min. After four washes with PBS, sections were mounted on precleaned slides with Immuno-Mount (Thermo Fisher Scientific). Images were acquired using a Zeiss LSM laser-scanning confocal microscope. Images for all conditions in individual experiments were analyzed by using identical acquisition parameters and were thresholded using identical values. The fluorescence intensities of labeled surface and internalized receptors were measured using ZEN software (Zeiss). Total and surface expression were normalized to the DAPI signal. Data are presented as mean  $\pm$  SEM. The average fluorescence intensity of group results was used to determine the statistical significance by *t*-test (two-tailed) with a  $p < 0.05$  being considered statistically significant.

## Electrophysiological Studies

### Animals and Housing Conditions

Electrophysiological testing was performed at the Medical College of Wisconsin on A350V IQSEC2 and wild type IQSEC2 males at 18–20 weeks of age. Animals were housed 1–5 per cage in a 12 h light-dark cycle with food and water *ad libitum*. Experiments were conducted during the light phase.

### Slice Preparation

Animals were anesthetized by isoflurane inhalation and decapitated. Coronal brain slices (360–400  $\mu$ m thick) were cut using a vibrating slicer (Leica VT1200, Nussloch, Germany). Slices were prepared in a choline-based solution containing 110 mM choline chloride, 2.5 mM KCl, 1.25 mM  $\text{NaH}_2\text{PO}_4$ , 0.5 mM  $\text{CaCl}_2$ , 7 mM  $\text{MgSO}_4$ , 26 mM  $\text{NaHCO}_3$ , 11 mM glucose, 11.6 mM sodium ascorbate, and 3.1 mM sodium pyruvate. Slices were cut in the midline to produce two individual slices from each section. The slices were incubated for 30 min in a sucrose-based solution containing 78 mM NaCl, 68 mM sucrose, 26 mM  $\text{NaHCO}_3$ , 2.5 mM KCl, 1.25 mM  $\text{NaH}_2\text{PO}_4$ , 2 mM  $\text{CaCl}_2$ , 2 mM  $\text{MgCl}_2$ , and 25 mM glucose. Slices were then allowed to recover for at least 60 min in artificial cerebrospinal fluid (ACSF) containing 119 mM NaCl, 2.5 mM KCl, 4 mM  $\text{CaCl}_2$ , 4 mM  $\text{MgCl}_2$ , 1 mM  $\text{NaH}_2\text{PO}_4$ , 26 mM  $\text{NaHCO}_3$ , and 11 mM glucose, at pH 7.4 and 290 mOsm. All solutions were saturated with carbogen (95%  $\text{O}_2$  and 5%  $\text{CO}_2$ ) at room temperature.

### Input/Output Curve

Field potential evoked responses were recorded from the dendritic region of CA1 pyramidal neurons, with bipolar stimulation at the Schaffer collateral fibers, using Multiclamp 700A amplifier (Axon instruments). All recordings were made in circulating ACSF saturated with carbogen at 30°C. Fiber volleys and fEPSP (field excitatory post-synaptic potentials) slopes were calculated using Clampfit 10.7. Input/output (I/O) curves were

generated from A350V IQSEC2 ( $n = 4$ ) and wild type IQSEC2 ( $n = 5$ ) male mice. One-tailed Student's *t*-test was used to determine significance ( $p \leq 0.05$ ).

## Behavioral Tests

### Animals and Housing Conditions

Behavioral testing was performed on A350V IQSEC2 and wild type (WT) IQSEC2 male and female mice on the same genetic background (C57BL/6J) at 5–7 weeks of age. Animals were housed in groups of 2–5 per cage in a reversed 12 h light-dark cycle (dim light at 9:30 am, lights off at 10:00 am) with food and water available *ad libitum*. The housing room was maintained at  $23 \pm 2^\circ\text{C}$ . Experiments were conducted during the dark phase, under red lighting conditions ( $< 5$  lux), between 10 am and 7 pm. All behavioral testing experiments were performed by the same two individuals who were blinded to the genotype of the animals. Any single animal was only handled by a single individual throughout these studies. Animals were handled for two consecutive days prior to the testing day except for the three-chamber sociability and social novelty tests (see below for details). On the testing day, mice were transferred to the testing room and were acclimated for an hour before the experiment commenced. All animal experiments were conducted in accordance with the United States Public Health Service's Policy on Humane Care and Use of Laboratory Animals and approved by the Institutional Animal Care and Use Committee of Technion – Israel Institute of Technology (IL1691117).

### Behavioral Analysis

For all the experiments, the arena or apparatus was cleaned after each trial with 70% ethanol and then with double-distilled water. All experiments were video-recorded by a camera (GUPPY PRO F-125B CCD) located above the arena and analyzed using Ethovision XT software version 10.1 (Noldus, Wageningen, The Netherlands), except for the Rotarod test which was recorded and analyzed using MATLAB R2017a (The Mathworks, Natick, MA, United States).

### Open Field Test

5–6 week old mice were placed in the center of a squared box arena (40  $\times$  40  $\times$  35 cm) made of white Derlin plastic and explored the novel environment for 5 min (Prut and Belzung, 2003). Velocity and distance were measured to assess locomotor activity. Anxiety-like behavior was measured by calculating the time spent in the center as compared to the perimeter of the arena. The arena was divided into 25 equal squared tiles with the center of the arena defined as the nine central tiles (40% of the arena) with each corner defined as a single tile.

### Rotarod

Assessment of motor coordination was done using the Rotarod test (Med Associates Inc., Georgia, VT, United States) (Karl et al., 2003). 5–6 week old mice were placed on a 32 mm diameter rod accelerating from 4 to 40 revolutions per minute (rpm) and latency to fall and end speed were measured. The test was performed on two consecutive days, each day consisting of four

trials which lasted up to 6 min with an inter-stimulus interval of 10 min during which mice were placed in their home-cage.

### Three-Chamber Sociability and Social Novelty Tests

Social interaction was measured in order to assess autistic-like behavior using a three-chamber test (Moy et al., 2004). Subject mice were assessed for the tendency to prefer an unfamiliar conspecific mouse (social stimulus; *Stranger 1*) over a novel object and over another unfamiliar mouse (novel social stimulus; *Stranger 2*). The arena (70 × 29 × 35 cm) was comprised of three chambers (side chambers 26 × 29 × 35 cm). 6–7 week old mice (subject and stimulus) were habituated to the testing room for 1 h on three consecutive days prior to the test day. Stimulus mice were further habituated to the wire cages (10.8 cm in height and 10.2 cm diameter; Galaxy Cup, Spectrum Diversified Designs, Inc., Streetsboro, OH, United States) for 20 min each day. On the test day, subject mice were habituated to the apparatus for 10 min and were allowed to explore all three empty chambers. Time spent in each chamber was measured to assess chamber bias. Following habituation, subject mice were assessed for social preference for 10 min by allowing interaction with *Stranger 1* placed inside a wire cage in one chamber and a novel object placed inside an identical wire cage in the opposite chamber. Stimulus mice location was counterbalanced across trials to prevent chamber bias. Next, the novel object was replaced with *Stranger 2* and social novelty was assessed for 10 min during which the subject mouse was able to choose between a novel mouse and an already familiar mouse. Time spent in each chamber and in close interaction were measured for both the preference and novelty experiments. Stimulus mice were conspecific C57BL/6J mice from different litters, and were age, sex and weight-matched to the subject mice and to each other.

### Morris Water Maze

The Morris water maze test was used to assess spatial learning and memory (Vorhees and Williams, 2006). 6–7 week old mice were placed in a 120 cm circular diameter pool filled with water and a 15 cm diameter transparent platform that was placed at the Southwest (SW) quadrant, submerged 1 cm below the water surface. Water was maintained at 22.0 ± 1°C and made opaque by adding a dried milk powder. Mice were trained for four consecutive days, each day consisted of four trials with an inter-stimulus interval of 15 min during which mice were placed in their home-cage. During training, mice were released from a different quadrant in each trial and were given 60 s to find the platform. If the mice did not find the platform within 60 s, the experimenter guided the animal to the platform. After reaching the platform, mice were left on the platform for 10 s. On the 5th day a probe trial was performed in which the platform was removed from the maze, mice were released at the Northeast quadrant and given 60 s to explore the maze. Time spent in the SW quadrant served as an index of long-term memory.

### Statistical Analysis of Behavioral Tests

All data were analyzed using MATLAB R2017a (The Mathworks, Natick, MA, United States). Summary statistics are presented as means ± SEM. Lilliefors test was used to determine normality.

Two-tailed Student's *t*-tests were used on normally distributed data. Mann–Whitney *U*-test was used to analyze data when sample size was not sufficient to establish normality.

## RESULTS

### In a Cell-Free System *in vitro* Wild Type IQSEC2 Binds Significantly Better to Apocalmodulin as Compared to A350V and Calcium Increases Binding of Both Wild Type and Mutant IQSEC2 to Calmodulin

As the A350V IQSEC2 mutation is in the IQ domain of IQSEC2 (Figure 1A) and the IQ domains of many proteins have been demonstrated to bind to calmodulin (Bahler and Rhoads, 2002) we first sought to determine how the A350V mutation would affect calmodulin binding to IQSEC2. Investigation of this interaction in a cell-free system *in vitro* using luciferase tagged IQSEC2 and calmodulin coupled to sepharose allowed for the precise control of calcium concentration which is known to dramatically affect the conformation and interactions of calmodulin with other proteins. In this system luciferase activity associated with calmodulin sepharose was used a quantitative readout of the calmodulin-IQSEC2 interaction. The IQ motif is present in over 100 proteins and in some cases preferentially binds to calcium-calmodulin while in other cases it binds preferentially to calcium-free calmodulin (apocalmodulin) (Bahler and Rhoads, 2002). Prior work on the IQSEC2-calmodulin interaction using myc-tagged wild type IQSEC2 and calmodulin sepharose (Myers et al., 2012) reported that apocalmodulin bound to IQSEC2 and that the addition of 2 mM calcium (thereby generating calcium-calmodulin) dramatically decreased the binding of calmodulin to IQSEC2. However, when we assessed the effect of calcium on the IQSEC2 calmodulin interaction we observed that calcium increased the binding of calmodulin to IQSEC2. Upon reviewing the buffers used by our group and that of Myers in assessing binding of IQSEC2 to calmodulin, we discovered that we differed in the concentration of Triton X-100 used in the binding and wash buffers. As shown in Figure 1B, at 0.1% Triton X-100, 100 μM calcium was associated with a several fold increase in binding of calmodulin to wild type IQSEC2 while at 0.5% Triton X-100, 100 μM calcium was associated with a several fold decrease in binding of calmodulin to wild type IQSEC2. Triton X-100 binds to most proteins via both hydrophobic and polar interactions (Singh and Kishore, 2006) and may thereby disrupt protein-protein interactions at high concentrations. An example of a calmodulin-interacting protein that is important for the calmodulin-IQ interaction is PEP-19 which binds to the C-terminal domain of calmodulin and electrostatically steers it to interact with the IQ domain (Wang and Putkey, 2016). We interpreted these results as indicating that normally calcium stimulates calmodulin binding to IQSEC2 and that the results of Myers showing calcium reduces the binding of calmodulin to IQSEC2 were artifacts related to the high Triton concentration used.

Therefore, for our *in vitro* studies comparing the interaction between calmodulin and wild type IQSEC2 as compared to mutant IQSEC2 we used low (0.1%) Triton X-100. In the absence of added calcium (5 mM EGTA) we observed that apocalmodulin bound significantly better to wild type IQSEC2 than A350V IQSEC2 ( $146 \pm 18$  vs.  $48 \pm 8$  luciferase units for wild type IQSEC2 as compared to A350V IQSEC2;  $n = 6$  experiments, unpaired *t*-test,  $p < 0.001$ ). We assessed the binding of wild type or A350V luciferase-IQSEC2 to calmodulin over a wide range of calcium concentrations. The  $K_d$  of calcium for calmodulin is  $1 \mu\text{M}$  and it has been demonstrated that at free calcium concentrations of less than 200 nM all calmodulin exists as apocalmodulin and there is no calcium-calmodulin (Persechini and Cronk, 1999). As shown for a representative experiment in **Figure 1C** for both wild type and A350V IQSEC2,

calcium resulted in an increase in the binding of calmodulin to IQSEC2 with a similar calcium dose-response relationship (half-maximal binding of calcium-calmodulin for IQSEC2 at a free calcium concentration of approximately  $1 \mu\text{M}$  for both wild type and A350V IQSEC2). The binding of calcium calmodulin was significantly increased for A350V IQSEC2 as compared to wild type IQSEC2 at all calcium concentrations greater than 200 nM (A350V  $594 \pm 59.6$  vs. wild type  $271 \pm 41$  luciferase units,  $n = 11$ , unpaired *t*-test,  $p < 0.0005$ ). These data demonstrate that while A350V binds less efficiently than wild type IQSEC2 to apocalmodulin, the A350V mutant is capable of binding calcium-calmodulin equivalent to or even superior to wild type IQSEC2. As has been demonstrated for the binding of apocalmodulin and calcium calmodulin to myosin (Trybus et al., 2007) these data would suggest that the epitopes or

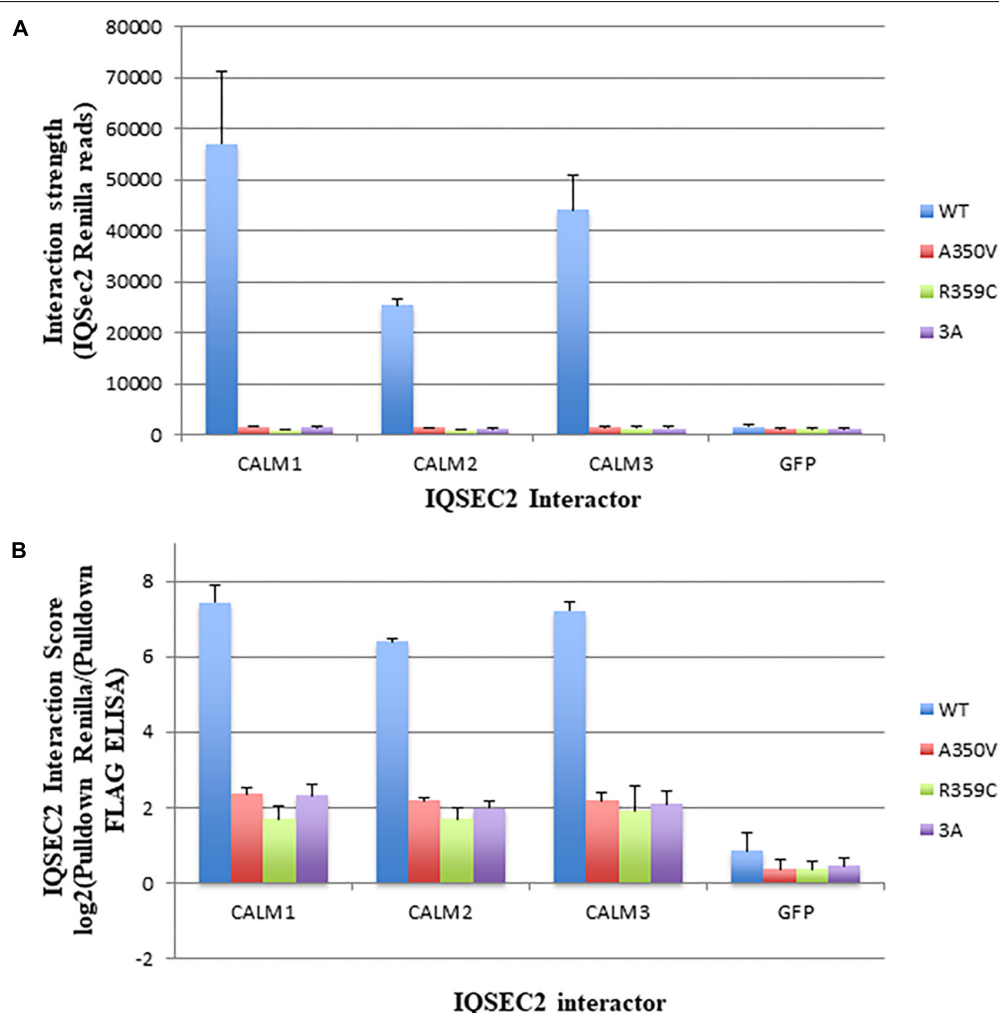


**FIGURE 2 |** Binding of wild type and mutant IQSEC2 to calmodulins in cells using the Lumier assay. **(A)** Interaction strength of wild type and mutant IQSEC2 proteins and calmodulins, measured as renilla luciferase-IQSEC2 activity after pulldown of calmodulin-FLAG proteins. Shown are mean and SD of 4 biological replicate wells for each pair of IQSEC2 calmodulin interactions. **(B)** Interaction score of wild type and mutant IQSEC2 proteins and calmodulins, measured as log2 of renilla luciferase-IQSEC2 activity after FLAG pulldown divided by pulldown FLAG ELISA, to normalize for the interactor levels. Shown are the mean and SD of 4 biological replicate wells for each pair of IQSEC2 calmodulin interactions. Data comparing A350V IQSEC2 and wild type IQSEC2 are representative of four independent experiments done on independent days and the data for the R359C and 3a mutants are representative of two independent experiments done on independent days.



conformations within IQSEC2 recognized by apocalmodulin and calcium-calmodulin are different.

### In Cells Wild Type IQSEC2 Binds More Effectively to Apocalmodulin Than A350V IQSEC2

We next sought to determine if we could demonstrate differences in the binding of apocalmodulin to wild type and A350V IQSEC2 in cells similar to what we found in a cell free system. In order to achieve this goal we assessed the binding of wild type and three mutant IQSEC2 renilla luciferase constructs (A350V, R359C, 3A) to three isoforms of human calmodulin in HEK293T cells using the Lumier assay as described in methods. In HEK cells, the intracellular calcium concentration is 50–100 nM so that all

calmodulin is present as apocalmodulin (Persechini and Cronk, 1999). We observed significantly stronger binding of wild type IQSEC2 to all three apocalmodulin proteins as compared to the three mutant IQSEC2 constructs. We observed 34, 15, and 36-fold differences between wild type and A350V IQSEC2 mutant with Calm1, Calm2 and Calm3, respectively (**Figure 2A**) with similar fold changes seen for IQSEC2 mutants R359C and 3A. Importantly, the interaction strength of the mutants with the apocalmodulins was very close to background interaction levels, as measured for interactions with GFP (**Figure 2A**) and GFP interaction was no different with wild type vs. mutant IQSEC2 (fold change of 1.07). Normalized interaction scores that take into account differences in the levels of the different interactors demonstrated 31, 14, and 31-fold higher interaction of wild type IQSEC2 with Calm1, Calm2 and Calm3, respectively, compared

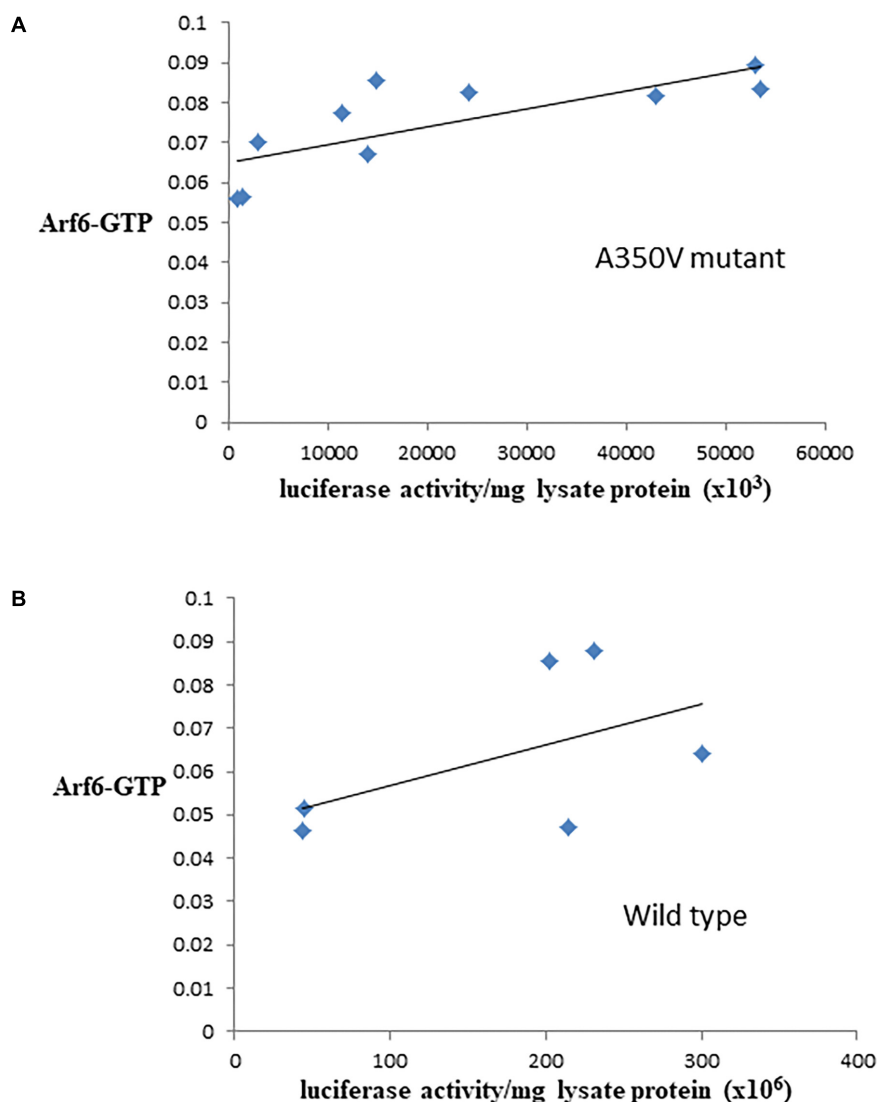


**FIGURE 3 |** Correlation between Arf6-GTP and luciferase in cell lines producing A350V (**A**) or wild type (**B**) IQSEC2 luciferase. Arf6-GTP was measured by ELISA (spectrophotometric units). The correlation between the relative amount of IQSEC2 and Arf6-GTP was significant for A350V ( $r = 0.77$ ,  $n = 10$ ,  $p = 0.009$ ) but not for WT IQSEC2 ( $r = 0.52$ ,  $n = 6$ ,  $p = 0.28$ ).

to A350V IQSEC2 (**Figure 2B** shown in log2 scale). We verified that the observed differences were not due to differences in cell viability or transfection efficiency as assessed by input luciferase activity of whole cell lysates. These data in cells are consistent with what was observed in a cell-free system, specifically that wild type IQSEC2 binds to apocalmodulin more effectively than A350V IQSEC2.

### Arf6 Activation Is Increased in A350V IQSEC2 Stable or Transiently Transfected Cells as Compared to Wild Type IQSEC2

The binding of calmodulin to IQSEC2 has been proposed to regulate IQSEC2 GEF activity for Arf6 promoting Arf6-GTP formation and thereby activating Arf6 (Shoubridge et al., 2010; Myers et al., 2012; Brown et al., 2016). Moreover, a R359C IQSEC2 mutation in the IQ calmodulin binding region of IQSEC2 has been associated with changes in IQSEC2 GEF activity for Arf6 (Shoubridge et al., 2010). Having demonstrated that the A350V affects the interaction of calmodulin for IQSEC2 we therefore set out to determine how the A350V mutation may affect the ability of IQSEC2 to promote Arf6-GTP. We assessed Arf6-GTP levels by ELISA in multiple stable transformants of HEK293T expressing different amounts of either wild type or A350V IQSEC2 as assessed by luciferase activity. We found, using equivalent amounts of protein extract, there was an approximately 25% increase in total Arf6-GTP in HEK293T cells expressing A350V IQSEC2 as compared to wild type IQSEC2 [ $0.075 \pm 0.004$  ( $n = 10$ ) vs.  $0.060 \pm 0.015$  ( $n = 6$ );  $p = 0.04$ ]. The stable cell lines expressing wild type or A350V IQSEC2 differed markedly in the relative amount of IQSEC2 (assessed by luciferase activity) which they produced with overall 5–200 fold more wild type IQSEC2 being produced than mutant IQSEC2 in these cell lines. When normalized for both protein and luciferase activity (i.e., comparing the GEF specific activity of A350V IQSEC2 to wild type IQSEC2) the A350V IQSEC2 protein promoted nearly 30-fold more Arf6-GTP than wild type IQSEC2 protein ( $1.6 \times 10^8 \pm 6.8 \times 10^{-9}$  vs.  $5.7 \times 10^{-10} \pm 1.7 \times 10^{-10}$ ,  $p = 0.058$ ). There was a highly significant correlation between the relative amount of A350V IQSEC2 and Arf6-GTP ( $r = 0.77$ ,  $p = 0.009$ ). This correlation was weaker in stable cell lines expressing different amounts of wild type IQSEC2 ( $r = 0.52$ ,  $p = 0.28$ ) (**Figures 3A,B**).

We also assessed activation of Arf6 (Arf6-GTP) by wild type, A350V, or R359C IQSEC2 in a GGA3 pulldown assay. HEK 293T cells were transiently transfected with constructs to express either wild type, A350V or R359C IQSEC2, and endogenous Arf6 activation was tested with or without treatment with the calcium ionophore ionomycin. Ionomycin has been previously demonstrated to increase IQSEC2 GEF activity and Arf6-GTP formation by stimulating calcium influx and thereby affecting the interaction of calmodulin with IQSEC2 (Myers et al., 2012). Cell lysates were incubated with beads coated with GGA3:GST to isolate the GTP-bound Arfs, and bound Arf6 was assessed by immunoblot (**Figure 4A**). Expression of wild type IQSEC2 resulted in  $3.87 \pm 0.89$  fold increase in Arf6 activation compared to sham transfected cells. Ionomycin treatment of cells

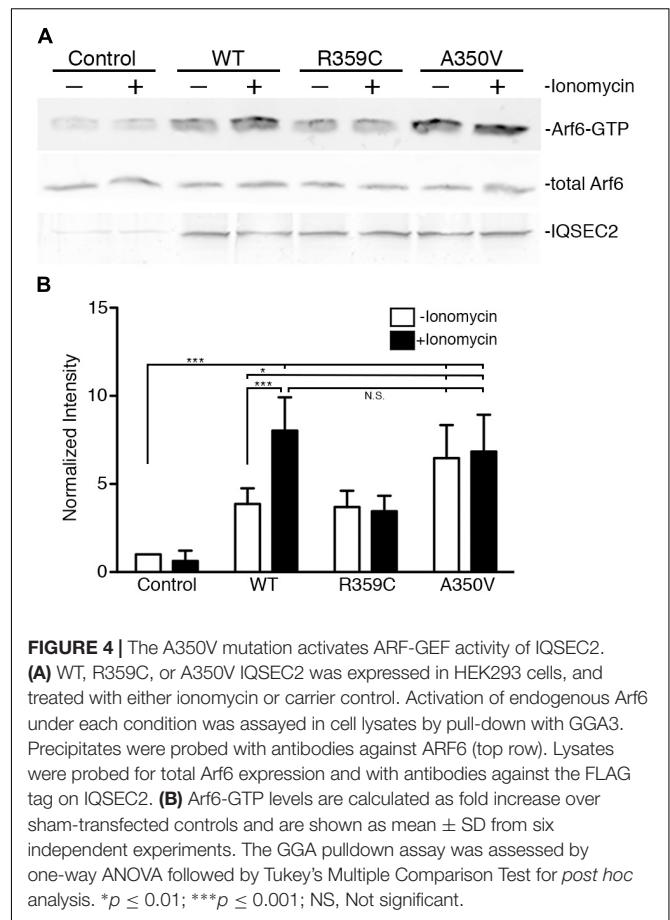


**FIGURE 4 |** The A350V mutation activates ARF-GEF activity of IQSEC2.

(A) WT, R359C, or A350V IQSEC2 was expressed in HEK293 cells, and treated with either ionomycin or carrier control. Activation of endogenous Arf6 under each condition was assayed in cell lysates by pull-down with GGA3. Precipitates were probed with antibodies against ARF6 (top row). Lysates were probed for total Arf6 expression and with antibodies against the FLAG tag on IQSEC2. (B) Arf6-GTP levels are calculated as fold increase over sham-transfected controls and are shown as mean  $\pm$  SD from six independent experiments. The GGA pull-down assay was assessed by one-way ANOVA followed by Tukey's Multiple Comparison Test for *post hoc* analysis. \* $p \leq 0.01$ ; \*\*\* $p \leq 0.001$ ; NS, Not significant.

containing wild type IQSEC2 further doubled Arf6 activation to an  $8.03 \pm 1.89$  fold increase. Transfection with R359C also caused an induction of Arf6-GTP, but this mutant was unresponsive to ionomycin treatment. Transfection of the A350V mutant strongly increased Arf6 activation to a level that was statistically indistinguishable from the cells both transfected with wild type IQSEC2 and treated with ionomycin. In the absence of ionomycin transfection with A350V significantly increased Arf6 activation as compared to wild type ( $p < 0.01$ ) and ionomycin did not further increase Arf6 activation by A350V (**Figure 4B**). These data demonstrate that the A350V mutation results in the constitutive activation of IQSEC2 GEF activity for Arf6.

### Surface AMPA Receptors Are Reduced in A350V Hippocampus

The GEF activity of IQSEC2, mediated through Arf6, has recently been demonstrated to be required for the activity dependent removal of AMPA receptors from the surface of hippocampal neurons (Brown et al., 2016). We therefore proposed that a constitutive increase in Arf6-GTP by A350V, as we have demonstrated *in vitro*, would result in a down regulation of surface AMPA receptors in hippocampi from A350V IQSEC2 mice as compared to wild type IQSEC2 mice. We assessed expression of total gluA1 and gluA2 receptors in hippocampus and whole brain by western blot from wild

type and A350V mice (age 6–8 weeks) and did not find any difference between the total receptor expression in these mice. We then sought to determine if the amount of surface expressed gluA1/2 was different between the wild type and A350V mice. First, by flow cytometry analysis (**Figures 5A,B**) we assessed gluA1/2 expression on the surface of neurons prepared from hippocampus as described in methods from 6 to 8 week old male mice and found a highly significant 30% reduction in the number of cells expressing surface gluA1/2 in A350V as compared to wild type IQSEC2 male mice (mean  $4.1\% \pm 0.5\%$  vs.  $3.1\% \pm 0.5\%$ ; median 3.9% vs. 2.7%,  $n = 10$  for wild type and mutant mice, respectively, paired  $t$ -test,  $p < 0.00001$ .) There was also a highly significant reduction in the total amount of gluA1/2 surface expression in those cells identified by flow cytometry as expressing surface gluA1/2 (median difference 51,  $p < 0.008$  by Wilcoxon signed rank test). Total (intracellular and extracellular) gluA1/2 was not significantly different between wild type and mutant mice assessed by flow cytometry. Second, using a surface cross linking assay coupled with western blot we assessed surface AMPA receptors (GluA1-4 subunits) in wild type and mutant hippocampi from male 6 to 8 week old mice and found that surface expression of GluA2 was significantly reduced in A350V IQSEC2 hippocampus as

compared to wild type IQSEC2 hippocampus (**Figure 6**) resulting in an overall significant change in the surface distribution of the different AMPA receptor subunits in the A350V mice (unpaired  $t$ -test; Two-tailed,  $t = 2.579$   $df = 8$ ,  $p = 0.0327$ ). There was no significant difference between A350V and wild type hippocampus in the amount of total GluA2 AMPA receptor or in the distribution of the total AMPA receptor subunits in these studies. Additionally, immunohistochemistry of surface expression of GluA2 in hippocampus (**Figure 7**) further confirmed that GluA2 AMPA receptor surface expression is reduced in A350V male mice compare to control wild type male mice. There was no significant difference in the amount of total GluA2 between A350V and wild type hippocampi as assessed by immunohistochemistry. Collectively, these data demonstrate that hippocampal surface GluA2 is decreased in A350V IQSEC2 mice.

### Basal Synaptic Transmission Is Decreased in the Hippocampus of A350V IQSEC2 Mice

In order to determine if the decrease in hippocampal surface AMPA expression was associated with a change in hippocampal

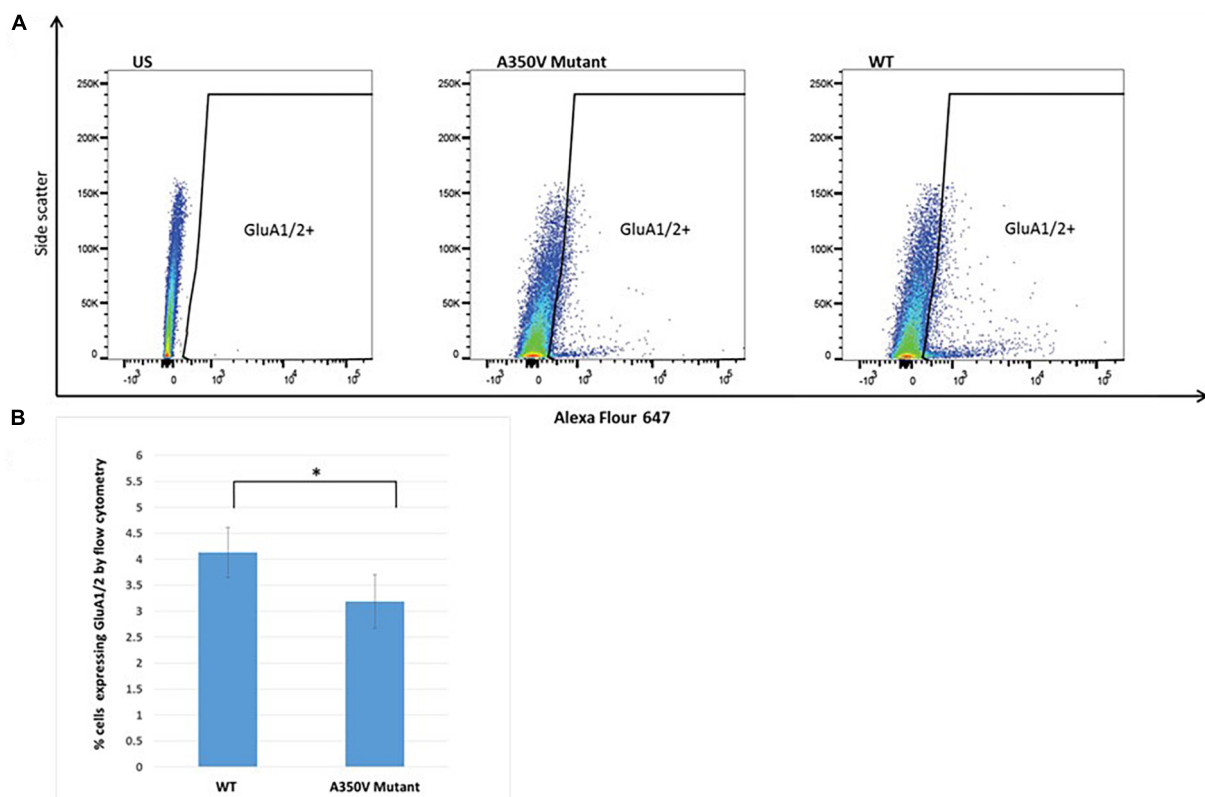


**FIGURE 5 |** Flow cytometry analysis of hippocampal derived cells for GluA1/2. **(A)** Representative dot plot of one of 10 experiments. US panel-unstained hippocampal cells. Mut and WT panels demonstrating staining with Alexa Flour 647 for extracellular GluA1/2 in single cell suspension of hippocampal cells from A350V and wild type mice, respectively, and window selected for identifying GluA1/2+ cells. **(B)** Summary of all experiments demonstrating significantly higher percentage of cells staining with GluA1/2 in wild type as compared to A350V mutant hippocampal neuronal preparations ( $4.1 \pm 0.5$  vs.  $3.1 \pm 0.5$ , paired  $t$ -test,  $n = 10$  independent experiments,  $*p < 0.00001$ ).

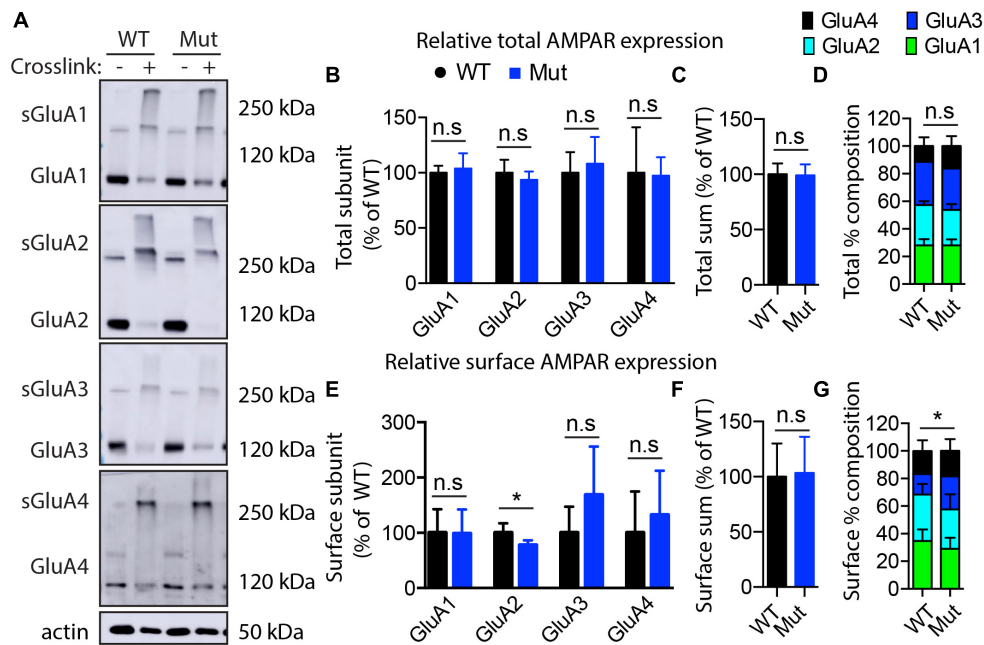


**FIGURE 6 |** Assessment of AMPA receptor subunits by surface cross-linking. **(A)** Representative images of immunoblots after  $\text{BS}_3$ -crosslinking of samples to assess surface (crosslinking “+”) and total protein expression of AMPA receptors (crosslinking “–”). Actin was used for normalization. **(B)** Quantification of relative total protein levels of AMPA receptor subunits in samples not crosslinked. Signal intensities normalized to actin signal and wild type as 100%. **(C)** Quantification of total sum of all AMPA receptor subunits in samples not crosslinked. **(D)** Quantification of AMPA receptor subunit percentage composition in samples not crosslinked. **(E)** Quantification of relative surface protein levels of AMPA receptor subunits in samples treated with  $\text{BS}_3$  (crosslinking “+”). Surface protein indicated by “s” on the blots in **(A)** Signal intensities of the bands at 250 kDa and above were normalized to actin signal and wild type as 100%. **(F)** Quantification of total sum of all AMPA receptor subunits at the membrane surface. **(G)** Quantification of surface AMPA receptor subunit percentage composition (significant differences in GluA2 composition). Optical densitometry quantification values represent the mean  $\pm$  SEM ( $n = 4-5$ , \* $p < 0.05$ , n.s.  $p > 0.05$ ,  $t$ -test, two-tailed).

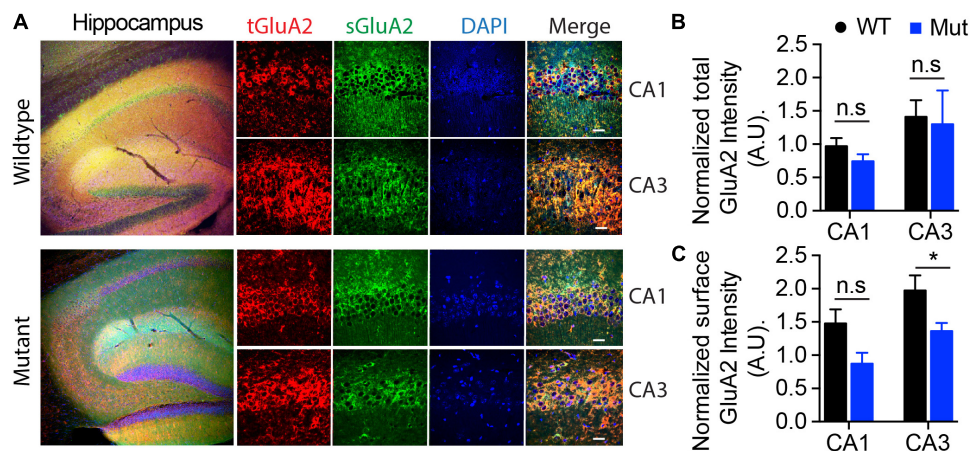


**FIGURE 7 |** Assessment of surface expression of AMPA receptor GluA2 in hippocampus by immunocytochemistry. **(A)** Representative images of immunohistochemistry of total (tGluA2) and surface (sGluA2) AMPA receptor GluA2 in wildtype and A350V IQSEC2 mutant hippocampi. Higher power representative images of the CA1 and CA3 regions are shown (right panel). Labeled scale bar for high-resolution images = 20  $\mu\text{m}$ . **(B)** Quantification of the normalized total GluA2 levels. Data represent mean  $\pm$  SEM,  $n = 5$  male mice in each group. No significant difference (n.s.)  $P > 0.05$ ,  $t$ -test, two-tailed. **(C)** Quantification of the normalized levels of surface GluA2 expression. Data represent mean  $\pm$  SEM,  $n = 5$  male mice in each group, \* $p < 0.05$ , n.s.  $p > 0.05$ ,  $t$ -test, two-tailed.

synaptic transmission we performed electrophysiological testing using coronal brain slices from A350V and WT IQSEC2 mice as described in methods. Evoked responses were recorded from the dendritic region of hippocampal CA1 pyramidal neurons.

An input/output curve representing synaptic responses (fEPSP slope/fiber volley) resulting from different stimulus intensities (**Figure 8**). Synaptic responses were significantly lower in A350V IQSEC2 mice as compared to WT IQSEC2 mice. These data



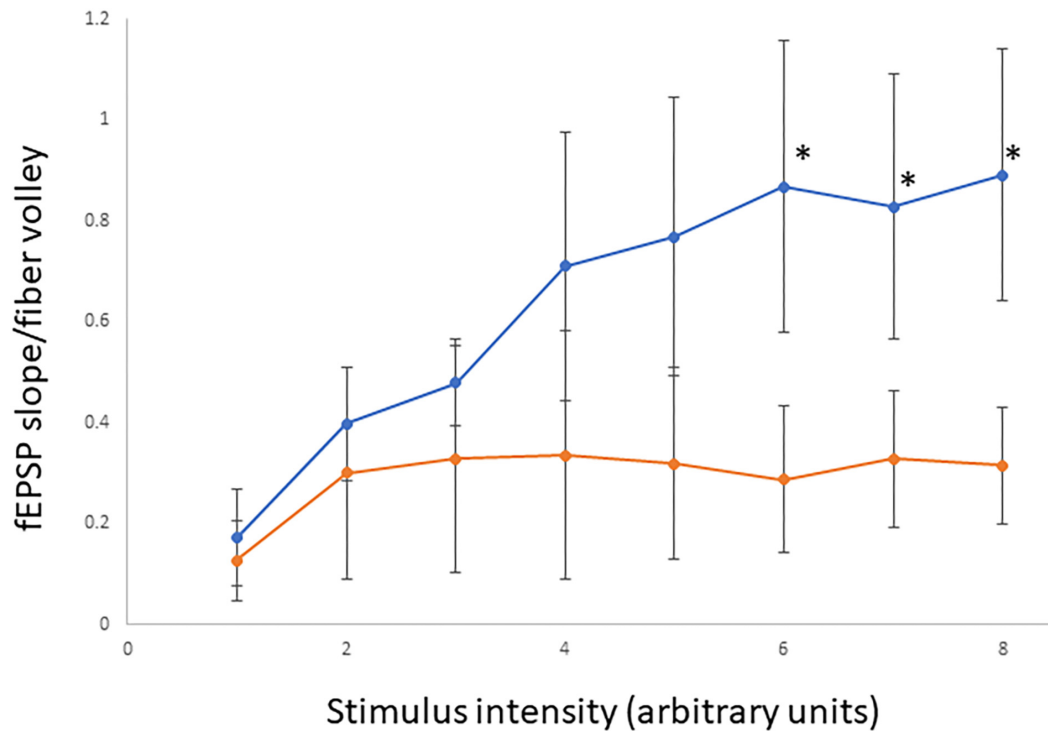


**FIGURE 8 |** Assessment of basal synaptic transmission in CA1 region of hippocampus. Input/output curves representing synaptic responses (fEPSP slope/fiber volley) resulting from different stimulus intensities. Stimulus intensity numbers are arbitrary units; where 1 is intensity that gives minimum response and 8 is intensity that produces maximum response. Synaptic responses were significantly lower in A350V IQSEC2 mice (orange) compared to WT IQSEC2 mice (blue). Data represent mean  $\pm$  SEM,  $n = 5$  wild type IQSEC2 mice and  $n = 4$  A350V IQSEC2 mice, \* $p \leq 0.05$ ,  $t$ -test, one-tailed.

demonstrate that basal hippocampal synaptic transmission is decreased in A350V IQSEC2 mice.

## Behavioral Phenotyping of A350V IQSEC2 Mice

In order to characterize the behavioral phenotype of the A350V IQSEC2 animal model, we examined anxiety-like behavior, locomotion, motor coordination, social behavior and learning abilities. Anxiety-like behavior was assessed in the open field test and we found no significant difference between A350V male mice ( $n = 13$ ) and WT littermates ( $n = 13$ ) in the time spent in the center of the arena relative to the perimeter [A350V: mean =  $0.215 \pm 0.02$ ; WT: mean =  $0.17 \pm 0.01$ , unpaired  $t$ -test;  $t(24) = 1.588$ ,  $p = 0.130$ ], suggesting that A350V show normal levels of anxiety-like behavior (Figure 9Ai). Locomotion (total distance traveled) was also assessed using the open field test (Figure 9Aii). There was a significant difference between A350V ( $n = 13$ ) and WT littermates ( $n = 13$ ) male mice when measuring the total distance traveled and velocity in the open field arena [unpaired  $t$ -test; distance:  $t(24) = -3.2805$ ,  $p < 0.01$ ; velocity:  $t(24) = -3.2851$ ,  $p < 0.01$ ]. This result was consistent with the increased locomotion found in A350V mice in the habituation phase of the three-chamber social preference test [unpaired  $t$ -test;  $t(24) = 2.3125$ ,  $p < 0.05$ ]. Motor coordination was assessed in the Rotarod test (Figure 9B). Both A350V and WT mice performed at similar levels with no significant difference between the two

groups in the time spent on the accelerating rotating rod. Social preference of A350V mice toward an unfamiliar conspecific mouse over an inanimate novel object was assessed using a three-chamber social arena (Figure 9C). Both A350V male mice ( $n = 13$ ) and WT ( $n = 13$ ) littermates preferred to spend more time in close interaction with a social stimulus (Stranger 1) over a novel object [paired  $t$ -test; A350V:  $t(12) = 2.535$ ,  $p < 0.05$ ; WT:  $t(12) = 4.671$ ,  $p < 0.001$ ]. However, A350V mice showed a trend toward social impairment as measured by a decreased time spent in close interaction with Stranger 1 compared to WT mice [unpaired  $t$ -test;  $t(24) = 1.743$ ,  $p = 0.094$ ]. Preference for social novelty (Figure 9D) was assessed by comparing the time spent in close interaction with a novel mouse to an already familiar mouse (Stranger 1). Both A350V ( $n = 9$ ) and WT ( $n = 12$ ) mice preferred an unfamiliar mouse (Stranger 2) relative to a previously encountered mouse (paired  $t$ -test; A350V:  $t(8) = 4.367$ ,  $p < 0.01$ ; WT:  $t(11) = 3.134$ ,  $p < 0.01$ ). However, A350V mice spent significantly more time in close interaction with a novel social stimulus (Stranger 2) over the familiar mouse compared to WT mice [unpaired  $t$ -test;  $t(19) = 2.294$ ,  $p < 0.05$ ]. Hippocampal-dependent memory was assessed using the Morris water maze test. Significant differences between female A350V ( $n = 5$ ) and WT ( $n = 5$ ) mice were found in the latency to reach the platform on the 1st and 4th days of training (Mann-Whitney  $U$ -test; Day 1:  $U = 16$ ,  $p < 0.05$ ; Day 4:  $U = 16$ ,  $p < 0.05$ ), as shown in the learning curve of each group (Figure 9Ei). In addition,

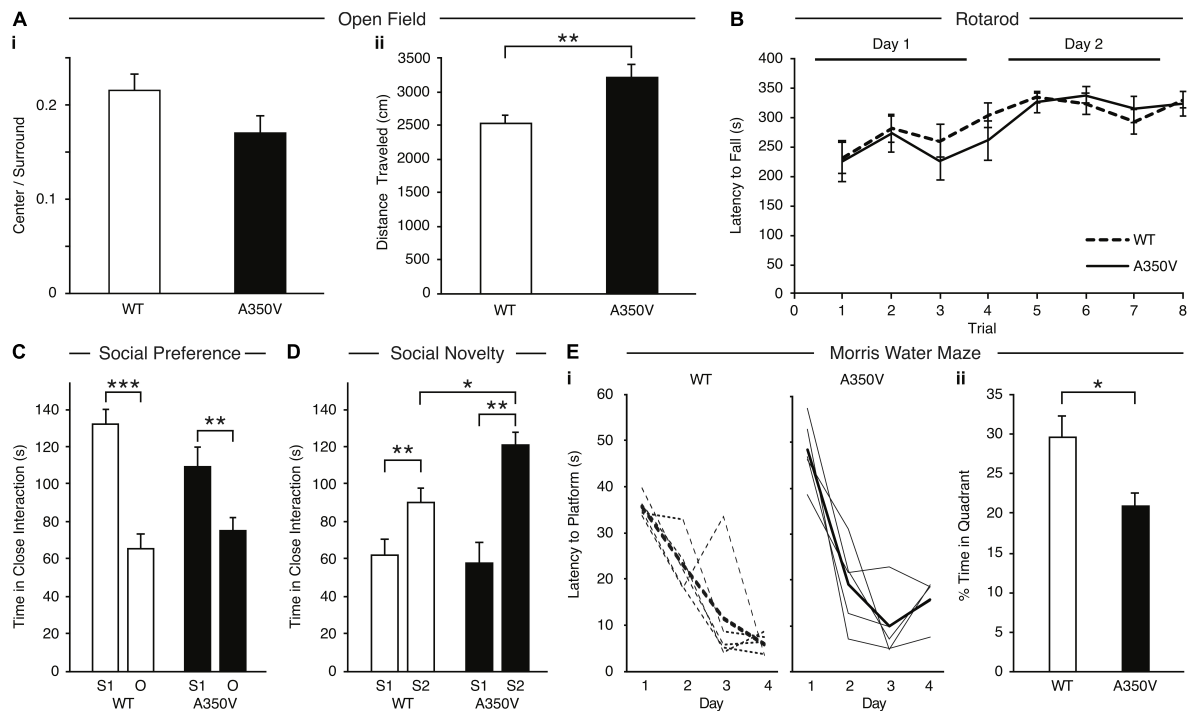


**FIGURE 9 |** Behavioral phenotype of A350V IQSEC2 mouse model. **(A)** A350V display normal levels of anxiety-like behavior (i) and increased locomotion activity in an open field test (ii) ( $n = 13$  wild type and A350V IQSEC2 mice). **(B)** Intact motor coordination in A350V relative to WT tested by the Rotarod test expressed as an equivalent learning curve and retention across two days in the two groups ( $n = 13$  wild type and A350V IQSEC2 mice). **(C)** Duration of time spent in close interaction with Stranger 1 (S1) and an object (O) in the three-chamber social preference test demonstrating both A350V and WT preferred interacting with S1 although this preference was less pronounced in A350V ( $n = 13$  wild type and A350V IQSEC2 mice). **(D)** Preference for social novelty expressed as the duration of time spent in close interaction with a previously encountered stranger animal (S1) relative to a novel stranger animal (S2) revealed a tendency to spend more time with S2 in WT and A350V, with significant enhancement of this preference for social novelty in A350V mice ( $n = 12$  wild type and 9 A350V IQSEC2 mice). **(E)** Learning and memory deficits in A350V mice shown by the latency to reach the hidden platform during training (i), shown for individual animals (thin lines) and averaged across the group (thick line) separately for WT and A350V mice and the percentage time spent in the target quadrant in a Morris water maze test (ii) ( $n = 5$  wild type and A350V IQSEC2 mice). Data indicate means  $\pm$  SEM. \* $p < 0.05$ , \*\* $p < 0.01$ , \*\*\* $p < 0.001$ .

time in the target quadrant during a probe trial was compared between female A350V ( $n = 5$ ) and WT ( $n = 5$ ) mice revealing a significant difference between the groups (Mann–Whitney  $U$ -test;  $U = 39.5$ ,  $p < 0.05$ ) (Figure 9Eii). Collectively, these data demonstrate that the A350V IQSEC2 mice model manifests some of the abnormalities found in the human index case with the A350V IQSEC2 mutation, specifically hyperactivity, abnormal social interactions and impaired cognitive function.

## DISCUSSION

This study provides new findings for understanding the regulation of IQSEC2 activity and the pathophysiology of a new IQSEC2 mutant (A350V) with implications for drug therapy. First, we have demonstrated that calcium increases the binding of IQSEC2 to calmodulin and we reconcile our data with previously reported conflicting results. Second, we report on the first mutation identified in humans associated with a constitutive activation of Arf6 due to a constitutive increase in IQSEC2 GEF activity. Third, we have demonstrated that surface GluA2 AMPA receptors are decreased in the brains of A350V IQSEC2 mice.

Finally, we demonstrate that A350V IQSEC2 mice have abnormal behavioral phenotypes with increased locomotion, abnormal social interactions and decreased learning.

We have demonstrated in two different systems, *in vitro* with cell extracts and in cells, that apocalmodulin can bind to IQSEC2 and that this binding is impaired with the A350V mutant. In a resting cell (i.e., HEK 293T cells, neurons) the cytoplasmic concentration of free calcium is 50–100 nM (Persechini and Cronk, 1999) with localized calcium concentrations of 1–10  $\mu$ M being achieved with an appropriate stimulus (i.e., NMDA receptor activation in neurons). The  $K_d$  of calcium for calmodulin is approximately 1  $\mu$ M with essentially no calcium-calmodulin being found in a cell with a free cytoplasmic calcium of less than 200 nM (Persechini and Cronk, 1999). Our demonstration that half-maximal interaction between calmodulin and IQSEC2 occurs at around 1  $\mu$ M calcium is therefore physiologically relevant.

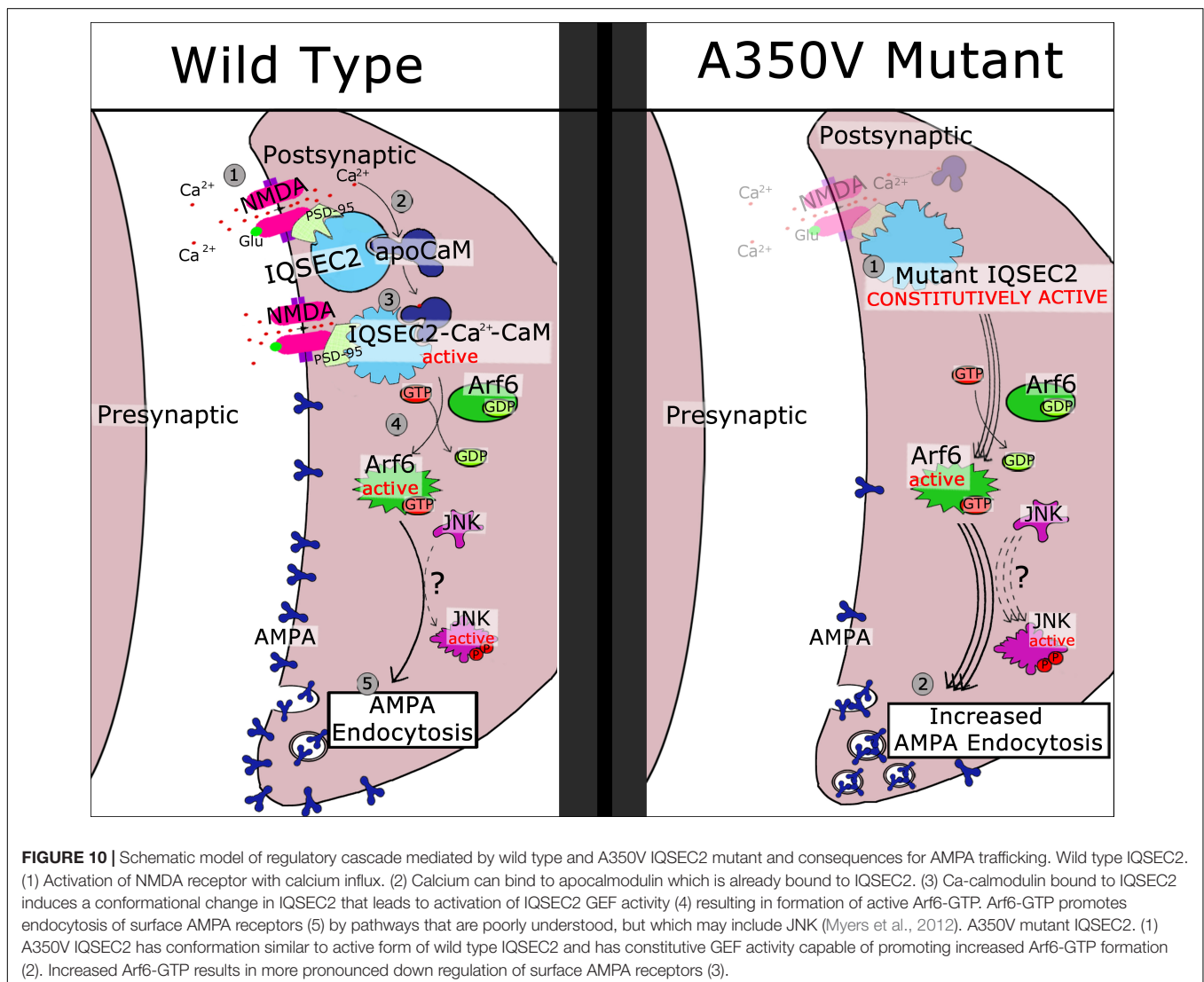
However, while A350V binds less efficiently to apocalmodulin as compared to wild type IQSEC2, the A350V mutant is capable of binding calcium-calmodulin equivalent to or even superior to wild type IQSEC2. Similar to myosin (Trybus et al., 2007) the epitope or conformation within the IQ region of IQSEC2

recognized by apocalmodulin and calcium calmodulin may be different. Our finding that A350V IQSEC2 can effectively bind to calcium-calmodulin but not apocalmodulin may suggest that the alpha helical distortion of the IQ domain in the A350V IQSEC2 mutant induced by the valine-for-alanine substitution introduces a change in the conformation of the IQ motif of IQSEC2 that is similar to the conformation of the IQ motif that is induced in wild type IQSEC2 by the binding of calcium calmodulin. The wild type IQSEC2 IQ motif may adopt a relaxed conformation in which apocalmodulin may bind when calcium-calmodulin is not present; however, in the A350V mutation the conformation of the IQ region may be locked in a conformation which will not allow it to assume a conformation permissive for apocalmodulin binding.

This is the first demonstration of a human disease resulting from a constitutive activation of Arf6 due to a constitutive increase in IQSEC2 GEF activity. We have shown that the IQSEC2 GEF activity for Arf6 is increased in cells expressing mutant A350V IQSEC2 as compared to wild type IQSEC2. Ionomycin treatment of cells expressing WT IQSEC2 induced

a significant increase in Arf6 activation, indicating a calcium-dependent regulation of Arf-GEF activity. The A350V mutant, however, already had a high level of basal activity that was comparable to WT IQSEC2 after treatment with ionomycin. All previously reported mutants of IQSEC2, including R359C, which is also located in the IQ region, have been noted to have decreased Arf6 GEF activity (Shoubbridge et al., 2010). We also show that the GEF activity of the R359C mutant is not elevated by ionomycin treatment, which suggests that deficits in calcium dependent regulation of this mutant may contribute to ID. As discussed above we propose that the constitutive activation of IQSEC2 GEF activity by the A350V mutation may be due to the mutation locking the IQ motif into the same conformation as wild type IQSEC2 bound to calcium-calmodulin (wherein IQSEC2 GEF activity is increased).

A key factor underlying the strength of individual excitatory synapses is the number of AMPA receptors at synapses. Trafficking of AMPA receptors to and from synapses plays a key role in synaptic transmission and in experience-dependent



synaptic plasticity and associative learning (Qin et al., 2005; Rumpel et al., 2005; McCormack et al., 2006; Hu et al., 2007; Matsu et al., 2008; Kielland et al., 2009; Zhu, 2009). NMDA receptor-induced removal of GluA1/2 AMPA receptors from synapses is a key step in the induction of long-term depression (LTD), and Arf6 activation is a necessary component of this type of plasticity (Scholz et al., 2010; Brown et al., 2016). IQSEC2 regulates AMPA receptor currents (Myers et al., 2012; Brown et al., 2016). The Arf-GEF activity of IQSEC2 is required for LTD, as ID-linked mutations in IQSEC2 that decrease its Arf-GEF activity impair its induction (Brown et al., 2016). This indicates that properly regulated activation of Arf6 by IQSEC2 is necessary for normal synaptic plasticity processes, including the regulated removal of AMPA receptors in LTD. Our findings here showing that increased Arf6 activity is associated with decreased GluA2 AMPA surface expression in A350V mutant brain tissue is consistent with the critical role of Arf6 in regulating the removal of AMPA receptors from the plasma membrane (Brown et al., 2016). Our demonstration that basal hippocampal synaptic transmission is decreased in A350V IQSEC2 mice is also consistent with a down-regulation of AMPA receptors in this model. Future experiments with specific AMPA receptor antagonists and positive allosteric modulators will attempt to prove that the decreased synaptic transmission in the A350V mice is due at least in part to a downregulation of AMPA receptors.

Based on the data presented here and previous work presented by others (Myers et al., 2012; Brown et al., 2016) we propose in **Figure 10** a model for the activation of wild type IQSEC2 by calcium as well as the pathophysiological consequences of the A350V IQSEC2 mutation. In the presence of wild type IQSEC2, the binding of glutamate to the NMDA receptor leads to calcium influx and a rise in free intracellular calcium. This calcium binds to calmodulin and the binding of calcium calmodulin to the IQ site on IQSEC2 induces the GEF activity of IQSEC2 allowing it to promote the formation of Arf6-GTP. Arf6-GTP, in turn, regulates endocytosis of surface AMPA receptors by pathways that are poorly understood, but which may include JNK (Myers et al., 2012). On the other hand, in the A350V IQSEC2 mutant, IQSEC2 GEF activity for Arf6 is constitutively activated resulting in persistently increased Arf6 activity, which may markedly downregulate surface AMPA receptors, specifically GluA2, (representing an exaggerated form of long-term depression). Thus, the normal processes for regulating AMPA receptor levels at synapses are compromised by the A350V IQSEC2 mutation. This hypothesis appears to provide a mechanistic basis for the defects in behavior and learning associated with the A350V IQSEC2 mutation. Furthermore, according to this hypothesis, treatment to restore the balance in AMPA transmission by blocking exaggerated AMPA downregulation may provide clinical benefit specifically an increase in learning potential. The size of the change in surface GluA2 AMPA induced by the A350V mutation is similar to what has been reported in mutations in the Thorase gene (Umanah et al., 2017; Piard et al., 2018) where pharmacological attempts to restore normal surface AMPA activity have shown therapeutic benefit in man (Ahrens-Nicklaus et al., 2017).

Behavioral phenotyping of the A350V IQSEC2 mice demonstrates increased locomotion, abnormal social interactions and learning impairments in the absence of motor coordination deficits. The increased preference for social novelty in the A350V mice described here, while different from what has been described in autism, has been described in other genetic encephalopathies with intellectual disability and abnormal social functioning such as Williams's syndrome (Martin et al., 2018; Ng et al., 2018). Our behavioral findings in the A350V mice appear to model some of the abnormal behaviors found in the human index case with the A350V mutation, specifically hyperactivity, abnormal social interactions with no inhibitions with strangers and impaired cognitive function. However, more complete behavioral phenotyping of the A350V IQSEC2 model will be required in order to properly define the spectrum of social interaction abnormalities, hyperactivity features, and the type of learning and memory impairment present in these mice. Decreases in surface AMPA receptors have been noted in other models of learning impairment (neurodevelopmental as well as Alzheimer's disease) and in models of social dysfunction (Guntupalli et al., 2016; Ahrens-Nicklaus et al., 2017; Umanah et al., 2017; Kim et al., 2018; Piard et al., 2018; Tian et al., 2018) and increasing AMPA transmission has shown benefit in these models (Lauterborn et al., 2016; Kim et al., 2018). Accordingly, strategies designed to restore surface AMPA in the A350V IQSEC2 mouse model may have a beneficial effect on cognitive and affective behavior and represents a potential actionable node for treatment in humans for the A350V IQSEC2 mutation.

## ETHICS STATEMENT

This study was carried out in accordance with the recommendations of the Technion Faculty of Medicine and the Medical College of Wisconsin Institutional Animal Care and Use Committees (IACUC) and approved by the IACUC committees.

## AUTHOR CONTRIBUTIONS

ER, RJ, KS-R, MS, MF, NL, RM, RW, RS, RP, DL, AK, IK, MC, NG, GU, and AL designed and performed the experiments, and analyzed the data. RS, RW, DL, NG, IK, GU, and AL wrote the manuscript. All authors were involved in revising the manuscript for important intellectual content and gave final approval of the version to be published.

## FUNDING

This work was funded in part by the Rappaport Research Institute to APL and NIH/NINDS NS099362 to GU.

## ACKNOWLEDGMENTS

This work is dedicated to Eviatar Haim Harir and his courageous parents Esther Zehava Harir and Avichai Shalom Harir.



## REFERENCES

- Ahrens-Nicklaus, R. C., Umanah, G. K. E., Sondheim, N., Deardorff, M. A., Wilkens, A. B., Conlin, L. K., et al. (2017). Precision therapy for a new disorder of AMPA receptor recycling due to mutations in ATAD1. *Neurol. Genet.* 3:e130. doi: 10.1212/NXG.0000000000000130
- Alexander-Bloch, A., McDougle, C., Ullman, Z., and Sweetser, D. (2016). IQSEC2 and X-linked syndromal intellectual disability. *Psychiatr. Genet.* 26, 101–108. doi: 10.1087/YPG.0000000000000128
- Awasthi, A., Ramachandran, B., Ahmed, S., Benito, E., Shinoda, Y., Nitzan, N., et al. (2018). Synaptotagmin-3 drives AMPA receptor endocytosis, depression of synapse strength, and forgetting. *Science* 363, eaav1483. doi: 10.1126/science.aav1483
- Bahler, M., and Rhoads, A. (2002). Calmodulin signaling via the IQ motif. *FEBS Lett.* 513, 107–113. doi: 10.1016/S0014-5793(01)03239-2
- Brown, J. C., Petersen, A., Zhong, L., Himelright, M. L., Murphy, J. A., Walikonis, R. S., et al. (2016). Bidirectional regulation of synaptic transmission by BRAG1/IQSEC2 and its requirement in long-term depression. *Nat. Commun.* 7:11080. doi: 10.1038/ncomms11080
- Choi, S., Ko, J., Lee, J. R., Lee, H. W., Kim, K., Chung, H. S., et al. (2006). ARF6 and EFA6A regulate the development and maintenance of dendrites. *J. Neurosci.* 26, 4811–4819. doi: 10.1523/JNEUROSCI.4182-05.2006
- Donaldson, J. G. (2003). Multiple roles for Arf6: sorting, structuring and signaling in the plasma membrane. *J. Biol. Chem.* 278, 41573–41576. doi: 10.1074/jbc.R300026200
- Fieremans, N., Van Esch, H., de Ravel, T., Van Driessche, J., Belet, S., Bauters, M., et al. (2015). Microdeletion of the escape genes KDM5C and IQSEC2 in a girl with severe intellectual disability and autistic features. *Eur. J. Med. Genet.* 58, 324–327. doi: 10.1016/j.ejmg.2015.03.003
- Guntupalli, S., Widagdo, J., and Anggono, V. (2016). Amyloid B induced dysregulation of AMPA receptor trafficking. *Neural Plast.* 2016, 1–12. doi: 10.1155/2016/3204519
- Heyne, H. O., Singh, T., Stamberger, H., Jamra, R. A., Caglayan, H., Craiu, D., et al. (2018). *De novo* variants in neurodevelopmental disorders with epilepsy. *Nat. Genet.* 50, 1048–1053. doi: 10.1038/s41588-018-0143-7
- Hinze, S. J., Jackson, M. R., Lie, S., Jolly, L., Field, M., Barry, S. C., et al. (2017). Incorrect dosage of IQSEC2, a known intellectual disability and epilepsy gene, disrupts dendritic spine morphogenesis. *Transl. Psychol.* 7:e1110. doi: 10.1038/tp.2017.81
- Hu, H., Real, E., Takamiya, K., Kang, M. G., Ledoux, J., Hugarir, R. L., et al. (2007). Emotion enhances learning via norepinephrine regulation of AMPA receptor trafficking. *Cell* 131, 160–173. doi: 10.1016/j.cell.2007.09.017
- Jaworski, J. (2007). ARF6 in the nervous system. *Eur. J. Cell Biol.* 86, 513–524. doi: 10.1016/j.ejcb.2007.04.007
- Kalscheuer, V. M., James, V. M., Himelright, M. L., Long, P., Oegema, R., Jensen, C., et al. (2016). Novel missense mutation A789V in IQSEC2 underlies X-linked intellectual disability in the MRX78 family. *Front. Mol. Neurosci.* 8:85. doi: 10.3389/fnmol.2015.00085
- Karl, T., Pabst, R., and Von Horsten, S. (2003). Behavioral phenotyping of mice in pharmacological and toxicological research. *Exp. Toxicol. Pathol.* 55, 69–83. doi: 10.1078/0940-2993-00301
- Kielland, A., Bochorishvili, G., Corson, J., Zhang, L., Rosin, D. L., Heggelund, P., et al. (2009). Activity patterns govern synapse specific AMPA-R trafficking between deliverable and synaptic pools. *Neuron* 62, 84–101. doi: 10.1016/j.neuron.2009.03.001
- Kim, J. W., Park, K., Kang, R. J., Gonzales, E. L. T., Kim, D. G., Oh, H. A., et al. (2018). Pharmacological modulation of AMPA receptor rescues social impairments in animal models of autism. *Neuropsychopharmacology* 44, 314–323. doi: 10.1038/s41386-018-0098-5
- Lauterborn, J. C., Palmer, L. C., Jia, Y., Pham, D. T., Hou, B., Wang, W., et al. (2016). Chronic Ampakine Treatments Stimulate Dendritic Growth and Promote Learning in Middle-Aged Rats. *J. Neurosci.* 36, 1636–1646. doi: 10.1523/JNEUROSCI.3157-15.2016
- Martin, L. A., Iceberg, E., and Allaf, G. (2018). Consistent hypersocial behavior in mice carrying a deletion of Gtf2i but no evidence of hyposocial behavior with Gtf2i duplication: implications for Williams-beuren syndrome and autism spectrum disorder. *Brain Behav.* 8:e00895. doi: 10.1002/brb3.895
- Matsu, N., Reijmers, L., and Mayford, M. (2008). Spine type specific recruitment of newly synthesized AMPA receptors with learning. *Science* 319, 1104–1107. doi: 10.1126/science.1149967
- McCormack, S. G., Stronetta, R. L., and Zhu, J. J. (2006). Synaptic AMPA receptor exchange maintains bidirectional plasticity. *Neuron* 50, 75–88. doi: 10.1016/j.neuron.2006.02.027
- Medin, T., Jensen, V., Skare, O., Storm-Mathisen, J., Hvalby, O., and Bergersen, L. H. (2018). Altered  $\alpha$ -amino-3-hydroxy-5-methyl-4-isoxazolepropionic acid (AMPA) receptor function and expression in hippocampus in a rat model of attention-deficit/hyperactivity disorder (ADHD). *Behav. Brain Res.* 360, 209–215. doi: 10.1016/j.bbr.2018.12.028
- Mignot, C., and Depienne, C. (2018). IQSEC2 related encephalopathy in males and females: a comparative study including 37 novel patients. *Genet. Med.* doi: 10.1038/s41436-018-0268-1 [Epub ahead of print].
- Moy, S. S., Nadler, J. J., Perez, A., Barabaro, R. P., Johns, J. M., Magnuson, T. R., et al. (2004). Sociability and preference for social novelty in five inbred strains: an approach to assess autistic-like behavior in mice. *Genes Brain Behav.* 3, 287–302. doi: 10.1111/j.1601-1848.2004.00076.x
- Murphy, J. A., Jense, O. N., and Walikonis, R. S. (2006). BRAG1 a Sec7 domain containing protein is a component of the postsynaptic density of excitatory synapses. *Brain Res.* 1120, 35–45. doi: 10.1016/j.brainres.2006.08.096
- Myers, K. R., Wang, G., Sheng, Y., Conger, K. K., Casanova, J. E., and Zhu, J. J. (2012). Arf6-GEF BRAG1 regulates JNK-mediated synaptic removal of GluA1-containing AMPA receptors: a new mechanism for nonsyndromic X-linked mental disorder. *J. Neurosci.* 32, 11716–11726. doi: 10.1523/JNEUROSCI.1942-12.2012
- Ng, P. R., Bellugi, E. U., and Trauner, M. D. (2018). Associations between social functioning, ADHD symptomatology, and emotion functioning in children with autism spectrum disorder and Williams syndrome. *Pediatr. Neurol.* 79, 69–71. doi: 10.1016/j.pediatrneurol.2017.10.022
- Parkinson, G. T., and Hanley, J. G. (2018). Mechanisms of AMPA receptor endosomal sorting. *Front. Mol. Neurosci.* 11:440. doi: 10.3389/fnmol.2018.00440
- Persechini, A., and Cronk, B. (1999). The relationship between the free concentrations of Ca<sup>2+</sup> and Ca<sup>2+</sup>-calmodulin in intact cells. *J. Biol. Chem.* 274, 6827–6830. doi: 10.1074/jbc.274.11.6827
- Petersen, A., Brown, J. C., and Gerges, N. Z. (2018). BRAG1/IQSEC2 as a regulator of small GTPase-dependent trafficking. *Small GTPases* doi: 10.1080/21541248.2017.1361898 [Epub ahead of print].
- Piard, J., Umanah, G. K. E., Harms, F. L., Abaide-Atristain, L., Amram, D., Chang, M., et al. (2018). A homozygous ATAD1 mutation impairs postsynaptic AMPA receptor trafficking and causes a lethal encephalopathy. *Brain* 141, 651–661. doi: 10.1093/brain/awx377
- Prut, L., and Belzung, C. (2003). The open field as a paradigm to measure the effects of drugs on anxiety like behaviors: a review. *Eur. J. Pharm.* 463, 3–33. doi: 10.1016/S0014-2999(03)01272-X
- Qin, Y., Zhu, Y., Baumgart, J. P., Stornetta, R. L., Seidenman, K., Mack, V., et al. (2005). State dependent Ras signaling and AMPA receptor trafficking. *Genes Dev.* 19, 2000–2015. doi: 10.1101/gad.342205
- Rumpel, S., LeDoux, J., Zador, A., and Malinow, R. (2005). Post synaptic receptor trafficking underlying a form of associative learning. *Science* 308, 83–88. doi: 10.1126/science.1103944
- Sakagami, H., Sanda, M., Fukaya, M., Miyazaki, T., Sukegawa, J., Yanagisawa, T., et al. (2008). IQ-ArfGEF/BRAG1 is a guanine nucleotide exchange factor for ARF6 that interacts with PSD-95 at post-synaptic density of excitatory synapses. *Neurosci. Res.* 60, 199–212. doi: 10.1016/j.neures.2007.10.013
- Scholz, R., Berberich, S., Rathgeber, L., Kolleker, A., Kohr, G., and Kornau, H. C. (2010). AMPA receptor signaling through BRAG2 and Arf6 critical for long term synaptic depression. *Neuron* 66, 768–780. doi: 10.1016/j.neuron.2010.05.003
- Shoubridge, C., Harvey, R. J., and Dudding-Byth, T. (2019). IQSEC2 mutation update and review of the female-specific phenotype spectrum including intellectual disability and epilepsy. *Hum. Mutat.* 2019, 5–24. doi: 10.1002/humu.23670
- Shoubridge, C., Tarpey, P. S., Abidi, F., Ramsden, S. L., Rujirabenjerd, S., Murphy, J. A., et al. (2010). Mutations in the guanine nucleotide exchange factor gene IQSEC2 cause nonsyndromic intellectual disability. *Nat. Genet.* 42, 486–488. doi: 10.1038/ng.588

- Singh, S. K., and Kishore, N. (2006). Thermodynamic insights into the binding of Triton X-100 to globular proteins: a colorimetric and spectroscopic investigation. *J. Phys. Chem.* 110, 9728–9737. doi: 10.1021/jp0608426
- Taipale, M., Krykbaeva, I., Koeva, M., Kayatekin, C., Westover, K. D., Karras, G. I., et al. (2012). Quantitative analysis of hsp90-client interactions reveals principles of substrate recognition. *Cell* 150, 987–1001. doi: 10.1016/j.cell.2012.06.047
- Tian, C., Kay, Y., Sadybekov, A., Rao, S., Katritch, V., and Herring, B. E. (2018). An intellectual disability-related missense mutation in Rac1 prevents LTP induction. *Front. Mol. Neurosci.* 11:223. doi: 10.3389/fnmol.2018.00223
- Trybus, K. M., Gushchin, M. I., Lui, H., Hazelwood, L., Kremetsova, E. B., Volkman, N., et al. (2007). Effect of calcium on calmodulin bound to the IQ motifs of Myosin V. *J. Biol. Chem.* 282, 23316–23325. doi: 10.1074/jbc.M701636200
- Umanah, G. K. E., Pignatelli, M., Yin, X., Chen, R., Crawford, J., Neifert, S., et al. (2017). Thorase variants are associated with defects in glutamatergic neurotransmission that can be rescued by perampanel. *Sci Transl Med* 9:eaa4985. doi: 10.1126/scitranslmed.aah4985
- Vorhees, C. V., and Williams, M. T. (2006). Morris water maze procedures for assessing spatial and related forms of learning and memory. *Nature protocols* 1, 848–858. doi: 10.1038/nprot.2006.116
- Wang, X., and Putkey, J. A. (2016). PEP-19 modulates calcium binding to calmodulin by electrostatic steering. *Nature communications* 7:13583. doi: 10.1038/ncomms13583
- Yang, X., Boehm, J. S., Yang, X., Salehi-Ashtiani, K., Hao, T., Shen, Y., et al. (2011). A public genome-scale lentiviral expression library of human ORFs. *Nat. Methods* 8, 659–661. doi: 10.1038/nmeth.1638
- Zerem, A., Haginoya, K., Lev, D., Blumkin, L., Kivity, S., Linder, I., et al. (2016). The molecular and phenotypic spectrum of IQSEC2-related epilepsy. *Epilepsia* 57, 1858–1869. doi: 10.1111/epi.13560
- Zhu, J. J. (2009). Activity dependent synapse specific AMPA receptor trafficking regulates transmission kinetics. *J. Neurosci.* 29, 6320–6335. doi: 10.1523/JNEUROSCI.4630-08.2009
- Zipper, R., Baine, S. D., Genizi, J., Maoz, H., Levy, N. S., and Levy, A. P. (2017). Developmental progression of intellectual disability, autism and epilepsy in a child with an IQSEC2 gene mutation. *Clin. Case Rep.* 5, 1639–1643. doi: 10.1002/ccr3.1139

**Conflict of Interest Statement:** The authors declare that the research was conducted in the absence of any commercial or financial relationships that could be construed as a potential conflict of interest.

Copyright © 2019 Rogers, Jada, Schragenheim-Rozales, Sah, Cortes, Florence, Levy, Moss, Walikonis, Palty, Shalgi, Lichtman, Kavushansky, Gerges, Kahn, Umanah and Levy. This is an open-access article distributed under the terms of the Creative Commons Attribution License (CC BY). The use, distribution or reproduction in other forums is permitted, provided the original author(s) and the copyright owner(s) are credited and that the original publication in this journal is cited, in accordance with accepted academic practice. No use, distribution or reproduction is permitted which does not comply with these terms.



# 27-Hydroxycholesterol Contributes to Lysosomal Membrane Permeabilization-Mediated Pyroptosis in Co-cultured SH-SY5Y Cells and C6 Cells

Si Chen<sup>†</sup>, Cui Zhou<sup>†</sup>, Huiyan Yu, Lingwei Tao, Yu An, Xiaona Zhang, Ying Wang, Yushan Wang and Rong Xiao\*

Beijing Key Laboratory of Environmental Toxicology, School of Public Health, Capital Medical University, Beijing, China

## OPEN ACCESS

### Edited by:

Juan Pablo de Rivero Vaccari,  
University of Miami, United States

### Reviewed by:

Alexandra Latini,  
Federal University of Santa Catarina,  
Brazil  
Shyam Gajavelli,  
University of Miami, United States

### \*Correspondence:

Rong Xiao  
xiaor22@ccmu.edu.cn

<sup>†</sup>These authors have contributed  
equally to this work

**Received:** 23 October 2018

**Accepted:** 15 January 2019

**Published:** 01 March 2019

### Citation:

Chen S, Zhou C, Yu H, Tao L, An Y, Zhang X, Wang Y, Wang Y and Xiao R (2019) 27-Hydroxycholesterol Contributes to Lysosomal Membrane Permeabilization-Mediated Pyroptosis in Co-cultured SH-SY5Y Cells and C6 Cells. *Front. Mol. Neurosci.* 12:14. doi: 10.3389/fnmol.2019.00014

**Purpose:** Emerging evidence suggests that 27-Hydroxycholesterol (27-OHC) causes neurodegenerative diseases through the induction of cytotoxicity and cholesterol metabolism disorder. The objective of this study is to determine the impacts of 27-OHC on lysosomal membrane permeabilization (LMP) and pyroptosis in neurons in the development of neural degenerative diseases.

**Methods:** In this study, SH-SY5Y cells and C6 cells were co-cultured *in vitro* to investigate the influence of 27-OHC on the function of lysosome, LMP and pyroptosis related factors in neuron. Lyso Tracker Red (LTR) was used to detect the changes of lysosome pH, volume and number. Acridine orange (AO) staining was also used to detect the LMP in neurons. Then the morphological changes of cells were observed by a scanning electron microscope (SEM). The content of lysosome function associated proteins [including Cathepsin B (CTSB), Cathepsin D (CTSD), lysosomal-associated membrane protein-1 (LAMP-1), LAMP-2] and the pyroptosis associated proteins [including nod-like receptor P3 (NLRP3), gasdermin D (GSDMD), caspase-1 and interleukin (IL)-1 $\beta$ ] were detected through Western blot.

**Results:** Results showed higher levels of lysosome function associated proteins, such as CTSB ( $p < 0.05$ ), CTSD ( $p < 0.05$ ), LAMP-1 ( $p < 0.01$ ), LAMP-2; ( $p < 0.01$ ) in 27-OHC treated group than that in the control group. AO staining and LTR staining showed that 27-OHC induced lysosome dysfunction with LMP. Content of pyroptosis related factor proteins, such as GSDMD ( $p < 0.01$ ), NLRP3 ( $p < 0.001$ ), caspase-1 ( $p < 0.01$ ) and IL-1 $\beta$  ( $p < 0.01$ ) were increased in 27-OHC treated neurons. Additionally, CTSB was leaked through LMP into the cytosol and induced pyroptosis. Results from the present study also suggested that the CTSB is involved in activation of pyroptosis.

**Abbreviations:** A $\beta$ ,  $\beta$ -amyloid; AO, acridine orange; AD, Alzheimer's disease; LMP, lysosomal membrane permeabilization; 24S-OHC, 24-hydroxycholesterol; 27-OHC, 27-hydroxycholesterol; 7-KC, 7-ketocholesterol; 7 $\beta$ -OHC, 7 $\beta$ -hydroxycholesterol; BBB, blood brain barrier; CTSB, cathepsin B; CTSD, cathepsin D; CNS, central nervous system; FBS, fetal bovine serum; GSDMD, gasdermin D; LTR, Lyso-Tracker Red; NLR, nod-like receptor.

**Conclusion:** Our data indicate that 27-OHC contributes to the pathogenesis of cell death by inducing LMP and pyroptosis in neurons.

**Keywords:** 27-hydroxycholesterol, lysosomal membrane permeabilization, pyroptosis, cell co-culture, SH-SY5Y cells and C6 cells

## INTRODUCTION

Cholesterol plays a key role in brain physiology and function. Its alterations in homeostasis and levels have been linked to neurodegeneration such as Alzheimer's disease (AD; Arenas et al., 2017). Evidences have suggested that increased occurrence of AD is associated with raised cholesterol level (Martins et al., 2009; Di Paolo and Kim, 2011). Cerebral cells synthesize all cholesterol found in central nervous system (CNS), since the blood brain barrier (BBB) makes cholesterol's metabolism in the brain independent to the rest of the organism (Costa et al., 2018). The question of how increased plasma cholesterol leads to the development of AD has yet to be answered.

In brain cholesterol pool, only the oxysterol metabolites of 27-hydroxycholesterol (27-OHC) and 24S-hydroxycholesterol (24S-OHC) can be exchanged with the blood circulation (Czuba et al., 2017). 27-OHC can cross the BBB from peripheral circulation to the brain with the greatest abundance. Its concentration is comparable to or slightly higher than other oxysterols in circulation (Nelson, 2018). In fact, several studies have already described increased levels of 27-OHC in serum (Popp et al., 2012) and cerebrospinal fluid (CSF; Besga et al., 2012) of AD patients not only as a reflection of the severity of disease but also the loss of metabolically active neurons and the degree of structural atrophy (Leoni et al., 2011; Popp et al., 2013), suggesting the critical role of 27-OHC in neuro-degeneration.

Hydrolytic enzymes capable of degrading macromolecules and cell components were contained in lysosomes, which are cytoplasmic membrane-enclosed organelles. Previous studies have shown the role of lysosome dysfunction in neurodegenerative diseases (Ferguson, 2018a,b). We also found the possible involvement of plasma 27-OHC increase in disorders of lysosome function and cholesterol metabolism in brain tissues of rats (Zhang et al., 2018). These studies reveal the possible role of 27-OHC in induction of lysosome dysfunction. However, the mechanism of how 27-OHC influences lysosome function still remains uncertain.

Partial and selective lysosomal membrane permeabilization (LMP) can induce controlled cell death (Galluzzi et al., 2018). As a form of lytic programmed cell death, pyroptosis is initiated by inflammasomes (Kovacs and Miao, 2017), which is composed of a nod-like receptor (NLR) family member, procaspase-1, and the adapter protein ASC usually. The best representative of NLR family member is NLRP3, which can be activated by different stimuli, such as lysosome destabilization. Previous research has shown that pyroptosis can be induced by cathepsin B (CTSB) that leaked through LMP into the cytosol (Orlowski et al., 2017). The CTSB release from LMP could lead to activation of NLRP3 inflammasome and NLRP3-dependent neuronal pyroptosis can result in

neurodegenerative diseases such as AD (Olsen and Singhrao, 2016; Li et al., 2018).

Cholesterol oxidation metabolites have been found to be one of the important factors inducing LMP (Boya, 2012). Cell experiments *in vitro* found that 7 $\beta$ -hydroxycholesterol (7 $\beta$ -OHC) and 7-ketocholesterol (7-KC) can induce cell death through LMP (Laskar et al., 2013; Yuan et al., 2016). However, whether 27-OHC, as one of the important oxysterols, can lead to LMP is still unclear.

We used the co-culture system to simulate a proper environment for the growth of neurons in the body to investigate the effect of 27-OHC. In the *in vitro* co-culture system neuron and astrocyte can support each other through the secretion of soluble factors among cells (Ma et al., 2015). In order to research the influence of 27-OHC on the function of lysosome and LMP which then induces pyroptosis in neuron, SH-SY5Y cells (human neuroblastoma cell line) and C6 cells (rat glial cell line) were co-cultured in this study.

## MATERIALS AND METHODS

### Reagents and Cell Culture

27-OHC was purchased from Santa Cruz Biotechnology Company (Dallas, TX, USA). Ten milligram 27-OHC was completely dissolved in 24.83 ml of absolute ethanol to 1,000  $\mu$ M as the stock solution. Then the stock solution was dispensed into a centrifuge tubes by 1 ml per tube, and blew dry with nitrogen gas. The tubes were finally preserved at  $-80^{\circ}\text{C}$ . Before each cell treatment, 27-OHC was first diluted in 0.08 ml ethanol and then added to culture medium to a final concentration of 5, 10 and 20  $\mu$ M, containing 0.04%, 0.08% and 0.16% ethanol (v/v).

SH-SY5Y cells (human neuroblastoma cell line) were purchased from Peking Union Medical College Cell Resource Center (CRC/PUMC) and C6 cells (rat glial cell line) were purchased from Cell Bank, Shanghai Institutes for Biological Sciences were grown in Dulbecco's modified eagles medium (DMEM) supplemented with 10% fetal bovine serum (FBS) and penicillin (100 U/ml)/streptomycin (100 U/ml) at  $37^{\circ}\text{C}$  in an atmosphere of  $\text{CO}_2$  (5%)/air (95%).

In order to simulate the environment in the brain, co-cultures of neuronal SH-SY5Y and astrocytic C6 cells were grown in a trans-well system with a 0.4  $\mu$ m pore size ( $4.0 \times 10^6$  pores/ $\text{cm}^2$ ). Neuronal SH-SY5Y cells ( $1.0 \times 10^6$  cells) were cultured in the lower compartment of a 6-well trans-well system, while astrocytic C6 cells ( $5.0 \times 10^5$  cells) were seeded in the insert. The insert and lower compartment are separated by polyester fiber film (Yang et al., 2005). The upper and lower compartments were cultured for 4 h separately, and then the insert was inoculated into a 6-well trans-well system. After 24 h, cells with DMEM were set as control and others were treated with 5, 10, and 20  $\mu$ M



27-OHC for 24 h.  $1.0 \times 10^7$  cells were collected and analyzed finally. The choice of 27-OHC concentration in the study was referenced from previous study of our group (Wang et al., 2016; An et al., 2017).

### Cathepsin Activity Fluorometric Assay

The enzymatic activities of CTSB and cathepsin D (CTSD) in SH-SY5Y cells and C6 cells were tested using the CTSB and CTSD activity fluorometric assay kit (NO. K140-100, NO. k143-100, Biovision, Milpitas, CA, USA). Briefly, cells were collected ( $1 \times 10^6$ ) by centrifugation. Lysed cells in 50  $\mu$ l of cell lysis buffer and incubated cells on ice for 10 min. Centrifuge at 20,000 g for 5 min, and then transferred the supernatant to a new tube. Added 50  $\mu$ l of cell lysate to the opaque black 96-well plate. Then 50  $\mu$ l of reaction buffer and 2  $\mu$ l of the 10 mM substrate Ac-RR-AFC were added to each sample. For negative control, added 2  $\mu$ l of inhibitor. Enspire multifunctional microplate reader was used with a 400-nm excitation and 505-nm emission filter to analyze fluorescence intensity for CTSB enzymatic activities, and with a 328-nm excitation and 460-nm emission filter for CTSD enzymatic activities after incubating at 37°C for 2 h in the dark.

### Lyso-Tracker Red Staining

Lysosomal staining was performed using Lyso-Tracker Red (LTR). After 24 h of treatment with 27-OHC in 20-mm glass-bottom dish, cells ( $1.0 \times 10^6$  cells/ml) were incubated with LysoTracker Red at 5 nmol/L for 30 min at 37°C and washed three times with phosphate-buffered saline (PBS). The cells were then inspected and photographed with the aid of a TCS SP8 STED confocal microscope (Leica; Germany).

### Acridine Orange Staining

After the designated treatments in 20-mm glass-bottom dish, cells ( $1.0 \times 10^6$  cells/ml) were incubated with medium containing 5  $\mu$ g/ml acridine orange (AO) for 15 min at 37°C and rinsed with PBS. Then the cells were imaged under the confocal microscope with the excitation wavelength set at 488 nm; two separate emission bands (505–570 nm and 615–754 nm) were obtained. Enspire multifunctional microplate reader was used to analyze fluorescence intensity after AO staining.

### Quantitative Analysis of the Integrity of Lysosomes

One-hundred microliter per well AO (5  $\mu$ g/ml in PBS) was added to 96-well plate for labeling cells for 5 min. After rinsing with PBS three times, the fluorescence intensity was analyzed using an Enspire multifunctional microplate reader with a 475-nm excitation and 520-nm emission filter for green fluorescence.

### Scanning Electron Microscopy

Cells were fixed with 2.5% glutaraldehyde for 3 h, and then rinsed with 0.1% PB three times. Then they were dehydrated through a graded series of ethanol (30, 50, 70, 95 and 100%) and dried by the tertiary butanol method. The samples were then mounted on metal stubs and dried in a silica gel vacuum desiccator. They were sputter coated with gold and examined under a Hitachi S-4800 scanning electron microscope (SEM) operating at 15 kV.

### Subcellular Fractionation

After 27-OHC exposure, SH-SY5Y cells were washed twice with PBS and collected using a cell scraper. The lysosome fractions were separated using a Lysosome Enrichment Kit (Bestbio, Shanghai, China) according to the manufacturer's instructions. In short, collected cells were resuspended with Lysosome Isolation Reagent A, and oscillated on ice for 10 min. Then the cells were homogenized 30–40 times in a Dounce homogenizer followed by centrifugation at 4,000 g for 10 min. Supernatant fractions were centrifuged at 20,000 g for 20 min and the supernatant was collected and labeled as cytosolic fraction. The resulting pellets were further spun at 20,000 g for 20 min after being resuspended with Lysosome Isolation Reagent B. The pellets were resuspended with Lysosome Isolation Reagent C (2  $\mu$ l of protease inhibitor cocktail per 200  $\mu$ l of reagent C) and added to the resulting pellets and oscillated on 4 for 15–30 min. The lysis was further spun at 12,000 g for 15 min and the supernatant was Lysosome total protein enriched fraction.

### Western Blot Analysis

Cells treated with DMEM in addition to 27-OHC with concentrations of 5  $\mu$ M, 10  $\mu$ M and 20  $\mu$ M respectively. After the treatments, cold PBS were used to wash cells and 0.1 ml cell lysis buffer was added to superstratum and substratum of transwell plate. Cell extracts were collected by centrifugation at 13,000 g for 15 min at 4°C. The BCA Protein Assay Kit was used to measure the protein concentration. Equal amount of proteins (20  $\mu$ g) were loaded on 8% or 10% SDS-acrylamide gels for separation by electrophoresis and then transferred onto PVDF membrane. After being blocked with 5% non-fat milk, immunoblots were probed with appropriate antibodies. The anti-CTSB (1:1,000, #31718) from Cell Signaling Technology, Danvers, MA, USA; anti-CTSD (1:1,000, #21327-1-AP) from proteintech, Rosemont, IL, USA; anti-lysosomal-associated membrane protein-1 (anti-LAMP-1; 1:1,000, #ab24170) from Abcam, USA; anti-LAMP-2 (1:1,000, #sc-71492) from Santa Cruz Biotechnologies, Dallas, TX, USA; anti-NLRP3 (1:1,000, #ab214185) from Abcam, USA; anti-gasdermin D (anti-GSDMD; 1:2,000, #orb390052) from biorbyt, UK; anti-interleukin (anti-IL)-1 $\beta$ ; 1:1,000, #sc-52012) from Santa Cruz Biotechnologies, Dallas, TX, USA; anti-caspase-1 (1:1,000, #ab1872) from Abcam, USA were used as primary antibodies.  $\beta$ -Actin was used as a control of total protein. After overnight incubation with primary antibodies and washing three times with TBST, the PVDF membranes were incubated with anti-rabbit IgG or anti-mouse IgG for 1 h. The membranes were then scanned using a Vilber Lourmat Fusion SL6 (Vilber; France), and the gray values were analyzed through ImageJ software at last. Each experiment was repeated at least three times.

### Statistical Analysis

The software SPSS 19.0 (Chicago, IL, USA) was used to analyze the data. All results were represented as means  $\pm$  SE of at least three independent experiments. One-way analysis of variance (ANOVA) and least significance difference (LSD) were used to

evaluate statistical significance of the difference between groups.  $P$  values  $< 0.05$  were considered as significant.

## RESULTS

### 27-OHC Caused Differential Regulation of Cathepsin B and D Protein and Activity in Co-cultures of SH-SY5Y Cells and C6 Cells

To observe the effect of 27-OHC on the function of lysosome, we examined the changes in protein content and enzymatic activity of CTSB and CTSD in SH-SY5Y cells and C6 cells. The active form of CTSB (24 and 27 kDa) was detected by western blot (Nagakannan and Eftekharpour, 2017). We found that 27-OHC treatment significantly regulated the protein content of CTSB and CTSD in both SH-SY5Y cells and C6 cells. In SH-SY5Y cells, the protein levels of CTSB and CTSD were up-regulated with treatments of both 10  $\mu$ M and 20  $\mu$ M 27-OHC (Figures 1A,B). In

C6 cells, CTSD protein level was up-regulated by treatment of 10  $\mu$ M 27-OHC, and both CTSB and CTSD protein content were significantly up-regulated by treatment with 20  $\mu$ M 27-OHC ( $p < 0.05$ ). To further confirm these changes in CTSB and CTSD protein activities, the commercially available enzymatic activity assay kits (Biovision, Milpitas, CA, USA) were used. We observed robust increased enzymatic activity of CTSB in both two cell lines with 27-OHC treatment. The enzymatic activity of CTSD was reduced in SH-SY5Y cells treated with 5  $\mu$ M, 10  $\mu$ M, and 20  $\mu$ M 27-OHC, while no significant change was observed in 27-OHC treated C6 cells (Figure 1C).

These data suggested that 27-OHC causes differential changes in protein content and activity of CTSB and CTSD in co-cultures of SH-SY5Y cells and C6 cells. The increase in CTSB levels in 27-OHC treated cells was coincided with the significant upregulation of CTSB activity. However, the new protein synthesis is independent of CTSD activity. Since previous

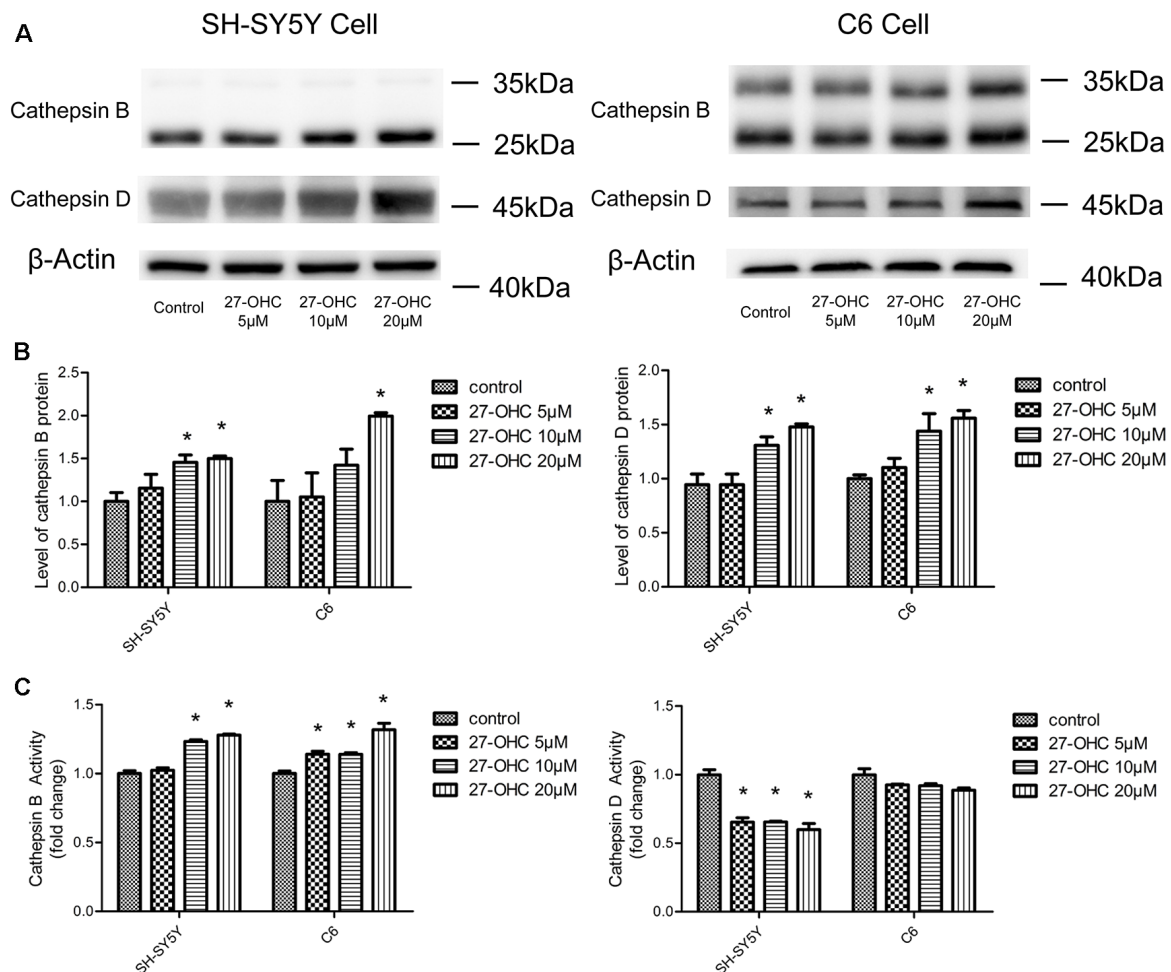


**FIGURE 1 |** 27-Hydroxycholesterol (27-OHC) treatment causes differential regulation of cathepsin B (CTSB) and cathepsin D (CTSD) protein and activity in co-cultures of SH-SY5Y cells and C6 cells. SH-SY5Y cells and C6 cells were treated with normal medium or 5  $\mu$ M, 10  $\mu$ M, 20  $\mu$ M 27-OHC. The protein levels of CTSD and CTSD were analyzed with western blotting (A,B). (C) The activities of CTSB and CTSD were measured by fluorometric method using commercially available kits. All data are presented as the means  $\pm$  SE.  $n = 3$ –4 for protein and  $n = 3$  for activity. \* $p < 0.05$  compared with the control group.

research has shown that the change of CTSD and CTSD is a specific indicator of lysosomes dysfunction (Ashtari et al., 2016;

Schultz et al., 2016), these results may indicate that 27-OHC could affect the lysosomal function of C6 and SH-SY5Y cells.

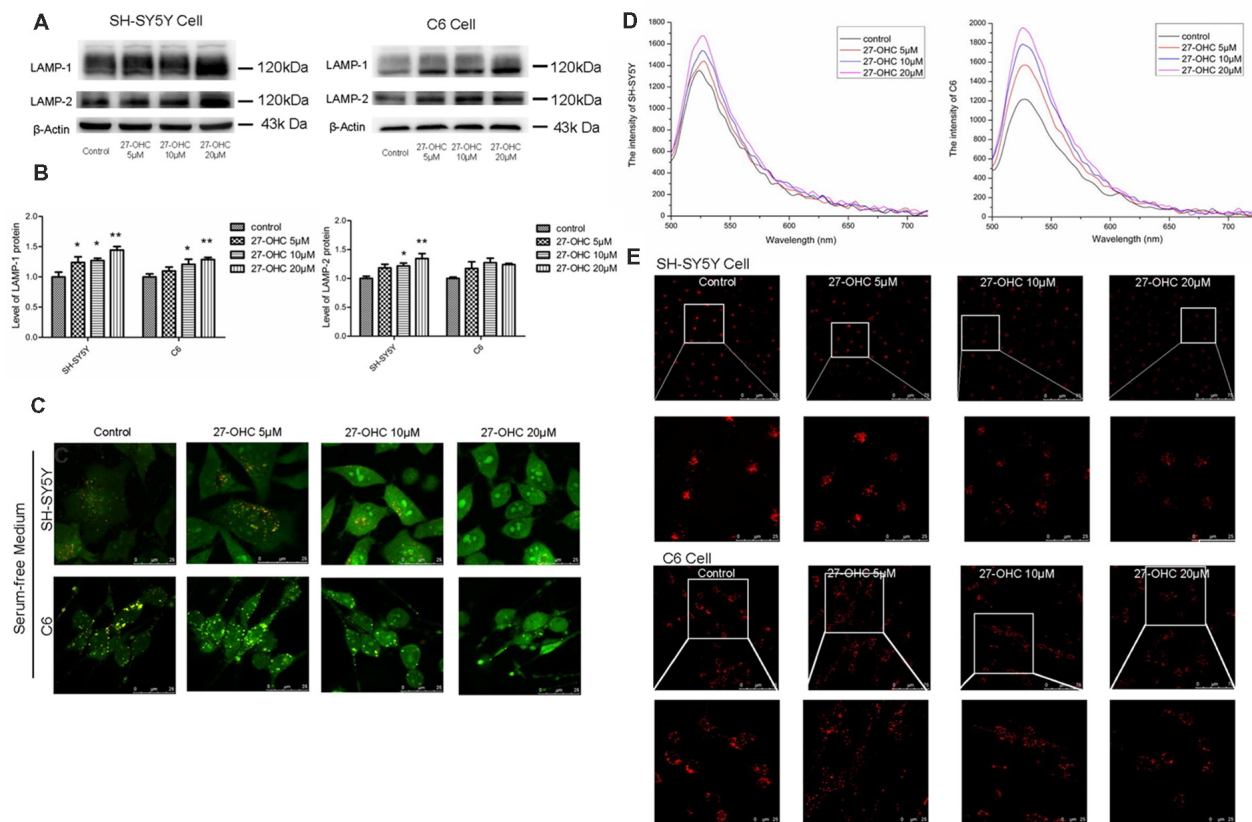


**FIGURE 2 |** 27-OHC causes lysosomal membrane permeabilization (LMP) in SH-SY5Y cells and C6 cells. **(A,B)** Representative western showed LAMP1 and LAMP2 levels in SH-SY5Y cells and C6 cells subjected to different concentrations 27-OHC (0, 5, 10, 20  $\mu$ M) for 24 h.  $\beta$ -Actin was used as a normalized protein. **(C)** SH-SY5Y cells and C6 cells were treated with normal culture medium or 27-OHC (5, 10, 20  $\mu$ M) for 24 h, stained with 5  $\mu$ g/ml acridine orange (AO) for 15 min and imaged under confocal microscope (scale bar: 25  $\mu$ m). **(D)** The spectrum of SH-SY5Y cells and C6 cells subjected to 27-OHC (0, 5, 10, 20  $\mu$ M) for 24 h;  $n \geq 100$  cells. **(E)** Effect of 27-OHC on lysosomes. SH-SY5Y cells and C6 cells were with 27-OHC (0, 5, 10, 20  $\mu$ M) for 24 h. The lysosomes were labeled by 5 nM Lyso-Tracker Red (LTR) and examined by confocal (scale bar: 75  $\mu$ m and 25  $\mu$ m). All the data were shown as mean  $\pm$  SE;  $n = 3-4$  for protein. \* $p < 0.05$ , \*\* $p < 0.01$  compared with control group.

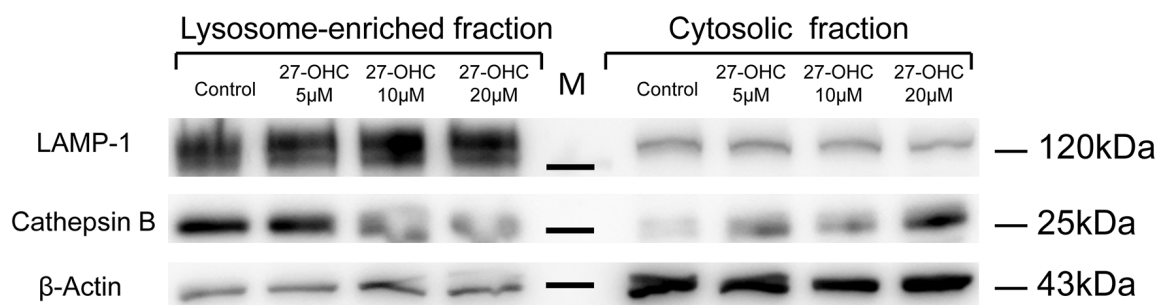


**FIGURE 3 |** 27-OHC causes CTSD leakage into the cytoplasm around the lysosomes with LMP in SH-SY5Y cells. 27-OHC treatment caused the spillage of CTSD into the cytosol. Cell fractionation was performed to separate lysosomal and cytosolic fractions in SH-SY5Y cells with 27-OHC treatment (0, 5, 10, 20  $\mu$ M) in serum-free medium for 24 h as indicated. Representative western blotting showing CTSD was detected in the different fractions.  $\beta$ -actin and LAMP1 were used as cytosolic and lysosomal markers.  $n = 3$  for experiment.

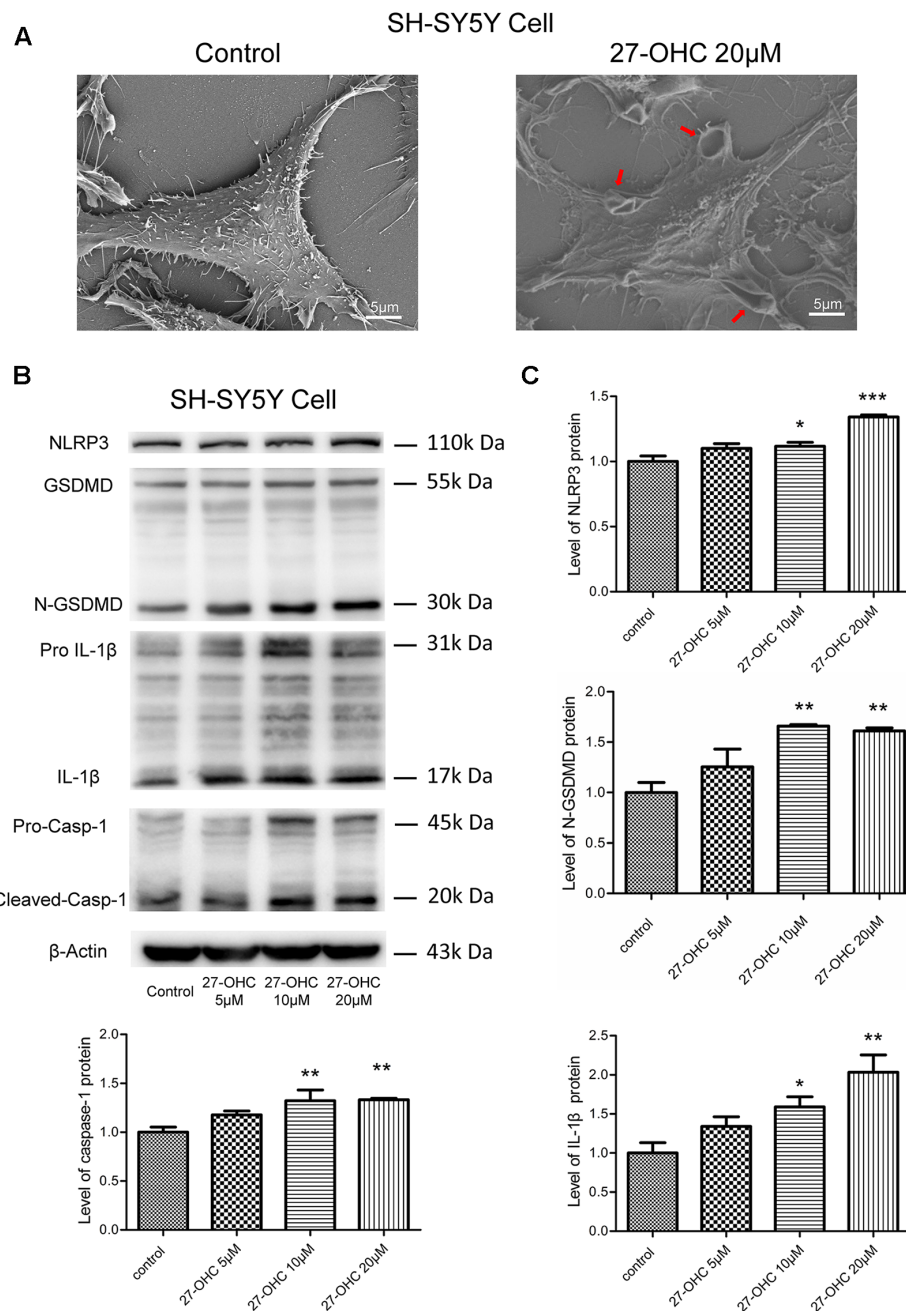


**FIGURE 4 |** 27-OHC treatment causes pyroptosis in SH-SY5Y cells. **(A)** The scanning electron microscope (SEM) showed SH-SY5Y cells swelling and membrane breakage after 27-OHC treatment, as indicated by the arrows. **(B,C)** The protein levels of nod-like receptor P3 (NLRP3), gasdermin D (GSDMD), Caspase-1, interleukin-1 $\beta$  (IL-1 $\beta$ ) was analyzed by western blotting. All the data were shown as mean  $\pm$  SE;  $n = 3-4$ . \* $p < 0.05$ , \*\* $p < 0.01$ , \*\*\* $p < 0.001$  compared with control group.

## Lysosomal Deficiency Caused by 27-OHC Treatment Was Shown as Lysosomal Membrane Permeabilization in SH-SY5Y Cells and C6 Cells

To determine whether lysosomal deficiency was associated with 27-OHC, we first tested lysosomal-associated membrane

proteins LAMP-1 and LAMP-2 after 27-OHC treatment. Administration of 27-OHC treatment remarkably increased the content of LAMP-1 protein in SH-SY5Y cells and C6 cells ( $p < 0.01$ ; **Figures 2A,B**) and LAMP-2 protein in SH-SY5Y cells ( $p < 0.01$ ; **Figures 2A,B**). However, there was no significant difference in the content of LAMP-2 protein between 27-OHC and control treatments in C6 cells.



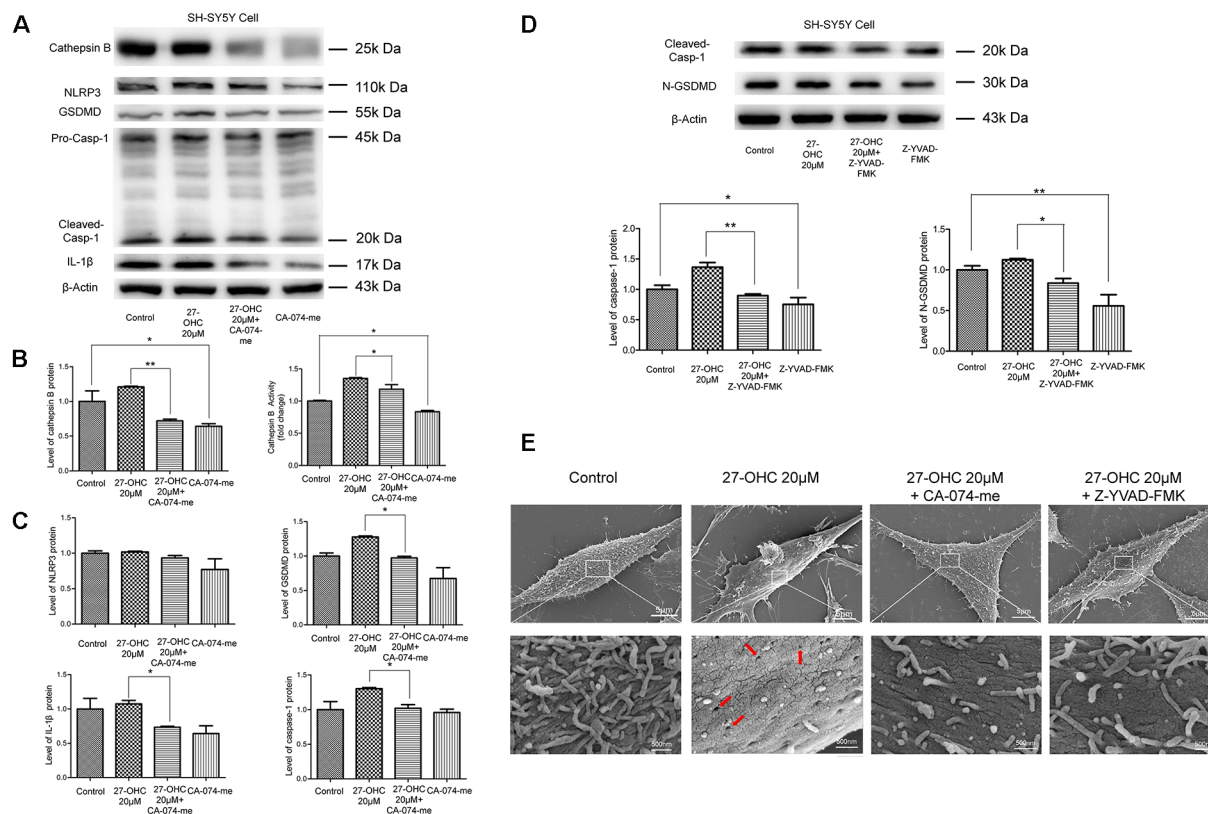


**FIGURE 5 |** LMP mediates the activation of pyroptosis after 27-OHC treatment in SH-SY5Y cells. **(A)** SH-SY5Y cells were treated with normal culture medium, 27-OHC (20  $\mu$ M), 27-OHC (20  $\mu$ M) + CA-074-me (15  $\mu$ M) and CA-074-me (15  $\mu$ M) for 24 h, and then the cell lysates were analyzed for pyroptosis markers by western blotting. **(B)** Densitometric analysis and activity results of CTBS. **(C)** Densitometric analysis of pyroptosis-associated proteins normalized to  $\beta$ -Actin is shown. **(D)** SH-SY5Y cells were treated with normal culture medium, 27-OHC (20  $\mu$ M), 27-OHC (20  $\mu$ M) + Z-YVAD-FMK (10  $\mu$ M) and Z-YVAD-FMK (10  $\mu$ M) for 24 h and the cell lysates analyzed for caspase-1 and GSDMD by western blotting. **(E)** SEM showed some pores on SH-SY5Y cells membranes after 27-OHC 20  $\mu$ M treatment (as indicated by the arrows) and absence/reduced pore formation after 27-OHC treatment with anti-CTSB or anti-GSDMD. All the data were shown as mean  $\pm$  SE;  $n = 3-4$ . \* $p < 0.05$ , \*\* $p < 0.01$  compared with control group.

These results indicated that in both cell lines 27-OHC treatment leads to enlargement of lysosomes (Nagakannan and Eftekharpour, 2017), which has been suggested to increase the possibility of lysosomes losing their integrity, leading to leakage of lysosomal content to the cytosol (Appelqvist et al., 2013).

To investigate whether 27-OHC treatment leading to lysosomal deficiency was associated with LMP induction, we used AO staining to detect the acid lysosomes (Hsieh et al., 2017). AO emits a granular red fluorescence in a normal lysosomal acidic environment, but a granular green fluorescence in neutral and slightly basic environment such as cytosol. Once the lysosomal integrity was destroyed, AO would relocate from lysosomes to cytosol and can then be detected by an enhanced green fluorescence, indicating the occurrence of LMP. We positioned distinct orange-red particles represents complete lysosome in control (Figure 2C). We noted decreased acidophilic lysosomes and an enhanced green fluorescence in the cytosol after treatment with 27-OHC in a dose-dependent manner in SH-SY5Y cells and C6 cells (Figure 2C). We used enspire multifunctional microplate reader to analyze

fluorescence intensity after AO staining. Green fluorescence was enhanced in both SH-SY5Y and C6 cells, which indicated that LMP was happening (Figure 2D).

To further examine the changes of lysosomal function caused by 27-OHC treatment, LTR was used to label lysosomes in live cells. As an acidotropic probe, the decreased LTR fluorescence reflected both a rise in pH of lysosomal and a reduction in number of lysosomes (Li et al., 2017). Treatment with 27-OHC markedly reduced the fluorescence intensity, indicating that 27-OHC treatment reduced intracellular acidic components and the number of lysosome (Figure 2E), and the possibility of LMP occurrence in SH-SY5Y cells and C6 cells.

### 27-OHC Caused Cathepsin B Leakage Into the Cytoplasm Around the Lysosomes With LMP in SH-SY5Y Cells

It is known that induction of LMP, translocation of CTBSB from lysosomes into cytosol can cause lysosomal membrane damage and initiate pyroptosis procedures (Gorojod et al., 2015; Orłowski et al., 2017). In order to determine whether CTBSB

leaks into the cytosol from lysosome upon induction of LMP, we carried out subcellular fractionation of SH-SY5Y cells to directly measure the location of CTSB. Western blotting results showed that 27-OHC treatment caused the spillage of CTSB into the cytosol which in a dose-dependent manner in SH-SY5Y cells (Figure 3). The results suggested that 27-OHC treatment increased the protein levels of CTSB and lead to its leakage into the cytosol around the lysosomes.

## 27-OHC Treatment Caused Pyroptosis in SH-SY5Y Cells

To investigate if 27-OHC treatment can lead to pyroptosis, we first analyzed morphological changes in SH-SY5Y cells after treatment with 20  $\mu$ M 27-OHC by means of SEM. Through comparing the 27-OHC treatment group with the control groups, we observed swelling and membrane breakage in SH-SY5Y cells (Figure 4A), presumably due to 27-OHC treatment.

Recent findings suggested that GSDMD is the executant of pyroptosis and is in charge of the secretion of matured IL-1 $\beta$  (He et al., 2015). Caspase-1 can cleave GSDMD to generate an N-terminal (N-GSDMD; 30–31-kDa) and a C-terminal fragment (C-GSDMD; 22-kDa), and only the N-terminal fragment of GSDMD can induce pyroptosis (Man and Kanneganti, 2015; Shi et al., 2015). Research also proposed that the NLRP3 inflammasome can control both caspase-1-mediated pyroptosis and secretion of mature IL-1 $\beta$  (He et al., 2016). We thus analyzed whether 27-OHC can modulate the content of NLRP3, GSDMD, caspase-1 and IL-1 $\beta$ . Western blotting was conducted in SH-SY5Y cells and an increase of IL-1 $\beta$  protein (17-kDa) triggered by 27-OHC after 24 h of stimulation was observed (Figures 4B,C). Pro-IL-1 $\beta$  have been cleaved or activated after 27-OHC treatment. We also found increased NLRP3, caspase-1 and the cleaved GSDMD N-terminal fragment (N-GSDMD) at 30 kDa with 27-OHC treatment compared to the control group (Figures 4B,C). These results showed that 27-OHC may cause pyroptosis in SH-SY5Y cells.

## LMP Mediated the Activation of Pyroptosis After 27-OHC Treatment in SH-SY5Y Cells

Recent researches have proposed that LMP can result in releases of CTSB into the cytosol and then activate NLRP3 (Duewell et al., 2010; Serrano-Puebla and Boya, 2016). Therefore, we analyzed the effect of LMP and/or CTSB on protein content of pyroptosis-associated proteins. We used CTSB inhibitor (CA-074-me, 15  $\mu$ M) to pretreat SH-SY5Y cells for 1 h at 37°C before 27-OHC treatment. The western blotting and activity results suggested decreased levels of CTSB when compared to the control group (Figures 5A,B). The protein content of GSDMD, caspase-1 and IL-1 $\beta$  were also examined. We found down regulation of protein content of all the three pyroptosis-associated proteins after co-treating with 27-OHC and CA-074-me. There were no statistically significant differences of NLRP3 protein content between each group, but the results revealed a clear decreased tendency (Figures 5A,C). To report this point more thoroughly, we used caspase-1 inhibitor (Z-YVAD-FMK, 10  $\mu$ M; Wang et al., 2015) to pretreat

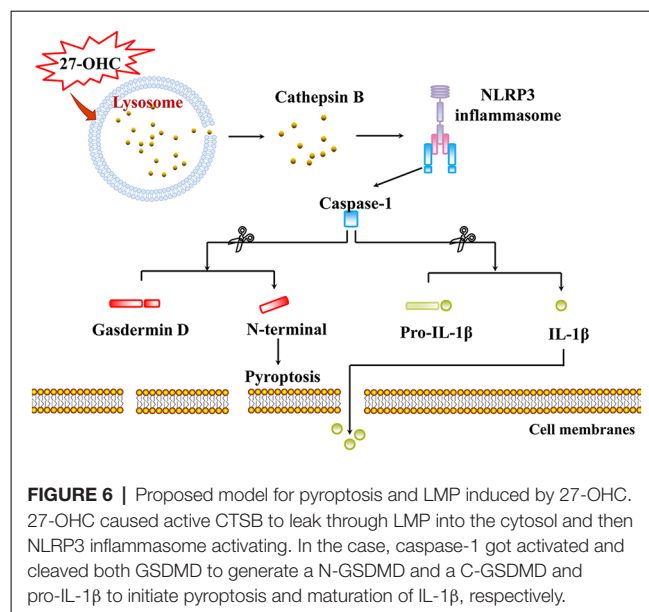


**FIGURE 6 |** Proposed model for pyroptosis and LMP induced by 27-OHC. 27-OHC caused active CTSB to leak through LMP into the cytosol and then NLRP3 inflammasome activating. In the case, caspase-1 got activated and cleaved both GSDMD to generate a N-GSDMD and a C-GSDMD and pro-IL-1 $\beta$  to initiate pyroptosis and maturation of IL-1 $\beta$ , respectively.

SH-SY5Y cells for 30 min at 37°C before 27-OHC treatment to suppress expression of GSDMD, which was proved to be effective through the results of western blot (Figure 5D). The results of SEM shown pores with size of 24–50 nm were formed on membranes after 27-OHC 20  $\mu$ M treatment by 500.0 nm scale bars. Beyond that, there is no/little pore on cell membranes with CA-074me and Z-YVAD-FMK treatment in SEM (Figure 5E). The results suggested that CTSB is implicated in activation of pyroptosis. The results are consistent with previous studies indicating that CTSB released from ruptured lysosomes can activate pyroptosis (Brojatsch et al., 2015; Yang et al., 2016).

## DISCUSSION

The amyloid hypothesis posits that  $\beta$ -amyloid (A $\beta$ ) is the pathological factor that initiates the onset and progression of AD (Tam et al., 2016). Earlier studies have shown that amyloid precursor protein (APP) is the source of A $\beta$ . And many studies indicated that nascent APP is cleaved after endocytosis from the cell surface into endosomes and subsequently into lysosomes. Recent research has demonstrated that APP degraded by lysosomal system (Hein et al., 2017). CTSB is a most abundant cysteine protease with potentially specific roles that cleaves APP and also degrades the A $\beta$ 42 peptide (Llorente et al., 2018) in the endo-lysosome system. Lysosomes are ubiquitous organelles that constitute the primary degradative compartments of the cell. They receive their substrates through endocytosis, phagocytosis or autophagy (Saftig and Klumperman, 2009). Thus, impairment of lysosomal function plays an important role in neuronal degeneration and in the pathogenesis of numerous neurodegenerative diseases (Cermak et al., 2016). Studies demonstrated that abnormalities of the endosomal-lysosomal system are also early pathological features in the AD brain (Barbero-Camps et al., 2018).

This study found that 27-OHC changed the levels of lysosome protein, CTSD and CTSD, and induced lysosome dysfunction in co-cultured SH-SY5Y cells and C6 cells. It revealed for the first time the effects of 27-OHC treatment on CTSD and CTSD *in vitro*. The effects of oxysteroids on structure and function of lysosomes have been proposed in a previous study (Boya, 2012). Excessive accumulation of oxysteroids in cells can lead to leakage of lysosomal membrane (Laskar et al., 2013; Yuan et al., 2016). However, as one of the important oxidation products of cholesterol, how 27-OHC influences the structure and function of lysosomes remains unknown. In our previous research, we found that increased level of plasma 27-OHC might affect the cholesterol metabolism and lysosome function *in vivo* (Zhang et al., 2018) and our previous study has demonstrated that excessive 27-OHC with concentrations of 7, 21 and 70  $\mu\text{M}$  in blood can impair spatial learning and memory and contributes to the perturbation of cholesterol metabolism in the rat brain (Zhang et al., 2015). Further studies on co-culture neurons have shown that 27-OHC can induce cytotoxicity and present a dose-effect and time-effect correlation (Wang et al., 2016). Wang found 5  $\mu\text{M}$ , 10  $\mu\text{M}$ , 20  $\mu\text{M}$  of 27-OHC treatment caused significant inhibition of cell viability and the loss of mitochondrial membrane potential (so the concentrations used 5  $\mu\text{M}$ , 10  $\mu\text{M}$ , 20  $\mu\text{M}$  of 27-OHC in our study). The present study found that 27-OHC treatment can up-regulate protein levels of CTSD and CTSD and activity of CTSD in both of SH-SY5Y cells and C6 cells in co-culture conditions. Up-regulation of CTSD and CTSD is a specific indicator of lysosomes dysfunction (Ashtari et al., 2016; Schultz et al., 2016). So the data obtained here confirmed that 27-OHC treatment can cause lysosomal dysfunction.

27-OHC treatment increased the protein content and accumulation of LAMP-1 and LAMP-2, which indicated the larger volume of lysosome (Nagakannan and Eftekharpour, 2017). The larger lysosomes are more prone to undergo membrane damage as had been verified in a previous study (Ono et al., 2003). In this research, we report that 27-OHC treatment can destroy the lysosomal membrane of SH-SY5Y cells and C6 cells accompany with the increased content of CTSD and CTSD and increased enzymatic activity of CTSD. For the result of reduced activity of CTSD, previous research has shown that CTSD will lose activity due to de-protonation of the residues in the active site at neutral pH, but remain stable structurally (Repnik et al., 2014). The results of AO and LTR have proved the induction of LMP by 27-OHC treatment (Figures 2C–E). The immediate consequence of LMP is leakage of lysosomal hydrolytic enzymes, which implies the release of CTSD and other lysosomal constituents from lysosome (Boya and Kroemer, 2008). And the detection results of protein content revealed that CTSD has leaked into the cytosol (Figure 3). Significantly, LTR showed more diffusion with the increasing concentration of 27-OHC-treatment, and such a distribution proved the burst of lysosome vesicles.

The previous study of our team found that 27-OHC treatment can cause cell death in co-cultured SH-SY5Y cells and C6 cells

(Wang et al., 2016). In the present study, we confirmed that 27-OHC treatment can cause lysosome damage and release of CTSD from lysosomes. Some research suggested that when LMP approaches a certain level, the nerve cells will change from the stable state to cell death state (Lipton, 2013; Ni et al., 2018). Research has shown that CTSD can remain active in neutral environment after LMP even if most hydrolytic enzymes are inactive under pH-neutral conditions (Boya, 2012).

Pyroptosis has been explored by many researchers recently. Some substances can induce cleavage and secretion of IL-1 family cytokines by stimulating the caspase-1-activating NLRP3 inflammasome, which results in pyroptosis. As the best-characterized inflammasome, studies found that NLRP3 was activated in AD (Saresella et al., 2016), which can be activated by cholesterol, cathepsin and also by the amyloid peptide (Düewell et al., 2010; Masters and O'Neill, 2011; Jo et al., 2016). The idea that cathepsins play an important role in the pathogenesis of neurodegenerative disorders has been long known in the scientific literature. Their changes in concentration, activity and localization are normally found in aging neurons and are considered as a cause of age-related neuropathologic changes (Cermak et al., 2016). Orłowski found due to LMP that active CTSD released into the cytoplasm can initiate pyroptosis procedures and lead to primary murine macrophages death eventually (Orłowski et al., 2017). However, whether LMP mediated the activation of pyroptosis after 27-OHC treatment in neurons was seldom reported. Therefore, we detected pyroptosis associated proteins including NLRP3, GSDMD, caspase-1 and IL-1 $\beta$  in the present study. The IL-1 $\beta$  is a well-known unconventionally secreted leaderless proteins with important extracellular functions (Rubartelli et al., 1990). We found that 27-OHC treatment caused pyroptosis in SH-SY5Y cells in co-culture system (Figure 4). In order to investigate the role of CTSD and/or LMP in pyroptosis in SH-SY5Y cell line, CA-074-me, an inhibitor of CTSD, was used to prohibit the activity of CTSD. We demonstrated that pyroptosis was partially prevented by CA-074-me, indicating that CTSD is involved in activation of pyroptosis (Figure 5). In general, our results showed that LMP plays a crucial role in 27-OHC-induced pyroptosis and consequently in CTSD mediated GSDMD cleavage and the resulting activation of the caspase-1 pathway. Meanwhile our results highlight the critical role of 27-OHC in pyroptosis of SH-SY5Y cells.

## CONCLUSION

We identified the role of 27-OHC in lysosome dysfunction in this research. Our data demonstrated that 27-OHC can induce LMP. We also found that CTSD leaked through LMP into the cytosol and induced NLRP3-dependent neuronal pyroptosis (Figure 6). Both references of the potential toxic effects of 27-OHC on lysosomes and their contribution to the pathogenesis of neurodegenerative diseases were provided in this study. Population-based studies and animal experiments are needed in further research to clarify the relationship between 27-OHC, lysosome dysfunction and neurodegenerative diseases. To our



knowledge, this is the first study indicating the lysosome dysfunction in 27-OHC treated neurons. We speculate that 27-OHC may cause pyroptosis through LMP of nerve cells.

## AUTHOR CONTRIBUTIONS

SC, CZ and RX designed the research. SC conducted the research and analyzed the data. SC and CZ wrote the manuscript. MJ and LJ gave technical support of SEM. XT provided linguistic assistance during the preparation of this manuscript. HY, LT,

YA, XZ, YuW and YiW gave auxiliary support, and RX had primary responsibility for the final content. All authors read and approved the final manuscript.

## FUNDING

This work was supported by the State Key Program of the National Natural Science Foundation of China (grant no. 81330065 and 81673149), and the National Natural Science Foundation of China (grant no. 81673149).

## REFERENCES

- An, Y., Zhang, D. D., Yu, H. L., Ma, W. W., Lu, Y. H., Liu, Q. R., et al. (2017). 27-Hydroxycholesterol regulates cholesterol synthesis and transport in C6 glioma cells. *Neurotoxicology* 59, 88–97. doi: 10.1016/j.neuro.2017.02.001
- Appelqvist, H., Waster, P., Kagedal, K., and Ollinger, K. (2013). The lysosome: from waste bag to potential therapeutic target. *J. Mol. Cell Biol.* 5, 214–226. doi: 10.1093/jmcb/mjt022
- Arenas, F., Garcia-Ruiz, C., and Fernandez-Checa, J. C. (2017). Intracellular cholesterol trafficking and impact in neurodegeneration. *Front. Mol. Neurosci.* 10:382. doi: 10.3389/fnmol.2017.00382
- Ashtari, N., Jiao, X., Rahimi-Balaei, M., Amir, S., Mehr, S. E., Yeganeh, B., et al. (2016). Lysosomal acid phosphatase biosynthesis and dysfunction: a mini review focused on lysosomal enzyme dysfunction in brain. *Curr. Mol. Med.* 16, 439–446. doi: 10.2174/1566524016666160429115834
- Barbero-Camps, E., Roca-Agujetas, V., Bartolessis, I., de Dios, C., Fernández-Checa, J. C., Mari, M., et al. (2018). Cholesterol impairs autophagy-mediated clearance of amyloid  $\beta$  while promoting its secretion. *Autophagy* 14, 1129–1154. doi: 10.1080/15548627.2018.1438807
- Besga, A., Cedazo-Minguez, A., Kåreholt, I., Solomon, A., Björkhem, I., Winblad, B., et al. (2012). Differences in brain cholesterol metabolism and insulin in two subgroups of patients with different CSF biomarkers but similar white matter lesions suggest different pathogenic mechanisms. *Neurosci. Lett.* 510, 121–126. doi: 10.1016/j.neulet.2012.01.017
- Boya, P. (2012). Lysosomal function and dysfunction: mechanism and disease. *Antioxid. Redox Signal.* 17, 766–774. doi: 10.1089/ars.2011.4405
- Boya, P., and Kroemer, G. (2008). Lysosomal membrane permeabilization in cell death. *Oncogene* 27, 6434–6451. doi: 10.1038/onc.2008.310
- Brojatsch, J., Lima, H. Jr., Palliser, D., Jacobson, L. S., Muehlbauer, S. M., Furtado, R., et al. (2015). Distinct cathepsins control necrotic cell death mediated by pyroptosis inducers and lysosome-destabilizing agents. *Cell Cycle* 14, 964–972. doi: 10.4161/15384101.2014.991194
- Cermak, S., Kosicek, M., Mladenovic-Djordjevic, A., Smiljanic, K., Kanazir, S., and Hecimovic, S. (2016). Loss of cathepsin B and L leads to lysosomal dysfunction, NPC-like cholesterol sequestration and accumulation of the key Alzheimer's proteins. *PLoS One* 11:e0167428. doi: 10.1371/journal.pone.0167428
- Costa, A. C., Joaquim, H., Nunes, V. S., Kerr, D. S., Ferreira, G. S., Forlenza, O. V., et al. (2018). Donepezil effects on cholesterol and oxysterol plasma levels of Alzheimer's disease patients. *Eur. Arch. Psychiatry Clin. Neurosci.* 268, 501–507. doi: 10.1007/s00406-017-0838-2
- Czuba, E., Steliga, A., Lietzau, G., and Kowianski, P. (2017). Cholesterol as a modifying agent of the neurovascular unit structure and function under physiological and pathological conditions. *Metab. Brain Dis.* 32, 935–948. doi: 10.1007/s11011-017-0015-3
- Di Paolo, G., and Kim, T. W. (2011). Linking lipids to Alzheimer's disease: cholesterol and beyond. *Nat. Rev. Neurosci.* 12, 284–296. doi: 10.1038/nrn3012
- Duewelling, P., Kono, H., Rayner, K. J., Sirois, C. M., Vladimer, G., Bauernfeind, F. G., et al. (2010). NLRP3 inflammasomes are required for atherogenesis and activated by cholesterol crystals. *Nature* 464, 1357–1361. doi: 10.1038/nature08938
- Ferguson, S. M. (2018a). Axonal transport and maturation of lysosomes. *Curr. Opin. Neurobiol.* 51, 45–51. doi: 10.1016/j.conb.2018.02.020
- Ferguson, S. M. (2018b). Neuronal lysosomes. *Neurosci. Lett.* doi: 10.1016/j.neulet.2018.04.005 [Epub ahead of print].
- Galluzzi, L., Vitale, I., Aaronson, S. A., Abrams, J. M., Adam, D., Agostinis, P., et al. (2018). Molecular mechanisms of cell death: recommendations of the Nomenclature Committee on Cell Death 2018. *Cell Death Differ.* 25, 486–541. doi: 10.1038/s41418-017-0012-4
- Gorjod, R. M., Alaimo, A., Porte Alcon, S., Pomilio, C., Saravia, F., and Kotler, M. L. (2015). The autophagic-lysosomal pathway determines the fate of glial cells under manganese-induced oxidative stress conditions. *Free Radic. Biol. Med.* 87, 237–251. doi: 10.1016/j.freeradbiomed.2015.06.034
- He, Y., Hara, H., and Nunez, G. (2016). Mechanism and regulation of NLRP3 inflammasome activation. *Trends Biochem. Sci.* 41, 1012–1021. doi: 10.1016/j.tibs.2016.09.002
- He, W. T., Wan, H., Hu, L., Chen, P., Wang, X., Huang, Z., et al. (2015). Gasdermin D is an executor of pyroptosis and required for interleukin-1 $\beta$  secretion. *Cell Res.* 25, 1285–1298. doi: 10.1038/cr.2015.139
- Hein, L. K., Apaja, P. M., Hattersley, K., Grose, R. H., Xie, J., Proud, C. G., et al. (2017). A novel fluorescent probe reveals starvation controls the commitment of amyloid precursor protein to the lysosome. *Biochim. Biophys. Acta Mol. Cell Res.* 1864, 1554–1565. doi: 10.1016/j.bbamcr.2017.06.011
- Hsieh, S. C., Wu, C. C., Hsu, S. L., and Yen, J. H. (2017). Molecular mechanisms of gallic acid-induced growth inhibition, apoptosis, and necrosis in hypertrophic scar fibroblasts. *Life Sci.* 179, 130–138. doi: 10.1016/j.lfs.2016.08.006
- Jo, E. K., Kim, J. K., Shin, D. M., and Sasakawa, C. (2016). Molecular mechanisms regulating NLRP3 inflammasome activation. *Cell. Mol. Immunol.* 13, 148–159. doi: 10.1038/cmi.2015.95
- Kovacs, S. B., and Miao, E. A. (2017). Gasdermins: effectors of pyroptosis. *Trends Cell Biol.* 27, 673–684. doi: 10.1016/j.tcb.2017.05.005
- Laskar, A., Andersson, R. G., and Li, W. (2013). Fodipir and its dephosphorylated derivative dipyridoxyl ethyldiamine are involved in mangafodipir-mediated cytoprotection against 7 $\beta$ -hydroxycholesterol-induced cell death. *Pharmacology* 92, 182–186. doi: 10.1159/000354601
- Leoni, V., Mariotti, C., Nanetti, L., Salvatore, E., Squitieri, F., Bentivoglio, A. R., et al. (2011). Whole body cholesterol metabolism is impaired in Huntington's disease. *Neurosci. Lett.* 494, 245–249. doi: 10.1016/j.neulet.2011.03.025
- Li, C., Liu, X., Liu, Q., Li, S., Li, Y., Hu, H., et al. (2017). Protection of taurine against PFOS-induced neurotoxicity in PC12 cells. *Adv. Exp. Med. Biol.* 975, 907–916. doi: 10.1007/978-94-024-1079-2\_72
- Li, S., Wang, M., Ojcius, D. M., Zhou, B., Hu, W., Liu, Y., et al. (2018). Leptospira interrogans infection leads to IL-1 $\beta$  and IL-18 secretion from a human macrophage cell line through reactive oxygen species and cathepsin B mediated-NLRP3 inflammasome activation. *Microbes Infect.* 20, 254–260. doi: 10.1016/j.micinf.2018.01.010
- Lipton, P. (2013). Lysosomal membrane permeabilization as a key player in brain ischemic cell death: a “lysosomocentric” hypothesis for ischemic brain damage. *Transl. Stroke Res.* 4, 672–684. doi: 10.1007/s12975-013-0301-2
- Llorente, P., Kristen, H., Sastre, I., Toledano-Zaragoza, A., Aldudo, J., Recuero, M., et al. (2018). A free radical-generating system regulates amyloid oligomers: involvement of cathepsin B. *J. Alzheimers Dis.* 66, 1397–1408. doi: 10.3233/jad-170159
- Ma, W. W., Li, C. Q., Yu, H. L., Zhang, D. D., Xi, Y. D., Han, J., et al. (2015). The oxysterol 27-hydroxycholesterol increases oxidative stress and



- regulate Nrf2 signaling pathway in astrocyte cells. *Neurochem. Res.* 40, 758–766. doi: 10.1007/s11064-015-1524-2
- Man, S. M., and Kanneganti, T. D. (2015). Gasdermin D: the long-awaited executioner of pyroptosis. *Cell Res.* 25, 1183–1184. doi: 10.1038/cr.2015.124
- Martins, I. J., Berger, T., Sharman, M. J., Verdile, G., Fuller, S. J., and Martins, R. N. (2009). Cholesterol metabolism and transport in the pathogenesis of Alzheimer's disease. *J. Neurochem.* 111, 1275–1308. doi: 10.1111/j.1471-4159.2009.06408.x
- Masters, S. L., and O'Neill, L. A. (2011). Disease-associated amyloid and misfolded protein aggregates activate the inflammasome. *Trends Mol. Med.* 17, 276–282. doi: 10.1016/j.molmed.2011.01.005
- Nagakannan, P., and Eftekharpour, E. (2017). Differential redox sensitivity of cathepsin B and L holds the key to autophagy-apoptosis interplay after Thioredoxin reductase inhibition in nutritionally stressed SH-SY5Y cells. *Free Radic. Biol. Med.* 108, 819–831. doi: 10.1016/j.freeradbiomed.2017.05.005
- Nelson, E. R. (2018). The significance of cholesterol and its metabolite, 27-hydroxycholesterol in breast cancer. *Mol. Cell. Endocrinol.* 466, 73–80. doi: 10.1016/j.mce.2017.09.021
- Ni, Y., Gu, W. W., Liu, Z. H., Zhu, Y. M., Rong, J. G., Kent, T. A., et al. (2018). RIP1K contributes to neuronal and astrocytic cell death in ischemic stroke via activating autophagic-lysosomal pathway. *Neuroscience* 371, 60–74. doi: 10.1016/j.neuroscience.2017.10.038
- Olsen, I., and Singhrao, S. K. (2016). Inflammasome involvement in Alzheimer's disease. *J. Alzheimers Dis.* 54, 45–53. doi: 10.3233/jad-160197
- Ono, K., Kim, S. O., and Han, J. (2003). Susceptibility of lysosomes to rupture is a determinant for plasma membrane disruption in tumor necrosis factor  $\alpha$ -induced cell death. *Mol. Cell. Biol.* 23, 665–676. doi: 10.1128/mcb.23.2.665-676.2003
- Orlowski, G. M., Sharma, S., Colbert, J. D., Bogoy, M., Robertson, S. A., Kataoka, H., et al. (2017). Frontline science: multiple cathepsins promote inflammasome-independent, particle-induced cell death during NLRP3-dependent IL-1 $\beta$  activation. *J. Leukoc. Biol.* 102, 7–17. doi: 10.1189/jlb.3hi0316-152r
- Popp, J., Lewczuk, P., Kölsch, H., Meichsner, S., Maier, W., Kornhuber, J., et al. (2012). Cholesterol metabolism is associated with soluble amyloid precursor protein production in Alzheimer's disease. *J. Neurochem.* 123, 310–316. doi: 10.1111/j.1471-4159.2012.07893.x
- Popp, J., Meichsner, S., Kölsch, H., Lewczuk, P., Maier, W., Kornhuber, J., et al. (2013). Cerebral and extracerebral cholesterol metabolism and CSF markers of Alzheimer's disease. *Biochem. Pharmacol.* 86, 37–42. doi: 10.1016/j.bcp.2012.12.007
- Repnik, U., Hafner Česen, M., and Turk, B. (2014). Lysosomal membrane permeabilization in cell death: concepts and challenges. *Mitochondrion* 19, 49–57. doi: 10.1016/j.mito.2014.06.006
- Rubartelli, A., Cozzolino, F., Talio, M., and Sitia, R. (1990). A novel secretory pathway for interleukin-1  $\beta$ , a protein lacking a signal sequence. *EMBO J.* 9, 1503–1510. doi: 10.1002/j.1460-2075.1990.tb08268.x
- Saftig, P., and Klumperman, J. (2009). Lysosome biogenesis and lysosomal membrane proteins: trafficking meets function. *Nat. Rev. Mol. Cell Biol.* 10, 623–635. doi: 10.1038/nrm2745
- Saresella, M., La Rosa, F., Piancone, F., Zoppis, M., Marventano, I., Calabrese, E., et al. (2016). The NLRP3 and NLRP1 inflammasomes are activated in Alzheimer's disease. *Mol. Neurodegener.* 11:23. doi: 10.1186/s13024-016-0088-1
- Schultz, M. L., Krus, K. L., and Lieberman, A. P. (2016). Lysosome and endoplasmic reticulum quality control pathways in Niemann-Pick type C disease. *Brain Res.* 1649, 181–188. doi: 10.1016/j.brainres.2016.03.035
- Serrano-Puebla, A., and Boya, P. (2016). Lysosomal membrane permeabilization in cell death: new evidence and implications for health and disease. *Ann. N Y Acad. Sci.* 1371, 30–44. doi: 10.1111/nyas.12966
- Shi, J., Zhao, Y., Wang, K., Shi, X., Wang, Y., Huang, H., et al. (2015). Cleavage of GSDMD by inflammatory caspases determines pyroptotic cell death. *Nature* 526, 660–665. doi: 10.1038/nature15514
- Tam, J. H., Cobb, M. R., Seah, C., and Pasternak, S. H. (2016). Tyrosine binding protein sites regulate the intracellular trafficking and processing of amyloid precursor protein through a novel lysosome-directed pathway. *PLoS One* 11:e0161445. doi: 10.1371/journal.pone.0161445
- Wang, X., Chu, G., Yang, Z., Sun, Y., Zhou, H., Li, M., et al. (2015). Ethanol directly induced HMGB1 release through NOX2/NLRP1 inflammasome in neuronal cells. *Toxicology* 334, 104–110. doi: 10.1016/j.tox.2015.06.006
- Wang, H., Yuan, L., Ma, W., Han, J., Lu, Y., Feng, L., et al. (2016). The cytotoxicity of 27-hydroxycholesterol in co-cultured SH-SY5Y cells and C6 cells. *Neurosci. Lett.* 632, 209–217. doi: 10.1016/j.neulet.2016.08.056
- Yang, I. H., Co, C. C., and Ho, C. C. (2005). Spatially controlled co-culture of neurons and glial cells. *J. Biomed. Mater. Res. A* 75, 976–984. doi: 10.1002/jbm.a.30509
- Yang, J., Zhao, Y., Zhang, P., Li, Y., Yang, Y., Yang, Y., et al. (2016). Hemorrhagic shock primes for lung vascular endothelial cell pyroptosis: role in pulmonary inflammation following LPS. *Cell Death. Dis.* 7:e2363. doi: 10.1038/cddis.2016.274
- Yuan, X. M., Sultana, N., Siraj, N., Ward, L. J., Ghafouri, B., and Li, W. (2016). Autophagy induction protects against 7-oxysterol-induced cell death via lysosomal pathway and oxidative stress. *J. Cell Death* 9, 1–7. doi: 10.4137/jcd.s37841
- Zhang, X., Lv, C., An, Y., Liu, Q., Rong, H., Tao, L., et al. (2018). Increased levels of 27-hydroxycholesterol induced by dietary cholesterol in brain contribute to learning and memory impairment in rats. *Mol. Nutr. Food Res.* 62:1700531. doi: 10.1002/mnfr.201700531
- Zhang, D. D., Yu, H. L., Ma, W. W., Liu, Q. R., Han, J., Wang, H., et al. (2015). 27-Hydroxycholesterol contributes to disruptive effects on learning and memory by modulating cholesterol metabolism in the rat brain. *Neuroscience* 300, 163–173. doi: 10.1016/j.neuroscience.2015.05.022

**Conflict of Interest Statement:** The authors declare that the research was conducted in the absence of any commercial or financial relationships that could be construed as a potential conflict of interest.

Copyright © 2019 Chen, Zhou, Yu, Tao, An, Zhang, Wang, Wang and Xiao. This is an open-access article distributed under the terms of the Creative Commons Attribution License (CC BY). The use, distribution or reproduction in other forums is permitted, provided the original author(s) and the copyright owner(s) are credited and that the original publication in this journal is cited, in accordance with accepted academic practice. No use, distribution or reproduction is permitted which does not comply with these terms.



# MicroRNAs in Microglia: How do MicroRNAs Affect Activation, Inflammation, Polarization of Microglia and Mediate the Interaction Between Microglia and Glioma?

Yawei Guo<sup>1†</sup>, Wenming Hong<sup>1,2†</sup>, Xinming Wang<sup>1</sup>, Pengying Zhang<sup>1</sup>, Heinrich Körner<sup>1</sup>, Jiajie Tu<sup>1\*</sup> and Wei Wei<sup>1\*</sup>

<sup>1</sup>Key Laboratory of Anti-inflammatory and Immune Medicine, Anhui Collaborative Innovation Center of Anti-inflammatory and Immune Medicine, Institute of Clinical Pharmacology, Anhui Medical University, Ministry of Education, Hefei, China,

<sup>2</sup>Department of Neurosurgery, The First Affiliated Hospital of Anhui Medical University, Hefei, China

## OPEN ACCESS

### Edited by:

Sung Jun Jung,  
Hanyang University, South Korea

### Reviewed by:

Wang-Xia Wang,  
University of Kentucky, United States  
David J. Loane,  
University of Maryland, United States

### \*Correspondence:

Jiajie Tu  
tujiajie@ahmu.edu.cn  
Wei Wei  
wwwei@ahmu.edu.cn

<sup>†</sup>These authors have contributed  
equally to this work

**Received:** 22 January 2019

**Accepted:** 26 April 2019

**Published:** 10 May 2019

### Citation:

Guo Y, Hong W, Wang X, Zhang P,  
Körner H, Tu J and Wei W  
(2019) MicroRNAs in Microglia: How  
do MicroRNAs Affect Activation,  
Inflammation, Polarization of  
Microglia and Mediate the Interaction  
Between Microglia and Glioma?  
*Front. Mol. Neurosci.* 12:125.  
doi: 10.3389/fnmol.2019.00125

The essential roles of microglia in maintaining homeostasis in the healthy brain and contributing to neuropathology are well documented. Emerging evidence suggests that epigenetic modulation regulates microglial behavior in both physiological and pathological conditions. MicroRNAs (miRNAs) are short, non-coding epigenetic regulators that repress target gene expression mostly *via* binding to 3'-untranslated region (3'-UTR) of mRNA in a Dicer-dependent manner. Dysregulation of certain miRNAs can contribute to microglial hyper-activation, persistent neuroinflammation, and abnormal macrophage polarization in the brain. These abnormal conditions can support the pathogenesis of neurological disorders such as glioma, Alzheimer's disease (AD), amyotrophic lateral sclerosis (ALS), stroke, ischemia, and spinal cord injury (SCI). However, the roles of miRNAs in microglia in health and neurological disease have not been systematically summarized. This review will first report the role of Dicer, a key endoribonuclease that is responsible for most miRNA biogenesis in microglia. Second, we will focus on recent research about the function of miRNAs in activation, inflammation and polarization of microglia, respectively. In addition, potential crosstalk between microglia and glioma cells *via* miRNAs will be discussed in this part. Finally, the role of two essential miRNAs, miR-124, and miR-155, in microglia will be highlighted.

**Keywords:** microRNA, microglia, activation, inflammation, polarization, glioma

## INTRODUCTION

Microglia are resident macrophages in the brain that contribute to immunological homeostasis in the central nervous system (CNS; Paolicelli et al., 2011; Schafer et al., 2012) and become activated during CNS pathology (Wake et al., 2009). To maintain homeostasis in the healthy CNS, microglia participate in brain (Paolicelli et al., 2011) and synaptic development (Tremblay et al., 2011) through active communication with neurons (Schafer et al., 2013). Emerging evidence suggests that microRNAs (miRNAs) have various essential roles in the normal brain (Boudreau et al., 2014) and have been implicated in neuropathological conditions (Brettschneider et al., 2015).

MiRNAs repress gene expression by binding to the 3'-untranslated region (3'-UTR; Tu et al., 2015), coding sequence (Fang and Rajewsky, 2011) or 5'UTR (Lee et al., 2009) of target genes. An individual miRNA can target hundreds of genes simultaneously (Hong et al., 2018) which makes its contribution to regulatory mechanism difficult to appreciate.

The specific roles of individual miRNAs in microglia have been extensively investigated (Amici et al., 2017). Activated microglia respond strongly to neurotransmitters (Town et al., 2005). In most pathological conditions of the CNS, microglia are highly activated (Ponomarev et al., 2005), suggesting that the transition from a resting to an activated state may play an important role in neuropathogenesis. Moreover, communication between microglia and neurons in chronic neuroinflammation has also been demonstrated in several neurodegenerative diseases (Suzumura, 2013). Additionally, the role of microglial polarization in M1 (pro-inflammation) and M2 (anti-inflammation) macrophages/microglia has been demonstrated in several CNS diseases (Jha et al., 2016; Geloso et al., 2017; Labandeira-Garcia et al., 2017; Lan et al., 2017). Finally, recent evidence has demonstrated that microglia abundantly infiltrate the microenvironment of glioma, a malignant brain tumor acting as tumor-associated macrophages (Hambardzumyan et al., 2016).

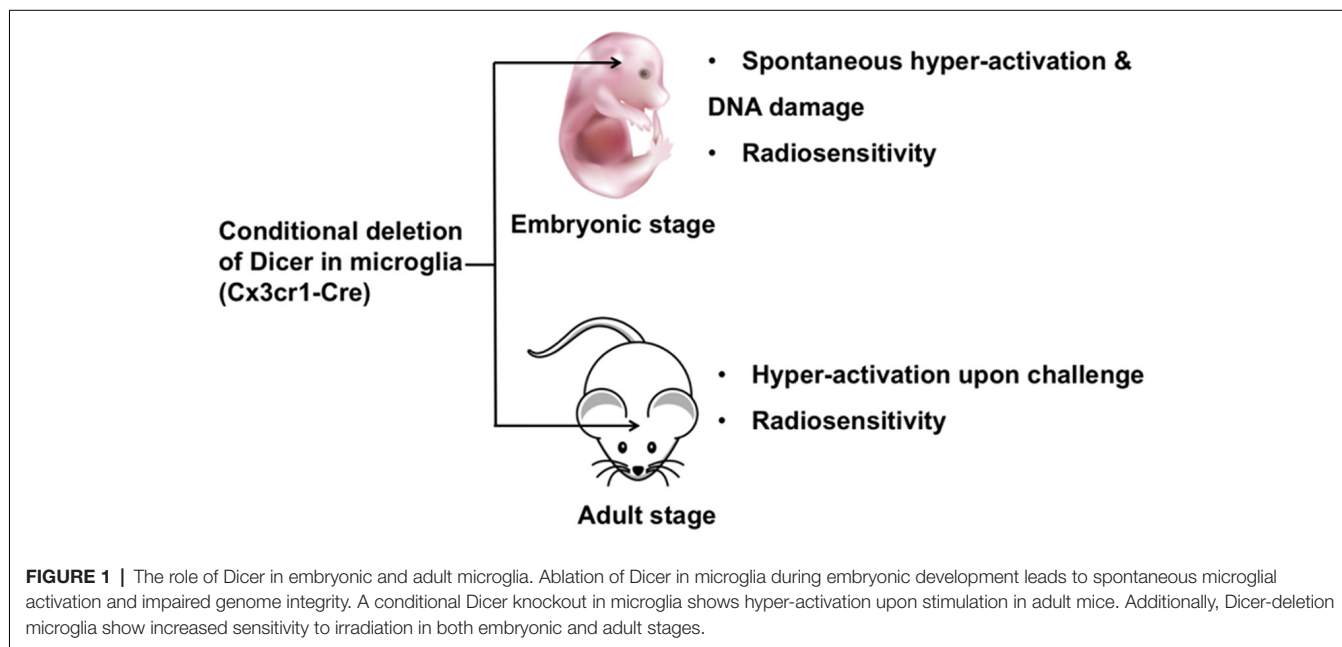
An improved understanding of the interactions between microglia and glioma could promote novel therapeutic strategies for glioma therapy. In this review, we will discuss in detail the dysregulation of miRNAs in microglia in both the healthy brain and CNS pathologies. The roles of specific miRNAs in mediating microglial activation, inflammation, and polarization signaling cascades will be summarized. The potential role of miRNAs in mediating a crosstalk between microglia and glioma and specifically, the roles of two well-studied miRNAs in microglia, miR-124 and miR-155 will be highlighted.

## Dicer KO Microglia

Dicer is responsible for most miRNA biogenesis by acting as endoribonuclease or helicase with an RNase motif and cleaving miRNA precursors into mature miRNAs (Cheloufi et al., 2010). Therefore, most miRNAs are downregulated in Dicer knockout cells. The consequences of this genetic ablation of Dicer are dramatic. A conditional Dicer knockout in microglia (Cx3cr1-Cre) showed hyper-activation upon stimulation. During embryonic development deletion of Dicer led to spontaneous microglial activation and impaired genome integrity. Furthermore, Dicer-negative microglia displayed a shift to an inflammatory state upon peripheral endotoxin challenge, thereby compromising hippocampal neuronal function. Additionally, Dicer-negative microglia showed increased sensitivity to irradiation (Varol et al., 2017). In summary, Dicer knockout microglia exhibited significant changes in normal functions in both prenatal and adult stages (**Figure 1**), suggesting that individual miRNAs play a role in microglia. It is critical to identify the specific miRNAs that are responsible for microglial dysfunction. Apart from Dicer, biogenesis of some miRNAs is dependent on the protein Argonaute (Cheloufi et al., 2010). Therefore, an investigation of the role of Argonaute in microglia will further clarify the function of miRNAs in brain. In the next section, we will summarize the versatile role of individual miRNAs in microglia.

## The Role of miRNAs in Microglial Activation

Microglial function is essential for neurodegenerative disorders including Parkinson's disease (PD), multiple sclerosis (MS) and Alzheimer's disease (AD; Grimmig et al., 2016; Hesse et al., 2016), all of which are closely associated with microglial activation (Lull and Block, 2010; Kandinov et al., 2011;



Tanaka et al., 2013; Reemst et al., 2016; Du et al., 2017; Sarlus and Heneka, 2017). In their resting state, microglia show beneficial effects *via* interactions with neurons, thus helping to maintain brain homeostasis. Upon brain injury or infection, microglia transform to an activated state and secrete neurotoxic mediators, such as reactive oxygen species (ROS), tumor necrosis factor alpha (TNF- $\alpha$ ), and interleukin-1 $\beta$  (IL-1 $\beta$ ; Belarbi et al., 2011; Krishnaswamy and Cooper, 2012; Mishra et al., 2012; Yang et al., 2013) which have harmful effects including disruption of neuronal function/synaptic transmission and neuronal oxidative stress/degeneration resulting in neuronal damage. Therefore, emerging evidence suggests that miRNAs can ameliorate degeneration by inhibiting microglial activation in the brain. A suppression of microglial activation could serve as a potential therapeutic approach to protect neurons and thus, treat or prevent neurodegenerative diseases (Lull and Block, 2010). The following section discusses the effects of miRNAs on microglial activation in preventing neuronal damage.

Intracerebroventricular injection of let-7c-5p mimics reduced infarction volume and ameliorated neurological defects *via* inhibition of microglia activation in a model of cerebral ischemia injury. These effects were mediated by inhibition of caspase-3 (Ni et al., 2015). Furthermore, it has been shown that microglial activation can induce ischemia, a condition that could be repressed by miR-203, which directly targeted MyD88 in microglia. A miR-203 overexpression or a MyD88 knockdown led to repression of NF- $\kappa$ B signaling and prevented subsequent microglial activation (Yang et al., 2015) ameliorating neuronal injury. Another microRNA, miR-145-5p, was shown to directly bind to the 3'-UTR of the mRNA of Nurr1, a member of the orphan nuclear receptor family that induces neuronal death and consequently, inhibited Nurr1-mediated microglial activation alleviating neuronal injury in acute cerebral ischemic/reperfusion in rats (Xie et al., 2017).

The miR-199b was shown to inhibit the IKK $\beta$ -NF- $\kappa$ B signaling pathway and to repress pro-inflammatory cytokines *via* modulation of microglial activation in a rat model of spinal cord injury (SCI; Zhou H. J. et al., 2016). These results imply that miR-199b is a potential therapeutic target for SCI. Additionally, miR-424 was found to be repressed in the plasma of patients with acute ischemic stroke, and in mouse plasma and brain tissues after ischemia. Treatment with miR-424 alleviated brain edema and cerebral infarction size after middle cerebral artery occlusion *via* repression of microglial activation and neuronal apoptosis. It was also demonstrated that miR-424 inhibited ionized calcium-binding adaptor molecule (iba) 1 and reduced pro-inflammatory TNF- $\alpha$  secretion. In addition, *in vitro* experiments further validated that miR-424 inhibited the activity of BV2, a microglial cell line (Zhao et al., 2013). Likewise, miR-7 inhibited microglial NLRP3 inflammasome activation *in vitro*. In contrast, anti-miR-7 induced inflammasome activation. Moreover, stereotactic injection of miR-7 mimics into the mouse striatum ameliorated microglial activation, concomitant with attenuation of dopaminergic neuron degeneration in a mouse model of PD (Zhou Y. et al., 2016) making miR-7 a potential target in PD therapy.

The miR-27a was found to be repressed in lipopolysaccharide (LPS)-activated microglia. It inhibited microglia-produced inflammatory cytokines, including IL-6, IL-1 $\beta$  and TNF- $\alpha$ , and interfered with the expression of TLR4 and interleukin-1 receptor-associated kinase 4 (IRAK4) by directly binding their 3'-UTRs. Downregulation of TLR4 or IRAK4 of the TLR4/MyD88 signaling pathway in microglia inhibited the downstream secretion of inflammatory mediators (Lv et al., 2017). Therefore, miR-27a could regulate LPS-activated production of inflammatory cytokines in microglia by modulating TLR4/IRAK4 activity. Hypoxic conditions were also shown to induce TLR4, to activate microglia, and to reduce miR-181c in the brain. Like miRNA27-a, miR-181c repressed microglial activation by directly targeting TLR4. Moreover, it repressed the production of inflammatory mediators of the NF- $\kappa$ B pathway (Zhang et al., 2015). Thus, miR-181c may play an important role in hypoxic microglial activation and neuroinflammation. The miR-181c-TLR4-NF- $\kappa$ B pathway may be a potential target for cerebral hypoxic diseases. Japanese encephalitis virus (JEV) infection was shown to activate the microglial cell line BV-2 and to upregulate the expression of inducible nitric oxide synthase (iNOS) and cyclooxygenase (COX) 2. miR-29b further increased JEV-induced microglial activation by targeting TNF- $\alpha$ -induced protein (TNFAIP) 3 and increasing the nuclear translocation of NF- $\kappa$ B (Thounaojam et al., 2014).

In amyotrophic lateral sclerosis (ALS), the NF- $\kappa$ B pathway is positively associated with microglial activation and motor neuron injury. The ubiquitin-editing enzyme A20 plays an important role in inhibiting the NF- $\kappa$ B pathway. miR-125b was shown to directly repress A20 and to consequently amplify NF- $\kappa$ B function in microglia in a P2X7 receptor-dependent manner (Parisi et al., 2016). These results highlight an important role for miR-125b in ALS *via* modulation of microglial activation and motor neuron injury. Methamphetamine-induced neurotoxicity is closely linked to microglial activation. Anti-miRNA143-mediated BBC3 induction restored methamphetamine-repressed microglial survival through the modulation of autophagy and apoptosis. BBC3 was also shown to be a direct target of miR-143 in microglia. As such, microinjection of anti-miR-143 into the hippocampus ameliorated methamphetamine-induced microglial activation. A similar result was demonstrated in heterozygous miR-143 mice (Zhang et al., 2016). Future work exploring the specific effects of miR-143-BBC3 on microglial activation is necessary to provide a better understanding of the mechanism of drug addiction. MiR-146a restored learning and memory impairment in an experimental mouse model of Postoperative cognitive dysfunction (POCD) by targeting interleukin-1 receptor-associated kinase 1 (IRAK1) and TNF-receptor-associated factor 6 (TRAF6). A reduced effect of miR-146a on the abnormal activation of microglia in the hippocampus indicates that miR-146a is a potential therapeutic target of POCD (Chen et al., 2019).

Interestingly, most of these microRNAs are related to the NF- $\kappa$ B pathway in microglia (**Figure 2**), indicating the central



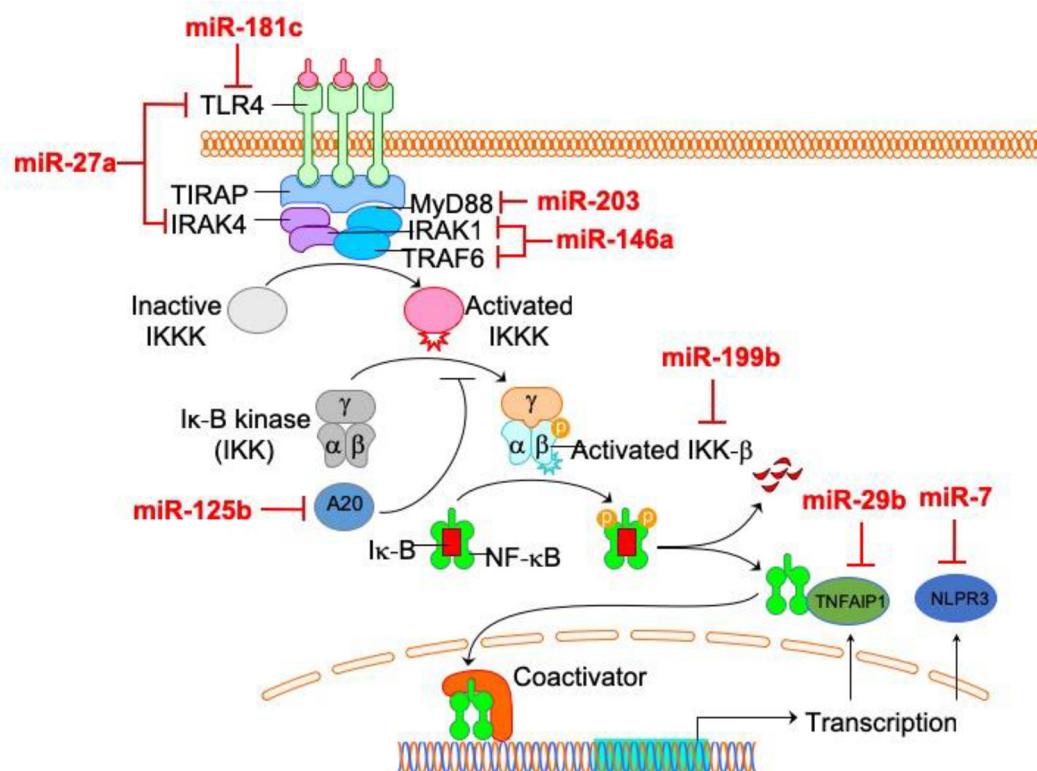


**FIGURE 2 |** The relationship between microRNAs (miRNAs) and NF-κB pathway in microglia. Among microglia activation-related miRNAs, the direct targets of most miRNAs (miR-27a, miR-181c, miR-203, miR-125b, miR-199, miR-29b, miR-7 and miR-146a) are within NF-κB pathway.

role of NF-κB pathway in microglia activation. Therefore, these findings suggest that miRNAs represent a novel group of NF-κB pathway-related targets regulating microglial activation and brain injury, thus offering a new therapeutic strategy for treating associated neuronal diseases. The modulation of microglial activation by adjusting the interaction between these miRNAs and the NF-κB pathway open new possibilities in the area of therapy for neurodegenerative disorders. By using the tools of gene therapy, miRNA-based “fine-tuning” therapy is a potential method to restore the abnormal activation of microglia.

## The Role of miRNAs in Microglia-Mediated Inflammation

Persistent CNS inflammation could be an underlying cause of cell death in many neurodegenerative diseases, such as HIV-induced dementia, PD, AD, and MS. Thus, microglia-mediated inflammation plays an essential role in neuropathogenesis. Nevertheless, the specific role of microglia in neuron inflammation is a still not entirely characterized. CNS inflammation involving microglia is a normal response to infection. However, when allowed to continue uncontrolled, inflammation may lead to pathological states. Therefore, during the inflammatory process, microglia switch from having a beneficial role to having a detrimental role by secreting cytotoxic molecules, including proinflammatory cytokines and reactive oxygen mediators. Thus, modulating microglia

in neuron inflammation is a potential therapeutic strategy for neurodegenerative disease. Indeed, there already exist a number of anti-inflammatory drugs that exert neuronal protective effects by modulating the status of microglia (Ajmone-Cat et al., 2010; Kwon et al., 2013). In recent years, several research groups have investigated the effect of miRNAs on microglia-mediated inflammation. Microglia activation also leads to inflammatory activities, but not all microglia-mediated inflammation is induced by microglia activation. Because we already discuss miRNA in microglia activation in previous section, we only discuss miRNAs in microglia inflammation while not activation.

Both TLR2 and TLR4 activation were shown to increase miR-146a in microglia. In response to TLR2 stimulation, miR-146a disrupted normal inflammatory responses, including NF-κB and JAK-STAT signaling pathways. Two phagocytic mediators of the oxidative burst, CYBA and NOS3, were predicted as direct targets of miR-146a (Saba et al., 2012). In addition, it was reported that in a transgenic reporter mouse, murine microglia specifically lost miR-9. Furthermore, injection of miR-9 vectors into rat brains induced transgene expression in microglia, which permitted direct visualization and isolation of inflammatory microglia without affecting circulation-derived monocytes/macrophages in rats with excitotoxic lesions. As such, miR-9 vectors have been useful in mechanism studies of microglial inflammation (Åkerblom et al., 2013). HIV-1 Tat C

exposure repressed miR-17 and induced NOX2/NOX4 and ROS production in human microglial cells. NOX2/NOX4 were shown to be direct targets of miR-17 in microglia (Jadhav et al., 2014). Thus, miR-17 may regulate intracellular ROS generation and subsequent neuroinflammatory responses.

miR-206 was shown to enhance LPS-induced inflammation and cause the release of amyloid- $\beta$  (an essential protein in AD) in microglia by directly binding to the 3'-UTR of Insulin-like growth factor (IGF) 1. A rescue assay demonstrated that IGF1 exposure could attenuate miR-206-induced inflammation in microglia, indicating that the miR-206/IGF1 signaling pathway may be associated with AD associated microglial inflammation (Xing et al., 2016). miR-26a was rapidly reduced after TLR4 stimulation in microglia and repressed the production of inflammatory cytokines. Furthermore, the ATF2 transcription factor linked to promote inflammation may be a direct target of miR-26a (Kumar et al., 2015), suggesting a role for miR-26a/ATF2-mediated regulation of proinflammatory cytokine production in microglia. miR-93 was significantly inhibited in cerebral ischemia reperfusion (CIR) mice brains. miR-93 overexpression reduced cerebral infarction volume and alleviated neurological deficits in CIR mice. Furthermore, miR-93 inhibited inflammatory responses and decreased the rate of cell apoptosis in CIR mice. Likewise, miR-93 was shown to inhibit IRAK4 and other pro-inflammatory genes in microglia (Tian et al., 2017).

Let-7a is involved in maintaining microglial function in inflammation-mediated injury. During inflammation, Let-7a was shown to inhibit the production of proinflammatory mediators, including iNOS, IL-6, and nitrite, while at the same time inducing anti-inflammatory genes such as brain derived neurotrophic factor (BDNF) and IL-4 in microglia (Cho et al., 2015). Another study showed that the anti-inflammatory factor Apoptosis signal-regulating kinase 1 (ASK1) induced Let-7a activity and consequently activated anti-inflammatory cytokines IL-10 and Mycs in microglia (Song and Lee, 2015). Therefore, Let-7a plays an important role in microglia-related inflammation. miR-32-5p was strongly upregulated in microglia from rats with spinal nerve ligation (SNL). Knockdown of miR-32-5p significantly reduced mechanical allodynia and heat hyperalgesia and decreased the production of inflammatory cytokines in SNL rats. Similarly, miR-32-5p inhibition ameliorated inflammatory cytokine production in LPS-treated microglia. Further investigations demonstrated that Dual-specificity phosphatase 5 (Dusp5) was directly repressed by miR-32. Dusp5 is involved in neuropathic pain and neuroinflammation (Yan et al., 2018). As such, miR-32-5p may induce neuroinflammation and neuropathic pain by modulating Dusp5 activity, suggesting novel therapeutic approaches targeting miR-32-5p-Dusp5 for the treatment of neuropathic pain.

Intracerebral hemorrhage (ICH) decreased miR-367 and increased IRAK4 in primary microglia. IRAK4 is a direct target of miR-367, which may inhibit the NF- $\kappa$ B pathway and block the secretion of related proinflammatory cytokines. Moreover, miR-367 inhibited the production of proinflammatory cytokines and reduced brain edema in ICH mice (Yuan et al., 2015).

Therefore, miR-367/IRAK4 represents a potential therapeutic target of neuroinflammation in ICH. Inhibition of miR-204 or SIRT overexpression inhibited LPS-mediated inflammation, proliferation of mouse microglial cells, and promoted apoptosis (Li et al., 2015). Therefore, miR-204 may inhibit microglia-related neuroinflammation in mice by modulating SIRT1. Hyperglycemia- (HG-) Amadori-glycated albumin- (AGA-) treated microglia leads to retinal inflammation, which can cause diabetic retinopathy (DR). In diabetic patients, miR-146b-3p was negatively correlated with adenosine deaminase (ADA) 2, which is a known inducer of retinal inflammation. Overexpression of miR-146b-3p repressed ADA2 and inhibited the production of inflammatory cytokines in microglia (Fulzele et al., 2015).

In summary, the above-mentioned studies stress the role of miRNAs as modulators of neuroinflammation and illustrate their potential as biomarkers and novel therapeutic targets in CNS diseases (Table 1) Thus, miRNAs may provide potential therapeutic strategies for treating cerebral inflammation.

## The Role of miRNAs in Microglial Polarization

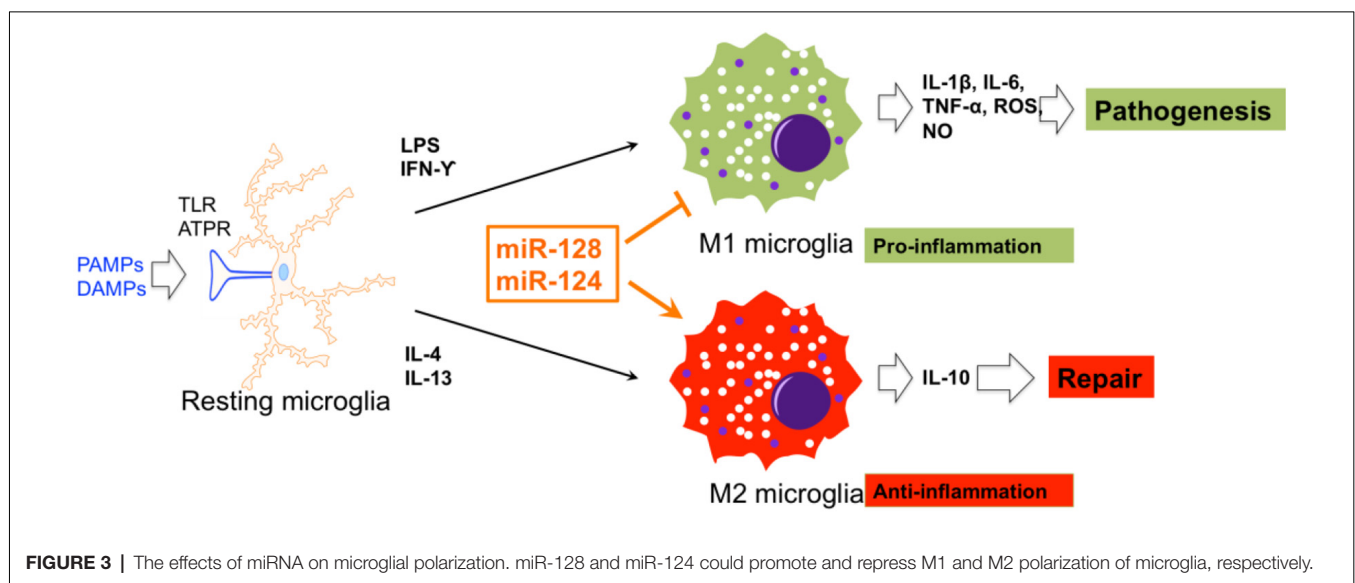
Classically, M1 and M2 microglia/macrophages show opposite phenotypes: M1 microglia/macrophages release destructive pro-inflammatory mediators while M2 microglia/macrophages produce protective factors (David and Kroner, 2011). However, the M1 and M2 concept are clearer for *in vitro* studies, while the polarization of microglia/macrophages is more intricate *in vivo* (Moore et al., 2013). M1/M2 classification are therefore a useful concept to identify the specific role of microglia/macrophages in neuropathogenesis (Boche et al., 2013), including SCI, stroke, and TBI (Kigerl et al., 2009; Hu et al., 2012; Wang et al., 2013).

In SCI mice, miR-128 was found to be downregulated in microglial BV2 cells. miR-128 markedly promoted the viability of microglia through downregulation of the microglial M1 phenotypic markers, CD86 and CD32, and up-regulation of the M2 phenotypic markers, Arginase (Arg) 1 and CD206. In addition, miR-128 repressed the secretion of inflammatory cytokines. It was also demonstrated that the anti-inflammatory function of miR-128 is mediated by the P38 pathway (Yang et al., 2017). miR-124 promoted neuronal survival and M2-like polarization of microglia. The neuroprotective function of miR-124 was exerted during the first week. Arg1<sup>+</sup> microglia were positively associated with functional improvement during the same course as miR-124 treatment (Hamzei Taj et al., 2016b). Therefore, miR-124 and miR-128 are two potential targets for functional recovery *via* regulation of microglial polarization (Figure 3).

Overall, the approach to regulate the polarization of microglia by targeting pro-inflammatory or anti-inflammatory miRNAs plays an essential role in plans for a therapy of CNS diseases. However, the main obstacle is how to directly deliver miRNAs to the CNS through the blood brain barrier (BBB) and how to prevent the degradation of exogenous miRNAs by lysosomal activities. With the development of new investigative methods and a better understanding of mechanisms of microglia

**TABLE 1** | The effect of microRNAs (miRNAs) on microglia activation and inflammation.

Funtion		miRNA	Target	Reference
Microglia activation	Promotion	miR-145	Nurr1	Xie et al. (2017)
		miR-29b	TNFAIP1	Thounaojam et al. (2014)
		miR-125b	A20	Parisi et al. (2016)
		miR-143	BBC3	Zhang et al. (2016)
	Repression	Let7c-5p	Casepase-3	Ni et al. (2015)
		miR-203	MyD88	Yang et al. (2015)
		miR-199b	IKK	Zhou H. J. et al. (2016)
		miR-424	CCND1/CDC25A/CDK6	Zhao et al. (2013)
		miR-7	Nlrp3	Zhou Y. et al. (2016)
		miR-27a	TLR4/TRAF4	Lv et al. (2017)
		miR-181c	TLR4	Zhang et al. (2015)
		miR-146a	IRAK1/TRAF6	Chen et al. (2019)
		miR-206	IGF1	Xing et al. (2016)
Microglia inflammation	Promotion	miR-36	Dusp5	Yan et al. (2018)
	Repression	miR-146	CYBA/NOS3	Saba et al. (2012)
		miR-17	NOX2/NOX4	Jadhav et al. (2014)
		miR-26a	ATF2	Kumar et al. (2015)
		miR-93	IRAK4	Tian et al. (2017)
		Let-7a	SIRT1	Cho et al. (2015) and Song and Lee (2015)
		miR-367	IRAK4	Yuan et al. (2015)
		miR-204	SIRT1	Li et al. (2015)
		miR-146b	ADA2	Fulzele et al. (2015)

**FIGURE 3** | The effects of miRNA on microglial polarization. miR-128 and miR-124 could promote and repress M1 and M2 polarization of microglia, respectively.

polarization, microglia polarization based molecular therapy will be potential future research field of neural diseases treatment.

### miRNA-Mediated Interaction Between Microglia and Glioma

In malignant glioma tissues, glioma cells foster a tumor-favorable microenvironment through interactions with other brain cells, including macrophages and microglia. Emerging evidence suggests that intracellular crosstalk between different cellular components within or near the glioma microenvironment occurs *via* transfer of oncogenic factors, including miRNA (Figure 4).

After resection, glioma often recurs due to the chemoradioresistance of glioma cells. Therefore, identification of the

tumor border composition is essential for prognosis in glioma. “miRNAome” expression was compared in tissues from the tumor, tumor border, and periphery by miRNA sequencing. miR-219-5p, miR-219-2-3p, and miR-338-3p were identified as the top three miRNAs in the tumor border, and all were closely associated with macrophages/microglia. Interestingly, the tumor suppressive role of miR-219 has been proven in glioma cells by targeting Sal-like protein (Sall4; Jiang et al., 2017) and epidermal growth factor receptor (EGFR; Rao et al., 2013). Similarly, miR-338 also showed inhibitory effects on glioma cells by repressing C-terminal binding protein 2 (CTBP2; Liu et al., 2017) and Forkhead box d1 (FOXO1; Ma et al., 2018). However, these studies only proved the roles of miR-219 and miR-338

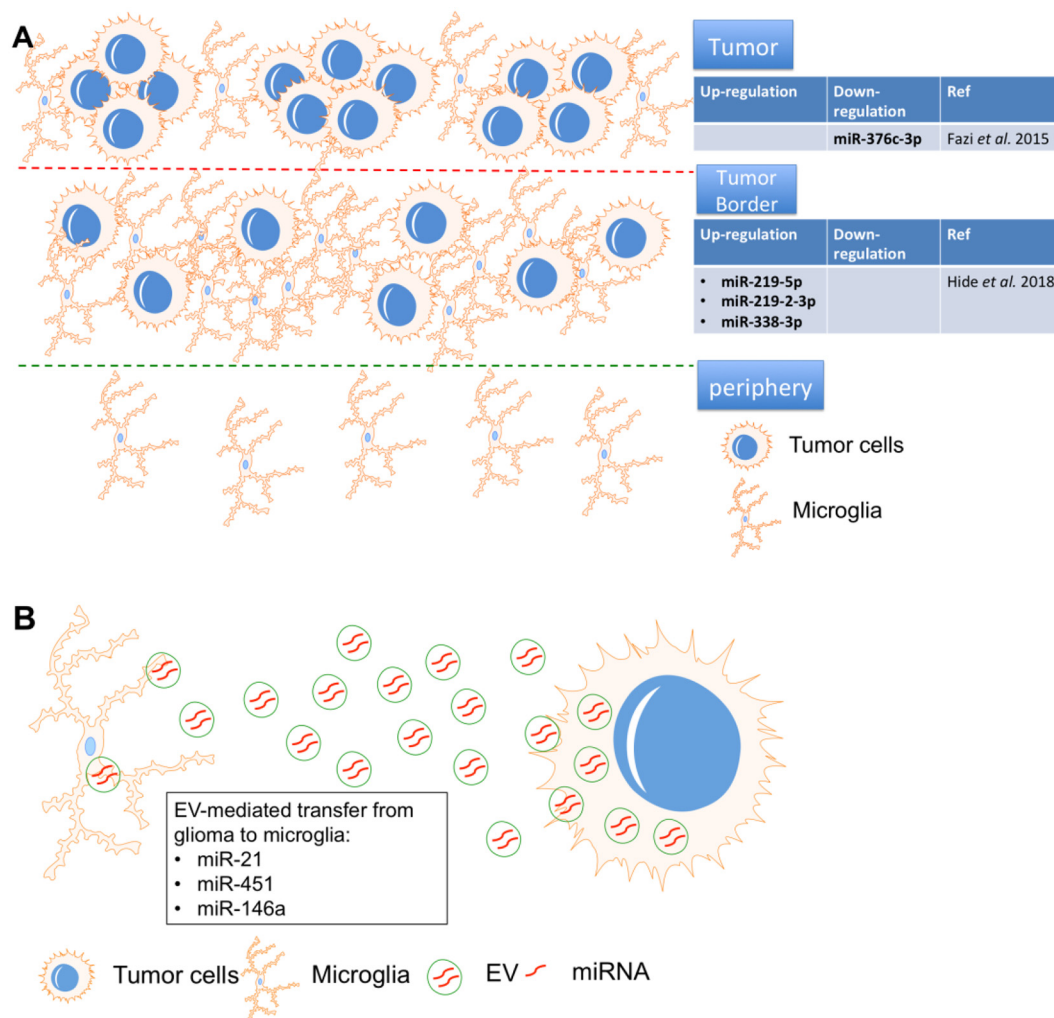


**FIGURE 4 |** MicroRNA-mediated interactions between microglia and glioma. **(A)** miR-219-5p, miR-219-2-3p, and miR-338-3p were identified as the top three miRNAs in the tumor border and miR-376c-3p was reduced in tumor samples, all were closely associated with macrophages/microglia. **(B)** miR-451, miR-21 and miR-146a in glioma-EVs were found to be transferred to microglia.

in glioma cells. The crosstalk between glioma cells and microglia *via* these two miRNAs should be systematically investigated in the future.

Macrophages and microglia strongly infiltrate the microenvironment of glioma tumor border, which is a potential target for recurrence (Hide et al., 2018). Using deep sequencing, another group found that the “miRNAome” in peritumoral areas is quite different from that of white matter but shares similarities with tumor tissue. The data revealed that miR-376c-3p was reduced in tumor samples compared to peritumoral tissues and in short-term tumors compared to long-term tumors (Fazi et al., 2015). miR-376c could repress the malignant behavior of glioma cells by repressing FOXP2 (Li et al., 2019) and circulating miR-376c was significantly down-regulated in serum from glioma patients when compared with healthy control (Huang et al., 2017), suggesting that miR-376c is a potential diagnostic marker and treatment target for glioma. Therefore, the specific

role of miR-376c the microenvironment of glioma also should be studied.

Due to complicated packaging and uptake by recipient cells, extracellular vesicle (EV)-mediated miRNA transfer is more complex than that of normal cytokines. To Elucidate the mechanism of EV-mediated miRNA silencing in recipient cells is crucial for combating gliomas. Intercellular communication within the glioma microenvironment is, at least partially, mediated by EVs containing miRNA. EV-secreted miRNAs are thought to be endocytosed, after which they may exert oncogenic effects in glioma (Rooj et al., 2016). Thus, EV-secreted miRNAs may provide novel diagnostic and prognostic biomarkers, and may even serve as therapy targets of glioma.

In one study, primary human glioma cell-released EVs were isolated and used to treat primary mouse microglia. Mouse glioma cells were implanted into mice brains, after which EV release and uptake by microglia/macrophages were investigated.



Proliferation of microglia/macrophages and production of immune suppressing cytokines were observed following uptake of glioma-EVs. Specifically, miR-451 and miR-21 in glioma-EVs were found to be efficiently transferred to microglia, while c-Myc mRNA was repressed in microglia at the same time. c-Myc has been shown to be a target of miR-451/miR-21, suggesting that EV-mediated miRNA silencing may be a functional link between glioma and microglia. Interestingly, in the brain, the release of EVs from glioma cells and the subsequent uptake by microglia/macrophages were directly visualized by researchers, as microglia/macrophages showed increased miR-21 and reduced c-Myc mRNA in the tumor-bearing brain (van der Vos et al., 2016). The interesting point is that the specific role of miR-21 (Moore and Zhang, 2010) and miR-451 in glioma is totally opposite. Circulating miR-21 dramatically increased in serum from glioma patients (Ivo D'Urso et al., 2015) and positively co-localized with angiogenesis marker VEGF in glioma tissue (Hermansen et al., 2016). In glioma cells, miR-21 exerted its oncogenic effects by promoting invasion (Gabriely et al., 2008) and repressing apoptosis (Quintavalle et al., 2013). Therefore, several groups already designed some tactics to fight against glioma by inhibiting miR-21 (Belter et al., 2016; Seo et al., 2019). However, miR-451 also functions as a tumor suppressor of glioma by repressing some key malignant cellular functions of glioma, such as proliferation, migration and apoptosis (Godlewski et al., 2010; Nan et al., 2010; Guo H. et al., 2016). Thus, EVs could be “oncogenic factor” or “tumor suppressor” by secreting different microRNAs (miR-21 or miR-451). It is critical to identify the specific inducer of secretion of oncogenic or anti-tumor miRNAs from EVs, which is a potential key step to elucidate the crosstalk between microglia and glioma cells in the tumor microenvironment.

miRNA could also directly mediate communication between glioma and microglia in the brain without contributions from EVs. Another study (Karthikeyan et al., 2018) demonstrated that the TGF- $\beta$  signaling pathway in glioma-associated microglia participated in glioma pathogenesis. TGF- $\beta$  activated in malignant glioma was shown to regulate glioma progression by modulating the Mothers against decapentaplegic homolog (SMAD) signaling pathway. SMAD4 has been shown to be a direct target of miR-146a, which was repressed in microglia treated with glioma-conditioned medium. Ectopic expression of miR-146a inhibited SMAD4 and another tumor-suppressor, MMP9, in microglia, and inhibited microglia migration towards glioma-conditioned medium. Moreover, glioma cell proliferation was reduced when treated with conditioned medium from SMAD4 downregulated or miR-146a up-regulated microglia. In addition, the tumor suppressive role of miR-146a also has been extensively studied in glioma cells (Mei et al., 2011; Lu et al., 2016; Li et al., 2018). A functional polymorphism in the pre-miR-146a gene [AG(C polymorphism (rs2910164)] is associated with risk and prognosis in glioma (Permuth-Wey et al., 2011). The therapeutical role of secreted miR-146a from marrow stromal cell (MSC) was also validated in glioma (Katakowski et al., 2013). Taken together, miR-146a-mediated crosstalk between microglia and glioma

promotes microglial migration and glioma cell viability, which is a promising target with dual effects (microglia and glioma cells).

## Two Well-Studied miRNAs in Microglia

### miR-124

miR-124 overexpression repressed motility and phagocytosis of apoptotic cells of microglia and caused residual apoptotic cell bodies to accumulate in the optic tectum. This *in vivo* study showed that miR-124 is essential for microglia development (Svahn et al., 2016). miR-124 is also required for maintaining the “resting” state of mouse monocytes. The *ex vivo* transfection of chitosan/miR-124 polyplex particles into rat microglia resulted in decreased inflammatory cytokine secretion, including ROS, TNF- $\alpha$ , and MHC-II. miR-124 particles were internalized by OX42- (rat macrophage marker) positive macrophages/microglia and reduced the number of ED-1- (rat macrophage marker) positive macrophages in the SCI (Louw et al., 2016).

Cocaine was found to inhibit miR-124 levels in microglia *in vitro*. miR-124 was also downregulated in isolated microglia from cocaine-administered mice (Guo M. L. et al., 2016). Cocaine-induced DNA methylation in the promoter region of miR-124 precursors, suggesting that cocaine exposure repressed miR-124 expression by inducing DNA methylation in the miR-124 promoter, which ultimately activates microglia in brain. Thus, epigenetic modification (e.g., DNA methylation in the promoter region) of miR-124 is a promising therapeutic approach in microglia-mediated cocaine addiction. D-4F (an apolipoprotein-A1 mimetic peptide) induced miR-124a and reduced matrix metalloproteinase-9, TNF- $\alpha$ , and TLR-4 in primary cortical neurons and microglia isolated from ischemic mice (Ning et al., 2017). The anti-inflammatory effects of D-4F were repressed in miR-124 knockdown primary neurons/microglia. D-4F treatment of type one diabetes mellitus (T1DM)-stroke increased miR-124 and promoted M2 macrophage polarization-mediated anti-inflammatory effects. miR-124 is highly expressed in neuronal cells but only shows a basal level in microglia. miR-124 could promote neuronal differentiation, modulate microglial activation, and keep microglia in a quiescent state. miR-124 also shifted pro-inflammatory M1 microglia/macrophages toward the anti-inflammatory M2 phenotype in the sub-acute phase of stroke (Hamzei Taj et al., 2016a), which suggests the ability to restore neurological deficits. Thus, miR-124 administration is a potential treatment for increasing rehabilitation change of stroke.

Morphine administration or inhibition of acetylcholine induced miR-124 expression in microglia and bone marrow-derived macrophages (Qiu et al., 2015). On the contrary, miR-124 promoted the inhibitory effects of morphine on innate immunity by suppressing TRAF6 and a subunit of NF- $\kappa$ B p65. Moreover, two additional transcriptional factors, Active protein (AP)-1 and cAMP response element-binding protein (CREB), were shown to repress miR-124, whereas p65 induced miR-124 transcription by targeting the miR-124 promoter. Therefore, a feedback loop seemingly formed between miR-124 and p65. Modulating miR-124 is a promising target for preventing

opioid-induced damage to microglia. The expression of miR-124 increased in M2 microglia. Furthermore, overexpression of miR-124 repressed the production of proinflammatory cytokines. A co-culture system of microglia and neurons (Yu et al., 2017) showed that M2 microglia protected neurons from injury. miR-124 was also shown to bind to the 3'-UTR of CCAAT enhancer binding protein alpha (C/EBP- $\alpha$ ). *In vivo*, miR-124 repressed expression of C/EBP- $\alpha$  and restored brain injury in ICH mice. Therefore, miR-124 prevents inflammatory damage in ICH by promoting M2 microglia polarization. In summary, miR-124 may represent a new therapeutic target for treatment of ICH.

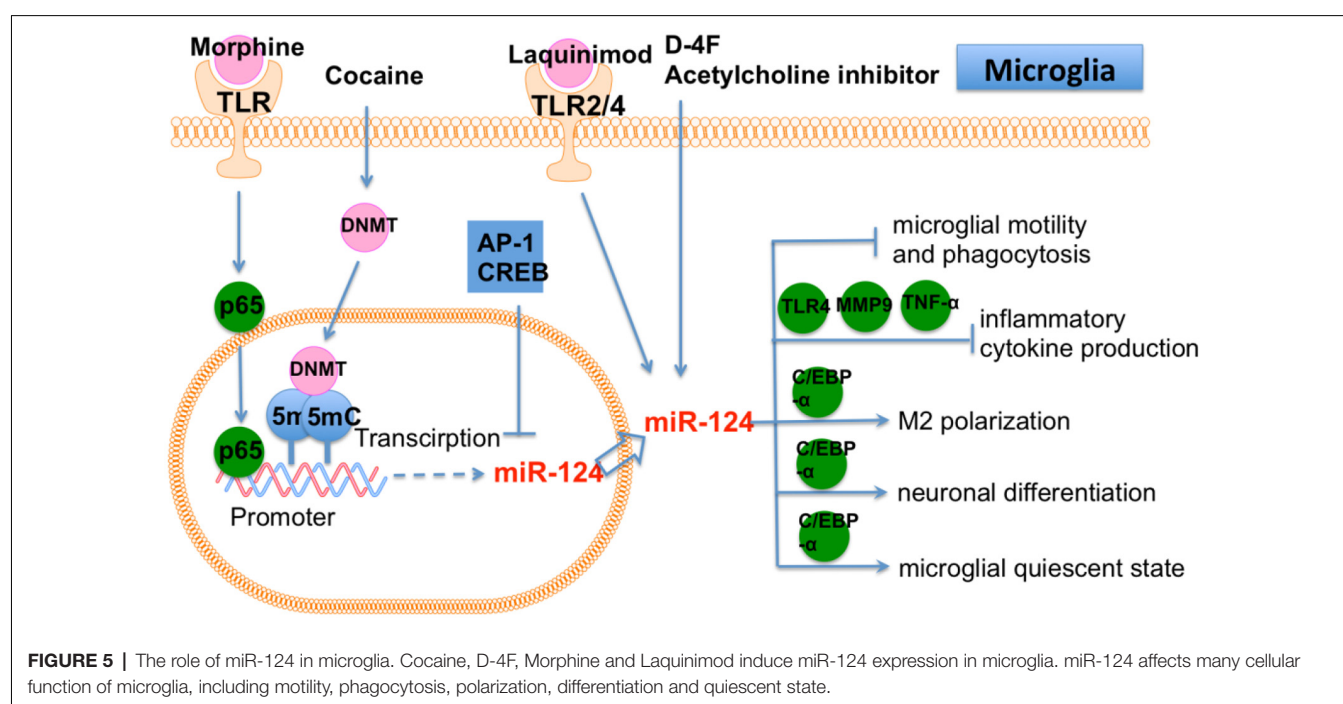
Laquinimod is an oral treatment for MS. Laquinimod reduced brain atrophy and prevented the decline of activated microglia induced by miR-124a (Mishra et al., 2014). Laquinimod also blocked several proinflammatory pathways in microglia, including JNK and AKT pathways. It was further demonstrated that miR-124 inhibited PU.1, an essential downstream target of C/EBP- $\alpha$ , leading these microglia to a quiescent CD45 (low), MHCII (low) phenotype. miR-124 decreased in microglia in experimental autoimmune encephalomyelitis (EAE). Peripheral infusion of miR-124 in EAE led to systemic deactivation of macrophages and T cells, which eventually ameliorated EAE. In addition, miR-124 inhibition in microglia led to the activated state (Ponomarev et al., 2011). miR-124 is required for microglia status in CNS (Figure 5).

The expression level of miR-124 in microglia seemed to reflect the physiological state of brain and the progression of CNS diseases. It would be worthwhile to further explore these observations and elucidate its potential as biomarker for CNS diseases. Based on previous findings that have been summarized

in the miR-124 related literatures, the specific function of miR-124 seems quite versatile in microglia depending upon different physiological and pathological conditions. This suggests that the role of miR-124 is contextual and mainly depends on the microenvironment of the brain in different brain tissues. Therefore, to further illuminate the regulatory role of miR-124 in brain, it will be necessary to pay more attention to the interaction between microglia and other cellular components in brain. In addition, miR-124 targets multiple targets simultaneously in brain (Figure 5). It is known that CNS diseases are often induced by multifactorial causes and the related treatment needs to act on a group of targets. Therefore, miR-124 is a potential therapy for the complexity of pathophysiological events that have been induced by multifactorial CNS diseases. Taken together, miR-124-based treatment is a potential therapy that may replace single-target therapy for the multifactorial CNS disease, which is definitely worth further investigation.

### miR-155

LPS, a proinflammatory TLR4 ligand, greatly induced the expression of miR-155 in primary murine microglia (Woodbury et al., 2015). LPS-induced neurogenic defects and microglial activation were restored in miR-155 knockout mice. In contrast, microglial proliferation was induced in miR-155 knockin mice. miR-155 overexpression in microglia was also shown to cause neurogenic effects on neural stem cell (NSC) amoeboid morphology in the dentate gyrus (DG). Therefore, miR-155 mediated LPS-induced neuroinflammation by modulating microglia. Another study showed that ectopic expression of miR-155 caused endothelial hyperplasia and up-regulated microglial proliferation/activation, while miR-155 knockout mice displayed vascular defects. Furthermore,



miR-155 was induced and microglia were activated in an oxygen-induced retinopathy (OIR) mouse model, which is characterized by abnormal angiogenesis. In addition, miR-155 knockout mice showed repressed microglial activation and abnormal vessel growth following ischemic insult. The CYR61 cysteine rich angiogenic inducer 61 (CCN1) gene is a direct target of miR-155. CCN1 encodes an extracellular matrix-associated integrin-binding protein that is essential for normal angiogenesis. Importantly, CCN1 knockout or double CCN1/miR-155 knockout mice showed retinal vascular dysfunction (Yan et al., 2015), highlighting an important role for miR-155-CCN1 in microglial activation and vascular abnormality.

Brains from 3xTg AD mice (a typical AD model) showed high levels of miR-155 expression (Guedes et al., 2014). Enhanced microglial activation was also observed in brains from AD mice. miR-155 and c-Jun were found to be increased in AD mice and Ab-activated microglia, which eventually resulted in the secretion of inflammatory cytokines. In addition, a c-Jun inhibitor was shown to repress miR-155 expression in activated microglia. Thus, miR-155 is a promising target to control neuroinflammation in AD.

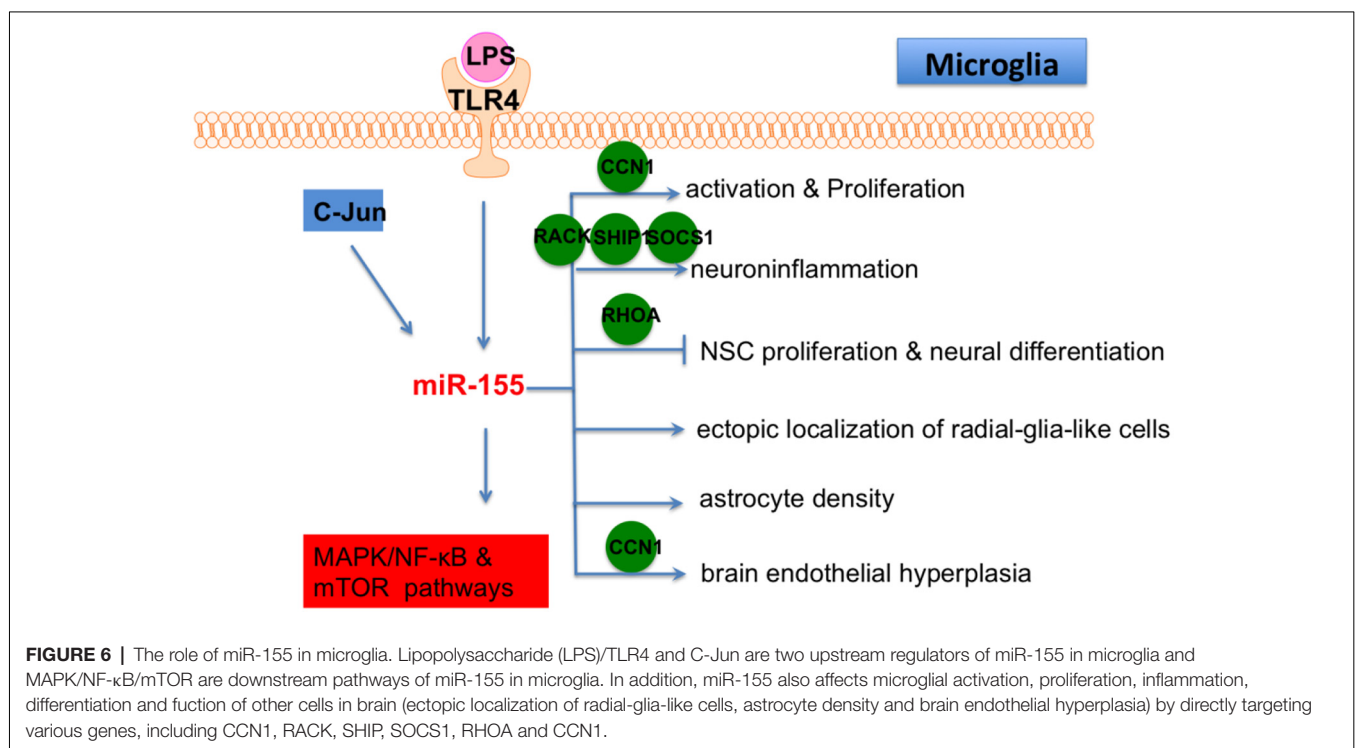
LPS-repressed suppressor of cytokine signaling 1 (SOCS-1) is involved in the suppression of inflammation and is a direct target of miR-155 (Cardoso et al., 2012). Knockdown of miR-155 induced SOCS-1 expression and led to downregulation of iNOS and nitric oxide production. Conditioned medium from a miR-155 knockdown microglia culture was shown to reverse neuronal cell death. Thus, miR-155 has a pro-inflammatory effect in microglia *via* repression of SOCS-1. LPS treatment also leads to miR-155 up-regulation in BV2 cells. LPS repressed

promoted apoptosis of BV2 cells and induced the production of pro-inflammatory cytokines. Meanwhile, miR-155 knockdown in BV2 cells rescued LPS-induced damage. Receptor of activated protein C kinase (RACK) 1 has been shown to be a target of miR-155 (Yin et al., 2017).

Taken together, these studies showed that miR-155 is a central regulator in CNS-related inflammation through its ability to affect microglia. Therefore, miR-155 should be strongly considered as a therapeutic target of neuroinflammatory disease in the future (**Figure 6**) because it regulates multiple functions of microglia, including activation, proliferation, inflammation and interacts with other cells in brain, such as NSC, astrocyte and endothelial cells. Collectively, these articles demonstrate that miR-155 is a pro-inflammatory factor in microglia and is necessary for the progression of neural diseases through repression of multiple targets, suggesting that miR-155 blockage is a potential neuroprotective target. An inhibition of miR-155 ameliorates the activity of dysfunctional microglia, implying that miR-155 has therapeutic effect on related neural diseases. As miR-155 associated pathogenesis is a novel concept in CNS diseases, many additional and essential mechanisms by which miR-155 regulates CNS pathogenesis will be discovered in the near future. With the systematical understanding of the specific role of miR-155 in microglia, we believe that miR-155 based therapy of neural diseases will become a promising direction.

## CONCLUSION

The roles of microglia in neuropathogenesis remain to be fully understood. However, there are several advantages of microglia



in the potential treatment of neurodegenerative diseases, such as EAE, CNS viral infection, and neuroinflammation. Available from clinical patients and *in vitro* cultures, microglia are an excellent tool for future gene therapy approaches for neuropathogenesis. In addition, distinguishing between resident microglia and monocyte-derived macrophages in pathological brain tissue is essential for the treatment of CNS diseases. Essential roles of miRNAs in microglial activation, inflammation, and differentiation/polarization have been widely demonstrated. Given the well-established roles of microRNAs in modulating gene expression, miRNA-based therapies could be considered as an attractive strategy to improve/recover microglial function and regulate genes/pathways in neuropathogenesis. Nevertheless, above-mentioned literatures mostly investigated the role of individual miRNAs, a dominant miRNA that plays the central role in microglia activation is yet to be identified. It is possible that key miRNA player in microglia activation differs in various pathological environment. Therefore, the central miRNA player in microglia activation may be emerged by simultaneous functional evaluation of all miRNAs that involved in the context of a specific neurological disease. In addition, since

miRNAs can bind multiple targets or signaling pathways simultaneously, the ‘fine-tuning’ capacity of miRNAs in microglia is also suitable for therapeutic intervention and maintaining brain homeostasis. However, we cannot ignore the potential “off-target effects” of miRNAs, which is a main obstacle for clinical application. In summary, the use of miRNAs as disease biomarkers or therapeutic targets in CNS represents a powerful and promising approach in the future.

## AUTHOR CONTRIBUTIONS

YG, JT and WW drafted the manuscript. WH, XW, PZ and HK revised the manuscript.

## FUNDING

This study was supported by the National Natural Science Foundation of China (81673444, 81330081), Natural Science Foundation of Anhui Province for young scholars (1708085QH200) and Grants for Scientific Research of BSKY from Anhui Medical University (4501041101).

## REFERENCES

- Ajmone-Cat, M. A., Bernardo, A., Greco, A., and Minghetti, L. (2010). Non-steroidal anti-inflammatory drugs and brain inflammation: effects on microglial functions. *Pharmaceuticals* 3, 1949–1964. doi: 10.3390/ph3061949
- Åkerblom, M., Sachdeva, R., Quintino, L., Wettergren, E. E., Chapman, K. Z., Manfre, G., et al. (2013). Visualization and genetic modification of resident brain microglia using lentiviral vectors regulated by microRNA-9. *Nat. Commun.* 4:1770. doi: 10.1038/ncomms2801
- Amici, S. A., Dong, J., and Guerau-de-Arellano, M. (2017). Molecular mechanisms modulating the phenotype of macrophages and microglia. *Front. Immunol.* 8:1520. doi: 10.3389/fimmu.2017.01520
- Belarbi, K., Tweedie, D., Arellano, C., Jopson, T., Greig, N., and Rosi, S. (2011). Inhibition of TNF- $\alpha$  protein synthesis restores neuronal function and reverses cognitive deficits induced by chronic neuroinflammation. *Alzheimers Dement.* 7:S649. doi: 10.1016/j.jalz.2011.05.1861
- Belter, A., Rolle, K., Piwecka, M., Fedoruk-wyszomirska, A., Naskręta-barciszewska, M. Z., and Barciszewski, J. (2016). Inhibition of miR-21 in glioma cells using catalytic nucleic acids. *Sci. Rep.* 6:24516. doi: 10.1038/srep24516
- Boche, D., Perry, V. H., and Nicoll, J. A. R. (2013). Review: activation patterns of microglia and their identification in the human brain. *Neuropathol. Appl. Neurobiol.* 39, 3–18. doi: 10.1111/nan.12011
- Boudreau, R. L., Jiang, P., Gilmore, B. L., Spengler, R. M., Tirabassi, R., Nelson, J. A., et al. (2014). Transcriptome-wide discovery of microRNA binding sites in human brain. *Neuron* 81, 294–305. doi: 10.1016/j.neuron.2013.10.062
- Brettschneider, J., Del Tredici, K., Lee, V. M. Y., and Trojanowski, J. Q. (2015). Spreading of pathology in neurodegenerative diseases: a focus on human studies. *Nat. Rev. Neurosci.* 16, 109–120. doi: 10.1038/nrn3887
- Cardoso, A. L., Guedes, J. R., Pereira de Almeida, L., and Pedrosa de Lima, M. C. (2012). miR-155 modulates microglia-mediated immune response by down-regulating SOCS-1 and promoting cytokine and nitric oxide production. *Immunology* 135, 73–88. doi: 10.1111/j.1365-2567.2011.03514.x
- Cheloufi, S., Dos Santos, C. O., Chong, M. M. W., and Hannon, G. J. (2010). A dicer-independent miRNA biogenesis pathway that requires Ago catalysis. *Nature* 465, 584–589. doi: 10.1038/nature09092
- Chen, L., Dong, R., Lu, Y., Zhou, Y., Li, K., Zhang, Z., et al. (2019). MicroRNA-146a protects against cognitive decline induced by surgical trauma by suppressing hippocampal neuroinflammation in mice. *Brain Behav. Immun.* 78, 188–201. doi: 10.1016/j.bbi.2019.01.020
- Cho, K. J., Song, J., Oh, Y., and Lee, J. E. (2015). MicroRNA-Let-7a regulates the function of microglia in inflammation. *Mol. Cell. Neurosci.* 68, 167–176. doi: 10.1016/j.mcn.2015.07.004
- David, S., and Kroner, A. (2011). Repertoire of microglial and macrophage responses after spinal cord injury. *Nat. Rev. Neurosci.* 12, 388–399. doi: 10.1038/nrn3053
- Du, L., Zhang, Y., Chen, Y., Zhu, J., Yang, Y., and Zhang, H. L. (2017). Role of microglia in neurological disorders and their potentials as a therapeutic target. *Mol. Neurobiol.* 54, 7567–7584. doi: 10.1007/s12035-016-0245-0
- Fang, Z., and Rajewsky, N. (2011). The impact of miRNA target sites in coding sequences and in 3'UTRs. *PLoS One* 6:e18067. doi: 10.1371/journal.pone.0018067
- Fazi, B., Felsani, A., Grassi, L., Moles, A., D'Andrea, D., Toschi, N., et al. (2015). The transcriptome and miRNome profiling of glioblastoma tissues and peritumoral regions highlights molecular pathways shared by tumors and surrounding areas and reveals differences between short-term and long-term survivors. *Oncotarget* 6, 22526–22552. doi: 10.18632/oncotarget.4151
- Fulzele, S., El-Sherbini, A., Ahmad, S., Sangani, R., Matragoon, S., El-Remessy, A., et al. (2015). MicroRNA-146b-3p regulates retinal inflammation by suppressing adenosine deaminase-2 in diabetes. *Biomed. Res. Int.* 2015:846501. doi: 10.1155/2015/846501
- Gabriely, G., Wurdinger, T., Kesari, S., Esau, C. C., Burchard, J., Linsley, P. S., et al. (2008). MicroRNA 21 promotes glioma invasion by targeting matrix metalloproteinase regulators. *Mol. Cell. Biol.* 28, 5369–5380. doi: 10.1128/mcb.00479-08
- Geloso, M. C., Corvino, V., Marchese, E., and Serrano, A. (2017). The dual role of microglia in ALS: mechanisms and therapeutic approaches. *Front. Aging Neurosci.* 9:242. doi: 10.3389/fnagi.2017.00242
- Godlewski, J., Bronisz, A., Nowicki, M. O., Chiocca, E. A., Godlewski, J., Bronisz, A., et al. (2010). microRNA-451: a conditional switch controlling glioma cell proliferation and migration. *Cell Cycle* 9, 2814–2820. doi: 10.4161/cc.9.14.12248
- Grimmig, B., Morganti, J., Nash, K., and Bickford, P. C. (2016). Immunomodulators as therapeutic agents in mitigating the progression of Parkinson's disease. *Brain Sci.* 6:E41. doi: 10.3390/brainsci6040041



- Guedes, J. R., Custódia, C. M., Silva, R. J., de Almeida, L. P., de Lima, M. C. P., and Cardoso, A. L. (2014). Early miR-155 upregulation contributes to neuroinflammation in Alzheimer's disease triple transgenic mouse model. *Hum. Mol. Genet.* 23, 6286–6301. doi: 10.1093/hmg/ddu348
- Guo, H., Nan, Y., Zhen, Y., Zhang, Y., Guo, L., and Yu, K. (2016). miRNA-451 inhibits glioma cell proliferation and invasion by downregulating glucose transporter 1. *Tumour Biol.* 37, 13751–13761. doi: 10.1007/s13277-016-5219-3
- Guo, M. L., Periyasamy, P., Liao, K., Kook, Y. H., Niu, F., Callen, S. E., et al. (2016). Cocaine-mediated downregulation of microglial miR-124 expression involves promoter DNA methylation. *Epigenetics* 11, 819–830. doi: 10.1080/15592294.2016.1232233
- Hambardzumyan, D., Gutmann, D. H., and Kettenmann, H. (2016). The role of microglia and macrophages in glioma maintenance and progression. *Nat. Neurosci.* 19, 20–27. doi: 10.1038/nn.4185
- Hamzei Taj, S., Kho, W., Aswendt, M., Collmann, F. M., Green, C., Adamczak, J., et al. (2016a). Dynamic modulation of microglia/macrophage polarization by miR-124 after focal cerebral ischemia. *J. Neuroimmune Pharmacol.* 11, 733–748. doi: 10.1007/s11481-016-9700-y
- Hamzei Taj, S., Kho, W., Riou, A., Wiedermann, D., and Hoehn, M. (2016b). MiRNA-124 induces neuroprotection and functional improvement after focal cerebral ischemia. *Biomaterials* 91, 151–165. doi: 10.1016/j.biomaterials.2016.03.025
- Hermansen, S. K., Nielsen, B. S., and Aaberg-jessen, C. (2016). miR-21 is linked to glioma angiogenesis: a co-localization study. *J. Histochem. Cytochem.* 64, 138–148. doi: 10.1369/0022155415623515
- Hesse, R., Wahler, A., Gummert, P., Kirschmer, S., Otto, M., Tuman, H., et al. (2016). Decreased IL-8 levels in CSF and serum of AD patients and negative correlation of MMSE and IL-1 $\beta$ . *BMC Neurol.* 16:185. doi: 10.1186/s12883-016-0707-z
- Hide, T., Komohara, Y., Miyasato, Y., Nakamura, H., Makino, K., Takeya, M., et al. (2018). Oligodendrocyte progenitor cells and macrophages/microglia produce glioma stem cell niches at the tumor border. *EBioMedicine* 30, 94–104. doi: 10.1016/j.ebiom.2018.02.024
- Hong, W., Zhang, P., Wang, X., Tu, J., and Wei, W. (2018). The effects of MicroRNAs on key signalling pathways and epigenetic modification in fibroblast-like synoviocytes of rheumatoid arthritis. *Mediators Inflamm.* 2018:9013124. doi: 10.1155/2018/9013124
- Hu, X., Li, P., Guo, Y., Wang, H., Leak, R. K., Chen, S., et al. (2012). Microglia/macrophage polarization dynamics reveal novel mechanism of injury expansion after focal cerebral ischemia. *Stroke* 43, 3063–3070. doi: 10.1161/strokeaha.112.659656
- Huang, Q., Wang, C., Hou, Z., Wang, G., Lv, J., Wang, H., et al. (2017). Serum microRNA-376 family as diagnostic and prognostic markers in human gliomas. *Cancer Biomark.* 19, 137–144. doi: 10.3233/cbm-160146
- Ivo D'Urso, P., Ivo D'Urso, O., Damiano Gianfreda, C., Mezzolla, V., Storelli, C., and Marsigliante, S. (2015). miR-15b and miR-21 as circulating biomarkers for diagnosis of glioma. *Curr. Genomics* 16, 304–311. doi: 10.2174/1389202916666150707155610
- Jadhav, V. S., Krause, K. H., and Singh, S. K. (2014). HIV-1 Tat C modulates NOX2 and NOX4 expressions through miR-17 in a human microglial cell line. *J. Neurochem.* 131, 803–815. doi: 10.1111/jnc.12933
- Jha, M. K., Lee, W. H., and Suk, K. (2016). Functional polarization of neuroglia: implications in neuroinflammation and neurological disorders. *Biochem. Pharmacol.* 103, 1–16. doi: 10.1016/j.bcp.2015.11.003
- Jiang, B., Li, M. I. N., Ji, F., and Nie, Y. (2017). MicroRNA-219 exerts a tumor suppressive role in glioma via targeting Sal-like protein 4. *Exp. Ther. Med.* 14, 6213–6221. doi: 10.3892/etm.2017.5292
- Kandinov, B., Koczyn, A. D., Rabinowitz, R., Nefussy, B., and Drory, V. E. (2011). Autonomic impairment in a transgenic mouse model of amyotrophic lateral sclerosis. *Auton. Neurosci.* 159, 84–89. doi: 10.1016/j.autneu.2010.09.002
- Karthikeyan, A., Gupta, N., Tang, C., Mallilankaraman, K., Silambarasan, M., Shi, M., et al. (2018). Microglial SMAD4 regulated by microRNA-146a promotes migration of microglia which support tumor progression in a glioma environment. *Oncotarget* 9, 24950–24969. doi: 10.18632/oncotarget.25116
- Katakowski, M., Buller, B., Zheng, X., Lu, Y., Rogers, T., Osobamiro, O., et al. (2013). Exosomes from marrow stromal cells expressing miR-146b inhibit glioma growth. *Cancer Lett.* 335, 201–204. doi: 10.1016/j.canlet.2013.02.019
- Kigerl, K. A., Gensel, J. C., Ankeny, D. P., Alexander, J. K., Donnelly, D. J., and Popovich, P. G. (2009). Identification of two distinct macrophage subsets with divergent effects causing either neurotoxicity or regeneration in the injured mouse spinal cord. *J. Neurosci.* 29, 13435–13444. doi: 10.1523/JNEUROSCI.3257-09.2009
- Krishnaswamy, A., and Cooper, E. (2012). Reactive oxygen species inactivate neuronal nicotinic acetylcholine receptors through a highly conserved cysteine near the intracellular mouth of the channel: implications for diseases that involve oxidative stress. *J. Physiol.* 590, 39–47. doi: 10.1113/jphysiol.2011.214007
- Kumar, A., Bhatia, H. S., De Oliveira, A. C. P., and Fiebich, B. L. (2015). microRNA-26a modulates inflammatory response induced by toll-like receptor 4 stimulation in microglia. *J. Neurochem.* 135, 1189–1202. doi: 10.1111/jnc.13364
- Kwon, Y. S., Pineda, E., Auvin, S., Shin, D., Mazarati, A., and Sankar, R. (2013). Neuroprotective and antiepileptogenic effects of combination of anti-inflammatory drugs in the immature brain. *J. Neuroinflammation* 10:30. doi: 10.1186/1742-2094-10-30
- Labandeira-Garcia, J. L., Rodríguez-Pérez, A. I., Garrido-Gil, P., Rodríguez-Pallares, J., Lanciego, J. L., and Guerra, M. J. (2017). Brain renin-angiotensin system and microglial polarization: implications for aging and neurodegeneration. *Front. Aging Neurosci.* 9:129. doi: 10.3389/fnagi.2017.00129
- Lan, X., Han, X., Li, Q., Yang, Q., and Wang, J. (2017). Modulators of microglial activation and polarization after intracerebral haemorrhage. *Nat. Rev. Neurol.* 13, 420–433. doi: 10.1038/nrneurol.2017.69
- Lee, I., Ajay, S. S., Yook, J. L., Kim, H. S., Hong, S. H., Kim, N. H., et al. (2009). New class of microRNA targets containing simultaneous 5'-UTR and 3'-UTR interaction sites. *Genome Res.* 19, 1175–1183. doi: 10.1101/gr.089367.108
- Li, S. H., Li, J. P., Chen, L., and Liu, J. L. (2018). miR-146a induces apoptosis in neuroblastoma cells by targeting BCL11A. *Med. Hypotheses* 117, 21–27. doi: 10.1016/j.mehy.2018.05.019
- Li, L., Sun, Q., Li, Y., Yang, Y., Yang, Y., Chang, T., et al. (2015). Overexpression of SIRT1 induced by resveratrol and inhibitor of miR-204 suppresses activation and proliferation of microglia. *J. Mol. Neurosci.* 56, 858–867. doi: 10.1007/s12031-015-0526-5
- Li, H., Xue, Y., Ma, J., Shao, L., Wang, D., Zheng, J., et al. (2019). SNHG1 promotes malignant biological behaviors of glioma cells via microRNA-154-5p/miR-376-3p-FOXP2-KDM5B participating positive feedback loop. *J. Exp. Clin. Cancer Res.* 38:59. doi: 10.1186/s13046-019-1063-9
- Liu, D., Zhao, H., Zou, Q., and Ma, Q. (2017). MiR-338 suppresses cell proliferation and invasion by targeting CTBP2 in glioma. *Cancer Biomark.* 20, 289–297. doi: 10.3233/cbm-170128
- Louw, A. M., Kolar, M. K., Novikova, L. N., Kingham, P. J., Wiberg, M., Kjems, J., et al. (2016). Chitosan polyplex mediated delivery of miRNA-124 reduces activation of microglial cells *in vitro* and in rat models of spinal cord injury. *Nanomedicine* 12, 643–653. doi: 10.1016/j.nano.2015.10.011
- Lu, X., Si, F., Zhang, S., and Liu, Z. (2016). Effect of miR-146a on glioma cell line proliferation in targeted-regulating MIF gene. *Int. J. Clin. Exp. Pathol.* 9, 2896–2902.
- Lull, M. E., and Block, M. L. (2010). Microglial activation and chronic neurodegeneration. *Neurotherapeutics* 7, 354–365. doi: 10.1016/j.nurt.2010.05.014
- Lv, Y. N., Ou-Yang, A. J., and Fu, L. S. (2017). MicroRNA-27a negatively modulates the inflammatory response in lipopolysaccharide-stimulated microglia by targeting TLR4 and IRAK4. *Cell. Mol. Neurobiol.* 37, 195–210. doi: 10.1007/s10571-016-0361-4
- Ma, X.-L., Feng, M., Wei, S., Jin, N., Bin, Z., Yu, L., et al. (2018). MicroRNA-338-5p plays a tumor suppressor role in glioma through inhibition of the MAPK-signaling pathway by binding to FOXD1. *J. Cancer Res. Clin. Oncol.* 144, 2351–2366. doi: 10.1007/s00432-018-2745-y
- Mei, J., Bachoo, R., and Zhang, C. (2011). MicroRNA-146a inhibits glioma development by targeting Notch1. *Mol. Cell. Biol.* 31, 3584–3592. doi: 10.1128/mcb.05821-11
- Mishra, A., Kim, H. J., Shin, A. H., and Thayer, S. A. (2012). Synapse loss induced by interleukin-1 $\beta$  requires pre- and post-synaptic mechanisms. *J. Neuroimmune Pharmacol.* 7, 571–578. doi: 10.1007/s11481-012-9342-7

- Mishra, M. K., Wang, J., Keough, M. B., Fan, Y., Silva, C., Sloka, S., et al. (2014). Laquinimod reduces neuroaxonal injury through inhibiting microglial activation. *Ann. Clin. Transl. Neurol.* 1, 409–422. doi: 10.1002/acn3.67
- Moore, K. J., Sheedy, F. J., and Fisher, E. A. (2013). Macrophages in atherosclerosis: a dynamic balance. *Nat. Rev. Immunol.* 13, 709–721. doi: 10.1038/nri3520
- Moore, L. M., and Zhang, W. (2010). Targeting miR-21 in glioma: a small RNA with big potential. *Expert Opin. Ther. Targets* 14, 1247–1257. doi: 10.1517/14728222.2010.527334
- Nan, Y., Han, L., Zhang, A., Wang, G., and Jia, Z. (2010). MiRNA-451 plays a role as tumor suppressor in human glioma cells. *Brain Res.* 1359, 14–21. doi: 10.1016/j.brainres.2010.08.074
- Ni, J., Wang, X., Chen, S., Liu, H., Wang, Y., Xu, X., et al. (2015). MicroRNA let-7c-5p protects against cerebral ischemia injury via mechanisms involving the inhibition of microglia activation. *Brain Behav. Immun.* 49, 75–85. doi: 10.1016/j.bbi.2015.04.014
- Ning, R., Venkat, P., Chopp, M., Zacharek, A., Yan, T., Cui, X., et al. (2017). D-4F increases microRNA-124a and reduces neuroinflammation in diabetic stroke rats. *Oncotarget* 8, 95481–95494. doi: 10.18632/oncotarget.20751
- Paolicelli, R. C., Bolasco, G., Pagani, F., Maggi, L., Scianni, M., Panzanelli, P., et al. (2011). Synaptic pruning by microglia is necessary for normal brain synaptic pruning by microglia is necessary for normal brain development. *Science* 333, 1456–1458. doi: 10.1126/science.1202529
- Parisi, C., Napoli, G., Amadio, S., Spalloni, A., Apolloni, S., Longone, P., et al. (2016). MicroRNA-125b regulates microglia activation and motor neuron death in ALS. *Cell Death Differ.* 23, 531–541. doi: 10.1038/cdd.2015.153
- Permuth-Wey, J., Thompson, R. C., Burton Nabors, L., Olson, J. J., and Browning Nabors, J. E. (2011). A functional polymorphism in the pre-miR-146a gene is associated with risk and prognosis in adult glioma. *J. Neurooncol.* 105, 639–646. doi: 10.1007/s11060-011-0634-1
- Ponomarev, E. D., Shriver, L. P., Maresz, K., and Dittel, B. N. (2005). Microglial cell activation and proliferation precedes the onset of CNS autoimmunity. *J. Neurosci. Res.* 81, 374–389. doi: 10.1002/jnr.20488
- Ponomarev, E. D., Veremeyko, T., Barteneva, N., Krichevsky, A. M., and Weiner, H. L. (2011). MicroRNA-124 promotes microglia quiescence and suppresses EAE by deactivating macrophages via the C/EBP- $\alpha$ -PU.1 pathway. *Nat. Med.* 17, 64–70. doi: 10.1038/nm.2266
- Qiu, S., Feng, Y., LeSage, G., Zhang, Y., Stuart, C., He, L., et al. (2015). Chronic morphine-induced microRNA-124 promotes microglial immunosuppression by modulating P65 and TRAF6. *J. Immunol.* 194, 1021–1030. doi: 10.4049/jimmunol.1400106
- Quintavalle, C., Donnarumma, E., Iaboni, M., Roscigno, G., Garofalo, M., Romano, G., et al. (2013). Effect of miR-21 and miR-30b/c on TRAIL-induced apoptosis in glioma cells. *Oncogene* 32, 4001–4008. doi: 10.1038/onc.2012.410
- Rao, S. A. M., Rao, M., Arimappamagan, A., Pandey, P., Santosh, V., Hegde, S., et al. (2013). miR-219-5p inhibits receptor tyrosine kinase pathway by targeting EGFR in glioblastoma. *PLoS One* 8:e63164. doi: 10.1371/journal.pone.0063164
- Reemst, K., Noctor, S. C., Lucassen, P. J., and Hol, E. M. (2016). The indispensable roles of microglia and astrocytes during brain development. *Front. Hum. Neurosci.* 10:566. doi: 10.3389/fnhum.2016.00566
- Rojo, A. K., Mineo, M., and Godlewski, J. (2016). MicroRNA and extracellular vesicles in glioblastoma: small but powerful. *Brain Tumor Pathol.* 33, 77–88. doi: 10.1007/s10014-016-0259-3
- Saba, R., Gushue, S., Huzarewich, R. L. C. H., Manguiat, K., Medina, S., Robertson, C., et al. (2012). MicroRNA 146a (miR-146a) is over-expressed during prion disease and modulates the innate immune response and the microglial activation state. *PLoS One* 7:e30832. doi: 10.1371/journal.pone.0030832
- Sarlus, H., and Heneka, M. T. (2017). Microglia in Alzheimer's disease. *J. Clin. Invest.* 127, 3240–3249. doi: 10.1172/JCI90606
- Schafer, D. P., Lehrman, E. K., Kautzman, A. G., Koyama, R., Mardinly, A. R., Yamasaki, R., et al. (2012). Microglia sculpt postnatal neural circuits in an activity and complement-dependent manner. *Neuron* 74, 691–705. doi: 10.1016/j.neuron.2012.03.026
- Schafer, D. P., Lehrman, E. K., and Stevens, B. (2013). The “quad-partite” synapse: microglia-synapse interactions in the developing and mature CNS. *Glia* 61, 24–36. doi: 10.1002/glia.22389
- Seo, Y., Suh, H., Bahal, R., Josowitz, A., Zhang, J., Song, E., et al. (2019). Nanoparticle-mediated intratumoral inhibition of miR-21 for improved survival in glioblastoma. *Biomaterials* 201, 87–98. doi: 10.1016/j.biomaterials.2019.02.016
- Song, J., and Lee, J. E. (2015). ASK1 modulates the expression of microRNA Let7A in microglia under high glucose *in vitro* condition. *Front. Cell. Neurosci.* 9:198. doi: 10.3389/fncel.2015.00198
- Suzumura, A. (2013). Neuron-microglia interaction in neuroinflammation. *Curr. Protein Pept. Sci.* 14, 16–20. doi: 10.2174/1389203711314010004
- Svahn, A. J., Giacomotto, J., Graeber, M. B., Rinkwitz, S., and Becker, T. S. (2016). miR-124 contributes to the functional maturity of microglia. *Dev. Neurobiol.* 76, 507–518. doi: 10.1002/dneu.22328
- Tanaka, S., Ishii, A., Ohtaki, H., Shioda, S., Yoshida, T., and Numazawa, S. (2013). Activation of microglia induces symptoms of Parkinson's disease in wild-type, but not in IL-1 knockout mice. *J. Neuroinflammation* 10:143. doi: 10.1186/1742-2094-10-143
- Thounaojam, M. C., Kaushik, D. K., Kundu, K., and Basu, A. (2014). MicroRNA-29b modulates Japanese encephalitis virus-induced microglia activation by targeting tumor necrosis factor  $\alpha$ -induced protein 3. *J. Neurochem.* 129, 143–154. doi: 10.1111/jnc.12609
- Tian, F., Yuan, C., Hu, L., and Shan, S. (2017). MicroRNA-93 inhibits inflammatory responses and cell apoptosis after cerebral ischemia reperfusion by targeting interleukin-1 receptor-associated kinase 4. *Exp. Ther. Med.* 14, 2903–2910. doi: 10.3892/etm.2017.4874
- Town, T., Nikolic, V., and Tan, J. (2005). The microglial “activation” continuum: from innate to adaptive responses. *J. Neuroinflammation* 2:24. doi: 10.1186/1742-2094-2-24
- Tremblay, M.-E., Stevens, B., Sierra, A., Wake, H., Bessis, A., and Nimmerjahn, A. (2011). The role of microglia in the healthy brain. *J. Neurosci.* 31, 16064–16069. doi: 10.1523/JNEUROSCI.4158-11.2011
- Tu, J., Liao, J., Luk, A. C. S., Tang, N. L. S., Chan, W. Y., and Lee, T. L. (2015). MicroRNAs mediated targeting on the Yin-yang dynamics of DNA methylation in disease and development. *Int. J. Biochem. Cell Biol.* 67, 115–120. doi: 10.1016/j.biocel.2015.05.002
- van der Vos, K. E., Abels, E. R., Zhang, X., Lai, C., Carrizosa, E., Oakley, D., et al. (2016). Directly visualized glioblastoma-derived extracellular vesicles transfer RNA to microglia/macrophages in the brain. *Neuro Oncol.* 18, 58–69. doi: 10.1093/neuonc/nov244
- Varol, D., Mildner, A., Blank, T., Shemer, A., Barashi, N., Yona, S., et al. (2017). Dicer deficiency differentially impacts microglia of the developing and adult brain. *Immunity* 46, 1030.e8–1044.e8. doi: 10.1016/j.immuni.2017.05.003
- Wake, H., Moorhouse, A. J., Jinno, S., Kohsaka, S., and Nabekura, J. (2009). Resting microglia directly monitor the functional state of synapses *in vivo* and determine the fate of ischemic terminals. *J. Neurosci.* 29, 3974–3980. doi: 10.1523/JNEUROSCI.4363-08.2009
- Wang, G., Zhang, J., Hu, X., Zhang, L., Mao, L., Jiang, X., et al. (2013). Microglia/macrophage polarization dynamics in white matter after traumatic brain injury. *J. Cereb. Blood Flow Metab.* 33, 1864–1874. doi: 10.1038/jcbfm.2013.146
- Woodbury, M. E., Freilich, R. W., Cheng, C. J., Asai, H., Ikezu, S., Boucher, J. D., et al. (2015). miR-155 is essential for inflammation-induced hippocampal neurogenic dysfunction. *J. Neurosci.* 35, 9764–9781. doi: 10.1523/JNEUROSCI.4790-14.2015
- Xie, X., Peng, L., Zhu, J., Zhou, Y., Li, L., Chen, Y., et al. (2017). miR-145-5p/Nurr1/TNF- $\alpha$  signaling-induced microglia activation regulates neuron injury of acute cerebral ischemic/reperfusion in rats. *Front. Mol. Neurosci.* 10:383. doi: 10.3389/fnmol.2017.00383
- Xing, H., Guo, S., Zhang, Y. I., Zheng, Z., and Wang, H. (2016). Upregulation of microRNA-206 enhances lipopolysaccharide-induced inflammation and release of amyloid- $\beta$  by targeting insulin-like growth factor 1 in microglia. *Mol. Med. Rep.* 14, 1357–1364. doi: 10.3892/mmr.2016.5369
- Yan, L., Lee, S., Lazzaro, D. R., Aranda, J., Grant, M. B., and Chaqour, B. (2015). Single and compound knock-outs of microRNA (miRNA)-155 and its angiogenic gene target CCN1 in mice alter vascular and neovascular growth in the retina via resident microglia. *J. Biol. Chem.* 290, 23264–23281. doi: 10.1074/jbc.M115.646950
- Yan, T., Zhang, F., Sun, C., Sun, J., Wang, Y., Xu, X., et al. (2018). miR-32-5p-mediated Dusp5 downregulation contributes to neuropathic pain.

- Biochem. Biophys. Res. Commun.* 495, 506–511. doi: 10.1016/j.bbrc.2017.11.013
- Yang, G., Parkhurst, C. N., Hayes, S., and Gan, W.-B. (2013). Peripheral elevation of TNF- $\alpha$  leads to early synaptic abnormalities in the mouse somatosensory cortex in experimental autoimmune encephalomyelitis. *Proc. Natl. Acad. Sci. U S A* 110, 10306–10311. doi: 10.1073/pnas.1222895110
- Yang, Z., Xu, J., Zhu, R., and Liu, L. (2017). Down-regulation of miRNA-128 contributes to neuropathic pain following spinal cord injury via activation of P38. *Med. Sci. Monit.* 23, 405–411. doi: 10.12659/msm.898788
- Yang, Z., Zhong, L., Zhong, S., Xian, R., and Yuan, B. (2015). MiR-203 protects microglia mediated brain injury by regulating inflammatory responses via feedback to MyD88 in ischemia. *Mol. Immunol.* 65, 293–301. doi: 10.1016/j.molimm.2015.01.019
- Yin, H., Song, S., and Pan, X. (2017). Knockdown of miR-155 protects microglia against LPS-induced inflammatory injury via targeting RACK1: a novel research for intracranial infection. *J. Inflamm.* 14:17. doi: 10.1186/s12950-017-0162-7
- Yu, A., Zhang, T., Duan, H., Pan, Y., Zhang, X., Yang, G., et al. (2017). MiR-124 contributes to M2 polarization of microglia and confers brain inflammatory protection via the C/EBP- $\alpha$  pathway in intracerebral hemorrhage. *Immunol. Lett.* 182, 1–11. doi: 10.1016/j.imlet.2016.12.003
- Yuan, B., Shen, H., Lin, L., Su, T., Zhong, L., and Yang, Z. (2015). MicroRNA367 negatively regulates the inflammatory response of microglia by targeting IRAK4 in intracerebral hemorrhage. *J. Neuroinflammation* 12:206. doi: 10.1186/s12974-015-0424-3
- Zhang, L., Li, Y. J., Wu, X. Y., Hong, Z., and Wei, W. S. (2015). MicroRNA-181c negatively regulates the inflammatory response in oxygen-glucose-deprived microglia by targeting Toll-like receptor 4. *J. Neurochem.* 132, 713–723. doi: 10.1111/jnc.13021
- Zhang, Y., Shen, K., Bai, Y., Lv, X., Huang, R., Zhang, W., et al. (2016). Mir143-BBC3 cascade reduces microglial survival via interplay between apoptosis and autophagy: implications for methamphetamine-mediated neurotoxicity. *Autophagy* 12, 1538–1559. doi: 10.1080/15548627.2016.1191723
- Zhao, H., Wang, J., Gao, L., Wang, R., Liu, X., Gao, Z., et al. (2013). MiRNA-424 protects against permanent focal cerebral ischemia injury in mice involving suppressing microglia activation. *Stroke* 44, 1706–1713. doi: 10.1161/strokeaha.111.000504
- Zhou, Y., Lu, M., Du, R. H., Qiao, C., Jiang, C. Y., Zhang, K. Z., et al. (2016). MicroRNA-7 targets Nod-like receptor protein 3 inflammasome to modulate neuroinflammation in the pathogenesis of Parkinson's disease. *Mol. Neurodegener.* 11:28. doi: 10.1186/s13024-016-0094-3
- Zhou, H. J., Wang, L. Q., Xu, Q. S., Fan, Z. X., Zhu, Y., Jiang, H., et al. (2016). Downregulation of miR-199b promotes the acute spinal cord injury through IKK $\beta$ -NF- $\kappa$ B signaling pathway activating microglial cells. *Exp. Cell Res.* 349, 60–67. doi: 10.1016/j.yexcr.2016.09.020

**Conflict of Interest Statement:** The authors declare that the research was conducted in the absence of any commercial or financial relationships that could be construed as a potential conflict of interest.

Copyright © 2019 Guo, Hong, Wang, Zhang, Körner, Tu and Wei. This is an open-access article distributed under the terms of the Creative Commons Attribution License (CC BY). The use, distribution or reproduction in other forums is permitted, provided the original author(s) and the copyright owner(s) are credited and that the original publication in this journal is cited, in accordance with accepted academic practice. No use, distribution or reproduction is permitted which does not comply with these terms.



# Monoamine Oxidases (MAOs) as Privileged Molecular Targets in Neuroscience: Research Literature Analysis

Andy Wai Kan Yeung<sup>1\*</sup>, Maya G. Georgieva<sup>2</sup>, Atanas G. Atanasov<sup>3,4\*</sup>  
and Nikolay T. Tzvetkov<sup>2\*</sup>

<sup>1</sup>Oral and Maxillofacial Radiology, Applied Oral Sciences, Faculty of Dentistry, The University of Hong Kong, Hong Kong, China, <sup>2</sup>Department of Biochemical Pharmacology and Drug Design, Institute of Molecular Biology Roumen Tsanev, Bulgarian Academy of Sciences, Sofia, Bulgaria, <sup>3</sup>The Institute of Genetics and Animal Breeding, Polish Academy of Sciences, Magdalenka, Poland, <sup>4</sup>Department of Pharmacognosy, University of Vienna, Vienna, Austria

## OPEN ACCESS

### Edited by:

Detlev Boison,  
Rutgers University, United States

### Reviewed by:

Claudia Binda,  
University of Pavia, Italy  
Hong Qing,  
Beijing Institute of Technology, China

### \*Correspondence:

Andy Wai Kan Yeung  
ndyeung@hku.hk  
Atanas G. Atanasov  
a.atanasov.mailbox@gmail.com  
Nikolay T. Tzvetkov  
ntzvetkov@gmx.de

**Received:** 05 April 2019

**Accepted:** 16 May 2019

**Published:** 29 May 2019

### Citation:

Yeung AWK, Georgieva MG,  
Atanasov AG and Tzvetkov NT  
(2019) Monoamine Oxidases (MAOs)  
as Privileged Molecular Targets in  
Neuroscience: Research Literature  
Analysis.  
*Front. Mol. Neurosci.* 12:143.  
doi: 10.3389/fnmol.2019.00143

**Background:** Monoamine oxidases (MAOs) were discovered nearly a century ago. This article aims to analyze the research literature landscape associated with MAOs as privileged class of neuronal enzymes (neuroenzymes) with key functions in the processes of neurodegeneration, serving as important biological targets in neuroscience. With the accumulating publications on this topic, we aimed to evaluate the publication and citation performance of the contributors, reveal the popular research themes, and identify its historical roots.

**Methods:** The electronic database of Web of Science (WoS) Core Collection was searched to identify publications related to MAOs, which were analyzed according to their publication year, authorship, institutions, countries/regions, journal title, WoS category, total citation count, and publication type. VOSviewer was utilized to visualize the citation patterns of the words appearing in the titles and abstracts, and author keywords. CRExplorer was utilized to identify seminal references cited by the MAO publications.

**Results:** The literature analysis was based on 19,854 publications. Most of them were original articles ( $n = 15,148$ , 76.3%) and reviews ( $n = 2,039$ , 10.3%). The top five WoS categories of the analyzed MAO publications were Pharmacology/Pharmacy ( $n = 4,664$ , 23.5%), Neurosciences ( $n = 4,416$ , 22.2%), Psychiatry ( $n = 2,906$ , 14.6%), Biochemistry/Molecular Biology ( $n = 2,691$ , 13.6%), and Clinical Neurology ( $n = 1,754$ , 8.8%). The top 10 institutions are scattered in the United States, UK, France, Sweden, Canada, Israel, and Russia, while the top 10 countries/regions with the most intensive research on the field of MAOs are the United States, followed by European and Asian countries. More highly cited publications generally involved neurotransmitters, such as dopamine (DA), serotonin, and norepinephrine (NE), as well as the MAO-A inhibitors moclobemide and clorgyline, and the irreversible MAO-B inhibitors selegiline and rasagiline.



**Conclusion:** Through decades of research, the literature has accumulated many publications investigating the therapeutic effects of MAO inhibitors (MAOIs) on various neurological conditions, such as Alzheimer's disease (AD), Parkinson's disease (PD), and depression. We envision that MAO literature will continue to grow steadily, with more new therapeutic candidates being tested for better management of neurological conditions, in particular, with the development of multi-target acting drugs against neurodegenerative diseases.

**Keywords:** molecular neuroscience, monoamine oxidase, tyramine, bibliometrics, history, Alzheimer's disease, Parkinson's disease, depression

## INTRODUCTION

Monoamine oxidases (MAOs, EC 1.4.3.4) were discovered by Mary L.C. Hare (later known as Mary Bernheim) nearly a century ago, back in 1928 (Hare, 1928). The discovery of the first MAO, originally called tyramine oxidase, has paved the way for researchers to study the potential of MAOs as biological targets and development of therapeutics, mainly related to neurological diseases (Zeller and Barsky, 1952; Slotkin, 1999; Youdim and Bakhle, 2006; Jo et al., 2012). MAOs are flavin adenine dinucleotide (FAD) co-factor-dependent enzymes localized on the mitochondrial outer membrane that catalyze the oxidation of endogenous and xenobiotic monoamines (**Figure 1A**). Therefore, MAOs play an important role in the central and peripheral nervous system (CNS and PNS) by modulating the levels of monoamine neurotransmitters (Setini et al., 2005). Two isoforms are present in most mammalian tissues, MAO-A and MAO-B. Although there is ~73% identity of the protein sequences, both MAOs are important for the inactivation of various neurotransmitters but display regional differences in enzyme activity, substrate specificity, and distribution in the human brain and periphery (Shih et al., 1999; Binda et al., 2002; Castagnoli et al., 2003). For example, serotonin (5-hydroxytryptamine, 5-HT) is preferably degraded by MAO-A (Tong et al., 2013), whereas MAO-B exhibits higher affinity toward benzylamine (BA) and phenylethylamine (PEA; Youdim and Bakhle, 2006; Jo et al., 2012; Tong et al., 2013). Catecholamines such as dopamine (DA), adrenaline (epinephrine), noradrenaline (norepinephrine, NE), tryptamine, and tyramine are substrates for both MAO isoforms (**Figure 1B**). However, DA is mainly metabolized by MAO-B in *substantia nigra*, where MAO-B is the main distributed isoform in glial cells and the increased MAO-B activity is associated with loss of DA in the human brain (Tzvetkov et al., 2017).

As MAOs play a key role in regulating neurotransmitter levels, altered MAO levels may associate with several neurological diseases. The abnormal MAO-A genotype is associated with Brunner syndrome (Brunner et al., 1993) and autism (Cohen et al., 2011). Furthermore, the elevated MAO-A levels may link to major depression (Meyer et al., 2006; Tong et al., 2013). Similarly, there seems to be an association between the increased MAO-B levels (~4-fold with aging) and neurodegenerative diseases, such as Alzheimer's disease (AD) and Parkinson's

disease (PD; Saura et al., 1994; Mallajosyula et al., 2009). The preferences in substrate (neurotransmitter) affinity are essential for the different clinical significance of both MAOs, e.g., *via* inhibiting the activity either of MAO-A or MAO-B by monoamine oxidase MAO inhibitors (MAOIs). Therefore, selective inhibition of MAO-A in the human brain is an established approach for the treatment of mental disorders, while selective MAO-B inhibitors are those used for treating of PD (Riederer et al., 2004a; Yamada and Yasuhara, 2004; Tzvetkov et al., 2017). Subsequently, a number of MAOIs have been developed and approved worldwide for the treatment of neurological or psychiatric diseases. For example, the irreversible non-selective MAOIs tranylcypromine, the selective MAO-A inhibitors such as the irreversible inhibitor clorgyline and the reversible inhibitor moclobemide are used to treat depression and anxiety (for structures, see **Figure 2**; Riederer et al., 2004b; Tzvetkov et al., 2017). A meta-analysis reported that selective MAO-A inhibitors have a better efficacy than tricyclic antidepressants for managing atypical depression (Henkel et al., 2006). Furthermore, the irreversible MAO-B inhibitors selegiline and rasagiline (first generation MAO-B inhibitors) are approved as monotherapy for early PD or in combination with levodopa in late-stage PD (Lakhan, 2007; Fowler et al., 2015). However, it is known that irreversible MAO inhibition may cause adverse pharmacological effects and safety complications (Kumar et al., 2016). In 2015, the reversible MAO-B inhibitor safinamide has been approved as an add-on drug to levodopa or to DA agonists for the treatment of motor complications in patients with mid-to late-stage or early PD, respectively (Deeks, 2015). In contrast, the reversible MAO-B inhibitor selegiline, a compound that was patented and investigated as a smoking-cessation agent, was discontinued in clinical phase III as a medication for the treatment of moderate AD (Borroni et al., 2017; Tzvetkov et al., 2019).

The resolution of the X-ray co-crystal structures of both human MAO-A and MAO-B with a number of irreversible and reversible inhibitors has not only gained new insight into the structure of these enzyme-ligand complexes, but also has newly inspired the research in the field of MAO inhibition as potential therapeutic approach in neurological diseases (Binda et al., 2002, 2004, 2007; De Colibus et al., 2005). Although electron paramagnetic resonance (EPR) experiments showed that human MAO-A and MAO-B isoenzymes are

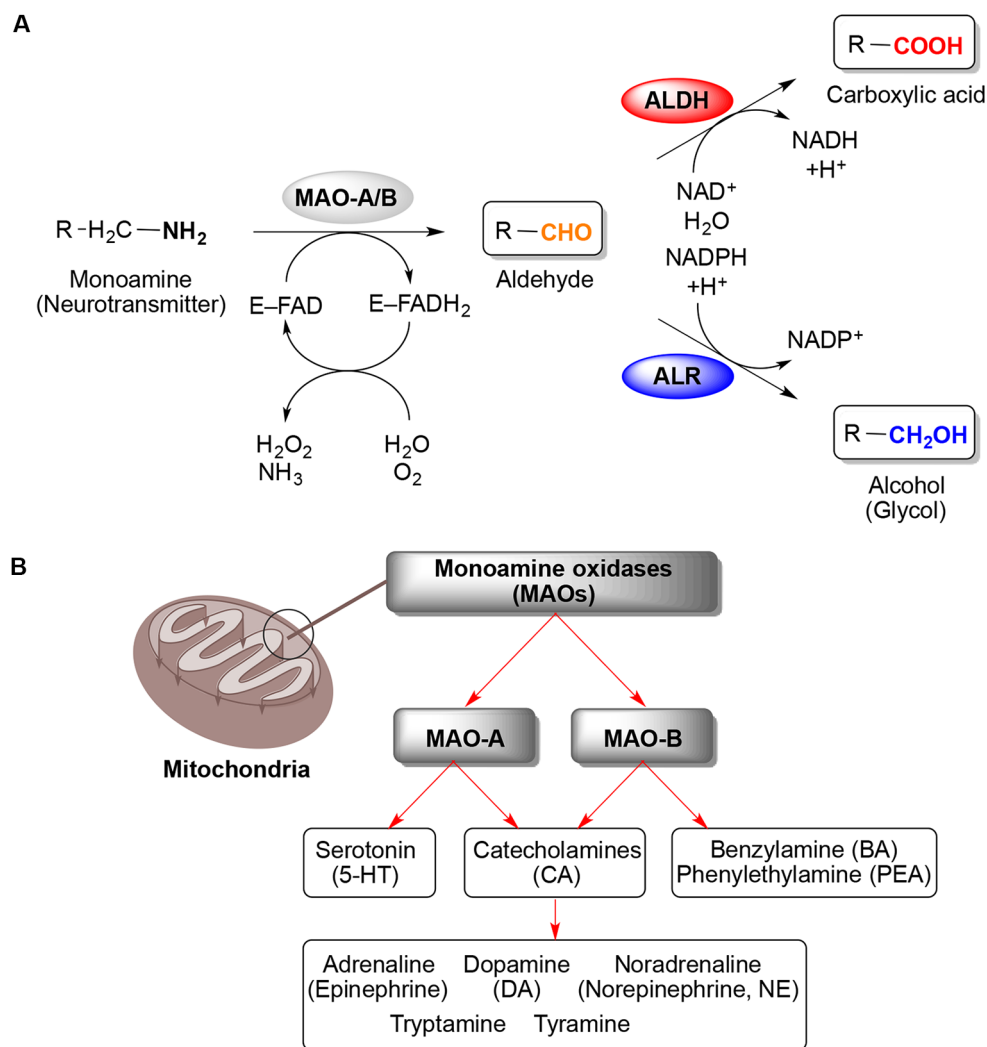
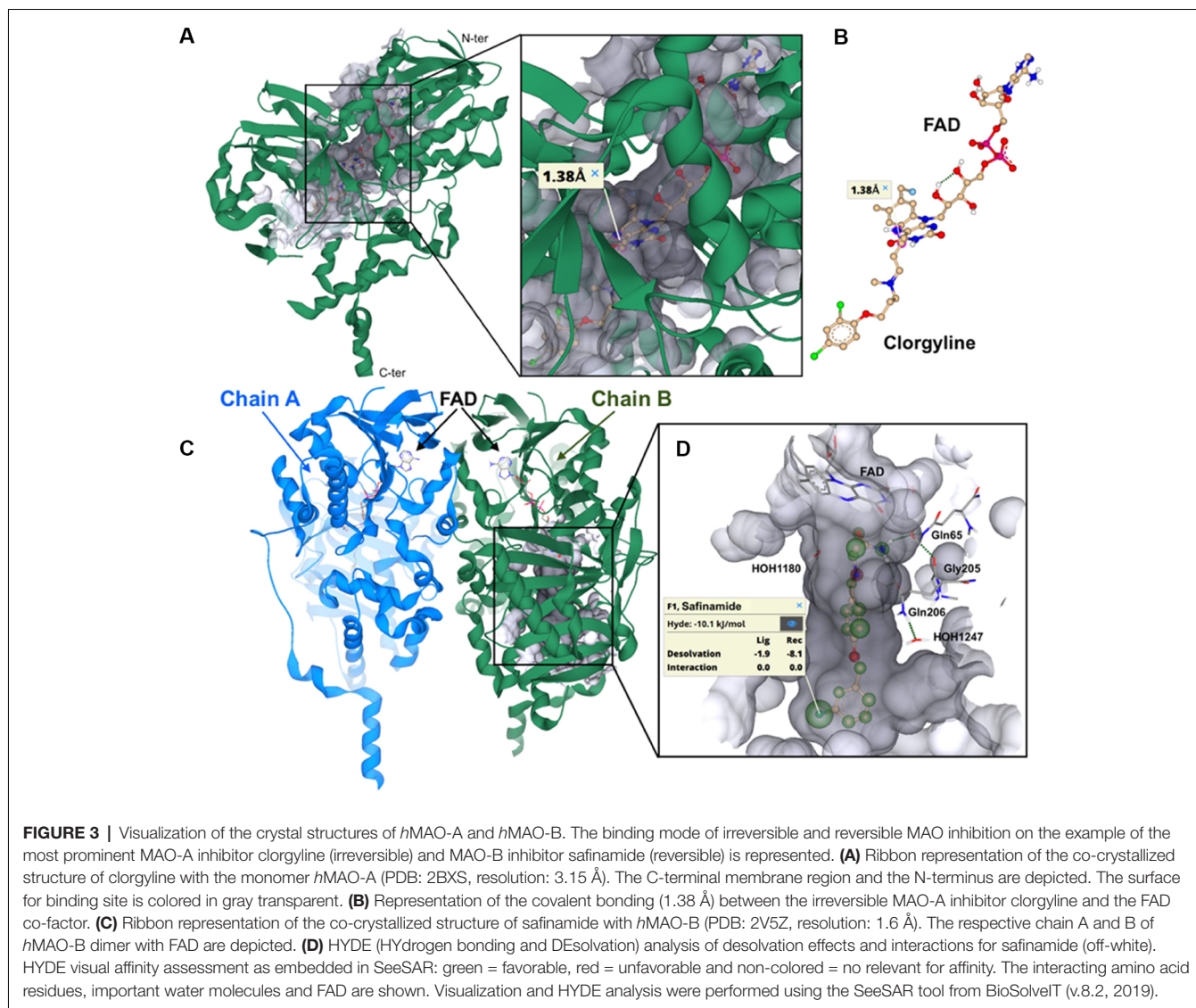


**FIGURE 1 |** Oxidative deamination of monoamines catalyzed by monoamine oxidases (MAOs) A and B. **(A)** General reaction scheme showing the binding of a monoamine (neurotransmitter) to the flavoenzyme (E-FAD) to yield the respective aldehyde and ammonia via reduction of the flavin adenine dinucleotide (FAD) co-factor toward FADH<sub>2</sub> (step 1), followed by conversion of the aldehyde (step 2) either to carboxylic acid via aldehyde dehydrogenase (ALDH) or into alcohol (glycol) by aldehyde reductase (ALR). **(B)** Localization of MAOs on the mitochondrial outer membrane and their specificities in the oxidative deamination of monoamine neurotransmitters (Maggiarani et al., 2017).

dimeric in their physiological forms (Kumar et al., 2016), the crystallographic studies revealed that the human MAO-A isoenzyme crystallizes as monomer (De Colibus et al., 2005; Son et al., 2008), whereas human MAO-B crystallizes as dimer (Binda et al., 2007). Furthermore, the active site of the human MAO-A consists of a single hydrophobic cavity with a volume of  $\sim 550 \text{ \AA}^3$ , while the bipartite cavity of human MAO-B has a volume of  $\sim 700 \text{ \AA}^3$ , divided into substrate binding site with the FAD co-factor ( $\sim 400 \text{ \AA}^3$ ) and entrance hydrophobic cavity ( $\sim 300 \text{ \AA}^3$ ; De Colibus et al., 2005). The X-ray structures of human MAO-A and human MAO-B complexes with the covalent (irreversible) bonded MAO-A inhibitor clorgyline and the non-covalent (reversible) MAO-B inhibitor safinamide, respectively, are showed in **Figure 3**.

In the current study, we aimed to analyze the research literature landscape concerning MAOs as privileged biological targets, in particular, in neuroscience from two bibliometric perspectives. First, we evaluated the publication and citation data of the literature, to identify the major contributors in terms of authors, institutions, countries/regions, and journals. By analyzing the words from titles, abstracts and keywords, we identified the hotspots of the field and revealed which themes were more investigated and cited in the period of time between 1928 and March 2019. Second, after performing the traditional citation analysis, we evaluated the cited references of the literature associated with the MAOs research. Cited reference analysis enables researchers to identify seminal publications that are important to a pre-defined body of literature, which may not be identified by traditional citation





of the human MAO-B enzyme in complex with safinamide (PDB code: 2V5Z; Binda et al., 2007) were obtained from the Protein Databank (PDB) and used for visualization of the binding modes for the respective ligands (inhibitors). The HYDE scoring function as embedded in SeeSAR considers the free energy by computing the difference between the unbound and bound states. H-bonds (approximate enthalpy) and dehydration (“desolvation”, approximate entropy) effects of all non-hydrogen/heavy atoms (HA), contributing to the overall Gibbs free energy ( $\Delta G$ ) are computed with respect to their accessibility to water before and after binding (Betz et al., 2016). After HYDE computations that run for very few seconds, SeeSAR visualizes the (HYDE-) estimated free energy of binding ( $\Delta G$ ); spherical “coronas” ranging from dark red (unfavorable) to dark green (favorable for affinity) visualize the contribution of an atom and its environment to the overall free energy of binding; corona sizes correlate with the amount of contribution (Schneider et al., 2012).

The extracted data was also imported into CRExplorer (v.1.9, 2018), a computer program that performs cited reference analysis (Thor et al., 2016), and outputs the results as a “reference publication year spectroscopy” (RPYS) that shows a waveform with high peaks in years when the seminal references were published (Slotkin, 1999; Marx et al., 2014; Yeung and Wong, 2019; Yeung et al., 2019c). For instance, the articles published in years 1926, 1927, 1928, 1929, and 1930 were cited by the publications within the dataset 45, 52, 146, 56, and 55 times, respectively. The 5-year median value was 55. Therefore, on the waveform there was a positive peak in 1928 with a magnitude of 91 (because the citation count for 1928 was 146, which positively deviated from its 5-year median by 91). We only considered references with >10% contributions to positive peaks with magnitude >50. We recorded their citations received from publications within the dataset and total citations as recorded by WoS.



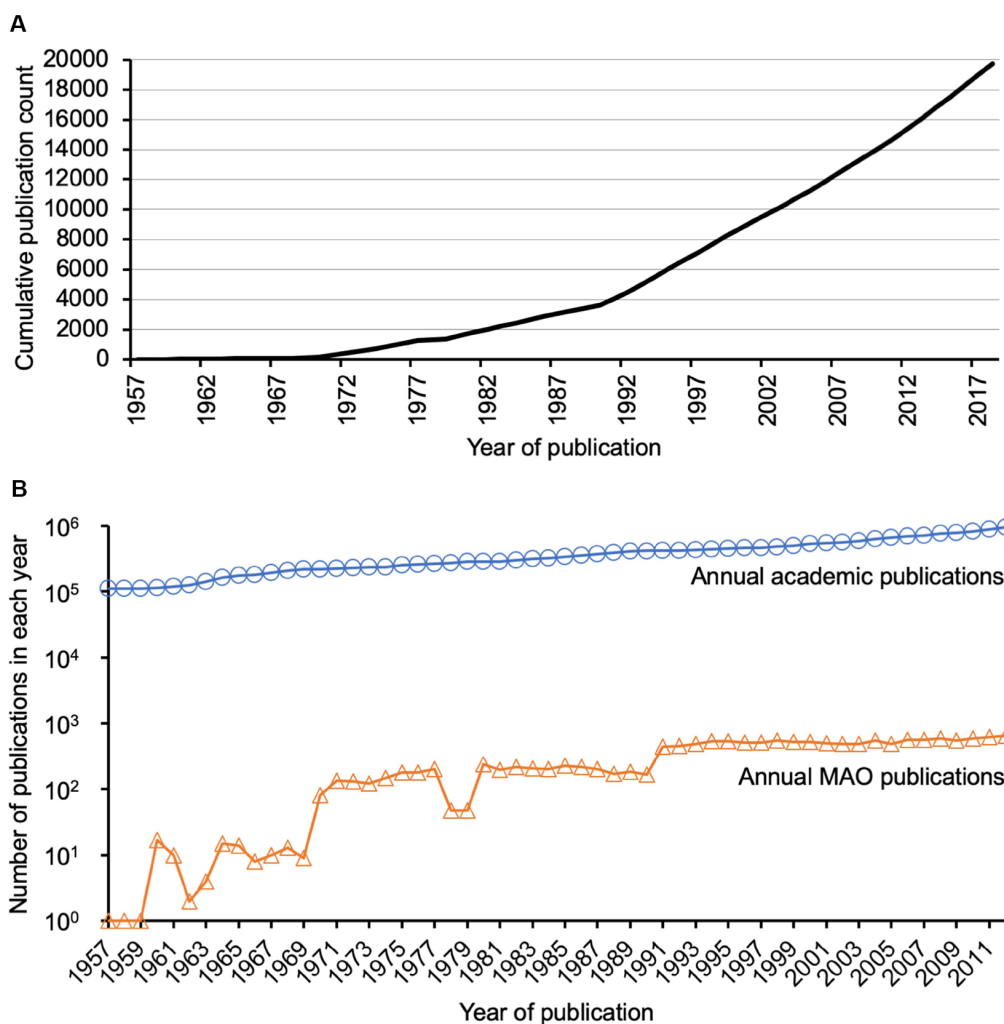


**FIGURE 4 |** Publication trend. **(A)** Publication trend of monoamine oxidase (MAO) publications. There has been a continuous research interest (apparent as a linear growth of publication counts) since the 1990s. **(B)** Detailed comparison of annual total academic publications and annual MAO publications. The former was extracted from PubMed database using MEDSUM (<http://webtools.mf.uni-lj.si/public/medsum.html>), because Web of Science does not allow such a search query.

## RESULTS AND DISCUSSION

In general, the literature search resulted in 19,854 publications, which were released in the period of time between 1928 and March 2019. **Figure 4** illustrates the continuous linear growth in MAO publications since the 1990's. The limited number of publications before the 1990's could be partly because of a lack of recording by WoS. The majority of the publications were original articles ( $n = 15,148$ , 76.3%) and reviews ( $n = 2,039$ , 10.3%). The remaining number of publications includes mainly meeting abstracts ( $n = 1,424$ ), but also proceedings ( $n = 865$ ), and brief articles ( $n = 378$ ). The publications were mainly written in English ( $n = 19,099$ , 96.2%). The top five WoS categories of the analyzed MAO publications were Pharmacology/Pharmacy ( $n = 4,664$ , 23.5%), Neurosciences ( $n = 4,416$ , 22.2%), Psychiatry ( $n = 2,906$ , 14.6%), Biochemistry/Molecular Biology ( $n = 2,691$ , 13.6%),

and Clinical Neurology ( $n = 1,754$ , 8.8%). This distribution was different for other topics such as anti-vascular endothelial growth factor (Yeung et al., 2019a) or antioxidant literature (Yeung et al., 2019b), in both of which Pharmacology/Pharmacy ranked third (7.3% and 11.8%, respectively); though these analyses also showed that original articles were the major publication type followed by review articles. The publications were contributed by over 46,000 authors from more than 7,200 institutions in 125 countries/regions and published in over 3,200 journals. All these data suggested the broad scientific community and importance of MAO research filed for neuroscience worldwide.

The top 10 most prolific authors have published at least 88 articles each, with CPP counts between 30.5 and 65.3 (**Table 1**). The top 10 institutions are scattered in the United States, UK, France, Sweden, Canada, Israel, and Russia, with CPP counts ranking from 9.2 to 54.3 (**Table 2**). The top 10

**TABLE 1** | The top 10 contributing authors.

Author	Number of publications (% of total)	Citations per publication
Moussa B.H. Youdim	247 (1.2%)	55.6
Lars Oreland	232 (1.2%)	34.8
Jean C. Shih	143 (0.7%)	53.4
Keith F. Tipton	117 (0.6%)	47.4
Dennis L. Murphy	107 (0.5%)	65.3
Neal Castagnoli Jr.	102 (0.5%)	36.5
Kevin Chen	102 (0.5%)	57.2
Merton Sandler	95 (0.5%)	33.2
Vivette Glover	91 (0.5%)	30.5
Peter Riederer	88 (0.4%)	46.1

**TABLE 2** | The top 10 contributing institutions.

Institution	Number of publications (% of total)	Citations per publication
National Institutes of Health (NIH USA)	528 (2.7%)	48.5
University of California	463 (2.3%)	48.6
University of London	349 (1.8%)	50.5
French National Institute of Health and Medical Research (INSERM)	321 (1.6%)	38.2
Harvard University	307 (1.5%)	54.3
Uppsala University	278 (1.4%)	27.5
University of Toronto	273 (1.4%)	34.3
French National Center for Scientific Research (CNRS)	270 (1.4%)	32.0
Technion-Israel Institute of Technology	266 (1.3%)	51.2
Russian Academy of Sciences	248 (1.2%)	9.2

**TABLE 3** | The top 10 contributing countries.

Country	Number of publications (% of total)	Citations per publication
USA	6,050 (30.5%)	37.4
UK	1,519 (7.7%)	35.3
China	1,374 (6.9%)	14.6
Japan	1,359 (6.8%)	20.9
Germany	1,219 (6.1%)	29.0
Italy	1,091 (5.5%)	31.5
Canada	1,058 (5.3%)	31.3
France	969 (4.9%)	28.3
Spain	794 (4.0%)	26.3
India	732 (3.7%)	14.9

countries/regions with the most intensive research on the field of MAOs are the United States, followed by European and Asian countries (Table 3). In terms of CPP, China and India were lagging behind the other eight countries. The huge publication shares of these countries are similar to the pattern observed in the scientific literature of neuroscience in general (Yeung et al., 2017; Yeung, 2018).

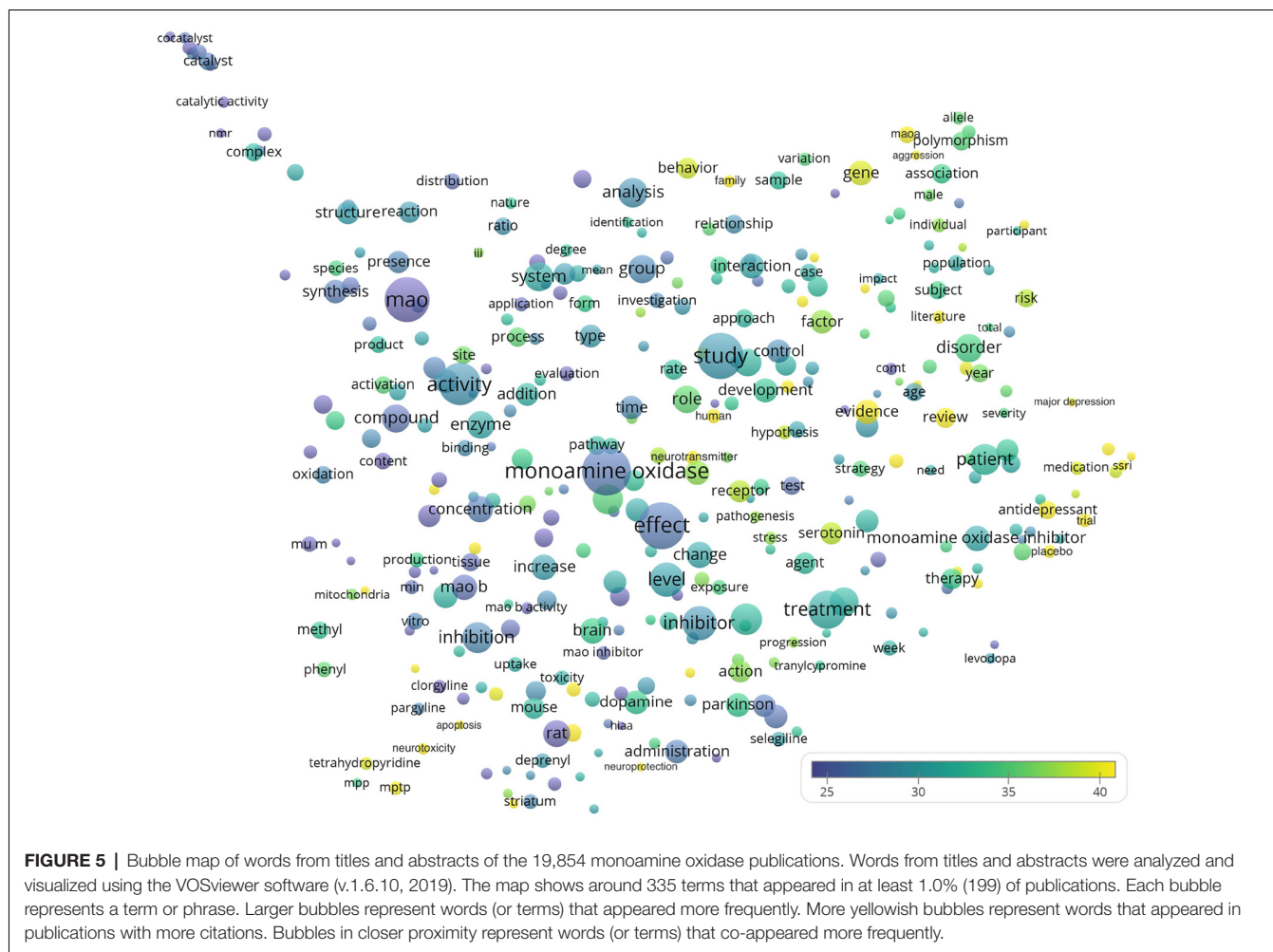
Most of the top 10 journals were specialized in pharmacology and neuroscience. Among them, *Journal of Neurochemistry* had the highest publication and CPP counts (Table 4).

**TABLE 4** | The top 10 contributing journals.

Journal	Number of publications (% of total)	Citations per publication
Journal of Neurochemistry	340 (1.7%)	50.8
Biochemical Pharmacology	272 (1.4%)	29.8
Journal of Neural Transmission	227 (1.1%)	22.6
Brain Research	215 (1.1%)	29.4
Biological Psychiatry	185 (0.9%)	38.3
European Journal of Pharmacology	183 (0.9%)	27.9
Life Sciences	176 (0.9%)	29.1
Neuroscience Letters	168 (0.8%)	19.7
British Journal of Pharmacology	167 (0.8%)	33.9
Psychopharmacology	153 (0.8%)	37.0

Figure 5 shows the words appearing in the title and abstracts of all analyzed 19,854 publications. Among the largest bubbles, several keywords were represented such as treatment ( $n = 4,189$ ; CPP = 30.9), disease ( $n = 2,957$ ; CPP = 31.9), inhibitor ( $n = 3,370$ ; CPP = 28.6), and monoamine oxidase inhibitor ( $n = 1,915$ ; CPP = 30.3). Meanwhile, examples of words with highest CPPs included reactive oxygen species (ROS;  $n = 239$ ; CPP = 50.4), major depression ( $n = 233$ ; CPP = 48.9), SSRI (selective serotonin reuptake inhibitor,  $n = 232$ ; CPP = 46.8), aggression ( $n = 282$ ; CPP = 45.6), substantia nigra ( $n = 268$ ; CPP = 44.9), apoptosis ( $n = 252$ ; CPP = 41.4), neuroprotection ( $n = 233$ ; CPP = 40.2), and neurotoxicity ( $n = 406$ ; CPP = 40.0).

The author keywords of the publications are visualized in Figure 6. The most frequently mentioned medical conditions and associated with such conditions chemicals/pharmaceuticals are listed in Tables 5, 6, respectively. PD, depression and AD were most frequently mentioned, which are consistent to previous analyses showing that PD and AD are among the most intensively investigated medical conditions in neuropharmacology (Yeung et al., 2018). The frequently mentioned chemicals/pharmaceuticals involved common neurotransmitters, such as DA, serotonin (5-hydroxytryptamine, 5-HT), and (NE, also known as noradrenaline, NA), MAOIs like selegiline, rasagiline, moclobemide, and clorgyline, as well as 1-methyl-4-phenyl-1,2,3,6-tetrahydropyridine (MPTP), which is a prodrug of 1-methyl-4-phenylpyridinium (MPP<sup>+</sup>), a mitochondrial neurotoxin leading to destruction of glial cells in *substantia nigra* and, therefore, associated with PD (Table 6, Figures 3, 7; Kopin, 1987; Edmondson et al., 2009; Tripathi et al., 2018). Furthermore, it is also suggested that *substantia nigra* is rich in DA, which may undergo enzymatic oxidation via the MAO-B enzyme to form ROS, which plays a key role in the development of PD (Fahn and Cohen, 1992; Jenner and Olanow, 1996). It is believed that the high activity of MAO-B will increase the peroxidative stress that similarly contributes to the formation of AD (Benzi and Moretti, 1995). Therefore, MAOIs and in particular reversible MAO-B inhibitors, have been extensively evaluated for their neuroprotective effects as single therapeutics or in combination with other medications for the treatment of AD and PD, while selective reversible MAO-A inhibitors



were successfully developed as antidepressants (Sano et al., 1997; Riederer et al., 2004a; Youdim and Bakhle, 2006). Many investigations have been conducted along these research directions, and thus accumulating publication counts. In recent years, dual inhibition of MAO-A/B is considered as privileged strategy in addition to other biological effects for the development of so called multi-target-directed ligands (MTDLs) for the treatment of neurodegenerative diseases, in particular, AD (Kumar et al., 2016; Tzvetkov and Atanasov, 2018). In addition, some research articles deal with the investigation of the key role of MAOs as potential drivers in non-neurological disorders, for example, mitochondrial dysfunctions associated with cardiac aging (Sheydina et al., 2011; Maggiorani et al., 2017).

Furthermore, we performed an analysis of the citation count of references per year for the whole investigated period of time 1928–2019. For this purpose, we applied the RPYS method as embedded in CRExplorer (Thor et al., 2016). **Figure 8** shows the RPYS plot for the cited reference analysis for each year and for each publication. Following the RPYS method, 16 positive peaks with magnitude  $>50$  for 17 separate years were found, as follows: 1928, 1934, 1937, 1949, 1951,

1957, 1965, 1968, 1972, 1976, 1980, 1985, 1995–1996, 2000, 2004, and 2006. From the figure, it seemed that the gray bars formed a bell that centered on the 2000–2010 years, meaning that many cited references were published during these years. Potential explanations could be that in those years the recombinant forms of MAO enzymes were available and the crystal structure solved, thus these important references were more cited. Meanwhile, there was a strong positive peak in 2000. Some references were cited >100 times by the analyzed MAO publications, though they did have >10% contributions to the peak. Two such exemplars were reporting inhibition of MAO by coumarin derivatives (Gnerre et al., 2000), and a potential association between MAOA gene polymorphism and variability in aggressiveness and impulsivity (Manuck et al., 2000). Nine seminal references fulfilled our predefined criteria of having >10% contributions to a positive peak with magnitude >50. All of them were published in 1972 or before (**Table 7**). The seminal paper by Mary Bernheim (Hare, 1928) was identified in the first positive peak. Another notable seminal reference was by Lowry et al. (1951), which described the technique of a biochemical assay to measure the total level of protein in a test solution. It should be noted that by analyzing

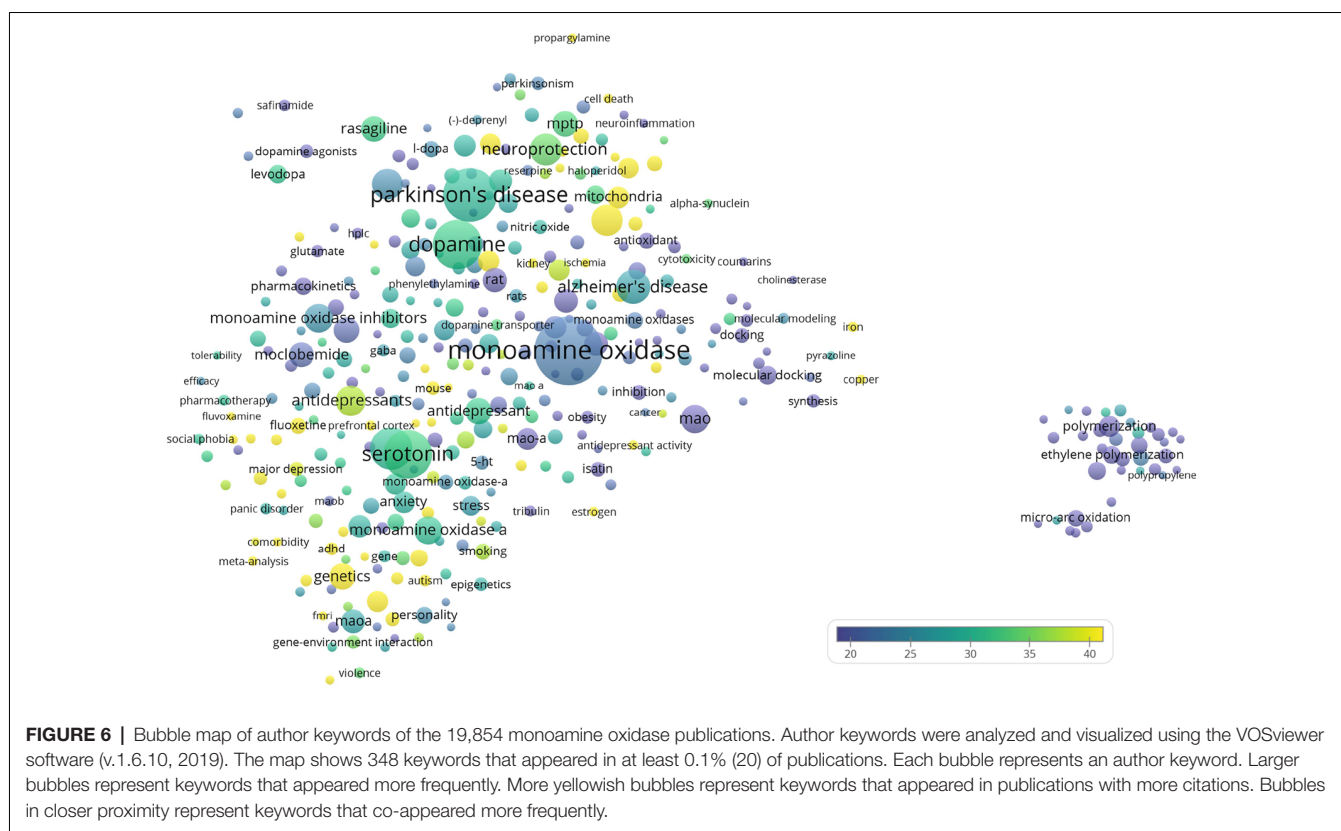


**TABLE 5 |** Medical and mental conditions mentioned in the author keywords of 0.5% ( $n = 100$ ) of the monoamine oxidase publications.

Medical condition	Number of publications (% of total)	Citations per publication
Parkinson's disease	789 (4.0%)	29.9
Depression	483 (2.4%)	30.2
Alzheimer's disease	316 (1.6%)	26.6
Anxiety	134 (0.7%)	29.0
Schizophrenia	125 (0.6%)	30.1
Aggression	120 (0.6%)	43.0

the cited references, we were able to identify not only the historical root of MAO but also articles reporting methods that became standard techniques in protein research field and thus highly cited by the MAO field. If only seminal papers regarding the MAO proteins were focused on, then these references were identified in four representative years: 1928, 1957, 1968, and 1972.

The current analysis has some limitations. First, the search strategy might limit the body of literature to be analyzed. Second, some MAO articles might not be indexed by the WoS database, especially the older ones. Alternative databases could be considered, such as Scopus, to identify additional publications, but data from multiple databases cannot be merged due to their differences in indexing and counting, and thus cannot be integrated in our analysis. Readers should also be aware of the general increase of scientific production along

**TABLE 6 |** Chemicals and pharmaceuticals mentioned in the author keywords of 0.5% ( $n = 100$ ) of the monoamine oxidase publications.

Chemical/pharmaceutical	Number of publications (% of total)	Citations per publication
Dopamine	665	31.7
Serotonin	649	32.1
Selegiline	257	24.4
MPTP (1-methyl-4-phenyl-1,2,3,6-tetrahydropyridine)	180	32.8
Rasagiline	178	32.1
Moclobemide	173	21.2
Norepinephrine	113	26.7
Clorgyline	110	22.9

the 20th century (**Figure 4B**), which was growing in a higher level compared to MAO publications in recent years (until 70s the trend was the opposite and the number of MAO articles was increasing more rapidly than the total number of academic articles). Nevertheless, the graph shows that the interest in these proteins is still very high. In general, the number of scientific articles, citations, journals, and institutions has been also progressively increasing. It would be interesting to normalize the results (publication and citation data of the MAO research field) with respect to these changing parameters. However, such normalization would be very complicated and hence not applicable for the current study. To the best of the authors' knowledge, a similar bibliometric analysis approach has not been done before so that in the future it can be



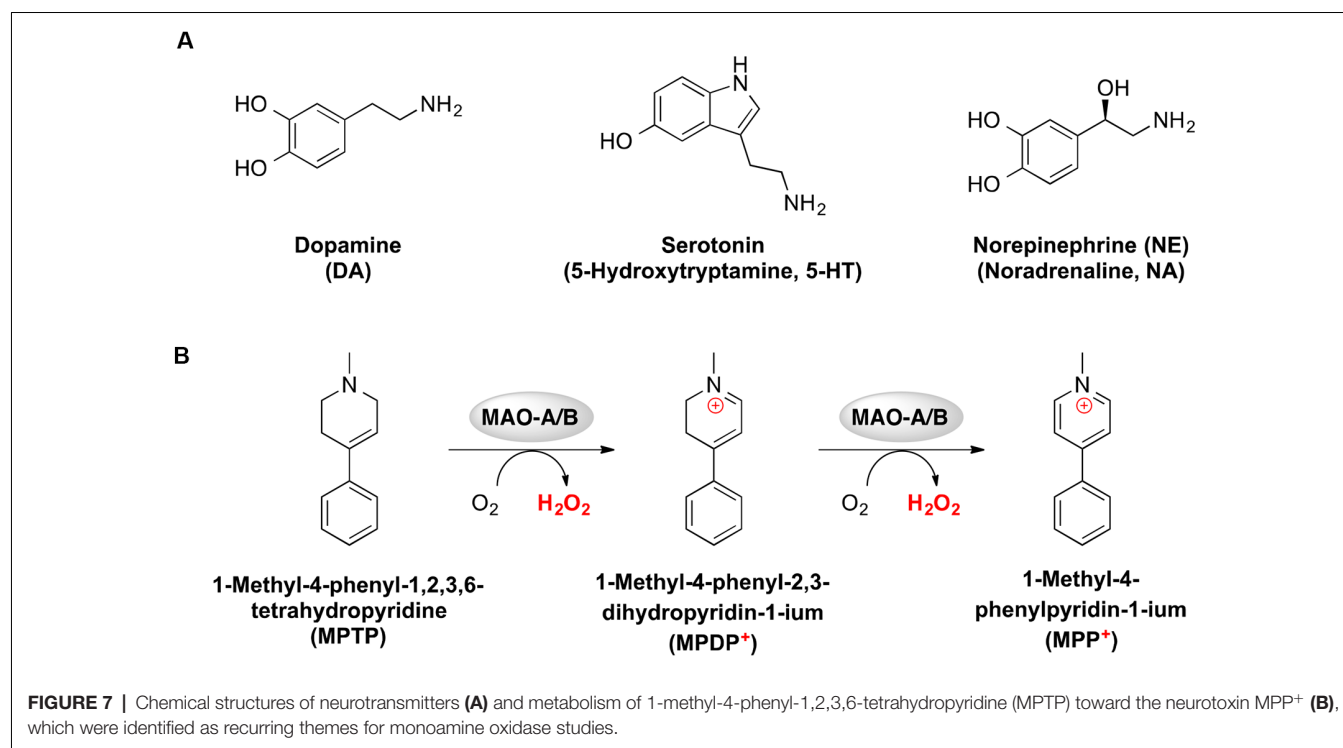
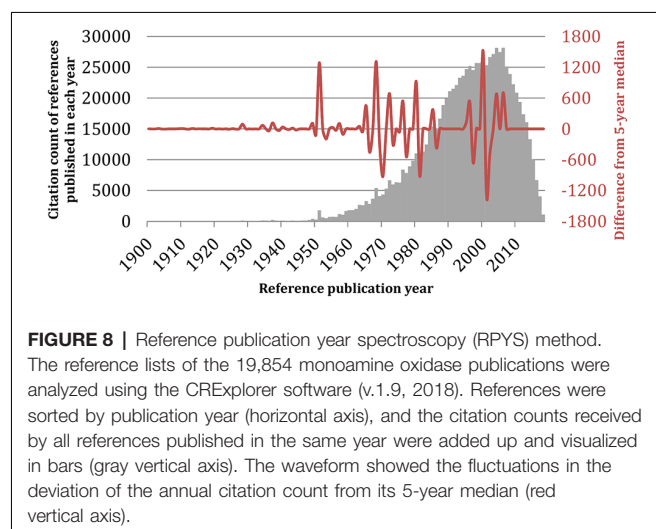


**TABLE 7 |** Seminal references of monoamine oxidase publications identified by the RPYS method.

Year	References	% Contribution to the peak	Citations by MAO publications	All-time total citations
1928	Hare (1928)	65.1	95	318*
1934	Lineweaver and Burk (1934)	50.3	77	12,422*
1937a	Blaschko et al. (1937a)	20.1	45	473*
1937b	Blaschko et al. (1937b)	10.7	24	197*
1949	Gornall et al. (1949)	16.2	62	16,989
1951	Lowry et al. (1951)	80.0	1,437	3,37,283
1957	Glennner et al. (1957)	12.0	140	685
1968	Johnston (1968)	22.5	1,218	1,596
1972	Knoll (1972)	10.3	688	1,014*

\*Citation count recorded from Google Scholar, as the publication is not indexed by Web of Science.



applied to other targets (e.g., specific proteins) to allow a better comparison.

In conclusion, the current MAO literature analysis highlights the popular research themes in the scientific literature related to MAOs and historical roots of MAO research as a quick guide for fellow researchers. Through decades of research, the literature has accumulated many publications investigating the therapeutic effects of at least two generations of MAOIs on various neurological conditions, such as AD, PD, and depression. The analyzed data showed that the United States is the major contributor, together with some European and Asian countries. Many of the articles were published in pharmacology and neuroscience journals. Publications involving the neurotransmitters DA, serotonin, and NE, as well as the MAO-A inhibitors moclobemide and clogyline, and the irreversible MAO-B inhibitors selegiline and rasagiline had over 20 citations per publication. We envision that the number of publications related to MAOs research will continue

to grow steadily, with more new drugs being tested for better management of neurological conditions, in particular, with the development of multi-target acting drugs against neurodegenerative diseases. Moreover, the analysis of the scientific literature suggested that in addition to the pivotal role of MAOs as biological targets in neuroscience, the research field will also be directed toward investigations of MAOIs as potential therapeutics for other pathophysiological processes associated with aging, such as increased sensitivity to apoptosis, increased production of mitochondrial ROS, and others.

## DATA AVAILABILITY

The datasets generated for this study are available on request to the corresponding author.

## REFERENCES

- Benzi, G., and Moretti, A. (1995). Are reactive oxygen species involved in Alzheimer's disease? *Neurobiol. Aging* 16, 661–674. doi: 10.1016/0197-4580(95)00066-n
- Betz, M., Wulsdorf, T., Krimmer, S. G., and Klebe, G. (2016). Impact of surface water layers on protein-ligand binding: how well are experimental data reproduced by molecular dynamics simulations in a thermolysin test case? *J. Chem. Inf. Model.* 56, 223–233. doi: 10.1021/acs.jcim.5b00621
- Bietz, S., Urbaczek, S., Schulz, B., and Rarey, M. (2014). Protoss: a holistic approach to predict tautomers and protonation states in protein-ligand complexes. *J. Cheminform.* 6:12. doi: 10.1186/1758-2946-6-12
- Binda, C., Hubálek, F., Li, M., Herzig, Y., Sterling, J., Edmondson, D. E., et al. (2004). Crystal structures of monoamine oxidase B in complex with four inhibitors of the N-propargylaminoindan class. *J. Med. Chem.* 47, 1767–1774. doi: 10.1021/jm031087c
- Binda, C., Newton-Vinson, P., Hubálek, F., Edmondson, D. E., and Mattevi, A. (2002). Structure of human monoamine oxidase B, a drug target for the treatment of neurological disorders. *Nat. Struct. Biol.* 9, 22–26. doi: 10.1038/nsb732
- Binda, C., Wang, J., Pisani, L., Caccia, C., Carotti, A., Salvati, P., et al. (2007). Structures of human monoamine oxidase B complexes with selective noncovalent inhibitors: safinamide and coumarin analogs. *J. Med. Chem.* 50, 5848–5852. doi: 10.1021/jm070677y
- Blaschko, H., Richter, D., and Schlossmann, H. (1937a). The oxidation of adrenaline and other amines. *Biochem. J.* 31, 2187–2196. doi: 10.1042/bj0312187
- Blaschko, H., Richter, D., and Schlossmann, H. (1937b). The inactivation of adrenaline. *J. Physiol.* 90, 1–17. doi: 10.1113/jphysiol.1937.sp003497
- Borroni, E., Bohrmann, B., Grueninger, F., Prinssen, E., Nave, S., Loetscher, H., et al. (2017). Sembragiline: a novel, selective monoamine oxidase type B inhibitor for the treatment of Alzheimer's disease. *J. Pharmacol. Exp. Ther.* 362, 413–423. doi: 10.1124/jpet.117.241653
- Brunner, H. G., Nelen, M. R., Van Zandvoort, P., Abeling, N. G., Van Gennip, A. H., Wolters, E. C., et al. (1993). X-linked borderline mental retardation with prominent behavioral disturbance: phenotype, genetic localization and evidence for disturbed monoamine metabolism. *Am. J. Hum. Genet.* 52, 1032–1039.
- Castagnoli, N., Petzer, J. P., Steyn, S., Castagnoli, K., Chen, J.-F., Schwarzschild, M. A., et al. (2003). Monoamine oxidase B inhibition and neuroprotection. *Neurology* 61, S62–S68. doi: 10.1212/01.WNL.0000095215.97585.59
- Cohen, I. L., Liu, X., Lewis, M., Chudley, A., Forster-Gibson, C., Gonzalez, M., et al. (2011). Autism severity is associated with child and maternal MAOA genotypes. *Clin. Genet.* 79, 355–362. doi: 10.1111/j.1399-0004.2010.01471.x
- De Colibus, L., Li, M., Binda, C., Lustig, A., Edmondson, D. E., and Mattevi, A. (2005). Three-dimensional structure of human monoamine oxidase A (MAO A): relation to the structures of rat MAO A and human MAO B. *Proc. Natl. Acad. Sci. U S A* 102, 12684–12689. doi: 10.1073/pnas.0505975102
- Deeks, E. D. (2015). Safinamide: first global approval. *Drugs* 75, 705–711. doi: 10.1007/s40265-015-0389-7
- Edmondson, D. E., Binda, C., Wang, J., Upadhyay, A. K., and Mattevi, A. (2009). Molecular and mechanistic properties of the membrane-bound mitochondrial monoamine oxidases. *Biochemistry* 48, 4220–4230. doi: 10.1021/bi900413g
- Fahn, S., and Cohen, G. (1992). The oxidant stress hypothesis in Parkinson's disease: evidence supporting it. *Ann. Neurol.* 32, 804–812. doi: 10.1002/ana.410320616
- Fowler, J. S., Logan, J., Volkow, N. D., Shumay, E., Mccall-Perez, F., Jayne, M., et al. (2015). Evidence that formulations of the selective MAO-B inhibitor, selegiline, which bypass first-pass metabolism, also inhibit MAO-A in the human brain. *Neuropsychopharmacology* 40, 650–657. doi: 10.1038/npp.2014.214
- Glenner, G. G., Burtner, H. J., and Brown, G. W. Jr. (1957). The histochemical demonstration of monoamine oxidase activity by tetrazolium salts. *J. Histochem. Cytochem.* 5, 591–600. doi: 10.1177/5.6.591
- Gnerre, C., Catto, M., Leonetti, F., Weber, P., Carrupt, P.-A., Altomare, C., et al. (2000). Inhibition of monoamine oxidases by functionalized coumarin derivatives: biological activities, QSARs and 3D-QSARs. *J. Med. Chem.* 43, 4747–4758. doi: 10.1021/jm001028o
- Gornall, A. G., Bardawill, C. J., and David, M. M. (1949). Determination of serum proteins by means of the biuret reaction. *J. Biol. Chem.* 177, 751–766.
- Hare, M. L. C. (1928). Tyramine oxidase: a new enzyme system in liver. *Biochem. J.* 22, 968–979. doi: 10.1042/bj0220968
- Henkel, V., Mergl, R., Allgaier, A.-K., Kohnen, R., Möller, H.-J., and Hegerl, U. (2006). Treatment of depression with atypical features: a meta-analytic approach. *Psychiatry Res.* 141, 89–101. doi: 10.1016/j.psychres.2005.07.012
- Jenner, P., and Olanow, C. W. (1996). Oxidative stress and the pathogenesis of Parkinson's disease. *Neurology* 47, S161–S170. doi: 10.1212/wnl.47.6\_suppl\_3.161s
- Jo, G., Sung, S. H., Lee, Y., Kim, B.-G., Yoon, J., Lee, H. O., et al. (2012). Discovery of monoamine oxidase A inhibitors derived from *in silico* docking. *Bull. Korean Chem. Soc.* 33, 3841–3844. doi: 10.5012/bkcs.2012.33.11.3841
- Johnston, J. P. (1968). Some observations upon a new inhibitor of monoamine oxidase in brain tissue. *Biochem. Pharmacol.* 17, 1285–1297. doi: 10.1016/0006-2952(68)90066-x
- Knoll, J. (1972). Some puzzling pharmacological effects of monoamine oxidase inhibitors. *Adv. Biochem. Psychopharmacol.* 5, 393–408.
- Kopin, I. J. (1987). MPTP: an industrial chemical and contaminant of illicit narcotics stimulates a new era in research on Parkinson's disease. *Environ. Health Perspect.* 75, 45–51. doi: 10.2307/3430575
- Kumar, B., Mantha, A. K., and Kumar, V. (2016). Recent developments on the structure-activity relationship studies of MAO inhibitors and their role in different neurological disorders. *RSC Adv.* 6, 42660–42683. doi: 10.1039/c6ra00302h

## AUTHOR CONTRIBUTIONS

All authors conceived the work. AY and NT acquired data and drafted the work. AY and AA analyzed data. AA, MG and NT critically revised the work. All authors have approved the final content of the manuscript.

## FUNDING

AA acknowledges the support by the Polish KNOW (Leading National Research Centre) Scientific Consortium “Healthy Animal—Safe Food” decision of Ministry of Science and Higher Education No. 05-1/KNOW2/2015. NT, MG and AA acknowledge the support by the Bulgarian National Science Fund (BNSF) under Grant No. KP-06-OPR 03/8.

- Lakhan, S. E. (2007). From a Parkinson's disease expert: rasagiline and the future of therapy. *Mol. Neurodegener.* 2:13. doi: 10.1186/1750-1326-2-13
- Lineweaver, H., and Burk, D. (1934). The determination of enzyme dissociation constants. *J. Am. Chem. Soc.* 56, 658–666. doi: 10.1021/ja01318a036
- Lowry, O. H., Rosebrough, N. J., Farr, A. L., and Randall, R. J. (1951). Protein measurement with the Folin phenol reagent. *J. Biol. Chem.* 193, 265–275.
- Maggiorani, D., Manzella, N., Edmondson, D. E., Mattevi, A., Parini, A., Binda, C., et al. (2017). Monoamine oxidases, oxidative stress, and altered mitochondrial dynamics in cardiac ageing. *Oxid. Med. Cell. Longev.* 2017:3017947. doi: 10.1155/2017/3017947
- Mallajosyula, J. K., Chinta, S. J., Rajagopalan, S., Nicholls, D. G., and Andersen, J. K. (2009). Metabolic control analysis in a cellular model of elevated MAO-B: relevance to Parkinson's disease. *Neurotox. Res.* 16, 186–193. doi: 10.1007/s12640-009-9032-2
- Manuck, S. B., Flory, J. D., Ferrell, R. E., Mann, J. J., and Muldoon, M. F. (2000). A regulatory polymorphism of the monoamine oxidase-A gene may be associated with variability in aggression, impulsivity and central nervous system serotonergic responsivity. *Psychiatry Res.* 95, 9–23. doi: 10.1016/s0165-1781(00)00162-1
- Marx, W., Bornmann, L., Barth, A., and Leydesdorff, L. (2014). Detecting the historical roots of research fields by reference publication year spectroscopy (RPYS). *J. Assoc. Inf. Sci. Technol.* 65, 751–764. doi: 10.1002/asi.23089
- Meyer, J. H., Ginovart, N., Boovariwala, A., Sagrati, S., Hussey, D., Garcia, A., et al. (2006). Elevated monoamine oxidase levels in the brain: an explanation for the monoamine imbalance of major depression. *Arch. Gen. Psychiatry* 63, 1209–1216. doi: 10.1001/archpsyc.63.11.1209
- Riederer, P., Danielczyk, W., and Grünblatt, E. (2004a). Monoamine oxidase-B inhibition in Alzheimer's disease. *Neurotoxicology* 25, 271–277. doi: 10.1016/S0161-813X(03)00106-2
- Riederer, P., Lachenmayer, L., and Laux, G. (2004b). Clinical applications of MAO-inhibitors. *Curr. Med. Chem.* 11, 2033–2043. doi: 10.2174/0929867043364775
- Sano, M., Ernesto, C., Thomas, R. G., Klauber, M. R., Schafer, K., Grundman, M., et al. (1997). A controlled trial of selegiline, alpha-tocopherol, or both as treatment for Alzheimer's disease. *N. Engl. J. Med.* 336, 1216–1222. doi: 10.1056/NEJM199704243361704
- Saura, J., Luque, J., Cesura, A., Da Prada, M., Chan-Palay, V., Huber, G., et al. (1994). Increased monoamine oxidase B activity in plaque-associated astrocytes of Alzheimer brains revealed by quantitative enzyme radioautography. *Neuroscience* 62, 15–30. doi: 10.1016/0306-4522(94)90311-5
- Schneider, N., Hindle, S., Lange, G., Klein, R., Albrecht, J., Briem, H., et al. (2012). Substantial improvements in large-scale redocking and screening using the novel HYDE scoring function. *J. Comput. Aided Mol. Des.* 26, 701–723. doi: 10.1007/s10822-011-9531-0
- Setini, A., Pierucci, F., Senatori, O., and Nicotra, A. (2005). Molecular characterization of monoamine oxidase in zebrafish (*Danio rerio*). *Comp. Biochem. Physiol. B Biochem. Mol. Biol.* 140, 153–161. doi: 10.1016/j.cbpc.2004.10.002
- Sheydina, A., Riordon, D. R., and Boheler, K. R. (2011). Molecular mechanisms of cardiomyocyte aging. *Clin. Sci.* 121, 315–329. doi: 10.1042/cs20110115
- Shih, J. C., Chen, K., and Ridd, M. J. (1999). Monoamine oxidase: from genes to behavior. *Annu. Rev. Neurosci.* 22, 197–217. doi: 10.1146/annurev.neuro.22.1.197
- Slotkin, T. A. (1999). Mary Bernheim and the discovery of monoamine oxidase. *Brain Res. Bull.* 50:373. doi: 10.1016/s0361-9230(99)00110-0
- Son, S.-Y., Ma, J., Kondou, Y., Yoshimura, M., Yamashita, E., and Tsukihara, T. (2008). Structure of human monoamine oxidase A at 2.2-Å resolution: the control of opening the entry for substrates/inhibitors. *Proc. Natl. Acad. Sci. U S A* 105, 5739–5744. doi: 10.1073/pnas.0710626105
- Thor, A., Marx, W., Leydesdorff, L., and Bornmann, L. (2016). Introducing CitedReferencesExplorer (CRExplorer): A program for reference publication year spectroscopy with cited references standardization. *J. Informetr.* 10, 503–515. doi: 10.1016/j.joi.2016.02.005
- Tong, J., Meyer, J. H., Furukawa, Y., Boileau, I., Chang, L.-J., Wilson, A. A., et al. (2013). Distribution of monoamine oxidase proteins in human brain: implications for brain imaging studies. *J. Cereb. Blood Flow Metab.* 33, 863–871. doi: 10.1038/jcbfm.2013.19
- Tripathi, A. C., Upadhyay, S., Paliwal, S., and Saraf, S. K. (2018). Privileged scaffolds as MAO inhibitors: retrospect and prospects. *Eur. J. Med. Chem.* 145, 445–497. doi: 10.1016/j.ejmech.2018.01.003
- Tzvetkov, N. T., and Atanasov, A. G. (2018). Natural product-based multitargeted ligands for Alzheimer's disease treatment? *Future Med. Chem.* 10, 1745–1748. doi: 10.4155/fmc-2018-0146
- Tzvetkov, N. T., Stämmler, H.-G., Hristova, S., Atanasov, A. G., and Antonov, L. (2019). (Pyrrolo-pyridin-5-yl) benzamides: BBB permeable monoamine oxidase B inhibitors with neuroprotective effect on cortical neurons. *Eur. J. Med. Chem.* 162, 793–809. doi: 10.1016/j.ejmech.2018.11.009
- Tzvetkov, N. T., Stämmler, H.-G., Neumann, B., Hristova, S., Antonov, L., and Gastreich, M. (2017). Crystal structures, binding interactions, and ADME evaluation of brain penetrant N-substituted indazole-5-carboxamides as subnanomolar, selective monoamine oxidase B and dual MAO-A/B inhibitors. *Eur. J. Med. Chem.* 127, 470–492. doi: 10.1016/j.ejmech.2017.01.011
- Van Eck, N. J., and Waltman, L. (2010). Software survey: VOSviewer, a computer program for bibliometric mapping. *Scientometrics* 84, 523–538. doi: 10.1007/s11192-009-0146-3
- Yamada, M., and Yasuhara, H. (2004). Clinical pharmacology of MAO inhibitors: safety and future. *Neurotoxicology* 25, 215–221. doi: 10.1016/s0161-813x(03)00097-4
- Yeung, A. W. K. (2018). Bibliometric study on functional magnetic resonance imaging literature (1995–2017) concerning chemosensory perception. *Chemosens. Percept.* 11, 42–50. doi: 10.1007/s12078-018-9243-0
- Yeung, A. W. K., Abdel-Daim, M. M., Abushouk, A. I., and Kadosono, K. (2019a). A literature analysis on anti-vascular endothelial growth factor therapy (anti-VEGF) using a bibliometric approach. *Naunyn Schmiedebergs Arch. Pharmacol.* 392, 393–403. doi: 10.1007/s00210-019-01629-y
- Yeung, A. W. K., Tzvetkov, N. T., El-Tawil, O. S., Bungau, S. G., Abdel-Daim, M. M., and Atanasov, A. G. (2019b). Antioxidants: scientific literature landscape analysis. *Oxid. Med. Cell. Longev.* 2019:8278454. doi: 10.1155/2019/8278454
- Yeung, A. W. K., Wong, N. S. M., and Leung, Y. Y. (2019c). Are coronectomy studies being cited? A bibliometric study. *J. Investig. Clin. Dent.* 10:e12366. doi: 10.1111/jicd.12366
- Yeung, A. W. K., Goto, T. K., and Leung, W. K. (2017). A bibliometric review of research trends in neuroimaging. *Curr. Sci.* 112, 725–734. doi: 10.18520/cs/v112/i04/725-734
- Yeung, A. W. K., Tzvetkov, N. T., and Atanasov, A. G. (2018). When neuroscience meets pharmacology: a neuropharmacology literature analysis. *Front. Neurosci.* 12:852. doi: 10.3389/fnins.2018.00852
- Yeung, A. W. K., and Wong, N. S. M. (2019). The historical roots of visual analogue scale in psychology as revealed by reference publication year spectroscopy. *Front. Hum. Neurosci.* 13:86. doi: 10.3389/fnhum.2019.00086
- Youdim, M. B., and Bakhle, Y. (2006). Monoamine oxidase: isoforms and inhibitors in Parkinson's disease and depressive illness. *Br. J. Pharmacol.* 147, S287–S296. doi: 10.1038/sj.bjp.0706464
- Zeller, E., and Barsky, J. (1952). *in vivo* inhibition of liver and brain monoamine oxidase by 1-Isonicotinyl-2-isopropyl hydrazine. *Proc. Soc. Exp. Biol. Med.* 81, 459–461. doi: 10.3181/00379727-81-19910

**Conflict of Interest Statement:** The authors declare that the research was conducted in the absence of any commercial or financial relationships that could be construed as a potential conflict of interest.

Copyright © 2019 Yeung, Georgieva, Atanasov and Tzvetkov. This is an open-access article distributed under the terms of the Creative Commons Attribution License (CC BY). The use, distribution or reproduction in other forums is permitted, provided the original author(s) and the copyright owner(s) are credited and that the original publication in this journal is cited, in accordance with accepted academic practice. No use, distribution or reproduction is permitted which does not comply with these terms.



# Inhibition of nSMase2 Reduces the Transfer of Oligomeric $\alpha$ -Synuclein Irrespective of Hypoxia

Valerie Sackmann<sup>1,2</sup>, Maitrayee Sardar Sinha<sup>1,2</sup>, Christopher Sackmann<sup>1,2</sup>, Livia Civitelli<sup>1,2</sup>, Joakim Bergström<sup>3</sup>, Anna Ansell-Schultz<sup>1,2</sup> and Martin Hallbeck<sup>1,2\*</sup>

<sup>1</sup> Department of Clinical Pathology, Linköping University, Linköping, Sweden, <sup>2</sup> Department of Clinical and Experimental Medicine, Linköping University, Linköping, Sweden, <sup>3</sup> Department of Public Health and Caring Sciences, Uppsala University, Uppsala, Sweden

## OPEN ACCESS

### Edited by:

Mauro Cozzolino,  
Institute of Translational  
Pharmacology (CNR), Italy

### Reviewed by:

Annalucia Serafino,  
Institute of Translational  
Pharmacology (CNR), Italy  
Jason Howitt,  
Florey Institute of Neuroscience  
and Mental Health, Australia

### \*Correspondence:

Martin Hallbeck  
martin.hallbeck@liu.se

**Received:** 21 May 2019

**Accepted:** 02 August 2019

**Published:** 28 August 2019

### Citation:

Sackmann V, Sinha MS, Sackmann C, Civitelli L, Bergström J, Ansell-Schultz A and Hallbeck M (2019) Inhibition of nSMase2 Reduces the Transfer of Oligomeric  $\alpha$ -Synuclein Irrespective of Hypoxia. *Front. Mol. Neurosci.* 12:200. doi: 10.3389/fnmol.2019.00200

Recently, extracellular vesicles (EVs), such as exosomes, have been proposed to play an influential role in the cell-to-cell spread of neurodegenerative diseases, including the intercellular transmission of  $\alpha$ -synuclein ( $\alpha$ -syn). However, the regulation of EV biogenesis and its relation to Parkinson's disease (PD) is only partially understood. The generation of EVs through the ESCRT-independent pathway depends on the hydrolysis of sphingomyelin by neutral sphingomyelinase 2 (nSMase2) to produce ceramide, which causes the membrane of endosomal multivesicular bodies to bud inward. nSMase2 is sensitive to oxidative stress, a common process in PD brains; however, little is known about the role of sphingomyelin metabolism in the pathogenesis of PD. This is the first study to show that inhibiting nSMase2 decreases the transfer of oligomeric aggregates of  $\alpha$ -syn between neuron-like cells. Furthermore, it reduced the accumulation and aggregation of high-molecular-weight  $\alpha$ -syn. Hypoxia, as a model of oxidative stress, reduced the levels of nSMase2, but not its enzymatic activity, and significantly altered the lipid composition of cells without affecting EV abundance or the transfer of  $\alpha$ -syn. These data show that altering sphingolipids can mitigate the spread of  $\alpha$ -syn, even under hypoxic conditions, potentially suppressing PD progression.

**Keywords:** Parkinson's disease, extracellular vesicles, neutral sphingomyelinase 2,  $\alpha$ -syn, hypoxia, cell-to-cell transmission, sphingomyelin, ceramide

## INTRODUCTION

Parkinson's disease (PD) is a progressive age-related movement disorder that results in the selective loss of midbrain dopaminergic neurons and widespread pathology at later stages of the disease (Braak et al., 2003). PD is also characterized by intracellular deposits of aggregated  $\alpha$ -synuclein ( $\alpha$ -syn), known as Lewy bodies and Lewy neurites, and research indicates that soluble oligomeric  $\alpha$ -syn ( $\alpha\alpha$ -syn) is the most toxic species [reviewed in Bengoa-Vergniory et al. (2017)]. Anatomical connections and cell-to-cell contact promote the accumulation of these aggregates.

**Abbreviations:**  $\alpha$ -syn, alpha-synuclein; AChE, acetylcholinesterase; Cer, ceramide; DHCer, dihydroceramide; dhSM, dihydrosphingomyelin; ESCRT, endosomal sorting complexes required for transport; EV, extracellular vesicle; GlcCer, glucosylceramide; HNE, 4-hydroxy-2-nonenal; KO, knockout; LacCer, lactosylceramide; nSMase2, neutral sphingomyelinase 2;  $\alpha\alpha$ -syn, oligomeric alpha-synuclein; PD, Parkinson's disease; siRNA, small interfering RNA; SM, sphingomyelin.



The mechanisms of this spreading, including the important role of cell-surface proteins (Reyes et al., 2019) and extracellular vesicles (EVs) (Russo et al., 2012), are beginning to be elucidated. Small EVs, specifically exosomes, are small membranous vesicles (30–150 nm) that are formed by the invagination and budding of endosomal multivesicular bodies from the membrane (Van Niel et al., 2006). These vesicles can serve as vehicles for transferring proteins, lipids, mRNA, and miRNA between cells. Intercellular communication involves the transfer of EVs and their functional biomolecular contents between cells and might be a prominent method by which  $\alpha$ -syn is transferred in PD.

The biogenesis of EVs depends on pathways that are either dependent or independent on endosomal sorting complexes required for transport (ESCRT) machinery [reviewed in Kowal et al. (2014)]. There are four neutral sphingomyelinase (nSMase) isoforms, nSMase1, nSMase2, nSMase3, and mitochondria-associated SMase, each encoded by the genes *SMPD* 2–5, respectively (Hofmann et al., 2000). However, nSMase2 is the most abundant sphingomyelinase isoform in the brain (Shamseddine et al., 2015). nSMase hydrolyzes sphingomyelin (SM), a type of sphingolipid, to produce ceramide (Cer), which forms EVs through the ESCRT-independent machinery pathway (Marsh and van Meer, 2008; Trajkovic et al., 2008). Although it was reported nearly half a century ago that SM accumulates in Lewy bodies (den Jager, 1969), little is known about how SM metabolism relates to the pathogenesis of PD. The importance of SM metabolism is supported by reports showing increased levels of Cer in the plasma of PD patients (Mielke et al., 2013; Xing et al., 2016; Savica et al., 2016). The regulation of Cer in the brains of PD patients seems more complex as both increased Cer levels in the visual cortex (Cheng et al., 2011) and decreased Cer levels in the anterior cingulate region (Abbott et al., 2014; Murphy et al., 2014) have been reported. The inhibition of nSMase2 has been shown to reduce the secretion of EVs [reviewed in Bienias et al. (2016)], but how nSMase2 influences PD pathogenesis in terms of protein accumulation and cell-to-cell transfer has not been studied so far.

Aging, which is associated with numerous changes in the brain, including alterations in enzymatic activities, lipid metabolism, and oxidative stress, is a major risk factor for neurodegenerative diseases such as PD (Anderton, 1997; Valli et al., 2015), and these alterations are known to induce  $\alpha$ -syn aggregation (Hashimoto et al., 1999; Scudamore et al., 2018). Oxidative stress can also cause the post-translational modification (PTM) of  $\alpha$ -syn, including modification by 4-hydroxy-2-nonenal (HNE), an end product of lipid peroxidation that promotes  $\alpha$ -syn oligomerization, aggregation, and cytotoxicity (Klucken et al., 2013). Furthermore, HNE PTMs have recently been reported to increase the secretion of EVs containing cytotoxic  $\alpha$ -syn (Zhang et al., 2018), and lipid vesicles affect the aggregation of HNE-modified  $\alpha$ -syn (Sardar Sinha et al., 2018). In addition, nSMase2 is sensitive to oxidative stress (Levy et al., 2006; Castillo et al., 2007) and has been shown to increase with age (Rutkute et al., 2007; Vozella et al., 2017).

This study investigated nSMase2 as a possible driving force for the progressive accumulation of  $\alpha$ -syn and its transfer between neuron-like cells. Since  $\alpha$ -syn PTMs can be induced by oxidative

stress (Duce et al., 2017), we investigated the influence of hypoxia on the SM–Cer pathway with regard to promoting  $\alpha$ -syn aggregation and transfer. For the first time, we showed that the inhibition of nSMase2 leads to a significant reduction in HNE-modified  $\alpha$ -syn aggregation and transfer between neuron-like cells. Hypoxia decreased nSMase2 protein levels but did not affect total EV abundance or alter the  $\alpha$ -syn transfer rate. These data provide evidence that SM metabolism may play a larger role in PD pathogenesis and support the need for additional investigations of sphingolipids in PD patients.

## MATERIALS AND METHODS

### Preparation of HNE- $\alpha$ -syn

For oligomerization, recombinant human  $\alpha$ -syn (AlexoTech) was prepared as previously described (Näsström et al., 2011; Domert et al., 2016; Sardar Sinha et al., 2018).  $\alpha$ -Syn was dissolved in 20 mM Tris-buffered saline (TBS) (pH 7.4), and 140  $\mu$ M  $\alpha$ -syn monomers were incubated with 2.8 mM HNE for 7 days at 37°C without agitation. After 7 days, the protein mixture was desalted by a Zeba desalt spin column (Thermo Scientific), equilibrated with Na<sub>2</sub>CO<sub>3</sub> (0.1 M, pH 8.5) and incubated with the fluorophore Alexa Fluor 700 (AF700) succinimidyl ester (final concentration of 1.58 mM, Life Technologies) for 1 h at room temperature with shaking.

Labeled HNE- $\alpha$ -syn was separated from free dye by size exclusion chromatography, which was also used to separate the labeled oligomers from the mixture. A Superose 6 PC 3.2/30 GL column (GE Healthcare) coupled to a liquid chromatography system (ÄKTA pure, GE Healthcare) was equilibrated with NH<sub>4</sub>HCO<sub>3</sub> (50 mM, pH 8.5), and 500  $\mu$ l of sample was injected into the column. To estimate the molecular weight of the  $\alpha$ -syn species, LMW gel filtration calibration kits (GE Healthcare) were used. Oligomeric and monomeric  $\alpha$ -syn species were eluted at a flow rate of 0.5 ml/min, collected, and lyophilized. The final pellet was resuspended in TBS buffer, and the protein concentration was determined using a Nanodrop (ND-1000 Spectrophotometer). The  $\alpha$ -syn used during the *in vitro* studies had a final concentration of 1  $\mu$ M and an incubation period of 3 h in serum-free culture media.

### Transmission Electron Microscopy

For transmission electron microscopy (TEM) analysis, 5  $\mu$ l of HNE-modified  $\alpha$ -syn was placed onto carbon-coated copper grids and incubated for 5–10 min. After removing the excess liquid, the grids were washed two times with deionized water prior to negative staining with 2% uranyl acetate for 30 s. The samples were analyzed with a JEM-1230-EX electron microscope (Jeol).

### Differentiation and 3D Coculture of SH-SY5Y Cells

Differentiation and coculture were performed as described previously, with minor modifications (Agholme et al., 2010; Nath et al., 2012; Domert et al., 2016; Sackmann et al., 2017).

All SH-SY5Y cells were cultured in complete culture media containing MEM-GlutaMAX (Gibco) supplemented with 10% fetal bovine serum (PAA Laboratories), 50 U/ml penicillin, 50  $\mu$ g/ml streptomycin, and 2 mM L-glutamine (all from Gibco) at 37°C with 5% CO<sub>2</sub>. Donor cells were differentiated with 10  $\mu$ M retinoic acid (RA; Sigma Aldrich) for 7 days and seeded at a density of 1400 cells/cm<sup>2</sup>. nSMase2 was inhibited in donor cells, as described below, and the cells were then treated with  $\alpha$ -syn, where applicable. For the coculture experiments, SH-SY5Y cells that stably expressed  $\beta$ -actin-GFP (Addgene plasmid #21948, provided by Ryohei Yasuda) were used to distinguish the recipient cells from the donor cells. Recipient cells were prepared by seeding RA-differentiated GFP cells at a density of 1700 cells/cm<sup>2</sup> and allowing them to further differentiate for 10 days in a 20% Extracellular Matrix (ECM) Gel coating (Corning) with a growth factor cocktail in serum-free culture media [50 ng/ml brain-derived neurotrophic factor (PeproTech), 10 ng/ml neuregulin  $\beta$ 1 (R&D Systems), 10 ng/ml nerve growth factor (R&D Systems), and 24 nM vitamin D<sub>3</sub> (Sigma-Aldrich)]. Finally, coculture was carried out by trypsinizing the donor cells, placing them on top of the recipient cells, and incubating the coculture for 24 h at 37°C to allow the formation of synaptic-like connections. A graphical schematic of the experimental setup is presented in **Figure 1**.

## siRNA Transfection

Donor cells were seeded 24 h before transfection. Small interfering RNA (siRNA) transfection was performed by targeting nSMase2 (*SMPD3* gene) with siRNA or negative control (All Stars Negative Control siRNA) using HiPerFect Transfection Reagent (all from Qiagen), according to the

manufacturer's instructions. A siRNA concentration of 20 nmol/L in Opti-MEM + GlutaMAX (Gibco) media was used for transfection, and the transfection period was 6 h, after which the transfection media was removed and the cells were incubated in serum-free culture media for an additional 42 h before the addition of  $\alpha$ -syn, where applicable. The selected predesigned FlexiTube siRNA target sequence was *SMPD3*, 5'-CACGAACGGCCTGTACGATGA-3'. Knockdown was verified by immunoblotting and RT-PCR, and a downregulation of 70% was considered sufficient.

## CRISPR/Cas9 Cells

CRISPR/Cas9 targets were designed against the *SMPD3* gene (Ensembl ENSG00000103056) using the software available on Benchling (Benchling Inc.). A guide RNA (gRNA) targeting exon 3, the first coding exon, was constructed using the gRNA sequence 5'-CATGGTCGAAGGCCTCGTCG-3', resulting in a truncated nSMase2 protein. The locus targeted by the gRNA occurs upstream of the nSMase2 catalytic domain, specifically residues D430 and K435, which are responsible for SM hydrolysis (Airolo et al., 2017). CRISPR/Cas9 plasmid design and assembly were performed according to the instructions of Ran et al. (Ran et al., 2013) using the plasmid pSpCas9(BB)-2A-GFP (PX458) (Addgene plasmid #48138, provided by Feng Zhang). Wild-type (WT) SH-SY5Y cells were transfected and single-cell sorted, and clonal cell lines were screened for anticipated changes to nSMase2 protein expression by Western blot and immunocytochemistry. As predicted, the selected clone was undetectable by nSMase2 antibodies (**Supplementary Figure S1**). The selected nSMase2 knockout (KO) clone was used in subsequent studies for differentiating cells into donor cells, as described above.

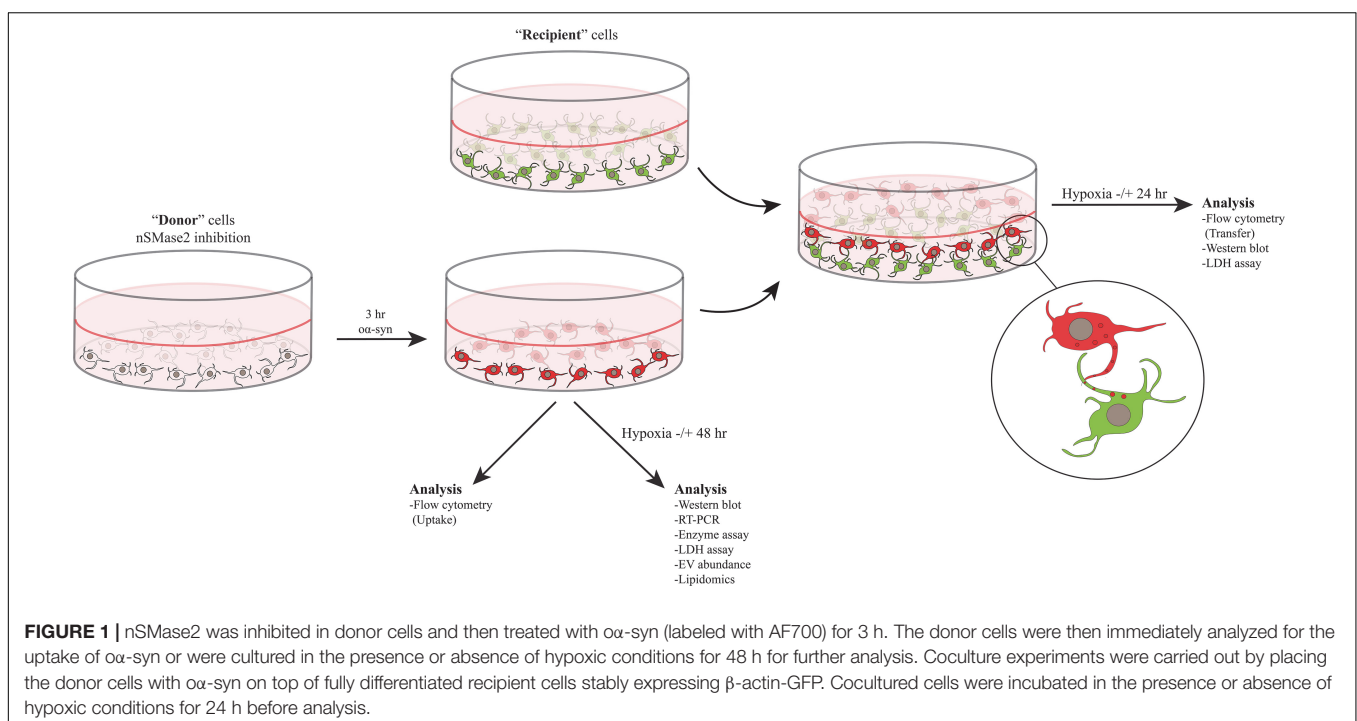


**FIGURE 1 |** nSMase2 was inhibited in donor cells and then treated with  $\alpha$ -syn (labeled with AF700) for 3 h. The donor cells were then immediately analyzed for the uptake of  $\alpha$ -syn or were cultured in the presence or absence of hypoxic conditions for 48 h for further analysis. Coculture experiments were carried out by placing the donor cells with  $\alpha$ -syn on top of fully differentiated recipient cells stably expressing  $\beta$ -actin-GFP. Cocultured cells were incubated in the presence or absence of hypoxic conditions for 24 h before analysis.

## Cambinol Treatment

Cambinol [5-(2-hydroxynaphthalen-1-ylmethyl)-6-phenyl-2-thioxo-2,3-dihydro-1H-pyrimidin-4-one; Sigma-Aldrich], a pharmaceutical inhibitor of nSMase2 (Figuera-Losada et al., 2015), was prepared at a stock concentration of 20 mM in DMSO and added to donor cells at a final concentration of 10  $\mu$ M for 48 h in serum-free culture media.

## Hypoxic Exposure

To produce oxidative stress, the cells were incubated in a hypoxic incubator set to 1% O<sub>2</sub>. For experiments analyzing donor cells alone, the cells were incubated for 48 h following siRNA transfection and/or  $\alpha$ -syn treatment. For coculture experiments, the cells were exposed to hypoxic conditions for 24 h after the establishment of the coculture.

## Western Blot

Cells were lysed with Tris-HCl (0.5 M, pH 6.8), 10% glycerol, and 2% SDS. For each sample, 20  $\mu$ g of protein and 0.1 M DTT was loaded on a 4–20% SDS ClearPAGE gel. EVs (isolated as described below) were lysed in RIPA buffer [50 mM Tris-HCl, 150 mM NaCl, 1% Triton X-100, 0.5% sodium deoxycholate, 0.1% SDS, 40  $\mu$ l/ml PhosSTOP (Roche) phosphatase inhibitor, and 10  $\mu$ l/ml Halt protease inhibitor (Thermo Fisher)] followed by vigorous vortexing. EV lysates were mixed with 4  $\times$  Laemmli loading buffer and DTT and loaded onto a 4–20% SDS ClearPAGE gel. The proteins were transferred onto nitrocellulose membranes (Invitrogen). The blots were incubated with the following antibodies, as indicated: mouse anti- $\beta$ -actin (1:10,000, A5441, Sigma-Aldrich), rabbit anti-nSMase2 (1:1,000, PA5-49140, Thermo Fisher), rabbit anti- $\alpha$ -syn (1:1,000, 701085, Invitrogen), mouse anti-pS129 (1:1000, 015-25191, Wako), and mouse anti-flotillin-1 (1:1,000, 610820, BD Transduction Laboratories). Goat anti-mouse HRP or goat anti-rabbit HRP (Dako) were used at a 1:2,000 dilution as a secondary antibody. The blots were visualized using Clarity ECL (BioRad) on a ChemiDoc MP imaging system (BioRad) and analyzed by ImageJ software.

## Semiquantitative RT-PCR

Total RNA was isolated using the RNeasy Mini Kit (Qiagen) and converted to cDNA using a High Capacity RNA to cDNA kit (ThermoFisher) following the manufacturer's instructions. Semiquantitative real-time PCR (RT-PCR) was performed using the TaqMan Gene Expression Kit and with FAM/MGB probes [SMPD3: Hs00920354\_m1; SMPD2: Hs00906924\_g1; SMPD1: Hs04183448\_m1; TSG101: Hs01121709\_m1; HGS: Hs00610371\_m1; STAM: Hs00989740\_m1; VPS4A: Hs00203085\_m1; CHMP4A: Hs00204331\_m1; ALIX (PDCD6IP): Hs00994346\_m1; FLOT2: Hs01080468\_g1; PLD2: Hs01093216\_m1; CD81: Hs01002167\_m1; SNCA: Hs01103383\_m1;  $\beta$ -actin (ACTB): Hs01060665\_g1; all from Applied Biosystems]. Reactions were carried out in triplicate using a 7500 Fast Real-Time PCR system (Applied Biosystems). The data were analyzed according to the comparative Ct method to determine the fold

change in the expression levels relative to the control samples, and statistics were performed on the  $\Delta\Delta C_t$  values.

## Flow Cytometry

$\alpha$ -syn uptake and transfer were quantified by flow cytometry. Cocultured cells were recovered from the ECM gel using Corning Recovery Solution (Corning) according to the manufacturer's instructions, while donor cells used to determine the uptake of  $\alpha$ -syn were trypsinized for 1 min. The cells were then resuspended in PBS and filtered through CellTrics 30- $\mu$ m filters (Sysmex), subsequently analyzed using a Beckman Coulter Gallios and analyzed with Kaluza 1.3 software. For transfer, forward and side scatter were gated to identify the cell population. WT and GFP-only controls were used to identify gating for AF700- and GFP-negative cells, and recipient cells with no transfer. Positive transfer was identified with double fluorescence. The ratio of transfer was normalized to the percentage of double fluorescent cells in the control coculture. The ratio of uptake was normalized to the percentage of AF700 cells, as this was performed in WT cells.

## Immunocytochemistry

Cells used for imaging were seeded on top of glass coverslips, fixed with 4% PFA in PBS, and permeabilized with incubation buffer (0.1% saponin and 5% FBS) for 20 min at room temperature. The cells were incubated with primary antibodies against C-terminal nSMase2 (PA5-49140, ThermoFisher) or N-terminal nSMase2 (SP4061, ECM BioSciences) at 1:500 in incubation buffer overnight at 4°C. This was followed by washing and incubation with Alexa Fluor 488 goat anti-rabbit (1:400; Life Technology) for 75 min at room temperature. After washing in PBS, the slides were mounted with ProLong containing DAPI (ThermoFisher). Images were acquired with a Zeiss LSM 700 inverted confocal microscope using a 20  $\times$  objective lens.

## LDH Toxicity Assay

Cytotoxicity was determined by the presence of lactate dehydrogenase (LDH) according to the manufacturer's instructions (Pierce) and analyzed at 490 nm and 650 nm using a VersaMax ELISA plate reader.

## nSMase Enzyme Activity Assay

nSMase enzymatic activity was determined using the nSMase assay kit from Echelon Biosciences following the manufacturer's instructions. Donor cells were harvested and washed with PBS; resuspended and lysed in 25 mM Tris-HCl, 150 mM NaCl, and 1% Triton X-100 (pH 7.4) and centrifuged at 10,000  $\times$  g for 10 min to remove cell debris. A sample volume of 50  $\mu$ l was mixed with reaction buffer, incubated for 4 h at 37°C, and analyzed by a Spark 10 M multimode microplate reader (Tecan Trading AG).

## Sphingolipid Analysis

For sphingolipid analysis, donor cells were extracted using butanol/methanol (BUME) as previously described (Löfgren et al., 2012). Internal standards [SM 12:0, Cer 17:0, glucosylceramide (GlcCer) 17:0 and lactosylceramide (LacCer)



17:0] were added during the extraction. Prior to analysis, the total extract was exposed to alkaline hydrolysis (0.1 M KOH in methanol) to remove phospholipids that could potentially cause ion suppression effects. The analysis of SM was performed using direct infusion on a QTRAP 5500 mass spectrometer (Sciex) equipped with a robotic nanoflow ion source, the TriVersa NanoMate (Advion BioSciences). Detection was achieved with precursor ion scanning in positive mode using  $m/z$  184 (phosphocholine) as a fragment ion (Brugger et al., 1997). The analysis of sphingolipids was performed using UPLC-MS/MS in positive mode, as previously described (Amrutkar et al., 2015). The BioRad BCA kit was used to determine the total cell protein concentration prior to hydrolysis.

## EV Isolation

Conditioned medium from 20 million donor cells was collected 48 h after  $\alpha$ -syn treatment under normoxic or hypoxic conditions. EVs were isolated by differential ultracentrifugation. The conditioned media was spun at  $2,000 \times g$  for 10 min to remove cells and cell debris, and the supernatant was spun at  $10,000 \times g$  for 30 min and  $100,000 \times g$  for 70 min. The EV pellet was washed with PBS and spun again at  $100,000 \times g$  for 70 min. The final EV pellet was resuspended in 75  $\mu$ l of PBS for quantification by FluoroCet, 100  $\mu$ l of PBS for nanoparticle tracking analysis (NTA), or 20  $\mu$ l of RIPA buffer for immunoblotting and stored at  $-80^\circ\text{C}$ . The EV size distribution was measured by NTA using the NanoSight NS300 system (Malvern Instruments).

## EV Abundance by FluoroCet

The FluoroCet quantitation kit (SBI) is designed to directly measure acetylcholinesterase (AChE) activity inside of EVs. After EVs were isolated as described above, the assay was performed following the manufacturer's instructions. The fluorometric assay was read at an excitation/emission of 530/590 nm using a Spark 10M multimode microplate reader.

## Statistical Analysis

The results are presented as the mean  $\pm$  standard error of the mean (SEM). The statistical significance was analyzed with GraphPad Prism 6 software using Student's  $t$  test for all experiments with the exception of lipidomic and RT-PCR analysis, which were completed using one-way ANOVA with Dunnett's multiple comparison test. Statistical significance was established at  $p \leq 0.05$ .

# RESULTS

## Inhibition of nSMase2 and Hypoxia

Parkinson's disease is a common neurodegenerative disease that is characterized by chronic oxidative stress in the brain (Blesa et al., 2015); however, to our knowledge, there are no previous studies investigating nSMase2 activation during hypoxia in human neurons. As the main model for this study, nSMase2 was knocked down in donor cells by either siRNA transfection in SH-SY5Y cells or by the generation of nSMase2 KO SH-SY5Y

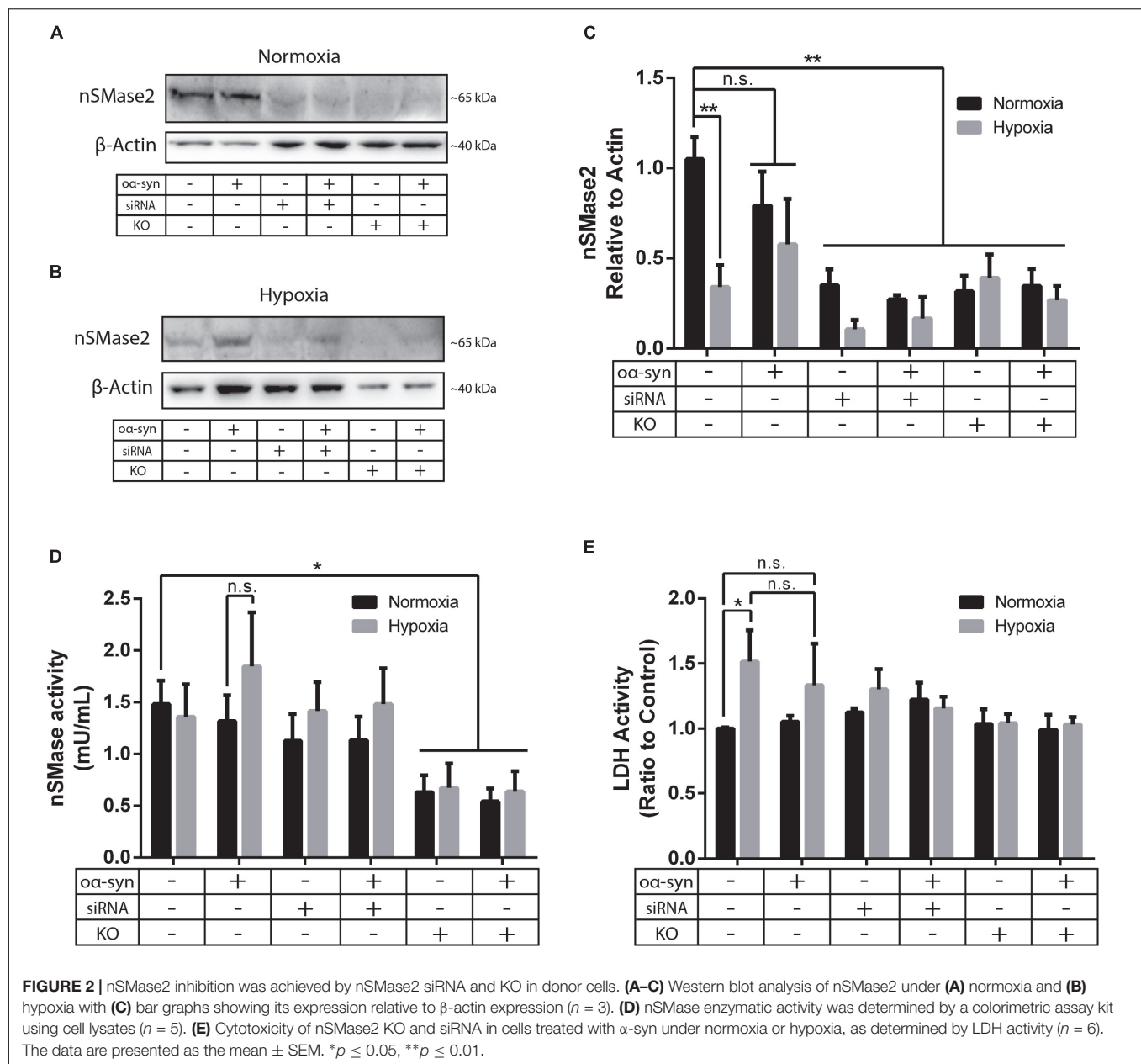
cells using CRISPR/Cas9. The loss of nSMase2 protein expression in nSMase2 KO cells was confirmed by immunoblotting and immunocytochemistry with N- and C-terminal specific antibodies (Figures 2A–C and Supplementary Figure S1), while siRNA treatment induced both a significant reduction in protein expression and gene downregulation (Figures 2A–C, 3). nSMase enzymatic activity was significantly decreased in KO cells ( $0.63 \pm 0.16$  mU/ml) compared to control cells ( $1.48 \pm 0.23$  mU/ml) (Figure 2D). However, siRNA-treated cells ( $1.13 \pm 0.25$  mU/ml) were not significantly modified, although it is possible that other nSMases are compensating from the acute transfection and are being detected in the assay. Based on these results, we established two different models of nSMase2 inhibition, specifically siRNA-treated cells with a reduction in total nSMase2 protein expression and KO cells with a reduction in total functional enzymatic protein levels.

As a model of oxidative stress, we exposed donor cells to hypoxic conditions of 1%  $\text{O}_2$  for 48 h. Hypoxia significantly reduced nSMase2 protein expression (Figures 2B,C), but nSMase enzymatic activity was not affected (Figure 2D). Compared to normoxia, hypoxia induced cell toxicity, which was completely mitigated by nSMase2 inhibition (Figure 2E), suggesting that a protective mechanism is in play when nSMase2 is reduced.

## nSMase2 Inhibition Prevents $\alpha$ -syn Aggregation

Next, we investigated the effect of nSMase2 inhibition on the aggregation of  $\alpha$ -syn, which was modified by the lipid peroxidation product HNE. The elevation of HNE has been observed in the brain during normal aging and is more pronounced in brain areas affected by PD pathology (Yoritaka et al., 1996; Castellani et al., 2002). PTMs caused by HNE contribute to the increased conversion of soluble  $\alpha$ -syn monomers into cytotoxic oligomers, as well as increased  $\alpha$ -syn secretion from cells (Näsström et al., 2011; Bae et al., 2013). Monomers of  $\alpha$ -syn were aggregated in the presence of HNE to produce  $\alpha$ -syn. Size exclusion chromatography was performed to characterize and purify  $\alpha$ -syn, which corresponded to an elution peak with a molecular weight of  $\sim 2000$  kDa (Supplementary Figure S2), as described previously (Sardar Sinha et al., 2018). The ultrastructural analysis of the oligomers showed a heterogeneous population of spherical, curvilinear, and ring-like structures (Supplementary Figure S2), as expected (Näsström et al., 2011; Sardar Sinha et al., 2018). Based on previous results from our lab (Domert et al., 2016; Reyes et al., 2019), donor cells were incubated with 1  $\mu$ M  $\alpha$ -syn for 3 h and analyzed after 48 h. The addition of  $\alpha$ -syn did not contribute to any changes in nSMase2 protein or gene expression under hypoxia or normoxia (Figures 2C, 3). The combination of hypoxia and  $\alpha$ -syn slightly increased nSMase enzymatic activity ( $1.85 \pm 0.52$  mU/ml vs. control  $1.48 \pm 0.23$  mU/ml), although this was not statistically significant (Figure 2D;  $p = 0.53$ ). In addition,  $\alpha$ -syn did not increase hypoxia-induced cytotoxicity (Figure 2E). However, the addition of  $\alpha$ -syn resulted in the significant aggregation of high molecular weight (MW)  $\alpha$ -syn (25–250 kDa) under both normoxic and hypoxic conditions,



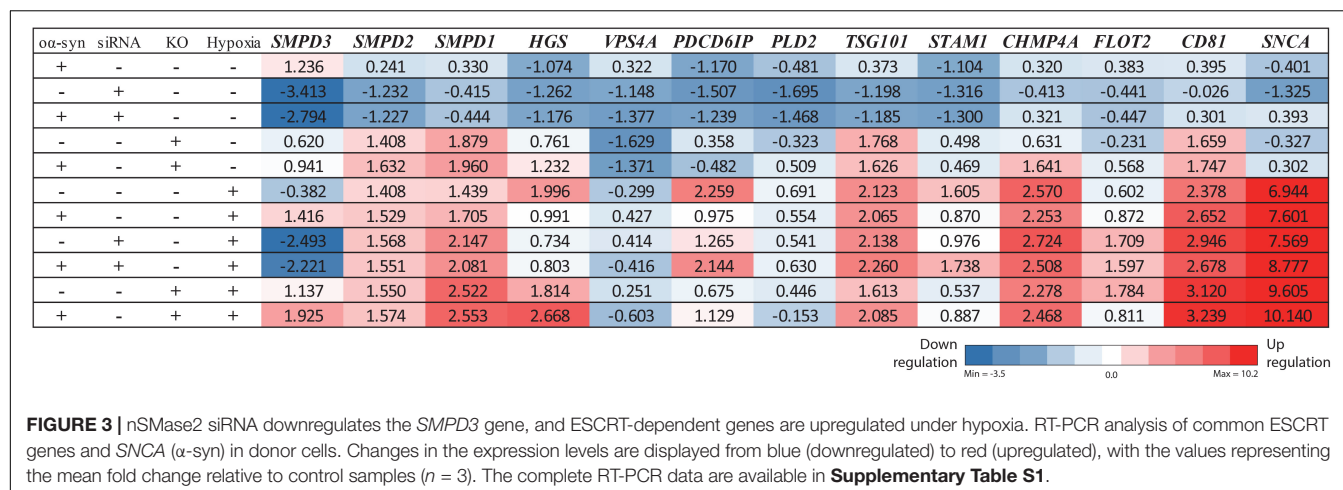


an effect that was significantly decreased in KO cells, even under hypoxic conditions (Figures 4A–C). A similar, but non-significant, decrease was also observed in cells subjected to siRNA. Monomeric ( $\sim 15$  kDa)  $\alpha$ -syn levels were not affected by any treatment, despite an increase in SNCA mRNA expression under hypoxia (Figures 3, 4D). Together, these data indicate that nSMase2 may impede the breakdown of aggregated high-molecular-weight  $\alpha$ -syn, both under normoxia and hypoxia.

## Hypoxia Promotes Longer Acyl Chain Lengths

As there have been conflicting results regarding sphingolipids in PD brains (Cheng et al., 2011; Fabelo and Martin, 2011;

Abbott et al., 2014; Murphy et al., 2014; Gegg et al., 2015; Bienias et al., 2016), we wanted to investigate whether inhibiting nSMase2 affects the lipid composition of sphingolipids after the addition of  $\alpha$ -syn in the absence or presence of hypoxia using UPLC-MS/MS. Hypoxia alone caused a significant decrease in SM ( $2.7 \pm 0.1$  pmol/mg vs. control  $4.1 \pm 0.6$  pmol/mg) and a decrease in Cer, although not significant ( $198.0 \pm 6.8$  pmol/mg vs. control  $300.1 \pm 35.7$  pmol/mg;  $p = 0.063$ ) (Figures 5A,B). The inhibition of nSMase2 alone, either by siRNA or KO, did not cause significant differences in total SM or Cer. In siRNA-treated cells, the combined treatment of  $\alpha$ -syn and hypoxia caused a significant reduction in total Cer when compared to the normoxic control ( $185.0 \pm 3.3$  pmol/mg vs. control  $300 \pm 35.7$  pmol/mg) (Figure 5B). Cer can also be synthesized by several other lipids,



such as dihydroceramide (DHCer), which is converted to Cer through *de novo* synthesis and is associated with slow cell proliferation and cell death [reviewed in Siddique et al. (2015)]. Interestingly, DHCer was significantly increased by hypoxia ( $38.88 \pm 1.77$  pmol/mg vs. control  $4.50 \pm 0.54$  pmol/mg), and the effect was mitigated by siRNA or  $\alpha$ -syn treatment but not by KO (**Figure 5C**). GlcCer, which can also be broken down into Cer, was not significantly dysregulated in any of the treatment groups (**Figure 5D**).

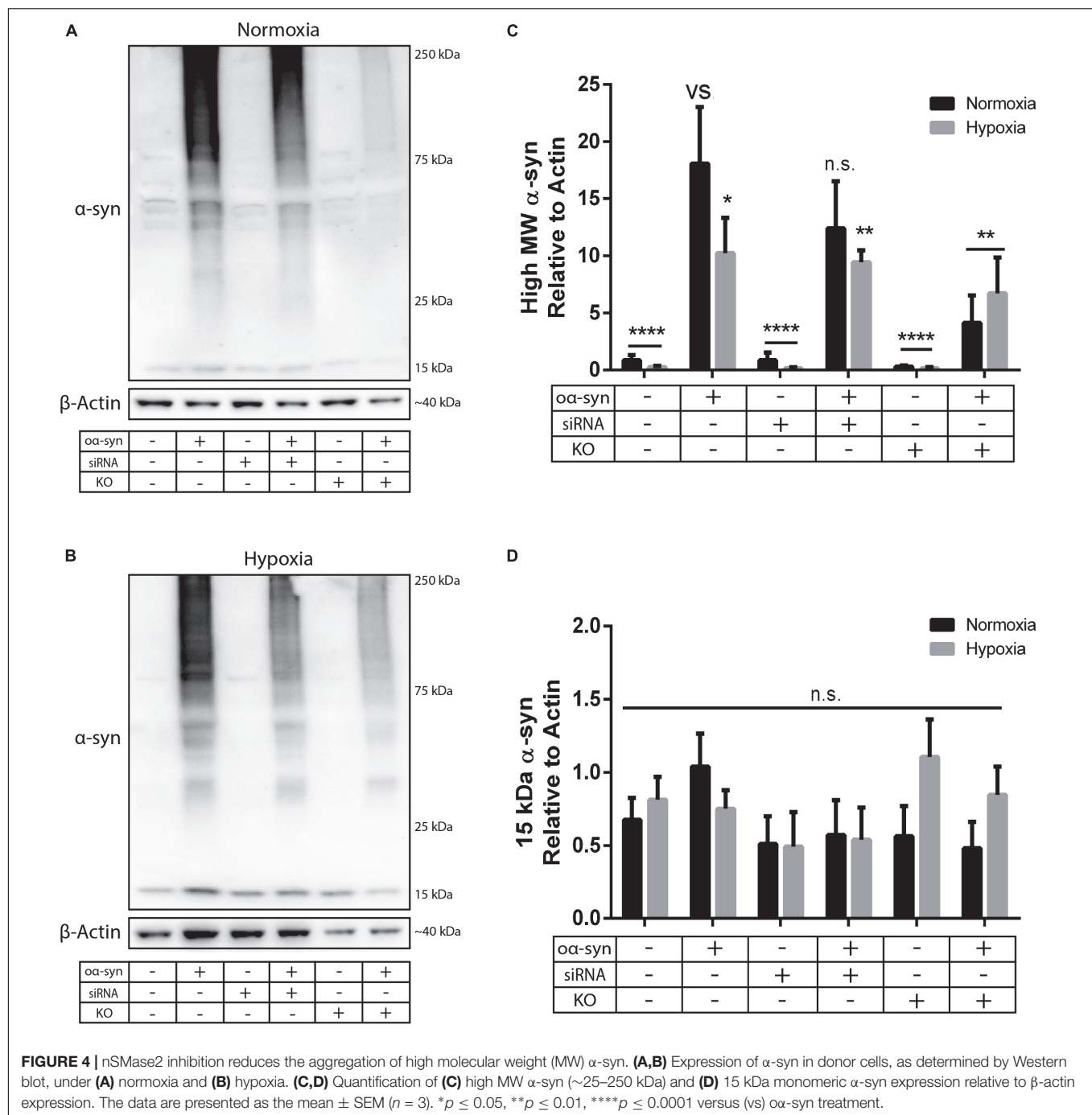
Cer acyl chain composition has been shown to shift toward shorter acyl chain lengths (C16–C20) in the anterior cingulate cortex in PD patients (Cheng et al., 2011; Abbott et al., 2014), while there is an increase in long-chain SM and Cer (C21–C24) in the visual cortex (Cheng et al., 2011). siRNA treatment resulted in an increased relative percentage of SM 16:0 ( $49.5 \pm 0.6\%$ ) and a decreased percentage of SM 24:0 ( $1.3 \pm 0.2\%$ ), while nSMase2 KO decreased the percentage of SM 24:1 ( $14.5 \pm 0.1\%$ ) relative to that in the control [SM 16:0 ( $46.4 \pm 0.6\%$ ), SM 24:0 ( $2.3 \pm 0.1\%$ ), and SM 24:1 ( $15.0 \pm 0.5\%$ )] (**Figure 5E**).  $\alpha$ -syn alone did not significantly change the sphingolipid composition, but nSMase2 KO combined with  $\alpha$ -syn treatment, for example, caused an increase in the percentage of dhSM 16:0 ( $2.6 \pm 0.1\%$ ) and Cer 24:1 ( $23.4 \pm 1.8\%$ ) compared to those in the control [dhSM 16:0 ( $0.5 \pm 0.1\%$ ) and Cer 24:1 ( $28.1 \pm 2.3\%$ )] (**Figures 5E,F**). Hypoxia alone caused a significant reduction in short acyl chain lengths [SM 16:0 ( $34.6 \pm 0.7\%$ ), Cer 16:0 ( $37.3 \pm 1.0\%$ ), DHCer 16:0 ( $26.7 \pm 1.0\%$ ), and GlcCer 16:0 ( $25.9 \pm 1.7\%$ )] relative to those in the control [SM 16:0 ( $46.4 \pm 0.6\%$ ), Cer 16:0 ( $48.1 \pm 2.5\%$ ), DHCer 16:0 ( $45.5 \pm 1.3\%$ ), and GlcCer 16:0 ( $34.0 \pm 2.8\%$ )] (**Figures 5E–H**). Consequently, hypoxic conditions alone also promoted longer acyl chain lengths [SM 24:0 ( $8.7 \pm 0.5\%$ ), Cer 24:1 ( $33.1 \pm 0.9\%$ ), DHCer 24:1 ( $38.6 \pm 1.4\%$ ), and GlcCer 22:0 ( $20.6 \pm 1.1\%$ )] relative to those in the control [SM 24:0 ( $2.3 \pm 0.1\%$ ), Cer 24:1 ( $28.1 \pm 2.3\%$ ), DHCer 24:1 ( $20.0 \pm 0.7\%$ ), and GlcCer 22:0 ( $15.2 \pm 0.6\%$ )] (**Figures 5E–H**). KO and siRNA treatment, as well as  $\alpha$ -syn treatment, contributed to a shift of acyl chain length to shorter chains under hypoxia. Collectively, these data show that nSMase2 inhibition in combination with  $\alpha$ -syn alleviates the lipid shifts that are associated with hypoxic

conditions. The complete lipidomic analysis can be found in **Supplementary Table S2**.

## Transfer of $\alpha$ -syn Is Reduced by Inhibiting nSMase2

Due to the importance of nSMase2 in generating EVs through the ESCRT-independent pathway, we next investigated whether the inhibition of nSMase2 affects EV production and its effect on the transmissibility of  $\alpha$ -syn between neuron-like cells. First, we investigated whether  $\alpha$ -syn is found in the EVs. Conditioned media was collected from donor cells 48 h after  $\alpha$ -syn treatment, and EVs were isolated by step-gradient ultracentrifugation. The homogeneity of the EV pellets was confirmed by NTA, which showed a population of enriched vesicles with a mode diameter of  $71.61 \pm 4.93$  nm (**Supplementary Figure 3A**). Immunoblotting was used to confirm that the EV pellets were enriched with flotillin-1, a common EV marker, and contained  $\alpha$ -syn (**Supplementary Figure 3B**). For coculture experiments, cambinol, a commercially available nSMase2 inhibitor (Figuera-Losada et al., 2015), was also used to confirm our findings pharmacologically. EV abundance was quantified by directly measuring AChE activity, which is proportional to EV quantity (Savina et al., 2002; Gupta and Knowlton, 2007). After  $\alpha$ -syn treatment, nSMase2 KO, as well as cambinol treatment, resulted in significantly decreased AChE activity, while siRNA treatment reduced AChE activity, although not significantly ( $p = 0.11$ ) (**Figure 6A**). Hypoxia did not alter the level of AChE activity regardless of whether nSMase2 was knocked out, likely due to the compensation of related ESCRT-related genes (*TSG101*, *CHMP4A*, and *CD81*), which were shown to be upregulated in response to hypoxia (**Figure 3**).

Since we were able to determine that  $\alpha$ -syn is present in EVs and that nSMase2 reduction also reduced the number of EVs, we aimed to determine if the reduction in EVs also reduces the transfer of  $\alpha$ -syn between neuron-like cells. First, we evaluated whether inhibiting nSMase2 in donor cells impairs  $\alpha$ -syn uptake by analyzing the percentage of cells that take up fluorescently labeled  $\alpha$ -syn using flow cytometry. A reduction in nSMase2



by KO, siRNA, or cambinol did not alter the number of donor cells that readily took up the free  $\alpha$ -syn during the 3 h treatment (**Figure 6B**). Next, using our well-established donor/recipient coculture model (Agholme et al., 2010; Nath et al., 2012; Domert et al., 2016; Sackmann et al., 2017),  $\alpha$ -syn-loaded donor cells, in which nSMase2 was inhibited, were cocultured onto highly differentiated recipient cells for 24 h and analyzed by flow cytometry. All treatments that inhibited nSMase2 reduced the transfer of  $\alpha$ -syn between donor and recipient cells; KO cells exhibited a reduction of  $31 \pm 5\%$ , siRNA-treated cells exhibited

a reduction of  $57 \pm 6\%$ , and cambinol-treated cells exhibited a reduction of  $50 \pm 9\%$  (**Figure 6C**). Hypoxia did not alter the amount of  $\alpha$ -syn transfer between cells, nor did it influence  $\alpha$ -syn transfer in the nSMase2 KO lineage; the rates of transfer among KO cells and KO cells exposed to hypoxia were not significantly different.

Cocultured cells were vulnerable to hypoxia-induced toxicity (**Figure 6D**), which caused technical limitations for analyzing donor and recipient cells separately. Hypoxia-exposed cells exhibited an increase in monomeric  $\alpha$ -syn compared to that in

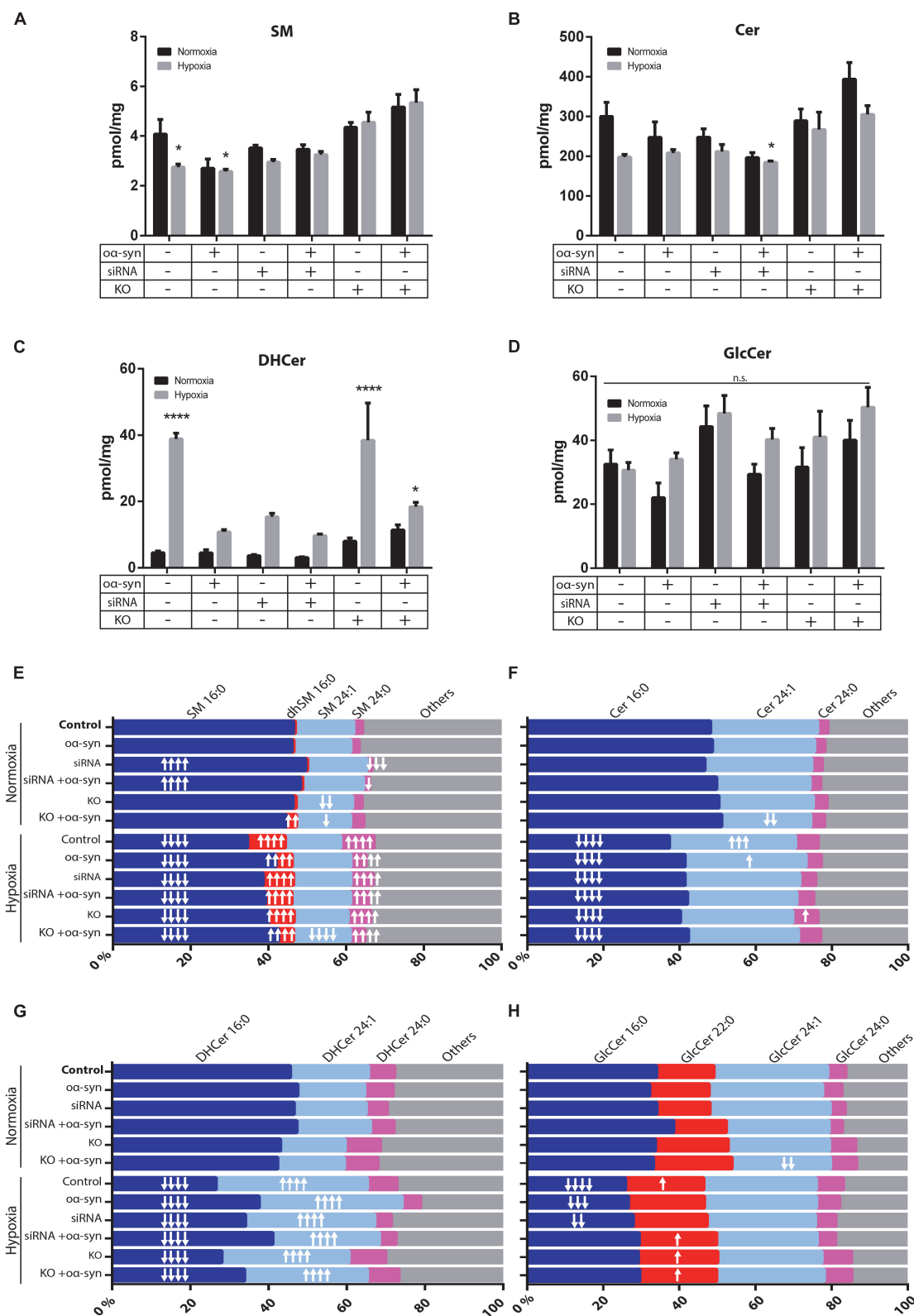


**FIGURE 5 |** nSMase2 inhibition and  $\alpha$ -syn alleviates acyl chain shift due to hypoxia. **(A–D)** Lipid extraction and UPLC-MS/MS analysis of **(A)** sphingomyelin (SM), **(B)** ceramide (Cer), **(C)** dihydroceramide (DHCer), and **(D)** glucosylceramide (GlcCer) in donor cells. The data are presented as the mean  $\pm$  SEM ( $n = 4$ ). \* $p \leq 0.05$ , \*\*\*\* $p \leq 0.0001$  relative to the normoxic control. **(E–H)** For acyl chain length alterations, the data are presented as the mole percentage of **(E)** SM, **(F)** Cer, **(G)** DHCer, and **(H)** GlcCer. (Continued)



**FIGURE 5 | Continued**

**(G)** DHCer, and **(H)** GlcCer relative to all acyl chains. Short chains are considered C16–C20, and long chains are considered C21–C24. “↑” denotes an increase and “↓” denotes a decrease, with  $\uparrow p \leq 0.05$ ,  $\uparrow\uparrow p \leq 0.01$ ,  $\uparrow\uparrow\uparrow p \leq 0.001$ , and  $\uparrow\uparrow\uparrow\uparrow p \leq 0.0001$  relative to the normoxic control with respective direction. Detailed lipid information is provided in **Supplementary Table S2**.

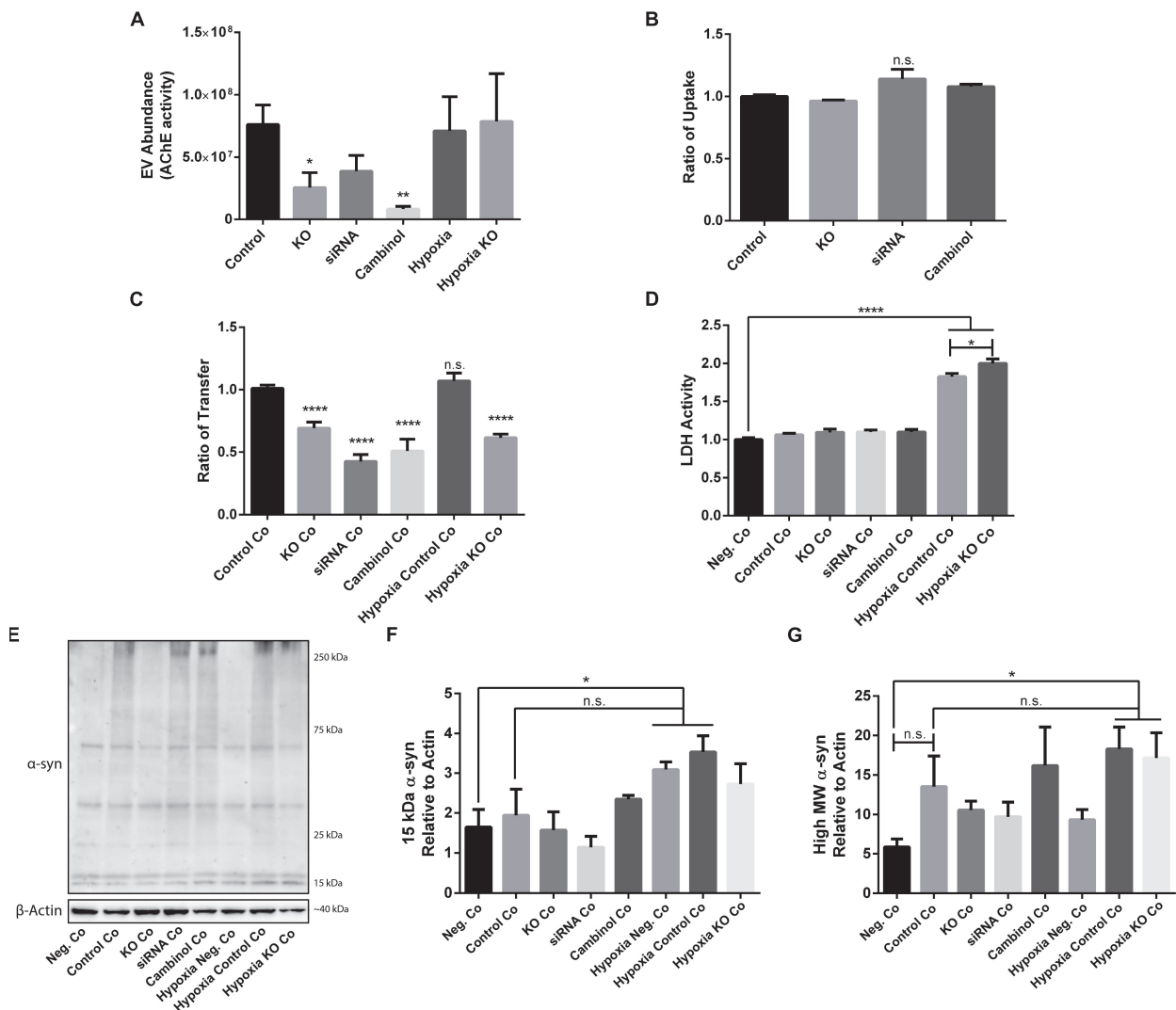


**FIGURE 6 |** nSMase2 expression is a critical component in the transmission of  $\alpha$ -syn between neuron-like cells. **(A)** EV abundance, as measured by the acetylcholinesterase (AChE) activity, of EVs isolated from donor cells treated with  $\alpha$ -syn ( $n = 4$ ). **(B,C)** Flow cytometry analysis of the  $\alpha$ -syn **(B)** ratio of uptake in donor cells and **(C)** ratio of transfer to recipient cells after 24 h of coculture (Co) ( $n = 6$ ). The provided ratios are relative to WT SH-SY5Y uptake and transfer, where the control = 1.0. **(D)** LDH assay demonstrating cytotoxicity after 24 h of coculture ( $n = 6$ ). **(E–G)** Western blot analysis of **(E)**  $\alpha$ -syn after 24 h of coculture and quantifications demonstrating the expression of **(F)** 15-kDa monomeric  $\alpha$ -syn and **(G)** high MW  $\alpha$ -syn (~25–250 kDa) relative to that of  $\beta$ -actin. The data are presented as the mean  $\pm$  SEM relative to the control ( $n = 3$ ). \* $p \leq 0.05$ , \*\* $p \leq 0.01$ , \*\*\* $p \leq 0.0001$ .

negative cocultures, but this increase was not significant when compared to control cocultures (**Figures 6E,F**). A similar effect was observed for high MW  $\alpha$ -syn (**Figures 6E,G**). nSMase2 KO did not provide any protection against hypoxia-induced cytotoxicity in cocultures; in fact, nSMase2 KO cocultures resulted in an increase in cell death compared to hypoxia-exposed cocultures (**Figure 6D**). nSMase2 KO cocultures displayed a minor reduction in monomeric and high MW  $\alpha$ -syn in the

presence and absence of hypoxia compared to that in control cocultures, although these differences were not significant (**Figures 6E–G**). Studies have shown that the phosphorylation of  $\alpha$ -syn at serine 129 (pS129) is a disease-specific modification found in Lewy bodies (Fujiwara et al., 2002) and that oxidative stress induces  $\alpha$ -syn pS129 (Takahashi et al., 2007). Our model showed a trend toward increased pS129 under hypoxic conditions; however, this increase did not achieve statistical

significance (**Supplementary Figure S4**). Taken together, these data indicate that  $\alpha$ -syn can be readily detected in EVs and that the depletion of the ESCRT-independent related protein nSMase2 causes a substantial reduction in protein propagation between cells. By reducing the production of EVs, we showed that  $\alpha$ -syn transmission was halved even when some EV production persisted. This alludes to the notion that, although other mechanisms of transfer are likely also at play, the cell-to-cell transfer of  $\alpha$ -syn relies heavily upon EVs produced through the ESCRT-independent pathway.

## DISCUSSION

This study is the first to investigate whether the inhibition of nSMase2 reduces the transfer of  $\alpha$ -syn between neuron-like cells. Furthermore, we also examined whether hypoxia contributes to  $\alpha$ -syn propagation in this system. Small EVs, such as exosomes, appear to play an important role in several pathological and physiological processes. EVs mediate the intercellular transfer of cell signaling products, and these particles can carry large aggregated proteins, including  $\alpha$ -syn (Alvarez-Erviti et al., 2011; Danzer et al., 2012; Delenclos et al., 2017). Additionally, exosomal  $\alpha$ -syn has been shown to be taken up more readily than free  $\alpha$ -syn (Danzer et al., 2012), with recent studies showing that exosomal  $\alpha$ -syn is found in the CSF (Stuendl et al., 2016) and plasma (Shi et al., 2014) of PD patients, further emphasizing the importance of these vesicles in the pathogenic propagation of  $\alpha$ -syn. EVs can be formed through different pathways; however, it is still unclear if these pathways produce distinct populations of EVs and if they depend on context-specific regulation [reviewed in Juan and F  rthauer (2018)]. One of the major pathways by which EVs are created involves the phosphodiesterase enzyme nSMase2, which hydrolyses SM to produce Cer and forms EVs through the ESCRT-independent pathway (Marsh and van Meer, 2008). Several studies have investigated SM metabolism in Alzheimer's disease [reviewed in Bienias et al. (2016)], and one of these studies found that inhibiting nSMase2 in APP/PS1 mice leads to a reduction in the number of EVs in the brain and serum, a reduction in amyloid- $\beta$ -42 concentration in plaques, and decreased levels of most Cer species in the serum (Dinkins et al., 2014). Furthermore, it has been shown that inhibiting nSMase2 prevents prion packaging by blocking EV formation (Guo et al., 2015), which is of particular interest given the evidence that misfolded  $\alpha$ -syn propagates in a prion-like manner (Luk et al., 2012). Until now, there has been a lack of knowledge in this area regarding PD. Our results showed that inhibiting nSMase2 reduces the amount of high MW  $\alpha$ -syn, indicating that nSMase2 is involved in promoting the fibrilization of  $\alpha$ -syn or preventing its clearance. Furthermore, inhibiting nSMase2 significantly reduced the amount of  $\alpha$ -syn that was transferred to recipient cells by 31–57%. This effect depends on the transfer mechanisms of the donor cell, not a failure to internalize exogenous  $\alpha$ -syn, as nSMase2 inhibition did not affect the uptake of  $\alpha$ -syn.

Oxidative stress is thought to be an underlying mechanism that leads to cellular dysfunction in PD patients [reviewed in

Hwang (2013)], and it has been shown that oxidative stress can activate nSMase2 production and induce apoptosis (Levy et al., 2006; Castillo et al., 2007). However, it is unclear if oxidative stress activates nSMase2 and Cer production in neuronal cells and if this is altered by the presence of  $\alpha$ -syn. Gu et al. determined that, in astrocytes, but not in neurons, nSMase activity increases following brain ischemia in rodents, which in turn leads to neuronal damage (Gu et al., 2013); however, here we show that nSMase2 is mildly sensitive to hypoxia in neuron-like cells. Contrary to this study, we observed that hypoxia reduces nSMase2 at the protein level in neuron-like cells, but this reduction does not correlate with a reduction in enzymatic activity. Oxidative stress may cause modifications that result in increased enzyme activation, even with lower levels of total protein, as it has been suggested that, under normal conditions, nSMase2 primarily exists as an inactive enzyme, while oxidative stress initiates its movement to the plasma membrane where it can generate Cer (Castillo et al., 2007). A similar effect was also observed in the siRNA-treated cells despite them having unaltered enzymatic activity even with reduced protein levels. Since the half-life of nSMase2 in HAE cells has been reported to be 20 h (Filosto et al., 2012), the remaining protein detected after 48 h may also be sufficient for the required enzymatic demands of cells. Levy et al. showed that oxidative stress increases Cer production, inducing cell death (Levy et al., 2006), while another study showed no changes in Cer in response to oxidative stress (Devlin et al., 2011). Others have reported that decreased Cer may be protective under hypoxia by promoting anti-apoptotic conditions (Epstein et al., 2009). In this study, under hypoxia, we observed a decrease in total Cer levels that correlated with an increase in cell death. DHCer is converted to Cer through *de novo* synthesis, correlated with the induction of autophagy [reviewed in Gr  sch et al. (2012)], and induced by hypoxia (Devlin et al., 2011; Testai et al., 2014). Accordingly, we observed an increase in DHCer after the induction of hypoxia, but this DHCer profile was mitigated after a reduction in nSMase2 and  $\alpha$ -syn treatment, presumably as a protective function to limit apoptosis, as previously described (Dinkins et al., 2014; Shi et al., 2014; Delenclos et al., 2017; Juan and F  rthauer, 2018). Currently, DHCer levels have only been evaluated in the plasma of PD patients (Guedes et al., 2017), but given our findings that reducing nSMase2 alleviates the hypoxia-induced DHCer increase, a further evaluation of this lipid in PD brains would be valuable. As oxidative stress is prevalent in PD, the pharmaceutical inhibition of nSMase2 might prove beneficial.

Changes in acyl chain lengths may be important because EV lipid rafts are influenced by the raft composition of the originating cell (Skotland et al., 2017) and may affect how  $\alpha$ -syn binds to them (Kubo et al., 2015). EVs incorporate the lipid rafts of the originating cell during their generation and are enriched in cholesterol, SM, glycosphingolipids, and phosphatidylserine (Bienias et al., 2016). Lipid rafts in PD patients have reduced total SM levels (Fabelo and Martin, 2011), which is similar to what we observed in whole cells under hypoxia, and therefore likely affect affecting lipid raft composition. Similarly, it has been shown that Cer acyl chain composition shifts toward shorter acyl chain lengths at the expense of longer chain lengths in the

anterior cingulate in PD brains (Abbott et al., 2014). However, we observed a significant reduction in the short chain SM 16:0, Cer 16:0, and GlcCer 16:0 and an increase in the long chains SM 24:0, Cer 24:1, DHCer 24:1, and GlcCer 22:0 under hypoxic conditions, while nSMase2 inhibition reduced this shift. In aged WT mice, an increase in Cer and SM long chains and a decrease in DHCer short chains have been observed (Vozella et al., 2017), and Cer long chains are associated with mitochondrial damage and cell death (Law et al., 2018); thus, this is a useful model for studying these changes *in vitro*. However, additional research in PD brains needs to be conducted to further elucidate which sphingolipids are dysregulated, as it has been speculated that lipid dysregulation may depend on the brain region investigated (Cheng et al., 2011; Fabelo and Martin, 2011; Abbott et al., 2014; Murphy et al., 2014; Gegg et al., 2015).

The  $\alpha$ -syn peptide has a high affinity for lipid rafts, and the lipid composition of these rafts changes the binding behavior of  $\alpha$ -syn, affecting its localization to synapses (Fortin et al., 2004; Kubo et al., 2005, 2015). Additionally, synthetic lipid vesicles prepared from neuroblastoma cells accelerate  $\alpha$ -syn aggregation (Marie et al., 2015), suggesting that the lipids in EVs themselves are instrumental to the self-aggregation properties of  $\alpha$ -syn. Our findings that  $\alpha$ -syn treatment induced an increase in high MW  $\alpha$ -syn (~25–250 kDa) in donor cells while nSMase2 KO cells displayed a significantly reduced amount of high MW  $\alpha$ -syn support and extend the importance of nSMase2, and therefore lipid generation and constitution, for  $\alpha$ -syn aggregation. Fussi et al. (2018) showed that inhibiting autophagosomes increases exosomal  $\alpha$ -syn secretion, presumably to reduce the intracellular  $\alpha$ -syn burden. We speculate that blocking EV formation may eliminate one pathway by which cells reduce their intracellular  $\alpha$ -syn burden and thus may upregulate lysosomal-autophagy pathways in an attempt to degrade the  $\alpha$ -syn within the cell. Another speculation is that  $\alpha$ -syn may be packed into larger microvesicles that are not as easily taken up by surrounding cells, as it has been reported that inhibiting nSMase2 increases the secretion of larger vesicles originating from the plasma membrane (Menck et al., 2017). Although oxidative stress has been shown to induce  $\alpha$ -syn aggregation (Hashimoto et al., 1999; Scudamore et al., 2018), we observed a minor reduction in  $\alpha$ -syn aggregation in response to hypoxia, but only in donor cells alone. We also observed an upregulation in  $\alpha$ -syn gene expression (SNCA) in donor cells under hypoxia but observed no changes in monomeric  $\alpha$ -syn protein expression, possibly due to a reduction in the overall rate of mRNA translation in cells under hypoxic conditions (Koritzinsky and Wouters, 2007). Interestingly,  $\alpha$ -syn treatment in donor cells also contributed to a shift back toward shorter acyl chain lengths, but only under hypoxia. Long acyl chains are more hydrophobic than shorter chains, which causes slower desorption from the plasma membrane (Fielding, 2007) and a disruption in lipid raft formation (Grösch et al., 2012).  $\alpha$ -Syn may cause a reduction in lipid complexity in favor of increased desorption in response to hypoxic stress as a cellular defense mechanism. Guitart et al. (2016) showed that the release of EVs carrying prion proteins results in improved survival of neurons under hypoxic conditions. Although we observed a decrease in  $\alpha$ -syn transfer

in KO cells under hypoxia, this decrease did not improve cell survival in this system.

It has been shown that hypoxia induces EV secretion (Michael et al., 2012; Kilic et al., 2018), but the degree of EV secretion varies depending on the cell model and method of hypoxia used (Tomazin, 2014; Ramteke et al., 2015). In the model used for this study, hypoxia upregulated many ESCRT-related genes, such as *TSG101*, *CHMP4A*, and *CD81*, which are some of the main components involved in the formation of EVs through ESCRT-dependent pathways (Van Niel et al., 2006; Baietti et al., 2012). However, the protein expression of *CD81* and *TSG101* has been shown to increase in response to hypoxia without affecting the number of total EVs generated (Ramteke et al., 2015), while *CHMP4A* upregulates hypoxia response elements (Shi et al., 2010) and may lead to a decrease in total EVs (Colombo et al., 2013). Our model displayed no change in EV abundance in response to hypoxia in control cells. This indicates that there is a shift toward different EV generation pathways, such as a greater reliance upon the ESCRT-dependent pathway, under hypoxia. This is particularly evident when nSMase2 is reduced; KO, siRNA, and cambinol all significantly reduced the transfer of  $\alpha$ -syn between cells, whereas under hypoxia, cells did not show a reduction in transfer or any reduction in EV abundance. Importantly, the high degree of  $\alpha$ -syn transfer was abolished even under hypoxia when nSMase2 was knocked out. Another study has also indicated that other nSMase isoforms play a role in EV biogenesis, but that the packing of aggregated proteins into EVs was specifically nSMase2 dependent (Guo et al., 2015). This provides strong evidence for the importance of the formation of EVs by nSMase2 as a critical pathway by which  $\alpha$ -syn is propagated between cells.

Our findings show that  $\alpha$ -syn transfer is significantly decreased when nSMase2 is reduced, providing a new avenue for exploring disease-modifying therapeutics for PD. Since these exosomal pathways have been implicated in the propagation of other neurodegenerative diseases, including Alzheimer's disease, tauopathies, and prion diseases, this could be a useful approach for generalized neuroprotective therapy. However, the direct mechanism by which this is accomplished requires further investigation. This study supports the need for a deeper investigation of sphingolipid metabolism in PD patients to further elucidate the lipid dysregulation and lipid-protein interactions observed in PD.

## CONCLUSION

In conclusion, we demonstrated that reducing nSMase2 significantly decreases the transfer of  $\alpha$ -syn between neuron-like cells and reduces  $\alpha$ -syn aggregation, even under hypoxic conditions. Inhibiting nSMase2 could be a beneficial strategy for reducing the pathogenesis of PD.

## DATA AVAILABILITY

All datasets generated for this study are included in the manuscript and/or the **Supplementary Files**.

## AUTHOR CONTRIBUTIONS

VS designed the experimental approach, performed the experiments, analyzed and interpreted the data, generated the figures, participated in the study design, and drafted the manuscript. MS conceived the hypothesis, participated in the study design, designed the experimental approach, and performed the experiments. CS performed the experiments and contributed to the writing of the manuscript. LC and JB performed some experiments. AA-S designed the experimental approach and interpreted the data. MH conceived the hypothesis, coordinated and led the study, and participated in the study design, data interpretation, and writing of the manuscript. All authors read and approved the manuscript.

## FUNDING

This work was supported by the Swedish Research Council (MH: 523-2013-2735), the Swedish Brain Foundation, the Research Foundation of the Swedish Parkinson's Disease Association, the Östergötland Research Foundation for Parkinson's Disease, the Parkinson Research Foundation, the Swedish Alzheimer's Foundation, the Hans-Gabriel and Alice Trolle-Wachtmeister Foundation for Medical Research, Konung Gustaf V:s och Drottning Victorias Frimurarestiftelse, the Swedish Dementia Foundation, the Linköping University Neurobiology Center, and the County Council of Östergötland. The funding agencies were not involved in the design or interpretation of the study.

## ACKNOWLEDGMENTS

We would like to thank Dr. Juan F. Reyes for his valuable input, Dr. Marcus Ståhlman at BioMS (University of Gothenburg) for

performing the UPLC-MS/MS lipid analysis, and Dr. Nazira Albargothy for critical proofreading of the manuscript.

## SUPPLEMENTARY MATERIAL

The Supplementary Material for this article can be found online at: <https://www.frontiersin.org/articles/10.3389/fnmol.2019.00200/full#supplementary-material>

**FIGURE S1** | Confirmation of the nSMase2 KO cell line. **(A,B)** KO was confirmed in the nSMase2 KO D3, D9, D12, and C12 clone lines by **(A)** Western blot analysis with an N-terminal antibody and **(B)** in the nSMase2 KO D3 clone line by immunofluorescence using C- and N-terminal antibodies. From these data, nSMase2 KO D3 was selected for use in further studies. Representative confocal images using DAPI (blue) and anti-nSMase2 conjugated to Alexa Fluor 488 (green) ( $n = 3$ ). The scale bar indicates 100  $\mu$ m.

**FIGURE S2** | Confirmation of oligomeric  $\alpha$ -syn preparations. **(A)** SEC analysis of  $\alpha$ -syn to confirm oligomer specificity. **(B)** TEM image of  $\alpha$ -syn depicting spherical, ring-like oligomers.  $\alpha$ -Syn peptides were heterogeneous in shape and size and could be categorized into three groups, namely, spherical, curvilinear, and ring-like oligomers, based on their shape. The scale bar indicates 500 nm.

**FIGURE S3** | Characterization of EVs isolated by step gradient ultracentrifugation. **(A)** Size distribution of EVs isolated from donor cells by NTA presented in a representative graph [mode particle size  $71.61 \pm 4.93$  nm ( $n = 8$ )]. **(B)** Western blot showing the expression of the common EV marker, flotillin-1, and  $\alpha$ -syn in EVs isolated from control cells (control EVs), EVs isolated from cells treated with  $\alpha$ -syn ( $\alpha$ -syn EVs), and cell lysates from control cells.

**FIGURE S4** | Phosphorylation of  $\alpha$ -syn at Ser129 is increased under hypoxia but does not achieve statistical significance. **(A)** Expression of pS129 after 24 h of coculture (Co), as determined by Western blot. **(B)** Quantification of the Western blot results relative to  $\beta$ -actin expression. The data are presented as the mean  $\pm$  SEM ( $n = 3$ ).

**TABLE S1** | Complete RT-PCR data presented as the  $\Delta C_t$  values  $\pm$  SEM ( $n = 3$ ).

**TABLE S2** | Sphingolipid analysis of SM, Cer, DHCer, GlcCer, and LacCer, as determined by UPLC-MS/MS, presented as pmol/mg or % mol  $\pm$  SEM ( $n = 4$ ).

## REFERENCES

- Abbott, S. K., Li, H., Muñoz, S. S., Knoch, B., Batterham, M., Murphy, K. E., et al. (2014). Altered ceramide acyl chain length and ceramide synthase gene expression in Parkinson's disease. *Mov. Disord.* 29, 518–526. doi: 10.1002/mds.25729
- Agholme, L., Lindström, T., Kågedal, K., Marcusson, J., and Hallbeck, M. (2010). An *in vitro* model for neuroscience: differentiation of SH-SY5Y cells into cells with morphological and biochemical characteristics of mature neurons. *J. Alzheimers Dis.* 20, 1069–1082. doi: 10.3233/JAD-2010-091363
- Airola, M. V., Shanbhogue, P., Shamseddine, A. A., Guja, K. E., Senkal, C. E., Maini, R., et al. (2017). Structure of human nSMase2 reveals an interdomain allosteric activation mechanism for ceramide generation. *Proc. Natl. Acad. Sci. U.S.A.* 114, E5549–E5558. doi: 10.1073/pnas.1705134114
- Alvarez-Erviti, L., Seow, Y., Schapira, A. H., Gardiner, C., Sargent, I. L., Wood, M. J. A., et al. (2011). Lysosomal dysfunction increases exosome-mediated alpha-synuclein release and transmission. *Neurobiol. Dis.* 42, 360–367. doi: 10.1016/j.nbd.2011.01.029
- Amrutkar, M., Cansby, E., Nuñez-Durán, E., Pirazzi, C., Ståhlman, M., Stenfeldt, E., et al. (2015). Protein kinase STK25 regulates hepatic lipid partitioning and progression of liver steatosis and NASH. *FASEB J.* 29, 1564–1576. doi: 10.1096/fj.14-264937
- Anderton, B. H. (1997). Changes in the ageing brain in health and disease. *Philos. Trans. R. Soc. Lond.* 352, 1781–1792. doi: 10.1098/rstb.1997.0162
- Bae, E.-J., Ho, D.-H., Park, E., Jung, J. W., Cho, K., Hong, J. H., et al. (2013). Lipid peroxidation product 4-hydroxy-2-nonenal promotes seeding-capable oligomer formation and cell-to-cell transfer of  $\alpha$ -synuclein. *Antioxid. Redox Signal.* 18, 770–783. doi: 10.1089/ars.2011.4429
- Baietti, M. F., Zhang, Z., Mortier, E., Melchior, A., Degeest, G., Geeraerts, A., et al. (2012). Syndecan-syntenin-ALIX regulates the biogenesis of exosomes. *Nat. Cell Biol.* 14, 677–685. doi: 10.1038/ncb2502
- Bengoa-Vergniory, N., Roberts, R. F., Wade-Martins, R., and Alegre-Abarrategui, J. (2017). Alpha-synuclein oligomers: a new hope. *Acta Neuropathol.* 134, 819–838. doi: 10.1007/s00401-017-1755-1
- Bienias, K., Fiedorowicz, A., Sadowska, A., Prokopiuk, S., and Car, H. (2016). Regulation of sphingomyelin metabolism. *Pharmacol. Rep.* 68, 570–581. doi: 10.1016/j.pharep.2015.12.008
- Blesa, J., Trigo-Damas, I., Quiroga-Varela, A., and Jackson-Lewis, V. (2015). Oxidative stress and Parkinson's disease. *Front. Neuroanat.* 9:91. doi: 10.3389/fnana.2015.00091
- Braak, H., Del Tredici, K., Rüb, U., De Vos, R. A., Jansen Steur, E. N., and Braak, E. (2003). Staging of brain pathology related to sporadic Parkinson's disease. *Neurobiol. Aging* 24, 197–211. doi: 10.1016/S0197-4580(02)00065-9
- Brugger, B., Erben, G., Sandhoff, R., Wieland, F. T., and Lehmann, W. D. (1997). Quantitative analysis of biological membrane lipids at the low picomole level by nano-electrospray ionization tandem mass spectrometry. *Proc. Natl. Acad. Sci. U.S.A.* 94, 2339–2344. doi: 10.1073/pnas.95.25.14863
- Castellani, R. J., Perry, G., Siedlak, S. L., Nunomura, A., Shimohama, S., Zhang, J., et al. (2002). Hydroxynonenal adducts indicate a role for lipid peroxidation in



- neocortical and brainstem Lewy bodies in humans. *Neurosci. Lett.* 319, 25–28. doi: 10.1016/S0304-3940(01)02514-9
- Castillo, S. S., Levy, M., Thaikoottathil, J. V., and Goldkorn, T. (2007). Reactive nitrogen and oxygen species activate different sphingomyelinases to induce apoptosis in airway epithelial cells. *Exp. Cell Res.* 313, 2680–2686. doi: 10.1016/j.yexcr.2007.04.002
- Cheng, D., Jenner, A. M., Shui, G., Fun Cheong, W., Mitchell, T. W., Nealon, J. R., et al. (2011). Lipid pathway alterations in Parkinson's disease primary visual cortex. *PLoS One* 6:e17299. doi: 10.1371/journal.pone.0017299
- Colombo, M., Moita, C., van Niel, G., Kowal, J., Vigneron, J., Benaroch, P., et al. (2013). Analysis of ESCRT functions in exosome biogenesis, composition and secretion highlights the heterogeneity of extracellular vesicles. *J. Cell Sci.* 126, 5553–5565. doi: 10.1242/jcs.128868
- Danzer, K. M., Kranich, L. R., Ruf, W. P., Cagsal-Getkin, O., Winslow, A. R., Zhu, L., et al. (2012). Exosomal cell-to-cell transmission of alpha synuclein oligomers. *Mol. Neurodegener.* 7:42. doi: 10.1186/1750-1326-7-42
- Delenclos, M., Trendafilova, T., Mahesh, D., Baine, A. M., Moussaud, S., Yan, I. K., et al. (2017). Investigation of endocytic pathways for the internalization of exosome-associated oligomeric alpha-synuclein. *Front. Neurosci.* 11:172. doi: 10.3389/fnins.2017.00172
- den Jager, W. A. (1969). Sphingomyelin in Lewy inclusion bodies in Parkinson's disease. *Arch. Neurol.* 21, 615–619. doi: 10.1001/archneur.1969.00480180071006
- Devlin, C. M., Lahm, T., Hubbard, W. C., Van Demark, M., Wang, K. C., Wu, X., et al. (2011). Dihydroceramide-based response to hypoxia. *J. Biol. Chem.* 286, 38069–38078. doi: 10.1074/jbc.M111.297994
- Dinkins, M. B., Dasgupta, S., Wang, G., Zhu, G., and Bieberich, E. (2014). Exosome reduction *in vivo* is associated with lower amyloid plaque load in the 5XFAD mouse model of Alzheimer's disease. *Neurobiol. Aging* 35, 1792–1800. doi: 10.1016/j.neurobiolaging.2014.02.012
- Domert, J., Sackmann, C., Severinsson, E., Agholme, L., Ingelsson, M., and Hallbeck, M. (2016). Aggregated alpha-synuclein transfer efficiently between cultured human neuron-like cells and localize to lysosomes. *PLoS One* 11:e0168700. doi: 10.1371/journal.pone.0168700
- Duce, J. A., Wong, B. X., Durham, H., Devedjian, J. C., Smith, D. P., and Devos, D. (2017). Post translational changes to  $\alpha$ -synuclein control iron and dopamine trafficking: a concept for neuron vulnerability in Parkinson's disease. *Mol. Neurodegener.* 12, 1–12. doi: 10.1186/s13024-017-0186-8
- Epstein, S., Hengartner, M. O., Menuz, V., Fornallaz-Mulhauser, M., Martinou, J.-C., Riezman, I., et al. (2009). Protection of *C. elegans* from anoxia by HYL-2 ceramide synthase. *Science* 324, 381–384. doi: 10.1126/science.1168532
- Fabelo, N., and Martin, V. (2011). Severe alterations in lipid composition of frontal cortex lipid rafts from Parkinson's disease and incidental Parkinson's disease. *Mol. Med.* 17, 1107–1118. doi: 10.2119/molmed.2011.00119
- Fielding, C. J. (ed.) (2007). *High-Density Lipoproteins: FROM Basic Biology to Clinical Aspects*. Weinheim: Wiley-VCH Verlag GmbH & Co.
- Figuera-Losada, M., Stathis, M., Dorskind, J. M., Thomas, A. G., Bandaru, V. V. R., Yoo, S. W., et al. (2015). Caminol, a novel inhibitor of neutral sphingomyelinase 2 shows neuroprotective properties. *PLoS One* 10:e0124481. doi: 10.1371/journal.pone.0124481
- Filosto, S., Ashfaq, M., Chung, S., Fry, W., and Goldkorn, T. (2012). Neutral sphingomyelinase 2 activity and protein stability are modulated by phosphorylation of five conserved serines. *J. Biol. Chem.* 287, 514–522. doi: 10.1074/jbc.M111.315481
- Fortin, D. L., Troyer, M. D., Nakamura, K., Kubo, S., Anthony, M. D., and Edwards, R. H. (2004). "Lipid rafts mediate the synaptic localization of  $\alpha$ -synuclein. *J. Neurosci.* 24, 6715–6723. doi: 10.1523/JNEUROSCI.1594-04.2004
- Fujiwara, H., Hasegawa, M., Dohmae, N., Kawashima, A., Masliah, E., Goldberg, M. S., et al. (2002). A-synuclein is phosphorylated in synucleinopathy lesions. *Nat. Cell Biol.* 4, 160–164. doi: 10.1038/ncb748
- Fussi, N., Höllerhage, M., Chakroun, T., Nykänen, N. P., Rösler, T. W., Koeglsperger, T., et al. (2018). Exosomal secretion of  $\alpha$ -synuclein as protective mechanism after upstream blockage of macroautophagy. *Cell Death Dis.* 9:757. doi: 10.1038/s41419-018-0816-2
- Gegg, M. E., Sweet, L., Wang, B. H., Shihabuddin, L. S., Sardi, S. P., and Schapira, A. H. V. (2015). No evidence for substrate accumulation in Parkinson brains with GBA mutations. *Mov. Disord.* 30, 1085–1089. doi: 10.1002/mds.26278
- Grösch, S., Schiffmann, S., and Geisslinger, G. (2012). Chain length-specific properties of ceramides. *Prog. Lipid Res.* 51, 50–62. doi: 10.1016/j.plipres.2011.11.001
- Gu, L., Huang, B., Shen, W., Gao, L., Ding, Z., Wu, H., et al. (2013). Early activation of NSMase2/ceramide pathway in astrocytes is involved in ischemia-associated neuronal damage via inflammation in rat hippocampi. *J. Neuroinflammation* 10:109. doi: 10.1186/1742-2094-10-109
- Guedes, L. C., Chan, R. B., Gomes, M. A., Conceição, V. A., Machado, R. B., Soares, T., et al. (2017). Serum lipid alterations in GBA-associated Parkinson's disease. *Parkinsonism Relat. Disord.* 44, 58–65. doi: 10.1016/j.parkreldis.2017.08.026
- Guitart, K., Loers, G., Buck, F., Bork, U., Melitta, S., and Kleene, R. (2016). Improvement of neuronal cell survival by astrocyte-derived exosomes under hypoxic and ischemic conditions depends on prion protein. *Glia* 64, 896–910. doi: 10.1002/glia.22963
- Guo, B. B., Bellingham, S. A., and Hill, A. F. (2015). The neutral sphingomyelinase pathway regulates packaging of the prion protein into exosomes. *J. Biol. Chem.* 290, 3455–3467. doi: 10.1074/jbc.M114.605253
- Gupta, S., and Knowlton, A. A. (2007). HSP60 trafficking in adult cardiac myocytes: role of the exosomal pathway. *Am. J. Physiol. Heart Circ. Physiol.* 292, H3052–H3056. doi: 10.1152/ajpheart.01355.2006
- Hashimoto, M., Hsu, L. J., Xia, Y., Takeda, A., Sisk, A., Sundsmo, M., et al. (1999). Oxidative stress induces amyloid-like aggregate formation of NACP/alpha-synuclein *in vitro*. *Neuroreport* 10, 717–721. doi: 10.1097/00001756-199903170-00011
- Hofmann, K., Tomiuk, S., Wolff, G., and Stoffel, W. (2000). Cloning and characterization of the mammalian brain-specific, Mg<sup>2+</sup>-dependent neutral sphingomyelinase. *Proc. Natl. Acad. Sci. U.S.A.* 97, 5895–5900. doi: 10.1073/pnas.97.11.5895
- Hwang, O. (2013). Role of oxidative stress in Parkinson's disease. *Exp. Neurobiol.* 22:11. doi: 10.5607/en.2013.22.1.11
- Juan, T., and Fürthauer, M. (2018). Biogenesis and function of ESCRT-dependent extracellular vesicles. *Semin. Cell Dev. Biol.* 74, 66–77. doi: 10.1016/j.semcdb.2017.08.022
- Kilic, T., Valinhas, A. T. S., Wall, I., Renaud, P., and Carrara, S. (2018). Label-free detection of hypoxia-induced extracellular vesicle secretion from MCF-7 cells. *Sci. Rep.* 8, 1–9. doi: 10.1038/s41598-018-27203-9
- Klucken, J., Helling, S., Schlachetzki, J. C. M., Winkler, J., Schäffer, T. E., Marcus, K., et al. (2013). Oxidative stress-induced posttranslational modifications of alpha-synuclein: specific modification of alpha-synuclein by 4-hydroxy-2-nonenal increases dopaminergic toxicity. *Mol. Cell. Neurosci.* 54, 71–83. doi: 10.1016/j.mcn.2013.01.004
- Koritzinsky, M., and Wouters, B. G. (2007). Hypoxia and regulation of messenger RNA translation. *Methods Enzymol.* 435, 247–273. doi: 10.1016/S0076-6879(07)35013-1
- Kowal, J., Tkach, M., and Théry, C. (2014). Biogenesis and secretion of exosomes. *Curr. Opin. Cell Biol.* 29, 116–125. doi: 10.1016/j.ccb.2014.05.004
- Kubo, S., Hatano, T., and Hattori, N. (2015). Lipid rafts involvement in the pathogenesis of Parkinson's disease. *Front. Biosci.* 20:4308. doi: 10.2741/4308
- Kubo, S., Nemani, V. M., Chalkley, R. J., Anthony, M. D., Hattori, N., Mizuno, Y., et al. (2005). A combinatorial code for the interaction of  $\alpha$ -synuclein with membranes. *J. Biol. Chem.* 280, 31664–31672. doi: 10.1108/eb013000
- Law, B. A., Liao, X., Moore, K. S., Southard, A., Roddy, P., Ji, R., et al. (2018). Lipotoxic very-long-chain ceramides cause mitochondrial dysfunction, oxidative stress, and cell death in cardiomyocytes. *FASEB J.* 32, 1403–1416. doi: 10.1096/fj.201700300R
- Levy, M., Castillo, S. S., and Goldkorn, T. (2006). NSMase2 activation and trafficking are modulated by oxidative stress to induce apoptosis. *Biochem. Biophys. Res. Commun.* 344, 900–905. doi: 10.1002/jps.21372
- Löfgren, L., Nilsson, R., Saarinen, S., Hansson, G. I., Ståhlman, M., and Forsberg, G.-B. (2012). The BUMe method: a novel automated chloroform-free 96-well total lipid extraction method for blood plasma. *J. Lipid Res.* 53, 1690–1700. doi: 10.1194/jlr.D023036
- Luk, K. C., Kehm, V., Carroll, J., Zhang, B., O'Brien, P., Trojanowski, J. Q., et al. (2012). Pathological  $\alpha$ -synuclein transmission initiates Parkinson-like neurodegeneration in non-transgenic mice. *Science* 338, 949–953. doi: 10.1126/science.1227157

- Marie, G., Dunning, C. J., Gaspar, R., Grey, C., Brundin, P., Sparr, E., et al. (2015). Acceleration of  $\alpha$ -synuclein aggregation by exosomes. *J. Biol. Chem.* 290, 2969–2982. doi: 10.1074/jbc.M114.585703
- Marsh, M., and van Meer, G. (2008). Cell biology: no ESCRTs for exosomes. *Science* 319, 1191–1192. doi: 10.1126/science.1155750
- Menck, K., Sönmez, C., Worst, T. S., Schulz, M., Dihazi, G. H., Streit, F., et al. (2017). Neutral sphingomyelinases control extracellular vesicles budding from the plasma membrane. *J. Extracell. Vesicles* 6:1378056. doi: 10.1080/20013078.2017.1378056
- Michael, M. Z., Gleadle, J. M., and King, H. W. (2012). Hypoxic enhancement of exosome release by breast cancer cells. *BMC Cancer* 12:421. doi: 10.1186/1471-2407-12-421
- Mielke, M. M., Maetzel, W., Haughey, N. J., Bandaru, V. V., Savica, R., Berg, D., et al. (2013). Plasma ceramide and glucosylceramide metabolism is altered in sporadic Parkinson's disease and associated with cognitive impairment: a pilot study. *PLoS One* 8:e73094. doi: 10.1371/journal.pone.0073094
- Murphy, K. E., Gysbers, A. M., Abbott, S. K., Tayebi, N., Kim, W. S., Sidransky, E., et al. (2014). Reduced glucocerebrosidase is associated with increased  $\alpha$ -synuclein in sporadic Parkinson's disease. *Brain* 137, 834–848. doi: 10.1093/brain/awt367
- Näsström, T., Fagerqvist, T., Barbu, M., Karlsson, M., Nikolajeff, F., Kasrayan, A., et al. (2011). The lipid peroxidation products 4-oxo-2-nonenal and 4-hydroxy-2-nonenal promote the formation of  $\alpha$ -synuclein oligomers with distinct biochemical, morphological, and functional properties. *Free Radic. Biol. Med.* 50, 428–437. doi: 10.1016/j.freeradbiomed.2010.11.027
- Nath, S., Agholme, L., Kurudenkandy, F. R., Granseth, B., Marcusson, J., and Hallbeck, M. (2012). Spreading of neurodegenerative pathology via neuron-to-neuron transmission of  $\beta$ -amyloid. *J. Neurosci.* 32, 8767–8777. doi: 10.1523/JNEUROSCI.0615-12.2012
- Ramteke, A., Ting, H., Agarwal, C., Mateen, S., Somasagara, R., Hussain, A., et al. (2015). Exosomes secreted under hypoxia enhance invasiveness and stemness of prostate cancer cells by targeting adherens junction molecules. *Mol. Carcinog.* 54, 554–565. doi: 10.1002/mc.22124
- Ran, F. A., Hsu, P. D., Wright, J., Agarwala, V., Scott, D. A., and Zhang, F. (2013). Genome engineering using the CRISPR-Cas9 system. *Nat. Protoc.* 8, 2281–2308. doi: 10.1038/nprot.2013.143
- Reyes, J. F., Sackmann, C., Hoffmann, A., Svenningsson, P., Winkler, J., Ingelsson, M., et al. (2019). Binding of  $\alpha$ -synuclein oligomers to Cx32 facilitates protein uptake and transfer in neurons and oligodendrocytes. *Acta Neuropathol.* 138, 23–47. doi: 10.1007/s00401-019-02007-x
- Russo, I., Bubacco, L., and Greggio, E. (2012). Exosomes-associated neurodegeneration and progression of Parkinson's disease. *Am. J. Neurodegener. Dis.* 1, 217–225.
- Rutkute, K., Asmis, R. H., and Nikolova-Karakashian, M. N. (2007). Regulation of neutral sphingomyelinase-2 by GSH: a new insight to the role of oxidative stress in aging-associated inflammation. *J. Lipid Res.* 48, 2443–2452. doi: 10.1194/jlr.M700227-JLR200
- Sackmann, V., Ansell, A., Sackmann, C., Lund, H., Harris, R. A., Hallbeck, M., et al. (2017). Anti-inflammatory (M2) macrophage media reduce transmission of oligomeric amyloid  $\beta$  in differentiated SH-SY5Y cells. *Neurobiol. Aging* 60, 173–182. doi: 10.1016/j.neurobiolaging.2017.08.022
- Sardar Sinha, M., Villamil Giraldo, A. M., Öllinger, K., Hallbeck, M., and Civitelli, L. (2018). Lipid vesicles affect the aggregation of 4-hydroxy-2-nonenal-modified  $\alpha$ -synuclein oligomers. *BBA Mol. Basis Dis.* 1864, 3060–3068. doi: 10.1016/j.bbadis.2018.06.020
- Savica, R., Murray, M. E., Persson, X. M., Kantarci, K., Parisi, J. E., Dickson, D. W., et al. (2016). Plasma sphingolipid changes with autopsy-confirmed Lewy body or Alzheimer's pathology. *Alzheimers Dement.* 3, 43–50. doi: 10.1016/j.dadm.2016.02.005
- Savina, A., Vidal, M., and Colombo, M. I. (2002). The exosome pathway in K562 cells is regulated by Rab11. *J. Cell Sci.* 115(Pt 12), 2505–2515. doi: 10.1083/jcb.149.1.1/a
- Scudamore, O., Ciossek, T., and Bank, B. (2018). Increased oxidative stress exacerbates  $\alpha$ -synuclein aggregation *in vivo*. *J. Neuropathol. Exp. Neurol.* 77, 443–453. doi: 10.1093/jnen/nly024
- Shamseddine, A. A., Airola, M. V., and Hannun, Y. A. (2015). Roles and regulation of neutral sphingomyelinase-2 in cellular and pathological processes. *Adv. Biol. Regul.* 57, 24–41. doi: 10.1016/j.bior.2014.10.002
- Shi, M., Liu, C., Cook, T. J., Bullock, K. M., Zhao, Y., Li, Y., et al. (2014). Plasma exosomal  $\alpha$ -synuclein is likely CNS-derived and increased in Parkinson's disease. *Acta Neuropathol.* 128, 639–650. doi: 10.1007/s00401-014-1314-y
- Shi, T., Dong, Y., Li, J., Gao, P., Fu, D., and Ma, D. (2010). High-throughput screening identifies CHMP4A associated with hypoxia-inducible factor 1. *Life Sci.* 87, 604–608. doi: 10.1016/j.lfs.2010.09.020
- Siddique, M. M., Li, Y., Chaurasia, B., Kaddai, V. A., and Summers, S. A. (2015). Dihydroceramides: from bit players to lead actors. *J. Biol. Chem.* 290, 15371–15379. doi: 10.1074/jbc.R115.653204
- Skotland, T., Sandvig, K., and Llorente, A. (2017). Progress in lipid research lipids in exosomes: current knowledge and the way forward. *Prog. Lipid Res.* 66, 30–41. doi: 10.1016/j.plipres.2017.03.001
- Stuendl, A., Kunadt, M., Kruse, N., Bartels, C., Moebius, W., Danzer, K. M., et al. (2016). Induction of  $\alpha$ -synuclein aggregate formation by CSF exosomes from patients with Parkinson's disease and dementia with Lewy bodies. *Brain* 139(Pt 2), 481–494. doi: 10.1093/brain/awv346
- Takahashi, M., Ko, L. W., Kulathingal, J., Jiang, P., Sevelev, D., and Yen, S. H. C. (2007). Oxidative stress-induced phosphorylation, degradation and aggregation of  $\alpha$ -synuclein are linked to upregulated CK2 and cathepsin D. *Eur. J. Neurosci.* 26, 863–874. doi: 10.1111/j.1460-9568.2007.05736.x
- Testai, F. D., Kilkus, J. P., Berdyshev, E., Gorshkova, I., Natarajan, V., and Dawson, G. (2014). Multiple sphingolipid abnormalities following cerebral microendothelial hypoxia. *J. Neurochem.* 131, 530–540. doi: 10.1111/jnc.12836
- Tomazin, K. (2014). Characterization of Exosomes From Glioma Cells Under Hypoxia and Oxidative Stress 41390. Available at: <http://lup.lub.lu.se/student-papers/record/5271385> doi: 10.1111/jnc.12836
- Trajkovic, K., Hsu, C., Chiantia, S., Rajendran, L., Wenzel, D., Wieland, F., et al. (2008). Ceramide triggers budding of exosome vesicles into multivesicular endosomes. *Science* 319, 1244–1247. doi: 10.1126/science.1153124
- Valli, A., Harris, A. L., and Kessler, B. M. (2015). Hypoxia metabolism in ageing. *Aging* 7, 465–466. doi: 10.18632/aging.100782
- Van Niel, G., Porto-Carreiro, I., Simoes, S., and Raposo, G. (2006). Exosomes: a common pathway for a specialized function. *J. Biochem.* 140, 13–21. doi: 10.1093/jb/mvj128
- Vozella, V., Basit, A., Misto, A., and Piomelli, D. (2017). Age-dependent changes in nervonic acid-containing sphingolipids in mouse hippocampus. *BBA Mol. Cell Biol. L.* 1862, 1502–1511. doi: 10.1016/j.bbalip.2017.08.008
- Xing, Y., Tang, Y., Zhao, L., Wang, Q., Qin, W., Ji, X., et al. (2016). Associations between plasma ceramides and cognitive and neuropsychiatric manifestations in Parkinson's disease dementia. *J. Neurol. Sci.* 370, 82–87. doi: 10.1016/j.jns.2016.09.028
- Yoritaka, A., Uchida, K., Stadtman, E. R., Hattori, N., Tanaka, M., and Mizuno, Y. (1996). Immunohistochemical detection of 4-hydroxynonenal protein adducts in Parkinson disease. *Proc. Natl. Acad. Sci. U.S.A.* 93, 2696–2701. doi: 10.1073/pnas.93.7.2696
- Zhang, S., Eitan, E., Wu, T. Y., and Mattson, M. P. (2018). Intercellular transfer of pathogenic  $\alpha$ -synuclein by extracellular vesicles is induced by the lipid peroxidation product 4-hydroxynonenal. *Neurobiol. Aging* 61, 52–65. doi: 10.1016/j.neurobiolaging.2017.09.016

**Conflict of Interest Statement:** The authors declare that the research was conducted in the absence of any commercial or financial relationships that could be construed as a potential conflict of interest.

Copyright © 2019 Sackmann, Sinha, Sackmann, Civitelli, Bergström, Ansell-Schultz and Hallbeck. This is an open-access article distributed under the terms of the Creative Commons Attribution License (CC BY). The use, distribution or reproduction in other forums is permitted, provided the original author(s) and the copyright owner(s) are credited and that the original publication in this journal is cited, in accordance with accepted academic practice. No use, distribution or reproduction is permitted which does not comply with these terms.



# Glucocorticoid-Driven NLRP3 Inflammasome Activation in Hippocampal Microglia Mediates Chronic Stress-Induced Depressive-Like Behaviors

**Xiujing Feng, Yuan Zhao, Tianyuan Yang, Manyu Song, Chaoran Wang, Yujie Yao and Honggang Fan\***

Heilongjiang Key Laboratory for Laboratory Animals and Comparative Medicine, College of Veterinary Medicine, Northeast Agricultural University, Harbin, China

## OPEN ACCESS

### Edited by:

Juan Pablo de Rivero Vaccari,  
University of Miami, United States

### Reviewed by:

Fabrizio Michetti,  
Catholic University of the Sacred  
Heart, Italy  
Nadine Ahmed Kerr,  
University of Miami, United States

### \*Correspondence:

Honggang Fan  
fanhonggang2002@163.com

**Received:** 13 June 2019

**Accepted:** 16 August 2019

**Published:** 29 August 2019

### Citation:

Feng X, Zhao Y, Yang T, Song M,  
Wang C, Yao Y and Fan H (2019)  
Glucocorticoid-Driven NLRP3  
Inflammasome Activation  
in Hippocampal Microglia Mediates  
Chronic Stress-Induced  
Depressive-Like Behaviors.  
*Front. Mol. Neurosci.* 12:210.  
doi: 10.3389/fnmol.2019.00210

Chronic stress is a key risk factor for depression, and microglia have been implicated in the pathogenesis of the disease. Recent studies show that the Nod-like receptor protein 3 (NLRP3) inflammasome is expressed in microglia and may play a crucial role in depression. However, the mechanism of NLRP3 inflammasome activation in hippocampal microglia and its role in depressive-like behaviors remain poorly understood. In this study, rats were subjected to 6 h of restraint stress per day for 21 days to produce a model of stress-induced depression. Behavioral tests and serum corticosterone were used to assess the success of the model. Furthermore, HAPI cells were pretreated with dexamethasone ( $5 \times 10^{-7}$  M) to assess stress-induced changes in microglial cells in culture. The microglial marker Iba-1, reactive oxygen species (ROS), nuclear factor kappa B (NF- $\kappa$ B) and key components of the NLRP3 inflammasome and its downstream inflammatory effectors (IL-1 $\beta$  and IL-18) were measured. Chronic stress induced depressive-like behavior, increased serum corticosterone levels and produced hippocampal structural changes. Chronic stress and dexamethasone both increased Iba-1 expression and ROS formation and also elevated levels of NF- $\kappa$ B, NLRP3, cleaved caspase-1, IL-1 $\beta$  and IL-18. After use of the NF- $\kappa$ B inhibitor BAY 117082 and knocked out NLRP3 *in vitro* decreased ROS formation and the expression of Iba-1, NF- $\kappa$ B and NLRP3 as well as levels of cleaved caspase-1, IL-1 $\beta$  and IL-18. These findings suggest that activation of the glucocorticoid receptor-NF- $\kappa$ B-NLRP3 pathway in hippocampal microglia mediates chronic stress-induced hippocampal neuroinflammation and depression-like behavior.

**Keywords:** stress, glucocorticoid, NLRP3 inflammasome, hippocampal microglia, neuroinflammation, depressive-like behaviors

## INTRODUCTION

Depression is a common mental disease with high morbidity, recurrence and mortality and is a serious global health problem (Yang et al., 2019). Stress, especially chronic stress, is considered an important risk factor for depression, and it severely impairs cognition and learning and memory functions (Hayden et al., 2010). Chronic stress activates hypothalamic-pituitary-adrenal (HPA)

axis, which results in persistent release of glucocorticoids throughout the brain (Rivier and Vale, 1983), especially the hippocampus (Zhao et al., 2015). The glucocorticoid receptor (GR), which is the main receptor for glucocorticoids, is highly expressed in the hippocampus (Joels, 2011). Furthermore, several studies have shown that the hippocampus, amygdala and the prefrontal cortex play major roles in depression (Price and Drevets, 2010). In particular, the hippocampus, a stress-sensitive limbic structure, is important for cognition and spatial memory, and these functions are impaired in depressive disorder (Austin et al., 2001). Thus, the hippocampus is intimately involved in the pathophysiology of depression.

Microglia are the resident immune cells in the CNS, and depression is increasingly considered a microglial disease (Yirmiya et al., 2015). Furthermore, preclinical studies show that microglia activation is involved in the pathogenesis of depression (Bollinger et al., 2016). Accumulating evidence indicates that microglial cells are widely distributed in the hippocampus and prefrontal cortex, which are brain regions that have a critical role in the regulation of mood and behavior (Lawson et al., 1990; Drevets et al., 2008). Furthermore, hippocampal microglial activation promotes the release of inflammatory factors, which results in the disruption of neuroplasticity and cognitive impairment, thereby contributing to the development of depression (Walker et al., 2013; Singhal and Baune, 2017). Microglial activation is a key mediator of neuroinflammatory processes (Tronel et al., 2017), and neuroinflammation plays a crucial role in the pathogenesis of depression (Zhang C. et al., 2019). In particular, HPA axis hyperactivity induces the overproduction of brain pro-inflammatory cytokines through microglial activation (Brites and Fernandes, 2015), and this phenomenon is consistently observed in subjects with depressive disorders (Zou et al., 2018). However, the mechanisms underlying chronic stress-induced hippocampal microglia activation and neuroinflammation in depression remain unclear.

Recent studies show that the Nod-like receptor protein 3 (NLRP3) inflammasome and related pathways are associated with the pathogenesis of depression (Xu et al., 2016; Gao et al., 2018). NLRP3 inflammasome activation is observed in animal models of depression (Zhang Y. et al., 2015) as well as in depressive patients (Alcocer-Gomez et al., 2014). One study shows that the antidepressant mechanism of silymarin may be associated with inhibition of neuroinflammation and NLRP3 inflammasome activation in CUMS-induced depression, at least in part proves that NLRP3 inflammasome activation is reduced by antidepressant treatment, and accordingly, it is a potential new target for the development of antidepressant strategies (Ashraf et al., 2019). Studies have shown that activation of P2X7 receptor and the NLRP3 inflammasome in hippocampal glial cells mediates depressive-like behavior induced by chronic stress (Yue et al., 2017). However, whether the NLRP3 inflammasome is activated in hippocampal microglia during chronic restraint stress and depression remains unclear.

Reactive oxygen species (ROS) are important activators of inflammation mediated by the NLRP3 inflammasome (Zhou et al., 2011). Furthermore, nuclear factor kappa B (NF- $\kappa$ B)-induced oligomerization of NLRP3 with apoptosis-associated

speck-like protein containing a CARD (ASC) and pro-caspase 1 forms the NLRP3 inflammasome (Gross et al., 2011). In response to stress, the activated NLRP3 inflammasome cleaves pro-caspase 1 to the mature caspase-1 p10 and p20. Subsequently, inactive pro-IL-1 $\beta$  and pro-IL-18 are converted into their active forms, IL-1 $\beta$  and IL-18 (Walsh et al., 2014). In addition, IL-1 $\beta$ , whose secretion is tightly controlled by the NLRP3 inflammasome, plays a critical role in the pathogenesis of depression (Park et al., 2015). Recent studies suggest that chronic glucocorticoid administration increases ROS levels in the brain (Uchiyama et al., 2016) and promotes NF- $\kappa$ B transcription (Pace and Miller, 2009). Moreover, glucocorticoids upregulate both mRNA and protein levels of NLRP3 in macrophages and microglia (Frank et al., 2014). However, it remains unclear whether glucocorticoid-induced neuroinflammation and depressive behavior in the chronic restraint stress model of depression involves microglial NLRP3 inflammasome activation.

We hypothesized that chronic stress-induced neuroinflammation and depressive behaviors are associated with activation of the GR-NF- $\kappa$ B-NLRP3 signaling pathway in hippocampal microglia. In this study, we used the chronic restraint stress-induced model of depression as well as cultured HAPI cells treated with dexamethasone (DEX, a glucocorticoids hormone) to investigate whether chronic stress-induced hippocampal neuroinflammation is mediated by the GR-NF- $\kappa$ B-NLRP3 pathway, and which might be a new target and offer new perspectives on depression research. The results also provide a theoretical basis for the development of new antidepressants.

## MATERIALS AND METHODS

### Animals

This study was approved by the ethical committee of Northeast Agricultural University (SRM-11), and experiments were carried out in accordance with the National Institutes of Health Guide for Care and Use of Laboratory Animals. For experiments, sixty adult (8 weeks old) male Wistar rats weighing 200–210 g (purchased from the Harbin Medical University Laboratory Animals Institutes, China) were housed at 22–24°C with appropriate humidity and a 12 h alternating light-dark cycle. Rats were housed in groups of 3 rats in standard polypropylene cages and *ad libitum* access to food and water. Animals were acclimated to the environment for 7 days before the beginning of the experiment.

### Experimental Design

Rats were randomly divided into two weight-matched groups: control group (C,  $n = 30$ ) and chronic stress group (CS,  $n = 30$ ). 12 rats in each group were used for behavioral experiments, and the remaining 18 were used for subsequent experiments. The chronic restraint stress procedure was performed between 9:00 and 15:00, as previously described (Zhao et al., 2013; Seo et al., 2017). Briefly, except rats in C group, all rats were daily restrained into a transparent plexiglass tube (26 cm long and 8 cm in diameter) for 6 h over 21 consecutive days (**Figures 1A,B**). During CS group rats were restrained, the rats in the C group



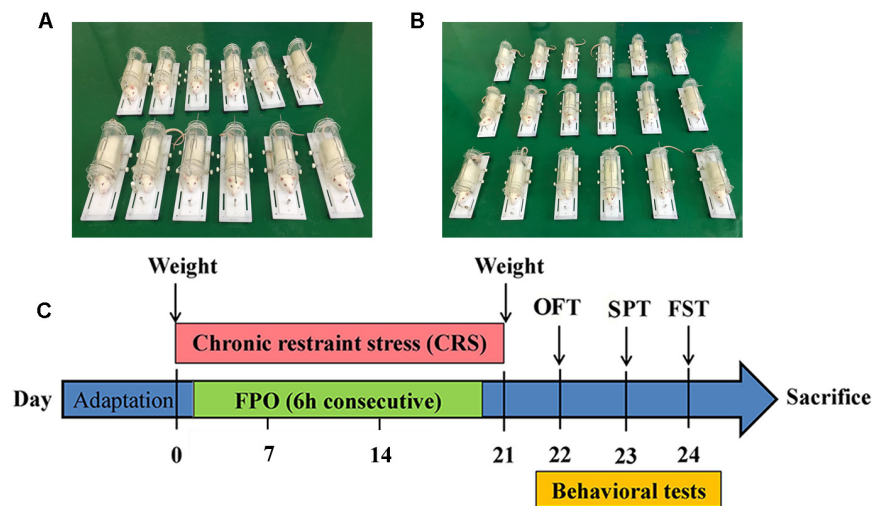


**FIGURE 1 |** The Wistar rats were challenged with chronic restraint stress with 6 h each day during 21 consecutive days. **(A)** Images of restrained rats ( $n = 12$ ) for behavioral testing, **(B)** Image of restrained rats ( $n = 18$ ) for subsequent experiments, **(C)** Schematic diagram showing the schedule of Body weight, Fecal pellet output (FPO), Sucrose preference test (SPT), Open field test (OFT), Forced swimming test (FST).

stay in their home cages without water and food. After stress, rats in the C and CS groups were given conventional feed and free drinking water. The body weights in the C and CS group were measured on the 0, 7, 14, and 21 days. The behavioral experiments started on day 22 to 24 after 21 consecutive days restrained. At least 24 h between each behavior (**Figure 1C**).

## Fecal Pellet Output

After 6 h of restraint stress, the number of pellets released during restraint in the CS rats was collected. Considering that rat isolation may cause a stress response, 3 rats in the C group were kept in a cage, and the fecal output of the C group represents the mean value for a group.

## Behavioral Tests

### Open Field Test

The open field test (OFT) was performed as previously described (Lee et al., 2014). The open-field box (100 cm × 100 cm × 40 cm) is made of wood and painted black inside. The bottom of the box is evenly divided into 25 squares. A camera was placed above the box to track and record rat performance. On day 22, rats were placed in the center of the open field box, and the rats' behavior was monitored for 3 min, including total distance, average speed, number of crossings and number of rearing. The device was cleaned with 70% ethanol thoroughly after each trial. Open field test was analyzed and recorded by Super Maze software (Shanghai Softmaze Information Technology Co., Ltd., Shanghai, China).

### Sucrose Preference Test

The sucrose preference test (SPT) was improved on the basis of predecessors (Overstreet, 2012). In a word, after deprivation of food and water for 12 h, rats were domesticated for 12 h, as two 1% sucrose bottles for 6 h, and then one of the 1% sucrose bottles was replaced with tap water for the next 6 h. On

the day of the experiment, rats were given a bottle of 200 ml tap water and a bottle of 200 ml 1% sucrose solution for 12 h (6 h light/6 h dark). After 6 h of testing, change the position of the two bottles to avoid position preference. Percentage (sucrose intake/sucrose intake plus water intake) is expressed as sucrose preference.

### Forced Swimming Test

The forced swimming test (FST) is performed as previously described and used to assess depressive-like behavior in animal models (Bogdanova et al., 2013; Lee et al., 2014). In this study, rats were placed individually into a vertical plexiglass cylinder measuring 45 cm height and 20 cm diameter containing water at  $25 \pm 1^\circ\text{C}$ , and the cylinder water depth of 30 cm. The swimming sessions consisted 20 min and the lasted 5 min was recorded as test session. The FST sessions in 5 min were recorded by a video camera for later analysis. After completion of the FST, the rats were removed from the water, well dried with paper towels, and returned to their warm cages.

## Blood and Tissue Samples Collection

On day 21, at the end of the last chronic restraint stress, except for the rats that performed the behavioral experiments, the remaining rats were immediately anesthetized with isoflurane (Yipin Pharmaceutical Co., Ltd., Hebei, China). Then blood samples were collected quickly by heart puncture, and the supernatant was collected by centrifugation at 3000 rpm for 10 min at  $4^\circ\text{C}$  and stored at  $-80^\circ\text{C}$  use for corticosterone assay. Simultaneously, brains were removed, brains ( $n = 6$ ) per group were placed in 10% paraformaldehyde for hematoxylin and eosin staining (H&E) and immunohistochemistry (IHC). Hippocampal areas were isolated, hippocampus ( $n = 6$ ) per group were placed in 3% glutaraldehyde to observe the changes of the ultrastructure of the hippocampus.

Hippocampus ( $n = 6$ ) per group were removed and immediately measured the concentration of ROS in the hippocampus, the rest of hippocampus were stored at  $-80^{\circ}\text{C}$  for subsequent experiments.

## Histological and Ultrastructural Observations

Once the hippocampus was fixed, hippocampus sections ( $3\text{ }\mu\text{m}$ ) were fixed in formalin for at least 24 h and embedded in paraffin prior to examination. The hippocampus sections were then stained using H&E (WUHAN XINXINJIALI Bio-tech Co., Ltd., Wuhan, China). After these procedures, sections were observed with light microscopy (TE2000, Nikon, Japan) and the camera (Canon, Tokyo, Japan) with the software was used for image capturing.

The hippocampus was cut into  $1\text{ mm}^3$  blocks, fixed in 3% glutaraldehyde for 48 h. The blocks were post fixed with 1% osmium tetroxide for 2 h. Afterward, the blocks were dehydrated in a graded series of acetone (50, 70, 90, and 100%) for 10 min each times. Then embedded in fresh pure Epon812 resin and allowed to polymerize at  $60^{\circ}\text{C}$  for 2 h. Samples were sectioned (60 nm) stained with lead citrate during 5 min. Samples were viewed and photographed with a transmission electron microscope (TEM, Tecnai-G212, FEI Company, Netherlands).

## Serum Corticosterone Assay

According to the kit instructions, the serum corticosterone levels were measured using Corticosterone ELISA Kit (Nanjing Jiancheng Bioengineering Institute, Nanjing, China).

## Immunohistochemistry Staining

After hippocampus tissue embedded in paraffin,  $3\text{ }\mu\text{m}$  thick sections were prepared for IHC. Dewaxing with xylene, hydration with different degrees of ethanol and incubation with 3%  $\text{H}_2\text{O}_2$  blocked the production of endogenous peroxidase. After incubation with goat serum, primary antibody anti-GR (1:400, Bioss antibodies, Beijing, China) was applied in blocking solution overnight at  $4^{\circ}\text{C}$ . After incubated with HRP- conjugated goat anti-rabbit IgG (1:100, Beyotime Biotechnology, Shanghai, China) for 30 min, and then reacted with DAB substrate for 5 min. The sections were counterstained with hematoxylin for 3 min. Images were captured using an Olympus microscope.

## Cell Culture and Drug Treatments

HAPI cells were purchased from the Cell Bank of the Chinese Academy of Sciences (Shanghai, China). Cells were cultured in DMEM medium (HyClone) supplemented with 10% FBS (BI), penicillin/streptomycin ( $100\text{ U/mL}$ ;  $100\text{ }\mu\text{g/mL}$ ) at  $37^{\circ}\text{C}$  in 5%  $\text{CO}_2$  atmosphere. The HAPI cells were seeded in 6-well plates or 96-well plates with  $8 \times 10^3$  cells/well and the culture medium was changed daily. The cell experiments were grouped as follows:

**Control group (CON):** The cells were incubated in complete medium without any treatment.

**Dexamethasone group (DEX):** The cells were incubated in complete medium for 24 h with  $5 \times 10^{-7}\text{ M}$  dexamethasone

(Sigma-Aldrich, San Francisco, CA, United States, D4902,  $\geq 97\%$ , dissolve in ethanol).

**NF- $\kappa\text{B}$  P65 inhibitor group (BAY):** The cells were pretreated with  $10\text{ }\mu\text{M}$  BAY117082 (Selleck.cn, Shanghai, China) for 30 min before incubated in complete medium for 24 h with  $5 \times 10^{-7}\text{ M}$  dexamethasone.

**NLRP3 knock out group (sgNLRP3):** The NLRP3 knock-out cells were incubated in complete medium for 24 h with  $5 \times 10^{-7}\text{ M}$  dexamethasone.

**Vehicle group (E):** The cells were incubated in complete medium for 24 h with ethanol. The final ethanol concentration did not exceed 0.2%.

## CRISPR/Cas9 Mediated Genome Editing

NLRP3 knock-out cells were generated using CRISPR/Cas9 technology. HAPI cells were seeded ( $5 \times 10^3$  cells/well) in 6-well plates and grown in DMEM supplemented with 10% FBS for 24 h at  $37^{\circ}\text{C}$  with 5%  $\text{CO}_2$ . The Cas9 and gRNA expressing plasmid PX459 V2.0 (gift from Linlin Li, Lanzhou Veterinary Research Institute, China) was used for gene editing. The CRISPR target sites were: ACGCTAATGATCGACTTCAA (NLRP3). HAPI were transfected with 500 ng plasmid and  $1.5\text{ }\mu\text{L}$  of Lipofectamine 2000 in Opti-MEM (Thermo Fisher Scientific) according to manufacturer's instructions. The transfection was stopped after 6 h by replacing the medium with fresh complete serum containing medium. The cells were selected 5 days after transfection with puromycin ( $1\text{ mg/mL}$ , LEAGENE, Beijing, China) and doxycycline ( $10\text{ }\mu\text{g}$ , LEAGENE, Beijing, China). Monoclonal build stable cell lines. The phenotype was confirmed by Western blot.

## Cell Counting Kit-8 (CCK-8) Assay

Cell viability was measured by using the CCK8 assay (Beyotime Institute of Biotechnology, Suzhou, China). To assess the effects of dexamethasone on cell proliferation, the cells were incubated in DMEM medium for 24 h at the concentration gradient from  $5 \times 10^{-6}\text{ M}$  to  $1 \times 10^{-8}\text{ M}$ .  $10\text{ }\mu\text{L}$  of CCK-8 solution reagent was added to  $100\text{ }\mu\text{L}$  of culture medium in each well. The absorbance of each well was read at a wavelength of 450 nm on a BioTek microplate reader (BioTek Instruments, Thermo Fisher Scientific, Winooski, VT, United States).

## LDH Release Assay

Released LDH in culture supernatants from damaged cells was measured with LDH assay kit (Beyotime Biotechnology, Nantong, China) by following manufacturer's instruction. Determination of absorption of samples at 490 nm using a BioTek microplate reader.

The calculation of % cytotoxicity followed the below equation, these values were subsequently normalized and expressed as a percentage of control.

% Cytotoxicity:  $[\text{Experimental (OD490)} - \text{Blank (OD490)}] \times 100 / [\text{Maximum LDH release (OD490)} - \text{Blank (OD490)}]$

## Measurement of Intracellular ROS Accumulation

Intracellular ROS accumulation was determined by an ROS assay kit (Beyotime Biotechnology, Shanghai, China) that utilizes DCFH-DA as a fluorescent probe. After dexamethasone treatment, cells were incubated with 10 mM of DCFH-DA at 37°C for 30 min. Intracellular ROS were determined by a fluorescence microscope at an excitation wavelength of 488nm and an emission wavelength of 525 nm.

## Immunofluorescence Staining

HAPI cells samples were prepared for immunofluorescence (IF) assays. The primary antibodies were anti-p-NF- $\kappa$ B P65 (1:100, Cell Signaling Technology, Danvers, MA) and anti-Iba-1 (1:100, Abcam, Cambridge, United Kingdom). Then the slides were mounted by using DAPI (Goodbio Technology, Co., Ltd.,

Wuhan, China). Images were acquired with a Nikon Eclipse Ni inverted microscope (TE2000, Nikon, Japan).

## Western Blot Analysis

Equal amounts of protein samples (28  $\mu$ g) were subjected to a SDS-PAGE and transferred to PVDF membranes. Membranes were blocked in 5% milk in TBST for 2 h followed by incubation with the following primary antibodies as follows: anti-p-NF- $\kappa$ B P65 (1:1000, Cell Signaling Technology), anti-NF- $\kappa$ B P65 (1:1000, Cell Signaling Technology), anti-Iba-1 (1:1000, Abcam), anti- $\beta$ -actin (1:7500, Bioss antibodies), anti-GR (1:1000, Bioss antibodies), anti-NLRP3 (1:1500), anti-ASC (1:500), anti-pro-caspase 1 (1:500), anti-caspase-1 p20 (1:750), anti-pro-IL-1 $\beta$  (1:10000), anti-IL-1 $\beta$  (1:750), anti-IL-18 (1:1000) and anti-Lamin B (1:750) both from Wanlei Biotechnology (Shenyang, China). After three times washing with TBST, the membranes were incubated with appropriate secondary antibody. The protein

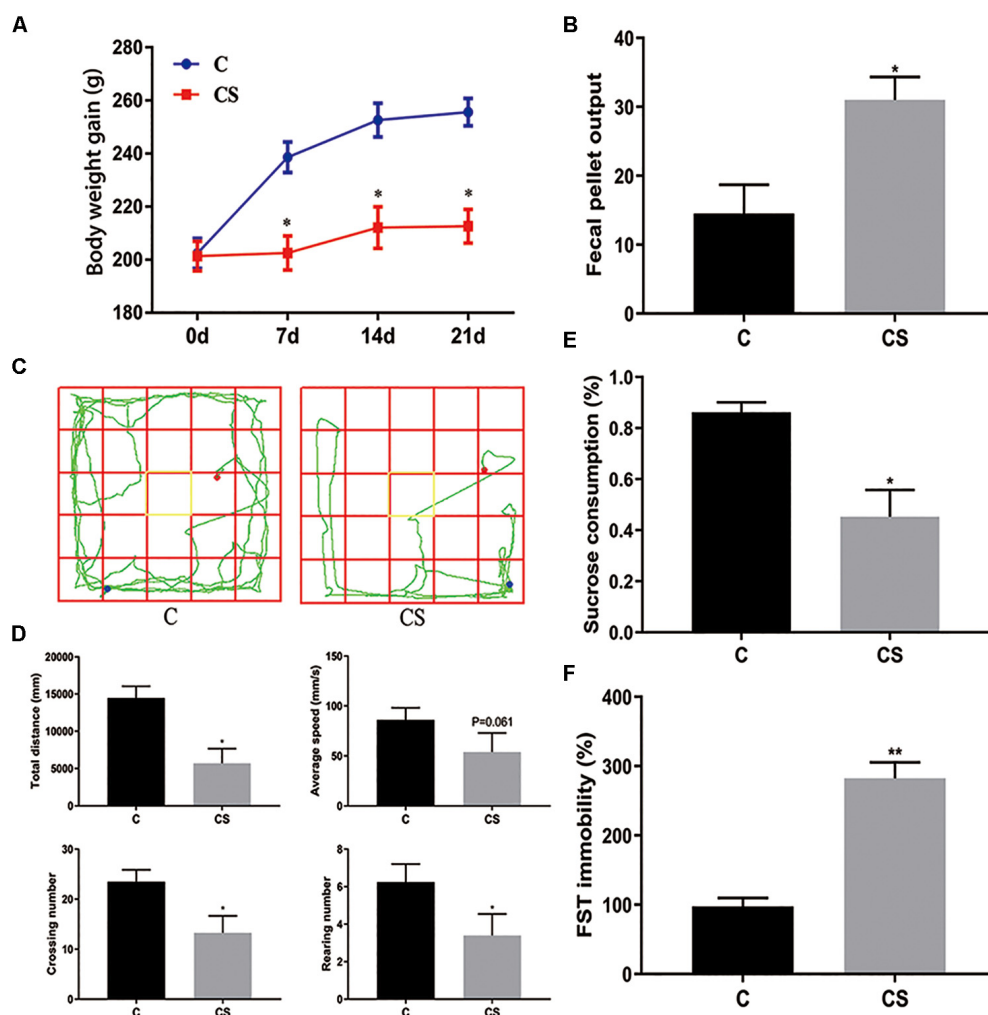


**FIGURE 2 |** Chronic stress induced depression-like behavior in rats. **(A)** Body weight gain, **(B)** Fecal Pellet Output, **(C)** OFT track diagram, **(D)** OFT data analysis, **(E)** Sucrose Preference Test (SPT), **(F)** Forced swimming test (FST). Values are presented as mean  $\pm$  SEM ( $n = 12$ ). \* $P < 0.05$ , \*\* $P < 0.01$  versus C group. Student's two-tailed  $t$ -test **(A,B,D-F)**.



bands were visualized by the ECL detection system (Thermo Scientific, Waltham, MA, United States) and quantified using Image J software. Nuclear and Cytoplasmic Protein Extraction Kit (Applygen Technologies, Co., Ltd., Beijing, China) was used to extract the cytoplasmic/nuclear proteins of NF- $\kappa$ B P65 according to the manufacturer's protocol.

## Statistical Analysis

Data were expressed as mean  $\pm$  SEM (standard error means). Unpaired two-tailed Student's *t*-test was used to two groups' comparison. One-way analysis of variance (ANOVA) followed by Tukey's *post hoc* test was used to multi-group comparison. Statistical analysis and Graphs were made using PASW Statistics 18 software (SPASS, IL, United States) and GraphPad Prism 8 software (GraphPad Software Inc., San Diego, CA, United States), respectively. IHC intensity was quantified with Image-Pro Plus software (Media Cybernetics, Rockville, MD, United States).  $P < 0.05$  was considered to be statistically significant.

## RESULTS

### Chronic Stress Affects Body Weight and Fecal Output and Causes Behavioral Deficits in Rats

The body weight of rats was measured every 7 days (**Figure 2A**). Compared with the C group, weight gain was significantly reduced in the CS group. In addition, we assessed the physiological response to restraint stress by measuring daily fecal output. As shown in **Figure 2B**, the number of feces pellets was increased in the CS group. To verify the success of the model, we conducted behavioral experiments. In the OFT (**Figures 2C,D**), the total distance traveled, the number of crossings and rearing times in the CS group were significantly reduced, with no difference in average speed. In the SPT (**Figure 2E**), sucrose consumption in the CS group was reduced. In the FST (**Figure 2F**), immobility time in the CS group was increased significantly, indicating behavioral

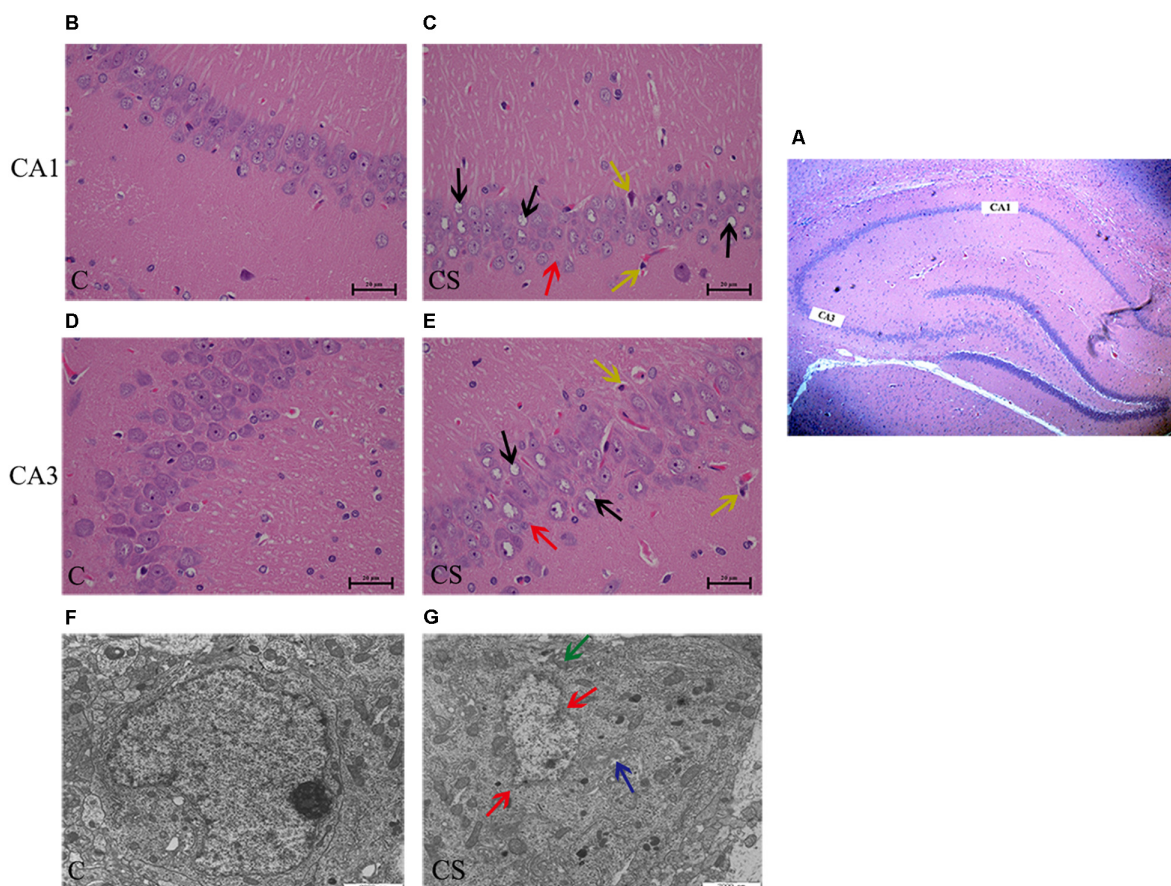


**FIGURE 3 |** Chronic stress caused hippocampus microstructure and ultrastructure injury. **(A)** CA1 and CA3 regions of hippocampal ( $\times 40$ ), **(B,D)** C group showed the normal cells morphology in CA1 and CA3 region, **(C,E)** CS group showed the structures of neuronal cells were mussy and the cells morphology changed in CA1 and CA3 region. The red arrows ( $\rightarrow$ ) represent neurons displayed an irregular arrangement, enlarged pericellular spaces, the black arrows ( $\rightarrow$ ) represent vacuolization of nerve cells and disappearance of nuclei, the yellow arrows ( $\rightarrow$ ) represents neuronal pyknosis and the coloring became deeper ( $\times 400$ ,  $n = 6$ ). **(F)** Ultrastructure of the hippocampus in C group, **(G)** Pathologic presentation of the ultrastructure of the hippocampus in CS group. (Scale bar = 2  $\mu$ m,  $n = 6$ ). The red arrows ( $\rightarrow$ ) represent nucleus contraction, local rupture, the green arrows ( $\rightarrow$ ) represent mitochondrial swelling and the blue arrows ( $\rightarrow$ ) represent mild dilatation of endoplasmic reticulum.



despair. These results suggest successful production of the rat model of depression.

## Chronic Stress Results in Histopathological and Ultrastructural Changes in the Hippocampus

In the CA1 and CA3 regions of the hippocampus (Figure 3A), the neurons were arranged in an orderly manner, with clear

profiles and distinct nuclei and nucleoli in the C group (Figures 3B,D). Hippocampal neurons displayed an irregular arrangement, enlarged pericellular spaces (red arrows), an unclear nuclear structure, the absence of clearly visible nucleoli (black arrows), and neuronal pyknosis (yellow arrows) in the CS group (Figures 3C,E).

Transmission electron microscopy showed that, in the C group (Figure 3F), the nuclear membrane was complete, without evidence of abnormalities in the mitochondria, endoplasmic

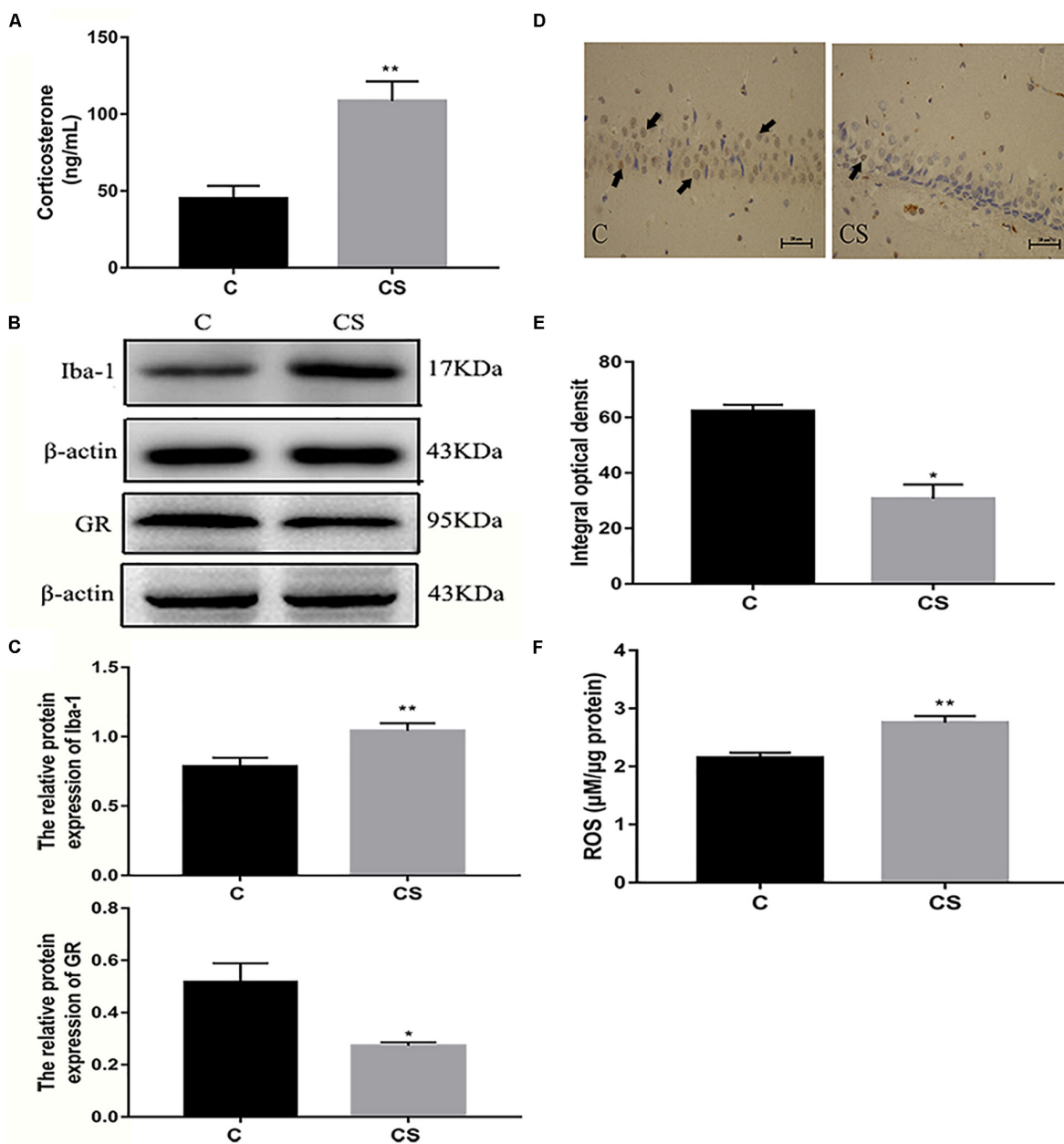
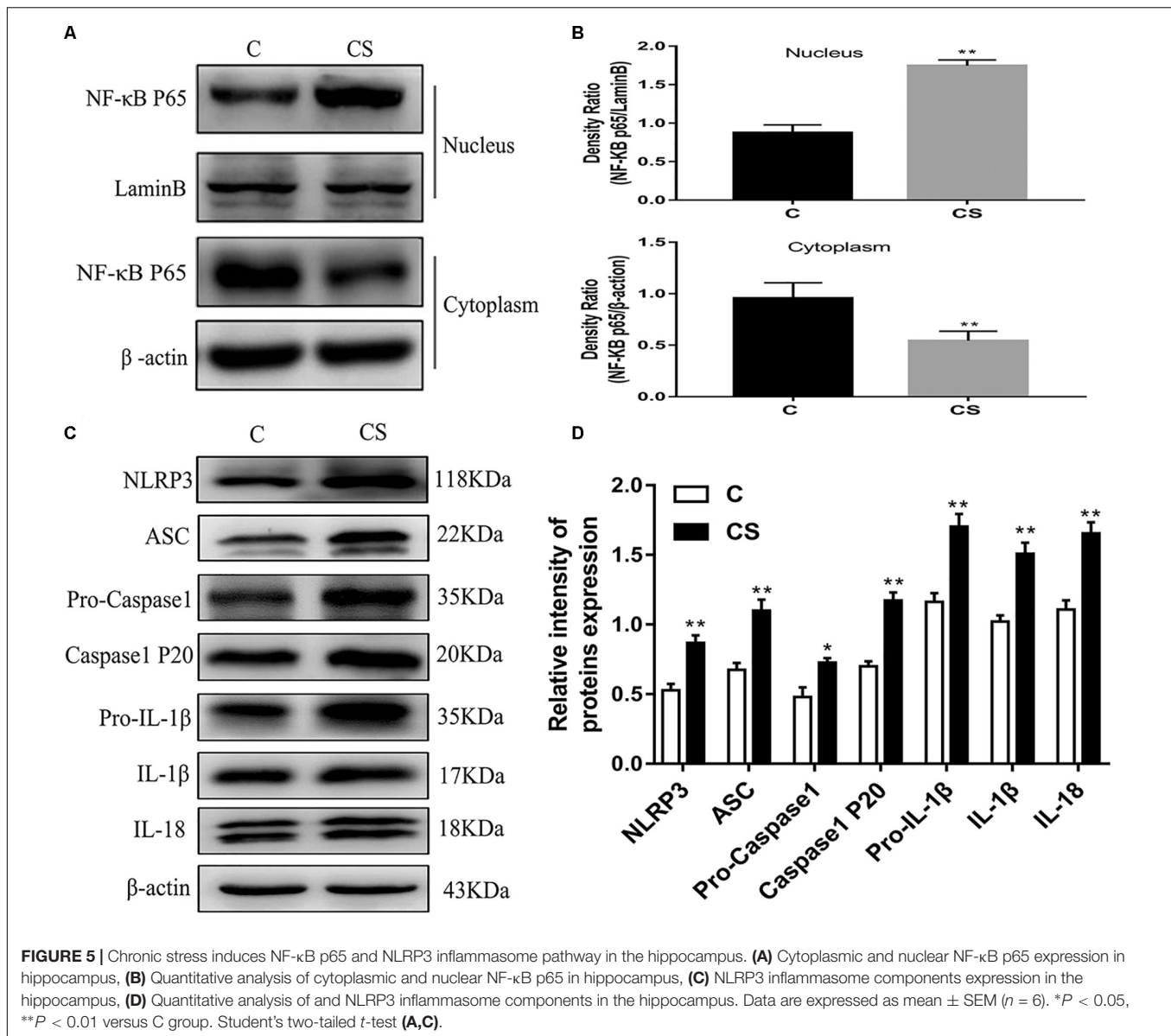


**FIGURE 4 |** Chronic stress induced the increase of glucocorticoid level, ROS content and Iba-1 expression in hippocampus of rats. (A) Serum corticosterone levels, (B) The GR and Iba-1 expressions in hippocampus, (C) Quantitative analysis of GR and Iba-1 in hippocampus, (D) Immunohistochemistry (IHC) of GR in hippocampal CA1 cells, the black arrows (→) represents positive cells, (E) The percentages of GR positive in hippocampal CA1 cells, (F) The content of ROS in hippocampal. Data are expressed as mean ± SEM ( $n = 6$ ). \* $P < 0.05$ , \*\* $P < 0.01$  versus C group. Scale bar = 20  $\mu$ m. Student's two-tailed  $t$ -test (A,C,E,F).



reticulum or other organelles. In the CS group (Figure 3G), the hippocampus showed signs of pathological changes, including nuclear shrinkage, rupture of the nuclear membrane (red arrows), swelling/degeneration of mitochondria (green arrows) and disappearance of the crests and mild dilation of the endoplasmic reticulum lumen (blue arrows).

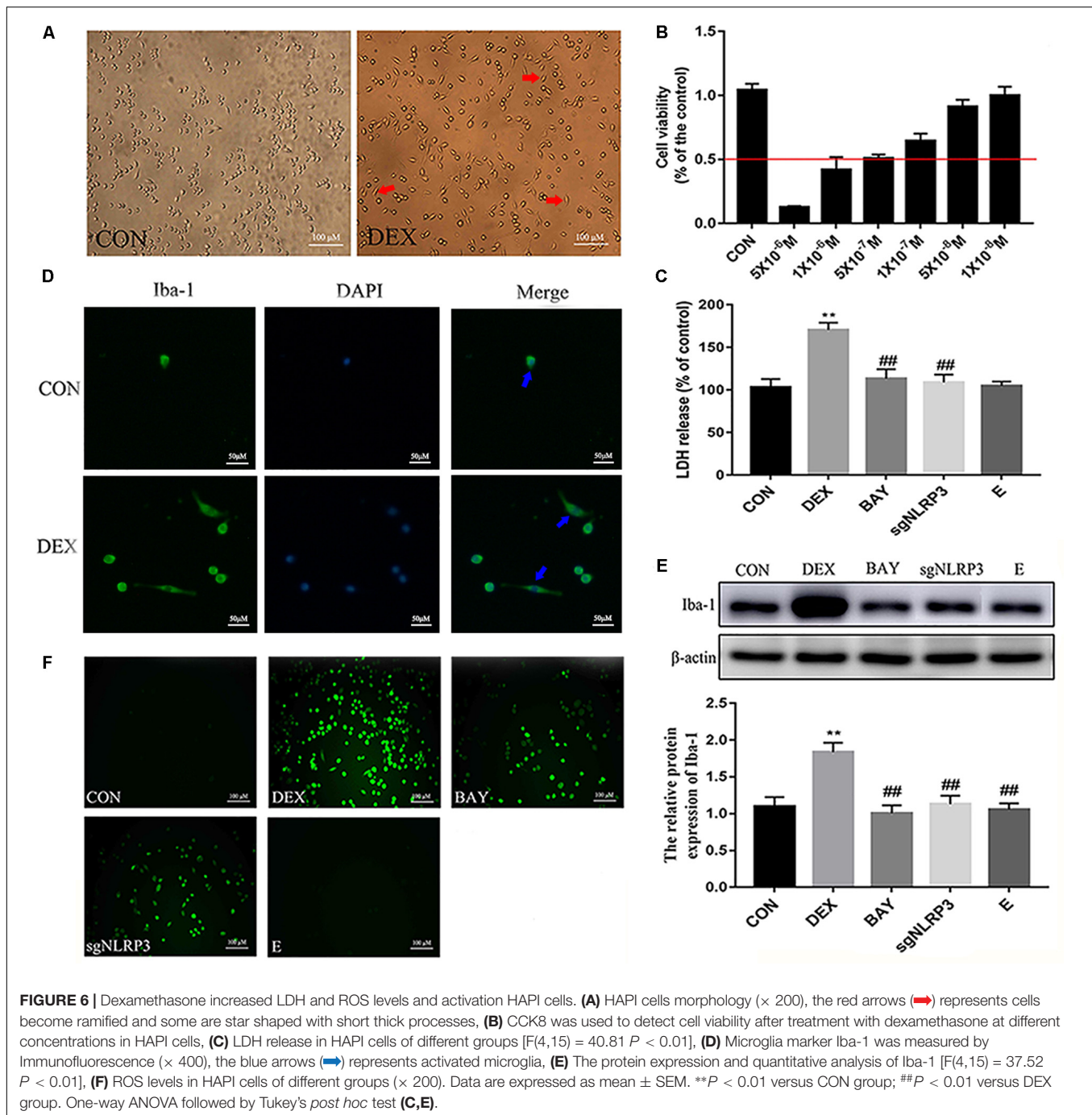
### Chronic Stress Induces Glucocorticoid Release and ROS Production

We speculated that chronic restraint stress would induce corticosterone release, which can be used as an index of HPA activation. Compared with the C group, serum corticosterone levels were increased in the CS group (Figure 4A). Activation of the HPA axis indicates that the rats did not adapt to daily exposure to the homotypic stressor. The expression of Iba-1 in the

hippocampus was significantly higher in the CS group compared with the C group, while the expression of GR in the hippocampus was significantly reduced in the CS group compared with the C group (Figures 4B,C). Immunohistochemical analysis showed that the percentage of GR-positive cells (black arrows) was reduced in the hippocampal CA1 region in the CS group compared with the C group (Figures 4D,E). Furthermore, ROS content was significantly increased in the hippocampus in the CS group compared with the C group (Figure 4F).

### Chronic Stress Induces NF-κB and NLRP3 Inflammasome Activation in the Hippocampus

To investigate whether NF-κB and the NLRP3 inflammasome are activated in the hippocampus of rats exposed to chronic

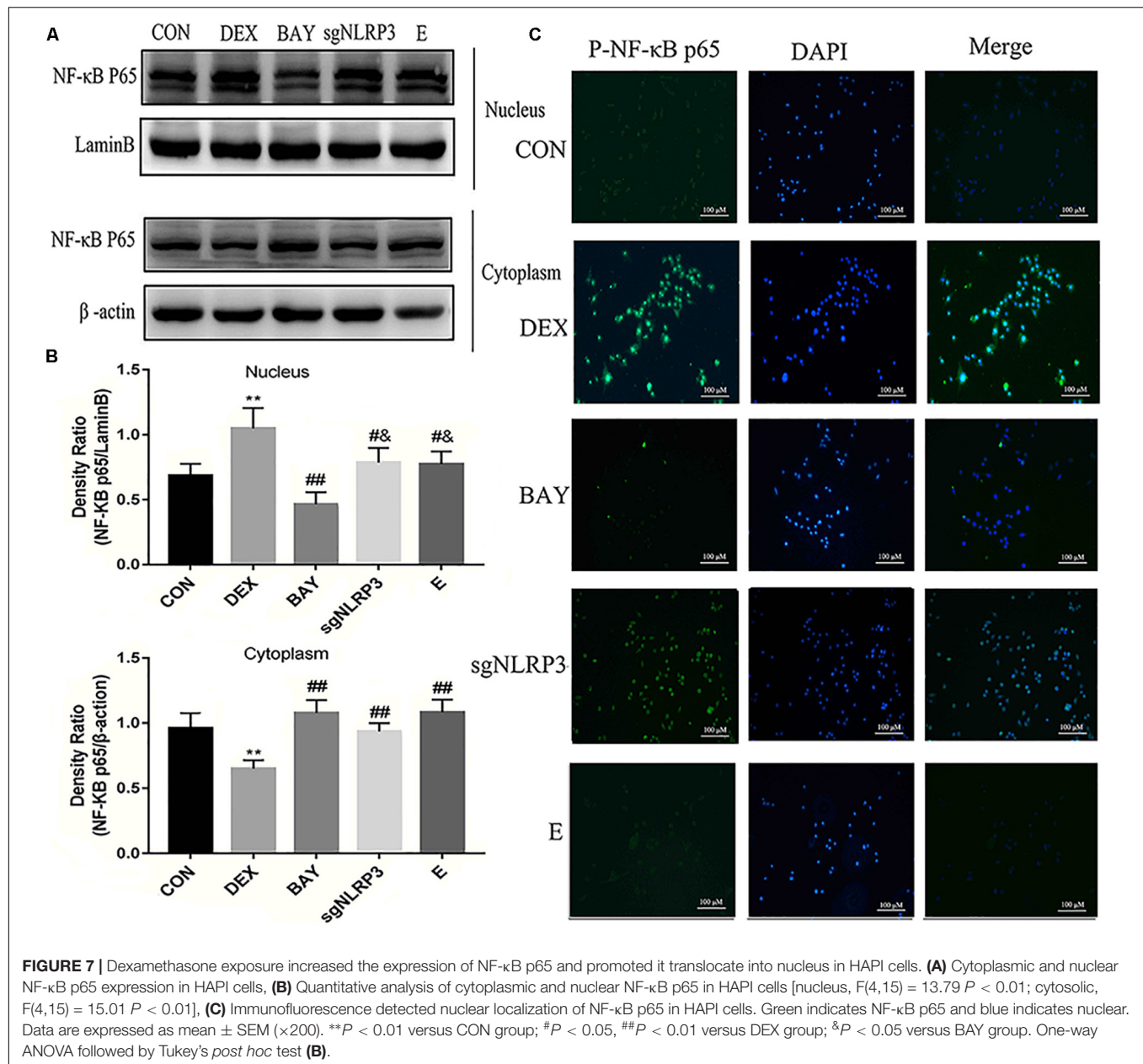


restraint stress, we measured the protein expression levels of NF- $\kappa$ B and NLRP3 inflammasome components. Nuclear NF- $\kappa$ B p65 was significantly increased and cytoplasmic NF- $\kappa$ B p65 was significantly decreased in the CS group compared with the C group (Figures 5A,B). The expression levels of NLRP3 inflammasome components (NLRP3, ASC and pro-caspase 1) as well as caspase-1 p20, IL-1 $\beta$  and IL-18 were significantly increased in the CS group compared to the C group, (Figures 5C,D). These results suggest that chronic stress induces NF- $\kappa$ B p65 expression and nuclear translocation, activates the

NLRP3 inflammasome and stimulates the production of IL-1 $\beta$  and IL-18.

### HAPI Cell Morphology and Optimum Concentration of Dexamethasone

HAPI cell morphology is shown in Figure 6A. HAPI cells in the CON group were mostly round, with high refraction and small dark nuclei. In contrast, cells in the DEX group were ramified, some with a star shaped and short thick processes (red arrows).



To evaluate the optimum concentration of dexamethasone for HAPI cells, the CCK8 assay was performed. HAPI cells were exposed to dexamethasone at different concentrations ( $5 \times 10^{-6}$  M,  $1 \times 10^{-6}$  M,  $5 \times 10^{-7}$  M,  $1 \times 10^{-7}$  M,  $5 \times 10^{-8}$  M,  $1 \times 10^{-8}$  M) for 24 h. As shown in **Figure 6B**, the  $5 \times 10^{-7}$  M concentration resulted in  $\sim 50\%$  viability.

### Dexamethasone Increases LDH and ROS Levels in HAPI Cells

To further explore changes in cell viability, we examined LDH released into the cell culture medium. As shown in **Figure 6C**, LDH release was significantly increased in the DEX group, while it was significantly decreased in the BAY and sgNLRP3 groups.

The expression of the microglia marker Iba-1 was investigated by immunofluorescence (**Figure 6D**) and western blot (**Figure 6E**). After dexamethasone exposure, Iba-1 expression was increased in HAPI cells (blue arrows), while it was significantly decreased in the BAY and sgNLRP3 groups. We also evaluated the levels of ROS in HAPI cells by immunofluorescence (**Figure 6F**). ROS levels were significantly increased in the DEX group, while they were significantly reduced in the BAY and sgNLRP3 groups.

### Dexamethasone Activates NF-κB/NLRP3 Inflammasome Pathway in HAPI Cells

NF-κB may function as the upstream transcriptional activator of NLRP3. To further clarify the role of the NF-κB-NLRP3



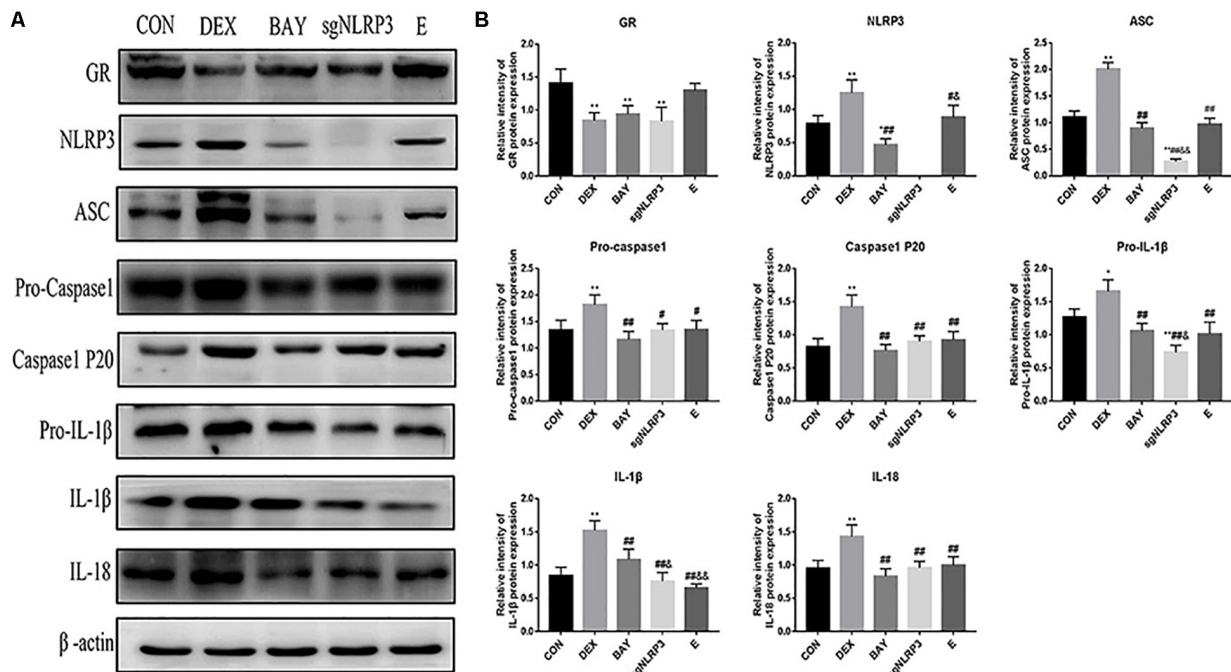


**FIGURE 8 |** Dexamethasone exposure increased the expression of NLRP3 inflammasome pathway in HAPI cells. **(A)** The protein expressions of GR and NLRP3 inflammasome components and its downstream inflammatory factors, **(B)** Quantitative analysis of GR [F(4,15) = 11.13  $P < 0.01$ ] and NLRP3 inflammasome components NLRP3 [F(4,15) = 47.79  $P < 0.01$ ], ASC [F(4,15) = 135.38  $P < 0.01$ ], pro-caspase 1 [F(4,15) = 8.83  $P < 0.01$ ], caspase-1 p20 [F(4,15) = 17.27  $P < 0.01$ ] and its downstream inflammatory factors pro-IL-1 $\beta$  [F(4,15) = 22.85  $P < 0.05$ ], IL-1 $\beta$  [F(4,15) = 29.09  $P < 0.01$ ], IL-18 [F(4,15) = 12.76  $P < 0.01$ ]. Data are expressed as mean  $\pm$  SEM. \* $P < 0.05$ , \*\* $P < 0.01$  versus CON group; # $P < 0.05$ , ## $P < 0.01$  versus DEX group; & $P < 0.05$ , && $P < 0.01$  versus BAY group; \$ $P < 0.05$ , \$\$ $P < 0.01$  versus sgNLRP3 group. One-way ANOVA followed by Tukey's *post hoc* test **(B)**.

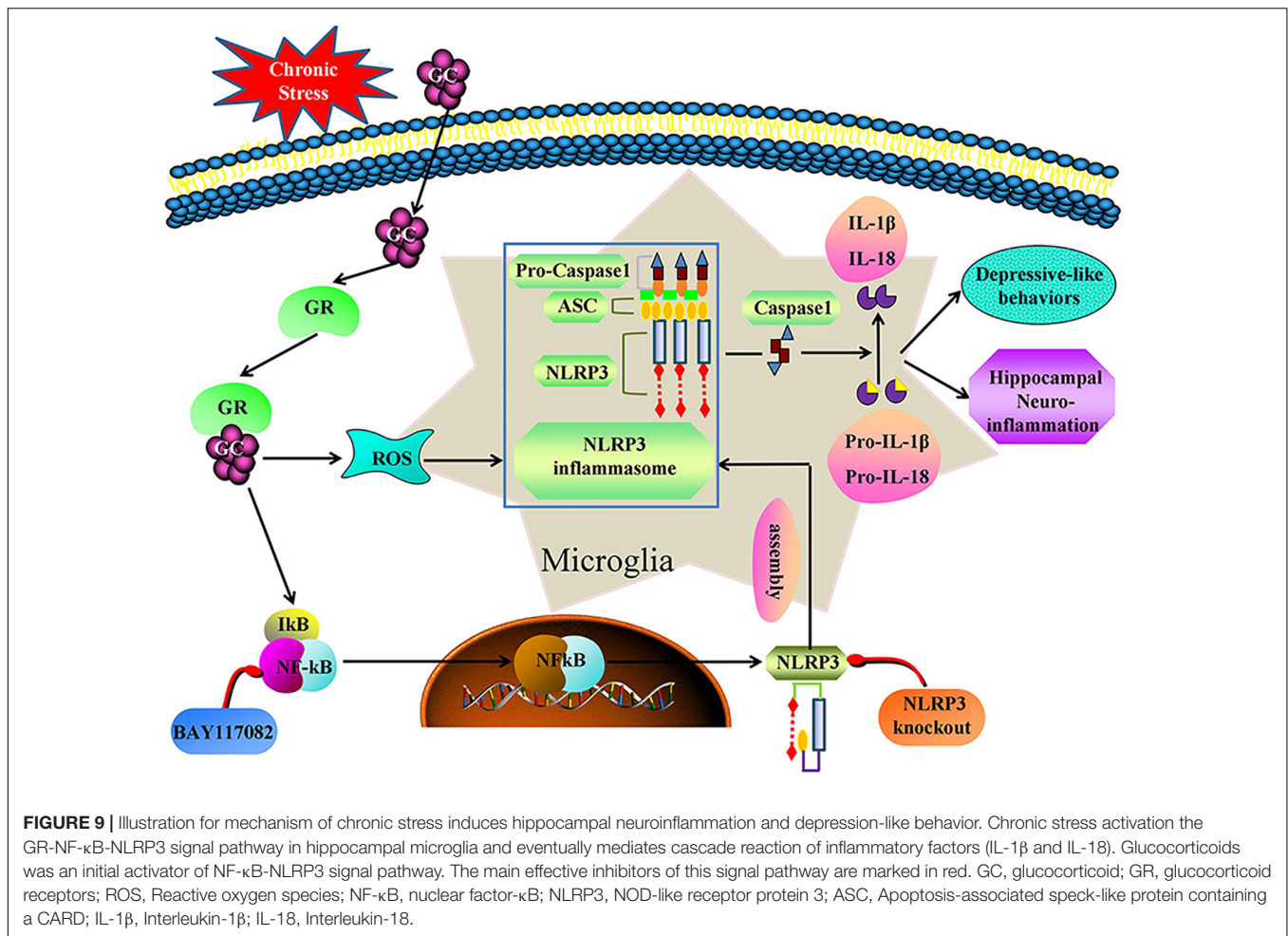
inflammasome pathway in microglial, we used the NF- $\kappa$ B p65 inhibitor BAY117082 and knocked out the NLRP3 gene using the CRISPR/Cas9 technique. Compared with the CON group, nuclear NF- $\kappa$ B p65 levels were increased, while cytoplasmic NF- $\kappa$ B p65 expression decreased in the DEX group. Compared with the DEX group, nuclear NF- $\kappa$ B p65 was decreased, while cytoplasmic NF- $\kappa$ B p65 was increased in the BAY, sgNLRP3 and E groups. Compared with the BAY group, nuclear NF- $\kappa$ B p65 was increased, while cytoplasmic NF- $\kappa$ B p65 was unaffected in the sgNLRP3 and E groups (**Figures 7A,B**). Immunofluorescence analysis showed that after dexamethasone treatment, NF- $\kappa$ B p65 translocated to the nuclei in HAPI cells (**Figure 7C**). In the BAY group, nuclear entry of NF- $\kappa$ B p65 was reduced compared with the CON group. In the sgNLRP3 group, NF- $\kappa$ B p65 translocation into the nucleus was significantly decreased compared with the DEX group, while there was no significant difference from the CON group.

We measured protein levels of GR, NLRP3 inflammasome components, caspase-1 p20, IL-1 $\beta$  and IL-18 in HAPI cells (**Figures 8A,B**). Compared with the CON group, the expression of GR was significantly decreased in the DEX, BAY and sgNLRP3 groups. NLRP3 inflammasome components, caspase-1 p20, pro-IL-1 $\beta$ , IL-1 $\beta$  and IL-18 were significantly upregulated in the DEX group compared with the CON group. NLRP3 inflammasome components, caspase-1 p20, pro-IL-1 $\beta$ , IL-1 $\beta$  and IL-18 were significantly downregulated in the BAY group compared with the

DEX group, while there was no significant difference from the CON group, except for NLRP3. ASC, pro-caspase 1, caspase-1 p20, pro-IL-1 $\beta$ , IL-1 $\beta$  and IL-18 were significantly downregulated in the sgNLRP3 group compared with the DEX group, while there was no significant difference from the CON group, except for ASC and pro-IL-1 $\beta$ . Taken together, these results demonstrate that dexamethasone induces NF- $\kappa$ B p65 expression and nuclear translocation, which in turn activates the NLRP3 inflammasome and triggers an inflammatory cascade.

## DISCUSSION

Numerous studies show that rats exposed to chronic restraint stress, consisting of a daily 6-h restraint period for 21 consecutive days, exhibit long-lasting depressive-like behavior (Donohue et al., 2006; Qiao et al., 2016). In the current study, we used this chronic restraint stress model of depression. Dexamethasone treatment of HAPI cells (a rat microglial cell line) was used to mimic depression and validate the *in vivo* findings. Firstly, we confirmed that chronic stress caused depression-like behavior in rats. Secondly, chronic stress induced excessive activation of the HPA (i.e., increased serum corticosterone concentration). Thirdly, increased glucocorticoid concentration may be the initial trigger of hippocampal microglia activation and neuroinflammation.



Fourthly, chronic stress elevated ROS levels, upregulated NF-κB, and activated the NLRP3 inflammasome in the hippocampus. Finally, NF-κB inhibitors and NLRP3 knockout showed that NF-κB is a major activator of the NLRP3 inflammasome in microglia and the inflammatory cascade, which induce microglia neuroinflammation. Thus, the GR-NF-κB-NLRP3 signaling pathway in microglia triggers a cascade of downstream inflammatory factors that mediates chronic stress-induced hippocampal neuroinflammation and depressive behavior.

Chronic stress induces depression-like behaviors in animals, including anhedonia (reduced sucrose preference) (Chiba et al., 2012), which is a core symptom of human depression (Hill et al., 2012). Here, we found that exposure to chronic stress induced depressive-like behavior in the SPT, OFT and FST, which mainly showed reduced sucrose consumption (SPT), reduced total distance traveled, number of crossings and rearing (OFT), and increased immobility time (FST). These results are consistent with previous reports on the behavioral effects of chronic stress (Cridder et al., 2018). Notably, we observed pathomorphological changes in the hippocampal regions. Therefore, chronic stress causes hippocampal damage that may underlie the depressive-like behavior.

Stress-induced glucocorticoid release is a neuroendocrine response to danger (Frank et al., 2013). The GR plays a major role in the adaptive stress response. However, stress-induced glucocorticoid hyper-secretion is associated with altered GR signaling (Finsterwald and Alberini, 2014). In the present study, we found that chronic stress exposure causes elevated corticosterone levels and a reduction in GR expression in the hippocampus. Studies have shown that SH-SY5Y cells exposed to dexamethasone mimic the hypersecretion of glucocorticoids in depression *in vitro* (Lim et al., 2018). Therefore, HAPI cells exposed to dexamethasone were used in this study to mimic glucocorticoid-induced neuroinflammation and depression. Dexamethasone treatment downregulated the GR. Both the *in vitro* and *in vivo* results suggest a link between chronic stress, glucocorticoids, GR signaling, and depression.

Overexposure to glucocorticoids may induce oxidative and inflammatory imbalance in the brain, thereby impairing neurogenesis and neuronal plasticity (Leonard and Maes, 2012). Corticosterone increases ROS levels in the brain, downregulates antioxidant enzymes, and induces depressive-like behavior (Sato et al., 2010). Our results that chronic stress increases levels of ROS in the hippocampus are in agreement with previous studies. Studies have also shown that chronic stress enhances NF-κB

signaling induced by cholinergic depletion in the hippocampus, thereby increasing the expression of pro-inflammatory factors (Lee et al., 2018). This is in line with our current finding that chronic stress induces NF- $\kappa$ B expression and promotes NF- $\kappa$ B translocation to the nucleus in the hippocampus. Furthermore, dexamethasone increased levels of ROS and promoted NF- $\kappa$ B translocation to the nucleus in HAPI cells *in vitro*. Collectively, these results suggest that glucocorticoids signal through the GR to increase ROS levels and NF- $\kappa$ B nuclear translocation, promote transcription of downstream genes, and initiate the inflammatory response.

Microglia, the resident immune cells of the CNS, are markedly activated after stress exposed in brain regions associated with depression (Franklin et al., 2018). It has been reported that excessive activation of microglia increases the expression of inflammatory markers in the hippocampus of depressive individuals (Zhang Y. et al., 2016). Microglial activation is observed in the hippocampus after exposure to restraint stress in rodents (Tynan et al., 2010). In the present study, we discovered that microglia in the hippocampus were activated by chronic restraint stress, as shown by increased Iba-1 expression. Dexamethasone also similarly activated HAPI cells *in vitro*. Our findings are consistent with previous studies showing that chronic stress-induced depression is associated with increased numbers of Iba-1-positive cells in the hippocampus (Koo et al., 2018) and that activated microglia play an important role in neuroinflammation (Wang et al., 2018).

Accumulating evidence indicates that the NLRP3 inflammasome is involved in neuroinflammation, neurodegenerative disorders (Jang et al., 2016; Zhang P. et al., 2016) and neuropsychiatric disorders such as depression (Jeon et al., 2017). Studies show that both NF- $\kappa$ B and ROS can activate the NLRP3 inflammasome. NF- $\kappa$ B translocates to the nucleus binding with DNA and triggers the transcription of pro-IL-1 $\beta$ , pro-IL-18 and NLRP3 (Choi and Ryter, 2014). ROS triggers the assembly of the NLRP3 inflammasome complex by recruiting ASC and pro-caspase 1 (Hu and Chai, 2016), driving a pro-inflammatory response that ultimately leads to cell damage (Gurung et al., 2015). *In vivo* results indicate that chronic stress activates NLRP3 inflammasome, which are expressed as NLRP3 expression, caspase-1 cleavage, and subsequent IL-1 $\beta$  and IL-18 generation. *In vitro* studies also show that dexamethasone activates NLRP3 inflammasome in HAPI cells. Interestingly, a recent study showed NF- $\kappa$ B was reported to be an ROS-sensitive transcription factor that mediated NLRP3 inflammasome activation (Li et al., 2014). Another study showed that NLRP3 deficiency significantly abolishes depressive behavior in mice under immobilization stress (Alcocer-Gomez and Cordero, 2014).

To further clarify the roles of NF- $\kappa$ B and the NLRP3 inflammasome in depression, we inhibited NF- $\kappa$ B and knocked out the NLRP3 gene *in vitro*. Western blot results confirmed successful knockdown of NLRP3 gene (**Supplementary Figure S1**). Downregulation of NF- $\kappa$ B and NLRP3 reduced ROS levels, inhibited microglial activation, decreased Iba-1 expression, inhibited NF- $\kappa$ B nuclear translocation, and reduced NLRP3 inflammasome activation. These findings

indicate that ROS and NF- $\kappa$ B-induced activation of the NLRP3 inflammasome in microglia contributes to hippocampal injury and the development of depression. Consistent with previous study, activated NLRP3 inflammasomes in microglia are involved in CMS-induced depression-like behavior in rats (Wang et al., 2018). Therefore, microglia and the NLRP3 inflammasome may have potential as drug targets for the treatment of depression. A better understanding of the anti-inflammatory properties of antidepressants may help advance therapy for neurodegenerative and psychiatric diseases associated with microglial hyperactivation.

In summary, HAPI cells were pretreated with dexamethasone to assess stress-induced changes in microglia cells in culture. Compared with *in vivo* results, it was first demonstrated that increased glucocorticoid concentration is the initial trigger for microglial activation and neuroinflammation. Secondly, it was proved that NF- $\kappa$ B is function as the upstream transcriptional activator of NLRP3. Finally, it was further confirmed that NLRP3 inflammasome activation in microglia mediates chronic stress-induced hippocampal neuroinflammation.

There are a number of limitations to this study. First, only limited animal models can properly express psychiatric symptoms (Suzuki et al., 2019), although chronic restraint stress has been widely used to induce depression and anxiety-like behavior in animal models (Huang et al., 2015), it may not adequately mimic depression in humans. Second, the production and release of IL-1 $\beta$  and IL-18 are regulated by active caspase-1. However, the activation of caspase-1 is promoted by various NLR family members, including NLRP1, NLRP3, NLRP4 (Eder, 2009). Further study is therefore needed to evaluate the impact of other inflammasome subtypes on the activation and release of IL-1 $\beta$  and IL-18. In our study, we only focus on the role of NLRP3 in the process of depression.

## CONCLUSION

We demonstrate that, chronic stress causes hippocampal neuroinflammation and depression-like behavior by activating the GR-NF- $\kappa$ B-NLRP3 signaling pathway in microglia (summarized in **Figure 9**). Our study provides fresh insight into the pathogenesis of depression and provides new therapeutic targets for the treatment of the disease. Inhibiting glucocorticoid release, NF- $\kappa$ B nuclear transcription, NLRP3 inflammasome activation and restoring microglial homeostasis in the hippocampus are novel strategies for the development of effective treatments for the management of depression in humans.

## DATA AVAILABILITY

All datasets used to support the results of this study are included in the manuscript without any reservations.

## ETHICS STATEMENT

**Animal Subjects:** The animal study was reviewed and approved by the ethical committee of Northeast



Agricultural University (SRM-11), and experiments were carried out in accordance with the National Institutes of Health Guide for Care and Use of Laboratory Animals.

## AUTHOR CONTRIBUTIONS

HF and XF contributed to study design. XF, YZ, and CW carried out the experiment. MS, YY, and TY contributed to data statistical analysis. XF wrote the manuscript. All authors read and approved the final manuscript.

## REFERENCES

- Alcocer-Gomez, E., and Cordero, M. D. (2014). NLRP3 inflammasome: a new target in major depressive disorder. *CNS. Neurosci. Ther.* 20, 294–295. doi: 10.1111/cns.12230
- Alcocer-Gomez, E., de Miguel, M., Casas-Barquero, N., Nunez-Vasco, J., Sanchez-Alcazar, J. A., Fernandez-Rodriguez, A., et al. (2014). NLRP3 inflammasome is activated in mononuclear blood cells from patients with major depressive disorder. *Brain Behav. Immun.* 36, 111–117. doi: 10.1016/j.bbi.2013.10.017
- Ashraf, A., Mahmoud, P. A., Reda, H., Mansour, S., Helal, M. H., Michel, H. E., et al. (2019). Silymarin and silymarin nanoparticles guard against chronic unpredictable mild stress induced depressive-like behavior in mice: involvement of neurogenesis and NLRP3 inflammasome. *J. Psychopharmacol.* 33, 615–631. doi: 10.1177/0269881119836221
- Austin, M. P., Mitchell, P., and Goodwin, G. M. (2001). Cognitive deficits in depression: possible implications for functional neuropathology. *Br. J. Psychiatry* 178, 200–206. doi: 10.1192/bjp.178.3.200
- Bogdanova, O. V., Kanekar, S., D'Anci, K. E., and Renshaw, P. F. (2013). Factors influencing behavior in the forced swim test. *Physiol. Behav.* 118, 227–239. doi: 10.1016/j.physbeh.2013.05.012
- Bollinger, J. L., Bergeon Burns, C. M., and Wellman, C. L. (2016). Differential effects of stress on microglial cell activation in male and female medial prefrontal cortex. *Brain Behav. Immun.* 52, 88–97. doi: 10.1016/j.bbi.2015.10.003
- Brites, D., and Fernandes, A. (2015). Neuroinflammation and depression: microglia activation, extracellular microvesicles and microRNA dysregulation. *Front. Cell. Neurosci.* 9:476. doi: 10.3389/fncel.2015.00476
- Chiba, S., Numakawa, T., Ninomiya, M., Richards, M. C., Wakabayashi, C., and Kunugi, H. (2012). Chronic restraint stress causes anxiety- and depression-like behaviors, downregulates glucocorticoid receptor expression, and attenuates glutamate release induced by brain-derived neurotrophic factor in the prefrontal cortex. *Prog. Neuropsychopharmacol. Biol. Psychiatry* 39, 112–119. doi: 10.1016/j.pnpbp.2012.05.018
- Choi, A. J., and Ryter, S. W. (2014). Inflammasomes: molecular regulation and implications for metabolic and cognitive diseases. *Mol. Cell.* 37, 441–448. doi: 10.14348/molcells.2014.0104
- Crider, A., Feng, T., Pandya, C. D., Davis, T., Nair, A., Ahmed, A. O., et al. (2018). Complement component 3a receptor deficiency attenuates chronic stress-induced monocyte infiltration and depressive-like behavior. *Brain Behav. Immun.* 70, 246–256. doi: 10.1016/j.bbi.2018.03.004
- Donohue, H. S., Gabbott, P. L., Davies, H. A., Rodriguez, J. J., Cordero, M. I., Sandi, C., et al. (2006). Chronic restraint stress induces changes in synapse morphology in stratum lacunosum-moleculare CA1 rat hippocampus: a stereological and three-dimensional ultrastructural study. *Neuroscience* 140, 597–606. doi: 10.1016/j.neuroscience.2006.02.072
- Drevets, W. C., Price, J. L., and Furey, M. L. (2008). Brain structural and functional abnormalities in mood disorders: implications for neurocircuitry models of depression. *Brain Struct. Funct.* 213, 93–118. doi: 10.1007/s00429-008-0189-x
- Eder, C. (2009). Mechanisms of interleukin-1 beta release. *Immunobiology* 214, 543–553. doi: 10.1016/j.imbio.2008.11.007

## FUNDING

This work was supported by a National Natural Science Foundation of China (Grant Nos. 31802251 and 31772806) and National Key Research and Development Project of China (Grant No. 2016YFD0501008).

## SUPPLEMENTARY MATERIAL

The Supplementary Material for this article can be found online at: <https://www.frontiersin.org/articles/10.3389/fnmol.2019.00210/full#supplementary-material>

- Finsterwald, C., and Alberini, C. M. (2014). Stress and glucocorticoid receptor-dependent mechanisms in long-term memory: from adaptive responses to psychopathologies. *Neurobiol. Learn. Mem.* 112, 17–29. doi: 10.1016/j.nlm.2013.09.017
- Frank, M. G., Hershman, S. A., Weber, M. D., Watkins, L. R., and Maier, S. F. (2014). Chronic exposure to exogenous glucocorticoids primes microglia to pro-inflammatory stimuli and induces NLRP3 mRNA in the hippocampus. *Psychoneuroendocrinology* 40, 191–200. doi: 10.1016/j.psyneuen.2013.11.006
- Frank, M. G., Watkins, L. R., and Maier, S. F. (2013). Stress-induced glucocorticoids as a neuroendocrine alarm signal of danger. *Brain Behav. Immun.* 33, 1–6. doi: 10.1016/j.bbi.2013.02.004
- Franklin, T. C., Wohleb, E. S., Zhang, Y., Fogaca, M., Hare, B., and Duman, R. S. (2018). Persistent increase in microglial RAGE contributes to chronic stress-induced priming of depressive-like behavior. *Biol. Psychiatry* 8, 50–60. doi: 10.1016/j.biopsych.2017.06.034
- Gao, H., Zhu, X., Xi, Y., Li, Q., Shen, Z., and Yang, Y. (2018). Anti-depressant-like effect of atractylenolide I in a mouse model of depression induced by chronic unpredictable mild stress. *Exp. Ther. Med.* 15, 1574–1579. doi: 10.3892/etm.2017.5517
- Gross, O., Thomas, C. J., Guarda, G., and Tschopp, J. (2011). The inflammasome: an integrated view. *Immunol. Rev.* 243, 136–151. doi: 10.1111/j.1600-065X.2011.01046.x
- Gurung, P., Lukens, J. R., and Kanneganti, T. D. (2015). Mitochondria: diversity in the regulation of the NLRP3 inflammasome. *Trends. Mol. Med.* 21, 193–201. doi: 10.1016/j.molmed.2014.11.008
- Hayden, E. P., Klein, D. N., Dougherty, L. R., Olino, T. M., Dyson, M. W., Durbin, C. E., et al. (2010). The role of brain-derived neurotrophic factor genotype, parental depression, and relationship discord in predicting early-emerging negative emotionality. *Psychol. Sci.* 21, 1678–1685. doi: 10.1177/0956797610385357
- Hill, M. N., Hellemans, K. G., Verma, P., Gorzalka, B. B., and Weinberg, J. (2012). Neurobiology of chronic mild stress: parallels to major depression. *Neurosci. Biobehav. Rev.* 36, 2085–2117. doi: 10.1016/j.neubiorev.2012.07.001
- Hu, Z., and Chai, J. (2016). Structural mechanisms in NLR inflammasome assembly and signaling. *Curr. Top. Microbiol. Immunol.* 397, 23–42. doi: 10.1007/978-3-319-41171-2\_2
- Huang, P., Li, C., Fu, T., Zhao, D., Yi, Z., and Lu, Q. (2015). Flupirtine attenuates chronic restraint stress-induced cognitive deficits and hippocampal apoptosis in male mice. *Behavioural. Brain Res.* 288, 1–10. doi: 10.1016/j.bbr.2015.04.004
- Jang, J., Park, S., Jin Hur, H., Cho, H. J., Hwang, I., Pyo Kang, Y., et al. (2016). 25-hydroxycholesterol contributes to cerebral inflammation of X-linked adrenoleukodystrophy through activation of the NLRP3 inflammasome. *Nat. Commun.* 7:13129. doi: 10.1038/ncomms13129
- Jeon, S. A., Lee, E., Hwang, I., Han, B., Park, S., Son, S., et al. (2017). NLRP3 Inflammasome contributes to lipopolysaccharide-induced depressive-like behaviors via indoleamine 2,3-dioxygenase induction. *Int. J. Neuropsychopharmacol.* 20, 896–906. doi: 10.1093/ijnp/pyx065
- Joels, M. (2011). Impact of glucocorticoids on brain function: relevance for mood disorders. *Psychoneuroendocrinology* 36, 406–414. doi: 10.1016/j.psyneuen.2010.03.004



- Koo, Y. S., Kim, H., Park, J. H., Kim, M. J., Shin, Y. I., and Choi, B. T. (2018). Indoleamine 2,3-dioxygenase-dependent neurotoxic kynurenine metabolism contributes to poststroke depression induced in mice by ischemic stroke along with spatial restraint stress. *Oxid. Med. Cell. Longev.* 2018:2413841. doi: 10.1155/2018/2413841
- Lawson, L. J., Perry, V. H., Dri, P., and Gordon, S. (1990). Heterogeneity in the distribution and morphology of microglia in the normal adult mouse brain. *Neuroscience* 39, 151–170. doi: 10.1016/0306-4522(90)90229-w
- Lee, S. Y., Cho, W. H., Lee, Y. S., and Han, J. S. (2018). Impact of chronic stress on the spatial learning and GR-PKAc-NF-kappaB signaling in the hippocampus and cortex in rats following cholinergic depletion. *Mol. Neurobiol.* 55, 3976–3989. doi: 10.1007/s12035-017-0620-5
- Lee, V., Sarkar, J., and Maguire, J. (2014). Loss of gabrd in CRH neurons blunts the corticosterone response to stress and diminishes stress-related behaviors. *Psychoneuroendocrinology* 41, 75–88. doi: 10.1016/j.psyneuen.2013.12.011
- Leonard, B., and Maes, M. (2012). Mechanistic explanations how cell-mediated immune activation, inflammation and oxidative and nitrosative stress pathways and their sequels and concomitants play a role in the pathophysiology of unipolar depression. *Neurosci. Biobehav. Rev.* 36, 764–785. doi: 10.1016/j.neubiorev.2011.12.005
- Li, B., Abdalrahman, A., Lai, Y., Janicki, J. S., Ward, K. W., Meyer, C. J., et al. (2014). Dihydro-CDDO-trifluoroethyl amide suppresses inflammatory responses in macrophages via activation of Nrf2. *Biochem. Biophys. Res. Commun.* 444, 555–561. doi: 10.1016/j.bbrc.2014.01.101
- Lim, D. W., Um, M. Y., Han, T., Lee, J., Kim, Y. T., Cho, S., et al. (2018). Standardized citrus unshiu peel extract ameliorates dexamethasone-induced neurotoxicity and depressive-like behaviors in mice. *Metab. Brain. Dis.* 33, 1877–1886. doi: 10.1007/s11011-018-0294-3
- Overstreet, D. H. (2012). Modeling depression in animal models. *Methods Mol. Biol.* 829, 125–144. doi: 10.1007/978-1-61779-458-2\_7
- Pace, T. W., and Miller, A. H. (2009). Cytokines and glucocorticoid receptor signaling. Relevance to major depression. *Ann. N.Y. Acad. Sci.* 1179, 86–105. doi: 10.1111/j.1749-6632.2009.04984.x
- Park, H. J., Shim, H. S., An, K., Starkweather, A., Kim, K. S., and Shim, I. (2015). IL-4 inhibits IL-1beta-induced depressive-like behavior and central neurotransmitter alterations. *Mediators. Inflamm.* 2015, 1–9. doi: 10.1155/2015/941413
- Price, J. L., and Drevets, W. C. (2010). Neurocircuitry of mood disorders. *Neuropsychopharmacology* 35, 192–216. doi: 10.1038/npp.2009.104
- Qiao, H., Li, M. X., Xu, C., Chen, H. B., An, S. C., and Ma, X. M. (2016). Dendritic spines in depression: what we learned from animal models. *Neural. Plast.* 2016, 1–26. doi: 10.1155/2016/8056370
- Rivier, C., and Vale, W. (1983). Modulation of stress-induced ACTH release by corticotropin-releasing factor, catecholamines and vasopressin. *Nature* 305, 325–327. doi: 10.1038/305325a0
- Sato, H., Takahashi, T., Sumitani, K., Takatsu, H., and Urano, S. (2010). Glucocorticoid generates ROS to induce oxidative injury in the hippocampus, leading to impairment of cognitive function of rats. *J. Clin. Biochem. Nutr.* 47, 224–232. doi: 10.3164/jcbn.10-58
- Seo, M. K., Choi, C. M., McIntyre, R. S., Cho, H. Y., Lee, C. H., Mansur, R. B., et al. (2017). Effects of escitalopram and paroxetine on mTORC1 signaling in the rat hippocampus under chronic restraint stress. *BMC Neurosci.* 18:39. doi: 10.1186/s12868-017-0357-0
- Singhal, G., and Baune, B. T. (2017). Microglia: an interface between the loss of neuroplasticity and depression. *Front. Cell. Neurosci.* 11:270. doi: 10.3389/fncel.2017.00270
- Suzuki, H., Ohgidani, M., Kuwano, N., Chretien, F., Lorin de la Grandmaison, G., and Onaya, M. (2019). Suicide and microglia: recent findings and future perspectives based on human studies. *Front. Cell. Neurosci.* 13:31. doi: 10.3389/fncel.2019.00031
- Tronel, C., Largeau, B., Santiago Ribeiro, M. J., Guilloteau, D., Dupont, A. C., and Arlicot, N. (2017). Molecular targets for PET imaging of activated microglia: the current situation and future expectations. *Int. J. Mol. Sci.* 18, E802. doi: 10.3390/ijms18040802
- Tynan, R. J., Naicker, S., Hinwood, M., Nalivaiko, E., Buller, K. M., Pow, D. V., et al. (2010). Chronic stress alters the density and morphology of microglia in a subset of stress-responsive brain regions. *Brain Behav. Immun.* 24, 1058–1068. doi: 10.1016/j.bbi.2010.02.001
- Uchiyama, Y., Tanaka, K., Asano, T., Tamura, F., and Mizushima, T. (2016). Superoxide dismutase overexpression protects against glucocorticoid-induced depressive-like behavioral phenotypes in mice. *Biochem. Biophys. Res. Commun.* 469, 873–877. doi: 10.1016/j.bbrc.2015.12.085
- Walker, F. R., Nilsson, M., and Jones, K. (2013). Acute and chronic stress-induced disturbances of microglial plasticity, phenotype and function. *Curr. Drug. Targets.* 14, 1262–1276. doi: 10.2174/13894501113149990208
- Walsh, J. G., Muruve, D. A., and Power, C. (2014). Inflammasomes in the CNS. *Nat. Rev. Neurosci.* 15, 84–97. doi: 10.1038/nrn3638
- Wang, Y. L., Han, Q. Q., Gong, W. Q., Pan, D. H., Wang, L. Z., Hu, W., et al. (2018). Microglial activation mediates chronic mild stress-induced depressive- and anxiety-like behavior in adult rats. *J. Neuroinflammation.* 15:21. doi: 10.1186/s12974-018-1054-3
- Xu, Y., Sheng, H., Bao, Q., Wang, Y., Lu, J., and Ni, X. (2016). NLRP3 inflammasome activation mediates estrogen deficiency-induced depression- and anxiety-like behavior and hippocampal inflammation in mice. *Brain. Behav. Immun.* 56, 175–186. doi: 10.1016/j.bbi.2016.02.022
- Yang, J., Liu, R., Lu, F., Xu, F., Zheng, J., Li, Z., et al. (2019). Fast green FCF attenuates lipopolysaccharide-induced depressive-like behavior and downregulates TLR4/Myd88/NF-kappaB signal pathway in the mouse hippocampus. *Front. Pharmacol.* 10:501. doi: 10.3389/fphar.2019.00501
- Yirmiya, R., Rimmerman, N., and Reshef, R. (2015). Depression as a microglial disease. *Trends. Neurosci.* 38, 637–658. doi: 10.1016/j.tins.2015.08.001
- Yue, N., Huang, H., Zhu, X., Han, Q., Wang, Y., Li, B., et al. (2017). Activation of P2X7 receptor and NLRP3 inflammasome assembly in hippocampal glial cells mediates chronic stress-induced depressive-like behaviors. *J. Neuroinflammation.* 14:102. doi: 10.1186/s12974-017-0865-y
- Zhang, C., Zhang, Y. P., Li, Y. Y., Liu, B. P., Wang, H. Y., Li, K. W., et al. (2019). Minocycline ameliorates depressive behaviors and neuro-immune dysfunction induced by chronic unpredictable mild stress in the rat. *Behav. Brain Res.* 356, 348–357. doi: 10.1016/j.bbr.2018.07.001
- Zhang, Y., Liu, L., Liu, Y. Z., Shen, X. L., Wu, T. Y., Zhang, T., et al. (2015). NLRP3 inflammasome mediates chronic mild stress-induced depression in mice via neuroinflammation. *Int. J. Neuropsychopharmacol.* 18, 1–8. doi: 10.1093/ijnp/ppy006
- Zhang, P., Shao, X. Y., Qi, G. J., Chen, Q., Bu, L. L., Chen, L. J., et al. (2016). Cdk5-dependent activation of neuronal inflammasomes in parkinson's disease. *Mov. Disord.* 31, 366–376. doi: 10.1002/mds.26488
- Zhang, Y., Su, W. J., Chen, Y., Wu, T. Y., Gong, H., and Shen, X. L. (2016). Effects of hydrogen-rich water on depressive-like behavior in mice. *Sci. Rep.* 6:23742. doi: 10.1038/srep23742
- Zhao, J. Q., Peng, L. Z., Zheng, W. H., Wang, R. K., Zhang, L., Yang, J., et al. (2015). Chemically bonding of amantadine with gardenamide enhances the neuroprotective effects against corticosterone-induced insults in PC12 Cells. *Int. J. Mol. Sci.* 16, 22795–22810. doi: 10.3390/ijms160922795
- Zhao, X., Seese, R. R., Yun, K., Peng, T., and Wang, Z. (2013). The role of galanin system in modulating depression, anxiety, and addiction-like behaviors after chronic restraint stress. *Neuroscience* 246, 82–93. doi: 10.1016/j.neuroscience.2013.04.046
- Zhou, R., Yazdi, A. S., Menu, P., and Tschopp, J. (2011). A role for mitochondria in NLRP3 inflammasome activation. *Nature* 469, 221–225. doi: 10.1038/nature09663
- Zou, W., Feng, R., and Yang, Y. (2018). Changes in the serum levels of inflammatory cytokines in antidepressant drug-naïve patients with major depression. *Plos One* 13:e0197267. doi: 10.1371/journal.pone.0197267

**Conflict of Interest Statement:** The authors declare that the research was conducted in the absence of any commercial or financial relationships that could be construed as a potential conflict of interest.

Copyright © 2019 Feng, Zhao, Yang, Song, Wang, Yao and Fan. This is an open-access article distributed under the terms of the Creative Commons Attribution License (CC BY). The use, distribution or reproduction in other forums is permitted, provided the original author(s) and the copyright owner(s) are credited and that the original publication in this journal is cited, in accordance with accepted academic practice. No use, distribution or reproduction is permitted which does not comply with these terms.



# Structural Insights Into TDP-43 and Effects of Post-translational Modifications

Liberty François-Moutal<sup>1,2</sup>, Samantha Perez-Miller<sup>1,2</sup>, David D. Scott<sup>1,2</sup>, Victor G. Miranda<sup>1,2</sup>, Niloufar Mollasalehi<sup>1,2,3</sup> and May Khanna<sup>1,2\*</sup>

<sup>1</sup> Department of Pharmacology, College of Medicine, University of Arizona, Tucson, AZ, United States, <sup>2</sup> Center for Innovation in Brain Science, Tucson, AZ, United States, <sup>3</sup> Department of Chemistry and Biochemistry, University of Arizona, Tucson, AZ, United States

## OPEN ACCESS

### Edited by:

Serena Carra,  
University of Modena and Reggio  
Emilia, Italy

### Reviewed by:

Fabian M. Feiguin,  
International Centre for Genetic  
Engineering and Biotechnology, Italy  
Miguel Mompeán,  
Spanish National Research Council  
(CSIC), Spain

### \*Correspondence:

May Khanna  
maykhanna@email.arizona.edu

**Received:** 05 September 2019

**Accepted:** 25 November 2019

**Published:** 17 December 2019

### Citation:

François-Moutal L, Perez-Miller S, Scott DD, Miranda VG, Mollasalehi N and Khanna M (2019) Structural Insights Into TDP-43 and Effects of Post-translational Modifications. *Front. Mol. Neurosci.* 12:301. doi: 10.3389/fnmol.2019.00301

Transactive response DNA binding protein (TDP-43) is a key player in neurodegenerative diseases. In this review, we have gathered and presented structural information on the different regions of TDP-43 with high resolution structures available. A thorough understanding of TDP-43 structure, effect of modifications, aggregation and sites of localization is necessary as we develop therapeutic strategies targeting TDP-43 for neurodegenerative diseases. We discuss how different domains as well as post-translational modification may influence TDP-43 overall structure, aggregation and droplet formation. The primary aim of the review is to utilize structural insights as we develop an understanding of the deleterious behavior of TDP-43 and highlight locations of established and proposed post-translation modifications. TDP-43 structure and effect on localization is paralleled by many RNA-binding proteins and this review serves as an example of how structure may be modulated by numerous compounding elements.

**Keywords:** TDP-43 = TAR DNA-binding protein 43, structure, post-translational modification, subdomains, RRM domain

## INTRODUCTION

Transactive response DNA binding protein (TDP-43), initially discovered in 1995 as a modulator of HIV-1 gene expression (Ou et al., 1995), is a highly conserved member of the heteronuclear ribonucleotide binding protein (hnRNP) family (Purice and Taylor, 2018). The TARDBP gene is located at chromosomal locus 1p36.22 and is comprised of six exons and while several TDP-43 isoforms have been identified, these have not been well-studied (Wang et al., 2004; Strong et al., 2007; D'Alton et al., 2015).

Since its discovery, TDP-43 has been shown to be involved in nearly all aspects of RNA metabolism (reviewed in Lagier-Tourenne et al., 2010; Ratti and Buratti, 2016) and is thought to be associated with more than 6000 RNA species. Of particular interest, TDP-43 has been shown to regulate its own mRNA (Ayala et al., 2011), the alternative splicing of hnRNPA1 mRNA (Deshaies et al., 2018), key cryptic exon splicing of *C9orf72* (Buratti et al., 2001) -the well-known hexanucleotide GGGGCC repeat expansion and the most frequent genetic cause of Amyotrophic Lateral Sclerosis (ALS) and Frontotemporal Lobar Degeneration (FTLD) (Balendra and Isaacs, 2018), Tau splicing resulting in accumulation of disease-associated isoform (Gu et al., 2017, 2018).

Although predominantly in the nucleus, TDP-43 is also present at low levels throughout the cell, including cytoplasm (Ayala et al., 2008) and mitochondria (Wang et al., 2016; Davis et al., 2018).

Accumulation of insoluble, TDP-43-positive inclusions in the cytoplasm has emerged as a hallmark of ALS-FTLD. In these inclusions, TDP-43 is usually hyperphosphorylated, polyubiquitinated, and found as a mix of full-length and fragmented protein (Neumann et al., 2006, 2009; Nonaka et al., 2009b). Although it is generally accepted that TDP-43 localization to the cytoplasm is a mechanism of pathology, Moss et al. were not able to reproduce cellular pathologies by simply delocalizing TDP-43 to the cytoplasm (Wobst et al., 2017).

Although TDP-43 mutations are only associated with a small fraction of cases (Buratti, 2015), TDP-43-positive inclusions are found in the vast majority of postmortem neuronal tissue from confirmed ALS-FTLD patients (Arai et al., 2006; Neumann et al., 2009; Ling et al., 2013). Inclusions of similar histopathology are also found in other neurodegenerative disorders as well (Amador-Ortiz et al., 2007; Hasegawa et al., 2007; Leverenz et al., 2007; Nakashima-Yasuda et al., 2007; Geser et al., 2008). Additionally, both loss and excess of TDP-43 are toxic, confirming that this is an essential protein and suggesting tight regulation of expression and localization (Kraemer et al., 2010; Wu et al., 2010; Ayala et al., 2011; Budini and Buratti, 2011; Polymenidou et al., 2011; Wegorzewska and Baloh, 2011). However, despite intense research, there is no clear consensus about what causes TDP-43 mislocalization and aggregation, nor how it contributes to neuronal toxicity. For potential pathways involved in the aberrant behavior of TDP-43 we refer the reader to several recent reviews (Janssens and Van Broeckhoven, 2013; Prasad et al., 2019).

Like other RNA binding proteins (RBPs), TDP-43 has a beads-on-a string architecture consisting of multiple, independent functional domains and many sites of post-translational modification. Despite its relatively small size (43 kDa), structural determination of the full-length protein has been a challenge, likely due to the large portion of the protein that is intrinsically disordered. Estimates of intrinsically disordered regions (IDR) range from 15–30% of the total protein and 36–66% of the C-terminal domain (Mészáros et al., 2018). Nevertheless, 3-dimensional structures of the N-terminal domain, the RNA-binding domains, and segments of the C-terminal domain have become available in recent years. The primary aim of this review is to consolidate the insights that these structures bring to our developing understanding of the functions and deleterious behavior of TDP-43 and to highlight the location of both established and proposed post-translational modifications.

## Structure Overview

TDP-43 is composed of a well folded N-terminal domain (NTD), two highly conserved RNA recognition motifs (RRM1 and RRM2), and a glycine-rich C-terminal domain (**Figure 1**).

### The N-Terminal Domain and Nuclear Localization Signal

#### *Organization/oligomerization of the N-terminal domain (NTD, amino acids 1–77)*

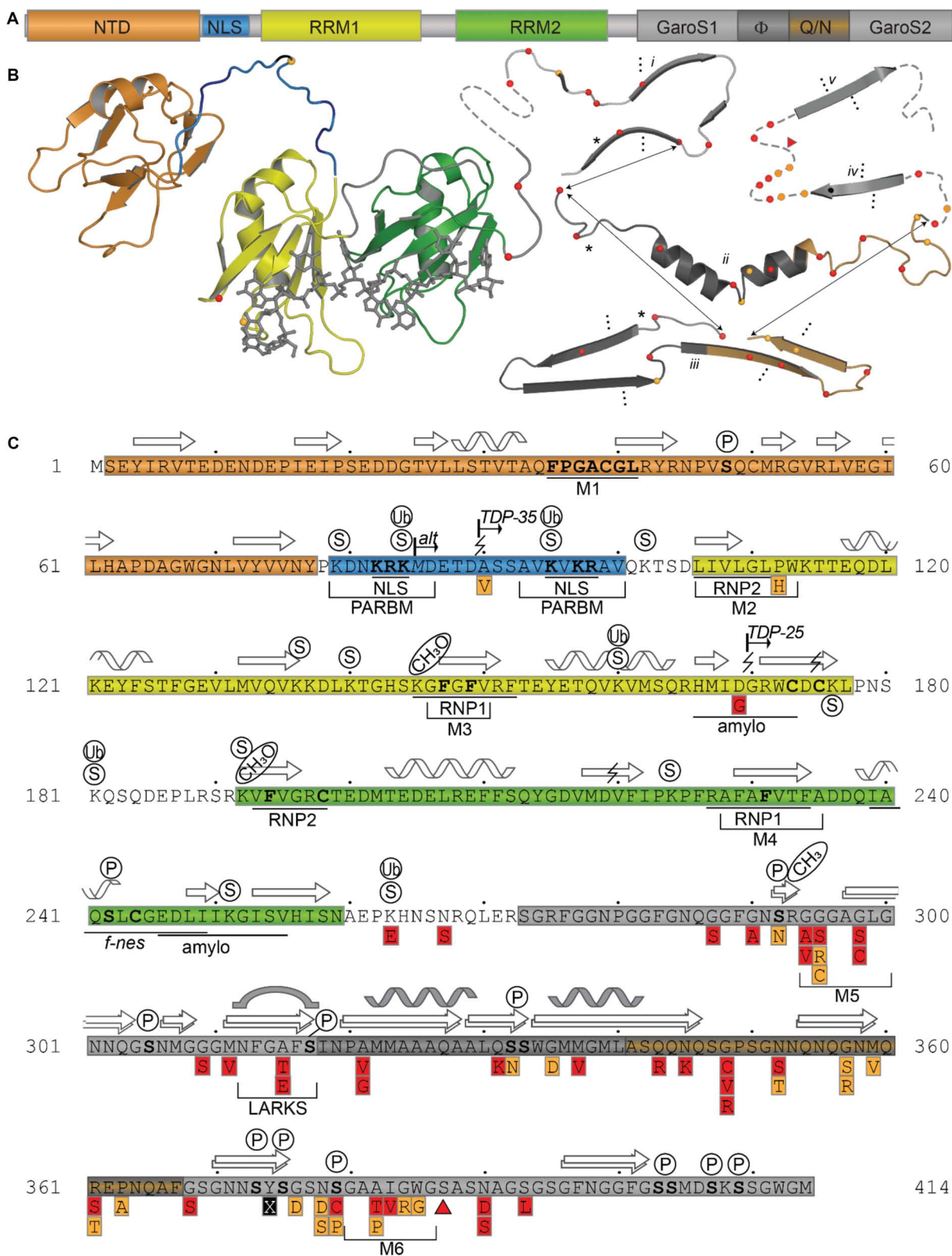
The TDP-43 N-terminal domain has been shown to form dimers and higher-order oligomers both *in vitro* and in the cell (Shiina et al., 2010; Chang et al., 2012; Wang et al., 2013;

Zhang et al., 2013; Afroz et al., 2017; Jiang et al., 2017; Mompeán et al., 2017; Sun et al., 2018; Wang A. et al., 2018) with a single dissociation constant of approximately 70  $\mu$ M, indicating absence of cooperativity in binding of subunits (Wang A. et al., 2018). Unlike pathological aggregates, which are hyperphosphorylated and ubiquitinated (Arai et al., 2006; Hasegawa et al., 2008), reversible formation of TDP-43 polymers through the NTD has been shown to be required for splicing activity (Afroz et al., 2017; Jiang et al., 2017; Mompeán et al., 2017; Wang A. et al., 2018) and to contribute to phase separation *via* liquid-droplet formation (Afroz et al., 2017; Wang A. et al., 2018), thought to contribute to formation of cytoplasmic stress granules (SGs) (Molliex et al., 2015). The NTD is also the site of one of three predicted mitochondrial targeting sequences (Wang et al., 2016), conserved phosphosite Ser 48 (Rigbolt et al., 2011; Wang A. et al., 2018), as well as potential, albeit weak, nucleotide binding (Chang et al., 2012; Qin et al., 2014; Mompeán et al., 2016; Wang L. et al., 2018). Thus far, five 3-dimensional structures of the NTD have been published, including three monomeric (Mompeán et al., 2016c, 2017; Jiang et al., 2017) and two dimeric structures (Afroz et al., 2017; Wang A. et al., 2018). Structural alignment shows that the overall folds are highly similar, with backbone root-mean-square deviations (RMSD) of 0.5–2.5 Å for individual subunits (**Table 1**).

The NTD monomer consists of six  $\beta$ -strands and a single  $\alpha$ -helix arranged in a ubiquitin-like  $\beta$ -grasp fold, similar to the DIX domain of Axin 1 (Mompeán et al., 2016c; **Figure 2A**). The DIX domain is known to facilitate both homo- and hetero-oligomerization (Kishida et al., 2015). Consistent with this, the dimeric NTD structures revealed a head-to-tail configuration of subunits (Afroz et al., 2017; Wang A. et al., 2018; **Figure 2B**). As noted by Wang A. et al. (2018) these two structures are very similar overall, differing by a moderate rotation and shift between subunits, likely due to differences in experimental conditions. In both cases, the interface is formed mainly by charged and polar residues (Afroz et al., 2017; Wang A. et al., 2018). Comparison with the monomeric structures shows that upon dimerization, a surface-accessible and mobile loop becomes more structured as it participates in the interface (**Figures 2A,B**). Phosphosite Ser 48 is also shifted toward the interface where it is involved in hydrogen bonding interactions (**Figures 2C,D**). It has been shown that mimicking phosphorylation at this site disrupts self-association of the NTD and affects splicing function (Wang A. et al., 2018). Additionally, one of three mitochondrial targeting sequences (F35 – L41) occurs in the loop following the  $\alpha$ -helix (**Figures 2A,B**), discussed in more detail below (see section “Mitochondrial Targeting”). Finally, crystal-packing symmetry in the X-ray structure suggests that the NTD alone can form a superhelical structure (Afroz et al., 2017), but the relevance of this supra-assembly for higher-order oligomerization of the full-length protein is unclear.

#### *The TDP-43 linker and nuclear localization signal (NLS, amino acids 78–100)*

The canonical, positively charged, bi-dentate nuclear localization signal (NLS, **Figure 1**) occurs in the linker between the NTD and the RNA-binding domains. The NLS is recognized by



27

FIGURE 1 | Continued



**FIGURE 1 | TDP-43 Structure and Sequence Features. (A)** Domain map showing relative sizes of the N-terminal domain (NTD, *orange*), linker containing nuclear localization signal (NLS, *blue*), RNA-recognition motif 1 (RRM1, *yellow*), RNA-recognition motif 2 (RRM2, *green*), and the C-terminal subdomains identified by Mompeán et al. (2016a): Gly-aromatic-Ser-rich regions (GaroS, *light gray*), hydrophobic region ( $\Phi$ , *dark gray*), glutamine-arginine-rich region (Q/N, *orange gray*). **(B)** Representative structures with variant sites shown as spheres and colored as in panels A and C. NTD (5mrg), RRM1-RRM2 with RNA as gray sticks (4bs2), CTD fragments *i* [6n3c (Cao et al., 2019)], *ii* [2n3x (Jiang et al., 2016)], *iii* [6n3a (Guenther et al., 2018a)], *iv* [5wia (Guenther et al., 2018a)], *v* [5wiq (Guenther et al., 2018a)]. Asterisk marks LARKS/Omega Loop. Arrows indicate residues that correspond among three shown polymorphs. Ellipses indicate tendency to form fibrils (*i*, *iii*) or steric zipper structures (*iv*, *v*). **(C)** Annotated primary sequence. Post-translational modifications shown in circles above sequence (P, phosphorylation site PhosphoSitePlus (Hornbeck et al., 2015)); S, SUMOylation sites identified by high-throughput studies (Hendriks et al., 2015, 2017); CH3, monomethylation site (Guo et al., 2014). Alternative start site at M85 [alt (Nishimoto et al., 2010)]. Caspase digestion sites [lightning bolts (Zhang et al., 2007; Rohn, 2008; Li et al., 2015; Chiang et al., 2016)]. Proposed mitochondrial targeting sequences (M1, M3, and M5) (Wang et al., 2016). Bipartite nuclear localization signal (NLS) (Winton et al., 2008) overlapping with the Poly-ADP-ribose (PAR) binding motif (PARBM) (McGurk et al., 2018). Conserved ribonucleotide interacting motifs (RNP1, RNP2) (Buratti et al., 2001). Amyloidogenic regions (amylo) (Shodai et al., 2012, 2013). Non-functional (former) nuclear export signal [f-nes (Archbold et al., 2018; Ederle et al., 2018; Pinarbasi et al., 2018)]. Sequence variants compiled using the ClinVar database (April 2019) (Landrum et al., 2016) and a review by Buratti et al. (Buratti, 2015), shown in red boxes if linked to disease, orange if clinical significance is not clear. Site of insertion/deletion [triangle (Solski et al., 2012)] and premature stop (X) also shown. Dots above sequence mark every 10 residues.

Importin- $\alpha$  for active transport of TDP-43 into the nucleus (Winton et al., 2008; Nishimura et al., 2010; Archbold et al., 2018; Pinarbasi et al., 2018). However, the NLS can be disrupted by caspase cleavage at Asp 89 (Suzuki et al., 2011) or by initiation at the alternative start site, Met 85 (Nishimoto et al., 2010; Xiao et al., 2015) resulting in accumulation of TDP-43 in the cytoplasm, an event generally agreed to result in formation of insoluble aggregates (Winton et al., 2008; Shenouda et al., 2018). In one study, the SNP A90V was shown to result in mild disruption of the NLS and low-level mislocalization (Winton et al., 2008). However, this SNP was also identified in one healthy control in the same study and two additional healthy persons in another study (Sreedharan et al., 2008), leaving the clinical significance of this substitution in doubt.

Only one structure to date contains the entire linker and this structure shows that the NLS is quite mobile (Figure 2E). The flexibility of this linker leads us to speculate that the connection between the NTD and RNA-binding domains is dynamic, allowing the arrangement of these domains to change with NTD-self association, RNA binding, post-translational modifications, and/or interactions with other proteins.

### Nucleic acid binding by the NTD and linker

Several studies have hinted at the ability of TDP-43 NTD to interact with nucleic acids (Chang et al., 2012; Qin et al., 2014; Mompeán et al., 2016c). While Chang et al. (2012) did not find a significant binding for TDP-43-NTD<sub>1–105</sub> to single stranded DNA (TG)<sub>6</sub>, the presence of TDP-43-NTD<sub>1–105</sub> did increase by three-fold the affinity of TDP-43 for this nucleic acid sequence compared to RRM only. An independent study proposed, using HSQC-NMR, the ability of the folded form to bind ssDNA (TG)<sub>6</sub>, RNA (UG)<sub>6</sub> but not ss(TT)<sub>6</sub>, suggesting a specificity component in the binding (Qin et al., 2014). While Qin et al. (2014) did not observe a binding event implicating the NLS (81–102), a third study showed a binding of this positively charged region to both ss(TG)<sub>6</sub> and ss(TT)<sub>6</sub> and report a  $K_d < 150 \mu\text{M}$  (Mompeán et al., 2016c). Even though the nucleotide binding interface of the NTD remains to be determined, it seems clear that the TDP-43 NTD and NLS serve as a structural support for nucleic

acid binding and might contribute to specificity toward certain nucleic acid sequences.

## The RNA-Recognition Motifs (RRM1-RRM2)

### RRM-nucleic acid binding

The RNA-recognition motifs of TDP-43 span amino acids 106–177 (RRM1) and 192–259 (RRM2), each of which contain two highly conserved short sequence motifs known as RNP-1 (octameric sequence: KGFGFVRF in RRM1 and RAFAFVTF in RRM2) and RNP-2 (hexameric sequence: LIVLGL in RRM1 and VFVGRC in RRM2) (Figure 1) required for nucleic acid binding. To date, there are four structures of RRM1, two structures of RRM2 and one of the tandem RRM1-RRM2. These structures are highly similar, with RMSD ranging from 0.84 to 1.37 Å (Table 1).

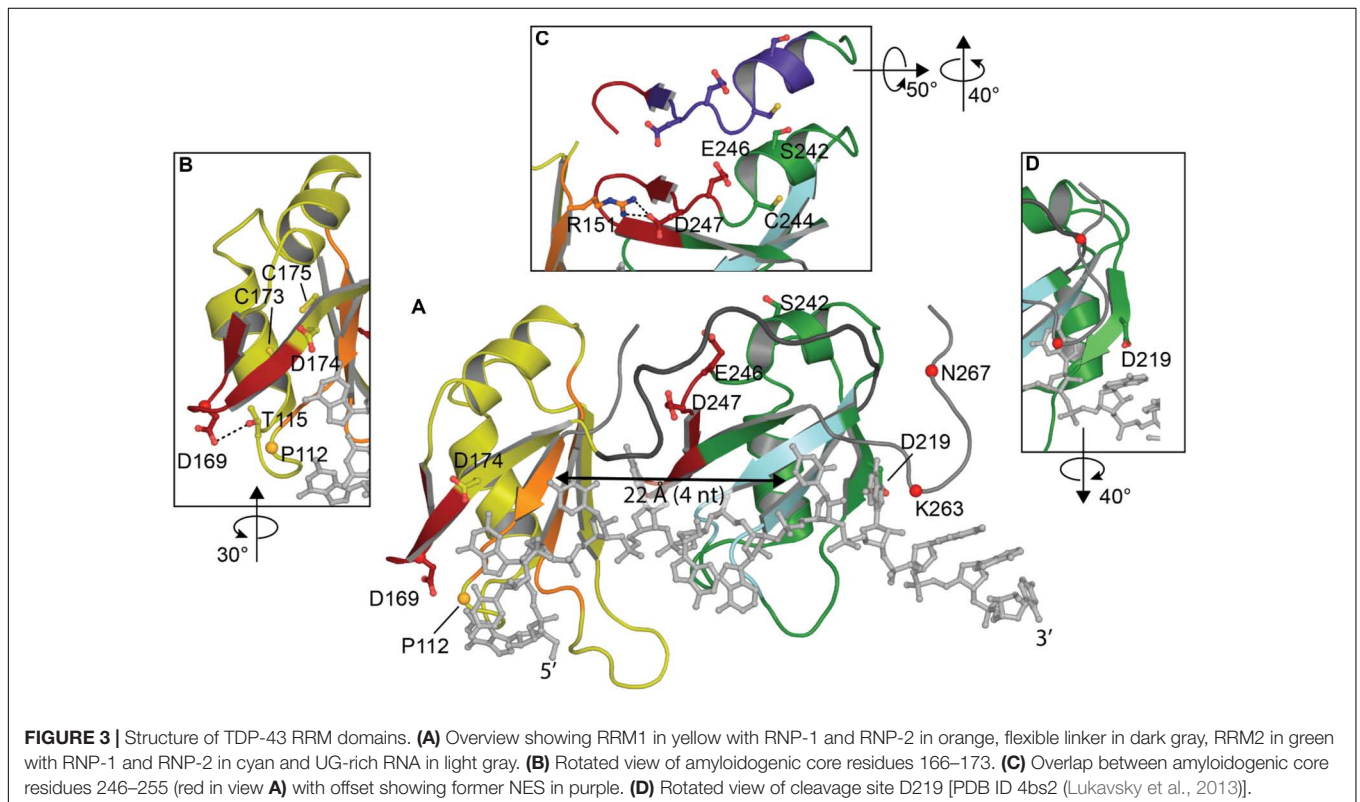
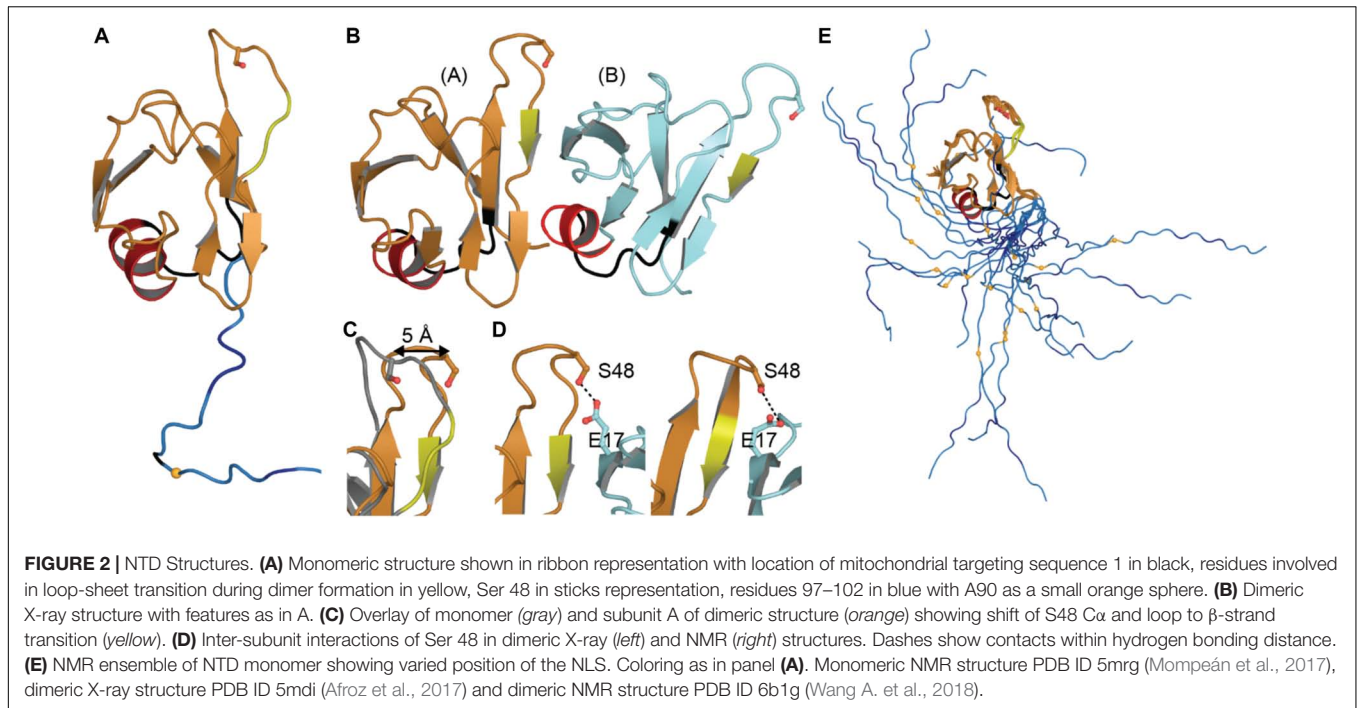
Both RRMs fold into a 5-stranded beta sheet stacked against two alpha helices with the conserved RNA-binding aromatic and hydrophobic residues located in the  $\beta$ -sheets, shown to form stacking interactions with the bases and the sugar rings of single-stranded RNA or DNA. These tandem RRM domains bind nucleic acid in the 5' to 3' direction, opposite to typical tandem RRMs (Lukavsky et al., 2013; Kuo et al., 2014; Figure 3A). Interestingly, compared to typical 4-stranded RRMs, the TDP-43 RRM1 and RRM2 both contain a supplementary  $\beta$ -strand thought to be necessary for structure stability (Shodai et al., 2013).

Studies have consistently shown preferential binding of TDP-43 to (TG)/(UG) sequences (Buratti et al., 2001; Kuo et al., 2009; Sephton et al., 2011; Colombrita et al., 2012; Bhardwaj et al., 2013; Lukavsky et al., 2013; Furukawa et al., 2016). RRM1 is known to be sufficient and essential for proper nucleic acid binding as its affinity is in the low nanomolar range for the canonical UG-rich sequence, while RRM2 is not (Kuo et al., 2009; Furukawa et al., 2016). RRM1 was shown to be able to bind other motifs, consistent with (Kuo et al., 2014), A3(GG)4A3, via a distinct binding site implicating Arg151 (Sephton et al., 2011). R151A did not impact sequence recognition of the RRM1-RRM2 tandem construct while substitution of E246 or D247 (Lukavsky et al., 2013) were able to decrease the specificity for RNA sequences. The authors concluded that E246 and especially D247 were crucial in the structure of RRM2 and the

**TABLE 1** | TDP-43 domain structures.

PDB code	Technique (resolution)	Observed amino acids	Notes	Observed oligomeric state	Backbone RMSD	References
<b>N-terminal domain</b>						
2n4p	NMR	1–77	6-His tag	Monomer	0.46	Mompeán et al., 2016c
5mdi	X-ray (2.1 Å)	2–79	6-His tag, C39/C50-dimethylarsinoyl	Dimer	1.50 (A) 1.63 (B)	Afroz et al., 2017
5mrg	NMR	1–102	6-His tag	Monomer	–	Mompeán et al., 2017
5 × 4f	NMR	1–77	C39/C50S, GB1 tag	Monomer	2.43	Jiang et al., 2017
6b1g	NMR	1–80	Y4R (A), S48E (B)	Dimer	1.78 (A) 1.45 (B)	Wang A. et al., 2018
<b>RRM domains</b>						
4bs2	NMR	102–269 (RRM1-RRM2)	With UG-rich RNA 5'-R(*GP*UP*GP*UP*GP*AP*AP*UP*GP*AP*AP*UP)-3'	Monomer		Lukavsky et al., 2013
2cqq	NMR	96–185 (RRM1)		Monomer	1.37a	–
4iuf	X-ray (2.75 Å)	103–179 (RRM1)	With 5'-D(*GP*TP*TP*GP*(XUA)P*GP*CP*GP*T)-3'	Monomer	1.02a	Kuo et al., 2014
4y00	X-ray (3.00 Å)	103–168(RRM1)	D169G, with (5'-D(P*TP*TP*GP*AP*GP*CP*GP*T)-3')	Monomer	0.97a	Chiang et al., 2016
4y0f	X-ray (2.65 Å)	103–180 (RRM1)	With (5'-D(*GP*TP*TP*GP*AP*GP*CP*GP*TP*T)-3')	Monomer	1.00a	Chiang et al., 2016
1wf0	NMR	193–267 (RRM2)	E200G	Monomer	1.13b	–
3d2w	X-ray (1.65 Å)	192–261 (RRM2 mouse)	With (5'-D(*DGP*DTP*DTP*DGP*DAP*DGP*DCP*DGP*DTP*DT)-3')	Homo 2-mer	0.84b	Kuo et al., 2009
<b>C-terminal domain</b>						
2n2c	NMR	307–348		Monomer		–
2n3x	NMR	311–360		Monomer		Jiang et al., 2016
2n4g	NMR	311–360	G335D	Monomer		Jiang et al., 2016
2n4h	NMR	311–360	Q343R	Monomer		Jiang et al., 2016
5whn	X-ray (1.1 Å)	312–317		Homo 15-mer		Guenther et al., 2018a
5whp	X-ray (1.0 Å)	312–317	A315T	Homo 10-mer		Guenther et al., 2018a
5wia	X-ray (1.0 Å)	370–375		Homo 10-mer		Guenther et al., 2018a
5wiq	X-ray (1.25 Å)	396–402		Homo 10-mer		Guenther et al., 2018a
5wkb	Electron crystallography (1.0 Å)	312–317	A315E	Homo 10-mer		Guenther et al., 2018a
5wkd	X-ray (1.8 Å)	300–306		Homo 10-mer		Guenther et al., 2018a
6cb9	X-ray (1.1 Å)	328–333		Homo 10-mer		Guenther et al., 2018a
6cew	X-ray (1.2 Å)	321–326		Homo 12-mer		Guenther et al., 2018a
6cf4	Electron crystallography (0.75 Å)	312–317	Phosphorylated A315T	Homo 10-mer		Guenther et al., 2018a
6cfh	Electron crystallography (1.5 Å)	333–343		Homo 20-mer		Guenther et al., 2018a
6n3a	Electron microscopy (3.3 Å)	311–360		Homo 10-mer		Cao et al., 2019
6n3b	Electron microscopy (3.8 Å)	312–352		Homo 10-mer		Cao et al., 2019
6n3c	Electron microscopy (3.3 Å)	288–314	A315E	Homo 20-mer		Cao et al., 2019
6n37	Electron microscopy (3.8 Å)	312–347		Homo 10-mer		Cao et al., 2019
<b>RRM2 amyloidogenic core</b>						
5w50	X-ray (1.4 Å)	248–253		Homo 12-mer		Guenther et al., 2018b
5w52	Electron crystallography (1.4 Å)	247–257		Homo 10-mer		Guenther et al., 2018b
5w7v	Electron microscopy (3.8 Å)	247–257		Triple- helical fibril		Guenther et al., 2018b

\*Structural alignment of all backbone atoms reported as the root-mean-square deviation (RMSD) in Å. NTD alignment to 5mrg core residues 1–77. RRM alignment to 4bs2 RRM1 (102–179)<sup>a</sup> or 4bs2 RRM2 (190–262)<sup>b</sup>. In the case of multiple copies in the asymmetric unit, the average RMSD is reported.



nucleic acid binding. Indeed, D247 is stabilizing the RRM1-RRM2 orientation when RNA is bound to the protein by making a salt bridge with Arg151 of RRM1 (Lukavsky et al., 2013; Figure 3C).

The recognition of nucleic acid sequences is achieved by an interaction between the two RRMs, which is typical of proteins that contain several RRMs, and RRM2 is being considered as a switch to regulate the sequence-specificity in the substrate

binding of TDP-43 by hiding Arg151 (Sephton et al., 2011). Cooperation between RRM1 and RRM2 also explains why TDP-43 affinity for nucleic acids increases with the length. Kuo et al. reported a large affinity increase between 4 and 6 nucleotides long, which approximately corresponds to the distance between both nucleic acid binding sites ( $\sim 22$  Å) (Shodai et al., 2013; **Figure 3A**). Additionally, the RRMs are connected by a highly flexible loop (178–191), thought to confer adaptability to different nucleic acid partners by allowing different orientations of the RRM domains (Auweter et al., 2006; Furukawa et al., 2016).

Although it is believed that TDP-43 binds thousands of different transcripts, there are only co-structures with UG or TG repeat RNA and DNA. Given that RRM1 was suggested to bind non-UG/TG rich sequences *via* a site distinct from RNP sequences, structural characterization of TDP-43 with non-canonical motifs might yield interesting novel data on TDP-43 binding to nucleic acid.

### Amyloidogenic cores

Although RRM1-2 are structurally well-folded and mostly known for interaction with nucleic acids, several studies have now suggested the presence of amyloidogenic cores and the ability of these domains to misfold and participate in either nucleation or propagation of TDP-43 aggregation in ALS (Shodai et al., 2012, 2013). Two regions of interest have been identified in ALS patients but not in well-folded non-pathological TDP-43: residues 166–173 in RRM1 (Shodai et al., 2013) and 246–255 in RRM2 (Shodai et al., 2012).

Residues 166–173 in RRM1 occur in a reasonably accessible loop (50% accessibility) (**Figure 3B**). Intriguingly, one of the two disease linked mutation in the RRM domain is D169G. While this mutation had no effect on TDP-43 RNA binding, the mutation stabilized TDP-43 and induced a loss of hydrogen bond with T115 resulting in a local conformational change (Chiang et al., 2016). D169G seemed to have no impact on aggregate formation but rather increased caspase cleavage (Shodai et al., 2013; Chiang et al., 2016).

Residues 246–255 in RRM2 lie between RRM1 and RRM2 and are not exposed in the folded state (27% accessibility) (**Figure 3C**). *In vitro* experiments have shown the ability of peptides encompassing residues 246–255 to participate in the formation fibrillar structures (Saini and Chauhan, 2011). The minimal sequence EDLIKGISV is necessary and deletion of the first as well as the second residues resulted in reduced aggregation (Saini and Chauhan, 2011). Moreover, substitution of E246 or D247 to glycine residues in the RRM2 protein induced the formation of fibrils (Shodai et al., 2012). A recent structural study showed the ability of 247-DLIKGISVHI-257 peptide to present amyloid polymorphism characterized by different backbone conformations as well as seven distinct steric zipper arrangements, a common structural feature of amyloid proteins (Guenther et al., 2018b; **Table 1**).

Interestingly, those two regions, 166–173 and 246–255, are the target of several pathological modifications- caspase cleavage, oxidation, ubiquitination. Those post-translational modifications will be discussed later in the manuscript (see section “Post-translational Modifications”).

### Former NES

Until 2018, TDP-43 was thought to have a Nuclear Export Signal in RRM2: 239-IAQSLCGEDLI-249, that was predicted to be a substrate of the nuclear export factor exportin-1 (XPO1/CRM1) (Ayala et al., 2008; Winton et al., 2008). The lack of experimental validation, the poor fit of this sequence to the XPO1/CRM1 consensus sequence ( $\Phi 1-X_{2,3}-\Phi 2-X_{2,3}-\Phi 3-X-\Phi 4$ , where  $\Phi n$  represents Leu, Val, Ile, Phe, or Met and X can be any amino acid), the fact that most validated NES are found in unstructured regions, contrary to the location within the well-folded RRM2, and the limited surface accessibility of some residues in TDP-43 NES sequence, led three independent groups to further investigate TDP-43 export to cytoplasm. They all found that (i) inhibition of XPO1 either by siRNA or inhibitors (leptomycin B - LMB-, as well as selective inhibitors of nuclear export -SINE) or overexpression of XPO1 had no effect on TDP-43 localization to cytoplasm, (ii) TDP-43 NES fused to GFP or YFP did not induce a specific localization to cytoplasm of the constructs (Archbold et al., 2018; Ederle et al., 2018; Pinarbasi et al., 2018). Moreover, Pinarbasi et al. (2018) showed weak affinity of TDP-43 “NES” for XPO1, in the micromolar range. While Archbold et al. (2018) suggested, with limited effect, a redundant mechanism of active nuclear export, implicating XPO7 (Exportin 7) and NXF1 (Nuclear RNA export factor 1), both Ederle et al. (2018) and Pinarbasi et al. (2018) showed a passive diffusion mechanism, slowed down by size and inhibited by newly synthesized RNA binding.

Interestingly, mutations in TDP-43 NTD, L27A and L28A, both leading to monomeric TDP-43, decreased and abolished TDP-43 splicing function, respectively, and induced a partial or complete cytoplasm localization (Mompéan et al., 2017). Foglieni et al. (2017) also showed, using split-GFP technology which allows detection of weak and/or transient species, that dimeric TDP-43 was only nuclear. Since passive retention in the nucleus was recently suggested as the preferred way to retain proteins in the nucleus (Wühr et al., 2015), it is likely that dimeric species of TDP-43 bound to RNA and other RNA related machineries will be nuclear and the free monomeric protein will be able to diffuse out to the cytoplasm. This may explain how TDP-43 shuttles between nucleus and cytoplasm in a transcription-dependent manner (Ayala et al., 2008).

In light of this, results showing that the TDP-43-“ $\Delta$ NES” (I239A/L243A, L248A/I249A/I250A) did not induce TDP-43-related toxicity in *Drosophila* and cell lines (Winton et al., 2008; Ritson et al., 2010) remain puzzling. Pinarbasi et al. (2018) suggested that contrary to early hypothesis stipulating that TDP-43- $\Delta$ NES inhibited TDP-43 cytoplasmic distribution, the neuroprotective effect of TDP-43- $\Delta$ NES arises from the disruption of TDP-43 splicing function. The authors compared TDP-43- $\Delta$ NES to the F147/149 L mutation, also able to disrupt splicing function and to alleviate overexpressed TDP-43 toxicity in *D. melanogaster*. This might seem surprising at first, since, contrary to F147 and F149, I239, L243, L248, I249, and I250 are not localized at the RNA interface (**Figure 3C**). But, those residues are localized at the interface between RRM1 and RRM2 and any modification of those contacts seems to lead to loss



of RNA binding, similar to D247 mutations. However, E246 and D247 mutations resulted in a misfolded TDP-43 protein, reduced TDP-43 solubility and induced protein aggregation (Shodai et al., 2012).

Since part of the “NES” overlaps with the amyloidogenic core 2 (residues 246–255, **Figure 3C**), we hypothesized those mutations would modify the amyloidogenicity of this sequence. We used Aggrescan, an online software that predicts amyloidogenic cores and was previously used on TDP-43 (Garnier et al., 2017). The comparison of TDP-43-WT versus TDP-43-“ $\Delta$ NES” shows a suppression of the known amyloidogenic core at residues 244–255 (**Figure 4**), exposed in ALS patients (Saini and Chauhan, 2011; Shodai et al., 2012). Nevertheless, without thorough structural analysis of the effects of those mutations on TDP-43, no clear conclusions can be drawn.

### The Aggregation-Prone C-Terminal Domain (CTD, Amino Acids 260–414)

TDP-43 CTD is the site of about 50 disease-linked mutations (Mackenzie and Rademakers, 2008) as well as most of the phosphorylation sites (**Figure 1**), and has thus been examined extensively, but due to its disordered nature, all structural studies of the CTD have been of fragments. The TDP-43 CTD has been shown to be required for TDP-43 splicing activity (Ayala et al., 2005; Freibaum et al., 2010; Conicella et al., 2016), including autoregulation (Ayala et al., 2011), and is the site of interaction with several protein partners such as UBQLN2 (Cassel and Reitz, 2013), FMRP (Majumder et al., 2016) and hnRNP (Buratti et al., 2005; D’Ambrogio et al., 2009).

### Organization of the CTD

The CTD is able to form secondary structural elements that have been observed by crystallography and electron microscopy (**Table 1**) and distinct subdomains have been established: two Gly-aromatic-Ser-rich (GaroS) regions, and an amyloidogenic

core divided into a hydrophobic region, and Q/N-rich region (Mompeán et al., 2016a; **Figure 1**).

The GaroS regions (residues 273–317 and 368–414) are similar to regions in FUS (Murray et al., 2017) proposed to interact within RNA granules (Mompeán et al., 2016a) and contributing to the formation of hydrogels (Kato et al., 2012).

The hydrophobic region (residues 318–340) can adopt a helical structure or Thioflavin T-positive filaments consistent with cross- $\beta$  architecture (Jiang et al., 2013, 2016; Mompeán et al., 2014; Lim et al., 2016). The first structure determined in a lipid-like environment showed an omega-loop-helix structure ( $\Omega$ -loop-helix, residues 320–343) (Lim et al., 2016). This was confirmed with a slightly longer construct determined under non-lipid conditions that showed a helix-turn-helix (**Figure 5**) that was disrupted by G335D and Q343R mutations (Jiang et al., 2016).

Likewise, Q/N rich regions (residues 341–369) were observed to form amyloid and amyloid-like aggregates (Mompeán et al., 2014). More recent structural studies identified six segments that form classic steric zippers and contribute to pathogenic aggregation (Guenther et al., 2018a; **Figure 5**), confirming the helix-to-sheet transition of the hydrophobic region and identifying additional aggregation-prone segments. This study also showed that the Omega-loop region, required for neurotoxicity (Zhu et al., 2014) can form Low complexity Aromatic-Rick Kinked Structures (LARKS) which can be affected by mutation and phosphorylation (Guenther et al., 2018a,b). These segments stack into kinked beta sheets, forming reversible (Velcro-like) associations thought to play a role in protein interactions and were hypothesized to play a role in reversible association of the CTD as well as pathogenic aggregation by bringing adjacent amyloid-forming segments together (Guenther et al., 2018a). Finally, multiple lines of evidence strongly suggest that the Q/N region also forms extended  $\beta$ -hairpin structures (Mompeán et al., 2014, 2015, 2016a; Cao et al., 2019). This was

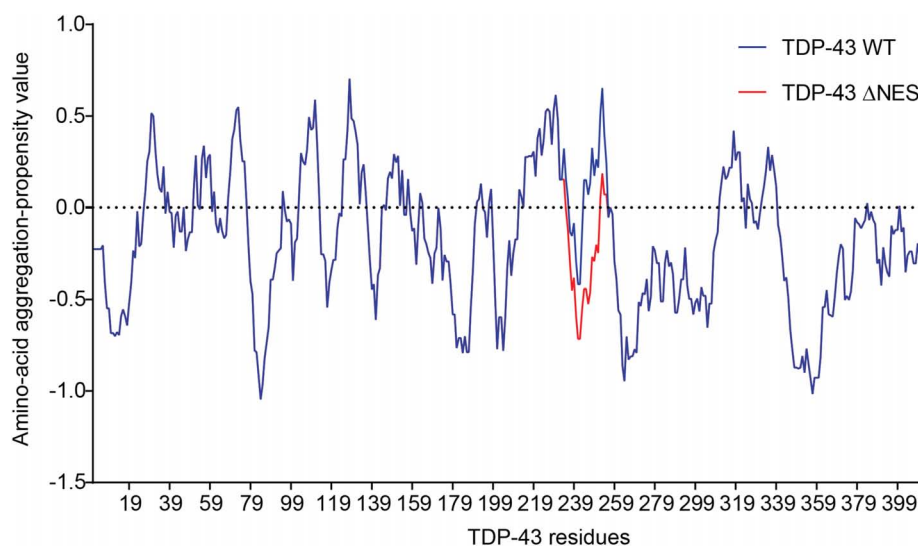
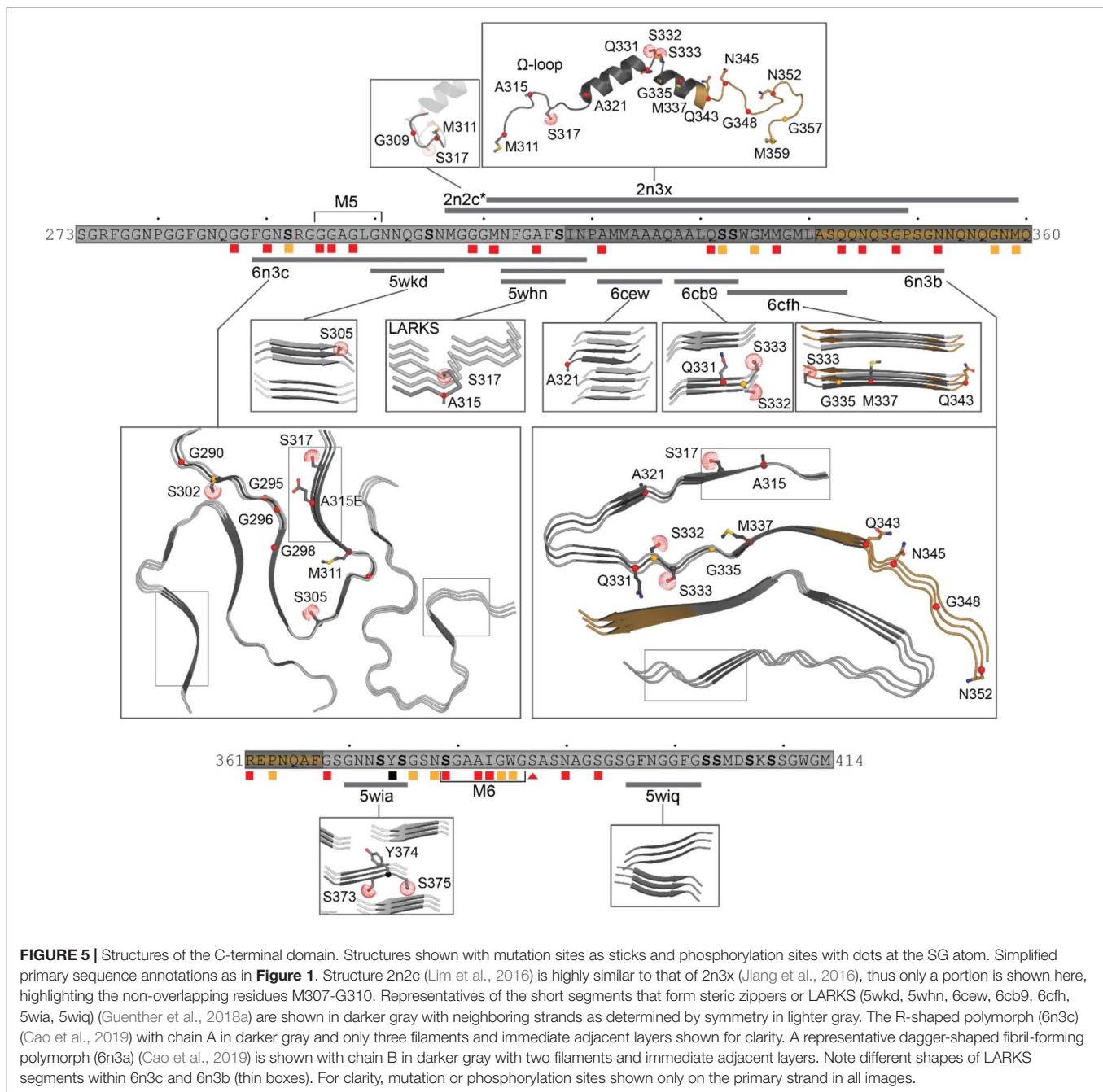


**FIGURE 4 |** Prediction of amyloidogenicity of TDP-43 and TDP-43-“ $\Delta$ NES.” Those mutations reduce the aggregation prone characteristic of the 244–255 region.



confirmed by very recent work describing the structures of two significantly longer regions using cryo-EM, both of which form irreversible fibrils (Cao et al., 2019). The first segment (residues 286–331), contains an ALS linked mutation (A315E) and folds into an R-shaped motif (**Figure 5**). The second segment (residues 311–360) exhibited three polymorphs with different inter-fibril contacts, but all sharing a common dagger-shaped motif at the core (**Figure 5**). Interestingly, structural alignment of the overlapping regions resulted in severe steric clashes, suggesting that the two folds cannot occur simultaneously in a single TDP-43 molecule. The authors further suggested

a disease specific foldome of TDP-43 fibrils, as observed with Tauopathies.

Taken together, these studies suggest that the C-terminal domain of TDP-43 transiently adopts a range of well-ordered shapes, many of which are capable of self-association. Mutations and post-translational modifications may change the kinetics of these states, influencing the balance between fibril formation and dissolution, as implied by Cao et al. (2019) who showed that mutations within the fibril interface delayed aggregation, supporting the argument that mutations will affect which shape is adopted by the CTD.

### Liquid-liquid phase separation and aggregation

Conflicting data exists for the contribution of the CTD to TDP-43 aggregation. Multiple studies point to the C-terminus essential to aggregation and pathology (Dewey et al., 2010; Guo et al., 2011; Budini et al., 2012; Jiang et al., 2013, 2016; Mompeán et al., 2014; Prasad et al., 2018). Others have shown that the CTD is not sufficient, but rather that the CTD combined with the RRM2 is required for significant accumulation of aggregates in cellular models (Johnson et al., 2008; Yang et al., 2010; Fallini et al., 2012; Wang et al., 2013). And indeed, as discussed above, the RRM domains contain amylogenic sequence elements that contribute to aggregation (Shodai et al., 2012, 2013; Chiang et al., 2016; Guenther et al., 2018b) and constructs lacking the CTD have been shown to aggregate as well (Zacco et al., 2019).

Further complicating the picture is the recent identification of the role of reversible self-association, generally termed LLPS (liquid-liquid phase separation) which is thought to initiate formation of SGs and to which both the NTD and CTD seem to contribute (Conicella et al., 2016; Schmidt and Rohatgi, 2016; Afroz et al., 2017; Li et al., 2018; Wang A. et al., 2018; Wang L. et al., 2018; Babinchak et al., 2019). The conditions under which TDP-43 undergoes LLPS are highly sensitive to the conditions of the experiment (Conicella et al., 2016; Li et al., 2018; Wang L. et al., 2018). Moreover, interaction between the CTD and charged nucleic acids, specifically ssDNA, can increase the CTD's ability to undergo LLPS, thought to occur *via* the many aromatic and pi interactions (Wang L. et al., 2018). Despite a lack of direct modulation of LLPS formation by charged residues, it was found that arginine residues played an integral role in changing the material properties and dynamics of the droplets formed by TDP-43. Interestingly, Mompeán et al. (2016b) suggested that electrostatic repulsion modulates the formation of TDP-43 aggregation.

The link between LLPS and aggregation is unclear, but several studies provide compelling evidence that time is a key factor. LLPS is important for formation of membraneless organelles, including stress granules [SGs, recently reviewed in Gomes and Shorter (2019)]. As SGs age, they tend to lose their dynamic nature, as a result of formation of protein fibrils thought to contribute to development of irreversible structures (Holehouse and Pappu, 2018; Vogler et al., 2018; Wang A. et al., 2018; Babinchak et al., 2019; Zhang et al., 2019).

In contrast, a recent study showed the ability of TDP-43 to undergo long-lasting liquid-demixing in a stress granule-independent fashion by either increasing cytoplasmic TDP-43, exposure to amyloid-like TDP-43, or arsenite stress (Gasset-Rosa et al., 2019). The authors further show the conversion, upon additional arsenite stress, of those TDP-43 droplets into solid-like structures, that further recruit components of the nucleocytoplasmic transport machinery, leading to impaired nuclear transport. This is thought to accelerate TDP-43 nuclear depletion and result in cell death.

In addition, some mutations within the CTD were shown to alter propensity for LLPS (Jiang et al., 2016), in addition to altering splicing function (Fratta et al., 2018).

### Post-translational Modifications of TDP-43

TDP-43 undergoes a significant number of post-translational modifications (Figure 1). Most of them are associated with pathological TDP-43 and are a hallmark feature of TDP-43 proteinopathy. Another recent review that focuses on a mechanistic perspective has described several post-translational modification of TDP-43 in a context of health and disease (Buratti, 2018). Our goal is to bring a structural point of view on those modifications.

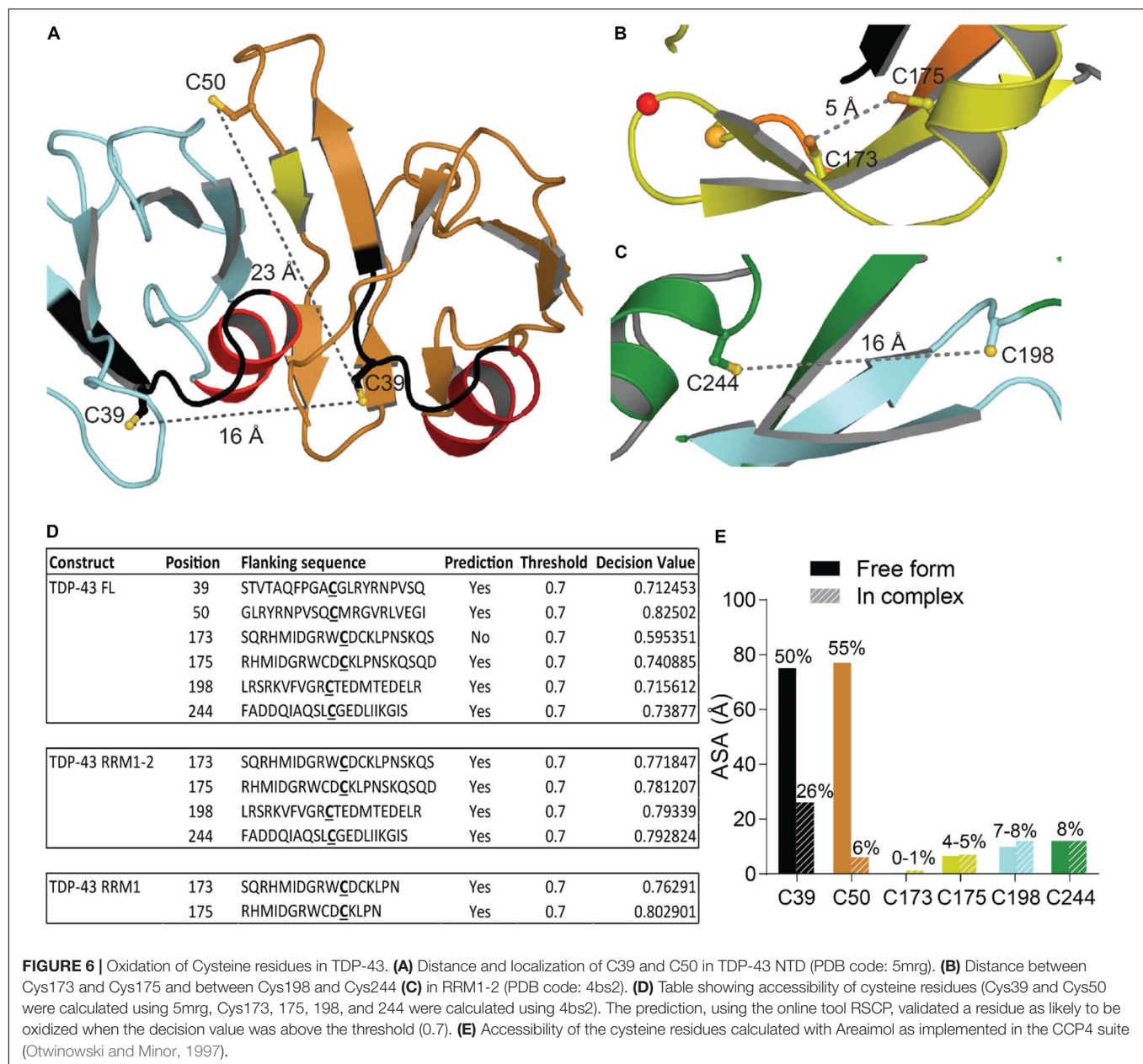
#### Oxidation

Oxidative stress is a hallmark feature of neurodegenerative diseases and ALS was suggested as a cysteninopathy, an aberration of cysteine residues modifications (Valle and Carri, 2017). It has been hypothesized that the generation of ROS could trigger some TDP-43 pathology (Cohen et al., 2012). The authors treated cells with various stressors that generate ROS using different pathways, i.e., H<sub>2</sub>O<sub>2</sub>, arsenite, heat shock and cadmium, and found a dramatic shift in TDP-43 solubility, attributed to a direct modification of TDP-43 *via* cysteine oxidation. All TDP-43 cysteine residues were suggested as targets: Cys173, Cys175, Cys198, and Cys244 as the major redox-regulated cysteine residues and Cys39 and Cys50 to a much lesser extent. The authors further reported intramolecular and intermolecular disulfide bonding implicating Cys173, Cys175, Cys198, and Cys244. Since Cys39 and Cys50 are about 22–24 Å apart (Figure 6A), intramolecular disulfide bonding between those two residues is very challenging and a study on NTD oxidation did not describe any aggregation (Chang et al., 2013). Cys39 and Cys50 are known to be in the dimeric interface of TDP-43 NTD and mutations of those residues into Serine induced a weaker oligomerization compared to wild-type, suggesting those cysteines to have contribution into assembly (Wang A. et al., 2018).

The distance between Cys173 and Cys175 is 5.1 Å and between Cys198 and Cys244 is 15.5 Å, intramolecular disulfide bond formation seems unlikely on a native TDP-43 structure (Figures 6B,C). An independent study demonstrated the sequential oxidation of RRM1, with Cys173 being preferentially oxidized and leading to a conformational change allowing Cys175 to be modified and a subsequent formation of cross-linked dimers (Chang et al., 2013). It is worth noting that Cys173 is the least accessible of the six cysteine residues and the least likely to be oxidized in the full-length protein, based on predictions by RSC oxidation prediction, an online web server able to predict the occurrence of redox-sensitive cysteine within the protein sequence (Sun et al., 2016; Figure 6D).

Analysis of the tandem RRM1-RRM2 structure (Lukavsky et al., 2013) shows that Cys173 and Cys175 make contacts with residues in the RRM1. Loss of those contacts by oxidation could explain the exposure of amyloidogenic residues 166–173, since Cys173 and 175 were shown to control both correct and aberrant folding of TDP-43 in ALS depending on the freedom of their thiol group (Shodai et al., 2013).





Given the proximity between oxidation sites and the disease-exposed regions of TDP-43 retrieved in ALS patients (166–173 and 246–255) as well as cleavage sites, the early misfolding of TDP-43 by oxidation, upstream of ubiquitination, phosphorylation, and fragmentation, as suggested in Cohen et al. (2012), is an attractive hypothesis. Moreover, disease-linked mutations G348C and S379C, which introduce new cysteine residue in TDP-43, were shown to undergo oxidation, generating cross-linked TDP-43 species, further supporting the role of early oxidation in TDP-43 misfunction (Cohen et al., 2012).

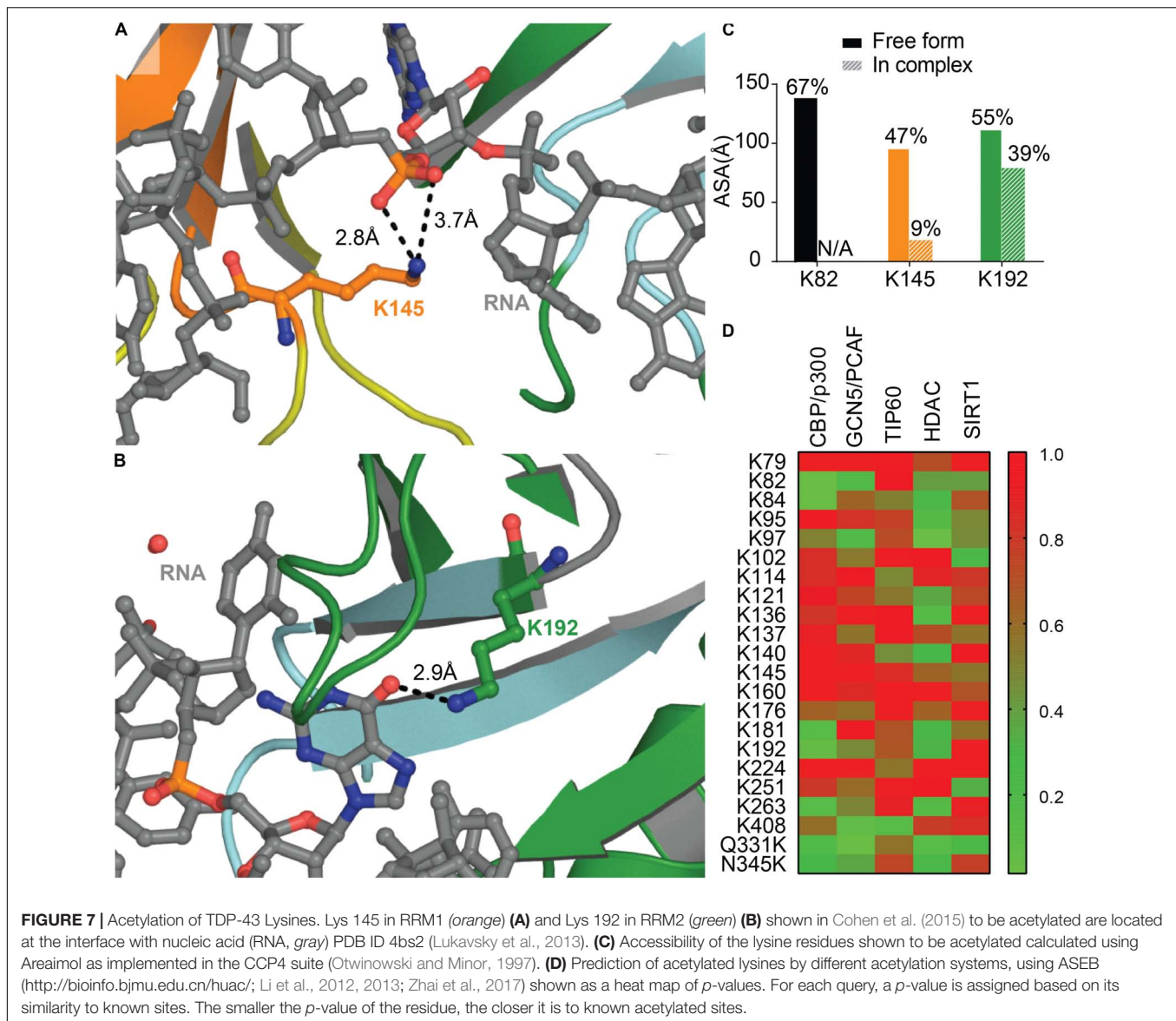
## Acetylation

Lysine acetylation is a post-translational modification associated with various pathways including RNA processing, cytoskeleton

association, and cellular signaling among others [see Narita et al. (2019) for an exhaustive list]. Recently, acetylation has been associated with aggregating proteins such as Tau (Irwin et al., 2012), Huntingtin (Arbez et al., 2017), and SOD1 (Abdolvahabi et al., 2015).

A recent study identified two main sites of acetylation in TDP-43, Lys145, and Lys192 (**Figures 7A,B**; Cohen et al., 2015). Generating acetylation mimics (K145Q and/or K192Q) led to the formation of nuclear speckles, and cytoplasmic aggregates when the TDP-43-nuclear localization signal was impaired (TDP-43  $\Delta$ NLS). The acetylation-null mutant (TDP43-2KR) was diffuse, even when TDP-43 NLS was impaired, supporting acetylation of TDP-43 as a pathological modification of the protein. TDP-43 K145Q mutant exhibited decreased nucleic acid binding that





translated into decreased splicing function (Cohen et al., 2015). This is not surprising, K145 is part of RRM1 RNP-1 motif and K192 of RRM2 RNP-2, they are both moderately accessible in the free protein (Figure 7C), and acetylation is a PTM known to modulate protein-nucleic acid binding (Arbely et al., 2011; Ren et al., 2016) by neutralizing the electrostatic interface.

Nevertheless, residues K145 and K192 were not found acetylated in a recent study using mass spectrometry on TDP-43 inclusions in ALS brains of two different patients (Kametani et al., 2016). The authors describe instead Lys82 as being modified, hence suggesting heterogeneity between patients. Acetylation at Lys82, found in TDP-43 NLS, could impair proper shuttling to the nucleus and act as a pathological event. Prediction of acetylation sites using ASEB (A Web Server for KAT-specific Acetylation Site Prediction<sup>1</sup>) (Li et al., 2012, 2013;

Zhai et al., 2017) shows a high potential of Lys82 as well as Lys192 (Figure 7D), while K145 were less likely to be modified. The implication of those two Lysines in disease remains to be further examined. We also probed for mutations that could enhance acetylation, Q331K and N345K, and found that they both are predicted as possible sites of acetylation. It would be intriguing to look for these acetylation sites in the brain of patients with these acetylation enhancing mutations.

### Zinc Binding

A recent study described the ability of zinc ions to bind TDP-43 with an affinity in the micromolar range. Binding of Zinc was shown to decrease TDP-43 thermostability and formed Thioflavin-T-positive aggregates, reminiscent of amyloid nuclei (Garnier et al., 2017). Zinc treated SY5Y neuronal-like cells recapitulated several hallmarks of TDP-43 proteinopathy including reduced expression, formation of

<sup>1</sup><http://bioinfo.bjmu.edu.cn/huac/>

small nuclear inclusions, and diffuse cytosolic localization. The treatment, however, did not cause formation of CTD fragments, ubiquitination or phosphorylation of TDP-43 (Caragounis et al., 2010). Although an indirect route was not ruled out, especially *via* the generation of ROS through NMDA- or mitochondrial-mediated pathways by  $Zn^{2+}$ , zinc ions are also known to bind and promote *in vitro* aggregation of Tau (Huang et al., 2014), alpha-synuclein ( $\alpha$ Syn) (Valiente-Gabioud et al., 2012) and Amyloid- $\beta$  Peptide ( $A\beta$ ) (Alies et al., 2016). Altered zinc homeostasis is also suggested as a risk factor for several neurodegenerative disorders such as ALS or Alzheimer's disease [see review (Szewczyk, 2013)]. Even though this is still a matter of debate given the relatively poor affinity of zinc for those proteins (in the micromolar range), direct contribution of zinc to TDP-43 aggregation could lead to complexes actively producing ROS similar to  $A\beta$  and  $\alpha$ Syn (Atrián-Blasco et al., 2018), and further amplifying toxicity.

The predicted binding sites of  $Zn^{2+}$  in TDP-43 RRM domains (Garnier et al., 2017) contain Cys residues, modified upon oxidative stress (Cohen et al., 2012), and especially Cys173 and Cys175 in RRM1 (Chang et al., 2013; **Figure 6B**) that govern aberrant self-assembly at amyloidogenic cores (Shodai et al., 2013). Even though  $Zn^{2+}$  binding is well-known to protect cysteine residues from oxidation, it has been suggested that some metal-binding cysteines could undergo redox modifications (Pace and Weerapana, 2014). Complexing those Cys residues by zinc ions might have an effect similar to oxidation and might lead to misfolding of the protein.

## SUMOylation

SUMOylation is a post-translational modification where a small ubiquitin-like modifier (SUMO) sequence is added to a Lysine residue within a SUMO-interaction motif, CKXE/D, C being a large hydrophobic amino acid. SUMOylation was suggested to be a pathological event in ALS, since superoxide dismutase 1 (SOD1), Fused in Sarcoma (FUS) and TDP-43 were found SUMOylated (Dangoumau et al., 2013; Foran et al., 2013) which resulted in an increase aggregation of those proteins. In addition, TDP-43 aggregated in inclusions was found SUMO positive following overexpression in mouse primary neurons (Seyfried et al., 2010).

To date, there is still no confirmation on where the modification occurs on TDP-43, all the SUMOylated sites described in **Figure 8A** were found in two high-throughput studies (Hendriks et al., 2014; Lumpkin et al., 2017). Prediction site SUMOPlot confirmed K136 as being the most likely to be SUMOylated (**Figure 8B**) which is consistent with the suggestion in Dangoumau et al. (2013). But given the poor surface accessibility of K136 SUMO motif (30% in the free protein and 27% when TDP-43 is in complex with RNA), SUMOylation at this site is unlikely on a native structure and SUMOylation at residues K84 or K140 seem more likely to occur on a folded TDP-43. While experimental data is necessary to validate the SUMOylation sites, we can speculate that SUMOylation of K84 would disrupt TDP-43 NLS and active transport from cytoplasm to nucleus and SUMOylation at K136 would be the most detrimental by affecting interactions between RRM1 and RRM2 domains as well as RNA binding (**Figures 8C,D**).

## Phosphorylation

Abnormal phosphorylation of TDP-43 in ALS has been described as a hallmark feature of cytoplasmic aggregates in ALS/FTLD (Arai et al., 2006; Hasegawa et al., 2008). Indeed, phosphorylation on serine residues 403/404 and/or 409/410 is considered a consistent reference marker of disease (Neumann et al., 2009). Most pathological phosphorylations that occur in the CTD of the protein (Hasegawa et al., 2008; **Figure 1**), are thought to happen as a later event, and to accumulate on the protein as it is trapped in the cytoplasm over time, depicting attempt from the cellular machinery to trigger degradation (Fang et al., 2014; Kametani et al., 2016; Zhang et al., 2019).

The effect of phosphorylation on TDP-43 remains unclear and largely debated. Several studies point out the propensity of phospho-null mutant to increase aggregation while phosphomimic mutant had the opposite effect (Brady et al., 2011; Li et al., 2011). On the contrary, another group has reported increased accumulation of TDP-43 following phosphorylation by truncated Casein Kinase 1 $\delta$  (Nonaka et al., 2016). Phosphorylation at T153 and Y155 by MAPK/ERK Kinase was not associated with protein accumulation and TDP-43 remained soluble but its capacity to bind nucleic acid was reduced, which could be consistent with a second RNA binding site on RRM1 (Li et al., 2017) (see section "RRM-Nucleic Acid Binding").

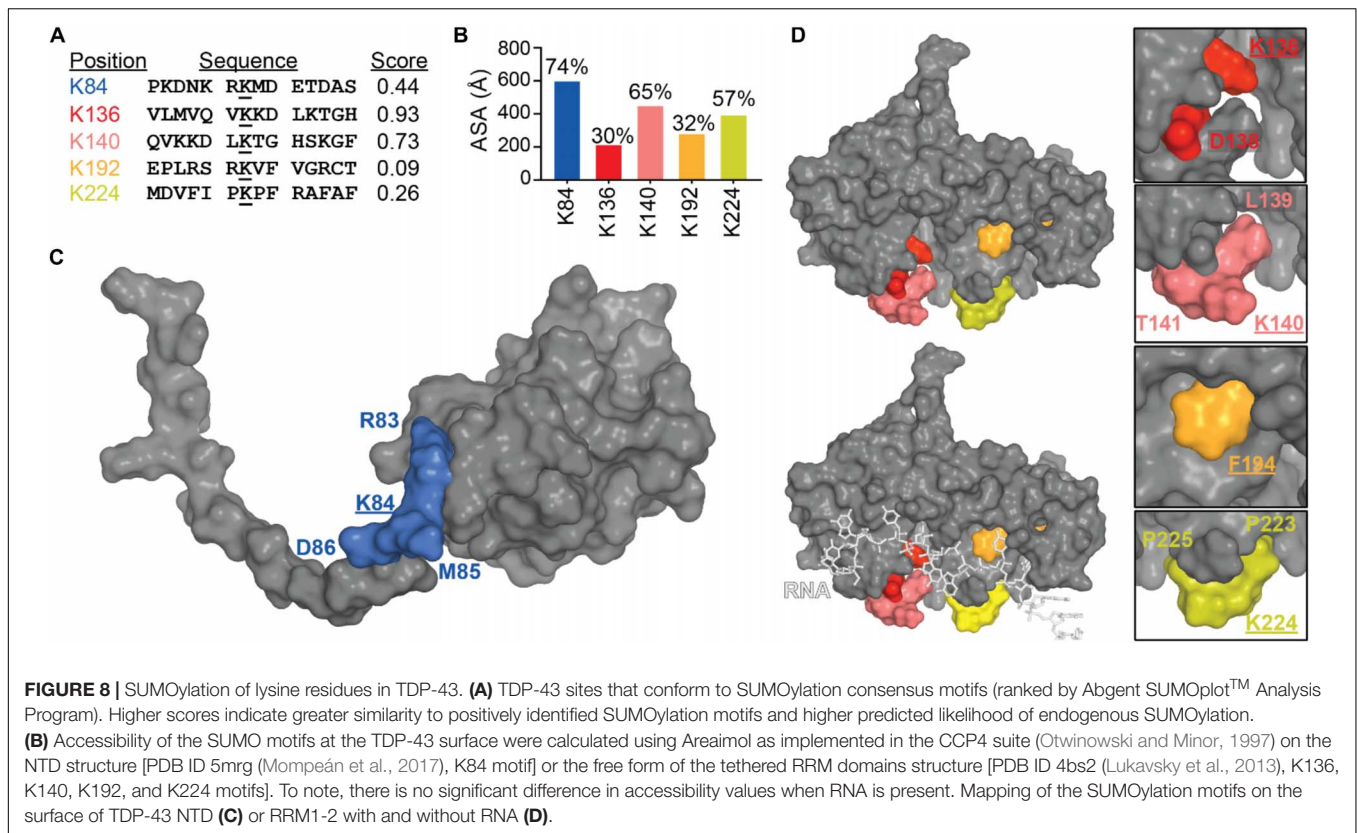
Another example is the recently reevaluated ALS mutation, S375G, linked to early onset disease (Newell et al., 2019). This mutation was shown to remove a phosphorylation site resulting in increased nuclear localization compared to wild-type TDP-43. Interestingly, the phosphomimic mutant, S375E, exhibited cytotoxicity and increased cytoplasmic accumulation. The authors suggested the necessity of a reversible phosphorylation in the regulation TDP-43 cellular redistribution.

Finally, about half of the known disease-linked mutations in TDP-43 will either create potential phosphorylated sites (new Ser or Thr residues), remove phosphorylation sites (elimination of Ser or Thr residues) or introduce a phosphomimic residue (Asp and Glu) (**Figure 1**), arguing that pathogenesis based on phosphorylation alone is possible but is probably correlated with the site of phosphorylation and/or the phosphorylation machinery.

## Ubiquitination

Ubiquitination was one of the first pathological modifications of TDP-43 that was discovered (Arai et al., 2006; Neumann et al., 2006; Nonaka et al., 2009a). This post-translational modification results in the covalent attachment of a small regulatory protein (8.6 kDa) -ubiquitin- catalyzed by a sequential cascade of enzymes, similarly to SUMOylation, and is well-known for its role into protein degradation.

A recent mutagenesis study coupled with mass spectrometry was able to find several ubiquitinated sites and suggested a proteasome and autophagosome targeting function of TDP-43 ubiquitination (von Zweyendorf et al., 2018). The authors validated K84 and K95 as being modified and showed only K84 to affect nuclear import while K95 seemed to impact CTD phosphorylation. To note, those two modifications seemed to have no effect on TDP-43 solubility. Residues



K160, K181, and K263 in the RRM domains, were also validated, but the authors did not pursue further those sites. Mapping of those residues as well as surface accessibility calculations (**Figure 9**) indicate that (i) K263 is the most accessible to modification (which is consistent with predictions using UbPred<sup>2</sup>) (Radivojac et al., 2010), and modification of this residue could result in direct RNA binding reduction, (ii) K181 modification would be detrimental to TDP-43 structure possibly by modifying interactions between RRM1 and RRM2 especially *via* loss of contact with the critical residue D247 (see RRM domains section for discussion of this residue) or by affecting RRM-NTD interactions since it is close to the linker and (iii) K160 modification would be the less detrimental, even though it has potential contacts with F127 and T157. The authors further noticed a lack of ubiquitination localized in the CTD when considering the full-length TDP-43, which was surprising at first since they previously observed major ubiquitination in a CTF fragment of TDP-43 (residues 193–414) (Hans et al., 2014). Thus, this observation suggests CTD ubiquitination might only occur post TDP-43 cleavage. While ALS-linked mutations Q331K and N345K did not induce further ubiquitination, K263E, very surprisingly led to enhanced ubiquitination that was attributed to ubiquitination to redundant sites (Hans et al., 2014). Interestingly, K263E exhibits higher propensity to form aggregates (Bhandare and Ramaswamy, 2018).

<sup>2</sup><http://www.ubpred.org>

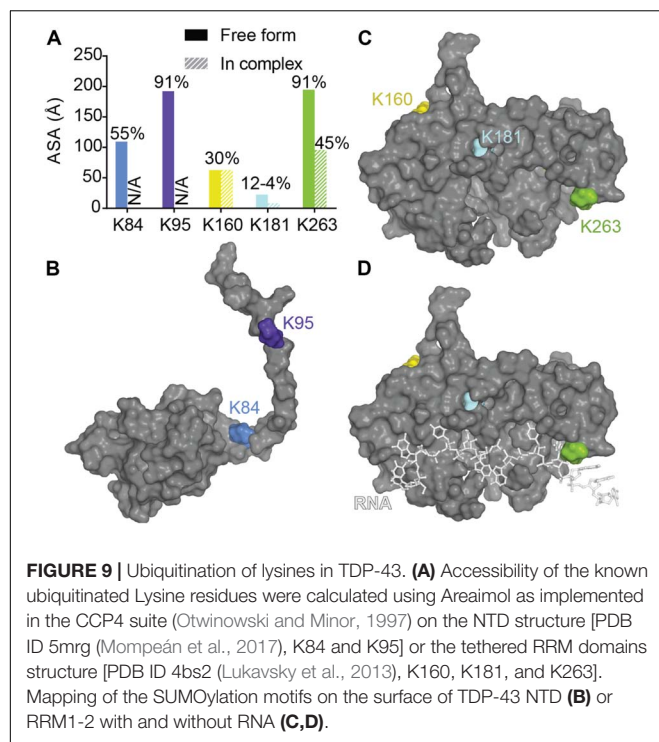
## Cleavage

An additional consistently observed aberration is the accumulation of fragmented TDP-43 in cytoplasmic aggregates (Neumann et al., 2006; Zhang et al., 2007, 2009; Che et al., 2015; Berning and Walker, 2019). These fragments appear to be the result of caspase cleavage at several sites (**Figure 1**). Cleavage at D89-A90 results in a 35 kDa fragment (TDP-35) that lacks the NTD and disrupts the NLS but is correctly folded (Che et al., 2015). Sites at D169-G170 and D174-C175 are both associated with the 25 kDa fragment (TDP-25) which lacks the NTD, NLS and most of RRM1 (Li et al., 2015; Chiang et al., 2016; **Figure 3B**). Additional sites occur at M218-D219 and E246-D247 (Igaz et al., 2009; Nonaka et al., 2009b; **Figure 3C**). All of these cleavage events lead to disruption or elimination of TDP-43 NLS, trapping the protein in the cytoplasm (Cicardi et al., 2018) and enhancing protein aggregation (Kitamura et al., 2016). Notably, D169-G170, D174-C175, and E246-D247 are located at or in the amyloidogenic cores and as such, cleavage might help in exposing those sequences. Alternatively, early unfolding initiated by other PTMs, for example oxidation of Cys 173 or Cys 244, might result in exposure of those regions, increasing cleavage activity. Further, disease-linked mutations, A90V and D169G (Chiang et al., 2016), link those cleavage sites to pathological forms of TDP-43.

## PARYlation

Poly-ADP-ribose is a post translational modification that conjugates several ADP-ribosyl units by members of the





poly(ADP-ribose) polymerase (PARP) family, to generate long and highly negatively charged linear or branched polymers (Teloni and Altmeyer, 2016), in PAR-binding modules. One of the PAR-binding modules is the PAR-binding motif (PBM, typically [HKR]1-X2-X3-[AIQVY]4-[KR]5-[KR]6-[AILV]7-[FILPV]8) where Lys, Asp and Glu can be modified [see (Teloni and Altmeyer, 2016) for full review, and (Gibson and Kraus, 2012) for structural insight]. Multiple PBMs can be found in the same protein and can increase interaction of target protein with PAR conjugation system (Krietsch et al., 2013). PARYlation has been linked to DNA damage repair, unfolded protein response and cellular stress response among other [see (Gupte et al., 2017) for a full list and description]. Interestingly, mammalian stress granules have been shown to contain PAR (Catara et al., 2017).

In a search for genetic modifier of TDP-43 toxicity, McGurk et al. (2018) found that downregulation of tankyrase (a PAR catalase) reduced degeneration of the *Drosophila* eye linked to expression of human TDP-43. Sequence alignment led McGurk et al. (2018) to find two regions of interest with 80 and 63% of fitting to the canonical PBM, which turned out to overlap with the bipartite NLS of TDP-43 (Figure 1) and which they experimentally validated. Not only did expression of TDP-43-ΔPBM induce a cytoplasmic localization of the protein, it also excluded the protein from stress granule assembly. Such a PARYlation, close to TDP-43 NLS, may serve as steric hindrance to mask TDP-43 NLS and is coherent with the need to avoid active shuttling to nucleus when the protein is needed in stress granules.

Moreover, TDP-43 was able to form LLPS in the presence of PAR while TDP-43-ΔPBM produced an aberrant phase transition. ALS associated TDP-43 fragments (TDP-35 and TDP-25), lacking partially or totally the PAR binding, were

not able to co-localize to stress granules nor undergo correct liquid phase demixing.

## Mitochondrial Targeting

Several studies have found TDP-43 localization to mitochondria (Mori et al., 2008; Wang et al., 2016, 2017; Davis et al., 2018) but others have failed to find such an association (Onesto et al., 2016; Kawamata et al., 2017). Nevertheless, one study was able to predict several mitochondrial targeting sequences in TDP-43, named M1-M6 (Wang et al., 2016; Table 2, Figures 1, 10) and experimentally validated three of them as main mitochondrial signals (M1, M3, and M5). Deletion of each of those three signals greatly reduced TDP-43 mitochondrial localization, but did not abolish it, suggesting the need for multiple sequences in the import process. It was further proposed that mitochondrial import of TDP-43 occurred through TOM70/TIM22 complexes, known to mediate translocation of proteins that do not carry a classical matrix-targeting signal and has been shown to bind multiple internal mitochondrial motifs (Backes et al., 2018).

With the likely exception of M5, located in the unstructured CTD of TDP-43, none of the mitochondrial signal are surface accessible in the well-folded protein (Table 2). While this is consistent with a very limited -if any- mitochondrial localization of TDP-43 in normal conditions (Wang et al., 2016), the question remains as to how TDP-43 gets translocated in mitochondria in a pathological context. We suggest that several events, among others, could contribute to this state. (1) TDP-43 abnormally interacts with the mitochondrial chaperone Hsp60 in ALS (Freibaum et al., 2010). Fused in sarcoma (FUS) protein, another ALS-linked protein, was also shown to have pathological interaction with Hsp60 which increases its mitochondrial localization (Deng et al., 2015). Increased Hsp60 binding could explain exacerbated mitochondrial localization. (2) The heat shock protein Hsp70 is known to be implicated in mitochondrial import (Young et al., 2003) and to bind TDP-43 as well as dissolve TDP-43 aggregates and rescue toxicity (Udan-Johns et al., 2014; Kitamura et al., 2018). It has been shown that Hsp70 is reduced and mislocalized to aggregates in SOD1 mutants mice (ALS model) (Liu et al., 2005; Chen et al., 2016). Moreover, defects in cytosolic Hsp70 led to enhanced entry of misfolded proteins into mitochondria and elevated mitochondrial stress in yeast, which is believed to translate into humans (Ruan et al., 2017). An abnormal Hsp70 could lead to exacerbated mislocalization of TDP-43 in mitochondria. (3) Interestingly, the M3 mitochondrial sequences is localized at the nucleic acid binding site (RNP-2 of RRM1) and accessibility of the mitochondrial signals are greatly affected by RNA binding

**TABLE 2 |** Accessibility of mitochondrial signals.

	Validated	Free protein	In complex with RNA
<b>M1</b> 35-FPGACGL-41	Yes	26%	N/A
<b>M3</b> 146-GFGFV-150	Yes	13%	1.4%
<b>M5</b> 293-RGGGA <sup>u</sup> GLG-300	Yes	N/A	N/A

*Underlined is mutation linked to increased mitochondrial localization.*



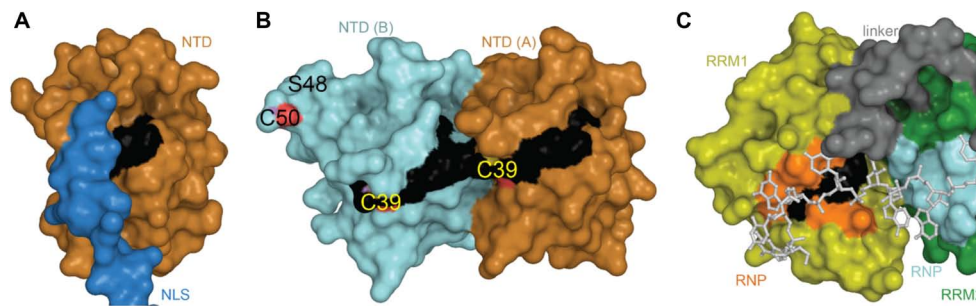


**FIGURE 10 |** Mitochondrial targeting sequences in TDP-43. **(A)** M1 in the NTD monomeric structure [PDB ID 5mrg (Mompeán et al., 2017)]. **(B)** M1 in the dimeric structure [PDB ID 5mdi (Afroz et al., 2017)] **(C)** M3 in RRM1, overlapping with RNP-1 (orange) [PDB ID 4bs2 (Lukavsky et al., 2013)]. Location of mitochondrial targeting signals shown in black. RNA is in light gray.

(Table 2). Since RNA was shown recently to be neuroprotective (Coyne et al., 2014; Mann et al., 2019), loss of RNA binding could hence promote TDP-43 to localize in mitochondria. (4) Mutations in TDP-43 could contribute to mislocalization to the mitochondria. G298S, occurring in M5, was shown to increase mitochondrial import in patient fibroblasts and cell lines (Wang et al., 2016). This mutation might thus make the mitochondrial signal more accessible. Alternatively, misfolding or unfolding, either local or total, of TDP-43 could help in exposing the mitochondrial targeting sequences and subsequent interaction with mitochondrial import machinery. For example, C39 occurs in M1 and has been shown to be oxidized, which might help in TDP-43 unfolding. Although the crystal structure of the dimeric TDP-43 NTD, which contain dimethylarsino-modified C39 and C50, does show a small increase in the distance between the monomers compared to the dimeric NMR structure, M1 is not significantly more surface exposed (Afroz et al., 2017; Wang A. et al., 2018; Figure 10). Another example would be acetylation at K145, localized just at the N-terminus of the M3 signal and is the first residues of RNP-1 in RRM1. Finally, phosphorylation of TDP-43 was shown to increase mitochondrial localization (Wang et al., 2016) since the phospho-mimic G298D induced increased mitochondrial TDP-43 and phospho-null G298A reduced it.

## CONCLUDING REMARKS

TDP-43 is an essential protein, found in all higher eukaryotes (Wang et al., 2004). It is ubiquitously expressed throughout CNS development and into adulthood (Huang et al., 2010), mainly in the nucleus (Wang et al., 2002; Casafont et al., 2009) and in the cytoplasm and mitochondria to a lesser extent. TDP-43 is mislocalized in the cytoplasm of cells in the presence of mutations in the context of neurodegenerative diseases. Possible mechanisms of pathophysiology include mislocalization due to excessive PTMs, aggregation, segregation of RNA in stress granules. All these mechanisms are driven or modulated by effects on the three-dimensional structure of TDP-43.

Solving the three-dimensional structure of the entire protein has been challenging due to large disordered domain and flexible linkers between domains. Differentially dissected

constructs of TDP-43 have been used to try to classify TDP-43 interdomain interactions, if any, in order to understand the full protein structure-function relationship. Characterization of these constructs using NMR concluded that TDP-43 has dynamic interdomain interactions and implied an interaction between N-terminus and C-terminus that contributes to its pathology (Wang et al., 2012; Wei et al., 2016). But overall, inter-domain characterization is still underdeveloped. Further structural advances may be possible with Cryo-EM, but the flexible domains will still be problematic. It is more likely that defining direct binding partners of TDP-43 will be more fruitful in defining structural elements not defined in the apo protein. It is also clear from this review, many PTMs will undoubtedly change the protein structure as well as influence binding to other partners.

An additional unanswered question is how full-length protein as higher order oligomers is implicated in RNA splicing. It is typical of RNA-binding proteins with multiple RRM motifs for increased specificity and affinity to form higher order oligomers; hnRNP proteins, for example, bind in tandem to RNA. For TDP-43, polymerization through the NTD has been shown to be implicated in splicing (Afroz et al., 2017). Moreover, while it was shown that TDP-43 CTD is implicated in its splicing function *via* flexible prion-like folding (Wang et al., 2012), a recent study suggested that the ability of TDP-43 to phase separate does not impact its splicing function (Schmidt et al., 2019). A better understanding of the oligomerization foldome of TDP-43 and how it relates to splicing will be necessary to define how the core TDP-43 function (RNA binding) may be modulated by other structural regions.

Another level of complexity arises from the contribution of the CTD to the diseased state that includes a wide variety of mutations clustered in this domain. Indeed, each mutation could contribute to proteinopathy through different mechanisms; no common mechanism has been elucidated thus far. Potentially, mutations in this region could modify the intrinsic properties of the CTD resulting in a shift between LLPS, SG, and aggregate formation of the protein. Alternatively, other mutations could modify the post-translational modification pattern.

From the intense literature on PTM, it is clear that defining the hierarchy between PTMs and various structural motifs from

within and from exogenous proteins and how this will influence TDP-43 will be of therapeutic interest. With the advent of better proteomics of patient-derived cells, asking if TDP-43's extensive PTMs (or which ones) detected in patients correlate with disease onset or if they result from the accumulation of insults will be critical. Coupled with better definition of the structure of TDP-43 and determining if PTM modifications are the cause or a result of the disease will define how we tackle our targeting strategies toward successful therapeutics.

## REFERENCES

- Abdolvahabi, A., Shi, Y., Rhodes, N. R., Cook, N. P., Martí, A. A., and Shaw, B. F. (2015). Arresting amyloid with coulomb's law: acetylation of ALS-linked SOD1 by aspirin impedes aggregation. *Biophys. J.* 108, 1199–1212. doi: 10.1016/j.bpj.2015.01.014
- Afroz, T., Hock, E. M., Ernst, P., Foglieni, C., Jambeau, M., Gilhespy, L. A. B., et al. (2017). Functional and dynamic polymerization of the ALS-linked protein TDP-43 antagonizes its pathologic aggregation. *Nat. Commun.* 8:45. doi: 10.1038/s41467-017-00062-0
- Alies, B., Conte-Daban, A., Sayen, S., Collin, F., Kieffer, I., Guillon, E., et al. (2016). Zinc(II) binding site to the Amyloid- $\beta$  peptide: insights from spectroscopic studies with a wide series of modified peptides. *Inorg. Chem.* 55, 10499–10509. doi: 10.1021/acs.inorgchem.6b01733
- Amador-Ortiz, C., Lin, W. L., Ahmed, Z., Personett, D., Davies, P., Duara, R., et al. (2007). TDP-43 immunoreactivity in hippocampal sclerosis and Alzheimer's disease. *Ann. Neurol.* 61, 435–445. doi: 10.1002/ana.21154
- Arai, T., Hasegawa, M., Akiyama, H., Ikeda, K., Nonaka, T., Mori, H., et al. (2006). TDP-43 is a component of ubiquitin-positive tau-negative inclusions in frontotemporal lobar degeneration and amyotrophic lateral sclerosis. *Biochem. Biophys. Res. Commun.* 351, 602–611. doi: 10.1016/j.bbrc.2006.10.093
- Arbely, E., Natan, E., Brandt, T., Allen, M. D., Veprintsev, D. B., Robinson, C. V., et al. (2011). Acetylation of lysine 120 of p53 endows DNA-binding specificity at effective physiological salt concentration. *Proc. Natl. Acad. Sci. U.S.A.* 108, 8251–8256. doi: 10.1073/pnas.1105028108
- Arbez, N., Ratovitski, T., Roby, E., Chighladze, E., Stewart, J. C., Ren, M., et al. (2017). Post-translational modifications clustering within proteolytic domains decrease mutant huntingtin toxicity. *J. Biol. Chem.* 292, 19238–19254. doi: 10.1074/jbc.M117.782300
- Archbold, H. C., Jackson, K. L., Arora, A., Weskamp, K., Tank, E. M. H., Li, X., et al. (2018). TDP43 nuclear export and neurodegeneration in models of amyotrophic lateral sclerosis and frontotemporal dementia. *Sci. Rep.* 8:4606. doi: 10.1038/s41598-018-22858-w
- Atrián-Blasco, E., Gonzalez, P., Santoro, A., Alies, B., Faller, P., and Hureau, C. (2018). Cu and Zn coordination to amyloid peptides: from fascinating chemistry to debated pathological relevance. *Coord. Chem. Rev.* 371, 38–55. doi: 10.1016/j.ccr.2018.04.007
- Auweter, S. D., Fasan, R., Reymond, L., Underwood, J. G., Black, D. L., Pitsch, S., et al. (2006). Molecular basis of RNA recognition by the human alternative splicing factor Fox-1. *EMBO J.* 25, 163–173. doi: 10.1038/sj.emboj.7600918
- Ayala, Y. M., De Conti, L., Avendaño-Vázquez, S. E., Dhir, A., Romano, M., D'Ambrogio, A., et al. (2011). TDP-43 regulates its mRNA levels through a negative feedback loop. *EMBO J.* 30, 277–288. doi: 10.1038/emboj.2010.310
- Ayala, Y. M., Pantano, S., D'Ambrogio, A., Buratti, E., Brindisi, A., Marchetti, C., et al. (2005). Human, *Drosophila*, and *C. elegans* TDP43: nucleic acid binding properties and splicing regulatory function. *J. Mol. Biol.* 348, 575–588.
- Ayala, Y. M., Zago, P., D'Ambrogio, A., Xu, Y.-F., Petrucelli, L., Buratti, E., et al. (2008). Structural determinants of the cellular localization and shuttling of TDP-43. *J. Cell Sci.* 121, 3778–3785. doi: 10.1242/jcs.038950
- Babinchak, W. M., Haider, R., Dumm, B. K., Sarkar, P., Surewicz, K., Choi, J. K., et al. (2019). The role of liquid-liquid phase separation in aggregation of the TDP-43 low-complexity domain. *J. Biol. Chem.* 294, 6306–6317. doi: 10.1074/jbc.RA118.007222

## AUTHOR CONTRIBUTIONS

All authors have made significant contribution and revised the manuscript critically for important intellectual content.

## ACKNOWLEDGMENTS

We would like to acknowledge funding for NM (Grant No. T32 GM008804).

- Backes, S., Hess, S., Boos, F., Woellhaf, M. W., Gödel, S., Jung, M., et al. (2018). Tom70 enhances mitochondrial preprotein import efficiency by binding to internal targeting sequences. *J. Cell Biol.* 217, 1369–1382. doi: 10.1083/jcb.201708044
- Balendra, R., and Isaacs, A. M. (2018). C9orf72-mediated ALS and FTD: multiple pathways to disease. *Nat. Rev. Neurol.* 14, 544–558. doi: 10.1038/s41582-018-0047-2
- Berning, B. A., and Walker, A. K. (2019). The pathobiology of TDP-43 C-terminal fragments in ALS and FTL. *Front. Neurosci.* 13:335. doi: 10.3389/fnins.2019.00335
- Bhandare, V. V., and Ramaswamy, A. (2018). The proteinopathy of D169G and K263E mutants at the RNA Recognition Motif (RRM) domain of tar DNA-binding protein (tdp43) causing neurological disorders: a computational study. *J. Biomol. Struct. Dyn.* 36, 1075–1093. doi: 10.1080/07391102.2017.1310670
- Bhardwaj, A., Myers, M. P., Buratti, E., and Baralle, F. E. (2013). Characterizing TDP-43 interaction with its RNA targets. *Nucleic Acids Res.* 41, 5062–5074. doi: 10.1093/nar/gkt189
- Brady, O. A., Meng, P., Zheng, Y., Mao, Y., and Hu, F. (2011). Regulation of TDP-43 aggregation by phosphorylation and p62/SQSTM1. *J. Neurochem.* 116, 248–259. doi: 10.1111/j.1471-4159.2010.07098.x
- Budini, M., and Buratti, E. (2011). TDP-43 autoregulation: implications for disease. *J. Mol. Neurosci.* 45, 473–479. doi: 10.1007/s12031-011-9573-8
- Budini, M., Buratti, E., Stuan, C., Guarnaccia, C., Romano, V., De Conti, L., et al. (2012). Cellular model of TAR DNA-binding Protein 43 (TDP-43) aggregation based on its C-terminal Gln/Asn-rich region. *J. Biol. Chem.* 287, 7512–7525. doi: 10.1074/jbc.M111.288720
- Buratti, E. (2015). Functional Significance of TDP-43 Mutations in Disease. *Adv. Genet.* 91, 1–53. doi: 10.1016/bs.adgen.2015.07.001
- Buratti, E. (2018). TDP-43 post-translational modifications in health and disease. *Expert Opin. Ther. Targets.* 22, 279–293. doi: 10.1080/14728222.2018.1439923
- Buratti, E., Brindisi, A., Giombi, M., Tisminețky, S., Ayala, Y. M., and Baralle, F. E. (2005). TDP-43 binds heterogeneous nuclear ribonucleoprotein A/B through its C-terminal tail: an important region for the inhibition of cystic fibrosis transmembrane conductance regulator exon 9 splicing. *J. Biol. Chem.* 280, 37572–37584. doi: 10.1074/jbc.M505557200
- Buratti, E., Dörk, T., Zuccato, E., Pagani, F., Romano, M., and Baralle, F. E. (2001). Nuclear factor TDP-43 and SR proteins promote in vitro and in vivo CFTR exon 9 skipping. *EMBO J.* 20, 1774–1784. doi: 10.1093/emboj/20.7.1774
- Cao, Q., Boyer, D. R., Sawaya, M. R., Ge, P., and Eisenberg, D. S. (2019). Cryo-EM structures of four polymorphic TDP-43 amyloid cores. *Nat. Struct. Mol. Biol.* 26, 619–627. doi: 10.1038/s41594-019-0248-4
- Caragounis, A., Price, K. A., Soon, C. P. W., Filiz, G., Masters, C. L., Li, Q. X., et al. (2010). Zinc induces depletion and aggregation of endogenous TDP-43. *Free Radic. Biol. Med.* 48, 1152–1161. doi: 10.1016/j.freeradbiomed.2010.01.035
- Casafont, I., Bengoechea, R., Tapia, O., Berciano, M. T., and Lafarga, M. (2009). TDP-43 localizes in mRNA transcription and processing sites in mammalian neurons. *J. Struct. Biol.* 167, 235–241. doi: 10.1016/j.jsb.2009.06.006
- Cassel, J. A., and Reitz, A. B. (2013). Ubiquitin-2 (UBQLN2) binds with high affinity to the C-terminal region of TDP-43 and modulates TDP-43 levels in H4 cells: characterization of inhibition by nucleic acids and 4-aminoquinolines. *Biochim. Biophys. Acta Proteins Proteom.* 1834, 964–971. doi: 10.1016/j.bbapap.2013.03.020
- Catara, G., Grimaldi, G., Schembri, L., Spano, D., Turacchio, G., Lo Monte, M., et al. (2017). PARP1-produced poly-ADP-ribose causes the PARP12

- translocation to stress granules and impairment of Golgi complex functions. *Sci. Rep.* 7:14035. doi: 10.1038/s41598-017-14156-8
- Chang, C., Wu, T. H., Wu, C. Y., Chiang, M., Toh, E. K., Hsu, Y. C., et al. (2012). The N-terminus of TDP-43 promotes its oligomerization and enhances DNA binding affinity. *Biochem. Biophys. Res. Commun.* 425, 219–224. doi: 10.1016/j.bbrc.2012.07.071
- Chang, C. K., Chiang, M. H., Toh, E. K. W., Chang, C. F., and Huang, T. H. (2013). Molecular mechanism of oxidation-induced TDP-43 RRM1 aggregation and loss of function. *FEBS Lett.* 587, 575–582. doi: 10.1016/j.febslet.2013.01.038
- Che, M. X., Jiang, L. L., Li, H. Y., Jiang, Y. J., and Hu, H. Y. (2015). TDP-35 sequesters TDP-43 into cytoplasmic inclusions through binding with RNA. *FEBS Lett.* 589, 1920–1928. doi: 10.1016/j.febslet.2015.06.009
- Chen, H. J., Mitchell, J. C., Novoselov, S., Miller, J., Nishimura, A. L., Scotter, E. L., et al. (2016). The heat shock response plays an important role in TDP-43 clearance: evidence for dysfunction in amyotrophic lateral sclerosis. *Brain* 139, 1417–1432. doi: 10.1093/brain/aww028
- Chiang, C. H., Grauffel, C., Wu, L. S., Kuo, P. H., Doudeva, L. G., Lim, C., et al. (2016). Structural analysis of disease-related TDP-43 D169G mutation: linking enhanced stability and caspase cleavage efficiency to protein accumulation. *Sci. Rep.* 6:21581. doi: 10.1038/srep21581
- Cicardi, M. E., Cristofani, R., Rusmini, P., Meroni, M., Ferrari, V., Vezzoli, G., et al. (2018). Tdp-25 routing to autophagy and proteasome ameliorates its aggregation in amyotrophic lateral sclerosis target cells. *Sci. Rep.* 8:12390. doi: 10.1038/s41598-018-29658-2
- Cohen, T. J., Hwang, A. W., Restrepo, C. R., Yuan, C. X., Trojanowski, J. Q., and Lee, V. M. Y. (2015). An acetylation switch controls TDP-43 function and aggregation propensity. *Nat. Commun.* 6:5845. doi: 10.1038/ncomms6845
- Cohen, T. J., Hwang, A. W., Unger, T., Trojanowski, J. Q., and Lee, V. M. Y. (2012). Redox signalling directly regulates TDP-43 via cysteine oxidation and disulphide cross-linking. *EMBO J.* 31, 1241–1252. doi: 10.1038/emboj.2011.471
- Colombrita, C., Onesto, E., Megiorni, F., Pizzuti, A., Baralle, F. E., Buratti, E., et al. (2012). TDP-43 and FUS RNA-binding proteins bind distinct sets of cytoplasmic messenger RNAs and differently regulate their post-transcriptional fate in motoneuron-like cells. *J. Biol. Chem.* 287, 15635–15647. doi: 10.1074/jbc.M111.333450
- Conicella, A. E., Zerze, G. H., Mittal, J., and Fawzi, N. L. (2016). ALS Mutations disrupt phase separation mediated by  $\alpha$ -Helical structure in the TDP-43 low-complexity C-Terminal domain. *Structure* 24, 1537–1549. doi: 10.1016/j.str.2016.07.007
- Coyne, A. N., Siddegowda, B. B., Estes, P. S., Johannesmeyer, J., Kovalik, T., Daniel, S. G., et al. (2014). Futsch/MAP1B mRNA Is a translational target of TDP-43 and is neuroprotective in a *Drosophila* Model of amyotrophic lateral sclerosis. *J. Neurosci.* 34, 15962–15974. doi: 10.1523/JNEUROSCI.2526-14.2014
- D'Alton, S., Altshuler, M., and Lewis, J. (2015). Studies of alternative isoforms provide insight into TDP-43 autoregulation and pathogenesis. *Rna* 21, 1419–1432. doi: 10.1261/rna.047647.114
- D'Ambrógio, A., Buratti, E., Stuaní, C., Guarnaccia, C., Romano, M., Ayala, Y. M., et al. (2009). Functional mapping of the interaction between TDP-43 and hnRNP A2 in vivo. *Nucleic Acids Res.* 37, 4116–4126. doi: 10.1093/nar/gkp342
- Dangoumau, A., Veyrat-Durebex, C., Blasco, H., Praline, J., Corcia, P., Andres, C. R., et al. (2013). Protein SUMOylation, an emerging pathway in amyotrophic lateral sclerosis. *Int. J. Neurosci.* 123, 366–374. doi: 10.3109/00207454.2012.761984
- Davis, S. A., Itaman, S., Khalid-Janney, C. M., Sherard, J. A., Dowell, J. A., Cairns, N. J., et al. (2018). TDP-43 interacts with mitochondrial proteins critical for mitophagy and mitochondrial dynamics. *Neurosci. Lett.* 678, 8–15. doi: 10.1016/j.neulet.2018.04.053
- Deng, J., Yang, M., Chen, Y., Chen, X., Liu, J., Sun, S., et al. (2015). FUS Interacts with HSP60 to promote mitochondrial damage. *PLoS Genet.* 11:e1005357. doi: 10.1371/journal.pgen.1005357
- Deshaies, J. E., Shkreta, L., Moszczynski, A. J., Sidibé, H., Semmler, S., Fouillen, A., et al. (2018). TDP-43 regulates the alternative splicing of hnRNP A1 to yield an aggregation-prone variant in amyotrophic lateral sclerosis. *Brain* 141, 1320–1333. doi: 10.1093/brain/awy062
- Dewey, C. M., Cenik, B., Sephton, C. F., Dries, D. R., Mayer, P., Good, S. K., et al. (2010). TDP-43 Is directed to stress granules by sorbitol, a novel physiological osmotic and oxidative stressor. *Mol. Cell. Biol.* 31, 1098–1108. doi: 10.1128/MCB.01279-10
- Ederle, H., Funk, C., Abou-Ajram, C., Hutten, S., Funk, E. B. E., Kehlenbach, R. H., et al. (2018). Nuclear egress of TDP-43 and FUS occurs independently of Exportin-1/CRM1. *Sci. Rep.* 8:7084. doi: 10.1038/s41598-018-25007-5
- Fallini, C., Bassell, G. J., and Rossoll, W. (2012). The ALS disease protein TDP-43 is actively transported in motor neuron axons and regulates axon outgrowth. *Hum. Mol. Genet.* 5:e15878. doi: 10.1371/journal.pone.0015878
- Fang, Y. S., Tsai, K. J., Chang, Y. J., Kao, P., Woods, R., Kuo, P. H., et al. (2014). Full-length TDP-43 forms toxic amyloid oligomers that are present in frontotemporal lobar dementia-TDP patients. *Nat. Commun.* 5:4824. doi: 10.1038/ncomms5824
- Foglieni, C., Papin, S., Salvadè, A., Afroz, T., Pinton, S., Pedrioli, G., et al. (2017). Split GFP technologies to structurally characterize and quantify functional biomolecular interactions of FTD-related proteins. *Sci. Rep.* 7:14013. doi: 10.1038/s41598-017-14459-w
- Foran, E., Rosenblum, L., Bogush, A. I., and Trotti, D. (2013). Sumoylation of critical proteins in amyotrophic lateral sclerosis: emerging pathways of pathogenesis. *NeuroMolecular Med.* 15, 760–770. doi: 10.1007/s12017-013-8262-x
- Fratta, P., Sivakumar, P., Humphrey, J., Lo, K., Ricketts, T., Oliveira, H., et al. (2018). Mice with endogenous TDP-43 mutations exhibit gain of splicing function and characteristics of amyotrophic lateral sclerosis. *EMBO J.* 37, e98684.
- Freibaum, B. D., Chitta, R. K., High, A. A., and Taylor, J. P. (2010). Global analysis of TDP-43 interacting proteins reveals strong association with RNA splicing and translation machinery. *J. Proteome Res.* 9, 1104–1120. doi: 10.1021/pr901076y
- Furukawa, Y., Suzuki, Y., Fukuoka, M., Nagasawa, K., Nakagome, K., Shimizu, H., et al. (2016). A molecular mechanism realizing sequence-specific recognition of nucleic acids by TDP-43. *Sci. Rep.* 6:20576. doi: 10.1038/srep20576
- Garnier, C., Devred, F., Byrne, D., Puppo, R., Roman, A. Y., Malesinski, S., et al. (2017). Zinc binding to RNA recognition motif of TDP-43 induces the formation of amyloid-like aggregates. *Sci. Rep.* 7:6812. doi: 10.1038/s41598-017-07215-7
- Gasset-Rosa, F., Lu, S., Yu, H., Chen, C., Melamed, Z., Guo, L., et al. (2019). Cytoplasmic TDP-43 De-mixing independent of stress granules drives inhibition of nuclear import, loss of nuclear TDP-43, and cell death. *Neuron* 102, 339.e7–357.e7. doi: 10.1016/j.neuron.2019.02.038
- Geser, F., Winton, M. J., Kwong, L. K., Xu, Y., Xie, S. X., Igaz, L. M., et al. (2008). Pathological TDP-43 in parkinsonism-dementia complex and amyotrophic lateral sclerosis of Guam. *Acta Neuropathol.* 115, 133–145. doi: 10.1007/s00401-007-0257-y
- Gibson, B. A., and Kraus, W. L. (2012). New insights into the molecular and cellular functions of poly(ADP-ribose) and PARPs. *Nat. Rev. Mol. Cell Biol.* 13, 411–424. doi: 10.1038/nrm3376
- Gomes, E., and Shorter, J. (2019). The molecular language of membraneless organelles. *J. Biol. Chem.* 294, 7115–7127.
- Gu, J., Chen, F., Iqbal, K., Gong, C. X., Wang, X., and Liu, F. (2017). Transactive response DNA-binding protein 43 (TDP-43) regulates alternative splicing of tau exon 10: implications for the pathogenesis of tauopathies. *J. Biol. Chem.* 292, 10600–10612. doi: 10.1074/jbc.M117.783498
- Gu, J., Wang, W., Miao, S., Chen, F., Wu, F., Hu, W., et al. (2018). Protein Phosphatase 1 dephosphorylates TDP-43 and suppresses its function in tau exon 10 inclusion. *FEBS Lett.* 592, 402–410. doi: 10.1002/1873-3468.12976
- Guenther, E. L., Cao, Q., Trinh, H., Lu, J., Sawaya, M. R., Cascio, D., et al. (2018a). Atomic structures of TDP-43 LCD segments and insights into reversible or pathogenic aggregation. *Nat. Struct. Mol. Biol.* 25, 463–471. doi: 10.1038/s41594-018-0064-2
- Guenther, E. L., Ge, P., Trinh, H., Sawaya, M. R., Cascio, D., Boyer, D. R., et al. (2018b). Atomic-level evidence for packing and positional amyloid polymorphism by segment from TDP-43 RRM2. *Nat. Struct. Mol. Biol.* 25, 311–319. doi: 10.1038/s41594-018-0045-5
- Guo, A., Gu, H., Zhou, J., Mulhern, D., Wang, Y., Lee, K. A., et al. (2014). Immunoaffinity enrichment and mass spectrometry analysis of protein methylation. *Mol. Cell. Proteomics.* 13, 372–387. doi: 10.1074/mcp.O113.027870
- Guo, W., Chen, Y., Zhou, X., Kar, A., Ray, P., Chen, X., et al. (2011). An ALS-associated mutation affecting TDP-43 enhances protein aggregation, fibril



- formation and neurotoxicity. *Nat. Struct. Mol. Biol.* 18, 822–830. doi: 10.1038/nsm.2053
- Gupte, R., Liu, Z., and Kraus, W. L. (2017). Parps and adp-ribosylation: recent advances linking molecular functions to biological outcomes. *Genes Dev.* 31, 101–126. doi: 10.1101/gad.291518.116
- Hans, F., Fiesel, F. C., Strong, J. C., Jackel, S., Rasse, T. M., Geisler, S., et al. (2014). UBE2E ubiquitin-conjugating enzymes and ubiquitin isopeptidase y regulate TDP-43 protein ubiquitination. *J. Biol. Chem.* 289, 19164–19179. doi: 10.1074/jbc.M114.561704
- Hasegawa, M., Arai, T., Akiyama, H., Nonaka, T., Mori, H., Hashimoto, T., et al. (2007). TDP-43 is deposited in the guam parkinsonism-dementia complex brains. *Brain* 130(Pt 5), 1386–1394. doi: 10.1093/brain/awm065
- Hasegawa, M., Arai, T., Nonaka, T., Kametani, F., Yoshida, M., Hashizume, Y., et al. (2008). Phosphorylated TDP-43 in frontotemporal lobar degeneration and amyotrophic lateral sclerosis. *Ann. Neurol.* 64, 60–70. doi: 10.1002/ana.21425
- Hendriks, I. A., D'Souza, R. C. J., Yang, B., Verlaan-De Vries, M., Mann, M., and Vertegaal, A. C. O. (2014). Uncovering global SUMOylation signaling networks in a site-specific manner. *Nat. Struct. Mol. Biol.* 21, 927–936. doi: 10.1038/nsm.2890
- Hendriks, I. A., Lyon, D., Young, C., Jensen, L. J., Vertegaal, A. C. O., and Nielsen, M. L. (2017). Site-specific mapping of the human SUMO proteome reveals co-modification with phosphorylation. *Nat. Struct. Mol. Biol.* 24, 325–336. doi: 10.1038/nsm.3366
- Hendriks, I. A., Treffers, L. W., Verlaan-deVries, M., Olsen, J. V., and Vertegaal, A. C. O. (2015). SUMO-2 orchestrates chromatin modifiers in response to DNA damage. *Cell Rep.* 10, 1778–1791. doi: 10.1016/j.celrep.2015.02.033
- Holehouse, A. S., and Pappu, R. V. (2018). Functional implications of intracellular phase transitions. *Biochemistry.* 57, 2415–2423. doi: 10.1021/acs.biochem.7b01136
- Hornbeck, P. V., Zhang, B., Murray, B., Kornhauser, J. M., Latham, V., and Skrzypek, E. (2015). PhosphoSitePlus, 2014: mutations, PTMs and recalibrations. *Nucleic Acids Res.* 43, D512–D520. doi: 10.1093/nar/gku1267
- Huang, C., Xia, P. Y., and Zhou, H. (2010). Sustained Expression of TDP-43 and FUS in motor neurons in rodent's lifetime. *Int. J. Biol. Sci.* 6, 396–406. doi: 10.7150/ijbs.6.396
- Huang, Y., Wu, Z., Cao, Y., Lang, M., Lu, B., and Zhou, B. (2014). Zinc binding directly regulates tau toxicity independent of tau hyperphosphorylation. *Cell Rep.* 8, 831–842. doi: 10.1016/j.celrep.2014.06.047
- Igaz, L. M., Kwong, L. K., Chen-Plotkin, A., Winton, M. J., Unger, T. L., Xu, Y., et al. (2009). Expression of TDP-43 C-terminal fragments in vitro recapitulates pathological features of TDP-43 proteinopathies. *J. Biol. Chem.* 284, 8516–8524. doi: 10.1074/jbc.M809462200
- Irwin, D. J., Cohen, T. J., Grossman, M., Arnold, S. E., Xie, S. X., Lee, V. M. Y., et al. (2012). Acetylated tau, a novel pathological signature in Alzheimer's disease and other tauopathies. *Brain* 135, 807–818. doi: 10.1093/brain/aww013
- Janssens, J., and Van Broeckhoven, C. (2013). Pathological mechanisms underlying TDP-43 driven neurodegeneration in FTL-ALS spectrum disorders. *Hum. Mol. Genet.* 22, R77–R87. doi: 10.1093/hmg/ddt349
- Jiang, L. L., Che, M. X., Zhao, J., Zhou, C. J., Xie, M. Y., Li, H. Y., et al. (2013). Structural transformation of the amyloidogenic core region of TDP-43 protein initiates its aggregation and cytoplasmic inclusion. *J. Biol. Chem.* 288, 19614–19624. doi: 10.1074/jbc.M113.463828
- Jiang, L. L., Xue, W., Hong, J. Y., Zhang, J. T., Li, M. J., Yu, S. N., et al. (2017). The N-terminal dimerization is required for TDP-43 splicing activity. *Sci. Rep.* 7:6196. doi: 10.1038/s41598-017-06263-3
- Jiang, L. L., Zhao, J., Yin, X. F., He, W. T., Yang, H., Che, M. X., et al. (2016). Two mutations G335D and Q343R within the amyloidogenic core region of TDP-43 influence its aggregation and inclusion formation. *Sci. Rep.* 6:23928. doi: 10.1038/srep23928
- Johnson, B. S., McCaffery, J. M., Lindquist, S., and Gitler, A. D. (2008). A yeast TDP-43 proteinopathy model: exploring the molecular determinants of TDP-43 aggregation and cellular toxicity. *Proc. Natl. Acad. Sci. U.S.A.* 105, 6439–6444. doi: 10.1073/pnas.0802082105
- Kametani, F., Obi, T., Shishido, T., Akatsu, H., Murayama, S., Saito, Y., et al. (2016). Mass spectrometric analysis of accumulated TDP-43 in amyotrophic lateral sclerosis brains. *Sci. Rep.* 6:23281. doi: 10.1038/srep23281
- Kato, M., Han, T. W., Xie, S., Shi, K., Du, X., Wu, L. C., et al. (2012). Cell-free formation of RNA granules: low complexity sequence domains form dynamic fibers within hydrogels. *Cell.* 149, 753–767. doi: 10.1016/j.cell.2012.04.017
- Kawamata, H., Peixoto, P., Konrad, C., Palomo, G., Bredvik, K., Gerges, M., et al. (2017). Mutant TDP-43 does not impair mitochondrial bioenergetics in vitro and in vivo. *Mol. Neurodegener.* 12:37.
- Kishida, S., Yamamoto, H., Hino, S., Ikeda, S., Kishida, M., and Kikuchi, A. (2015). DIX domains of Dvl and axin are necessary for protein interactions and their ability to regulate  $\beta$ -Catenin stability. *Mol. Cell. Biol.* 19, 4414–4422. doi: 10.1128/mcb.19.6.4414
- Kitamura, A., Iwasaki, N., and Kinjo, M. (2018). Molecular chaperone HSP70 prevents formation of inclusion bodies of the 25-kDa C-terminal fragment of TDP-43 by preventing aggregate accumulation. *Cell Stress Chaperones* 23, 1177–1183. doi: 10.1007/s12192-018-0930-1
- Kitamura, A., Nakayama, Y., Shibasaki, A., Taki, A., Yuno, S., Takeda, K., et al. (2016). Interaction of RNA with a C-terminal fragment of the amyotrophic lateral sclerosis-associated TDP43 reduces cytotoxicity. *Sci. Rep.* 6, 19230. doi: 10.1038/srep19230
- Kraemer, B. C., Schuck, T., Wheeler, J. M., Robinson, L. C., Trojanowski, J. Q., Lee, V. M. Y., et al. (2010). Loss of Murine TDP-43 disrupts motor function and plays an essential role in embryogenesis. *Acta Neuropathol.* 119, 409–419. doi: 10.1007/s00401-010-0659-0
- Krietsch, J., Rouleau, M., Pic, É, Ethier, C., Dawson, T. M., Dawson, V. L., et al. (2013). Reprogramming cellular events by poly(ADP-ribose)-binding proteins. *Mol. Aspects Med.* 34, 1066–1087. doi: 10.1016/j.mam.2012.12.005
- Kuo, P. H., Chiang, C. H., Wang, Y. T., Doudeva, L. G., and Yuan, H. S. (2014). The crystal structure of TDP-43 RRM1-DNA complex reveals the specific recognition for UG- and TG-rich nucleic acids. *Nucleic Acids Res.* 42, 4712–4722. doi: 10.1093/nar/gkt1407
- Kuo, P. H., Doudeva, L. G., Wang, Y. T., Shen, C. K. J., and Yuan, H. S. (2009). Structural insights into TDP-43 in nucleic-acid binding and domain interactions. *Nucleic Acids Res.* 37, 1799–1808. doi: 10.1093/nar/gkp013
- Lagier-Tourenne, C., Polymenidou, M., and Cleveland, D. W. (2010). TDP-43 and FUS/TLS: emerging roles in RNA processing and neurodegeneration. *Hum. Mol. Genet.* 19, R46–R64. doi: 10.1093/hmg/ddq137
- Landrum, M. J., Lee, J. M., Benson, M., Brown, G., Chao, C., Chitipiralla, S., et al. (2016). ClinVar: public archive of interpretations of clinically relevant variants. *Nucleic Acids Res.* 44, D862–D868. doi: 10.1093/nar/gkv1222
- Leverenz, J. B., Yu, C. E., Montine, T. J., Steinbart, E., Bekris, L. M., Zabetian, C., et al. (2007). A novel progranulin mutation associated with variable clinical presentation and tau, TDP43 and alpha-synuclein pathology. *Brain* 130(Pt 5), 1360–1374. doi: 10.1093/brain/awm069
- Li, H. R., Chen, T. C., Hsiao, C. L., Shi, L., Chou, C. Y., and Huang, J. (2018). The physical forces mediating self-association and phase-separation in the C-terminal domain of TDP-43. *Biochim. Biophys. Acta Proteins Proteom.* 1866, 214–223. doi: 10.1016/j.bbapap.2017.10.001
- Li, H. Y., Yeh, P. A., Chiu, H. C., Tang, C. Y., and Tu, B. P. (2011). Hyperphosphorylation as a defense mechanism to reduce TDP-43 aggregation. *PLoS One* 6:e23075. doi: 10.1371/journal.pone.0023075
- Li, Q., Yokoshi, M., Okada, H., and Kawahara, Y. (2015). The cleavage pattern of TDP-43 determines its rate of clearance and cytotoxicity. *Nat. Commun.* 6:6183. doi: 10.1038/ncomms7183
- Li, T., Du, Y., Wang, L., Huang, L., Li, W., Lu, M., et al. (2012). Characterization and prediction of lysine (K)-acetyl-transferase specific acetylation sites. *Mol. Cell. Proteomics.* 11:M111.011080. doi: 10.1074/mcp.M111.011080
- Li, T., Song, B., Wu, Z., Lu, M., and Zhu, W. G. (2013). Systematic identification of Class I HDAC substrates. *Brief. Bioinform.* 15, 963–972. doi: 10.1093/bib/bbt060
- Li, W., Reeb, A. N., Lin, B., Subramanian, P., Fey, E. E., Knoverek, C. R., et al. (2017). Heat shock-induced phosphorylation of TAR DNA-binding protein 43 (TDP-43) by MAPK/ERK kinase regulates TDP-43 function. *J. Biol. Chem.* 292, 5089–5100. doi: 10.1074/jbc.M116.753913
- Lim, L., Wei, Y., Lu, Y., and Song, J. (2016). ALS-Causing mutations significantly perturb the self-assembly and interaction with nucleic acid of the intrinsically disordered prion-like domain of TDP-43. *PLoS Biol.* 14:e1002338. doi: 10.1371/journal.pbio.1002338
- Ling, S. C., Polymenidou, M., and Cleveland, D. W. (2013). Converging mechanisms in als and FTD: disrupted RNA and protein homeostasis. *Neuron.* 79, 416–438. doi: 10.1016/j.neuron.2013.07.033



- Liu, J., Shinobu, L. A., Ward, C. M., Young, D., and Cleveland, D. W. (2005). Elevation of the Hsp70 chaperone does not effect toxicity in mouse models of familial amyotrophic lateral sclerosis. *J. Neurochem.* 93, 875–882. doi: 10.1111/j.1471-4159.2005.03054.x
- Lukavsky, P. J., Daujotyte, D., Tollervey, J. R., Ule, J., Stuani, C., Buratti, E., et al. (2013). Molecular basis of UG-rich RNA recognition by the human splicing factor TDP-43. *Nat. Struct. Mol. Biol.* 20, 1443–1449. doi: 10.1038/nsmb.2698
- Lumpkin, R. J., Gu, H., Zhu, Y., Leonard, M., Ahmad, A. S., Clauser, K. R., et al. (2017). Site-specific identification and quantitation of endogenous SUMO modifications under native conditions. *Nat. Commun.* 8:1171. doi: 10.1038/s41467-017-01271-3
- Mackenzie, I. R. A., and Rademakers, R. (2008). The role of transactive response DNA-binding protein-43 in amyotrophic lateral sclerosis and frontotemporal dementia. *Curr. Opin. Neurol.* 21, 693–700. doi: 10.1097/WCO.0b013e3283168d1d
- Majumder, P., Chu, J. F., Chatterjee, B., Swamy, K. B. S., and Shen, C. K. J. (2016). Co-regulation of mRNA translation by TDP-43 and Fragile X Syndrome protein FMRP. *Acta Neuropathol.* 132, 721–738. doi: 10.1007/s00401-016-1603-8
- Mann, J. R., Gleixner, A. M., Mauna, J. C., Gomes, E., DeChellis-Marks, M. R., Needham, P. G., et al. (2019). RNA binding antagonizes neurotoxic phase transitions of TDP-43. *Neuron* 102, 321.e8–338.e8. doi: 10.1016/j.neuron.2019.01.048
- McGurk, L., Gomes, E., Guo, L., Mojsilovic-Petrovic, J., Tran, V., Kalb, R. G., et al. (2018). Poly(ADP-Ribose) prevents pathological phase separation of TDP-43 by promoting liquid demixing and stress granule localization. *Mol. Cell* 71, 703.e9–717.e9. doi: 10.1016/j.molcel.2018.07.002
- Mészáros, B., Erdős, G., and Dosztányi, Z. (2018). IUPred2A: context-dependent prediction of protein disorder as a function of redox state and protein binding. *Nucleic Acids Res.* 46, W329–W337. doi: 10.1093/nar/gky384
- Molliex, A., Temirov, J., Lee, J., Coughlin, M., Kanagaraj, A. P., Kim, H. J., et al. (2015). Phase separation by low complexity domains promotes stress granule assembly and drives pathological fibrillization. *Cell* 163, 123–133. doi: 10.1016/j.cell.2015.09.015
- Mompeán, M., Baralle, M., Buratti, E., and Laurents, D. V. (2016a). An amyloid-like pathological conformation of TDP-43 is stabilized by hypercooperative hydrogen bonds. *Front. Mol. Neurosci.* 9:125.
- Mompeán, M., Chakraborty, A., Buratti, E., and Laurents, D. V. (2016b). Electrostatic repulsion governs TDP-43 C-terminal domain aggregation. *PLoS Biol.* 14:e1002447. doi: 10.1371/journal.pbio.1002447
- Mompeán, M., Romano, V., Pantoja-Uceda, D., Stuani, C., Baralle, F. E., Buratti, E., et al. (2016c). The TDP-43 N-terminal domain structure at high resolution. *FEBS J.* 283, 1242–1260. doi: 10.1111/febs.13651
- Mompeán, M., Buratti, E., Guarnaccia, C., Brito, R. M. M., Chakraborty, A., Baralle, F. E., et al. (2014). Structural characterization of the minimal segment of TDP-43 competent for aggregation. *Arch. Biochem. Biophys.* 545, 53–62. doi: 10.1016/j.abb.2014.01.007
- Mompeán, M., Hervás, R., Xu, Y., Tran, T. H., Guarnaccia, C., Buratti, E., et al. (2015). Structural evidence of amyloid fibril formation in the putative aggregation domain of TDP-43. *J. Phys. Chem. Lett.* 6, 2608–2615. doi: 10.1021/acs.jpclett.5b00918
- Mompeán, M., Romano, V., Pantoja-Uceda, D., Stuani, C., Baralle, F. E., Buratti, E., et al. (2017). Point mutations in the N-terminal domain of transactive response DNA-binding protein 43 kDa (TDP-43) compromise its stability, dimerization, and functions. *J. Biol. Chem.* 292, 11992–12006. doi: 10.1074/jbc.M117.775965
- Mori, F., Tanji, K., Zhang, H. X., Nishihira, Y., Tan, C. F., Takahashi, H., et al. (2008). Maturation process of TDP-43-positive neuronal cytoplasmic inclusions in amyotrophic lateral sclerosis with and without dementia. *Acta Neuropathol.* 116, 193–203. doi: 10.1007/s00401-008-0396-9
- Murray, D. T., Kato, M., Lin, Y., Thurber, K. R., Hung, I., McKnight, S. L., et al. (2017). Structure of FUS protein fibrils and its relevance to self-assembly and phase separation of low-complexity domains. *Cell* 171, 615.e16–627.e16. doi: 10.1016/j.cell.2017.08.048
- Nakashima-Yasuda, H., Uryu, K., Robinson, J., Xie, S. X., Hurtig, H., Duda, J. E., et al. (2007). Co-morbidity of TDP-43 proteinopathy in Lewy body related diseases. *Acta Neuropathol.* 114, 221–229. doi: 10.1007/s00401-007-0261-2
- Narita, T., Weinert, B. T., and Choudhary, C. (2019). Functions and mechanisms of non-histone protein acetylation. *Nat. Rev. Mol. Cell Biol.* 20, 156–174. doi: 10.1038/s41580-018-0081-3
- Neumann, M., Kwong, L. K., Lee, E. B., Kremmer, E., Flatley, A., Xu, Y., et al. (2009). Phosphorylation of S409/410 of TDP-43 is a consistent feature in all sporadic and familial forms of TDP-43 proteinopathies. *Acta Neuropathol.* 117, 137–149. doi: 10.1007/s00401-008-0477-9
- Neumann, M., Sampathu, D. M., Kwong, L. K., Truax, A. C., Micsenyi, M. C., Chou, T. T., et al. (2006). Ubiquitinated TDP-43 in frontotemporal lobar degeneration and amyotrophic lateral sclerosis. *Science* 314, 130–133.
- Newell, K., Paron, F., Mompeán, M., Murrell, J., Salis, E., Stuani, C., et al. (2019). Dysregulation of TDP-43 intracellular localization and early onset ALS are associated with a TARDBP S375G variant. *Brain Pathol.* 29, 397–413. doi: 10.1111/bpa.12680
- Nishimoto, Y., Ito, D., Yagi, T., Nihei, Y., Tsunodo, Y., and Suzuki, N. (2010). Characterization of alternative isoforms and inclusion body of the TAR DNA-binding protein-43. *J. Biol. Chem.* 285, 608–619. doi: 10.1074/jbc.M109.022012
- Nishimura, A. L., Upunski, V., Troakes, C., Kathe, C., Fratta, P., Howell, M., et al. (2010). Nuclear import impairment causes cytoplasmic transactivation response DNA-binding protein accumulation and is associated with frontotemporal lobar degeneration. *Brain* 133, 1763–1771. doi: 10.1093/brain/awq111
- Nonaka, T., Arai, T., Buratti, E., Baralle, F. E., Akiyama, H., and Hasegawa, M. (2009a). Phosphorylated and ubiquitinated TDP-43 pathological inclusions in ALS and FTL-D-U are recapitulated in SH-SY5Y cells. *FEBS Lett.* 583, 394–400. doi: 10.1016/j.febslet.2008.12.031
- Nonaka, T., Kametani, F., Arai, T., Akiyama, H., and Hasegawa, M. (2009b). Truncation and pathogenic mutations facilitate the formation of intracellular aggregates of TDP-43. *Hum. Mol. Genet.* 18, 3353–3364. doi: 10.1093/hmg/ddp275
- Nonaka, T., Suzuki, G., Tanaka, Y., Kametani, F., Hirai, S., Okado, H., et al. (2016). Phosphorylation of TAR DNA-binding protein of 43 kDa (TDP-43) by truncated casein kinase 18 triggers mislocalization and accumulation of TDP-43. *J. Biol. Chem.* 291, 5473–5483. doi: 10.1074/jbc.M115.695379
- Onesto, E., Colombrina, C., Gumina, V., Borghi, M. O., Dusi, S., Doretti, A., et al. (2016). Gene-specific mitochondria dysfunctions in human TARDBP and C9ORF72 fibroblasts. *Acta Neuropathol. Commun.* 4:47. doi: 10.1186/s40478-016-0316-5
- Otwinowski, Z., and Minor, W. (1997). Processing of X-ray diffraction data collected in oscillation mode. *Methods Enzymol.* 276, 307–326. doi: 10.1016/s0076-6879(97)76066-x
- Ou, S. H., Wu, F., Harrich, D., García-Martínez, L. F., and Gaynor, R. B. (1995). Cloning and characterization of a novel cellular protein, TDP-43, that binds to human immunodeficiency virus type 1 TAR DNA sequence motifs. *J. Virol.* 69, 3584–3596.
- Pace, N. J., and Weerapana, E. (2014). Zinc-binding cysteines: diverse functions and structural motifs. *Biomolecules.* 4, 419–434. doi: 10.3390/biom4020419
- Pinarbasi, E. S., Cagatay, T., Fung, H. Y. J., Li, Y. C., Chook, Y. M., and Thomas, P. J. (2018). Active nuclear import and passive nuclear export are the primary determinants of TDP-43 localization. *Sci. Rep.* 8:7083. doi: 10.1038/s41598-018-25008-4
- Polymenidou, M., Lagier-Tourenne, C., Hutt, K. R., Huelga, S. C., Moran, J., Liang, T. Y., et al. (2011). Long pre-mRNA depletion and RNA missplicing contribute to neuronal vulnerability from loss of TDP-43. *Nat. Neurosci.* 14, 459–468. doi: 10.1038/nn.2779
- Prasad, A., Bharathi, V., Sivalingam, V., Girdhar, A., and Patel, B. K. (2019). Molecular Mechanisms of TDP-43 Misfolding and Pathology in amyotrophic lateral sclerosis. *Front. Mol. Neurosci.* 12:25. doi: 10.3389/fnmol.2019.00025
- Prasad, A., Sivalingam, V., Bharathi, V., Girdhar, A., and Patel, B. K. (2018). The amyloidogenicity of a C-terminal region of TDP-43 implicated in Amyotrophic Lateral Sclerosis can be affected by anions, acetylation and homodimerization. *Biochimie.* 150, 76–87. doi: 10.1016/j.biochi.2018.05.003
- Purice, M. D., and Taylor, J. P. (2018). Linking hnRNP function to ALS and FTD pathology. *Front. Neurosci.* 12:326. doi: 10.3389/fnins.2018.00326
- Qin, H., Lim, L.-Z., Wei, Y., and Song, J. (2014). TDP-43 N terminus encodes a novel ubiquitin-like fold and its unfolded form in equilibrium that can be shifted by binding to ssDNA. *Proc. Natl. Acad. Sci. U.S.A.* 111, 18619–18624. doi: 10.1073/pnas.1413994112

- Radičovac, P., Vacic, V., Haynes, C., Cocklin, R. R., Mohan, A., Heyen, J. W., et al. (2010). Identification, analysis, and prediction of protein ubiquitination sites. *Proteins Struct. Funct. Bioinforma.* 78, 365–380. doi: 10.1002/prot.22555
- Ratti, A., and Buratti, E. (2016). Physiological functions and pathobiology of TDP-43 and FUS/TLS proteins. *J. Neurochem.* 138(Suppl. 1), 95–111. doi: 10.1111/jnc.13625
- Ren, J., Sang, Y., Tan, Y., Tao, J., Ni, J., Liu, S., et al. (2016). Acetylation of Lysine 201 Inhibits the DNA-Binding Ability of PhoP to Regulate *Salmonella* Virulence. *PLoS Pathog.* 12:e1005458. doi: 10.1371/journal.ppat.1005458
- Rigbolt, K. T. G., Prokhorova, T. A., Akimov, V., Henningsen, J., Johansen, P. T., Kratchmarova, I., et al. (2011). System-wide temporal characterization of the proteome and phosphoproteome of human embryonic stem cell differentiation. *Sci. Signal* 4:rs3. doi: 10.1126/scisignal.2001570
- Ritson, G. P., Custer, S. K., Freibaum, B. D., Guinto, J. B., Geffel, D., Moore, J., et al. (2010). TDP-43 mediates degeneration in a novel *Drosophila* model of disease caused by mutations in VCP/p97. *J. Neurosci.* 30, 7729–7739. doi: 10.1523/JNEUROSCI.5894-09.2010
- Rohn, T. T. (2008). Caspase-cleaved TAR DNA-binding protein-43 is a major pathological finding in Alzheimer's disease. *Brain Res.* 1228, 189–198. doi: 10.1016/j.brainres.2008.06.094
- Ruan, L., Zhou, C., Jin, E., Kucharavy, A., Zhang, Y., Wen, Z., et al. (2017). Cytosolic proteostasis through importing of misfolded proteins into mitochondria. *Nature* 543, 443–446. doi: 10.1038/nature21695
- Saini, A., and Chauhan, V. S. (2011). Delineation of the core aggregation sequences of TDP-43 C-terminal fragment. *ChemBioChem* 12, 2495–2501. doi: 10.1002/cbic.201100427
- Schmidt, H. B., Barreau, A., and Rohatgi, R. (2019). Phase separation-deficient TDP43 remains functional in splicing. *Nat. Commun.* 10:4890. doi: 10.1038/s41467-019-12740-2
- Schmidt, H. B., and Rohatgi, R. (2016). In Vivo Formation of Vacuolated Multi-phase Compartments Lacking Membranes. *Cell Rep.* 16, 1228–1236. doi: 10.1016/j.celrep.2016.06.088
- Sephton, C. F., Cenik, C., Kucukural, A., Dammer, E. B., Cenik, B., Han, Y., et al. (2011). Identification of neuronal RNA targets of TDP-43-containing ribonucleoprotein complexes. *J. Biol. Chem.* 286, 1204–1215. doi: 10.1074/jbc.M110.190884
- Seyfried, N. T., Gozal, Y. M., Dammer, E. B., Xia, Q., Duong, D. M., Cheng, D., et al. (2010). Multiplex SILAC Analysis of a Cellular TDP-43 proteinopathy model reveals protein inclusions associated with SUMOylation and diverse polyubiquitin chains. *Mol. Cell. Proteomics* 9, 705–718. doi: 10.1074/mcp.M800390-MCP200
- Shenouda, M., Zhang, A. B., Weichert, A., and Robertson, J. (2018). Mechanisms associated with TDP-43 neurotoxicity in ALS/FTLD. *Adv. Neurobiol.* 20, 239–263. doi: 10.1007/978-3-319-89689-2\_9
- Shiina, Y., Arima, K., Tabunoki, H., and Satoh, J. I. (2010). TDP-43 dimerizes in human cells in culture. *Cell. Mol. Neurobiol.* 30, 641–652. doi: 10.1007/s10571-009-9489-9
- Shodai, A., Ido, A., Fujiwara, N., Ayaki, T., Morimura, T., Oono, M., et al. (2012). Conserved acidic amino acid residues in a second rna recognition motif regulate assembly and function of TDP-43. *PLoS One* 7:e52776. doi: 10.1371/journal.pone.0052776
- Shodai, A., Morimura, T., Ido, A., Uchida, T., Ayaki, T., Takahashi, R., et al. (2013). Aberrant assembly of RNA recognition motif 1 links to pathogenic conversion of TAR DNA-binding protein of 43 kDa (TDP-43). *J. Biol. Chem.* 288, 14886–14905. doi: 10.1074/jbc.M113.451849
- Solski, J. A., Yang, S., Nicholson, G. A., Luquin, N., Williams, K. L., Fernando, R., et al. (2012). A novel TARDBP insertion/deletion mutation in the flail arm variant of amyotrophic lateral sclerosis. *Amyotroph. Lateral Scler.* 13, 465–470. doi: 10.3109/17482968.2012.662690
- Sreedharan, J., Blair, I. P., Tripathi, V. B., Hu, X., Vance, C., Rogelj, B., et al. (2008). TDP-43 mutations in familial and sporadic amyotrophic lateral sclerosis. *Science* 319, 1668–1672.
- Strong, M. J., Volkening, K., Hammond, R., Yang, W., Strong, W., Leystra-Lantz, C., et al. (2007). TDP43 is a human low molecular weight neurofilament (hNFL) mRNA-binding protein. *Mol. Cell. Neurosci.* 35, 320–327. doi: 10.1016/j.mcn.2007.03.007
- Sun, M., Zhang, Q., Wang, Y., Ge, W., and Guo, D. (2016). Prediction of redox-sensitive cysteines using sequential distance and other sequence-based features. *BMC Bioinformatics.* 17:316. doi: 10.1186/s12859-016-1185-4
- Sun, Y., Medina-Cruz, A., Hadley, K. C., Galant, N. J., Law, R., Vernon, R. M., et al. (2018). Physiologically important electrolytes as regulators of TDP-43 aggregation and droplet-phase behavior. *Biochemistry.* 58, 590–607. doi: 10.1021/acs.biochem.8b00842
- Suzuki, H., Lee, K., and Matsuoka, M. (2011). TDP-43-induced death is associated with altered regulation of BIM and Bcl-xL and attenuated by caspase-mediated TDP-43 cleavage. *J. Biol. Chem.* 286, 13171–13183. doi: 10.1074/jbc.M110.197483
- Szewczyk, B. (2013). Zinc homeostasis and neurodegenerative disorders. *Front. Aging Neurosci.* 5:33.
- Teloni, F., and Altmeyer, M. (2016). Survey and summary readers of poly(ADP-ribose): designed to be fit for purpose. *Nucleic Acids Res.* 44, 993–1006. doi: 10.1093/nar/gkv1383
- Udan-Johns, M., Bengoechea, R., Bell, S., Shao, J., Diamond, M. I., True, H. L., et al. (2014). Prion-like nuclear aggregation of TDP-43 during heat shock is regulated by HSP40/70 chaperones. *Hum. Mol. Genet.* 23, 157–170. doi: 10.1093/hmg/ddt408
- Valiente-Gabioud, A. A., Torres-Monserrat, V., Molina-Rubino, L., Binolfi, A., Griesinger, C., and Fernández, C. O. (2012). Structural basis behind the interaction of Zn<sup>2+</sup> with the protein  $\alpha$ -synuclein and the A $\beta$  peptide: a comparative analysis. *J. Inorg. Biochem.* 117, 334–341. doi: 10.1016/j.jinorgbio.2012.06.011
- Valle, C., and Carri, M. T. (2017). Cysteine modifications in the pathogenesis of ALS. *Front. Mol. Neurosci.* 10:5. doi: 10.3389/fnmol.2017.00005
- Vogler, T. O., Wheeler, J. R., Nguyen, E. D., Hughes, M. P., Britson, K. A., Lester, E., et al. (2018). TDP-43 and RNA form amyloid-like myo-granules in regenerating muscle. *Nature* 563, 508–513. doi: 10.1038/s41586-018-0665-2
- von Zweydford, F., Kahle, P. J., Gloeckner, C. J., Eckert, M., and Hans, F. (2018). Identification and characterization of ubiquitinylation sites in TAR DNA-binding protein of 43 kDa (TDP-43). *J. Biol. Chem.* 293, 16083–16099. doi: 10.1074/jbc.RA118.003440
- Wang, A., Conicella, A. E., Schmidt, H. B., Martin, E. W., Rhoads, S. N., Reeb, A. N., et al. (2018). A single N-terminal phosphomimic disrupts TDP-43 polymerization, phase separation, and RNA splicing. *EMBO J.* 37, e97452. doi: 10.15252/embj.201797452
- Wang, L., Kang, J., Lim, L., Wei, Y., and Song, J. (2018). TDP-43 NTD can be induced while CTD is significantly enhanced by ssDNA to undergo liquid-liquid phase separation. *Biochem. Biophys. Res. Commun.* 499, 189–195. doi: 10.1016/j.bbrc.2018.03.121
- Wang, H.-Y., Wang, I.-F., Bose, J., and Shen, C.-K. J. (2004). Structural diversity and functional implications of the eukaryotic TDP gene family. *Genomics* 83, 130–139. doi: 10.1016/s0888-7543(03)00214-3
- Wang, I. F., Chang, H. Y., Hou, S. C., Liou, G. G., Way, T. D., and James Shen, C. K. (2012). The self-interaction of native TDP-43 C terminus inhibits its degradation and contributes to early proteinopathies. *Nat. Commun.* 3:766. doi: 10.1038/ncomms1766
- Wang, I. F., Reddy, N. M., and Shen, C. K. J. (2002). Higher order arrangement of the eukaryotic nuclear bodies. *Proc. Natl. Acad. Sci. U.S.A.* 99, 13583–13588. doi: 10.1073/pnas.212483099
- Wang, W., Arakawa, H., Wang, L., Okolo, O., Siedlak, S. L., Jiang, Y., et al. (2017). Motor-coordinative and cognitive dysfunction caused by mutant TDP-43 could be reversed by inhibiting its mitochondrial localization. *Mol. Ther.* 25, 127–139. doi: 10.1016/j.ymthe.2016.10.013
- Wang, W., Wang, L., Lu, J., Siedlak, S. L., Fujioka, H., Liang, J., et al. (2016). The inhibition of TDP-43 mitochondrial localization blocks its neuronal toxicity. *Nat. Med.* 22, 869–878. doi: 10.1038/nm.4130
- Wang, Y. T., Kuo, P. H., Chiang, C. H., Liang, J. R., Chen, Y. R., Wang, S., et al. (2013). The truncated C-terminal RNA recognition motif of TDP-43 protein plays a key role in forming proteinaceous aggregates. *J. Biol. Chem.* 288, 9049–9057. doi: 10.1074/jbc.M112.438564
- Wegorzewska, I., and Baloh, R. H. (2011). TDP-43-based animal models of neurodegeneration: new insights into ALS pathology and pathophysiology. *Neurodegener. Dis.* 8, 262–274. doi: 10.1159/000321547

- Wei, Y., Lim, L., Wang, L., and Song, J. (2016). Inter-domain interactions of TDP-43 as decoded by NMR. *Biochem. Biophys. Res. Commun.* 473, 614–619. doi: 10.1016/j.bbrc.2016.03.158
- Winton, M. J., Igaz, L. M., Wong, M. M., Kwong, L. K., Trojanowski, J. Q., and Lee, V. M. Y. (2008). Disturbance of nuclear and cytoplasmic TAR DNA-binding protein (TDP-43) induces disease-like redistribution, sequestration, and aggregate formation. *J. Biol. Chem.* 283, 13302–13309. doi: 10.1074/jbc.M800342200
- Wobst, H. J., Wesolowski, S. S., Chadchankar, J., Delsing, L., Jacobsen, S., Mukherjee, J., et al. (2017). Cytoplasmic relocalization of TAR DNA-binding protein 43 is not sufficient to reproduce cellular pathologies associated with ALS in vitro. *Front. Mol. Neurosci.* 10:46.
- Wu, L. S., Cheng, W., Hou, S. C., Yan, Y. T., Jiang, S. T., and Shen, C. K. J. (2010). TDP-43, a neuro-pathosignature factor, is essential for early mouse embryogenesis. *Genesis* 48, 56–62. doi: 10.1002/dvg.20584
- Wühr, M., Güttler, T., Peshkin, L., McAlister, G. C., Sonnett, M., Ishihara, K., et al. (2015). The nuclear proteome of a vertebrate. *Curr. Biol.* 25, 2663–2671. doi: 10.1016/j.cub.2015.08.047
- Xiao, S., Sanelli, T., Chiang, H., Sun, Y., Chakrabarty, A., Keith, J., et al. (2015). Low molecular weight species of TDP-43 generated by abnormal splicing form inclusions in amyotrophic lateral sclerosis and result in motor neuron death. *Acta Neuropathol.* 130, 49–61. doi: 10.1007/s00401-015-1412-5
- Yang, C., Tan, W., Whittle, C., Qiu, L., Cao, L., Akbarian, S., et al. (2010). The C-terminal TDP-43 fragments have a high aggregation propensity and harm neurons by a dominant-negative mechanism. *PLoS One*. 5:e15878. doi: 10.1371/journal.pone.0015878
- Young, J. C., Hoogenraad, N. J., and Hartl, F. U. (2003). Molecular chaperones Hsp90 and Hsp70 deliver preproteins to the mitochondrial import receptor Tom70. *Cell* 112, 41–50. doi: 10.1016/s0092-8674(02)01250-3
- Zacco, E., Graña-Montes, R., Martin, S. R., de Groot, N. S., Alfano, C., Tartaglia, G. G., et al. (2019). RNA as a key factor in driving or preventing self-assembly of the TAR DNA-binding protein 43. *J. Mol. Biol.* 431, 1671–1688. doi: 10.1016/j.jmb.2019.01.028
- Zhai, Z., Tang, M., Yang, Y., Lu, M., Zhu, W. G., and Li, T. (2017). Identifying human SIRT1 substrates by integrating heterogeneous information from various sources. *Sci. Rep.* 7:4614. doi: 10.1038/s41598-017-04847-7
- Zhang, P., Fan, B., Yang, P., Temirov, J., Messing, J., Kim, H. J., et al. (2019). Chronic optogenetic induction of stress granules is cytotoxic and reveals the evolution of ALS-FTD pathology. *Elife* 8:e39578. doi: 10.7554/eLife.39578
- Zhang, Y. J., Caulfield, T., Xu, Y. F., Gendron, T. F., Hubbard, J., Stetler, C., et al. (2013). The dual functions of the extreme N-terminus of TDP-43 in regulating its biological activity and inclusion formation. *Hum. Mol. Genet.* 22, 3112–3122. doi: 10.1093/hmg/ddt166
- Zhang, Y. J., Xu, Y. F., Cook, C., Gendron, T. F., Roettges, P., Link, C. D., et al. (2009). Aberrant cleavage of TDP-43 enhances aggregation and cellular toxicity. *Proc. Natl. Acad. Sci. U.S.A.* 106, 7607–7612. doi: 10.1073/pnas.0900688106
- Zhang, Y. J., Xu, Y. F., Dickey, C. A., Buratti, E., Baralle, F., Bailey, R., et al. (2007). Progranulin mediates caspase-dependent cleavage of TAR DNA binding protein-43. *J. Neurosci.* 27, 10530–10534. doi: 10.1523/jneurosci.3421-07.2007
- Zhu, L., Xu, M., Yang, M., Yang, Y., Li, Y., Deng, J., et al. (2014). An ALS-mutant TDP-43 neurotoxic peptide adopts an anti-parallel  $\beta$ -structure and induces TDP-43 redistribution. *Hum. Mol. Genet.* 23, 6863–6877. doi: 10.1093/hmg/ddu409

**Conflict of Interest:** The authors declare that the research was conducted in the absence of any commercial or financial relationships that could be construed as a potential conflict of interest.

Copyright © 2019 François-Moutal, Perez-Miller, Scott, Miranda, Mollasalehi and Khanna. This is an open-access article distributed under the terms of the Creative Commons Attribution License (CC BY). The use, distribution or reproduction in other forums is permitted, provided the original author(s) and the copyright owner(s) are credited and that the original publication in this journal is cited, in accordance with accepted academic practice. No use, distribution or reproduction is permitted which does not comply with these terms.



# Circulating Exosomal miRNA as Diagnostic Biomarkers of Neurodegenerative Diseases

Lin Wang<sup>1</sup> and Lijuan Zhang<sup>2\*</sup>

<sup>1</sup>Department of Emergency Medicine, Shengjing Hospital of China Medical University, Shenyang, China, <sup>2</sup>Department of Obstetrics and Gynecology, Shengjing Hospital of China Medical University, Shenyang, China

## OPEN ACCESS

### Edited by:

Yunjong Lee,  
Sungkyunkwan University,  
South Korea

### Reviewed by:

Je-Hyun Yoon,  
Medical University of South Carolina,  
United States  
Marco Venturin,  
University of Milan, Italy

### \*Correspondence:

Lijuan Zhang  
cmu\_lijuanzhang@163.com

**Received:** 30 December 2019

**Accepted:** 17 March 2020

**Published:** 15 April 2020

### Citation:

Wang L and Zhang L  
(2020) Circulating Exosomal miRNA  
as Diagnostic Biomarkers of  
Neurodegenerative Diseases.  
*Front. Mol. Neurosci.* 13:53.  
doi: 10.3389/fnmol.2020.00053

Neurodegenerative diseases (NDDs) are a group of diseases caused by chronic and progressive degeneration of neural tissue. The main pathological manifestations are neuronal degeneration and loss in the brain and/or spinal cord. Common NDDs include Alzheimer disease (AD), Parkinson disease (PD), Huntington disease (HD), and amyotrophic lateral sclerosis (ALS). The complicated pathological characteristics and different clinical manifestations of NDDs result in a lack of sensitive and efficient diagnostic methods. In addition, no sensitive biomarkers are available to monitor the course of NDDs, predict their prognosis, and monitor the therapeutic response. Despite extensive research in recent years, analysis of amyloid  $\beta$  (A $\beta$ ) and  $\alpha$ -synuclein has failed to effectively improve NDD diagnosis. Although recent studies have indicated circulating miRNAs as promising diagnostic biomarkers of NDDs, the miRNA in the peripheral circulation is susceptible to interference by other components, making circulating miRNA results less consistent. Exosomes are small membrane vesicles with a diameter of approximately 30–100 nm that transport proteins, lipids, mRNA, and miRNA. Because recent studies have shown that exosomes have a double-membrane structure that can resist ribonuclease in the blood, giving exosomal miRNA high stability and making them resistant to degradation, they may become an ideal biomarker of circulating fluids. In this review, we discuss the applicability of circulating exosomal miRNAs as biomarkers, highlight the technical aspects of exosomal miRNA analysis, and review studies that have used circulating exosomal miRNAs as candidate diagnostic biomarkers of NDDs.

**Keywords:** biomarker, exosomal miRNA, neurodegenerative disease, CSF, blood

## INTRODUCTION

Neurodegenerative diseases (NDDs) are a group of diseases caused by chronic and progressive degeneration of neural tissue. The main pathological manifestations are neuronal degeneration and loss in the brain and/or spinal cord (Amin Lari et al., 2019). Common NDDs include Alzheimer disease (AD), Parkinson disease (PD), Huntington disease (HD), and amyotrophic lateral sclerosis (ALS).

Exosomes are extracellular vesicles with a diameter of 30–100 nm. They are produced by a variety of cells in eukaryotes and contain proteins, lipids, mRNA, and miRNAs. Exosomes carry the components of their original cells and interact with adjacent or distant cells to perform information exchange between different cells under both physiological and pathological conditions (Zhang et al., 2015; Yang et al., 2017).



In recent years, studies have shown that misfolded proteins associated with the pathogenesis of NDDs, such as  $\alpha$ -synuclein ( $\alpha$ -syn), tau, and amyloid  $\beta$  (A $\beta$ ), can be transported through exosomes and thereby promote the transmission of these proteins between cells and to nonpathological areas, hastening disease progression (Asai et al., 2015; D'Anca et al., 2019; Hosaka et al., 2019; Jiang et al., 2019). In addition to the ability of misfolded proteins to accelerate the development of NDDs, exosomal miRNAs (ex-miRNAs) are also involved in the pathogenesis of NDDs. AD onset is related to inflammation, which may increase cell damage and cause neuronal death. For example, the levels of ex-let-7 are increased in the brains of AD patients, where it can activate Toll-like receptor and further promote the release of inflammatory factors by activating its downstream signal molecules, eventually leading to neuronal death (Winkler et al., 2014). BACE1 ( $\beta$ -site amyloid precursor protein-cleaving enzyme 1) protein is an endopeptidase that cleaves the  $\beta$ -amyloid precursor protein to generate neurotoxic  $\beta$ -amyloid peptide A $\beta$ <sub>1-42</sub> (Hanin et al., 2000). Wang et al. (2008) indicated the ex-miR-107 contributes to BACE1 posttranscriptional regulation, which was predicted to exacerbate pathology in AD patients (Wang et al., 2008; Van Giau and An, 2016). Ex-miR-125, ex-miR-210, ex-miR-450b, and ex-miR-669b promote mitochondrial dysfunction, immune system disturbance, and inflammatory activation through multiple signaling pathways to trigger manganese-dependent  $\alpha$ -syn overexpression and deposition and thereby play an important role in the pathogenesis of PD (Danzer et al., 2012; Harischandra et al., 2018). Ex-miRNA-7 reduces the expression of  $\alpha$ -syn protein, the major component of Lewy bodies in sporadic PD (Junn et al., 2009). Langfelder et al. (2018) suggested that miR-128, miR-132, and miR-218 may be significantly correlated with the CAG repeat expansion of HD. The exosomes of mutant superoxide dismutase 1 (SOD1) motor neurons are rich in ex-miR-124, which can activate microglia and the nuclear factor  $\kappa$ B signaling pathway to stimulate the release of numerous cytokines, such as interleukin 1 $\beta$ , tumor necrosis factor  $\alpha$ , major histocompatibility class II, and inducible nitric oxide synthase (Pinto et al., 2017). The expression levels of ex-miR-155, ex-miR-146a, and ex-miR-124 are increased in the later stage of ALS, further aggravating the inflammation reaction, leading to a disordered intracellular environment and motor neuron degeneration and necrosis (Pinto et al., 2017). Ex-miR-27a-3p was down-regulated in ALS patients. Xu et al. (2018) suggested the down-regulated ex-miR-27a-3p could mineralize osteoblasts by dysregulating Wnt signaling pathway.

The complicated pathological characteristics and different clinical manifestations of NDDs have led to insufficiently sensitive and efficient diagnostic biomarkers. In addition, no sensitive biomarkers designed to monitor the course of NDDs can predict the prognosis and observe the therapeutic response. Patients with high levels of A $\beta$ <sub>42</sub> in the peripheral blood have an increased risk of dementia after 5 years; in addition, peripheral blood levels of tau protein are higher in AD patients and significantly associated with future cognitive impairment (Fiandaca et al., 2015; McDade and Bateman,

2017). However, the relatively low levels of A $\beta$  and tau proteins in peripheral blood necessitate more sensitive detection techniques and increase the detection cost, which limits their application as diagnostic biomarkers of AD. Tabrizi et al. (2013) showed that the plasma levels of neurofilament light chain (NfL) were significantly increased in HD patients and closely associated with age and CAG repeat length. However, the NfL concentration failed to reflect the treatment effects of patients.

Recent studies have suggested that miRNAs in the peripheral circulation are important biomarkers for the evaluation of diseases, including NDDs. In patients with NDDs, specific miRNAs are differentially expressed in body fluids such as blood and interstitial fluids. The plasma levels of miR-206 were determined to be increased in AD and to display a close relationship with cognitive decline and memory deficits (Kenny et al., 2019). Bai et al. (2017) found that decreased levels of serum miR-29, especially miR-29a and miR-29c, were potential biomarkers of PD. Increased levels of miR-100-5p and decreased levels of miR-330-3p and miR-641 were correlated with the total functional capacity of HD patients (Díez-Planelles et al., 2016). The authors therefore suggested that the levels of these circulating miRNAs might be promising biomarkers for monitoring disease progression. De Felice et al. (2014) suggested that miR-338-3p was increased in peripheral leukocytes, serum, and cerebrospinal fluid (CSF) from sporadic ALS patients and considered the miRNA to be a potential biomarker for early diagnosis of sporadic ALS (Díez-Planelles et al., 2016).

MiRNAs are small RNA molecules that are widely studied because of their important posttranscriptional regulatory roles in gene expression in cells and can also be found in exosomes. These ex-miRNAs can be protected by exosomes from degradation by nucleases that are widespread in body fluids. This feature also enables disease diagnosis through the detection of the content of specific miRNAs in exosomes. Because of connecting to the central nervous system (CNS) directly, analysis of CSF can accurately reflect the biochemical changes of the CNS and is an accurate and effective body fluid specimen. However, obtaining CSF is invasive and increases the risk of intracranial infection and is not easily accepted by patients. Ex-miRNAs are also stable in blood and can be reliably detected at low concentrations using today's sensitive analytical methods; the study of ex-miRNAs in blood is a good sample for noninvasive early diagnosis and prognostic evaluation for NDD patients. In this review, we discuss the applicability of circulating ex-miRNAs as biomarkers, highlight the technical aspects of ex-miR analysis, and review published studies that have used circulating ex-miRNAs as candidate diagnostic biomarkers of NDDs.

## BIOLOGICAL CHARACTERISTICS OF EXOSOMES

Exosomes are phospholipid bilayer membrane vesicles with a diameter of approximately 30–100 nm. They are rich in protein, lipid, mRNA, and miRNA and are released

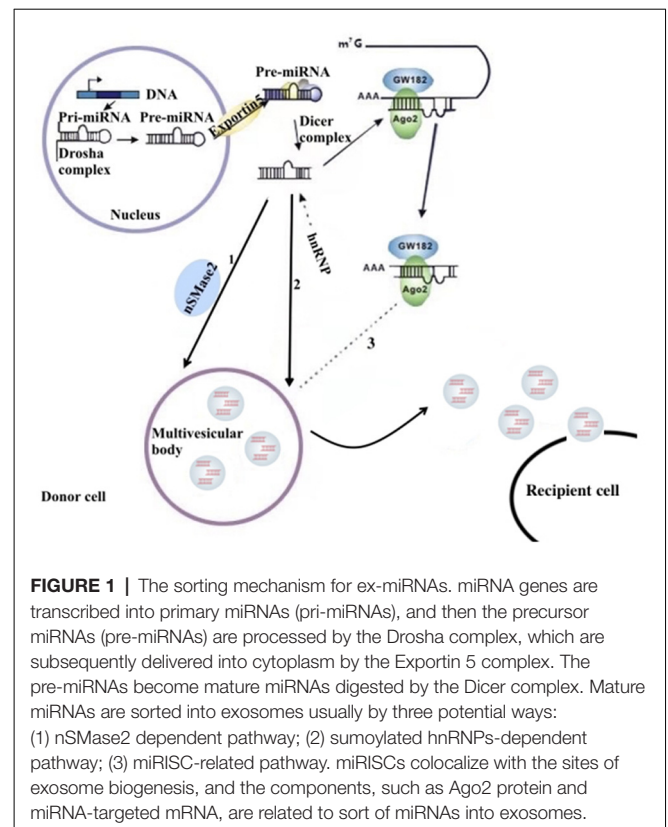
by membrane fusion into various extracellular and body fluids, such as urine, plasma, breast milk, and CSF. They act locally *via* autocrine and paracrine signaling or enter the blood system and travel to distant cells, directly acting on target cells through receptor ligand binding, endocytosis, and cytoplasmic membrane fusion and participating in complex intercellular material and information exchange (Saman et al., 2012; Kalani et al., 2014; Sarko and McKinney, 2017). Exosomes come from the endosome system. At present, exosome biogenesis is considered to begin with the formation of intraluminal vesicles in the multivesicular body (MVB; Trajkovic et al., 2008).

Exosome formation is roughly divided into three steps: (1) the cell membrane is sunken inward to form intracellular vesicles, namely, early endosomes; (2) early endosomes in turn form multivesicles with multiple vesicles in the cavity by means of endophytic buds to form MVBs; and (3) the MVBs combine with lysosomes: some vesicles within MVBs are degraded by lysosomes, whereas the remaining vesicles fuse with the cell membrane and are released to the outside of the cell in the form of exosomes (Grant and Donaldson, 2009; Shao et al., 2018).

## EXOSOME COMPOSITION AND miRNA SYNTHESIS AND PACKAGING

Exosomes are rich in proteins and lipids. According to the Exocarta database<sup>1</sup>, there are more than 8,000 exosome-related proteins and 184 lipids, of which more than 100 proteins are listed as exosomal biomarkers (Keerthikumar et al., 2015). Exosomes are mainly composed of two types of molecules: structural molecules and cargo molecules. Exosomes are released through the endosome pathway, and all contain tetraspanin proteins, Rab GTPases, TSG101, and heat shock proteins (Hsp70 and Hsp90; Stenmark, 2009; Hsu et al., 2010). Cargo molecules are lipids, proteins, and genetic material. Exosomes from different cells carry different proteins. Cells can also release prion-like proteins, such as A $\beta$ , tau,  $\alpha$ -syn, and misfolded SOD1, under different pathological and physiological conditions (Arellano-Anaya et al., 2015). The main role of lipid components in exosomes is to regulate exosomal sorting of miRNAs and proteins (Lamichhane et al., 2015). In addition to proteins and lipids, exosomes are also responsible for the transport of genetic material such as DNA, mRNA, miRNA, ribosomal RNA, circular RNA, and long noncoding RNA (Crescitelli et al., 2013). However, miRNA accounts for more than 50% of all exosomal RNA (Huang et al., 2013).

miRNAs are a type of endogenous noncoding RNA with regulatory function found in eukaryotes. In the nucleus, the miRNA gene transcribes into the initial miRNA (pri-miRNA) and then the pri-miRNA produces approximately 70 nucleotides with stem-ring structure under the shearing action of Drosha (pre-miRNA). In the cytoplasm, pre-miRNAs are cleaved by the RNase III enzyme Dicer to form a mature double-stranded miRNA containing approximately 21 nucleotides. In the cytoplasm, pre-miRNAs are cleaved by RNA polymerase



III to form a mature miRNA containing approximately 21 nucleotides. With the help of helicase, mature miRNAs can form RNA-induced silencing complex (RISC). Under the action of RISC and Argonaute proteins, miRNAs bind to target mRNA. One mature single-stranded miRNA remains in the complex, and the complementary mRNA sites regulate gene expression through base pairing (Higa et al., 2014). miRNAs in the nervous system constitute a complex network for regulating gene expression that plays an important role in the normal physiological regulation of the nervous system and the progression of NDDs (Properzi et al., 2015; Saraiva et al., 2017). The distribution of miRNAs into exosomes in the cytoplasm can be regulated by a variety of mechanisms. Possible pathways include: (1) the neutral sphingomyelinase 2 (nSMase 2)-dependent pathway; (2) the SUMOylated heterogeneous ribonucleoprotein nuclear (hnRNP)-dependent pathways; and (3) the 3'-terminal sequence-dependent pathways of miRNAs (Chevillet et al., 2014; Zhang et al., 2015; **Figure 1**).

Possible outcomes after exosomes are extracellularly released include: (1) their capture by nearby cells and reabsorption by their secretory cells; (2) their remote relocation, recognition by a cell, and fusion with its cell membrane; and (3) their entrance into the body fluid circulation and movement to other organs; the latter provides a solid foundation for their extraction and analysis. Common fluids for obtaining exosomes of the nervous system are the CSF and peripheral blood (Pant et al., 2012). Studies have found that the analysis of specific ex-miRNAs derived from the nervous system can reflect the physiological

<sup>1</sup><http://www.exocarta.org>

condition of the nervous system and provide a reference point for the diagnosis of NDDs.

## EXOSOME ISOLATION AND STORAGE

Since the discovery of exosomes, numerous studies have shown that exosomes can play an important role in the diagnosis and treatment of diseases. To facilitate the clinical application of exosomes, efficient separation and storage methods are essential. The current methods for isolating exosomes primarily comprise ultracentrifugation (Baranyai et al., 2015), the microfluidic chip method (Zhang et al., 2019), the antibody affinity capture method (Mathivanan et al., 2010), the polymer precipitation method (Cao F. et al., 2019), and gel exclusion chromatography (Hayashi et al., 2019). Of these, the most commonly used method is ultracentrifugation. The separation principle is based on particle size and density and involves low- and high-speed centrifugation. The method is simple and suitable for large-volume samples, but the equipment cost is high, and the recovery rate is unstable. At the same time, the disadvantages of repeated centrifugation, which may damage the vesicle membrane, limit its application (Helwa et al., 2017). The microfluidic chip method can construct a three-dimensional microenvironment based on exosome specificity and separate exosomes from the complex cell matrix. This method can obtain highly pure exosomes with high separation efficiency and automatic control. It is also an ideal method to separate exosomes (Cao H. et al., 2019). The antibody affinity capture method uses the antigens present in the exosomes and the highly specific affinity between the antibodies for separation. This method can also obtain high-purity exosomes and isolate different subtypes of exosomes (Popovic et al., 2018). The polymer precipitation method produces more heteroproteins and may yield particles of uneven size (Niu et al., 2017), whereas gel exclusion chromatography requires special equipment and has a long running time (Monguió-Tortajada et al., 2019), which is why these two methods are not widely used.

In addition, in terms of storage, it is extremely important to maintain the *in vitro* integrity of the exosomes. Exosomes prevent RNase degradation and are considered to be a stable source of miRNA (Koga et al., 2011). Indeed, ex-miRNAs have been shown to be stable for 5 years at  $-20^{\circ}\text{C}$ , unaffected for 2 weeks at  $4^{\circ}\text{C}$ , and resistant to freeze-thaw cycles (Weber et al., 2010). Therefore, exosomes, as a source of miRNAs, are efficient means for the storage and recovery of miRNAs under conditions that normally degrade free miRNAs (Thind and Wilson, 2016). Because of their availability and stability, ex-miRNAs are considered to be a new, noninvasive diagnostic biomarker of disease with potential for predicting prognosis. Two miRNA measurement techniques commonly used in research today are microarrays and reverse transcription-polymerase chain reaction (RT-PCR). Microarrays can provide the entire genome expression profiles of miRNAs, which can help to detect a large number of abnormal miRNAs. Compared with RT-PCR, microarrays have higher specificity but lower sensitivity (Mestdagh et al., 2014). Reverse transcription-PCR is more sensitive and suitable for monitoring low-level miRNAs. However, miRNAs have “isomiRs” (sequence heterogeneity at

the 3' and 5' ends), which may complicate the measurement, especially for RT-PCR (Lee et al., 2010).

Next-generation sequencing, a recently adopted and powerful method for measuring miRNA expression profiles, may prove clinically useful. This technique can accurately quantify miRNAs across the genome and distinguish between miRNAs that differ by only one nucleotide. Because no primers or probes are needed, it can detect new miRNAs (Liguori et al., 2018; Zhou et al., 2018).

In addition, the development of diagnostic biomarkers of NDDs based on circulating ex-miRNAs requires the consideration of multiple factors, such as source fluids, separation techniques, and quantitative methods. These factors should also be considered when published studies in this area are being compared (Figure 2).

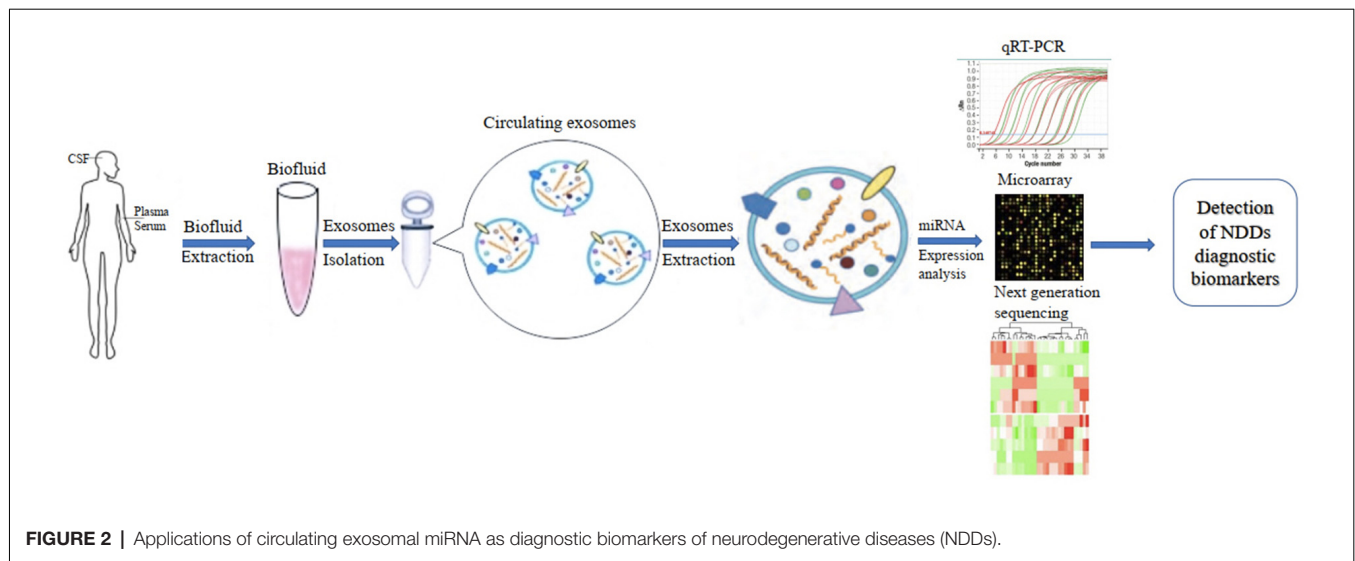
## CIRCULATING EX-miRNAs AS BIOMARKERS IN NDDs

The levels of miRNAs in peripheral blood are affected by multiple factors. In addition to sex, ethnicity, inflammatory factors, and lifestyle (Fan et al., 2015; Wagner et al., 2016; Pheiffer et al., 2018; Ludwig et al., 2019), they may also vary among sample types (whole blood, serum, and plasma; Blondal et al., 2013). Ex-miRNAs effectively avoid the above problems due to their stable expression, and the development and application of high-throughput sequencing technology to miRNA expression profiles have greatly improved diagnostic sensitivity (Cheng et al., 2013; Chen et al., 2017). The pathological changes in the nervous system microenvironment will affect the type and content of exosomes released by nerve cells, and miRNAs, as important components of neuroepigenetics, are often significantly altered as well, which suggests that ex-miRNAs are of considerable value as early diagnostic markers of NDDs (Table 1, Figure 3).

## EX-miRNAs AS BIOMARKERS IN AD

Lugli et al. (2015) successfully isolated exosomes from the plasma of AD patients and used high-throughput sequencing technology to compare their miRNA expression levels with those of a control group. They found that ex-miR-342-3p levels were significantly lower in AD patients and were highly correlated with several other low-expressing miRNAs. Decreased plasma levels of ex-miR-342-3p were also observed in AD patients by Rani et al. (2017); in addition, ex-miR-125a-5p, ex-miR-125b-5p, and ex-miR-451a levels were also lower in AD patients, and the levels of these ex-miRNA reductions correlated with the extent of cognitive impairment, which was assessed by Montreal Cognitive Assessment scores. Another plasma-based ex-miRNA study by Gámez-Valero et al. (2019) included 10 AD patients and 15 healthy controls. They used next-generation sequencing technology to identify significantly decreased levels of ex-miR-23a-3p, ex-let-7i-5p, ex-miR-126-3p, and ex-miR-151a-3p in AD patients, suggesting that the changes in the plasma levels of ex-miRNAs exhibited diagnostic value for AD.

Barbagallo et al. (2019), who compared the levels of ex-miRNAs in the serum of healthy controls and patients with

**TABLE 1 |** Circulating ex-miRNAs as biomarkers in neurodegenerative diseases (NDDs).

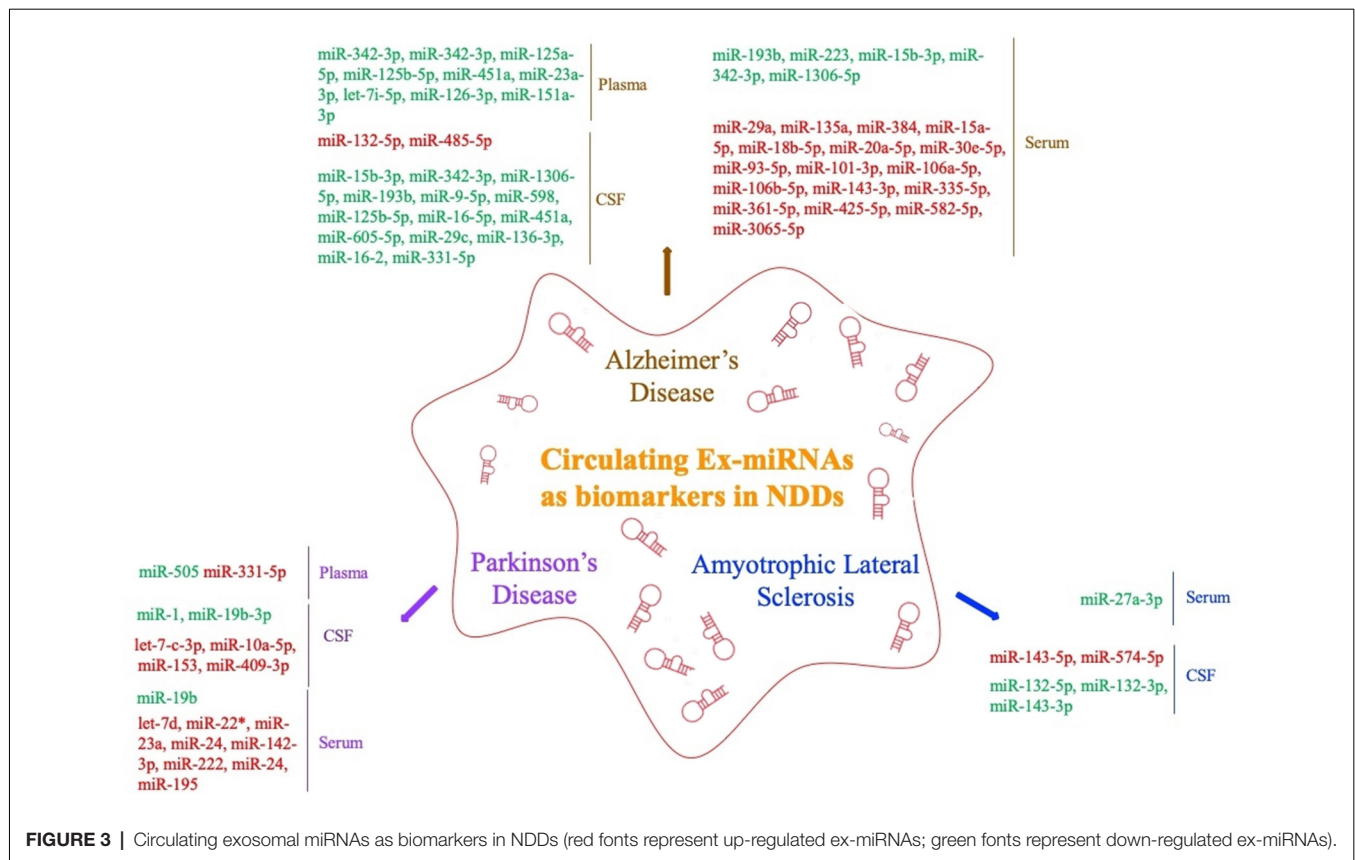
NDDs	Sample	Sample size	Validated changes		ROC curve analysis	References
			Up-regulated	Down-regulated		
AD	Plasma	46 P, 41 C		ex-miR-342-3p	N	Lugli et al. (2015)
	Plasma	97 P, 97 C		ex-miR-342-3p, ex-miR-125a-5p, ex-miR-125b-5p and ex-miR-451a	N	Rani et al. (2017)
	Plasma	10 P, 15 C		ex-miR-23a-3p, ex-let-7i-5p, ex-miR-126-3p and ex-miR-151a-3p	Y	Gómez-Valero et al. (2019)
	Serum	30 P, 30 C	ex-miR-29a		Y	Barbagallo et al. (2019)
	Serum	208 P, 228 C	ex-miR-135a, ex-miR-384	ex-miR-193b	Y	Yang et al. (2018)
	Serum	16 P, 22 C		ex-miR-223	Y	Wei et al. (2018)
	Serum	23 P, 23 C	ex-miR-15a-5p, ex-miR-18b-5p, ex-miR-20a-5p, ex-miR-30e-5p, ex-miR-93-5p, ex-miR-101-3p, ex-miR-106a-5p, ex-miR-106b-5p, ex-miR-143-3p, ex-miR-335-5p, ex-miR-361-5p, ex-miR-425-5p, ex-miR-582-5p, ex-miR-3065-5p	ex-miR-15b-3p, ex-miR-342-3p, ex-miR-1306-5p	N	Cheng et al. (2015)
	CSF	51 P, 84 C		ex-miR-193b	N	Liu et al. (2014)
	CSF	10 P, 10 C		ex-miR-9-5p, ex-miR-598	Y	Riancho et al. (2017)
	CSF	17 P, 12 C		ex-miR-125b-5p was increased, ex-miR-16-5p, ex-miR-451a, ex-miR-605-5p	Y	McKeever et al. (2018)
PD	CSF	27 P, 28 C	ex-miR-132-5p, ex-miR-485-5p	ex-miR-29c, ex-miR-136-3p, ex-miR-16-2, ex-miR-331-5p	Y	Gui et al. (2015)
	Plasma	52 P, 48 C	ex-miR-331-5p	ex-miR-505	Y	Yao et al. (2018)
	Serum	30 P, 30 C	ex-let-7d, ex-miR-22*, ex-miR-23a, ex-miR-24, ex-miR-142-3p, and ex-miR-222		Y	Barbagallo et al. (2019)
	Serum	109 P, 43 C	ex-miR-24, ex-miR-195	ex-miR-19b	Y	Cao et al. (2017)
	CSF	47 P, 27 C	ex-let-7-c-3p, ex-miR-10a-5p, ex-miR-153, and ex-miR-409-3p	ex-miR-1, ex-miR-19b-3p	N	Gui et al. (2015)
ALS	Serum	10 P, 20 C		ex-miR-27a-3p	N	Xu et al. (2018)
	CSF	22 P, 24 C	ex-miR-143-5p, ex-miR-574-5p	ex-miR-132-5p, ex-miR-132-3p, ex-miR-143-3p	N	Freischmidt et al. (2013)

CSF, Cerebrospinal fluid; P, patients; C, Controls; ROC, receiver operating characteristic; Y, yes; N, no.

different types of NDDs, found that ex-miR-29a levels were significantly increased in AD patients [area under the curve (AUC), 0.71; 95% confidence interval (CI), 0.577–0.843], with

43.0% sensitivity and 97.0% specificity and a stronger fold change and higher *p* value than free miR-29a in serum. Yang et al. (2018) used quantitative RT (qRT)-PCR to measure the





serum levels of three ex-miRNAs—ex-miR-135a, ex-miR-193b, and ex-miR-384 in 101 mild cognitive impairment (MCI) and 107 dementia of Alzheimer type (DAT) patients. They found with high sensitivity and specificity that the levels of ex-miR-135a (AUC, 0.981; 95% CI, 0.951–0.995) and ex-miR-384 (AUC, 0.870; 95% CI, 0.816–0.914) were increased in DAT patients and that ex-miR-193b (AUC, 0.798; 95% CI, 0.736–0.914) was decreased. Moreover, they further determined that the combination of the three miRNAs would be better for the early diagnosis of AD than any single one. The serum levels of ex-miR-223 were also found to be dysregulated in AD patients, with Wei et al. (2018) suggesting that the level of ex-miR-223 (AUC, 0.875; 95% CI, 0.7779–0.9721) was significantly decreased in AD patients and might act as a biomarker to distinguish AD patients from individuals without dementia. Cheng et al. (2015) explored serum-derived differentially expressed ex-miRNAs in a study of AD patients and identified 14 significantly upregulated ex-miRNAs (ex-miR-15a-5p, ex-miR-18b-5p, ex-miR-20a-5p, ex-miR-30e-5p, ex-miR-93-5p, ex-miR-101-3p, ex-miR-106a-5p, ex-miR-106b-5p, ex-miR-143-3p, ex-miR-335-5p, ex-miR-361-5p, ex-miR-425-5p, ex-miR-582-5p, and ex-miR-3065-5p) and 3 significantly downregulated ex-miRNAs (ex-miR-15b-3p, ex-miR-342-3p, and ex-miR-1306-5p). Although all ex-miRNAs were validated by qRT-PCR analysis, their study lacked receiver operating characteristic (ROC) curve analysis and enrolled fewer patients with MCI. Nonetheless, their results contribute to the study of serum-derived ex-miRNAs as markers for AD diagnosis.

By comparing ex-miR-193b levels between the normal population and patients with MCI and DAT, Liu et al. (2014) found that ex-miR-193b levels were significantly lower in patients with MCI and DAT than in the people in the control group. However, the difference in the levels of miR-193b in whole blood was not statistically significant. In addition, ex-miR-193b levels were lower in DAT patients than in MCI patients. This study suggested that specific ex-miRNAs can be used as diagnostic biomarkers to reflect AD disease progression. Another study that examined the levels of free miRNAs and ex-miRNAs in the CSF of AD patients found that ex-miR-9-5p and ex-miR-598 levels were significantly downregulated. However, free miR-9-5p and miR-598 were detected in up to 50% and 75% of healthy control CSF samples, respectively, but they were not present in any AD CSF sample. This difference suggested that ex-miRNAs may be more reliable as potential biomarkers of AD (Riancho et al., 2017).

Researchers have also strived to distinguish between young- and late-onset AD (YOAD/LOAD). McKeever et al. (2018) collected CSF samples from 17 YOAD patients, 13 LOAD patients, and 12 healthy controls; they found that CSF-derived ex-miR-125b-5p was increased in YOAD patients, whereas ex-miR-16-5p, ex-miR-451a, and ex-miR-605-5p were decreased. In addition, the altered levels of ex-miR-125b-5p, ex-miR-451a, and ex-miR-605-5p were similar in both LOAD and YOAD patients when compared with the healthy controls. Another study reported decreased levels of ex-miR-29c, ex-miR-136-3p,

ex-miR-16-2, and ex-miR-331-5p but increased levels of ex-miR-132-5p and ex-miR-485-5p in the CSF of AD patients (Gui et al., 2015).

## EX-miRNAs AS BIOMARKERS IN PD

PD is the second most common NDDs in the elderly. The incidence of PD increases with age. Compared with the direct detection of biomarkers such as DJ-1,  $\alpha$ -syn, and miRNA in the CSF or blood, exosome detection is more stable and more reliable and can better reflect PD severity (Hartfield et al., 2012; Saito, 2017). Cerebrospinal fluid and plasma exosomes are rich in miRNA and provide a stable protective environment for genetic material. The expression levels of miRNA are significantly altered in PD, indicating that these nucleic acids play a major role in the pathogenesis of PD and may become biological markers of PD.

Yao et al. (2018) compared the diagnostic value of plasma-derived ex-miRNAs in patients with PD. Their study included 52 PD patients and 48 healthy controls. The analysis was verified by qRT-PCR and showed that the ex-miR-331-5p expression level was significantly increased and the ex-miR-505 expression level significantly decreased in PD patients, with AUCs of 0.849 and 0.898, respectively, suggesting that these two ex-miRNAs are potentially useful for the early diagnosis of PD.

Barbagallo et al. (2019) isolated ex-miRNA from the serum of 30 PD patients and compared it with that of 30 healthy controls to try to explore the differential expression of ex-miRNAs in PD patients. The results were verified by TaqMan RT-PCR analysis. The expression levels of ex-let-7d, ex-miR-22\* (asterisk indicates anti-sense miR), ex-miR-23a, ex-miR-24, ex-miR-142-3p, and ex-miR-222 were significantly increased in the serum of PD patients. In addition, ROC curve analysis revealed that these six ex-miRNAs are ideal biomarkers for the diagnosis of PD, but the researchers also mentioned that, because of the small number of patients enrolled, subsequent larger multicenter studies were needed to verify their conclusions. Another differential expression study of serum-derived ex-miRNA was performed by Cao et al. (2017). Comparison of the levels of 24 ex-miRNAs from the serum of 109 PD patients and healthy controls showed that the levels of ex-miR-24 (AUC, 0.908; 95% CI, 0.850–0.949) and ex-miR-195 (AUC, 0.697; 95% CI, 0.617–0.770) were increased, and ex-miR-19b (AUC, 0.753; 95% CI, 0.675–0.820) decreased in PD patients, indicating the possible use of ex-miRNA as a novel strategy for the diagnosis of PD.

Gui et al. (2015) performed the only differential expression analysis of ex-miRNA derived from the CSF of PD patients. The study included 47 PD patients, 28 AD patients, and 27 healthy controls. The researchers verified 16 differentially expressed ex-miRNAs from 746 miRNAs. Among the 11 downregulated ex-miRNAs, the levels of ex-miR-1 and ex-miR-19b-3p were significantly decreased in the CSF of PD patients, whereas the levels of ex-let-7-c-3p, ex-miR-10a-5p, ex-miR-153, and ex-miR-409-3p were significantly increased. The researchers further compared the expression levels of ex-miRNAs in the CSF of AD patients, with the results showing that the expression levels of ex-let-7-c-3p, ex-miR-10a-5p, ex-miR-153, and ex-miR-409-3p were significantly higher, and the levels of ex-miR-1 and ex-miR-

19b-3p significantly lower, in the CSF of PD patients than those of AD patients. The final results of the study suggested that the expression of CSF-derived ex-miRNAs in PD patients not only had potential diagnostic value for PD, but also could help to identify different types of NDDs.

## EX-miRNAs AS BIOMARKERS IN HD

HD is a hereditary and slowly progressing NDD. Diagnosis mainly relies on family genetic history and genetic testing. Although HD is an untreatable disease, biomarkers that might provide early diagnostic clues or reflect disease progression are still important for patients. Progress has been made in circulating biomarkers of diagnosis of HD, with plasma NfL reported to be significantly increased in HD patients (Tabrizi et al., 2013). Leukocyte telomere length values were significantly decreased in HD and might be a reliable biomarker to track HD progression (Scarabino et al., 2019). In the PREDICT-HD study, the researchers suggested that six miRNAs—miR-135b-3p, miR-140-5p, miR-520f-3p, miR-3928-5p, miR-4317, and miR-8082—were significantly increased in presymptomatic HD patients and could be potential biomarkers for the early diagnosis of HD (Reed et al., 2018). Gaughwin et al. (2011) found that the level of plasma miR-34b was significantly decreased in presymptomatic HD patients compared with healthy controls, suggesting miR-34b as a new potential biomarker of HD that can be stably expressed in plasma and detected before clinical symptoms occur. No study has explored ex-miRNAs as biomarkers for the diagnosis of HD. However, previous studies have found that miR-124 expression decreases in HD patients and can lead to upregulation of REST expression, thereby inhibiting the expression of brain-derived neurotrophic factor and indicating that abnormal expression of miR-124 plays a key role in the pathogenesis of HD (Cheng et al., 2009; Das et al., 2013; Hwang and Zukin, 2018).

Lee et al. (2017) developed an exosome-based delivery method (Exo-124) to treat HD in an animal model (R6/2 transgenic HD mice). Although they did not achieve the desired improvement in motor symptoms, their research into a new exosome-based system for miRNA delivery in NDDs is nonetheless valuable.

## EX-miRNAs AS BIOMARKERS IN ALS

ALS is one of the NDDs entailing selective upper and lower motor neuron damage. The main clinical manifestations of ALS are rapidly progressing muscle weakness and atrophy and ultimately death due to respiratory failure caused by respiratory muscle weakness. The early symptoms of ALS are not specific, and it can be easily confused with various diseases such as cervical spondylosis and myasthenia gravis. It lacks specific biomarkers, which makes clinical diagnosis difficult, and has a high rate of misdiagnosis (Worms, 2001). Because the molecules contained in exosomes are specific and related to their source cells and pathological conditions, exosomes can reflect the physiological and pathological changes of the original cells, including proteins, mRNA, and miRNA, and have potential biomarker functions (Bang and Thum, 2012). The serum levels of miR-1234-3p and miR-1825 have been reported to be significantly decreased in

ALS patients, with the miR-1825 decrease observed in both sporadic ALS and familial ALS patients and the miR-1234-3p decrease restricted to patients with sporadic ALS (Freischmidt et al., 2015). The plasma levels of miR-130a-3p, miR-151b, and miR-221-3p were also reported to be decreased in sporadic ALS patients and positively correlated with sporadic ALS progression, suggesting that these miRNAs could be useful not only as biomarkers for diagnosis, but also for monitoring disease progression (Liguori et al., 2018).

A study of serum-derived ex-miRNA as a biomarker for ALS diagnosis performed by Xu et al. (2018) enrolled 10 ALS patients and 20 healthy controls. By comparing the two groups, they found that ex-miR-27a-3p levels were significantly decreased in ALS patients. The researchers concluded that ex-miR-27a-3p might be a potential diagnostic biomarker of ALS. However, because the study did not further analyze the data using ROC statistics, specific analysis is needed before this test can be applied in the clinic. Freischmidt et al. (2013) determined the expression levels of ex-miRNAs in the CSF and serum of 22 patients with sporadic ALS and compared them with those of 24 healthy controls. Ex-miR-132-5p, ex-miR-132-3p, and ex-miR-143-3p were significantly decreased, and ex-miR-143-5p and ex-miR-574-5p significantly increased in ALS patients, suggesting that these ex-miRNAs are potential biomarkers for ALS diagnosis. In addition, all of these ex-miRNAs can be combined with TDP-43 *in vitro*, proving that miRNA dysfunction may participate in ALS pathogenesis by affecting TDP-43.

## ADVANTAGES AND DISADVANTAGES OF EX-miRNA AS DIAGNOSTIC BIOMARKERS FOR NDDs

The stable expression of ex-miRNAs and their resistance to the influence of external factors that might affect their expression, coupled with the development and application of high-throughput sequencing technology for determining the expression profiles of miRNAs, greatly improve the sensitivity of ex-miRNA diagnosis (Cheng et al., 2013). Some studies have compared ex-miRNAs with currently recognized methods for diagnosing NDDs to further illustrate their accuracy as NDD biomarkers. Cheng et al. (2015) analyzed the plasma ex-miRNAs of AD patients and identified a group of abnormally expressed ex-miRNAs. Compared with other diagnostic methods such as neuropsychology and neuroimaging, the sensitivity and specificity of ex-miRNAs were 87% and 77%, respectively, which showed that the specific ex-miRNAs had potential value as biomarkers for AD diagnosis. Liu et al. (2014) examined miR-193b levels in the peripheral blood of healthy controls, patients with MCI, and patients with DAT. By comparing ex-miR-193b, A $\beta$ , tau, p-tau, HCY, homocysteine; APOE, apolipoprotein E levels, the authors found that ex-miR-193b levels were significantly lower in MCI and DAT patients than in healthy controls; there were no significant differences in peripheral blood. In addition, ex-miR-193b expression was lower in DAT patients than in MCI patients, and ex-miR-193b was negatively correlated with A $\beta$ 42. This study indicated

that specific ex-miRNAs may have similar diagnostic efficacy to traditional biomarkers and could be used as potential diagnostic biomarkers to reflect AD disease progression. Thus, it can be seen that ex-miRNA have considerable potential as biomarkers for the diagnosis and prognosis prediction of NDDs.

In the field of NDD diagnosis, analysis of circulating ex-miRNAs is undoubtedly a novel and particularly exciting method. However, given the relatively late clinical start for exosomal research, it still faces significant practical problems. First, existing exosomal enrichment schemes differ in the yield of exosomal isolation and may also result in slightly different amounts of exosomes (Taylor et al., 2011; Rekker et al., 2014). These methods include ultracentrifugation, density gradient separation, immunoaffinity capture, size-exclusion chromatography, and commercial kits (Zhang et al., 2015). Depending on the sample tested, they may all isolate only small amounts of exosomes. In these cases, a large number of test samples may be required. However, a study has shown that as little as 250  $\mu$ l of human plasma might be sufficient for the isolation of an adequate quantity of ex-miRNAs (Huang et al., 2013). Some commercial reagents can simplify the process of exosomal extraction, but they are often too expensive to be widely used in clinical diagnosis. Second, there is no effective and rapid technical method to detect exosomes. Moreover, the method for long-term *in vitro* storage of exosomes requires optimization. Third, there is huge variation in the ex-miRNA expression results among different epidemiological studies of NDD patients in the progressive stage, indicating the need for a large sample of standardized and controllable epidemiological research data to determine the diagnostic efficacy.

However, for ex-miRNAs to become the diagnostic biomarker for NDDs, breakthroughs need to be made in the following aspects: (1) clarification of the relationship between ex-miRNAs and the occurrence and development of NDDs and further elucidation of disease pathogenesis; (2) development of more mature and reliable techniques for extracting ex-miRNAs from various body fluids for their application in clinical practice; and (3) using ex-miRNAs as a breakthrough point, identification of more specific miRNAs in various NDDs as biomarkers for early diagnosis, thereby boosting clinical diagnosis.

## CONCLUSIONS

Although still facing significant practical problems, the stable expression of ex-miRNAs has been a potential biomarker of NDDs. As a possible diagnostic biomarker of NDDs, ex-miRNAs cannot currently surpass the traditional clinical detection methods, but with technological and research development, their advantages as diagnostic biomarkers of NDDs will undoubtedly be gradually validated, providing a theoretical basis for the early detection and prevention of NDDs.

## AUTHOR CONTRIBUTIONS

This manuscript was primarily written by LW. The figure was produced by LW and LZ. LZ contributed to the editing of this review. Both authors read and approved the final manuscript.



## REFERENCES

- Amin Lari, A., Ghavanini, A. A., and Bokaei, H. R. (2019). A review of electrophysiological studies of lower motor neuron involvement in amyotrophic lateral sclerosis. *Neurol. Sci.* 40, 1125–1136. doi: 10.1007/s10072-019-03832-4
- Arellano-Anaya, Z. E., Huor, A., Leblanc, P., Lehmann, S., Provansal, M., Raposo, G., et al. (2015). Prion strains are differentially released through the exosomal pathway. *Cell. Mol. Life Sci.* 72, 1185–1196. doi: 10.1007/s00018-014-1735-8
- Asai, H., Ikezu, S., Tsunoda, S., Medalla, M., Luebke, J., Haydar, T., et al. (2015). Depletion of microglia and inhibition of exosome synthesis halt tau propagation. *Nat. Neurosci.* 18, 1584–1593. doi: 10.1038/nn.4132
- Bai, X., Tang, Y., Yu, M., Wu, L., Liu, F., Ni, J., et al. (2017). Downregulation of blood serum microRNA 29 family in patients with Parkinson's disease. *Sci. Rep.* 7:5411. doi: 10.1038/s41598-017-03887-3
- Bang, C., and Thum, T. (2012). Exosomes: new players in cell-cell communication. *Int. J. Biochem. Cell Biol.* 44, 2060–2064. doi: 10.1016/j.biocel.2012.08.007
- Baranyai, T., Herczeg, K., Onódi, Z., Voszka, I., Módos, K., Marton, N., et al. (2015). Isolation of exosomes from blood plasma: qualitative and quantitative comparison of ultracentrifugation and size exclusion chromatography methods. *PLoS One* 10:e0145686. doi: 10.1371/journal.pone.0145686
- Barbagallo, C., Mostile, G., Baglieri, G., Giunta, F., Luca, A., Raciti, L., et al. (2019). Specific signatures of serum mirnas as potential biomarkers to discriminate clinically similar neurodegenerative and vascular-related diseases. *Cell. Mol. Neurobiol.* doi: 10.1007/s10571-019-00751-y [Epub ahead of print].
- Blondal, T., Jensby Nielsen, S., Baker, A., Andreasen, D., Mouritzen, P., Wrang Teillum, M., et al. (2013). Assessing sample and miRNA profile quality in serum and plasma or other biofluids. *Methods* 59, S1–S6. doi: 10.1016/j.jymeth.2012.09.015
- Cao, F., Gao, Y., Chu, Q., Wu, Q., Zhao, L., Lan, T., et al. (2019). Proteomics comparison of exosomes from serum and plasma between ultracentrifugation and polymer-based precipitation kit methods. *Electrophoresis* 40, 3092–3098. doi: 10.1002/elps.201900295
- Cao, X. Y., Lu, J. M., Zhao, Z. Q., Li, M. C., Lu, T., An, X. S., et al. (2017). MicroRNA biomarkers of Parkinson's disease in serum exosome-like microvesicles. *Neurosci. Lett.* 644, 94–99. doi: 10.1016/j.neulet.2017.02.045
- Cao, H., Zhou, X., and Zeng, Y. (2019). Microfluidic exponential rolling circle amplification for sensitive microRNA detection directly from biological samples. *Sens. Actuators B Chem.* 279, 447–457. doi: 10.1016/j.snb.2018.09.121
- Chen, J. J., Zhao, B., Zhao, J., and Li, S. (2017). Potential roles of exosomal MicroRNAs as diagnostic biomarkers and therapeutic application in Alzheimer's disease. *Neural Plast.* 2017:7027380. doi: 10.1155/2017/7027380
- Cheng, L., Doecke, J. D., Sharples, R. A., Villemagne, V. L., Fowler, C. J., Rembach, A., et al. (2015). Prognostic serum miRNA biomarkers associated with Alzheimer's disease shows concordance with neuropsychological and neuroimaging assessment. *Mol. Psychiatry* 20, 1188–1196. doi: 10.1038/mp.2014.127
- Cheng, L., Quek, C. Y. J., Sun, X., Bellingham, S. A., and Hill, A. F. (2013). The detection of microRNA associated with Alzheimer's disease in biological fluids using next-generation sequencing technologies. *Front. Genet.* 4:150. doi: 10.3389/fgene.2013.00150
- Cheng, L. C., Pastrana, E., Tavazoie, M., and Doetsch, F. (2009). miR-124 regulates adult neurogenesis in the subventricular zone stem cell niche. *Nat. Neurosci.* 12, 399–408. doi: 10.1038/nn.2294
- Chevillet, J. R., Kang, Q., Ruf, I. K., Briggs, H. A., Vojtech, L. N., Hughes, S. M., et al. (2014). Quantitative and stoichiometric analysis of the microRNA content of exosomes. *Proc. Natl. Acad. Sci. U S A* 111, 14888–14893. doi: 10.1073/pnas.1408301111
- Crescitelli, R., Lässer, C., Szabó, T. G., Kittel, A., Eldh, M., Dianzani, I., et al. (2013). Distinct RNA profiles in subpopulations of extracellular vesicles: apoptotic bodies, microvesicles and exosomes. *J. Extracell. Vesicles* 2:20677. doi: 10.3402/jev.v2i0.20677
- D'Anca, M., Fenoglio, C., Serpente, M., Arosio, B., Cesari, M., Scarpini, E. A., et al. (2019). Exosome determinants of physiological aging and age-related neurodegenerative diseases. *Front. Aging Neurosci.* 11:232. doi: 10.3389/fnagi.2019.00232
- Danzer, K. M., Kranich, L. R., Ruf, W. P., Cagsal-Getkin, O., Winslow, A. R., Zhu, L., et al. (2012). Exosomal cell-to-cell transmission of  $\alpha$  synuclein oligomers. *Mol. Neurodegener.* 7:42. doi: 10.1186/1750-1326-7-42
- Das, E., Jana, N. R., and Bhattacharyya, N. P. (2013). MicroRNA-124 targets CCNA2 and regulates cell cycle in STHdh(Q111)/Hdh(Q111) cells. *Biochem. Biophys. Res. Commun.* 437, 217–224. doi: 10.1016/j.bbrc.2013.06.041
- De Felice, B., Annunziata, A., Fiorentino, G., Borra, M., Biffali, E., Coppola, C., et al. (2014). miR-338–3p is over-expressed in blood, CFS, serum and spinal cord from sporadic amyotrophic lateral sclerosis patients. *Neurogenetics* 15, 243–253. doi: 10.1007/s10048-014-0420-2
- Díez-Planelles, C., Sánchez-Lozano, P., Crespo, M. C., Gil-Zamorano, J., Ribacoba, R., González, N., et al. (2016). Circulating microRNAs in Huntington's disease: emerging mediators in metabolic impairment. *Pharmacol. Res.* 108, 102–110. doi: 10.1016/j.phrs.2016.05.005
- Fan, H.-M., Sun, X.-Y., Niu, W., Zhao, L., Zhang, Q.-L., Li, W.-S., et al. (2015). Altered microRNA expression in peripheral blood mononuclear cells from young patients with schizophrenia. *J. Mol. Neurosci.* 56, 562–571. doi: 10.1007/s12031-015-0503-z
- Fiandaca, M. S., Kapogiannis, D., Mapstone, M., Boxer, A., Eitan, E., Schwartz, J. B., et al. (2015). Identification of preclinical Alzheimer's disease by a profile of pathogenic proteins in neurally derived blood exosomes: a case-control study. *Alzheimers Dement.* 11, 600.e1–607.e1. doi: 10.1016/j.jalz.2014.06.008
- Freischmidt, A., Müller, K., Ludolph, A. C., and Weishaupt, J. H. (2013). Systemic dysregulation of TDP-43 binding microRNAs in amyotrophic lateral sclerosis. *Acta Neuropathol. Commun.* 1:42. doi: 10.1186/2051-5960-1-42
- Freischmidt, A., Müller, K., Zondler, L., Weydt, P., Mayer, B., von Arnim, C. A., et al. (2015). Serum microRNAs in sporadic amyotrophic lateral sclerosis. *Neurobiol. Aging* 36, 2660.e15–2620.e20. doi: 10.1016/j.neurobiolaging.2015.06.003
- Gámez-Valero, A., Campdelacreu, J., Vilas, D., Ispuerto, L., Reñé, R., Álvarez, R., et al. (2019). Exploratory study on microRNA profiles from plasma-derived extracellular vesicles in Alzheimer's disease and dementia with Lewy bodies. *Transl. Neurodegener.* 8:31. doi: 10.1186/s40035-019-0169-5
- Gaughwin, P. M., Ciesla, M., Lahiri, N., Tabrizi, S. J., Brundin, P., and Björkqvist, M. (2011). Hsa-miR-34b is a plasma-stable microRNA that is elevated in pre-manifest Huntington's disease. *Hum. Mol. Genet.* 20, 2225–2237. doi: 10.1093/hmg/ddr111
- Grant, B. D., and Donaldson, J. G. (2009). Pathways and mechanisms of endocytic recycling. *Nat. Rev. Mol. Cell Biol.* 10, 597–608. doi: 10.1038/nrm2755
- Gui, Y., Liu, H., Zhang, L., Lv, W., and Hu, X. (2015). Altered microRNA profiles in cerebrospinal fluid exosome in Parkinson disease and Alzheimer disease. *Oncotarget* 6, 37043–37053. doi: 10.18632/oncotarget.6158
- Haniu, M., Denis, P., Young, Y., Mendiaz, E. A., Fuller, J., Hui, J. O., et al. (2000). Characterization of Alzheimer's  $\beta$ -secretase protein BACE. A pepsin family member with unusual properties. *J. Biol. Chem.* 275, 21099–21106. doi: 10.1074/jbc.M002095200
- Harischandra, D. S., Ghaisas, S., Rokad, D., Zamanian, M., Jin, H., Anantharam, V., et al. (2018). Environmental neurotoxicant manganese regulates exosome-mediated extracellular miRNAs in cell culture model of Parkinson's disease: relevance to  $\alpha$ -synuclein misfolding in metal neurotoxicity. *Neurotoxicology* 64, 267–277. doi: 10.1016/j.neuro.2017.04.007
- Hartfield, E. M., Fernandes, H. J., Vowles, J., Cowley, S. A., and Wade-Martins, R. (2012). Cellular reprogramming: a new approach to modelling Parkinson's disease. *Biochem. Soc. Trans.* 40, 1152–1157. doi: 10.1042/bst20120159
- Hayashi, N., Doi, H., Kurata, Y., Kagawa, H., Atobe, Y., Funakoshi, K., et al. (2019). Proteomic analysis of exosome-enriched fractions derived from cerebrospinal fluid of amyotrophic lateral sclerosis patients. *Neurosci. Res.* doi: 10.1016/j.neures.2019.10.010 [Epub ahead of print].
- Helwa, I., Cai, J., Drewry, M. D., Zimmerman, A., Dinkins, M. B., Khaled, M. L., et al. (2017). A comparative study of serum exosome isolation using differential ultracentrifugation and three commercial reagents. *PLoS One* 12:e0170628. doi: 10.1371/journal.pone.0170628
- Higa, G. S., de Sousa, E., Walter, L. T., Kinjo, E. R., Resende, R. R., and Kihara, A. H. (2014). MicroRNAs in neuronal communication. *Mol. Neurobiol.* 49, 1309–1326. doi: 10.1007/s12035-013-8603-7
- Hosaka, T., Yamashita, T., Tamaoka, A., and Kwak, S. (2019). Extracellular RNAs as biomarkers of sporadic amyotrophic lateral sclerosis



- and other neurodegenerative diseases. *Int. J. Mol. Sci.* 20:E3148. doi: 10.3390/ijms20133148
- Hsu, C., Morohashi, Y., Yoshimura, S., Manrique-Hoyos, N., Jung, S., Lauterbach, M. A., et al. (2010). Regulation of exosome secretion by Rab35 and its GTPase-activating proteins TBC1D10A-C. *J. Cell Biol.* 189, 223–232. doi: 10.1083/jcb.200911018
- Huang, X., Yuan, T., Tschannen, M., Sun, Z., Jacob, H., Du, M., et al. (2013). Characterization of human plasma-derived exosomal RNAs by deep sequencing. *BMC Genomics* 14:319. doi: 10.1186/1471-2164-14-319
- Hwang, J. Y., and Zukin, R. S. (2018). REST, a master transcriptional regulator in neurodegenerative disease. *Curr. Opin. Neurobiol.* 48, 193–200. doi: 10.1016/j.conb.2017.12.008
- Jiang, R., Rong, C., Ke, R., Meng, S., Yan, X., Ke, H., et al. (2019). Differential proteomic analysis of serum exosomes reveals alterations in progression of Parkinson disease. *Medicine* 98:e17478. doi: 10.1097/md.00000000000017478
- Junn, E., Lee, K.-W., Jeong, B. S., Chan, T. W., Im, J.-Y., and Mouradian, M. M. (2009). Repression of  $\alpha$ -synuclein expression and toxicity by microRNA-7. *Proc. Natl. Acad. Sci. U S A* 106, 13052–13057. doi: 10.1073/pnas.0906277106
- Kalani, A., Tyagi, A., and Tyagi, N. (2014). Exosomes: mediators of neurodegeneration, neuroprotection and therapeutics. *Mol. Neurobiol.* 49, 590–600. doi: 10.1007/s12035-013-8544-1
- Keerthikumar, S., Gangoda, L., Liem, M., Fonseka, P., Atukorala, I., Ozcitti, C., et al. (2015). Proteogenomic analysis reveals exosomes are more oncogenic than ectosomes. *Oncotarget* 6, 15375–15396. doi: 10.18632/oncotarget.3801
- Kenny, A., McArdle, H., Calero, M., Rabano, A., Madden, S. F., Adamson, K., et al. (2019). Elevated plasma microRNA-206 levels predict cognitive decline and progression to dementia from mild cognitive impairment. *Biomolecules* 9:E734. doi: 10.3390/biom9110734
- Koga, Y., Yasunaga, M., Moriya, Y., Akasu, T., Fujita, S., Yamamoto, S., et al. (2011). Exosome can prevent RNase from degrading microRNA in feces. *J. Gastrointest. Oncol.* 2, 215–222. doi: 10.3978/j.issn.2078-6891.2011.015
- Lamichane, T. N., Raiker, R. S., and Jay, S. M. (2015). Exogenous DNA loading into extracellular vesicles via electroporation is size-dependent and enables limited gene delivery. *Mol. Pharm.* 12, 3650–3657. doi: 10.1021/acs.molpharmaceut.5b00364
- Langfelder, P., Gao, F., Wang, N., Howland, D., Kwak, S., Vogt, T. F., et al. (2018). MicroRNA signatures of endogenous Huntingtin CAG repeat expansion in mice. *PLoS One* 13:e0190550. doi: 10.1371/journal.pone.0190550
- Lee, S. T., Im, W., Ban, J. J., Lee, M., Jung, K. H., Lee, S. K., et al. (2017). Exosome-based delivery of miR-124 in a Huntington's disease model. *J. Mov. Disord.* 10, 45–52. doi: 10.14802/jmd.16054
- Lee, L. W., Zhang, S., Etheridge, A., Ma, L., Martin, D., Galas, D., et al. (2010). Complexity of the microRNA repertoire revealed by next-generation sequencing. *RNA* 16, 2170–2180. doi: 10.1261/rna.2225110
- Liguori, M., Nuzziello, N., Introna, A., Consiglio, A., Licciulli, F., D'Errico, E., et al. (2018). Dysregulation of MicroRNAs and target genes networks in peripheral blood of patients with sporadic amyotrophic lateral sclerosis. *Front. Mol. Neurosci.* 11:288. doi: 10.3389/fnmol.2018.00288
- Liu, C. G., Song, J., Zhang, Y. Q., and Wang, P. C. (2014). MicroRNA-193b is a regulator of amyloid precursor protein in the blood and cerebrospinal fluid derived exosomal microRNA-193b is a biomarker of Alzheimer's disease. *Mol. Med. Rep.* 10, 2395–2400. doi: 10.3892/mmr.2014.2484
- Ludwig, N., Hecksteden, A., Kahraman, M., Fehlmann, T., Laufer, T., Kern, F., et al. (2019). Spring is in the air: seasonal profiles indicate vernal change of miRNA activity. *RNA Biol.* 16, 1034–1043. doi: 10.1080/15476286.2019.1612217
- Lugli, G., Cohen, A. M., Bennett, D. A., Shah, R. C., Fields, C. J., Hernandez, A. G., et al. (2015). Plasma exosomal miRNAs in persons with and without Alzheimer disease: altered expression and prospects for biomarkers. *PLoS One* 10:e0139233. doi: 10.1371/journal.pone.0139233
- Mathivanan, S., Lim, J. W., Tauro, B. J., Ji, H., Moritz, R. L., and Simpson, R. J. (2010). Proteomics analysis of A33 immunoaffinity-purified exosomes released from the human colon tumor cell line LIM1215 reveals a tissue-specific protein signature. *Mol. Cell Proteomics* 9, 197–208. doi: 10.1074/mcp.900152-mcp200
- McDade, E., and Bateman, R. J. (2017). Stop Alzheimer's before it starts. *Nature* 547, 153–155. doi: 10.1038/547153a
- McKeever, P. M., Schneider, R., Taghdiri, F., Weichert, A., Multani, N., Brown, R. A., et al. (2018). MicroRNA expression levels are altered in the cerebrospinal fluid of patients with young-onset alzheimer's disease. *Mol. Neurobiol.* 55, 8826–8841. doi: 10.1007/s12035-018-1032-x
- Mestdagh, P., Hartmann, N., Baeriswyl, L., Andreasen, D., Bernard, N., Chen, C., et al. (2014). Evaluation of quantitative miRNA expression platforms in the microRNA quality control (miRQC) study. *Nat. Methods* 11, 809–815. doi: 10.1038/nmeth.3014
- Mongiui-Tortajada, M., Gálvez-Montón, C., Bayes-Genis, A., Roura, S., and Borràs, F. E. (2019). Extracellular vesicle isolation methods: rising impact of size-exclusion chromatography. *Cell. Mol. Life Sci.* 76, 2369–2382. doi: 10.1007/s00018-019-03071-y
- Niu, Z., Pang, R. T. K., Liu, W., Li, Q., Cheng, R., and Yeung, W. S. B. (2017). Polymer-based precipitation preserves biological activities of extracellular vesicles from an endometrial cell line. *PLoS One* 12:e0186534. doi: 10.1371/journal.pone.0186534
- Pant, S., Hilton, H., and Burczynski, M. E. (2012). The multifaceted exosome: biogenesis, role in normal and aberrant cellular function and frontiers for pharmacological and biomarker opportunities. *Biochem. Pharmacol.* 83, 1484–1494. doi: 10.1016/j.bcp.2011.12.037
- Pheiffer, C., Dias, S., Rheeder, P., and Adam, S. (2018). Decreased expression of circulating miR-20a-5p in south african women with gestational diabetes mellitus. *Mol. Diagn. Ther.* 22, 345–352. doi: 10.1007/s40291-018-0325-0
- Pinto, S., Cunha, C., Barbosa, M., Vaz, A. R., and Brites, D. (2017). Exosomes from NSC-34 cells transfected with hSOD1-G93A are enriched in miR-124 and drive alterations in microglia phenotype. *Front. Neurosci.* 11:273. doi: 10.3389/fnins.2017.00273
- Popovic, M., Mazzega, E., Toffoletto, B., and de Marco, A. (2018). Isolation of anti-extracellular vesicle single-domain antibodies by direct panning on vesicle-enriched fractions. *Microb. Cell Fact.* 17:6. doi: 10.1186/s12934-017-0856-9
- Properzi, F., Ferroni, E., Poleggi, A., and Vinci, R. (2015). The regulation of exosome function in the CNS: implications for neurodegeneration. *Swiss Med. Wkly.* 145:w14204. doi: 10.4414/sm.w.2015.14204
- Rani, A., O'Shea, A., Ianov, L., Cohen, R. A., Woods, A. J., and Foster, T. C. (2017). miRNA in circulating microvesicles as biomarkers for age-related cognitive decline. *Front. Aging Neurosci.* 9:323. doi: 10.3389/fnagi.2017.00323
- Reed, E. R., Latourelle, J. C., Bockholt, J. H., Bregu, J., Smock, J., Paulsen, J. S., et al. (2018). MicroRNAs in CSF as prodromal biomarkers for Huntington disease in the PREDICT-HD study. *Neurology* 90, e264–e272. doi: 10.1212/wnl.0000000000004844
- Rekker, K., Saare, M., Roost, A. M., Kubo, A.-L., Zarovni, N., Chiesi, A., et al. (2014). Comparison of serum exosome isolation methods for microRNA profiling. *Clin. Biochem.* 47, 135–138. doi: 10.1016/j.clinbiochem.2013.10.020
- Riancho, J., Vázquez-Higuera, J. L., Pozueta, A., Lage, C., Kazimierzczak, M., Bravo, M., et al. (2017). MicroRNA profile in patients with Alzheimer's disease: analysis of miR-9-5p and miR-598 in raw and exosome enriched cerebrospinal fluid samples. *J. Alzheimers Dis.* 57, 483–491. doi: 10.3233/jad-161179
- Saito, Y. (2017). DJ-1 as a biomarker of Parkinson's disease. *Adv. Exp. Med. Biol.* 1037, 149–171. doi: 10.1007/978-981-10-6583-5\_10
- Saman, S., Kim, W., Raya, M., Visnick, Y., Vinci, S., Saman, S., et al. (2012). Exosome-associated tau is secreted in tauopathy models and is selectively phosphorylated in cerebrospinal fluid in early Alzheimer disease. *J. Biol. Chem.* 287, 3842–3849. doi: 10.1074/jbc.m111.277061
- Saraiva, C., Esteves, M., and Bernardino, L. (2017). MicroRNA: basic concepts and implications for regeneration and repair of neurodegenerative diseases. *Biochem. Pharmacol.* 141, 118–131. doi: 10.1016/j.bcp.2017.07.008
- Sarko, D. K., and McKinney, C. E. (2017). Exosomes: origins and therapeutic potential for neurodegenerative disease. *Front. Neurosci.* 11:82. doi: 10.3389/fnins.2017.00082
- Scarabino, D., Veneziano, L., Peconi, M., Frontali, M., Mantuano, E., and Corbo, R. M. (2019). Leukocyte telomere shortening in Huntington's disease. *J. Neurol. Sci.* 396, 25–29. doi: 10.1016/j.jns.2018.10.024
- Shao, H., Im, H., Castro, C. M., Breakefield, X., Weissleder, R., and Lee, H. (2018). New technologies for analysis of extracellular vesicles. *Chem. Rev.* 118, 1917–1950. doi: 10.1021/acs.chemrev.7b00534
- Stenmark, H. (2009). Rab GTPases as coordinators of vesicle traffic. *Nat. Rev. Mol. Cell Biol.* 10, 513–525. doi: 10.1038/nrm2728
- Tabrizi, S. J., Scahill, R. I., Owen, G., Durr, A., Leavitt, B. R., Roos, R. A., et al. (2013). Predictors of phenotypic progression and disease onset in premanifest and early-stage Huntington's disease in the TRACK-HD study: analysis of

- 36-month observational data. *Lancet Neurol.* 12, 637–649. doi: 10.1016/s1474-4422(13)70088-7
- Taylor, D. D., Zacharias, W., and Gercel-Taylor, C. (2011). Exosome isolation for proteomic analyses and RNA profiling. *Methods Mol. Biol.* 728, 235–246. doi: 10.1007/978-1-61779-068-3\_15
- Thind, A., and Wilson, C. (2016). Exosomal miRNAs as cancer biomarkers and therapeutic targets. *J. Extracell. Vesicles* 5:31292. doi: 10.3402/jev.v5.31292
- Trajkovic, K., Hsu, C., Chiantia, S., Rajendran, L., Wenzel, D., Wieland, F., et al. (2008). Ceramide triggers budding of exosome vesicles into multivesicular endosomes. *Science* 319, 1244–1247. doi: 10.1126/science.1153124
- Van Giau, V., and An, S. S. A. (2016). Emergence of exosomal miRNAs as a diagnostic biomarker for Alzheimer's disease. *J. Neurol. Sci.* 360, 141–152. doi: 10.1016/j.jns.2015.12.005
- Wagner, K.-H., Cameron-Smith, D., Wessner, B., and Franzke, B. (2016). Biomarkers of aging: from function to molecular biology. *Nutrients* 8:E338. doi: 10.3390/nu8060338
- Wang, W.-X., Rajeev, B. W., Stromberg, A. J., Ren, N., Tang, G., Huang, Q., et al. (2008). The expression of microRNA miR-107 decreases early in Alzheimer's disease and may accelerate disease progression through regulation of  $\beta$ -site amyloid precursor protein-cleaving enzyme 1. *J. Neurosci.* 28, 1213–1223. doi: 10.1523/JNEUROSCI.5065-07.2008
- Weber, J. A., Baxter, D. H., Zhang, S., Huang, D. Y., Huang, K. H., Lee, M. J., et al. (2010). The microRNA spectrum in 12 body fluids. *Clin. Chem.* 56, 1733–1741. doi: 10.1373/clinchem.2010.147405
- Wei, H., Xu, Y., Xu, W., Zhou, Q., Chen, Q., Yang, M., et al. (2018). Serum exosomal miR-223 serves as a potential diagnostic and prognostic biomarker for dementia. *Neuroscience* 379, 167–176. doi: 10.1016/j.neuroscience.2018.03.016
- Winkler, C. W., Taylor, K. G., and Peterson, K. E. (2014). Location is everything: let-7b microRNA and TLR7 signaling results in a painful TRP. *Sci. Signal.* 7:pe14. doi: 10.1126/scisignal.2005407
- Worms, P. M. (2001). The epidemiology of motor neuron diseases: a review of recent studies. *J. Neurol. Sci.* 191, 3–9. doi: 10.1016/s0022-510x(01)00630-x
- Xu, Q., Zhao, Y., Zhou, X., Luan, J., Cui, Y., and Han, J. (2018). Comparison of the extraction and determination of serum exosome and miRNA in serum and the detection of miR-27a-3p in serum exosome of ALS patients. *Intractable Rare Dis. Res.* 7, 13–18. doi: 10.5582/iridr.2017.01091
- Yang, F., Liao, X., Tian, Y., and Li, G. (2017). Exosome separation using microfluidic systems: size-based, immunoaffinity-based and dynamic methodologies. *Biotechnol. J.* 12:1600699. doi: 10.1002/biot.201600699
- Yang, T. T., Liu, C. G., Gao, S. C., Zhang, Y., and Wang, P. C. (2018). The serum exosome derived MicroRNA-135a, -193b, and -384 were potential Alzheimer's disease biomarkers. *Biomed. Environ. Sci.* 31, 87–96. doi: 10.3967/bes2018.011
- Yao, Y. F., Qu, M. W., Li, G. C., Zhang, F. B., and Rui, H. C. (2018). Circulating exosomal miRNAs as diagnostic biomarkers in Parkinson's disease. *Eur. Rev. Med. Pharmacol. Sci.* 22, 5278–5283. doi: 10.26355/eurrev\_201808\_15727
- Zhang, J., Li, S., Li, L., Li, M., Guo, C., Yao, J., et al. (2015). Exosome and exosomal microRNA: trafficking, sorting, and function. *Genomics Proteomics Bioinformatics* 13, 17–24. doi: 10.1016/j.gpb.2015.02.001
- Zhang, P., Zhou, X., He, M., Shang, Y., Tetlow, A. L., Godwin, A. K., et al. (2019). Ultrasensitive detection of circulating exosomes with a 3D-nanopatterned microfluidic chip. *Nat. Biomed. Eng.* 3, 438–451. doi: 10.1038/s41551-019-0356-9
- Zhou, Y., Fujikura, K., Mkrtchian, S., and Lauschke, V. M. (2018). Computational methods for the pharmacogenetic interpretation of next generation sequencing data. *Front. Pharmacol.* 9:1437. doi: 10.3389/fphar.2018.01437

**Conflict of Interest:** The authors declare that the research was conducted in the absence of any commercial or financial relationships that could be construed as a potential conflict of interest.

Copyright © 2020 Wang and Zhang. This is an open-access article distributed under the terms of the Creative Commons Attribution License (CC BY). The use, distribution or reproduction in other forums is permitted, provided the original author(s) and the copyright owner(s) are credited and that the original publication in this journal is cited, in accordance with accepted academic practice. No use, distribution or reproduction is permitted which does not comply with these terms.

# Advantages of publishing in Frontiers



## OPEN ACCESS

Articles are free to read  
for greatest visibility  
and readership



## FAST PUBLICATION

Around 90 days  
from submission  
to decision



## HIGH QUALITY PEER-REVIEW

Rigorous, collaborative,  
and constructive  
peer-review



## TRANSPARENT PEER-REVIEW

Editors and reviewers  
acknowledged by name  
on published articles

## Frontiers

Avenue du Tribunal-Fédéral 34  
1005 Lausanne | Switzerland

**Visit us:** [www.frontiersin.org](http://www.frontiersin.org)

**Contact us:** [frontiersin.org/about/contact](http://frontiersin.org/about/contact)



## REPRODUCIBILITY OF RESEARCH

Support open data  
and methods to enhance  
research reproducibility



## DIGITAL PUBLISHING

Articles designed  
for optimal readership  
across devices



## FOLLOW US

@frontiersin



## IMPACT METRICS

Advanced article metrics  
track visibility across  
digital media



## EXTENSIVE PROMOTION

Marketing  
and promotion  
of impactful research



## LOOP RESEARCH NETWORK

Our network  
increases your  
article's readership